NASA TECHNICAL MEMORANDUM

NASA TM X-72818

COPY NO.

NASA TM X-72818

AERODYNAMIC CHARACTERISTICS OF A POWERED TILT-PROPROTOR WIND-TUNNEL MODEL

John C. Wilson, Raymond E. Mineck, and Carl E. Freeman

Langley Directorate,
U.S. Army Air Mobility R&D Lab

NATIONAL AERONAUTICS AND SPACE ADMINISTRATION
LANGLEY RESEARCH CENTER, HAMPTON, VIRGINIA 23665

1 Report No	2 Government Accession No	3. Recipient's Catalog No
NASA TM X-72818		

4 Title and Subtitle	5 Report Date
AERODYNAMIC CHARACTERISTICS OF A POWERED TILT-PROPROTOR WIND-TUNNEL MODEL	March 1976
	6 Performing Organization Code
7 Author(s)	8 Performing Organization Report No
*John C. Wilson, Raymond E. Mineck, and Carl E. Freeman	
9 Performing Organization Name and Address	10 Work Unit No.
NASA Langley Research Center Hampton, VA 23665	505-11-41-10
	11 Contract or Grant No
12 Sponsoring Agency Name and Address	13 Type of Report and Period Covered
National Aeronautics & Space Administration Washington, DC 20546	Technical Memorandum
	14 Sponsoring Agency Code

15 Supplementary Notes

*U.S. Army Air Mobility R&D Lab
Langley Directorate

16 Abstract

An investigation was conducted in the Langley V/STOL tunnel to determine the performance, stability and control, and rotor-wake interaction effects of a powered tilt-proprotor aircraft model with gimbal-hub rotors. Tests were conducted at representative flight conditions for hover, helicopter, transition, and airplane flight. Force and moment data were obtained for the complete model and for each of the two rotors. In addition to wind-speed variation, the angle of attack, angle of sideslip, rotor speed, rotor collective pitch, longitudinal cyclic pitch, rotor pylon angle, and configuration geometry were varied. The results, presented in graphical form, are available in tabular form to facilitate the validation of analytical methods of defining the aerodynamic characteristics of tilt-proprotor configurations. For the most part, the data are presented in this report without extensive analyses or correlations with theory.

17. Key Words (Suggested by Author(s))	18. Distribution Statement
Tilt-proprotor Wind-tunnel tests Wall corrections	Unclassified - Unlimited

19 Security Classif. (of this report)	20 Security Classif. (of this page)	21 No. of Pages	22 Price
Unclassified	Unclassified	270	$8.50

AERODYNAMIC CHARACTERISTICS OF A POWERED TILT-PROPROTOR WIND-TUNNEL MODEL

John C. Wilson, Raymond E. Mineck, and Carl E. Freeman

Langley Directorate
U.S. Army Air Mobility R&D Laboratory
NASA Langley Research Center
Hampton, Virginia 23665

SUMMARY

An investigation was conducted in the Langley V/STOL tunnel to determine the performance, stability and control, and rotor-wake interaction effects of a powered tilt-proprotor aircraft model with gimbal-hub rotors. Tests were conducted at representative flight conditions for hover, helicopter, transition and airplane flight. Force and moment data were obtained for the complete model and for each of the two rotors. In addition to wind-speed variation, the angle of attack, angle of sideslip, rotor speed, rotor collective pitch, longitudinal cyclic pitch, rotor pylon angle, and configuration geometry were varied. The results are presented in graphical form; they are also available in tabular form through a supplement to the present report to facilitate the validation of analytical methods of defining the aerodynamic characteristics of tilt-proprotor configurations.

It was found that the existing correction procedure for open and closed test-section configurations resulted in noticeable differences in corrected aerodynamic data.

INTRODUCTION

The tilt-proprotor VTOL aircraft configuration offers a means of combining the lift efficiency of the helicopter in hover with the cruise efficiency of the propeller-driven aircraft in forward flight. Two rotor concepts which are candidates for the tilt-proprotor configuration are the three-bladed-gimbaled rotor concept and the three-bladed-rigid, soft-in-plane, rotor concept. The evaluation of these candidates required aerodynamic tests as in reference 1 to provide data describing baseline trim characteristics, forces and moments, and

stability and control derivatives, to identify and explore potential problem areas, and to provide an experimental base for the validation of analytical methods of deriving stability and control characteristics. The flight range of particular interest is the low-speed/transition-flight from helicopter mode through low-speed proprotor mode, where the rotor shafts are essentially horizontal.

A wind-tunnel investigation was undertaken to evaluate the aerodynamics of the gimbaled rotor version of the tilt-proprotor configuration. A powered 1/10-scale model was tested in the Langley V/STOL tunnel. The rotors were driven through a common transmission by two electric motors. The model had three force and moment measuring balances: one to measure total loads and one in each pylon to measure rotor loads. Variations were made of angle of attack, wind speed, angle of yaw, pylon tilt angle, rotor speed, collective pitch, longitudinal cyclic pitch, elevator angle, horizontal tail incidence, and flap/aileron angle.

The capability of the model to provide data was facilitated by three balances, remote actuation of rotor controls for collective and cyclic pitch, strain gages on the rotor blades, and variation of configuration, i.e., pylon tilt angle, empennage, and removal of rotors. The data presented herein will permit the assessment of rotor wake effects on the wing and horizontal tail. Both gross and net hover performance, as affected by airframe download, ground proximity and flap/aileron settings were obtained. Control power as affected by differential collective pitch, mean longitudinal cyclic pitch, differential longitudinal cyclic pitch, and elevator angle were evaluated from hover throughout the transition flight speed range. Some testing was made with the horizontal and vertical tails off. This provided data to evaluate the influence of the rotor wake on the tail contributions to pitching-moment and yawing-moment characteristics. Stability derivatives related to angle of attack and angle of sideslip can also be determined from the data which is presented in graphical form. Comprehensive tabulations of the data are available in a supplement to this report. A request form for the supplement is found in the back of this report. For the most part, the data in this report are presented without correlation with theory.

SYMBOLS

A sketch of the axis systems used in this investigation showing the positive direction of forces, moments, and angles is presented in figure 1. Force and moment data are referred to both stability axis and body axis systems. A nominal center of gravity was defined as the origin of both axis systems. It should be noted that the position of the center of gravity would change as the pylon angle changes on the full-scale aircraft. The rotor force and moment data are referred to the rotor shaft axis system with the moment center located 22.16 cm (8.725 in.) from the rotor hub towards the conversion axis (center of pylon rotation).

The physical quantities in this paper are given in both the International System of Units (SI) and the U.S. Customary Units. Factors relating these two systems of units are presented in reference 2. The symbols and coefficients are as follows (symbols enclosed in parenthesis are used in the data tabulations).

a_{1s} lateral flapping, deg

A rotor disk area, πR^2, m^2 (ft^2)

AR aspect ratio, $\frac{b^2}{S}$

b wing span, m (in.)

b_{1s} longitudinal flapping, deg

b_r number of rotor blades

B_{1S}(BIAV) average longitudinal cyclic pitch of left and right rotors, measured from shaft, $\frac{B_{1S_R} + B_{1S_L}}{2}$, deg

B_{1S_L}(BIL) left rotor longitudinal cyclic pitch, measured from shaft, deg

B_{1S_R}(BIR) right rotor longitudinal cyclic pitch, measured from shaft, deg

c	local chord, m (in.)
$\bar{c}$	mean aerodynamic chord, m (in.)
c_r	rotor blade chord, cm (in.)
C_D(CD)	drag coefficient, $\frac{F_D}{q_\infty S}$ (stability axis)
C_{D_o}	profile drag coefficient, $C_D - \frac{C_L^2}{\pi e AR}$
C_H	rotor drag force coefficient, $\frac{H}{\rho_\infty A V_T^2}$
C_ℓ(CRM,CR)	rolling-moment coefficient about the center of gravity, $\frac{M_X}{q_\infty S b}$ (CRM for body axis, CR for stability axis)
$C_{\ell,s}$(CRS)	slipstream rolling-moment coefficient about the center of gravity, $\frac{M_X}{q_s S b}$ (stability axis)
C_L(CL)	lift coefficient, $\frac{F_L}{q_\infty S}$
$C_{L,s}$(CLS)	slipstream lift coefficient, $\frac{F_L}{q_s S}$
$C_{L,VT}$(CLVT)	lift coefficient, $\frac{F_L}{\rho_\infty A V_T^2}$
C_{L_α}	lift-curve slope, $\frac{dC_L}{d\alpha}$
C_m(CPM,CM)	pitching-moment coefficient about the center of gravity, $\frac{M_Y}{q_\infty S \bar{c}}$ (CPM for body axis, CM for stability axis)
$C_{m,s}$(CMS)	slipstream pitching-moment coefficient about the center of gravity, $\frac{M_Y}{q_s S \bar{c}}$ (stability axis)
C_n(CYM,CYW)	yawing-moment coefficient about the center of gravity, $\frac{M_Z}{q_\infty S b}$ (CYM for stability axis, CYW for body axis)

$C_{n,s}$(CYMS) slipstream yawing-moment coefficient about the center of gravity, $\frac{M_Z}{q_s Sb}$ (stability axis)

C_{NF}(CNF) normal-force coefficient, $\frac{F_N}{q_\infty S}$ (body axis)

C_Q(CQAV) average rotor torque coefficient, $\frac{Q_L + Q_R}{2\rho_\infty ARV_T^2}$

C_T average rotor thrust coefficient, $\frac{T_L + T_R}{2(\rho_\infty AV_T^2)}$

$C_{X,s}$(CXS) slipstream propulsive force coefficient, $\frac{-F_D}{q_s S}$

C_Y(CY) side-force coefficient, $\frac{F_Y}{q_\infty S}$, or rotor side-force coefficient, $\frac{Y}{\rho_\infty AV_T^2}$

$C_{Y,s}$(CSFS) slipstream side-force coefficient, $\frac{F_Y}{q_s S}$

D rotor diameter, m (ft)

e span efficiency factor

F_A(AF) axial force, N (lbf)

F_D drag force, N (lbf)

F_L lift force, N (lbf)

F_N(NF) normal force, N (lbf)

F_Y(SF) side force, N (lbf)

h height from ground to rotor hub, m (ft)

H	rotor drag force at hub, N (lbf)
i_t	tail incidence with respect to body axis, deg
M_X(RM)	rolling moment about the center of gravity, N-m (in.-lbf)
M_Y(PM)	pitching moment about the center of gravity, N-m (in.-lbf)
M_Z(YM)	yawing moment about the center of gravity, N-m (in.-lbf)
N	rotor speed, revolutions per minute
PM_L	left pylon pitching moment, N-m (in.-lbf)
PM_R	right pylon pitching moment, N-m (in.-lbf)
Q_L(QL)	left rotor torque, N-m (in.-lbf)
Q_R(QR)	right rotor torque, N-m (in.-lbf)
q_s(QS)	slipstream dynamic pressure, $q_\infty + \frac{T_L + T_R}{2A}$, N/m^2 (lbf/ft^2)
q_∞(Q)	free-stream dynamic pressure, $\frac{1}{2}\rho_\infty V_\infty^2$, N/m^2 (lbf/ft^2)
r	radial distance from hub, m (ft)
R	rotor radius, m (ft)
RM_L	left pylon rolling moment, N-m (in.-lbf)
RM_R	right pylon rolling moment, N-m (in.-lbf)
S	wing area, m^2 (ft^2)
t	airfoil thickness, m (ft)

T_L(TL)	left rotor thrust, N (lbf)
T_R(TR)	right rotor thrust, N (lbf)
V_∞	free-stream velocity, m/sec (ft/sec)
V_{FS}(V,FS)	full-scale flight speed, $\frac{3600\ V_\infty}{6080}$ (tip speed scale factor of 0.6), kts
V_T	tip speed, ΩR, m/sec (ft/sec)
X,Y,Z	axes
Y	rotor side force at hub, N (lbf)
α(ALC)	angle of attack (corrected for tunnel wall boundary effects), deg
$\Delta\alpha$(DALF)	angle-of-attack change caused by tunnel wall boundary effects, deg
α_p	pylon angle, angle between model reference and pylon shaft axis, deg
β	angle of sideslip, deg
δ_a	aileron deflection, trailing edge down positive, deg
δ_e	elevator deflection, deg
δ_f	flap deflection, deg
δ_3	pitch flap coupling angle, deg
$\Delta\theta_c$	differential blade collective pitch, $\theta_{cL} - \theta_{cR}$, deg
θ_c(THA)	average blade collective pitch, measured at tip $\frac{\theta_{cL} + \theta_{cR}}{2}$, deg

θ_{cL}(THL) left rotor collective pitch at blade tip, deg

θ_{cR} right rotor collective pitch at blade tip, deg

θ_{tw} blade twist, deg

μ(MU) rotor advance ratio, $\frac{V_\infty}{V_T}$

ρ_∞ free-stream density, kg/m^3 (slugs/ft^3)

σ rotor solidity, $\frac{b_r c_r R}{A}$

ϕ roll angle, deg

Ω rotor speed, rad/sec

Notation:

CG center of gravity

MODEL AND APPARATUS

Drawings of the model are presented in figures 2 and 3. Geometric characteristics are described in Table I. The model had a forward swept wing with plain flaps and ailerons and a proprotor nacelle (hereafter referred to as pylon) at each wing tip. The pylons, canted outward 4° from the vertical, could be manually adjusted with support struts to angles of 0° (airplane), 15°, 30°, 45°, 60°, 75°, and 90° (helicopter). The flaps and ailerons could be set with the trailing edge down 0°, 20°, 50°, and 62°, and on that aileron only, trailing edge up 20°. The horizontal stabilizer, which could be manually adjusted to incidence settings of 0° and $\pm$5°, was located about half way up the vertical stabilizer and was equipped with a remotely adjustable elevator.

The model construction, described in detail in reference 3, utilized steel, aluminum, wood, and fiberglass components. The fuselage had a steel backbone with aluminum bulkheads supporting aluminum fuselage shells forward of the wing

and fiberglass shells aft. The main gearbox for mechanically interconnecting the rotors and electric motors (rated at 21.63 KW (29 HP) each) for driving the proprotors was in the fuselage. The wing structure consisted of shaped wooden panels attached to an aluminum spar. The spar, a "torque box" formed by an aluminum channel with cover plates, contained the shafting from the main gearbox to the tip-mounted gearboxes in the pylons. The vertical stabilizers had a steel spar which attached to the fuselage steel backbone. Wooden panels provided the aerodynamic shape (airfoil) for the vertical and horizontal stabilizers. The horizontal had an aluminum spar.

The proprotors were counterotating up at the center. Each proprotor had three blades attached to a gimbaled hub. The blades were made of steel, aluminum, and plastic foam, all covered with fiberglass. As noted in Table I, they were highly twisted. Spanwise and chordwise mass distribution and stiffness were dynamically scaled based on a model tip speed of 0.6 times full-scale tip speed. The blades were provided with strain gages for monitoring beam, chord, and torsion loadings at the 27.3 percent radius station. The gimbal hub permitted flapping motion of the rotor, though hub springs moderately restrained the flapping motion. Flapping motion was measured on both rotors. The interconnection of both rotors through the 90^{o} gearboxes in the pylons, shafting in the wing, and main gearbox in the fuselage resulted in the same rate of rotation and phase relationship. Each rotor had independent controls for varying collective pitch and longitudinal cyclic pitch. Collective pitch range was -11^{o} to 33^{o} (at the blade tips) and the longitudinal cyclic range $\pm 12^{o}$.

The model was mounted on a strain-gage balance attached to a special sting support. The sting, shown in figure 4, by movement of the three joints in concert, kept the model on the centerline of the tunnel (for in-ground effect tests the whole sting was lowered) to minimize aerodynamic interference effects of the walls. The strain-gage balance measured all six components of the total forces and moments on the model. Angle of attack and angle of roll were measured with electronic inclinometers inside the model. Inside each pylon there was a three-component rotor balance to measure the rotor thrust, rotor pitching moment, and rotor rolling moment. The moment resolving center of the balance was located 22.0 cm (8.66 in.) from the center of the gimbaled hub.

Rotor torque was measured with strain gages on the rotor shaft. Electronic signals from torque, blade stress rotor flapping, and pitch link load were passed through slip-ring assemblies, one in each pylon.

Data were recorded on oscillographs and a digital data recording system. The oscillographs recorded the dynamic measurements passed through the slip-rings and the pylon balance signals. The digital system recorded the "static" data from the total force and moment balance, angle of attack, angle of roll, angle of yaw, and wind speed and also recorded the pylon strain-gage balance signals, rotor speed, and rotor torque signals.

TEST CONDITIONS

This investigation was conducted in the Langley V/STOL tunnel which is a closed return, atmospheric tunnel. The tunnel test section measures 4.42 m (14.50 ft) by 6.63 m (21.75 ft). The model was supported on a special sting which kept the model in the center of the tunnel for the various angles of pitch, roll, and yaw used in the investigation. The sting could be raised or lowered to permit testing in ground effect.

Before testing the model in the tunnel, the 1 g trim conditions of the full-scale aircraft were estimated using the computer program in reference 4. Variation of trim attitudes and control position were made about these trim positions. Later in the test program (after Run 176), the procedure was altered whereby trim position was established by varying thrust in an attempt to obtain scaled lift and drag at a specified attitude.

The model was tested with the rotors removed for several pylon angles to determine the unpowered aerodynamic characteristics. With the rotors installed, the model was tested in three flight modes: helicopter, conversion, and airplane. For helicopter mode, the pylons were set at 90° and 75° and the rotor speed was set at 1884 rpm. Flaps and ailerons were usually set at 50° and 20°, respectively. For some hover tests, the flaps and ailerons were varied from 0° to 62°. For conversion mode, the pylon angle was set at 60°, 30°, and 0°. Rotor speed was reduced to 1604 rpm. Flaps and aileron angles were 50° and 20°, respectively. For airplane mode, the rotor speed was reduced to approximately 1372 rpm. This low rotational speed was allowed to vary from 1350 to 1390 rpm

in an attempt to avoid model vibration problems. These vibration characteristics were most troublesome when the empennage was removed. After Run 175, some reduction of vibrations was achieved by installing a mass in the fuselage to represent the empennage mass when the empennage was removed.

Table II presents a tabulation of test conditions including configuration information, attitudes, control positions, and test run number. The effective full-scale flight speed is shown rather than the actual wind speed in the tunnel. The actual wind speed was 60 percent of the full-scale flight speed since the model rotors were operated with a tip speed of 60 percent of full-scale tip speed and the ratio of wind speed to tip speed was a primary test parameter. Table III presents the configuration code nomenclature used in Table II.

Since the Langley V/STOL tunnel test section is variable in configuration, tests were made with three wall configurations: closed test section, walls and ceiling removed (open), and closed test section with slots opened. There were four slots on the ceiling and floor and six on each wall (one at each corner) which provided a porosity, when wide open, of 10 percent. Most of the testing because of safety considerations was done with the closed test section for effective full-scale flight speeds 40 knots or greater. For testing with lower wind speeds, down to hover, the open test section was used. At the lower wind speeds, the data corrections for the open test section were less than those of the closed section.

The data corrections for the influence of the closed or open test section were applied with the aid of the formulae of references 5 and 6. Data obtained when the slots in the walls were opened had no corrections applied since appropriate analyses such as in references 5 and 6 are not readily available. However, it is concluded in reference 7, for the Boeing-Vertol V/STOL wind tunnel, that the slotted test section with 10 percent porosity, as in this test, should have negligible corrections.

PRESENTATION OF DATA

The results of the present investigation was presented in the following figures. The forces and moments are presented in engineering units and in various coefficient forms (see List of Symbols) for body axes and wind-tunnel

stability axes. The test run number shown provides a means of correlating test conditions also listed in Table II, with the selected data presented in figures 5 through 103. These figures are grouped as follows:

Since the oscillatory data recorded on the two oscillographs were used for monitoring of blade loads, only the flapping angle data were extracted and shown in the figures.

RESULTS

For the most part the data in this report are presented without detailed analyses or correlation with theory. Such correlation is presented in reference 4. As indicated, these data provide an experimental base for validation of analytical methods for deriving stability and control characteristics of the tilt-proprotor configuration tested. The presentation of the selected data will aid in the definition of other aerodynamic characteristics, forces and moments, and stability and control derivatives. The following sections are provided to describe highlights of the data presented.

Unpowered Aerodynamic Characteristics

Longitudinal. - Testing with the rotors off was conducted to provide a basis for evaluation of the incremental rotor effects on the wing and empennage. In figure 5, the pylon angle variation from 90° to 0° indicates that the lift-

curve slope C_{L_α} increases as the pylons become more effective as end plates at the wing tips. Also notable is the substantial decrease in drag as the pylon angle is decreased. The nonlinear variation (fig. 5) of pitching moment, only for $\alpha_p = 90°$, is borne out in figure 6; though for all pylon angles, pitching-moment variation is stable. Figure 6 shows that the effect of wind-speed variation (and the associated Reynolds number) is greatest for the high pylon angles, 75° and 90°, and only significant near stall. Though the influence of Reynolds number can be of concern for the low wind speeds of this test program, it should be less so for data away from stall which was true of most of the data.

Configuration changes, flap/aileron angles and empennage on and off, result in the data shown in figures 7 and 8. The flap/aileron deflection to 50°/20° provides a large increase in lift at the expense of greater drag but does not change the pitch stability. Removal of the horizontal tail results in the unstable pitching-moment variation. The data for the configuration with the empennage removed was used to evaluate the wing efficiency. The results are presented in figures 9 and 10. Since the horizontal tail is located well above the wing plane, elevator effectiveness is not appreciably affected by changes of horizontal tail incidence, angle of attack, or flap/aileron deflection (figs. 11, 12, and 13).

The windstream flow angle which would alter the true angle of attack was determined by testing the unpowered model upside down. As shown in figure 14, the angle correction is small, about 0.2°. This correction was not applied to the data.

Lateral. - As for the longitudinal aerodynamic characteristics, changes in pylon angle, horizontal-tail incidence, and aileron deflection did not result in unexpected lateral characteristics. (See figs. 16 through 21.) The primary variable of these figures is sideslip angle. In these figures, it is evident that for moderate angles of sideslip at an angle of attack of 10° or higher, wing stall takes place on the advanced wing panel. When the wing is not stalled, aileron effectiveness (fig. 18) is unaffected by sideslip significantly improves the yaw stability of the unpowered configuration (figs. 19 and 20); though yaw instability with the vertical tail off is moderate.

Removal of only the horizontal tail (fig. 21) results in a reduction of the effective dihedral.

Powered Aerodynamic Characteristics

Longitudinal. - The presentation of the data in figures 22 through 44 in the form of coefficients based on slipstream dynamic pressure was done to make the data more amenable to analyses. The wide range of wind speeds and the corresponding wide range of dynamic pressure would tend to obscure the effects of test variables if presented in the more commonly used coefficients based on free-stream dynamic pressure.

Figures 22 through 30 show all three longitudinal aerodynamic components, lift, pitch, and propulsive force as affected by the variables of collective pitch angle, longitudinal cyclic pitch angle, and angle of attack for the complete model configuration, with rotors on and empennage on. The test conditions and configuration characteristics compared include pylon angle, wind speed, and flap/aileron deflection. It can be seen that, in general, the predetermined control positions and attitudes for trimmed flight did not lead to very successful bracketing of trimmed flight conditions with sweeps of the variables of collective pitch, longitudinal cyclic pitch, and angle of attack. wever, the linear variations of the data permit moderate extrapolation and interpolation of the data.

Figures 31 through 45 deal with the effects of horizontal tail and elevator; therefore, only the longitudinal components of lift and pitching moment are presented.

Lateral. - As for the previous section, these data are also in the form of coefficients based on slipstream dynamic pressure. In figures 46 through 53, the primary variable is sideslip angle. The range of sideslip is from moderately positive sideslip angle to -16° of sideslip. Since the model is symmetrical about the fuselage centerline X-Z plane, the data can be expected to vary in a symmetrical fashion about the sideslip angle of 0°. There is little effect of power on yawing-moment stability; without the vertical tail there is moderate instability, and with the tail, the powered and unpowered yaw stability are similar. (See figs. 15 through 21.)

Differential collective pitch angle and differential cyclic pitch angles excursions resulted in the data shown in figures 54 through 57. Configuration and test conditions varied for these data include pylon angle, wind speed, and height above ground (in hover). Figure 58 shows rolling-moment characteristics due to roll angle, in and out of ground effect. Though the data are erratic because of complex flow beneath the model, it appears that as height above the ground is decreased, roll stability varies from neutral stability to negative stability at moderate heights to positive stability at the minimum height above the ground. According to reference 4, there is more than adequate control power (that is, differential collective pitch) to compensate for the unstable rolling moment.

Rotor Aerodynamic Characteristics

Rotor performance characteristics of thrust, torque, "H" force, "Y" force and flapping angles are presented in figures 59 through 77. The primary variables are collective pitch angle, longitudinal cyclic pitch, and angle of attack. The effects of configuration and test conditions include the effects of pylon angle, wind speed, and angle of attack. The H and Y force component data that are shown were obtained by correcting the rotor balance pitching and yawing-moment data for the effect of cyclic flapping and the resultant hub spring moments. There were minor differences in thrust and torque measurements between left and right rotors attributable to balance inaccuracy, differences in control settings (collective and cyclic pitch angles) and suspected differences in elastic properties of the rotor blades. However, the average values of thrust and torque tend to reduce the influence of these differences. The flapping angle data shown was obtained from the oscillograph records and were subject to errors on the order of $\pm 1°$. As for previous data, the general linearity of the data suggest that moderate extrapolation and interpolation is justified.

Rotor Effects

Longitudinal. - A purpose of this test program was to establish the effects of the tilt-proprotor performance and rotor wake on the total tilt-proprotor configuration. Figures 78 through 91 are presented to do this with comparisons of unpowered and powered longitudinal configuration data; though figures 78 and

79 are presented strictly for the powered flight in hover. In figure 78, it can be seen that when out of ground effect (when the rotor is approximately two rotor diameters above ground level), the gross rotor thrust required to hover is 10 percent greater than the net required thrust (for design flap/aileron setting of 50°/50°). The 10 percent is essentially a loss due to a down loading of wing panels below the rotor. This is consistent with the results shown in reference 8. As the height above the ground is decreased, the thrust loss is decreased eventually becoming a net thrust gain (3 percent) at minimum height above ground. Figure 79 indicates that the flap/aileron deflection design setting of 50°/50° may not be optimum because deflection of 62°/62° will reduce the thrust loss moderately. The reduction of projected area is almost negligible; therefore, the benefit accrues from alteration of flow patterns beneath the wing.

Figure 80 through 91 provide the comparison of unpowered and powered characteristics utilizing coefficients based on windstream dynamic pressure for flight speeds of 80 knots or higher. In general, pitch stability with the horizontal tail on was not affected appreciably for all pylon angles. With tail off, rotor thrust tends to stabilize pitch.

Lateral. - The lateral aerodynamic characteristics, unpowered and powered, are shown in figures 92 through 100. The sweeps of sideslip angle for these data were limited by the vibration problem which occurred when testing with the vertical tail off. The problem was reduced by adding mass to the fuselage tail cone. However, the amount of data obtained was limited by the problem; as a result, the comparisons of characteristics for vertical tail on and off are fewer than desired. In general, the figures indicate that the rotors provide a contribution to directional stability, and for the lower flight speeds and high pylon angles, the rotors decrease the effective dihedral. For higher flight speeds (that is, increasing to 120 knots and higher) and as pylon angle is decreased, the rotor effect becomes negligible. For a moderate range of sideslip about 0°, the directional stability is somewhat less than that at greater sideslip angles. This can be attributed to the reduced dynamic pressure at the tail due to the wake of the fuselage. There are no evident nonlinear variations of yawing moment, nor significant differences between unpowered and powered yawing-moment variations (which might be more likely at lower pylon angles) which

would indicate significant rotor-wake effect as the tail enters the wake of the rotor at high sideslip angle.

Wind-Tunnel Test-Section Configuration Effects

The Langley V/STOL tunnel test-section configuration was varied at low wind speeds to evaluate the influence of jet boundary on the model longitudinal characteristics. Comparisons of these characteristics for the three test-section configurations are shown in figures 101 through 103. The data for the closed test section (solid walls, ceiling and floor in place) and for the open test section (side walls and ceiling raised with only the floor in place) were corrected with the computational procedures described in references 5 and 6. Unfortunately, comparable wall-correction procedures for the slotted tunnel test section (for side-by-side rotors) are not available. However, for some tunnels, it is believed (refs. 7 and 9) that slotted walls with a 10 percent porosity can greatly reduce the wall effects. In figure 101, lift coefficients obtained with the slotted test section fall between the corrected data of the other two test sections. Where this is not the case, figures 101(a) and 101(c), the data for the closed and slotted tunnels in figure 101(a) can be discounted because of the likelihood that flow recirculation, i.e., upstream standing vortex, is adversely affecting the data, and in figure 101(c), the data for the slotted test section were obtained with an incorrect setting of collective pitch. It can be concluded that the corrections made with the analytical procedures of references 5 and 6 were not wholly successful.

CONCLUDING REMARKS

A wind-tunnel investigation of a powered model with a tilt-proprotor and gimbal hub rotors was conducted to determine aerodynamic performance, stability and control, and rotor wake interaction effects on the model components. Data were obtained for many combinations of test conditions, control positions, and configuration. For the most part, the data are presented in this report without extensive analyses or correlations with theory.

The tests in the Langley V/STOL tunnel provided an opportunity to evaluate three wind-tunnel test-section configurations for the determination of the aerodynamic influence of wind-stream boundary configuration. It was found that the existing correction procedure for open and closed test-section configurations resulted in noticeable differences in corrected aerodynamic data.

REFERENCES

1. Magee, John P.; Taylor, Robert B.; McHugh, Frank J.; Miller, Nelson; and Leon, N.: Wind Tunnel Test of a Powered, Tilt-Rotor Performance Model. AFFDL TR-71-62, vol. V, Oct. 1971

2. Mechtly, E. A.: The International System of Units - Physical Constants and Conversion Factors. NASA SP-7012 (Revised), 1972

3. Marr, R. L.; Ford, D. G.; and Ferguson, S. W.: Analysis of the Wind Tunnel Test of a Tilt Rotor Powered Force Model. Bell Helicopter Co. Rep. BHC 301-099-004, June 1974

4. Livingston, Charles L., et. al.: A Stability and Control Prediction Method for Helicopters and Stoppable Rotor Aircraft. AFFDL TR-69-123, March 1970

5. Heyson, Harry H.: FORTRAN Programs for Calculating Wind Tunnel Boundary Interference. NASA TM X-1740, 1969

6. Heyson, Harry H.: Use of Superposition in Digital Computers to Obtain Wind Tunnel Interference Factors for Arbitrary Configurations, With Particular Reference to V/STOL Models. NASA TR R-302, 1969

7. Harris, Franklin D.: Articulated Rotor Blade Flapping Motion at Low Advance Ratio. J. of the Am.Hel. Soc., vol. 1, no. 1, Jan. 1972

8. Fradenburg, Evan A.: Aerodynamic Factors Influencing Overall Hover Performance. AGARD Conference Proceedings 111, On Aerodynamics of Rotary Wings, Sep. 72.

9. Kraft, E. M.; and Lo, C. F.: A General Solution for Lift Interference in Rectangular Ventilated Wind Tunnels. AIAA Paper 73-209, 1973

TABLE I

GEOMETRY

	Wing	Horizontal tail	Vertical tail
Airfoil, root	64-318, a=0.8	64A012	64A015
tip	64-318, a=0.8	64A008	64A008
Span, m (ft)	1.958 (6.425)	1.015 (3.33)	
Area, m^2 (ft^2)	.656 (7.06)	.232 (2.50)	.190 (2.05)
Aspect ratio	5.85	4.5	1.6
Chord, root, cm (in.)	39.9 (15.7)		
tip, cm (in.)	27.2 (10.7)		
mac, cm (in.)	33.9 (13.34)	23.0 (9.07)	35.3 (13.90)
Incidence	2°	-5°,0°,+5°	0°
Leading-edge sweep	-6°	17°	35°
Dihedral	2°	0°	--
Flap area	.0369 (.397)		
Flap chord	.275 c		
Flaperon area	.0275 (.296)		
Flaperon chord	.275 c		
Elevator area		.0373 (.51)	
Elevator chord		.265 c	
Rotor			
Blades	3		
Diameter, cm (in.)	152.4 (60.0)		
Disk area/rotor, m^2 (ft^2)	1.825 (19.64)		
Solidity, σ	.1275		
Blade chord, cm (in.)	10.2 (4.0)		
Twist	-25°		
Airfoil section	64-212, a=0.3		
Precone	2.67°		
δ_3	-25°		

Table II

RUN SCHEDULE SUMMARY

*Pitch angles are approximate

Run no.	Run type (sweep)	Walls	V_{FS}	α_p	Configuration	RPM	h/D
1	Collective	Up	0	90	1-2-6	1884	2.00
2	"						
3	Cyclic						
4	Collect. & cyclic			75	1-2-5		
5	"			45	1-2-3	1604	
6	"			45			
7	Collective			0			
8	"			90	1-2-1	1884	
9	Cyclic				1-2-6		
10	Collective						1.83
11	Cyclic						
12	Collective		20				
13	Pitch						
14	Yaw (*Pitch = 1°)						
(15)	Void	--	--	--	--	--	--
16	Collective		40				
17	Pitch		40				
(18)	Void	--	--	--	--	--	--
19	Yaw (Pitch = -1°)		40				
20	Collective	Down	20				
21	"		40				
22	Pitch						
23	Cyclic						
24	Differential Coll.						1.84
25	Differential Cycl.						
26	Yaw (Pitch = -2°)						
27	Elevator						
(28)	Void	--	--	--	--	--	--
29	Pitch				2-0-6		
30	Yaw (Pitch = -2°)						
31	Collective						
32	"		80				
(33)	Void	--	--	--	--	--	--
34	Yaw (Pitch = 2°)						
(35)	Void	--	--	--	--	--	--
36	Pitch						
37	"				1-2-6		
38	"						
39	"						
40	Yaw (Pitch = 2°)						
41	Collective		120				
42	"		120				

Table II (continued)

*Pitch angles are approximate.

Run no.	Run type (sweep)	Walls	V_{FS}	α_p	Configuration	RPM	h/D
43	Collective	Down	100	90	1-2-6	1884	1.84
44	Elevator						
45	Cyclic						
46	Differential Coll.						
47	Pitch						
48	Cyclic		80				
49	Wind speed		40/120	75	1-2-5	1604	
50	"		40/120			1884	
51	Collective		40				
52	Pitch						
53	Elevator						
54	Cyclic						
55	Differential Coll.						
56	Differential Cycl.						
57	Collective		80				
58	Pitch						
59	Elevator						
60	Cyclic						
61	Collective		120				
62	Pitch						
63	Elevator						
64	Cyclic						
65	Differential Coll.						
66	Differential Cycl.						
67	Collective	Up	0	90	6-2-6		
68	Cyclic						
69	Differential Cycl.						
70	Roll						
71	Differential Coll.						
72	Collective						1.00
73	Pitch						
74	Cyclic						
75	Roll						
76	Elevator						
77	Differential Coll.						
78	Collective						.83
79	Roll						.83
80	Collective						.67
(81)	Void	--	--	--	--	--	--
82	Roll						.67
83	Collective						.53
84	Cyclic						
85	"						
86	Roll						
87	Elevator						1.84

Table II (continued)

Run No.	Run type (sweep)	Walls	V_{FS}	α_p	Configuration	RPM	h/D
88	Collective	Down	100	90	2-0-6	1884	1.84
89	Pitch		↓	↓	↓	↓	↓
90	Collective		40	75	2-0-5		
91	Pitch		↓	↓	↓		
92	Collective		80	↓	↓		
93	Pitch		80	↓	↓	↓	
94	Collective		120	60	1-2-4	1604	
95	Pitch		↓	↓	↓	↓	
96	Elevator		↓	↓	↓	↓	
97	Cyclic		↓	↓	↓	↓	
98	Differential Coll.		↓	↓	↓	↓	
99	Differential Cycl.		↓	↓	↓	↓	
100	Collective		140	↓	↓	↓	
101	Pitch		↓	↓	↓	↓	
102	Elevator		↓	↓	↓	↓	
103	Collective		120	30	1-2-2	↓	
104	Pitch		↓	↓	↓	↓	
105	Elevator		↓	↓	↓	↓	
106	Cyclic		↓	↓	↓	↓	
107	Differential Cycl.		↓	↓	↓	↓	
108	Collective		↓	60	2-0-4	↓	
109	Pitch		↓	↓	↓	↓	
110	Collective		140	↓	↓	↓	
111	Pitch		140	↓	↓	↓	
112	Collective		120	30	2-0-2	↓	
113	"		↓	↓	↓	↓	
114	"		↓	↓	↓	↓	
115	Pitch		↓	↓	↓	↓	
116	Collective		80	75	1-2-5	1884	
117	Pitch		↓	↓	↓	↓	
118	Elevator		↓	↓	↓	↓	
119	Collective		120	↓	2-0-5	↓	
120	Pitch		120	↓	↓	↓	
121	Collective		80	↓	↓	↓	
122	Pitch		80	↓	↓	↓	
123	Collective		20	90	2-0-6	↓	
124	Pitch		20	↓	↓	↓	
125	Collective		40	↓	↓	↓	
126	Pitch		40	↓	↓	↓	
127	Yaw (Pitch = 1^0)		20	↓	↓	↓	
128	Yaw (Pitch = -1^0)		40	↓	↓	↓	
(129)	Void	↓	↓	↓	1-2-6	↓	↓
ROTORS OFF							
130	Pitch	Down	80	90	3-2-6	0	1.84
131	"	↓	120	↓	↓	↓	↓
132	"	↓	160	↓	↓	↓	↓

Table II (continued)

Run no.	Run type (sweep)	Walls	V_{FS}	α_p	Configuration	RPM	h/D
133	Yaw (Pitch = 0°)	Down	160	90	3-2-6	0	1.84
134	Yaw (Pitch = 0°)		120				
135	Yaw (Pitch = 5°)		160				
136	Yaw (Pitch = 10°)						
137	Yaw (Pitch = -10°)						
138	Elevator						
(139)	Void						
140	Pitch						
141	Yaw (Pitch = 0°)						
142	Yaw (Pitch = 5°)						
143	Elevator		120				
144	"		160		3-3-6		
145	Pitch		160				
146	"		120	75	3-2-5		
147	"		160				
148	Yaw (Pitch = 1°)						
149	Yaw (Pitch = 10°)						
150	Pitch		120	60	3-2-4		
151	"		160				
152	Yaw (Pitch = 1°)		160				
153	Pitch		120	45	3-2-3		
154	"		160				
155	Yaw (Pitch = 1°)		160				
156	Pitch		120	30	3-2-2		
157	"		160				
158	Yaw (Pitch = 1°)						
159	Pitch			0	3-2-1		
160	Elevator				3-2-1		
161	Yaw (Pitch = 1°)				3-2-1		
162	Pitch				4-0-1		
163	Yaw (Pitch = 1°)				4-0-1		
164	"			30	4-0-2		
165	Pitch			30	4-0-2		
166	"			60	4-0-4		
167	Yaw (Pitch = 1°)			60	4-0-4		
168	Pitch			90	4-0-6		
169	Yaw (Pitch = 1°)						
170	Yaw (Pitch = 10°)						
171	"						
(172)	Void		--	--	--	--	--
(173)	"		--	--	--	--	--
(174)	"		--	--	--	--	--
(175)	"		--	--	--	--	--

Table II (continued)

Run no.	Run type (sweep)	Walls	V_{FS}	α_p	Configuration	RPM	h/D
SECOND TEST PHASE							
176	Collective	Down	40	90	1-2-6	1884	1.84
177	Pitch						
178	Yaw (Pitch = -1^0)						
179	Pitch				1-1-6		
180	"		80	75	1-1-5		
181	"				1-1-5		
182	"				1-2-5		
183	Collective						
184	Yaw (Pitch = 11^0)						
185	Collective		120	60	1-2-4	1604	
186	Pitch						
187	Yaw (Pitch = 8^0)						
188	Pitch				1-1-4		
189	"			30	1-1-2		
190	"		160		1-1-2		
191	Yaw (Pitch = 11^0)		120		1-2-2		
192	Collective						
193	Pitch						
194	Collective		160				
195	Cyclic						
196	Elevator						
197	Roll tare		0			0	
198	Yaw (Pitch = 3^0)		160			1604	
199	Roll tare		0			0	
200	Pitch		160			1604	
201	Roll tare		0	0	1-2-1	0	
202	Thrust calibration		0			0	
203	Collective		120			1604	
204	Pitch						
205	Yaw (Pitch = 11^0)						
206	Collective		160				
207	Pitch						
208	Yaw (Pitch = 3^0)						
209	Thrust calibration					0	
210	"					0	
211	Pitch		120		1-1-1	1604	
212	Elevator		120				
213	Pitch		160				
214	Elevator						
215	Collective				5-2-1	1372	
216	Pitch						
217	Elevator						
218	Collective		180				
219	Pitch						
220	Elevator				1-2-1		
221	Collective		120				

Table II (continued)

Run no.	Run type (sweep)	Walls	V_{FS}	α_p	Configuration	RPM	h/D
222	Pitch	Down	120	0	1-2-1	1372	1.84
223	Elevator	↓	↓	↓	↓	↓	↓
224	Yaw (Pitch = 11^{o})						
225	Collective		180				
226	Pitch		↓				
227	Yaw (Pitch = 1^{o})					↓	
228	Elevator		160			1604	
229	Elevator		120		↓	1604	
230	Pitch		120		1-1-1	1372	
231	"		180		↓	↓	
232	"		160		5-1-1		
233	"		180		5-1-1		
234	Yaw (Pitch = 8^{o})		160		5-2-1		
235	Yaw (Pitch = 2^{o})		180		↓		
236	Pitch		160				
237	"		160				
238	"		180		↓		
239	Yaw (Pitch = 10^{o})		120		9-2-1		
240	Pitch		↓	↓	9-2-1	↓	
241	"			30	2-0-2	1604	
242	"			↓	↓	↓	
243	"		160		↓		
244	Yaw (Pitch = 10^{o})		120		2-4-2		
245	Pitch		120		↓		
246	"		160				
247	Yaw (Pitch = 2^{o})		160	↓			
248	Pitch		120	0	2-4-1		
249	Yaw (Pitch = 11^{o})		120		↓		
250	Pitch		160				
251	Yaw (Pitch = 2^{o})		160	↓			
252	Pitch		120	60	2-4-4		
253	Yaw (Pitch = 8^{o})		↓	↓	↓		
254	Pitch						
255	Yaw (Pitch = 11^{o})	↓	↓	↓	↓		
256	Collective	Up	0	90	1-2-6		
257	Pitch		20		↓		
258	"		30				
259	"		40				
260	"		50				
261	"		60		↓		
262	"		20		1-1-6		
263	"		30		↓		
264	"		40				
265	"		50				
266	Yaw (Pitch = -3^{o})	↓	40	↓	↓	↓	↓

Table II (continued)

Run no.	Run type (sweep)	Walls	V_{FS}	α_p	Configuration	RPM	h/D
267	Pitch	Up	20	90	2-4-6	1884	1.84
268	"	↓	30	↓	↓	↓	↓
269	"		40				
270	"		50				
271	Yaw (Pitch = -3^o)		40		↓		
272	Pitch	Open-	20		1-2-6		
273	"	Slots	30		↓		
274	"	↓	40				
275	"		50				
276	"	↓	60				
277	"	Down	20				
278	"	↓	30				
279	"		40				
280	"		50				
281	" (Auto)		80				
282	" (Climb)		80				
283	" (Climb)	↓	40		↓		
284	Collective	Up	0		5-2-6		
285	" (δ_F/δ_A = 20/20)	↓	↓		9-2-6		
286	" (" = 50/50)				6-2-6		
287	" (" = 62/62)				9-2-6		
288	Roll(δ_F/δ_A=50/50)				6-2-6		1.0
289	" "				↓		.83
290	" "						.67
291	" "						.53
292	" "	↓	↓		↓		1.84
293	Pitch	Down	60		1-2-6		
294	"	↓	50	↓	1-2-6		
295	"		120	60	1-2-4	1604	
296	Yaw (Pitch = 8^o)		↓	60	1-2-4	↓	
297	Pitch			30	1-2-2		
298	Yaw (Pitch = 11^o)			↓	↓		
299	Pitch						
300	Yaw (Pitch = 3^o)						
301	Pitch						
302	"						
303	"						
304	"	↓	↓	↓	↓	↓	↓
(305)	Void						

Table II (continued)

Run no.	Run type (sweep)	Walls	V_{FS}	α_p	Configuration	RPM	h/D
ROTORS OFF							
306	Pitch	Down	60	90	3-?-6	0	1.84
307	"		120		3-2-6		
308	"		80		3-1-6		
309	"		160		3-1-6		
310	"		80	75	3-1-5		
311	"				3-1-5		
312	"				3-2-5		
313	Yaw (Pitch = 10^0)				3-2-5		
314	Pitch		60	90	3-2-6		
315	"		120				
316	Yaw (Pitch = -1^0)		60				
317	"		120				
318	Pitch		80		3-1-6		
319	"		120	60	3-1-4		
320	"			60	3-2-4		1.83
321	Yaw (Pitch = 7^0)			60	3-2-4		
322	Pitch			30	3-2-2		
323	Yaw (Pitch = 11^0)				3-2-2		
324	Pitch				3-1-2		
325	"			0	3-1-1		
326	"				3-2-1		
327	"						
328	Yaw (Pitch = 11^0)						
329	" (" = 2^0)						
330	" (" = 8^0)		160		6-2-1		
331	Pitch						
332	Elevator						
333	"						
334	Pitch(upside down)						
335	"		60				
336	Yaw (Pitch = 8^0) (RT ail. dwn)		160		9-2-1		
337	Yaw (Pitch = 8^0) (LT ail. dwn)		160		9-2-1		
(338)	Void		--	--	--		

Table II - (continued)

Run no.	Run type (sweep)	Walls	V_{FS}	α_p	Configuration	RPM	h/D
339	Pitch	Down	80	75	3-2-5	0	1.83
340	"		120	60	3-2-4		
341	"			30	3-2-2		
342	"				4-4-2		
343	"						
344	Yaw (Pitch = 0^o)						
345	Pitch			0	4-4-1		
346	"						
347	Yaw (Pitch = 11^o)						
348	Yaw (Pitch = 9^o)				6-4-1		
349	Pitch				6-4-1		
350	"			60	4-4-4		
351	Yaw (Pitch = 8^o)			60	4-4-4		
352	Pitch		60	90	4-4-6		
353	Yaw (Pitch = -1^o)		60				
354	"		120				
355	Pitch		120				
356	"		60	75	4-4-5		
357	"		80				
358	Yaw (Pitch = 10^o)		80				
359	Pitch		160				

Table III

Configuration Code

A - B - C

If A =	1	δ_F/δ_A = 50/20
	2	Horizontal tail off, δ_F/δ_A = 50/20
	3	Rotors off, δ_F/δ_A = 50/20
	4	Vertical tail off, δ_F/δ_A = 50/20
	5	δ_F/δ_A = 0/0
	6	Rotors off, δ_F/δ_A = 0/0
	9	Flap/Aileron settings other than 50/20, 50/50, 0/0
If B =	0	Horizontal tail off
	1	Horizontal tail incidence = -5^o
	2	Horizontal tail incidence = 0^o
	3	Horizontal tail incidence = $+5^o$
	4	Vertical tail off
If C =	1	Pylon angle = 0^o
	2	Pylon angle = 30^o
	3	Pylon angle = 45^o
	4	Pylon angle = 60^o
	5	Pylon angle = 75^o
	6	Pylon angle = 90^o

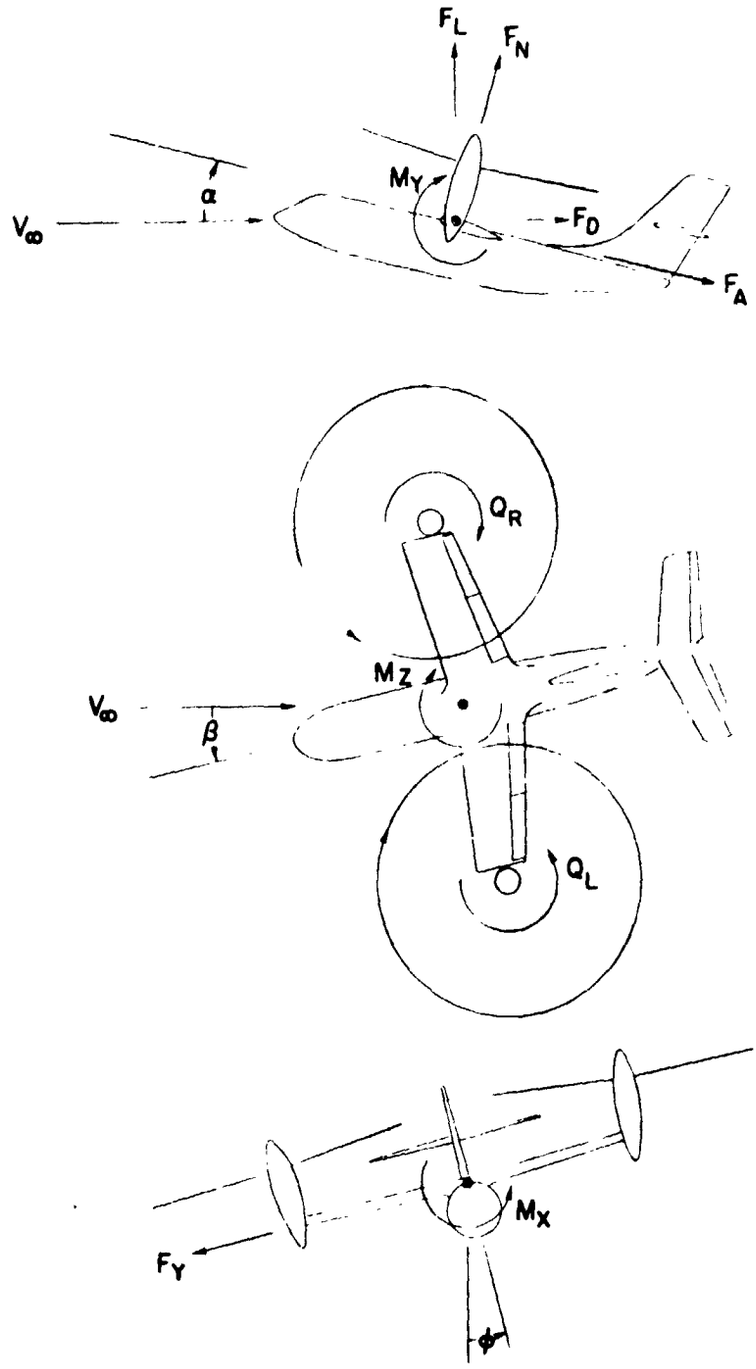

Figure 1. - System of axes. Positive directions of forces, moments, and angles are indicated by arrows.

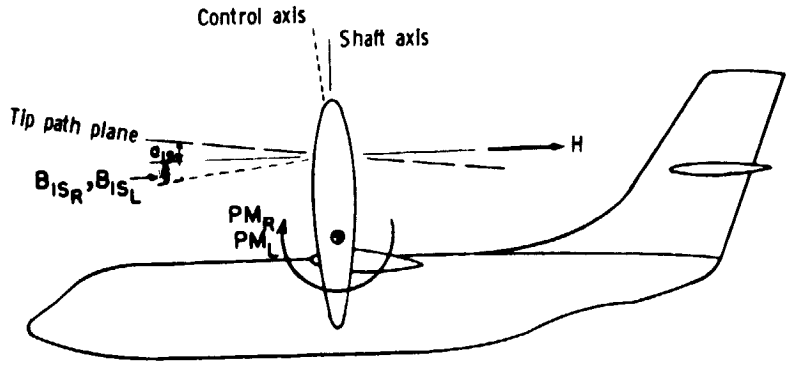

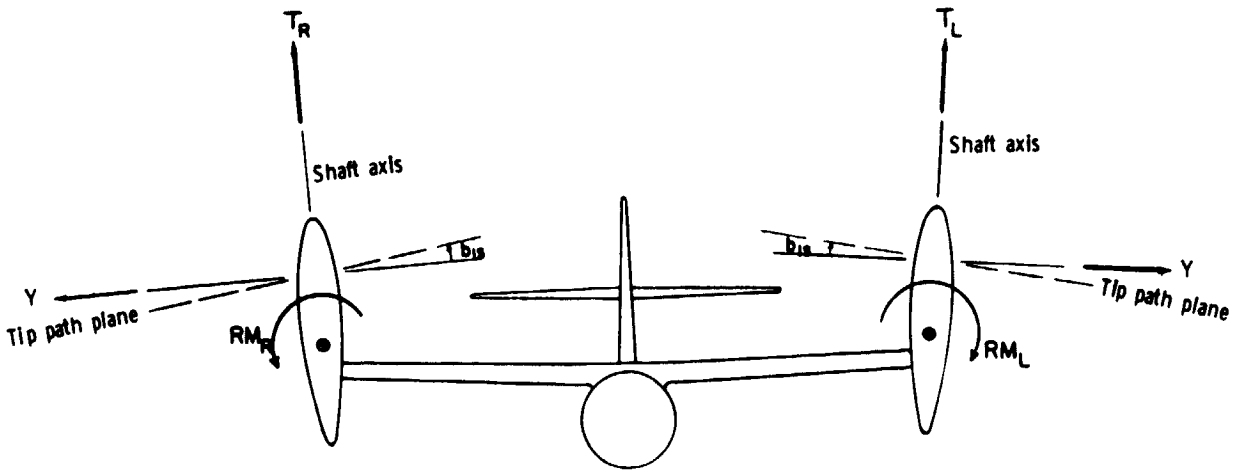

Figure 1. - Concluded.

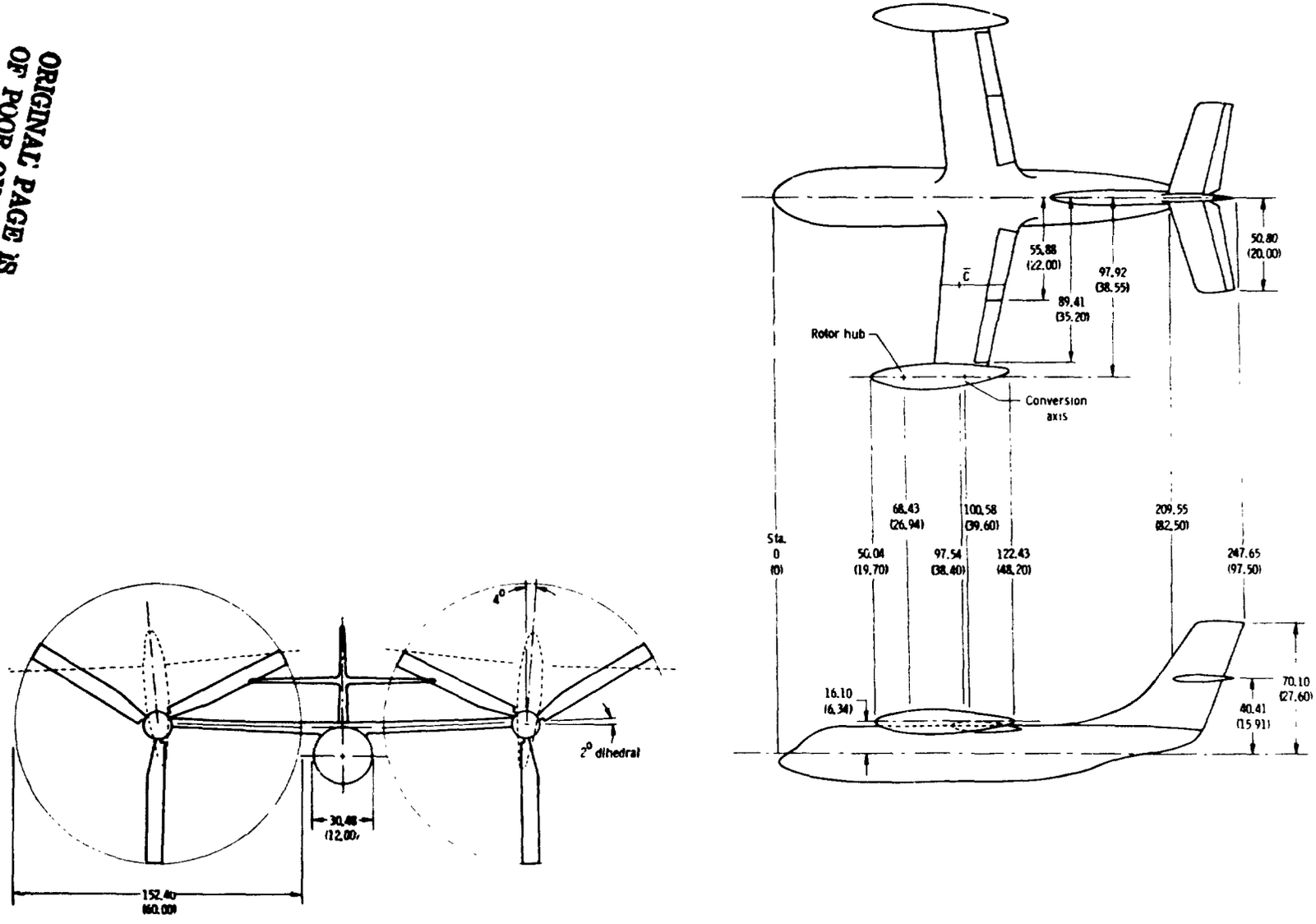

(a) Three-view drawing for $\alpha_p = 0^0$

Figure 2. - Details of the model. All dimensions shown in cm (in.) unless otherwise noted.

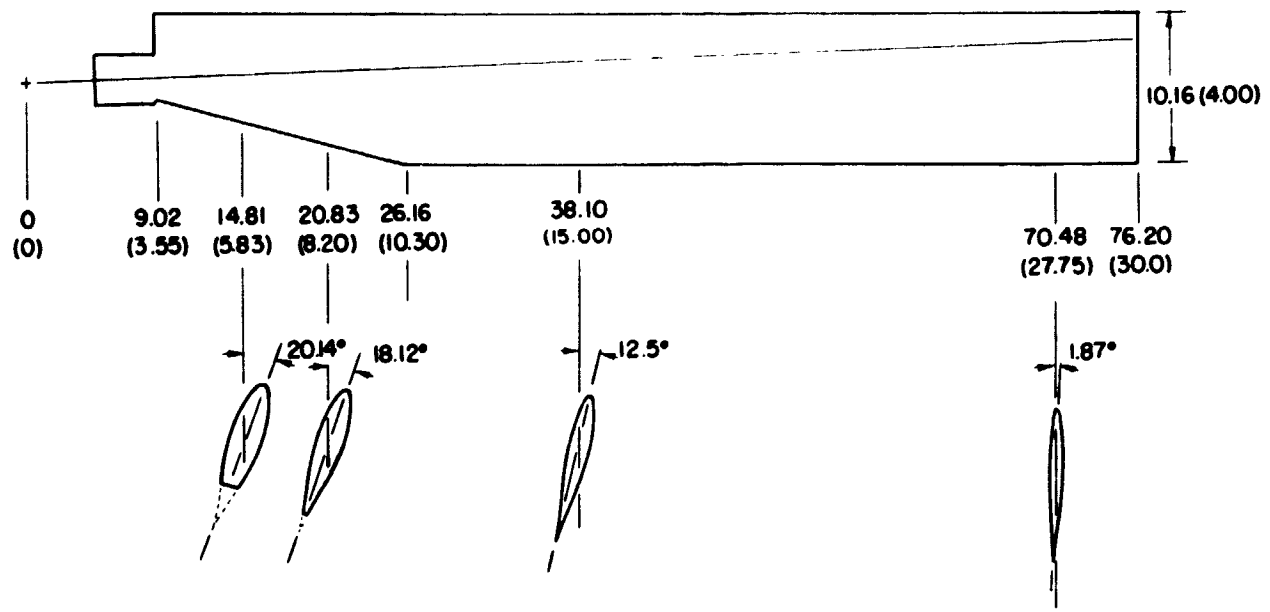

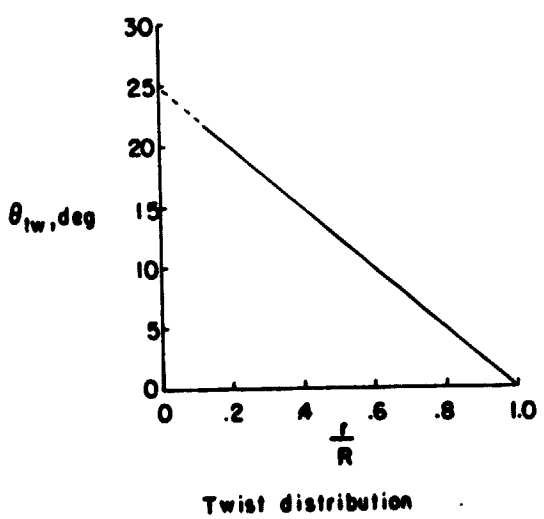

Twist distribution

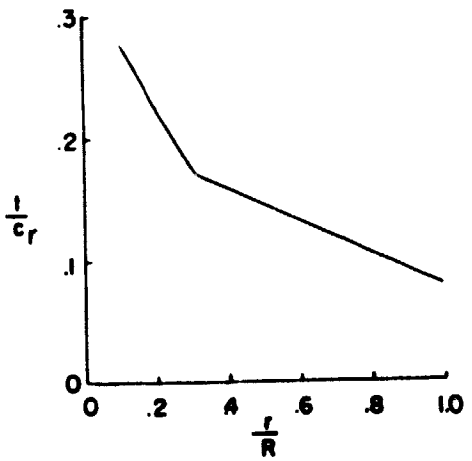

Thickness distribution

(b) Details of the proprotor blade

Figure 2. - Concluded.

Center of Gravity Location		
	Longitudinal	Vertical
90	101.3(39.9)	17.0(6.7)
75	100.6(39.6)	16.0(6.3)
60	99.8(39.3)	14.7(5.8)
45	99.1(39.0)	13.5(5.3)
30	98.3(38.7)	12.2(4.8)
0	96.5(38.0)	9.9(3.9)

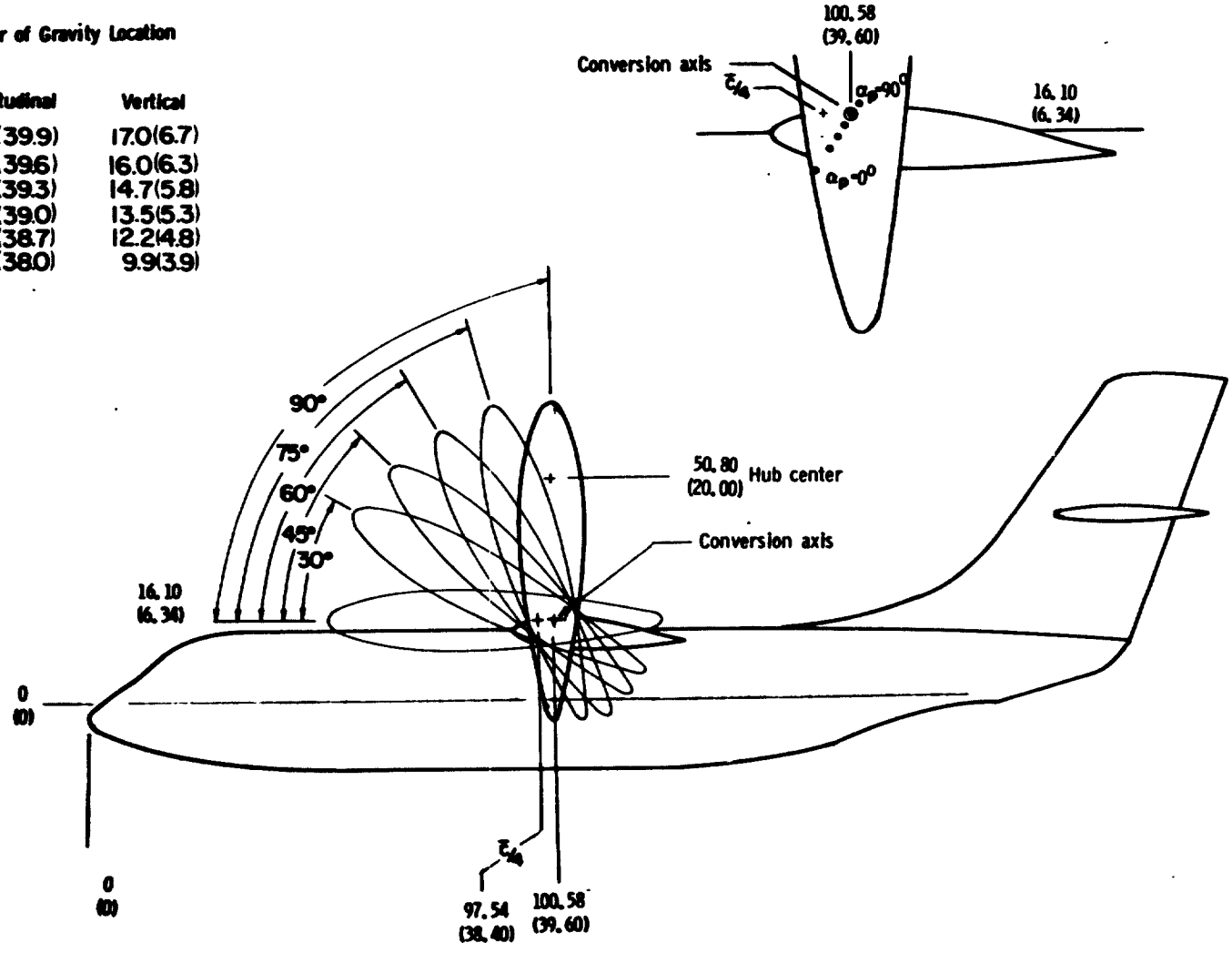

Figure 3. - Change in position of the assumed center of gravity with pylon angle. Dimensions in cm (in.).

(a) $\alpha_p = 0^o$

Figure 4. - Installation of tilt-proprotor model in the Langley V/STOL tunnel with various pylon angles.

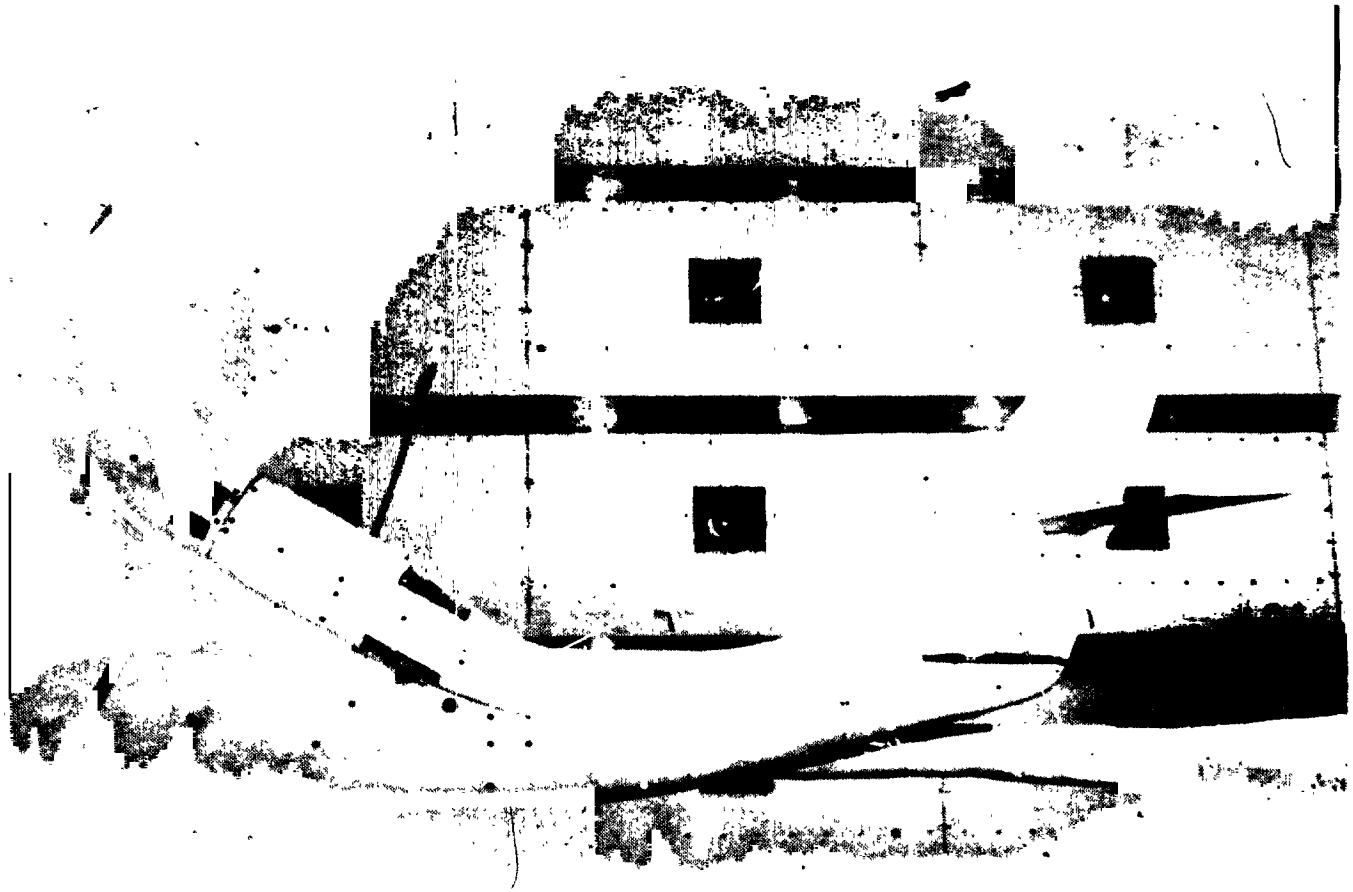

(b) $\alpha_p = 30^0$

Figure 4. - Continued.

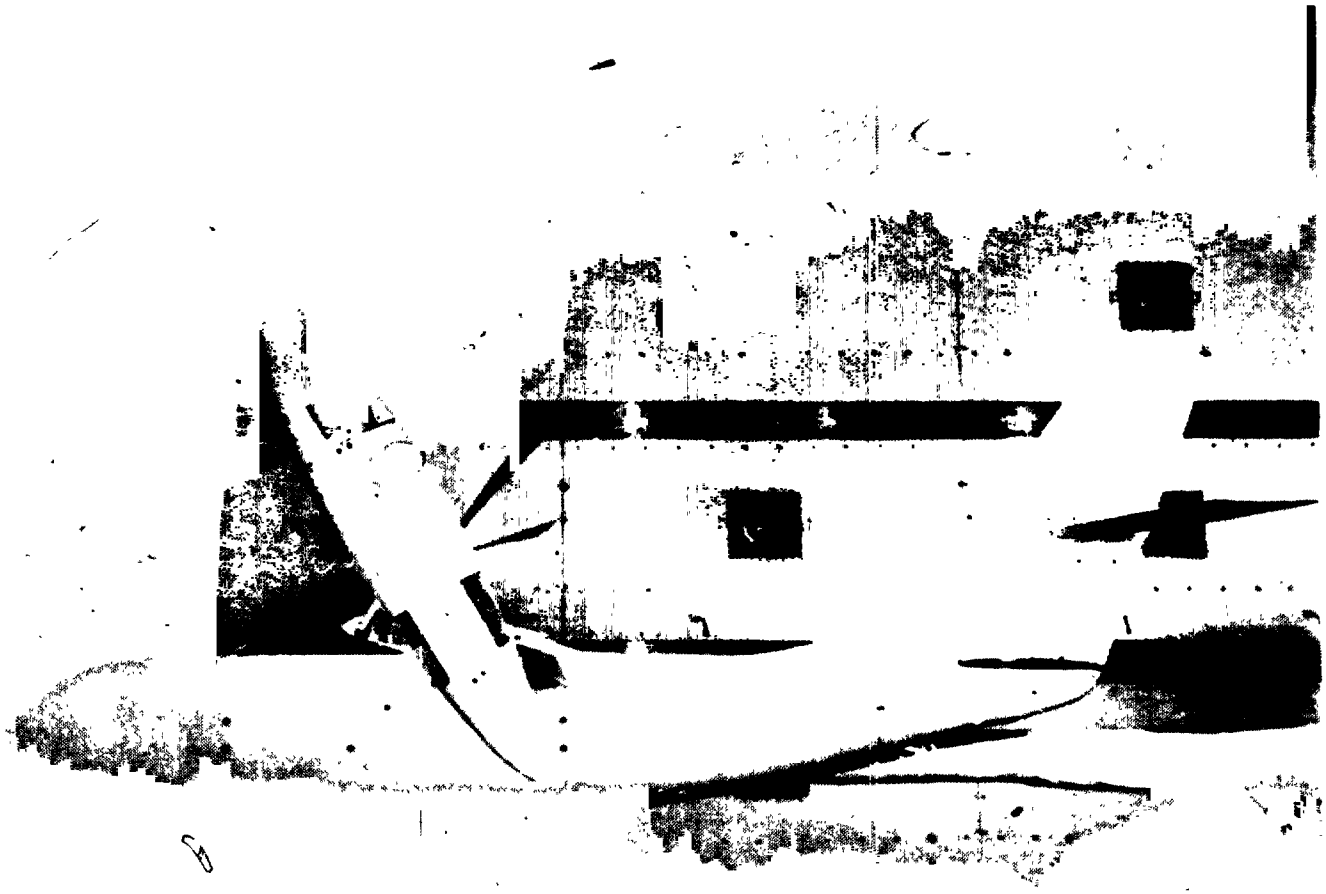

(c) $\alpha_p = 60^0$

Figure 4. - Continued.

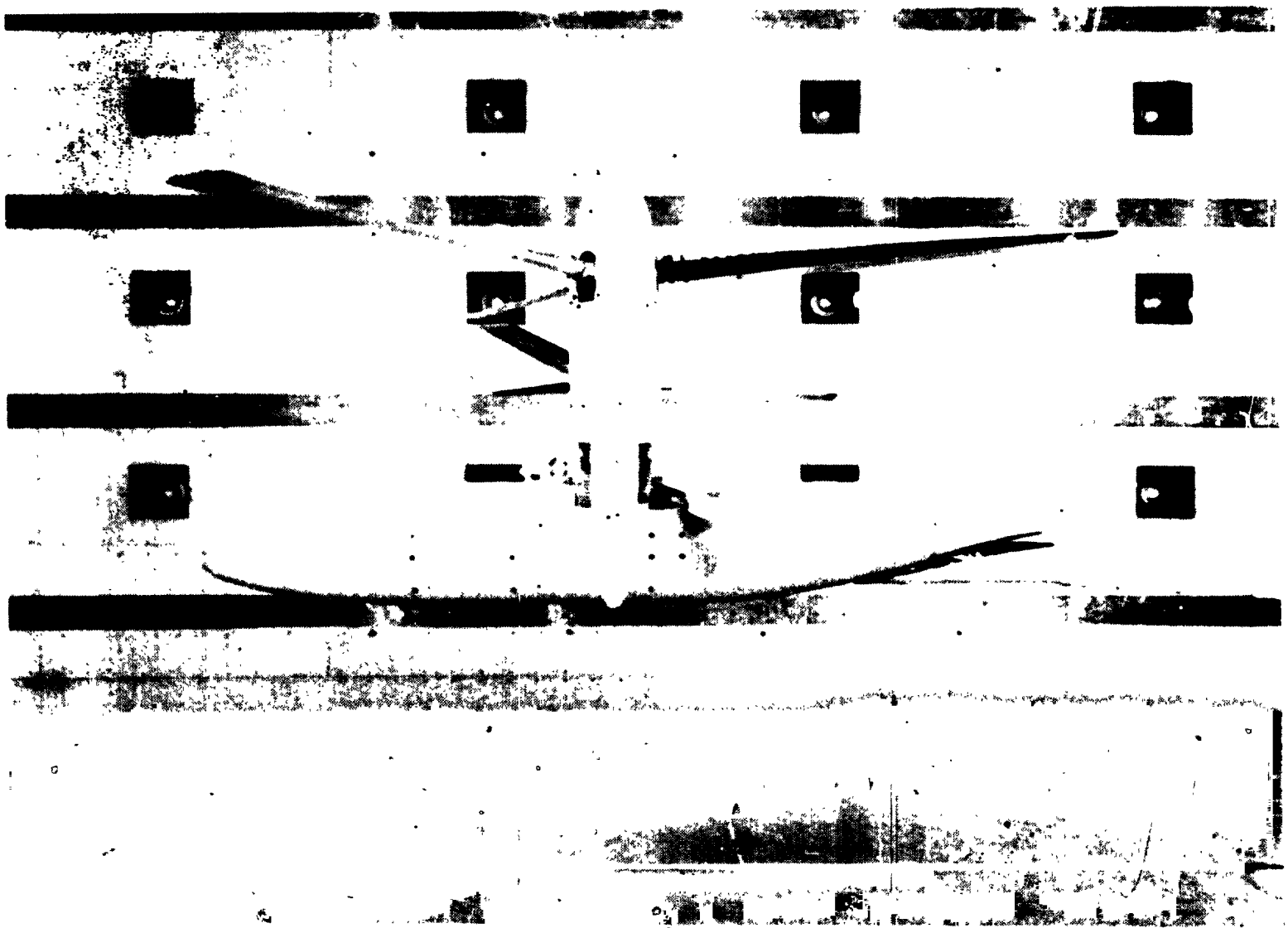

(d) $\alpha_p = 90^0$

Figure 4. - Concluded.

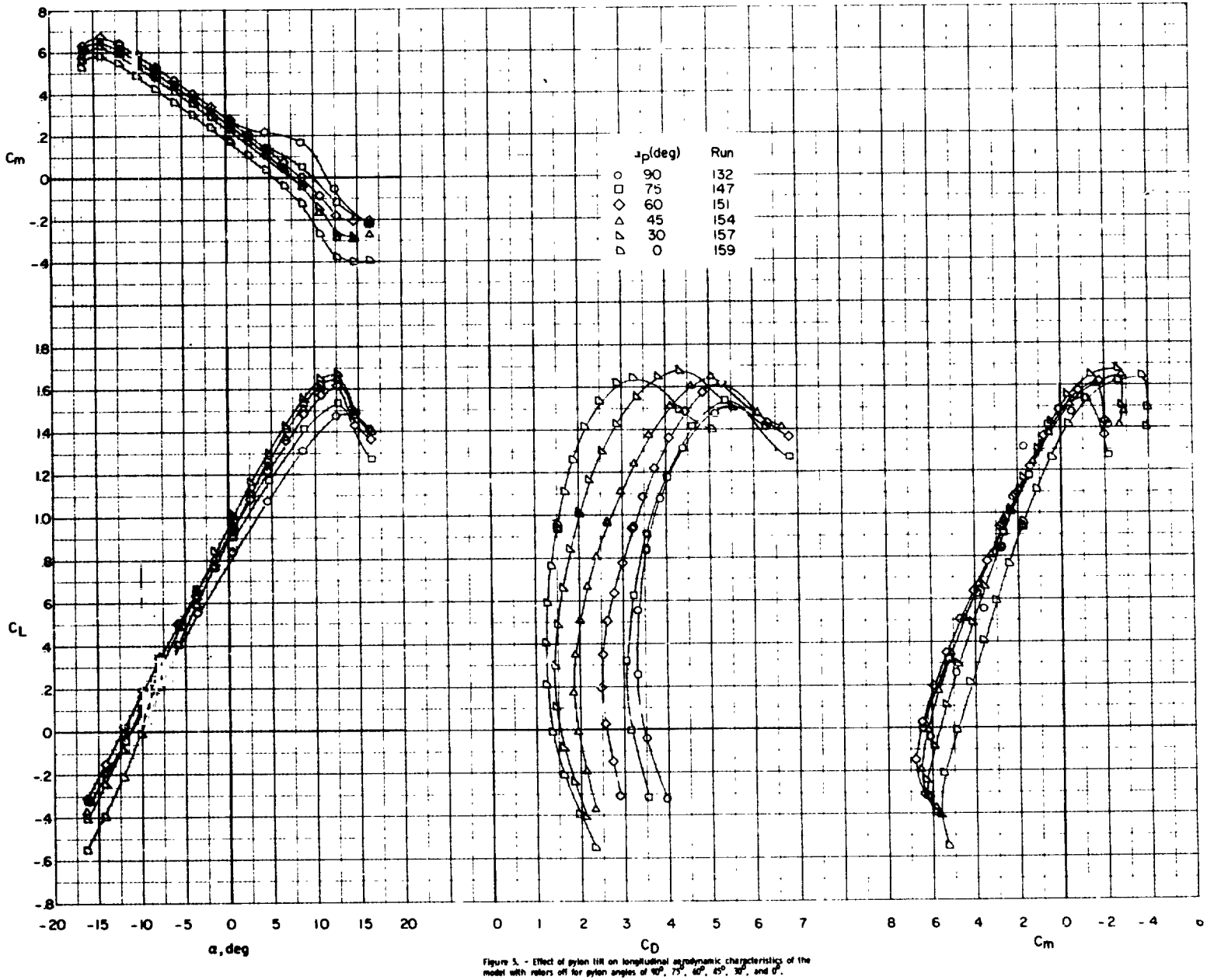

Figure 5. - Effect of pylon tilt on longitudinal aerodynamic characteristics of the model with rotors off for pylon angles of 90°, 75°, 60°, 45°, 30°, and 0°.

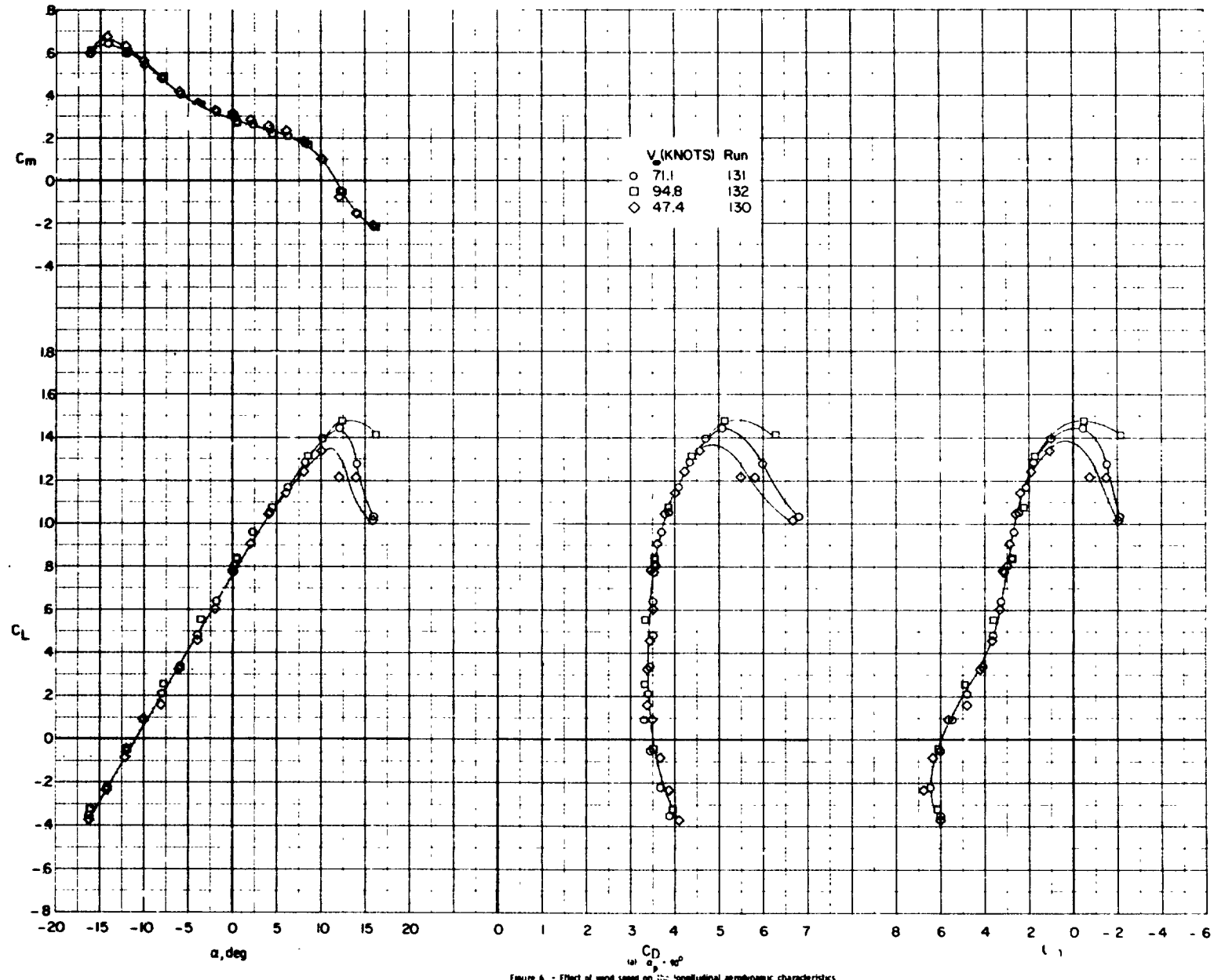

Figure 6. - Effect of wind speed on the longitudinal aerodynamic characteristics of the model with rotors off for pylon angles of 90°, 75°, 60°, 45°, 30°, and 0°.

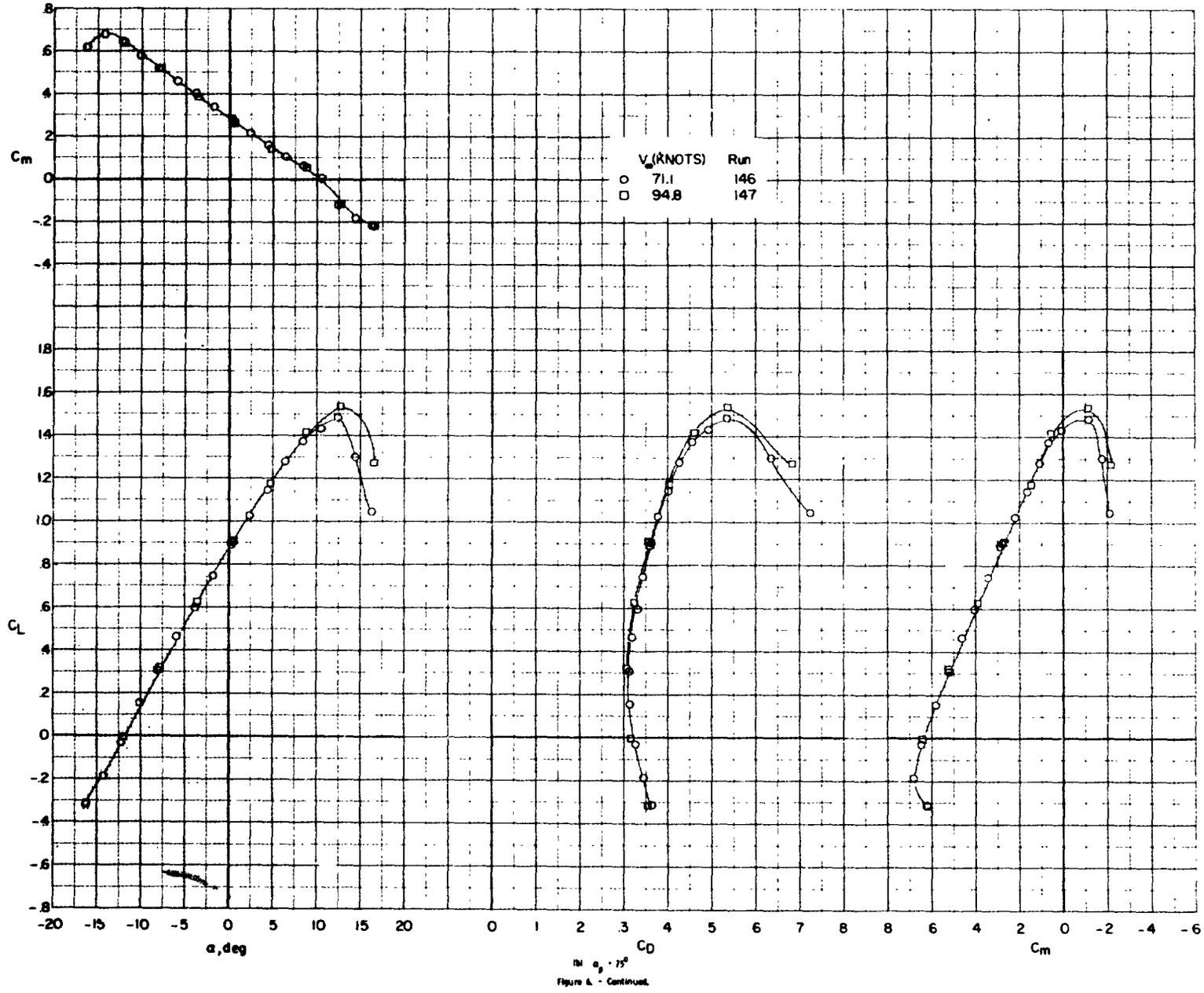

(b) $\alpha_p = 75°$

Figure 6. - Continued.

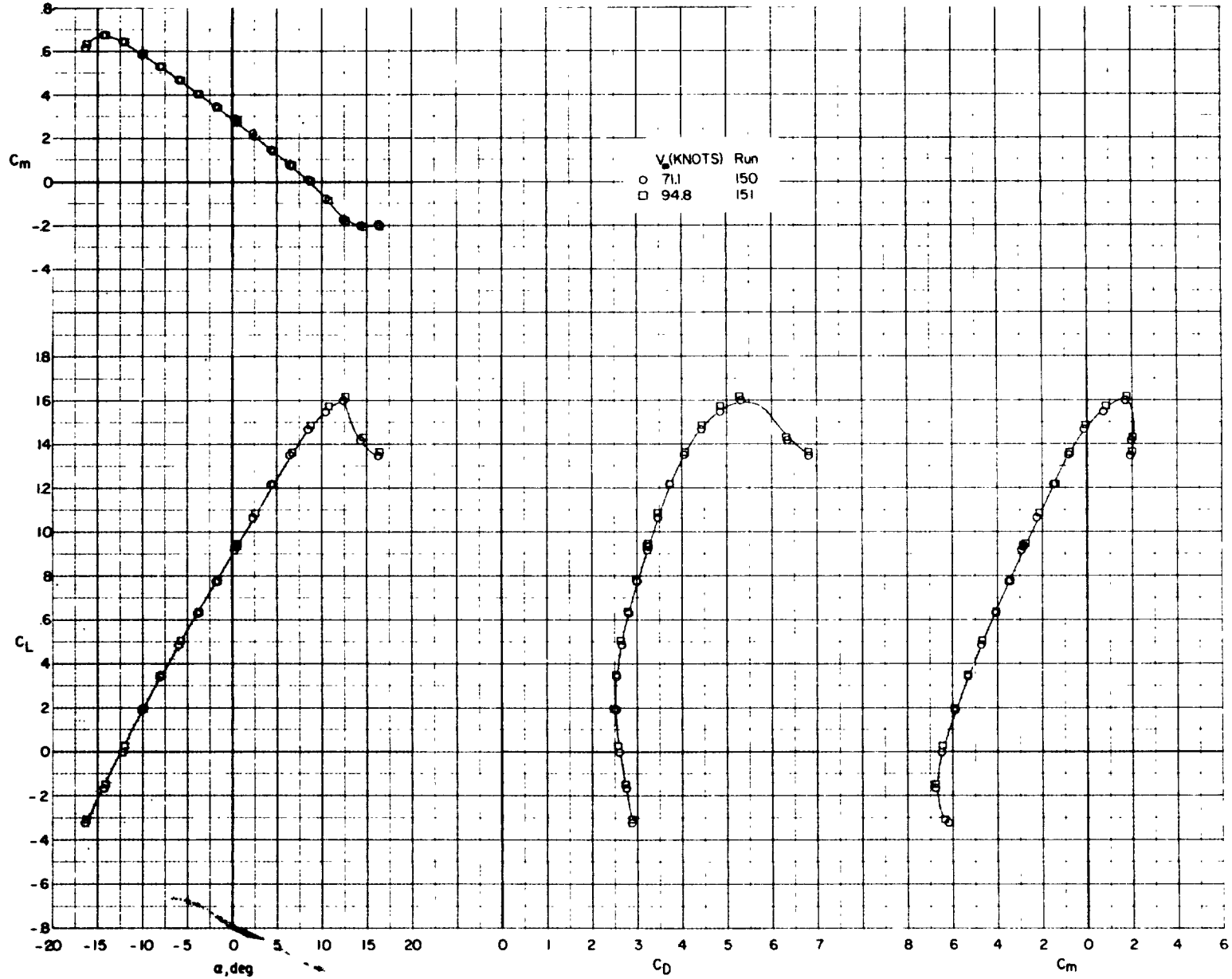

(c) $\alpha_p = 60°$

Figure 6. - Continued.

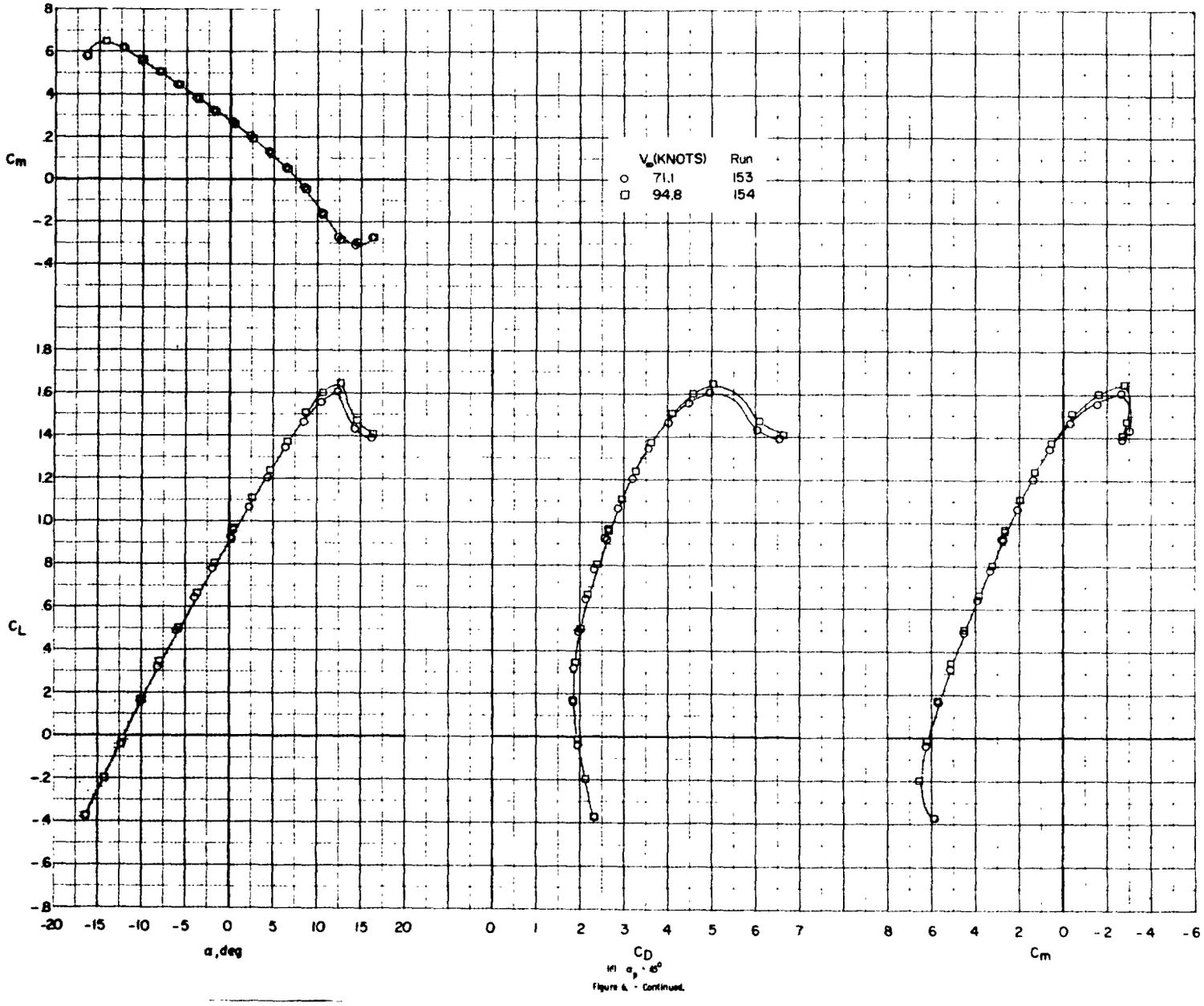

(c) $\alpha_p = 60°$

Figure 6. - Continued.

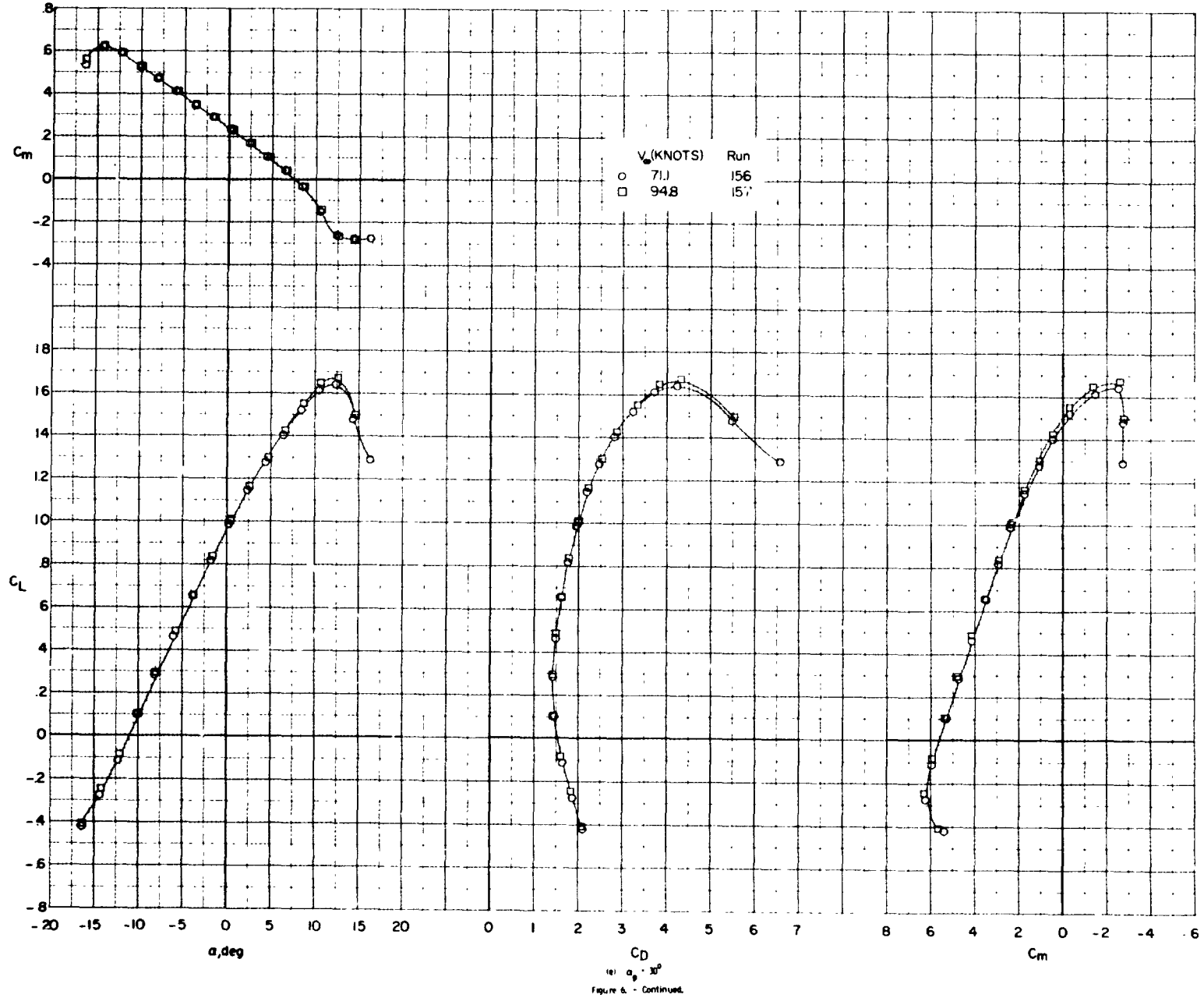

(e) $\alpha_g = 30^\circ$

Figure 6. - Continued.

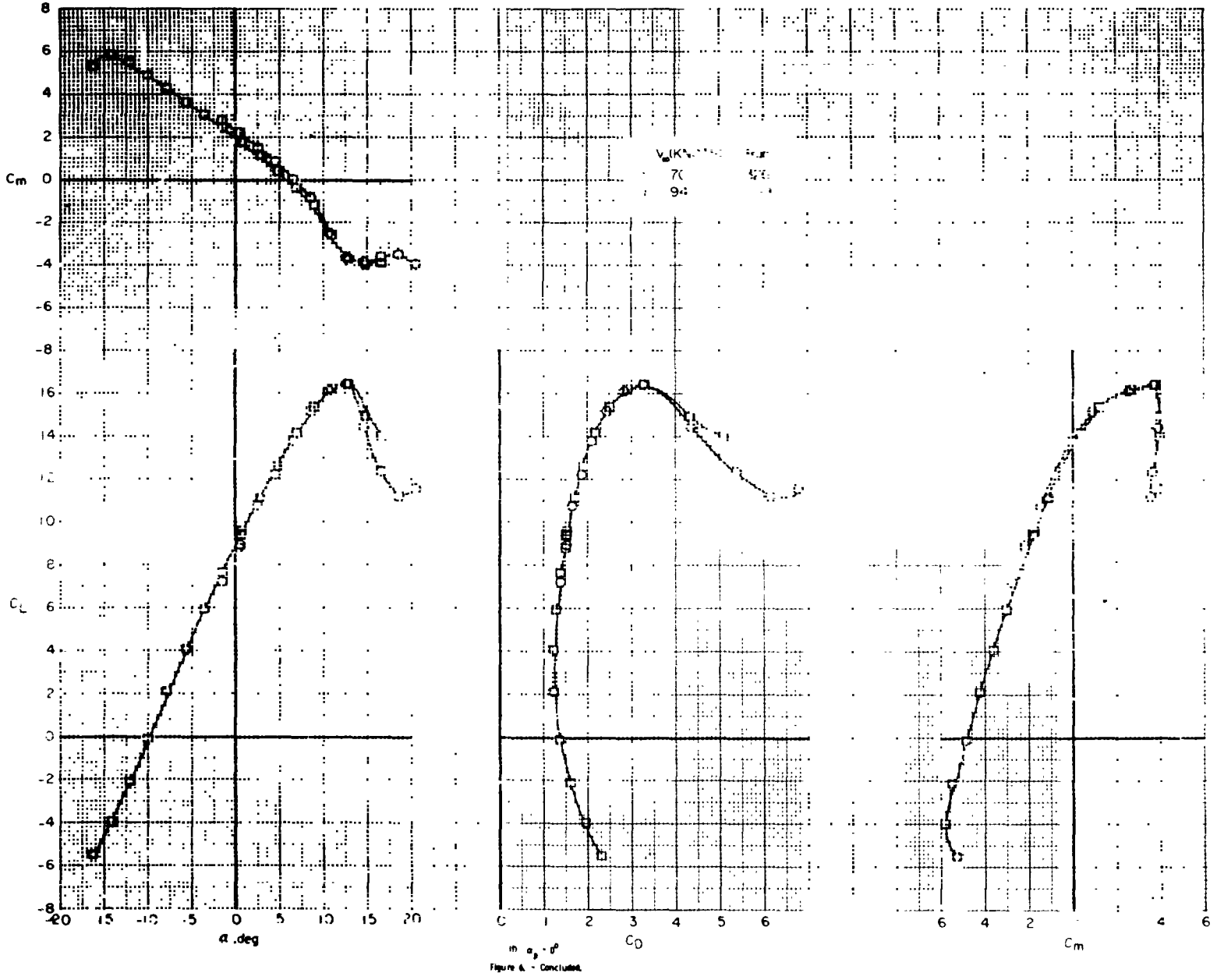

m α_p = 0°

Figure 6. - Concluded.

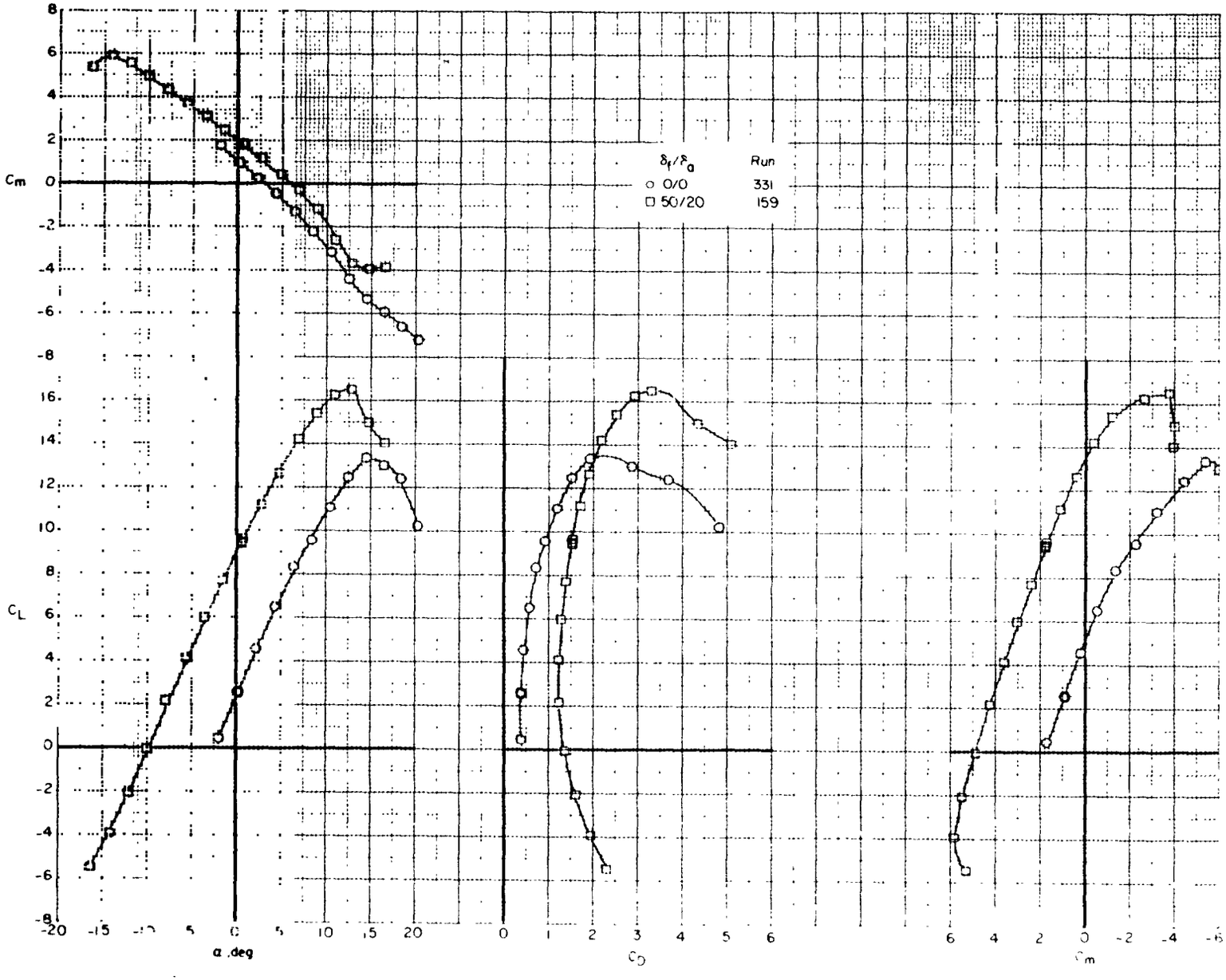
δ_f/δ_a Run
○ 0/0 331
□ 50/20 159
C_m
C_L
α ,deg
C_D
C_m

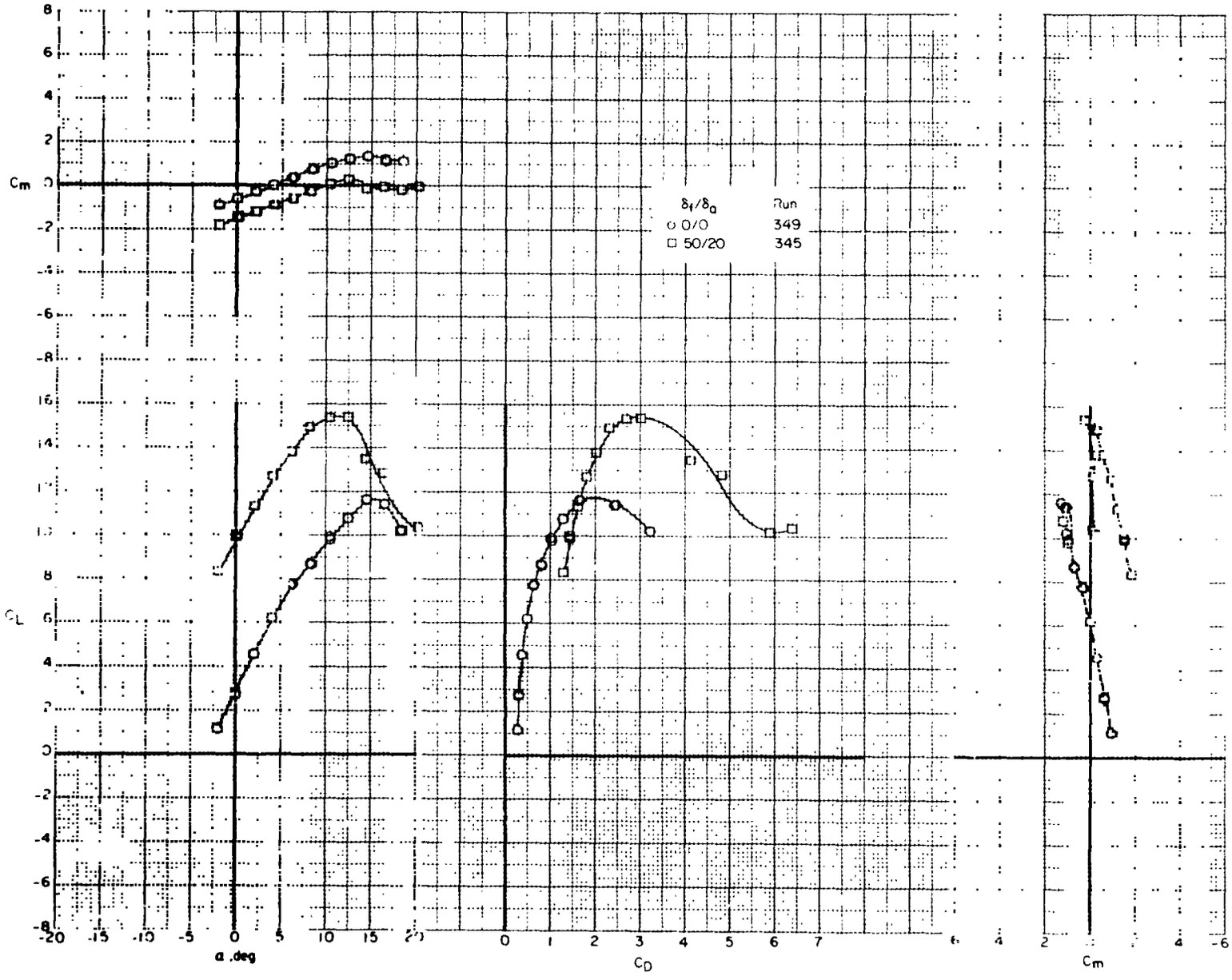

(b) Vertical and horizontal tails off

Figure 7 - Concluded.

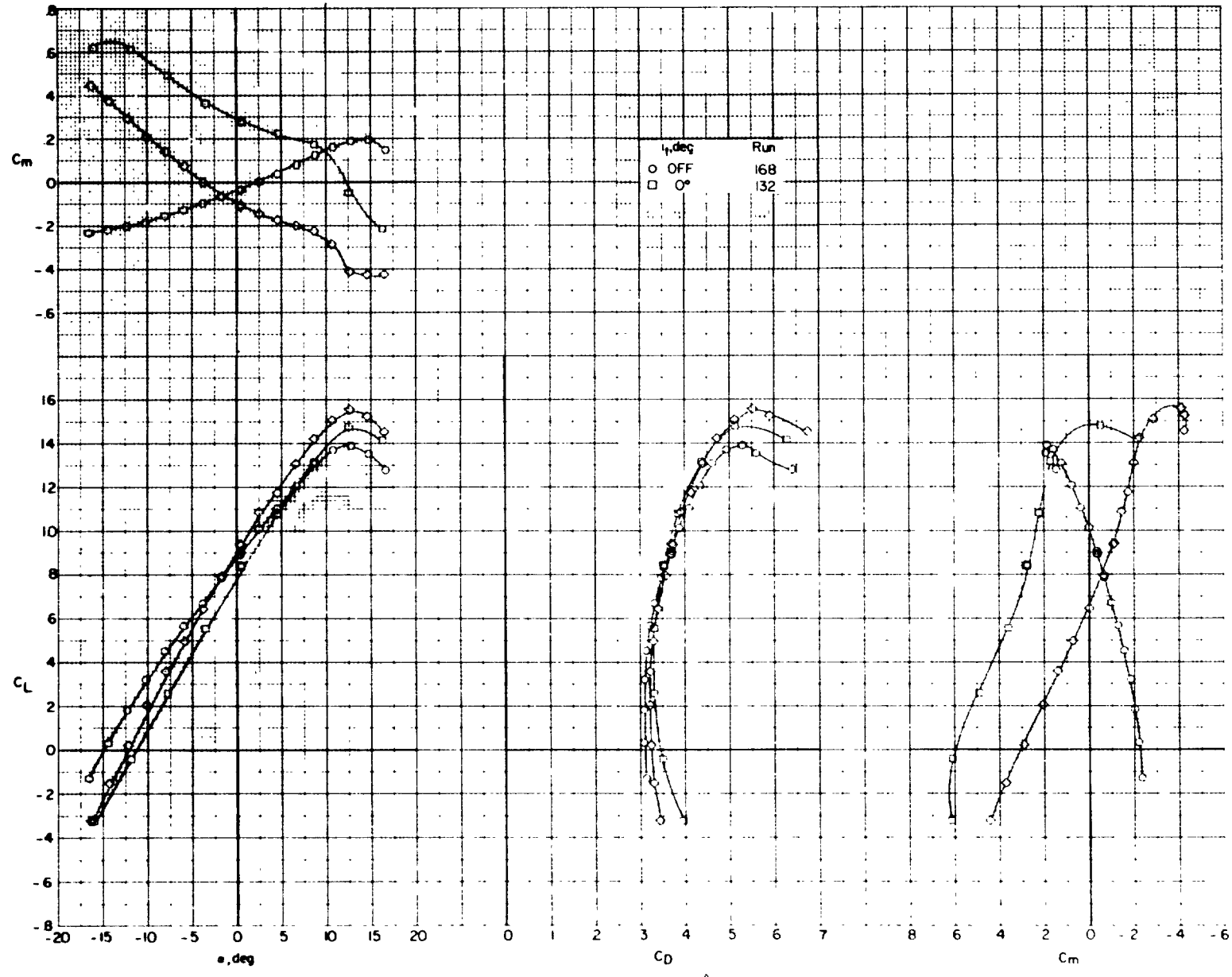

for α_p 90°

Figure 5. - Effect of tail configuration on longitudinal aerodynamic characteristics of the model with the rotors off for pylon angles 90°, 75°, 60°, 30°, and 0°.

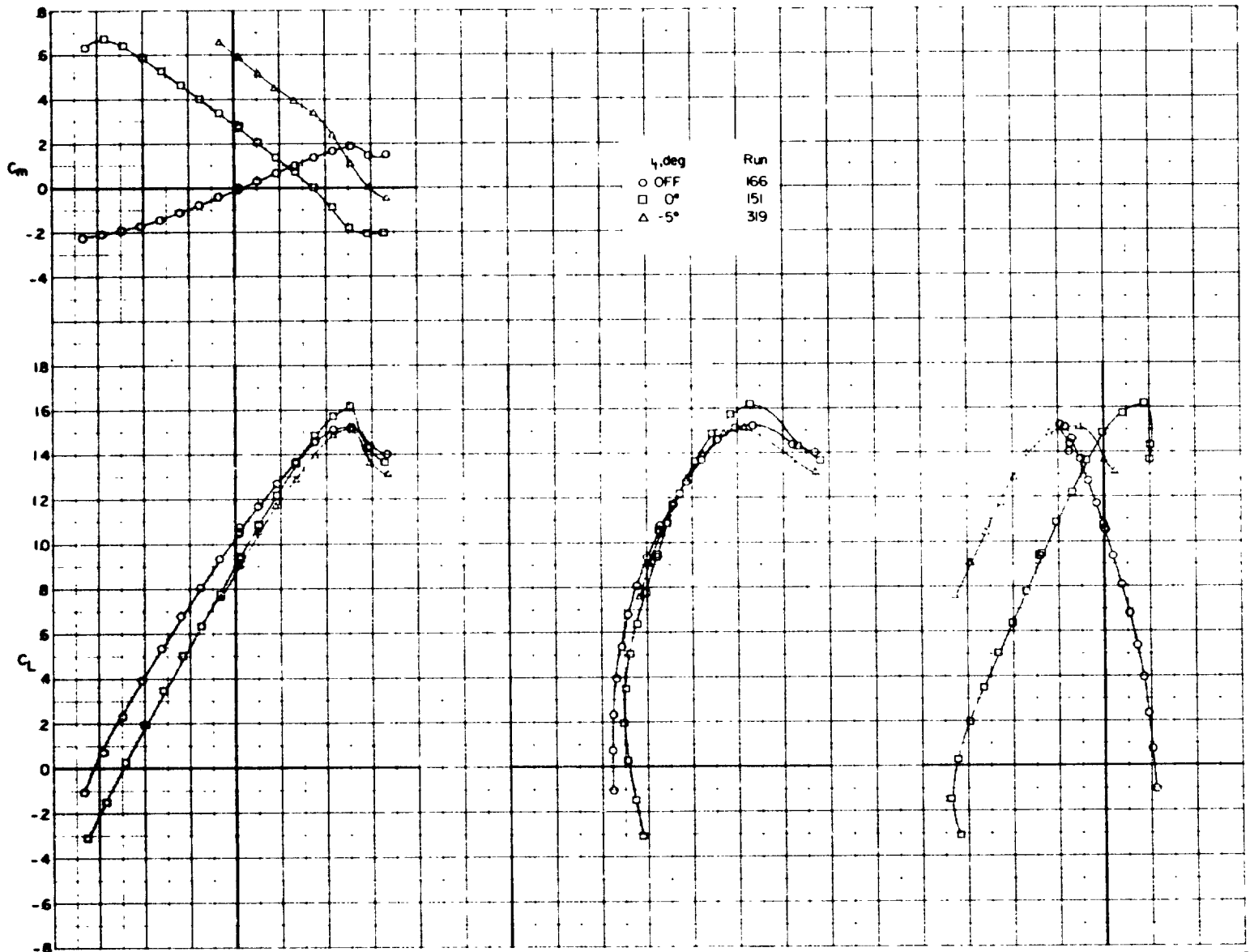

Figure 8. - Continued.

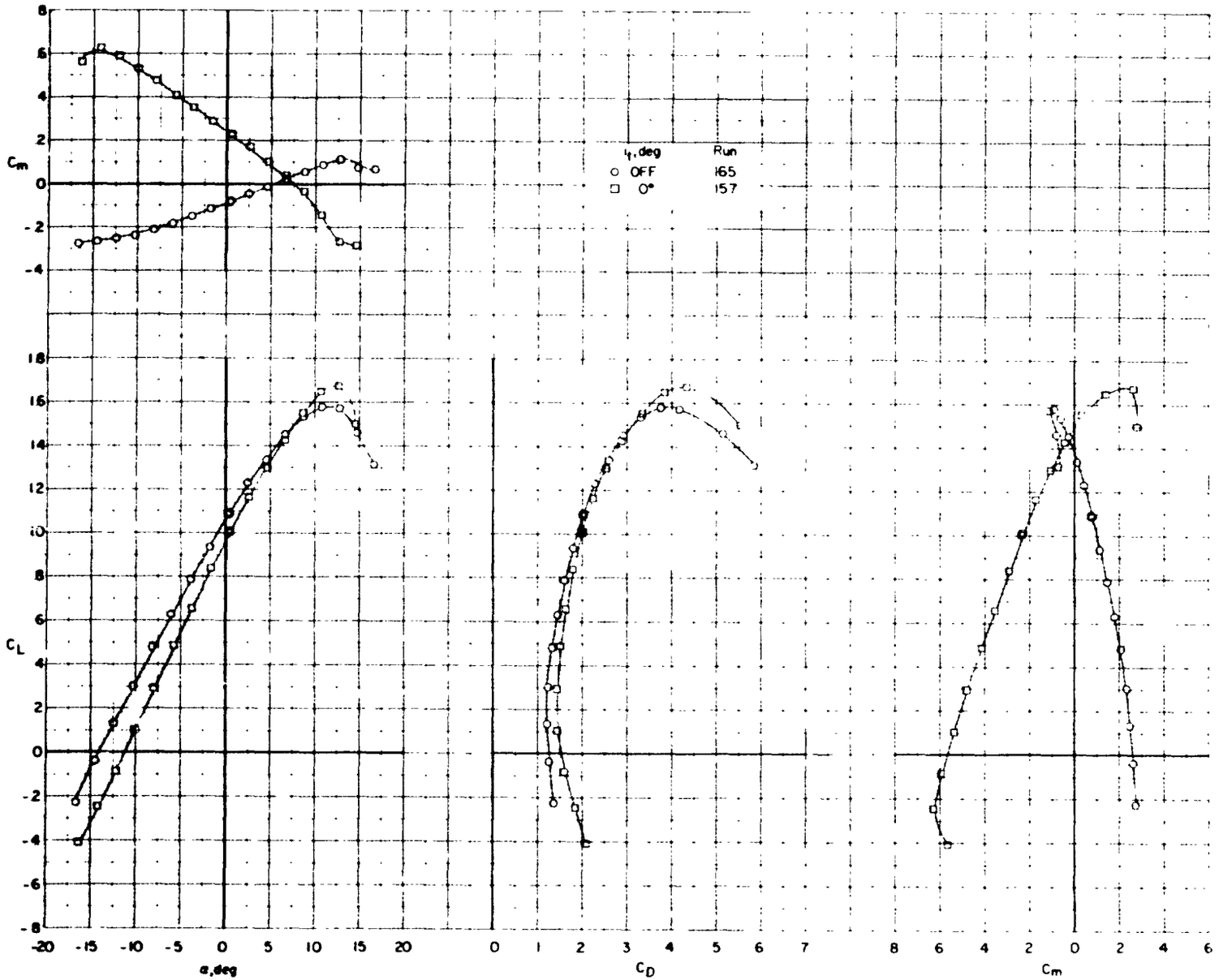

Figure 8. - Continued.

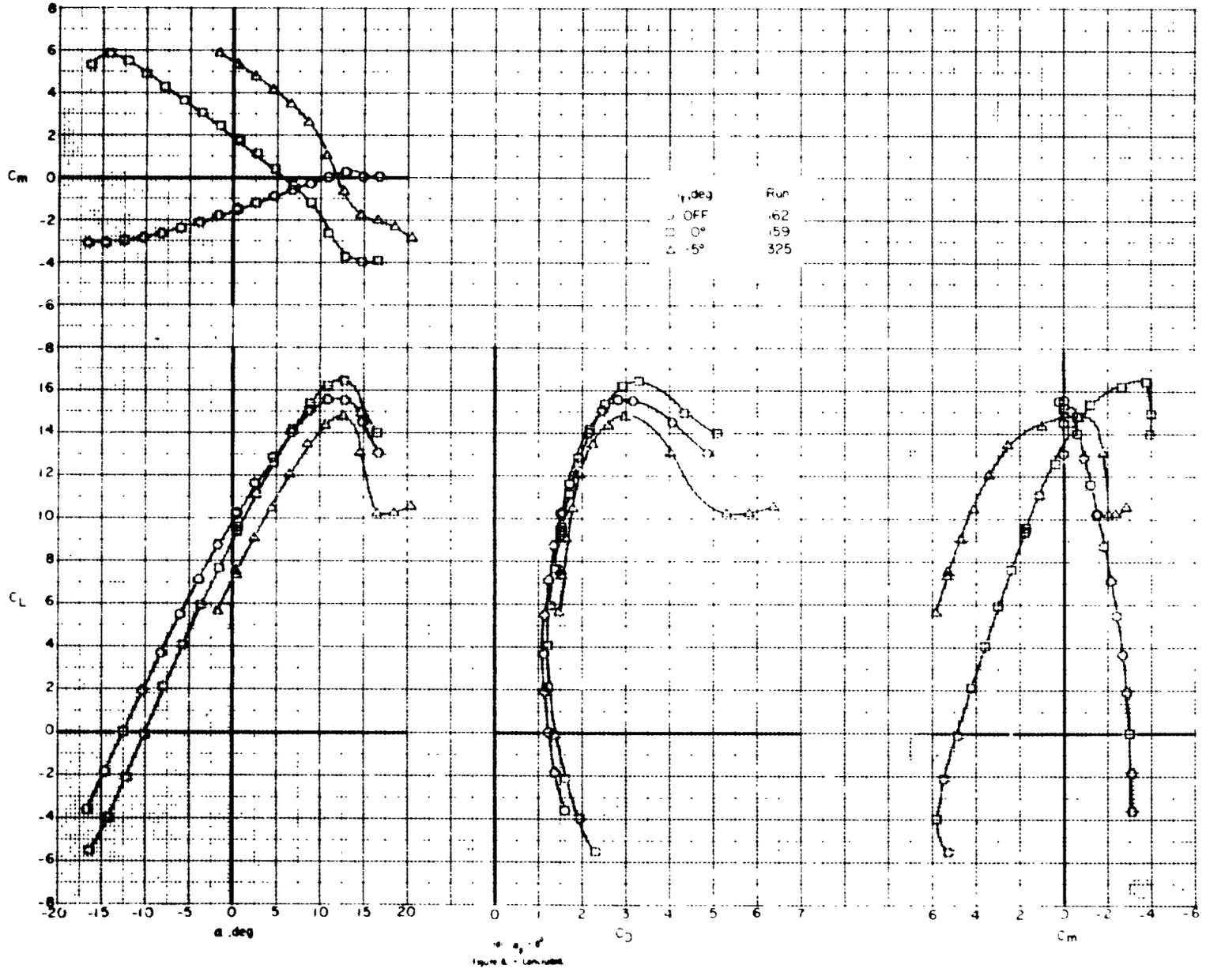
Cm
CL
α, deg
CD
Cm
Run
OFF
0°
-5°
162
159
325

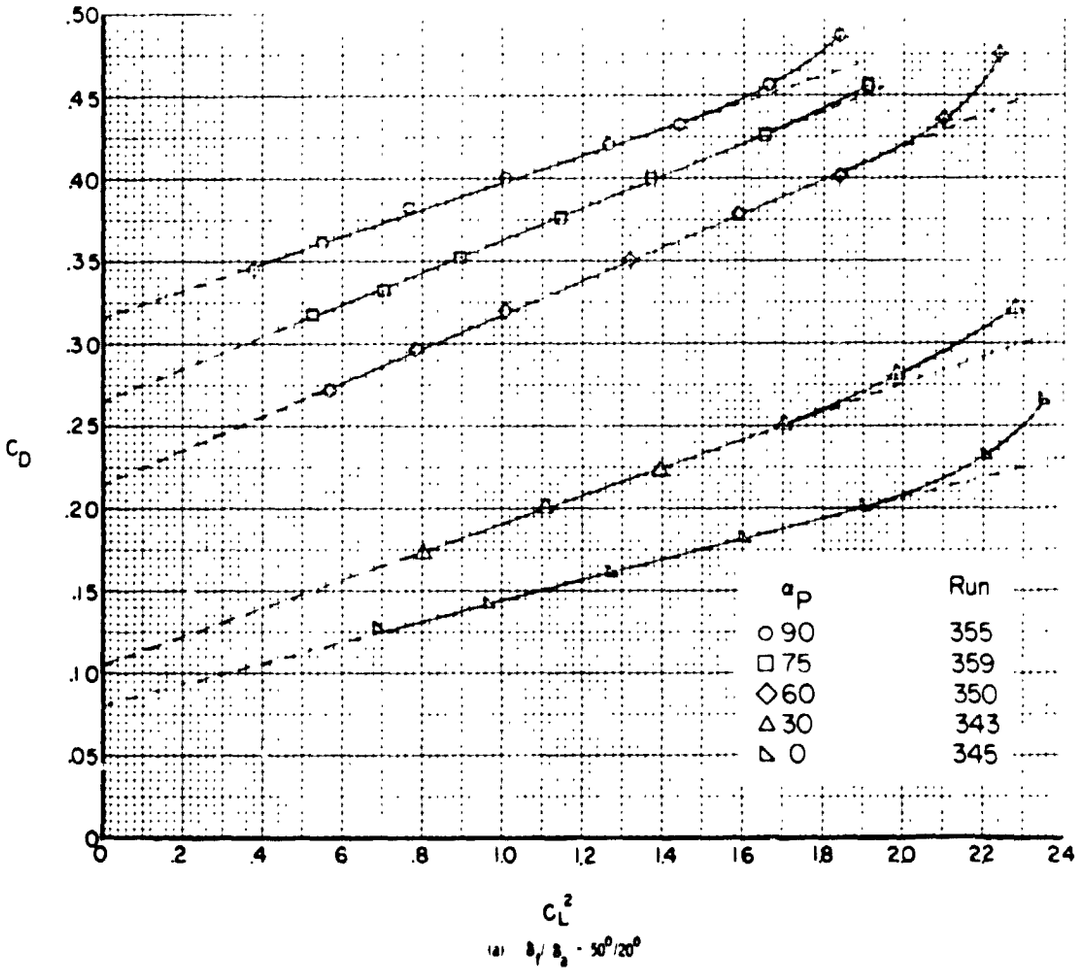

(a) $\delta_f / \delta_a = 50^0/20^0$

Figure 9. - Drag variation as a function of the square of lift coefficient for rotors off and vertical tail off for two flap/aileron deflections.

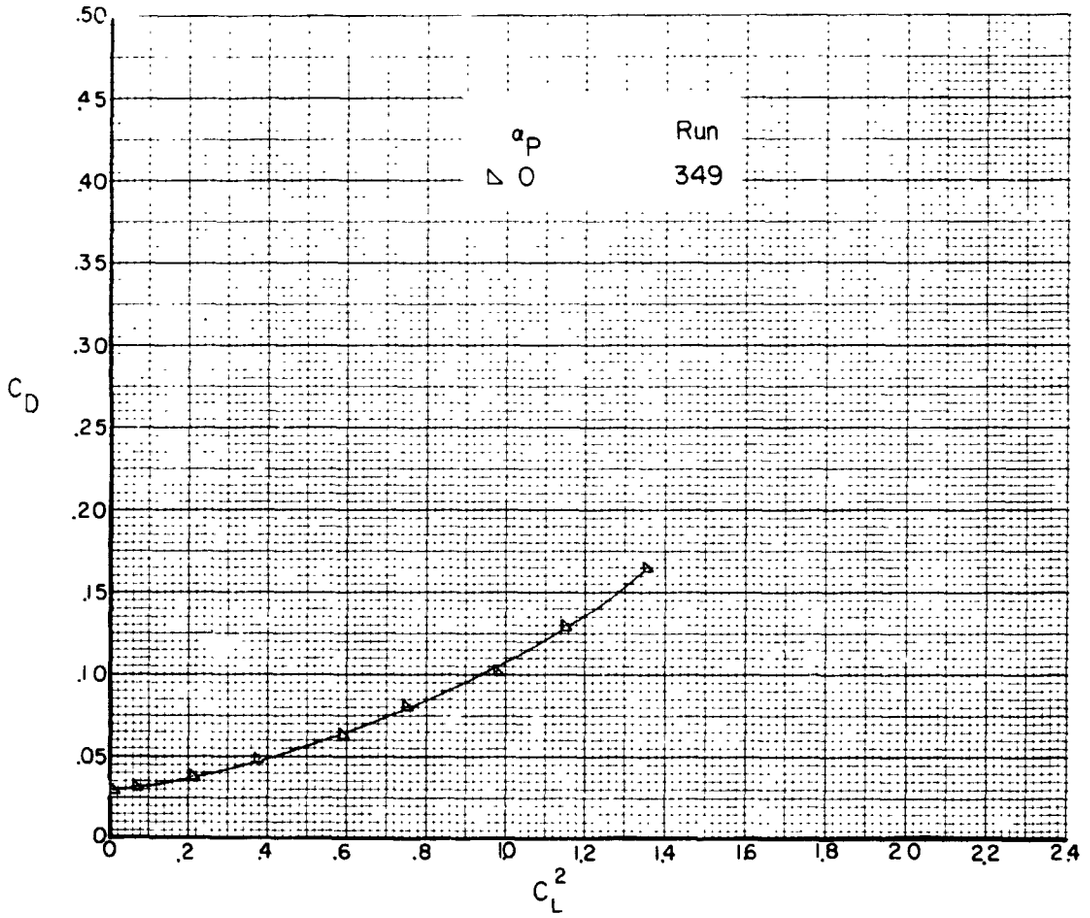

(b) $\delta_f/\delta_a = 0°/0°$

Figure 9. - Concluded.

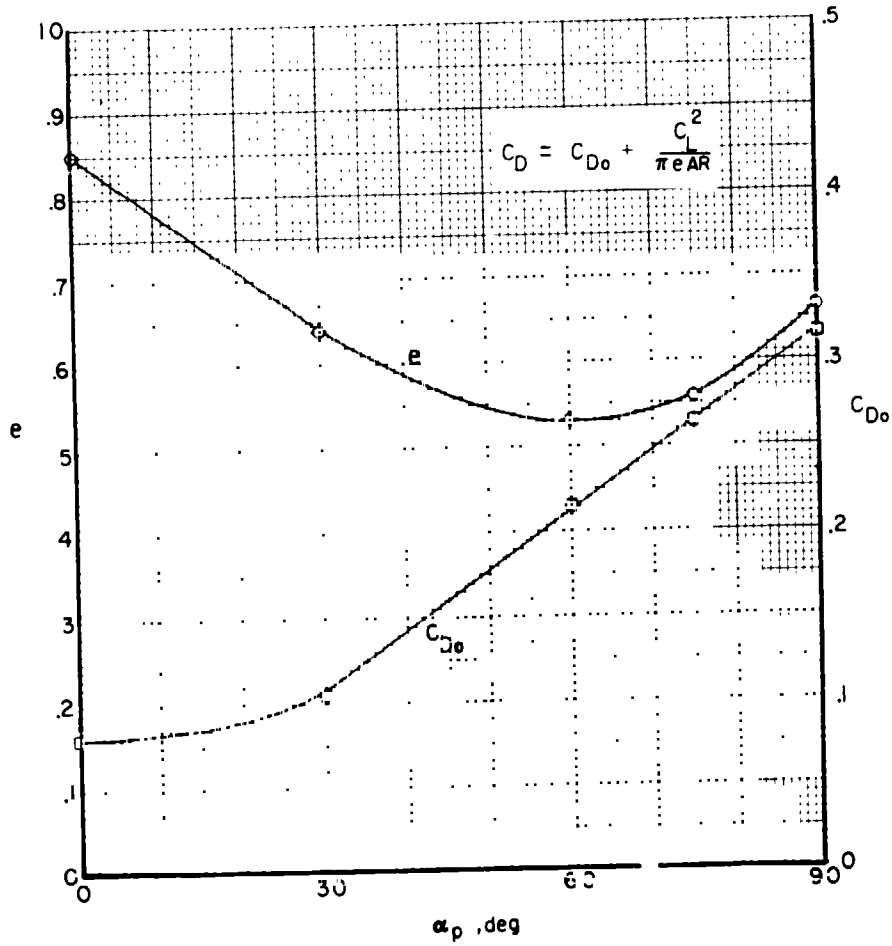

Figure 10. - Span efficiency and effective drag coefficient as a function of pylon angle for rotors and vertical tail off.

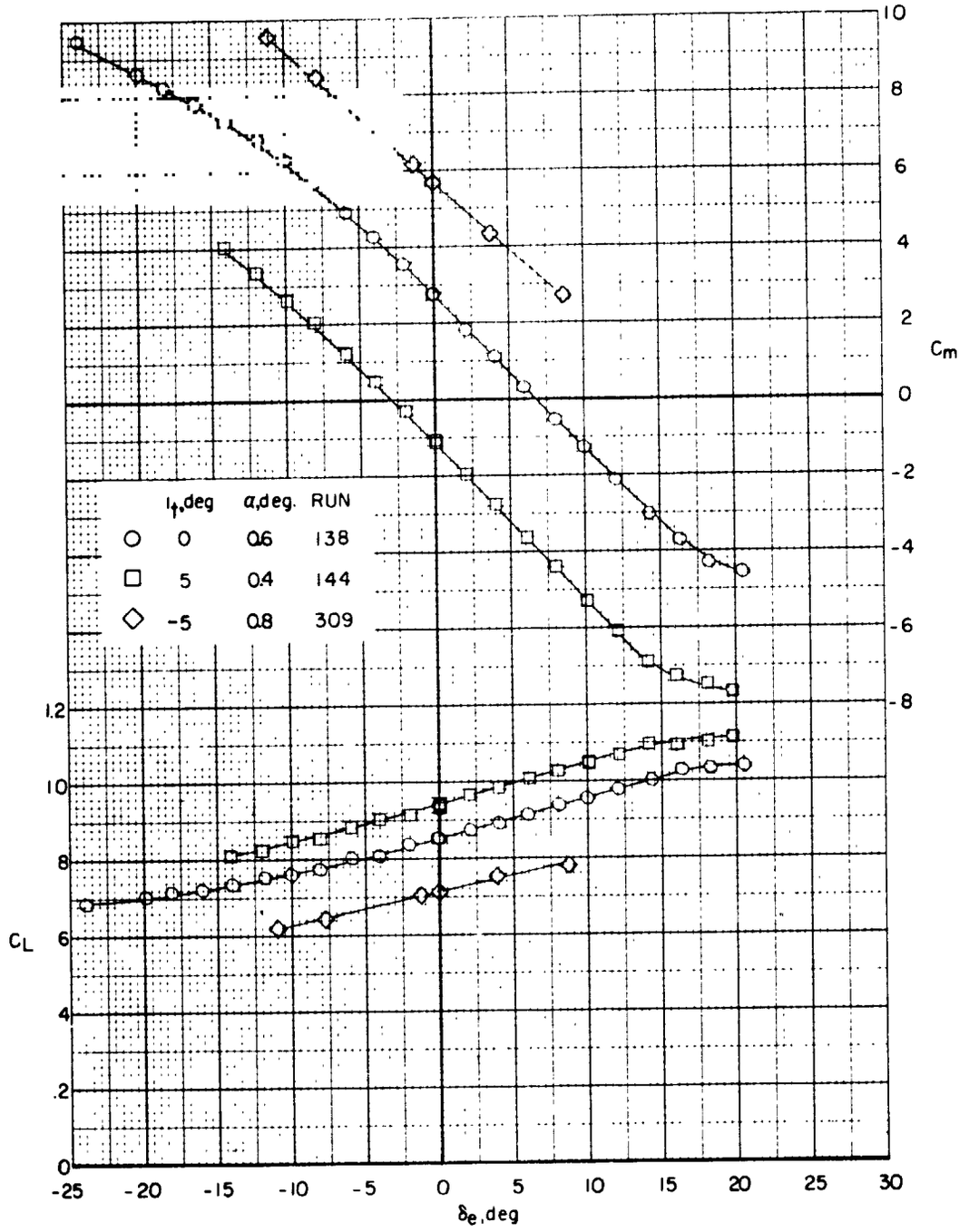

Figure 11. - Effect of elevator deflection on lift and pitching-moment characteristics for a pylon angle of 90° for three horizontal tail incidences (0°, 5°, -5°) and rotors off.

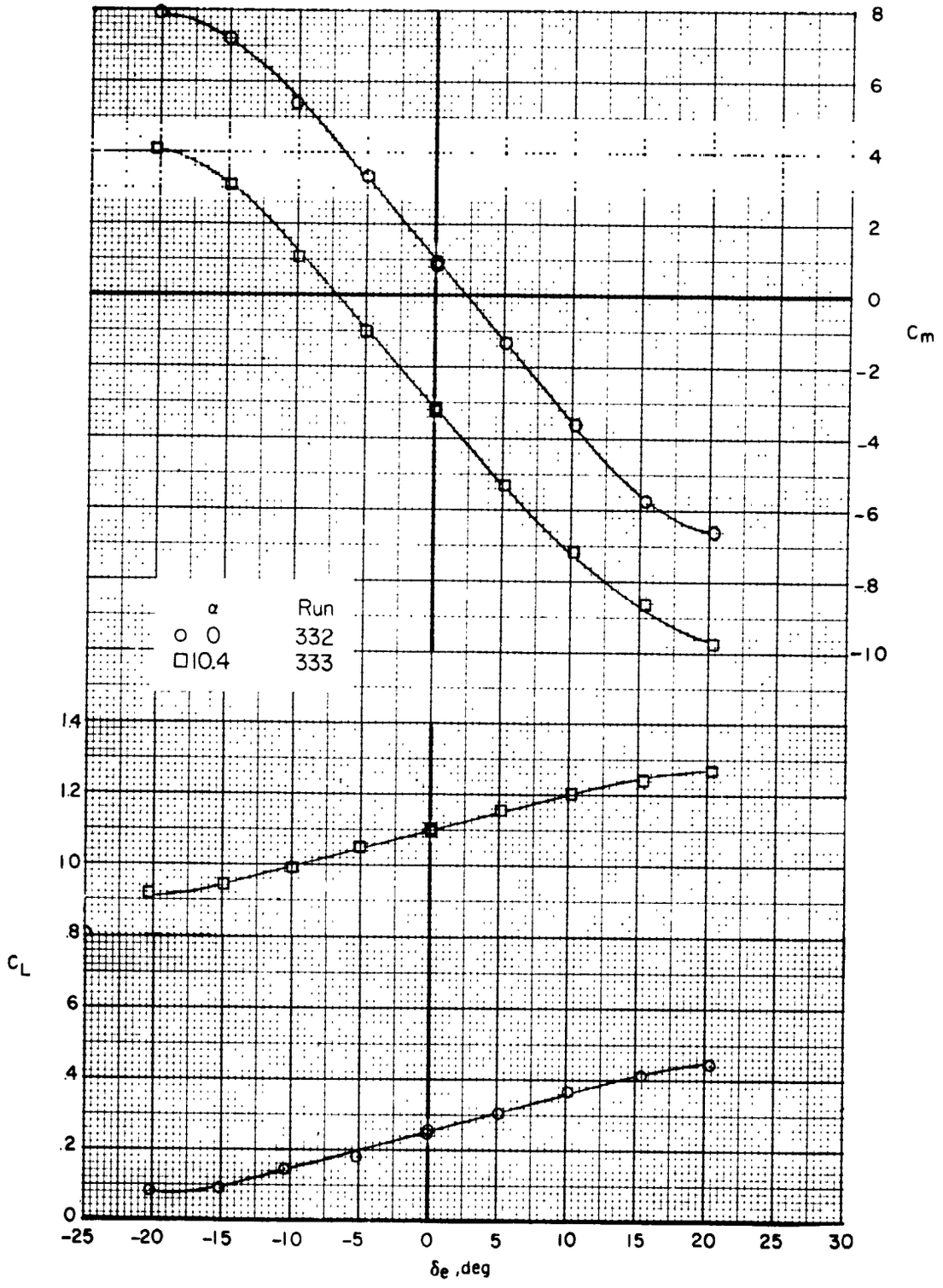

Figure 12. - Effect of elevator deflection on lift and pitching-moment characteristics for pylon angle 0^0 for two angles of attack (0^0 and 10.4^0) and rotors off.

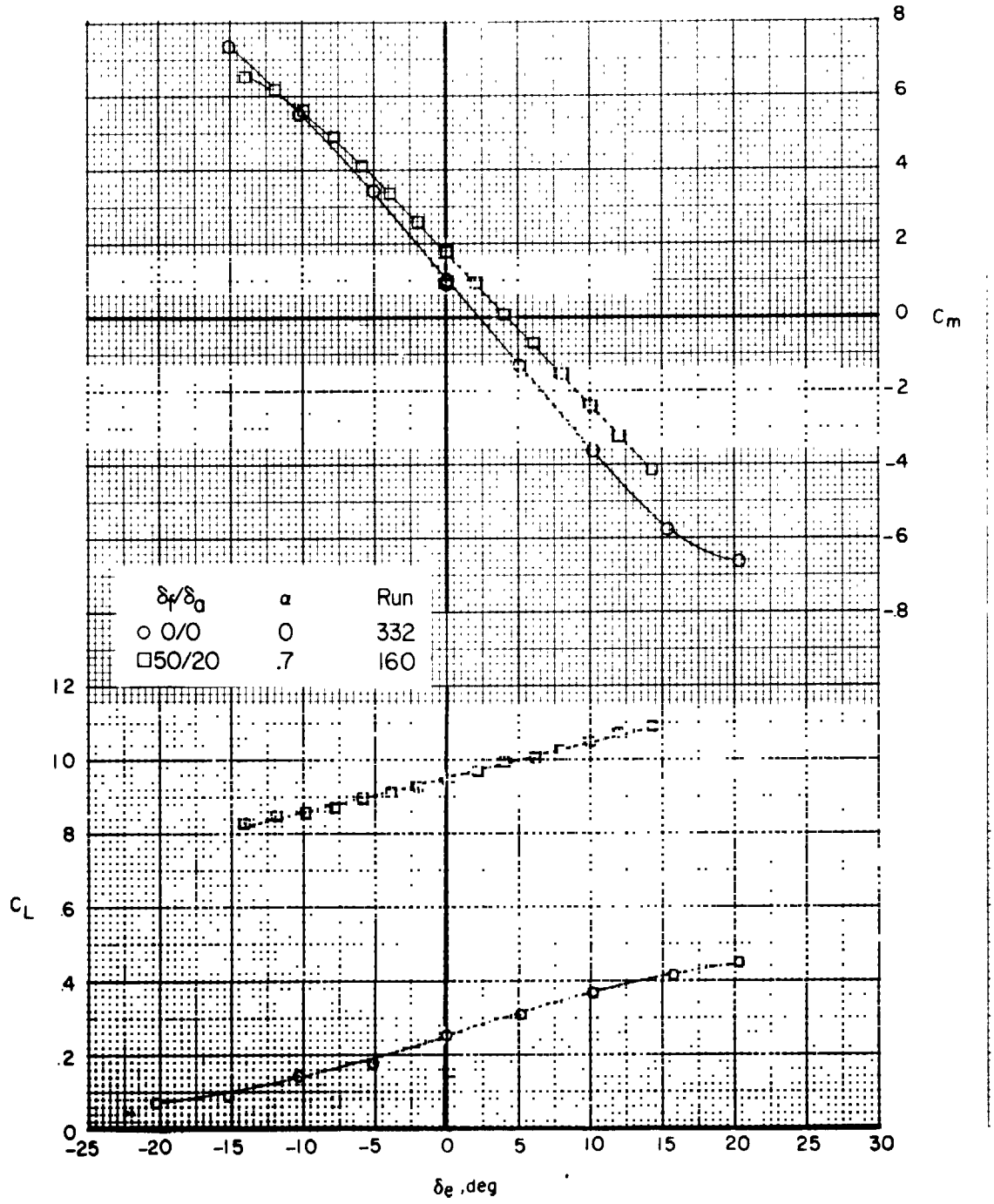

Figure 13. - Effect of flap/aileron deflection on elevator effectiveness for pylon angle 0° and rotors off.

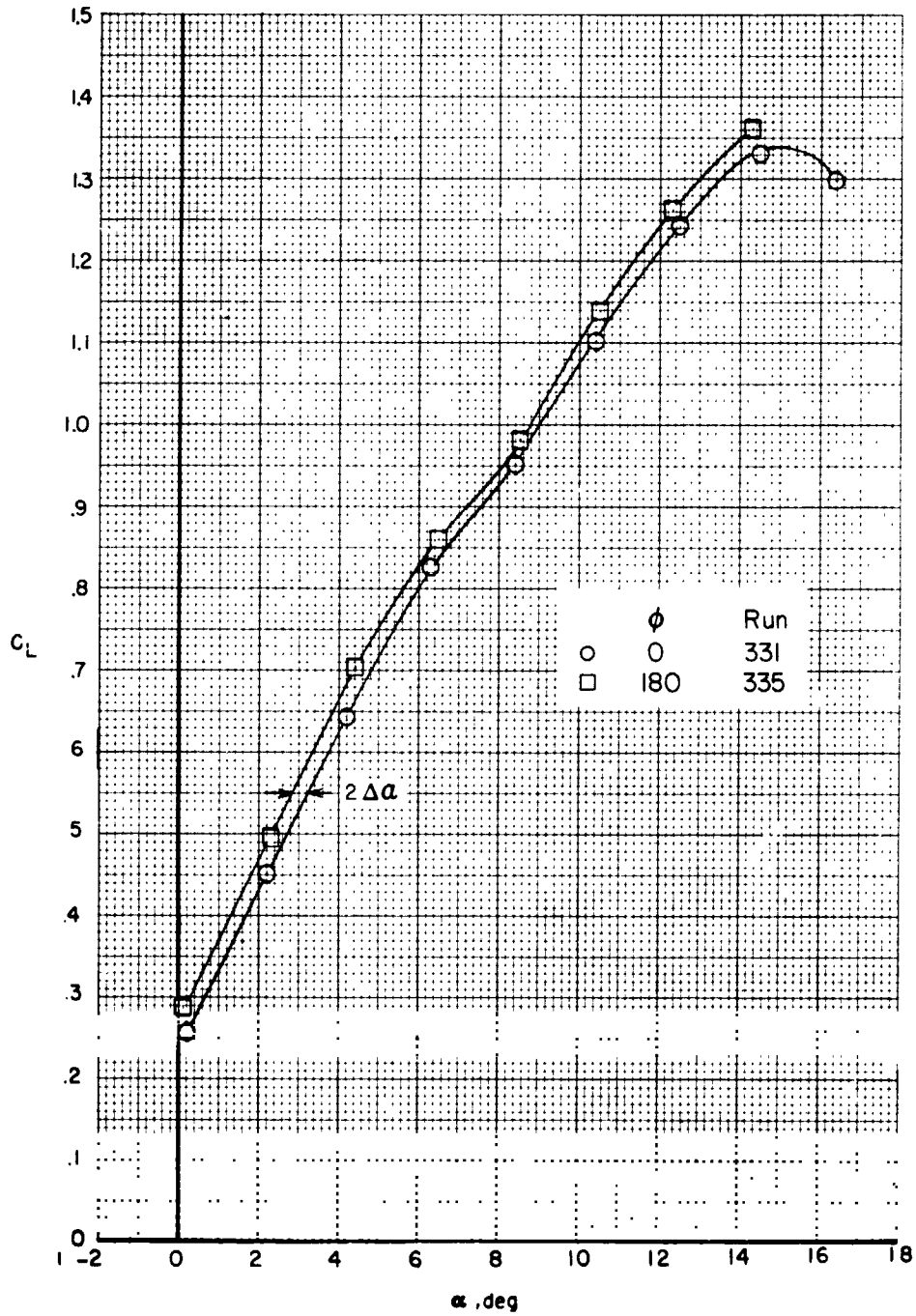

Figure 14. - Tunnel windstream flow angles as determined by testing of model at roll angles of 0^0 and 180^0.

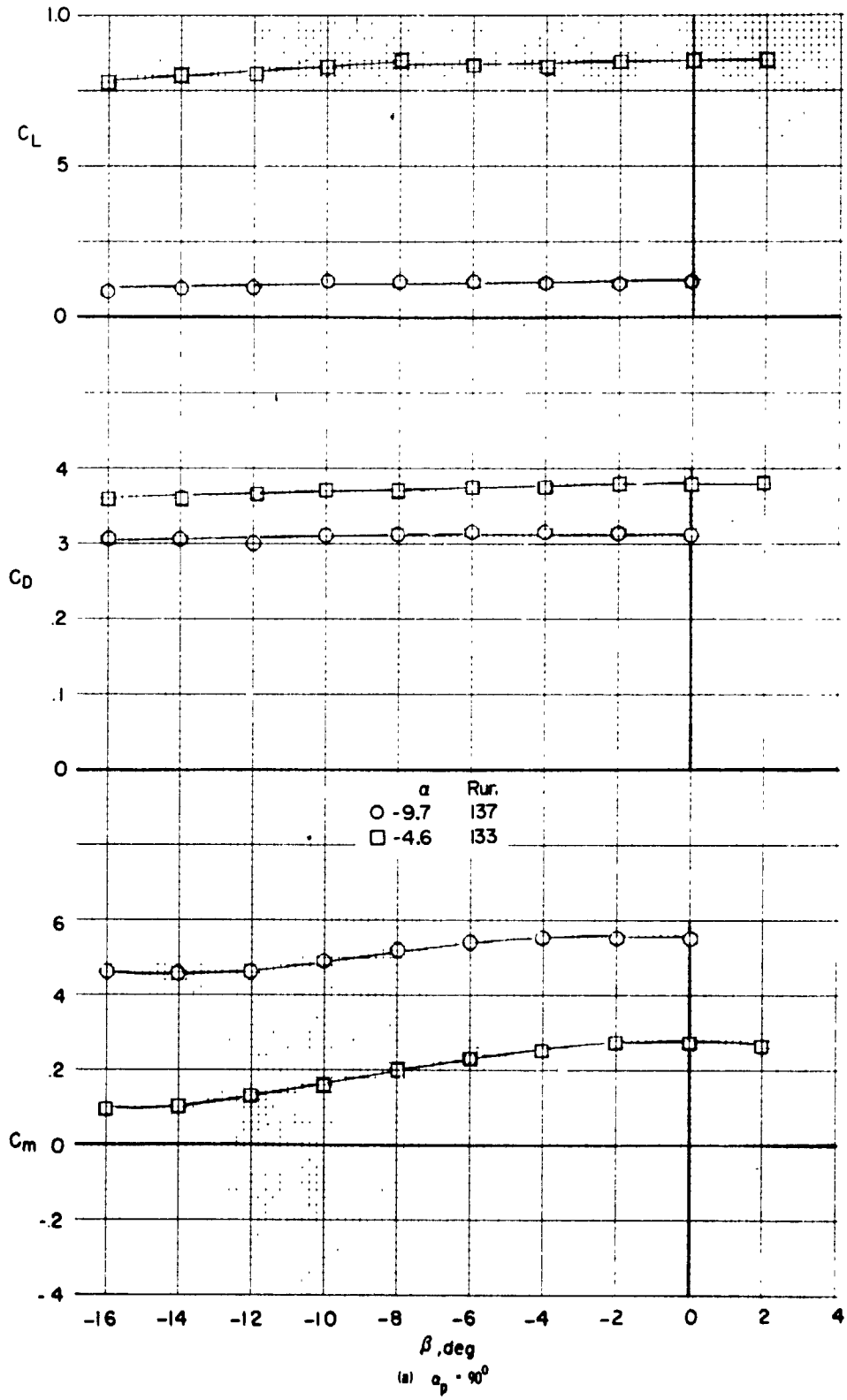

(a) $\alpha_p = 90^0$

Figure 15. - Effect of sideslip angle on longitudinal aerodynamic characteristics of the model with rotors off for pylon angles of 90^0, 75^0, and 0^0.

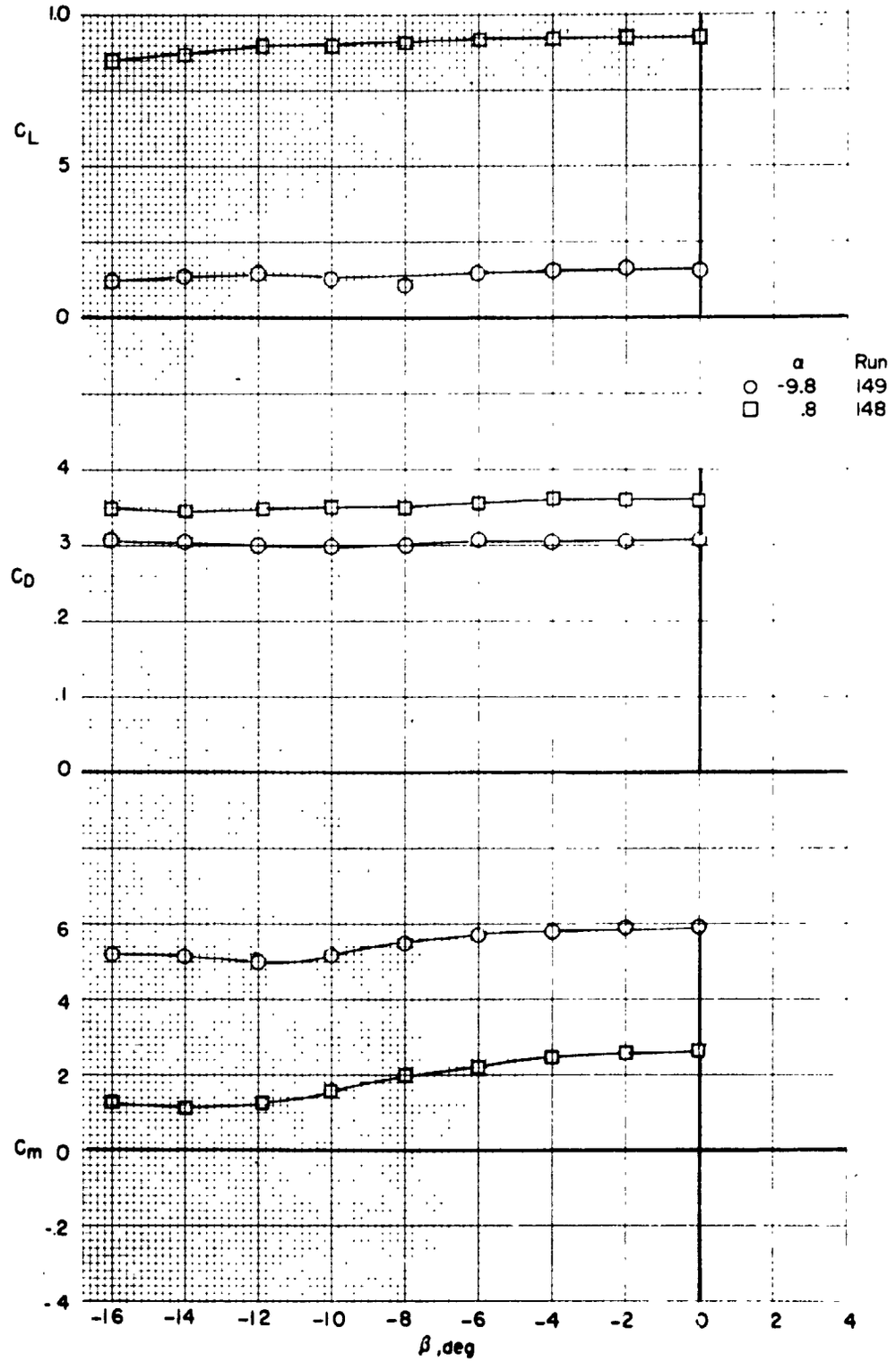

(b) $\alpha_\beta = 75^0$

Figure 15. - Continued.

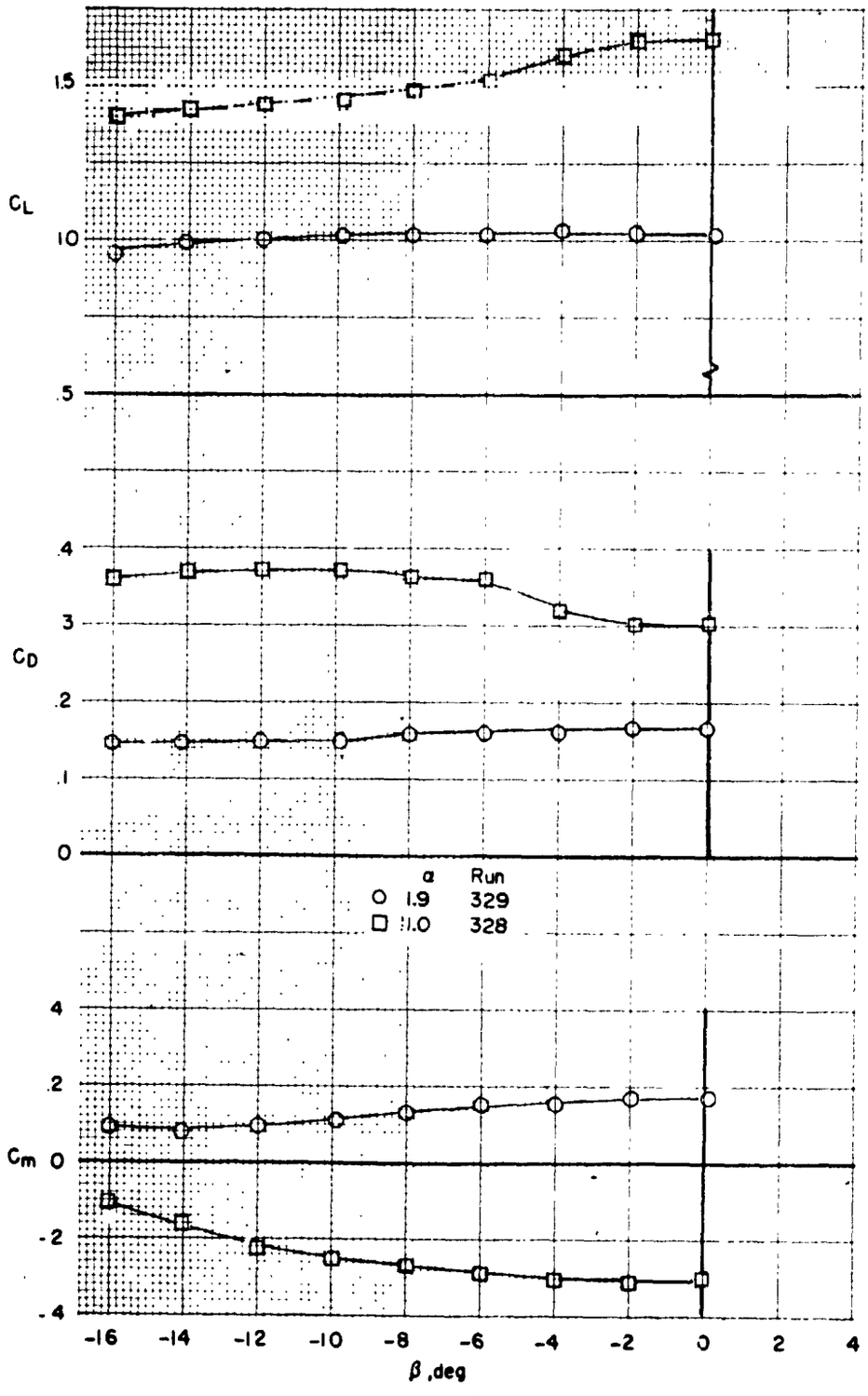

(c) $\alpha_p = 0^0$

Figure 15. - Concluded.

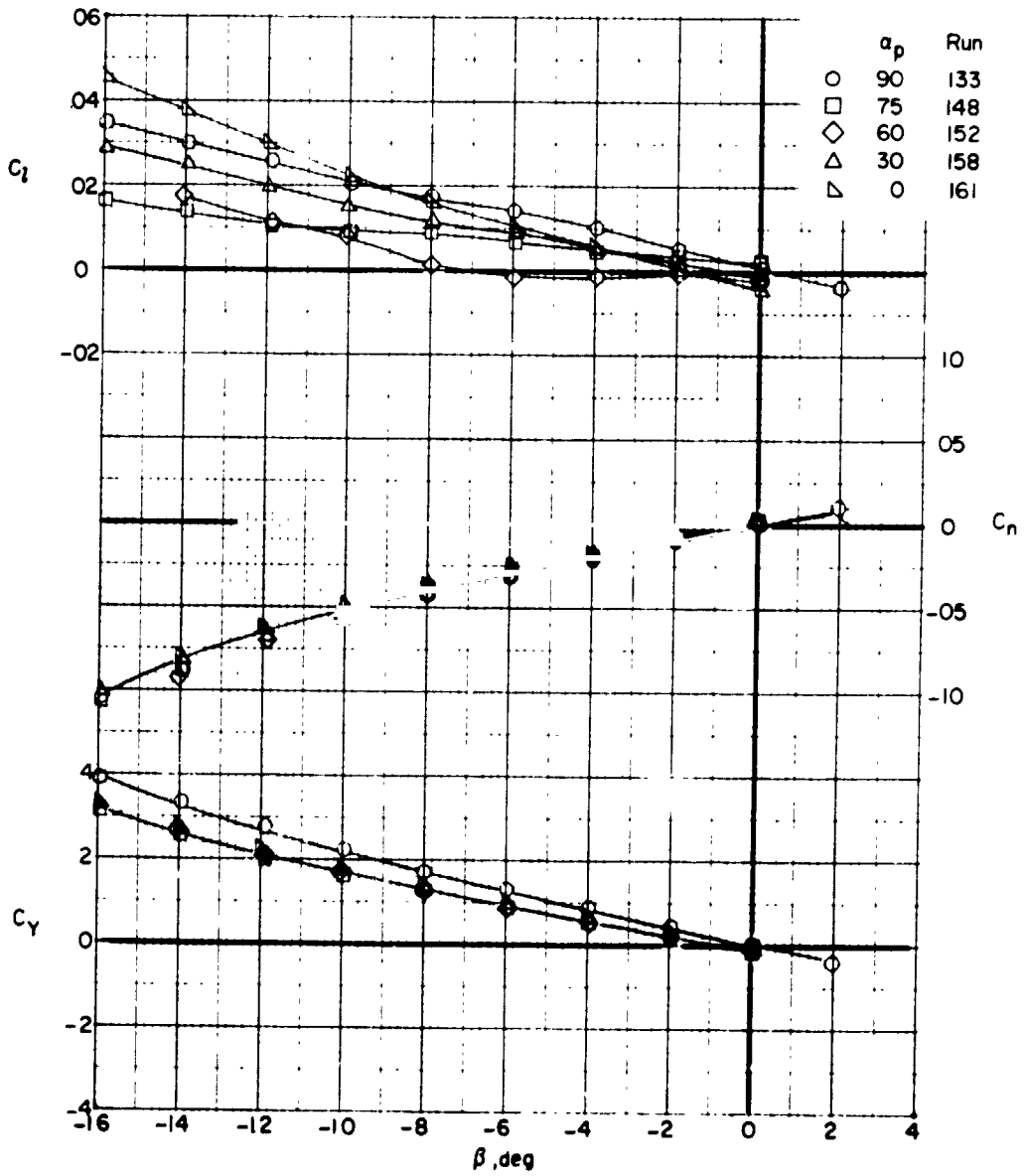

Figure 16. - Effect of pylon angle on lateral aerodynamic characteristics of the model with rotors off, $\mu = 0.6$.

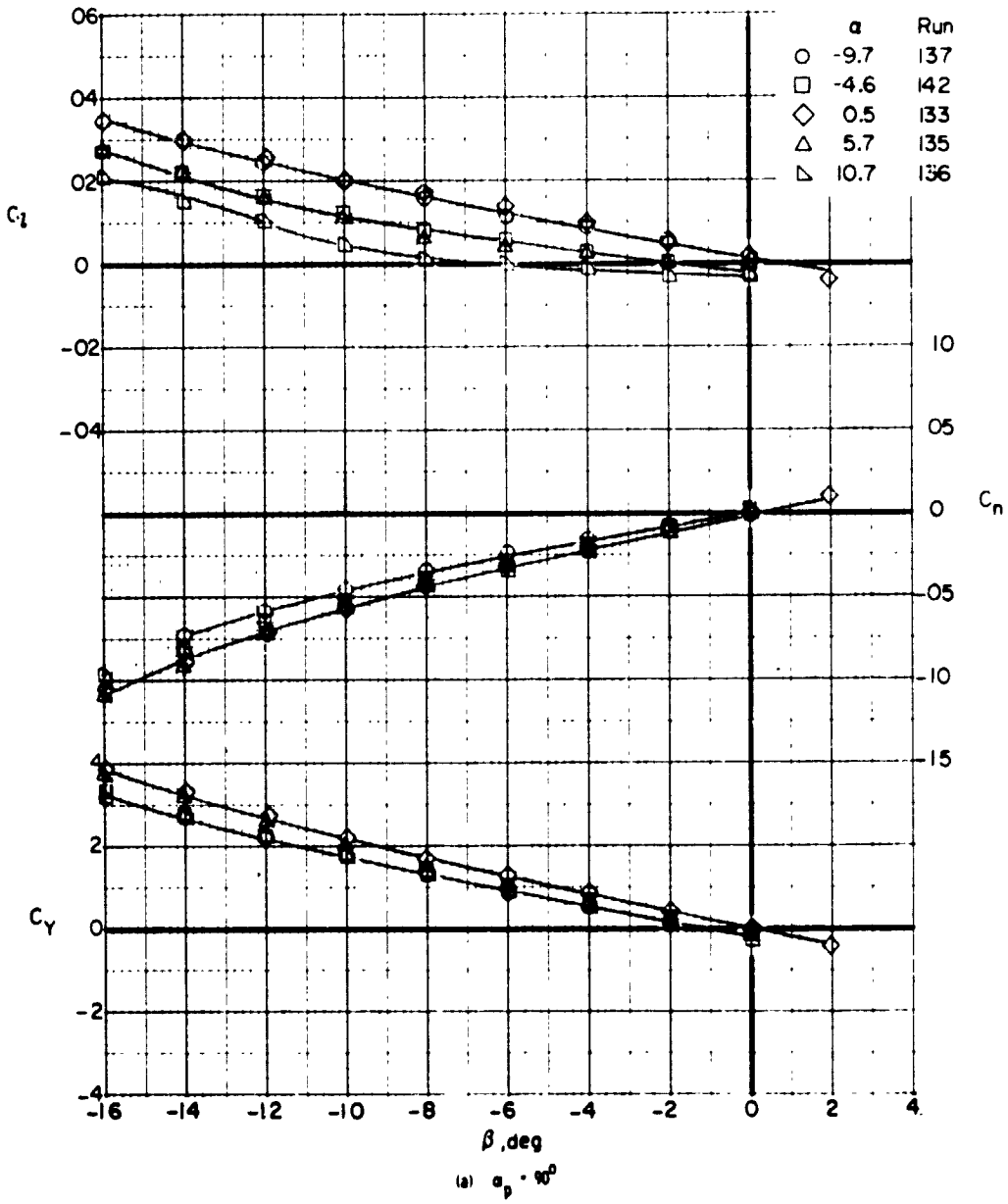

(a) $\alpha_p = 90^0$

Figure 17. - Effect of angle of attack on the lateral aerodynamic characteristics of the model with rotors off for pylon angles 90°, 75°, and 0°.

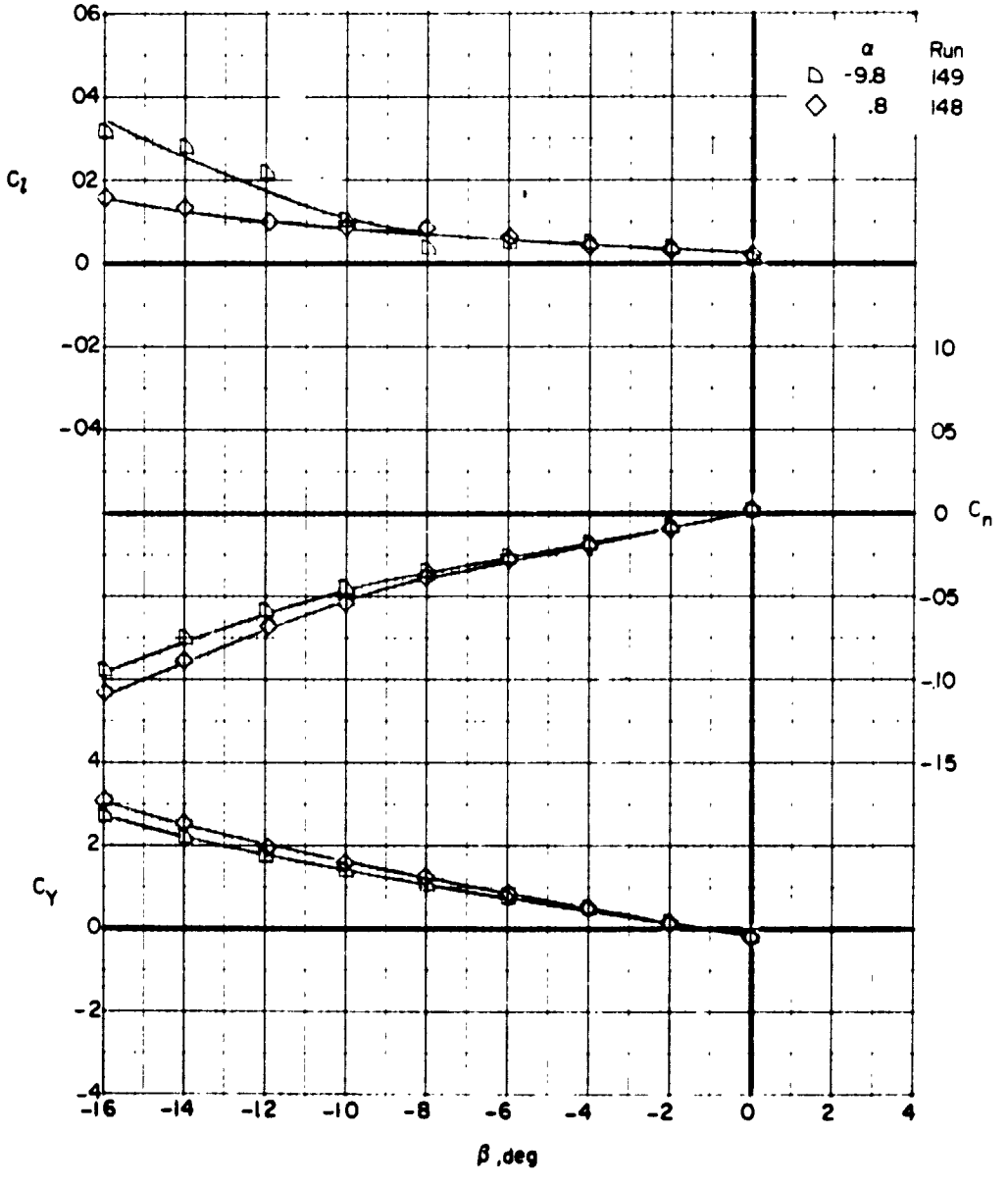

(b) $\alpha_p = 75^0$

Figure 17. - Continued.

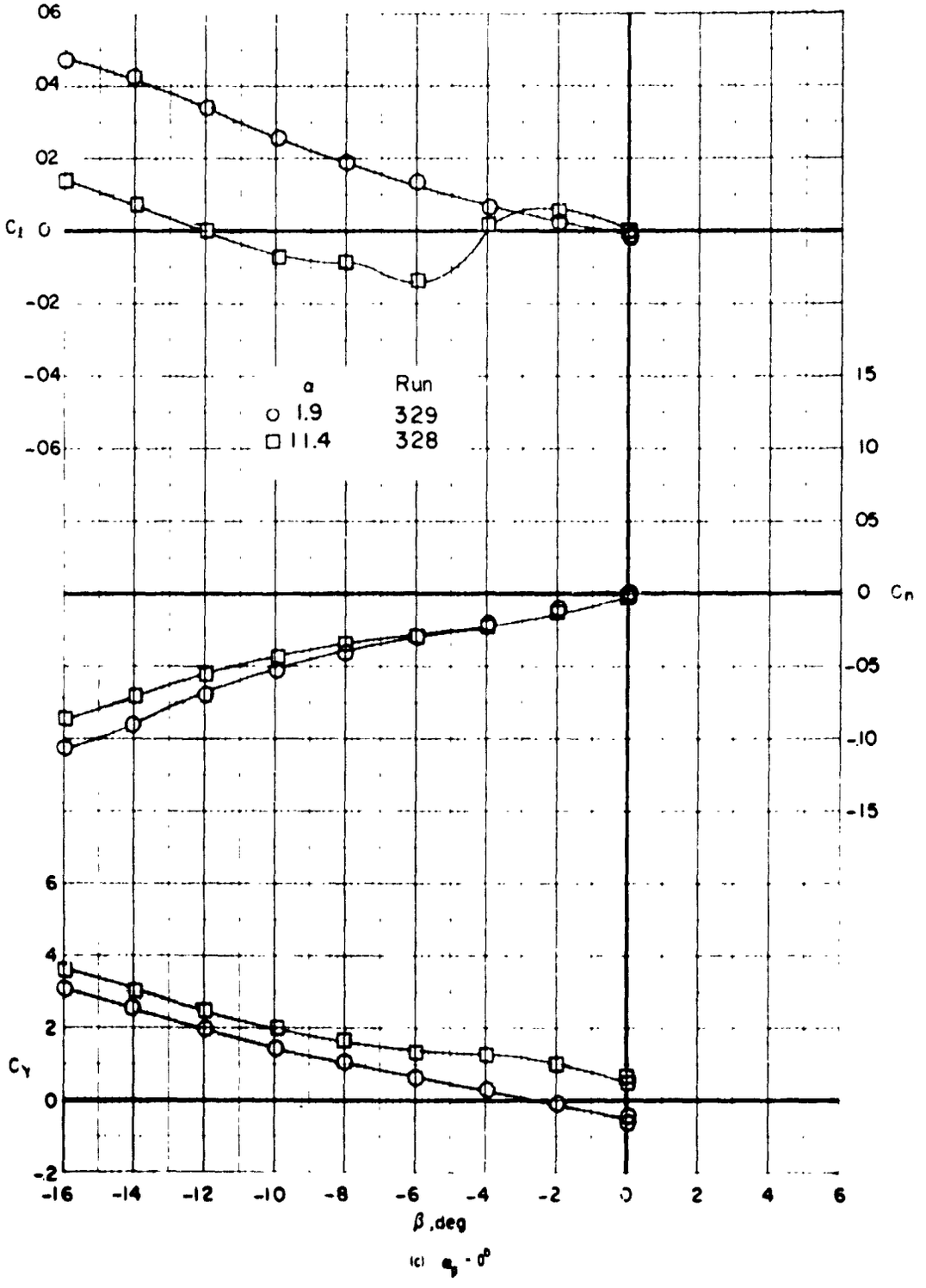

(c) $\alpha_p = 0^\circ$

Figure 17. - Concluded.

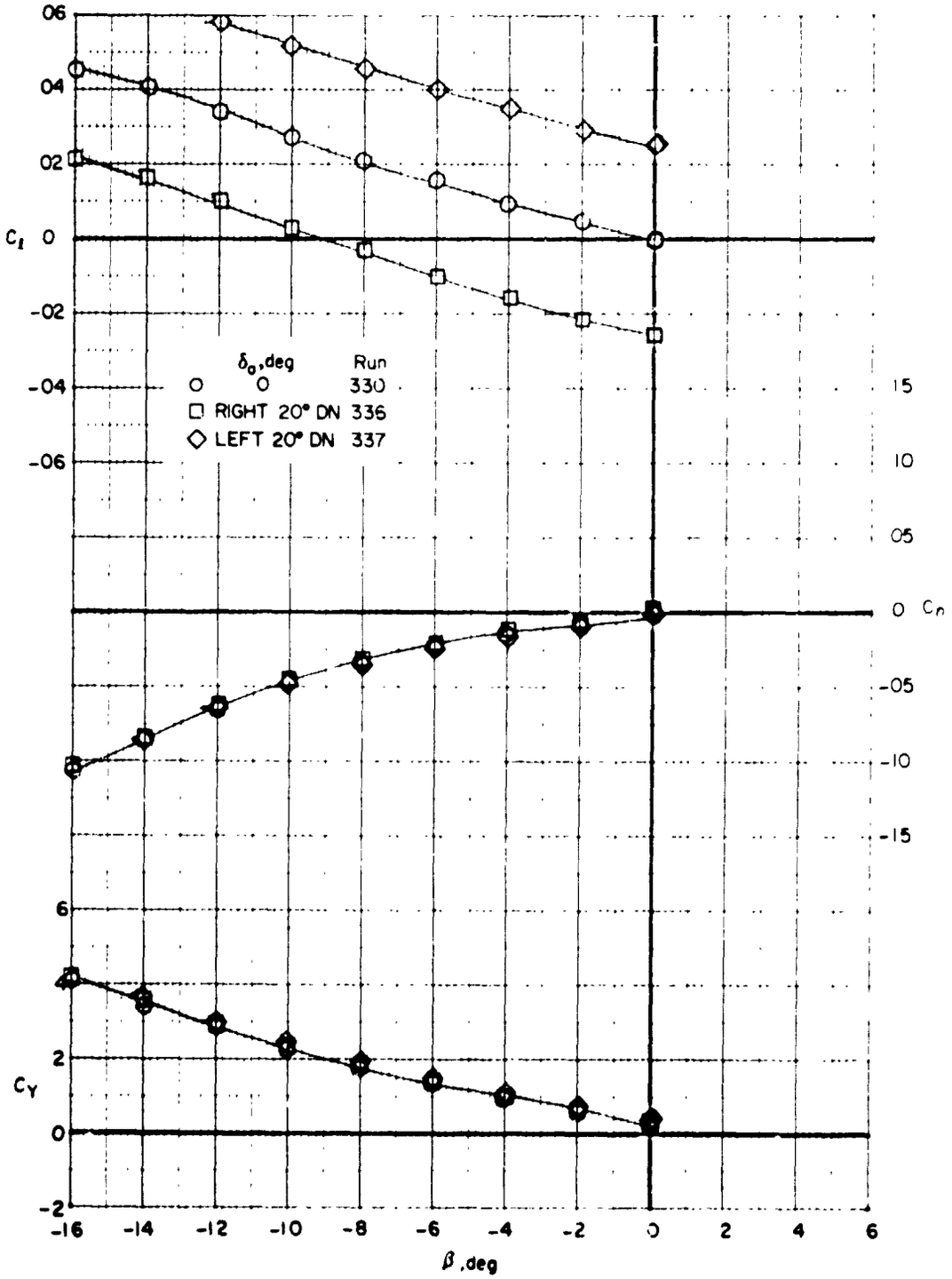

Figure 18. - Effect of aileron deflection on the lateral aerodynamic characteristics of the model, $\alpha = 0^0$, $\alpha_p = 0^0$, $\delta_e = 0^0$.

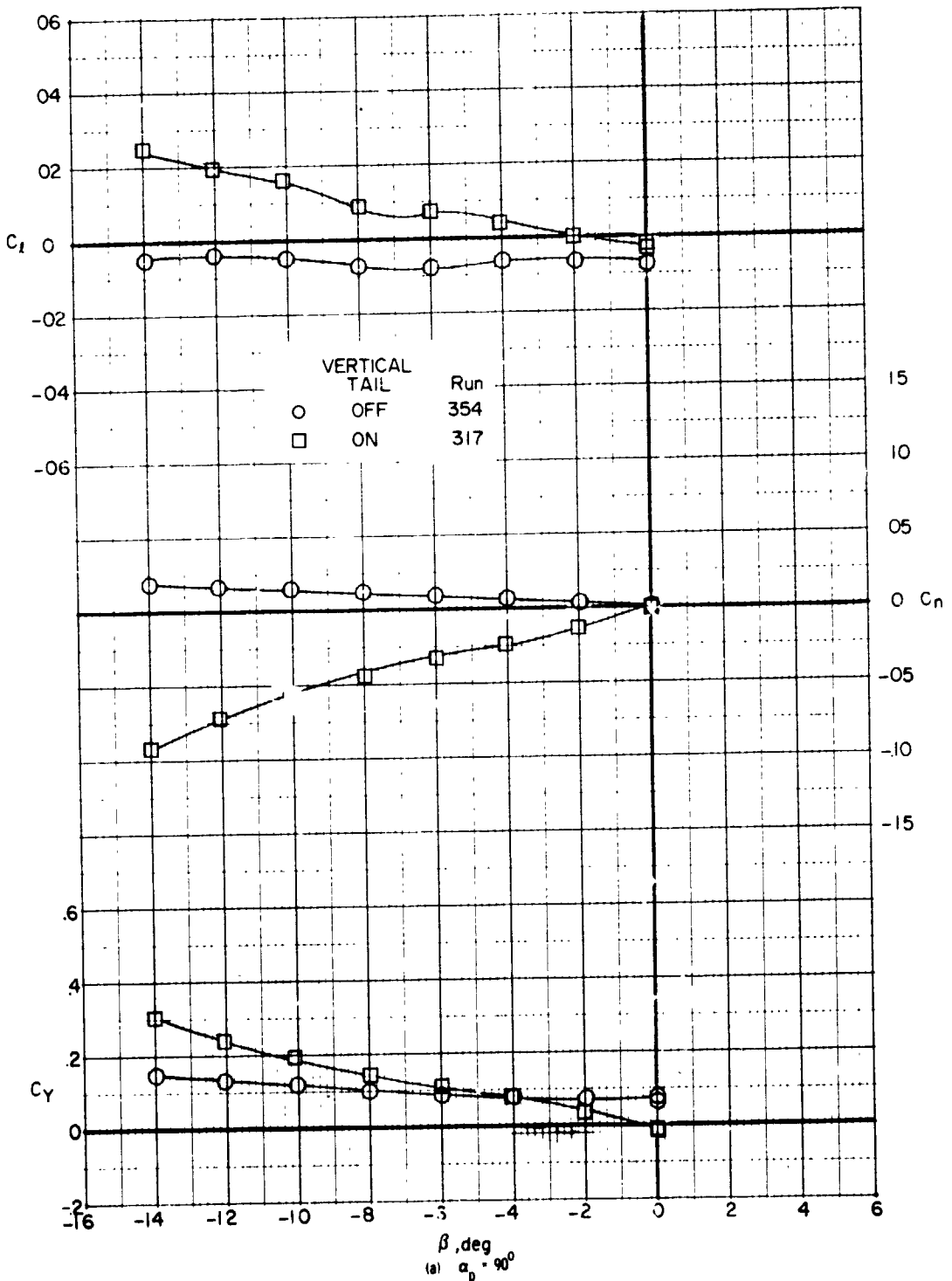

(a) $\alpha_p = 90^0$

Figure 19. - Effect of the vertical tail on the lateral aerodynamic characteristics for several pylon angles, $\delta_f = 50^0$, $\delta_a = 20^0$.

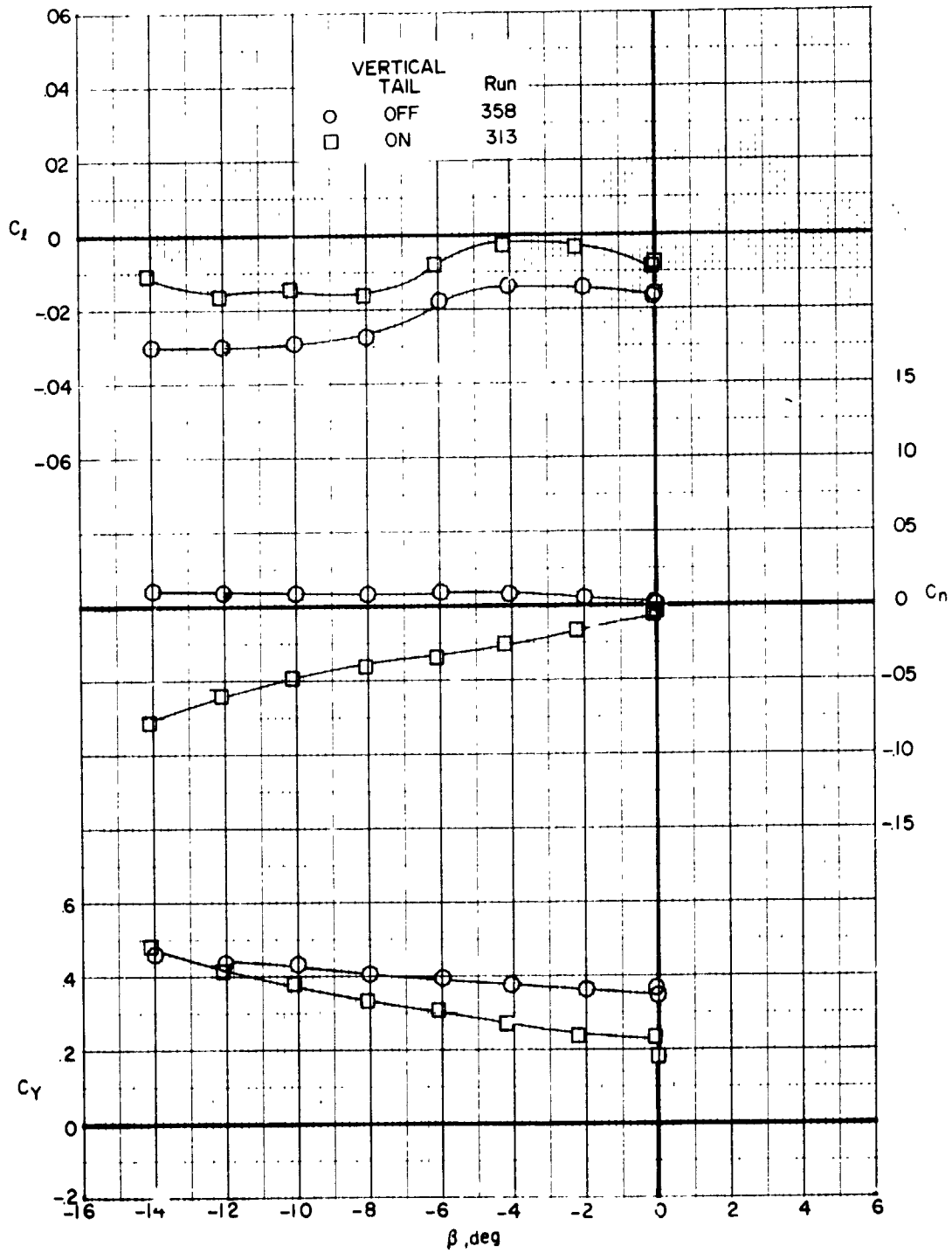

(b) $\alpha_p = 75^0$

Figure 19. - Continued.

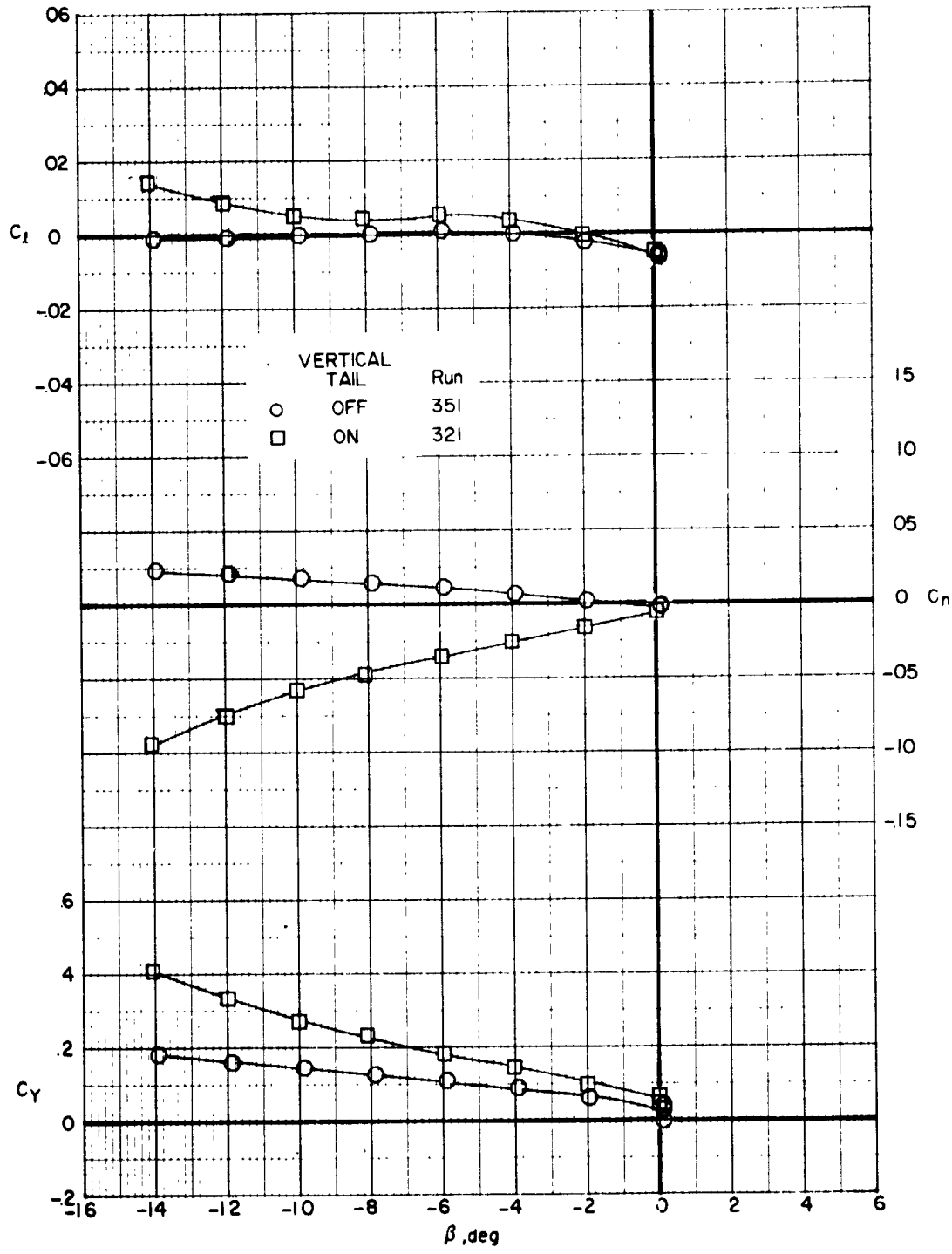

(c) $\alpha_p = 60^0$

Figure 19. - Continued.

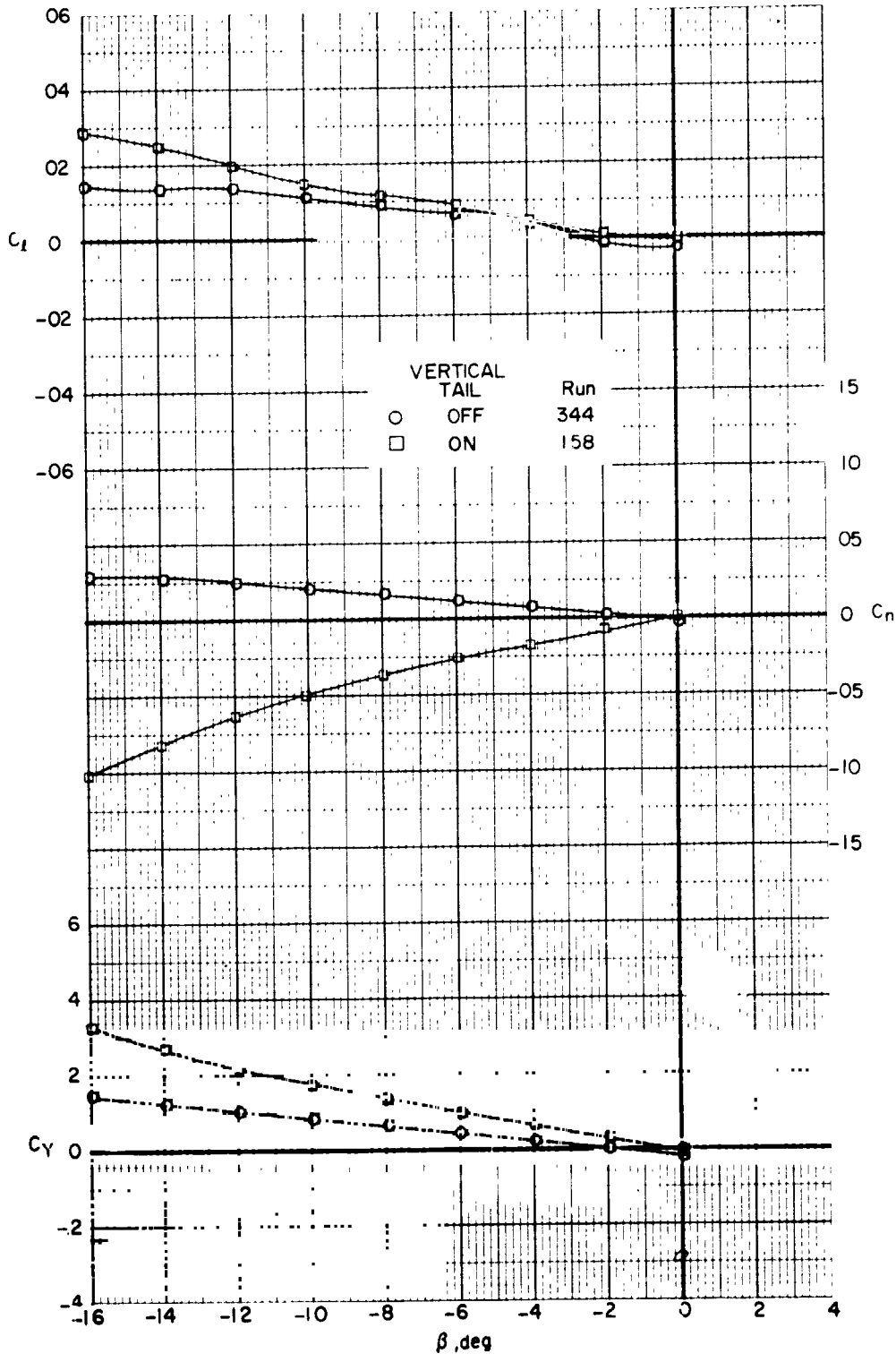

(d) $\alpha_p = 30^0$

Figure 19. Continued

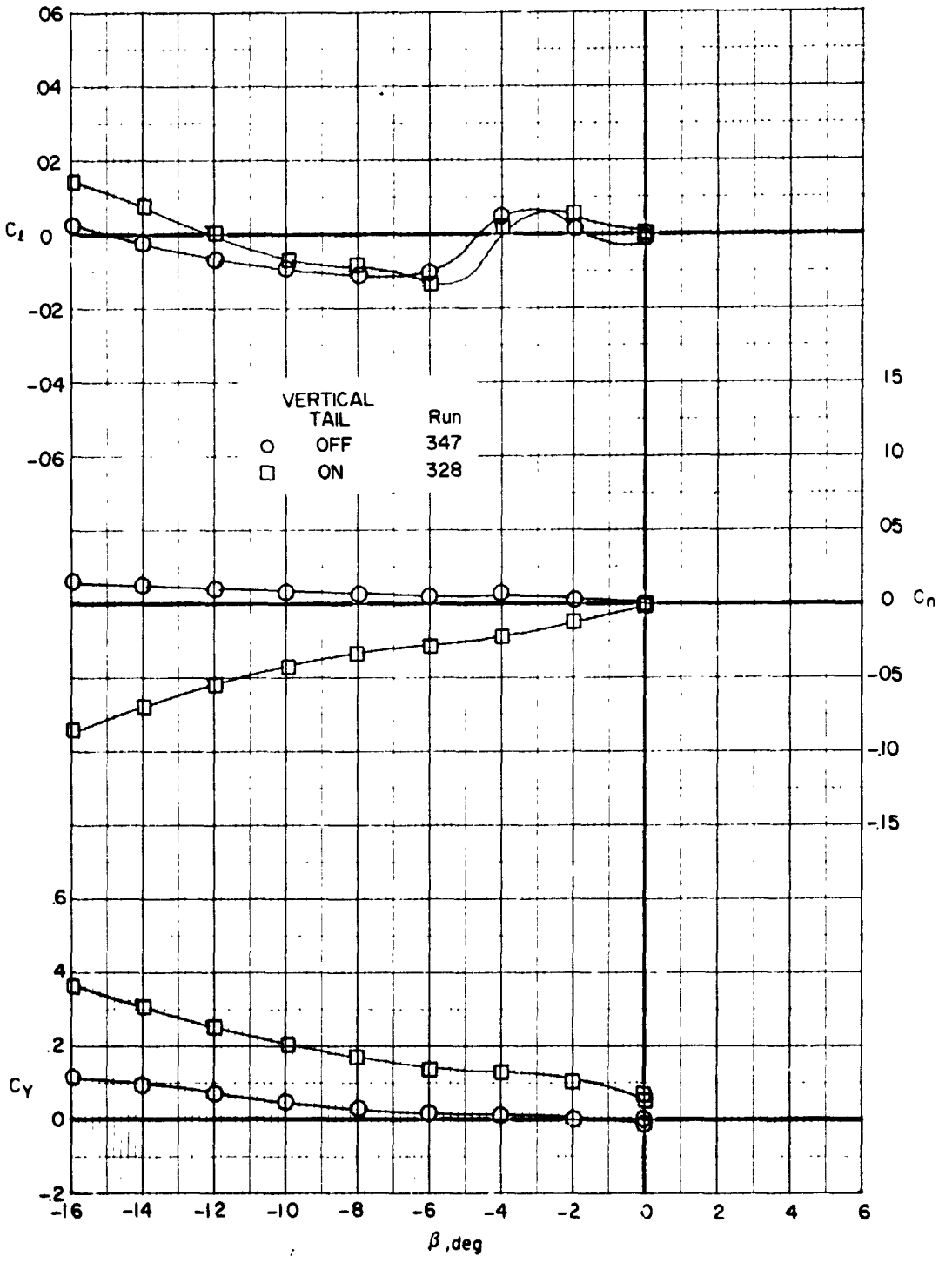

(e) α, σ'

Figure 19. Concluded.

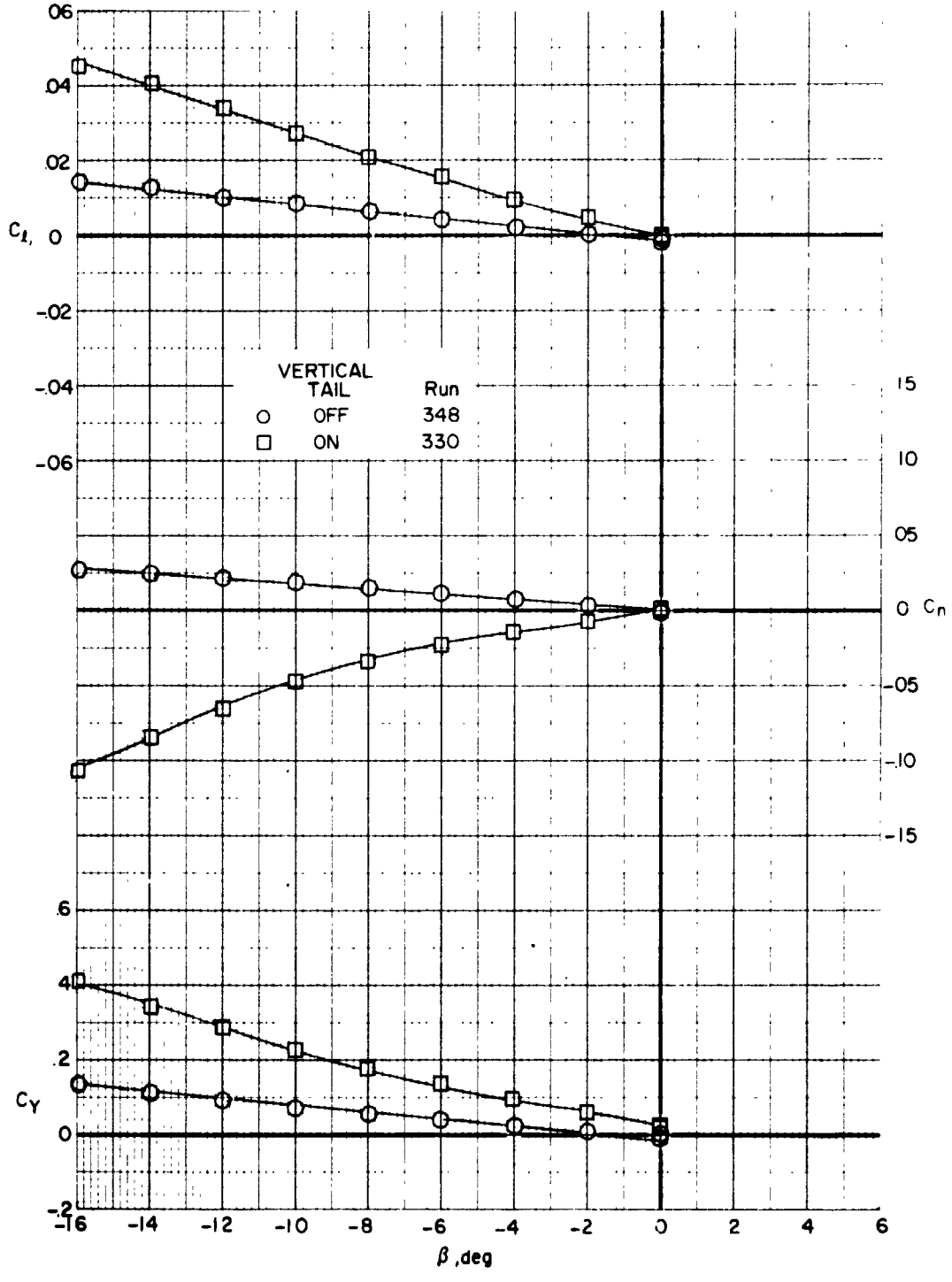

Figure 20. - Effect of the vertical tail on the lateral aerodynamic characteristics for $\alpha_p = 0^0$, $\delta_f = 0^0$, $\delta_a = 0^0$.

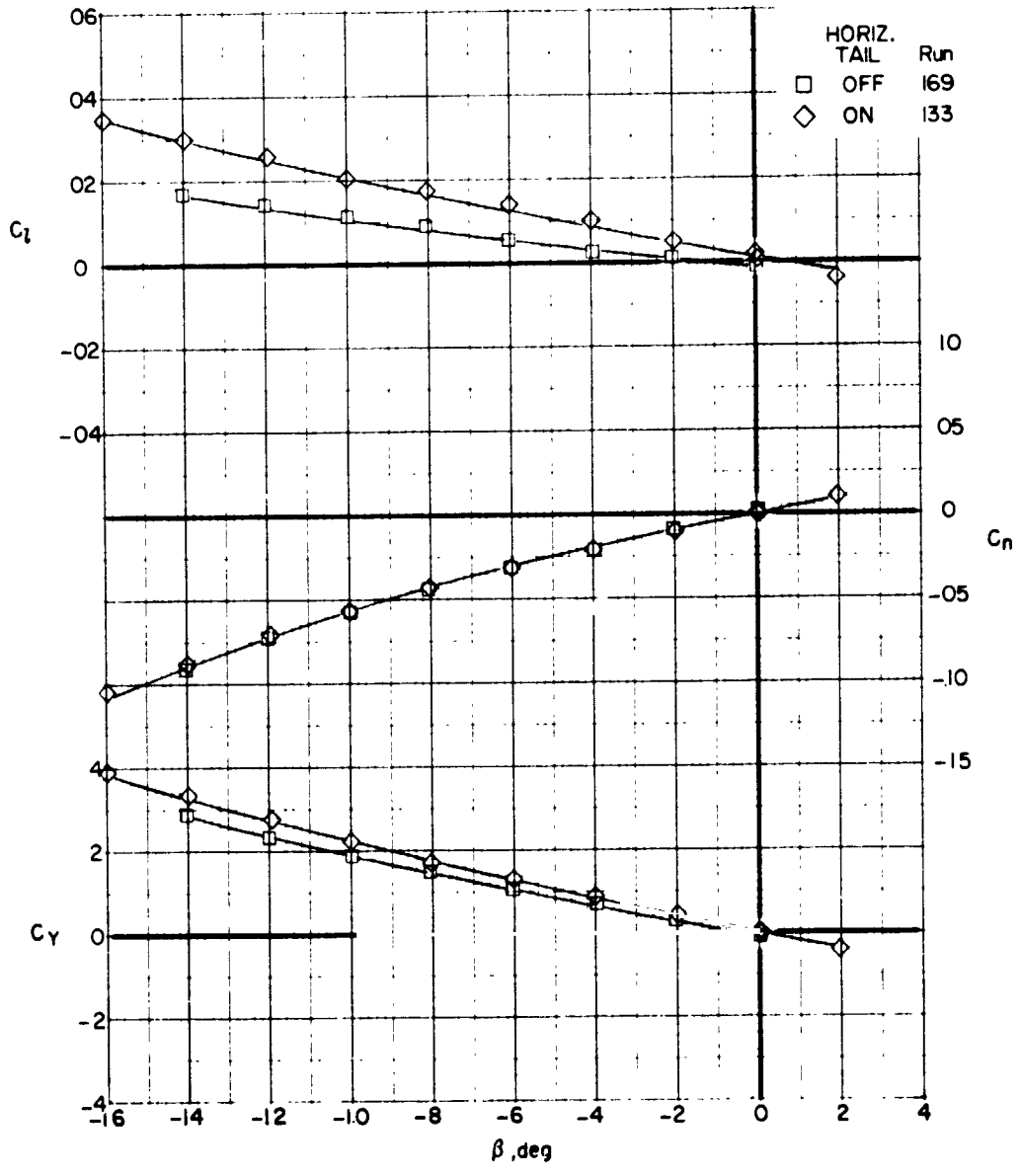

(a) $\alpha_p = 90^0$

Figure 21. - Effect of horizontal tail on lateral aerodynamic characteristics of the model with rotors off for pylon angles, 90^0, 60^0, 30^0, and 0^0.

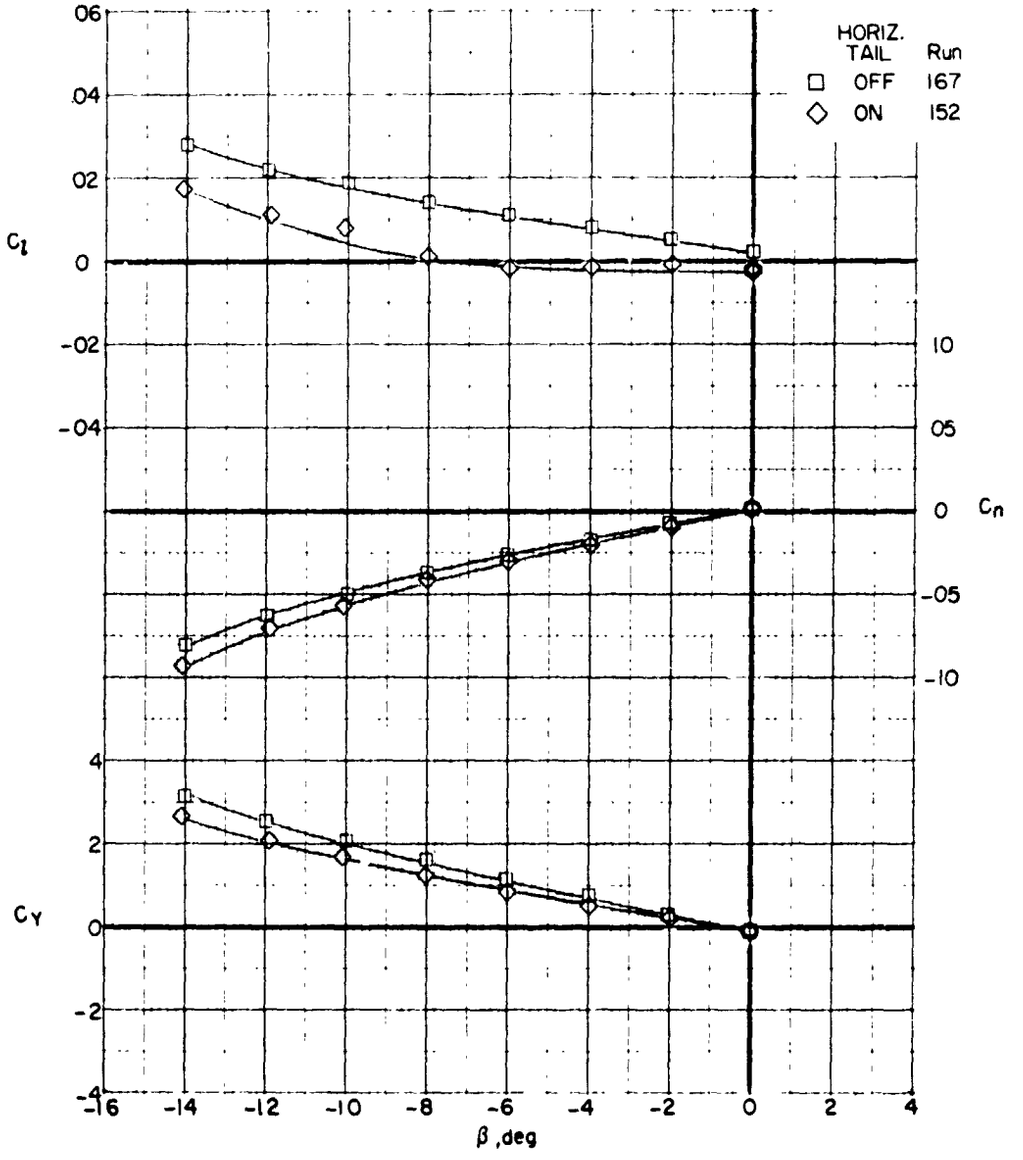

(b) $\alpha_p = 60^0$

Figure 21. - Continued.

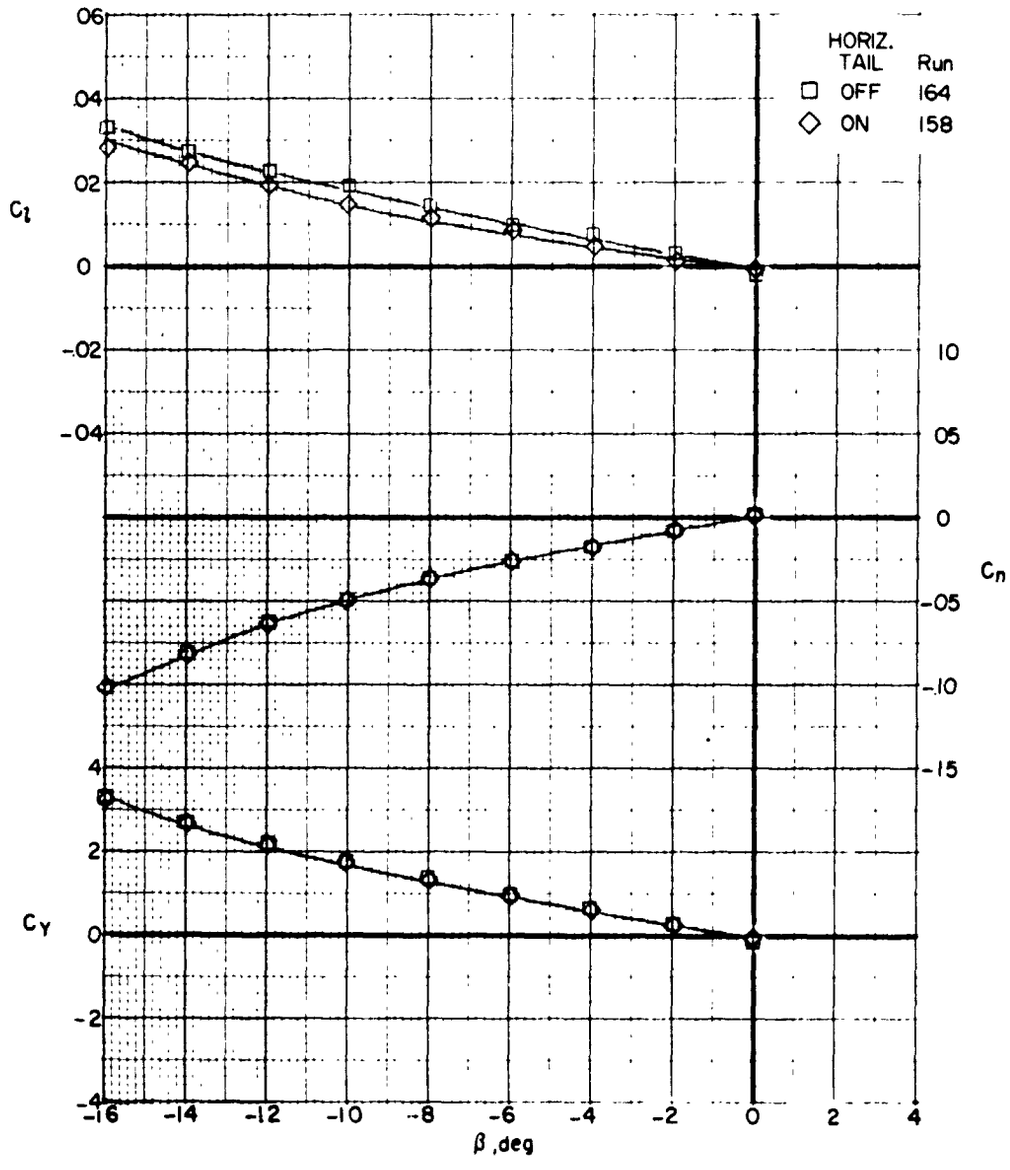

(c) $\alpha_p = 30^0$

Figure 21. - Continued.

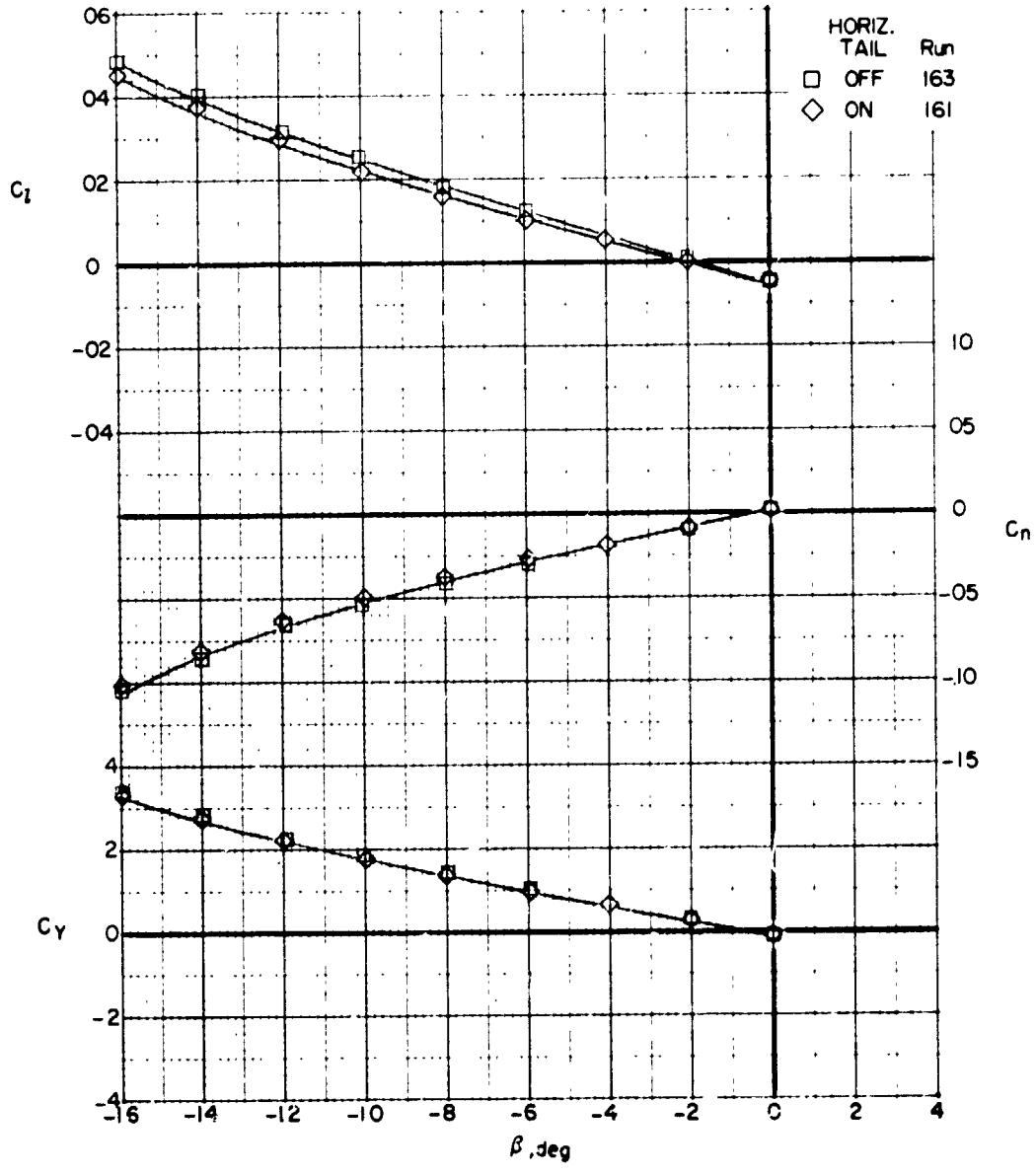

(d) $\alpha_p = 0^\circ$

Figure 21. - Concluded.

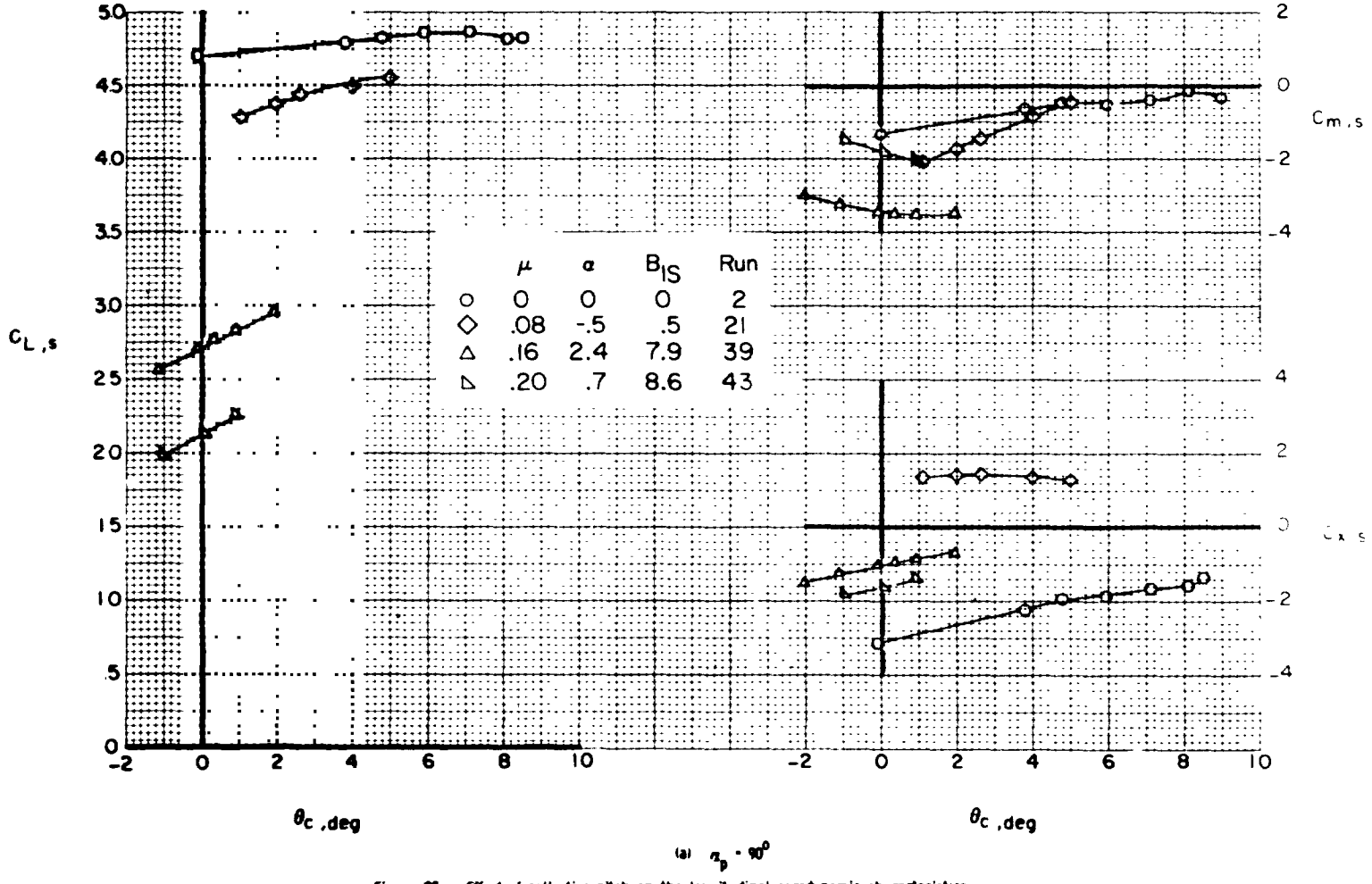

(a) $\alpha_p = 90^0$

Figure 22. - Effect of collective pitch on the longitudinal aerodynamic characteristics for several forward speeds, $\delta_1 = 50^0$, $\delta_3 = 20^0$.

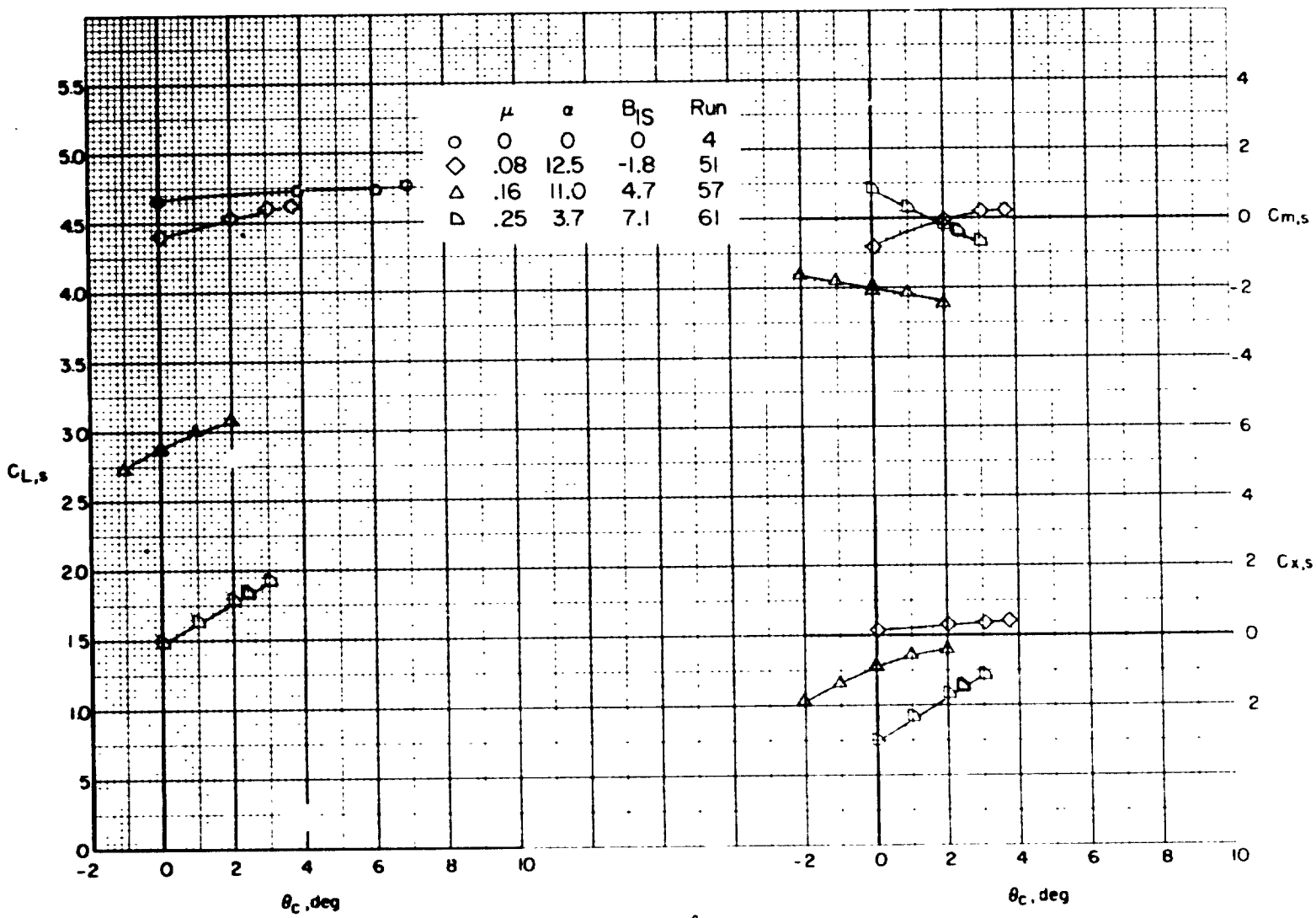

(b) $\alpha_p = 75^0$

Figure 22. - Continued

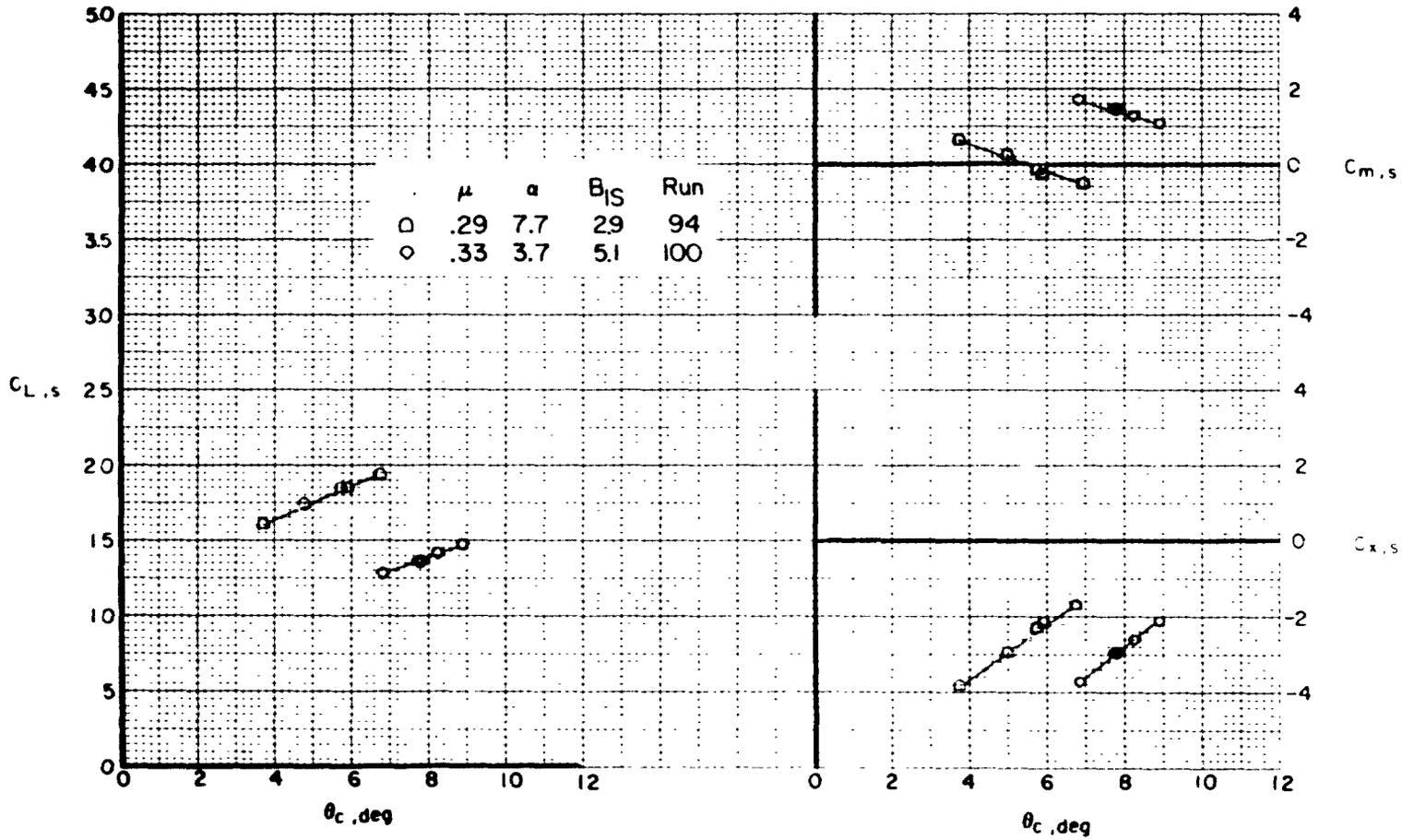

(c) $\alpha_p = 60^\circ$

Figure 22. - Continued.

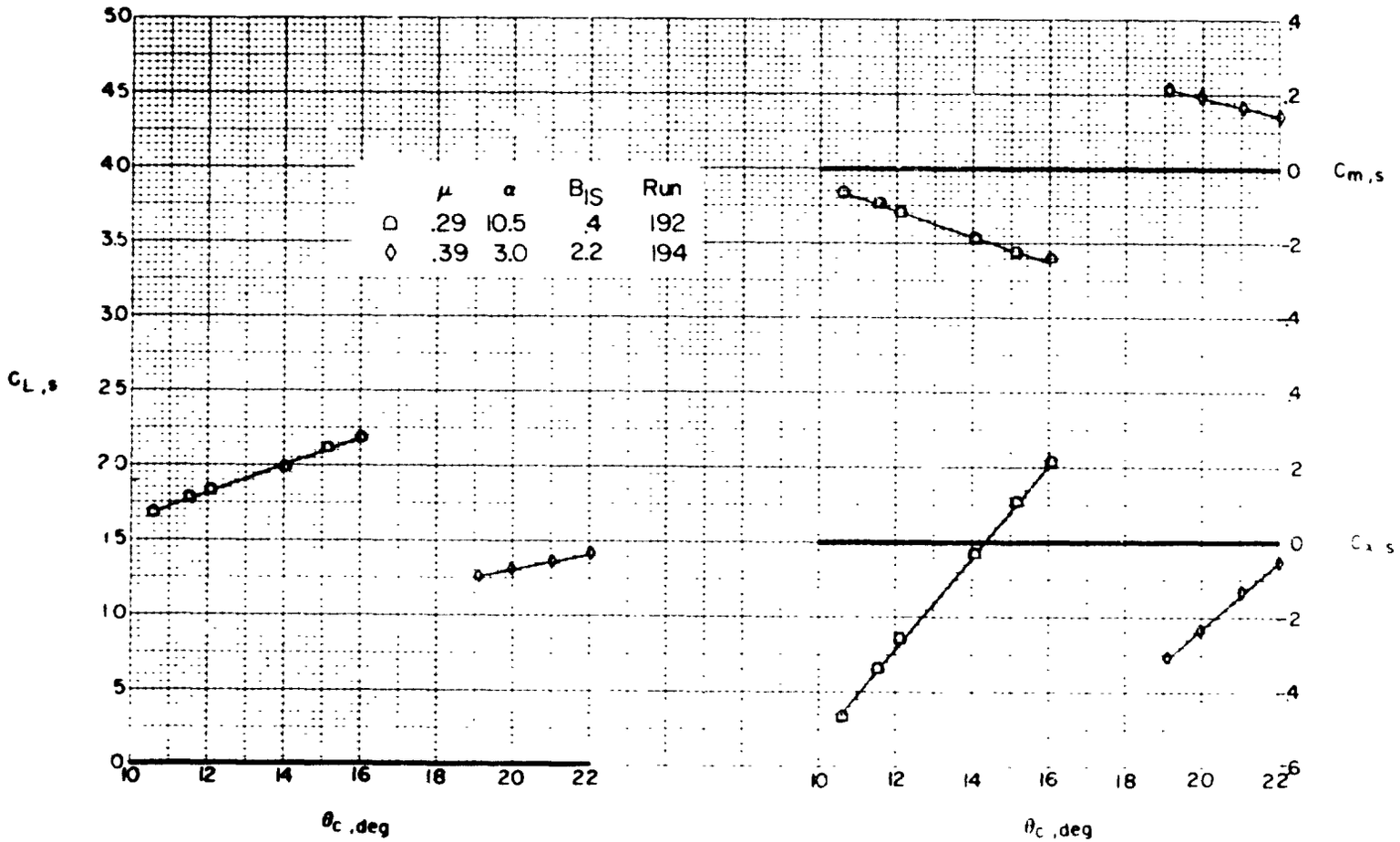

(d) $\alpha_p = 30^0$

Figure 22. - Continued.

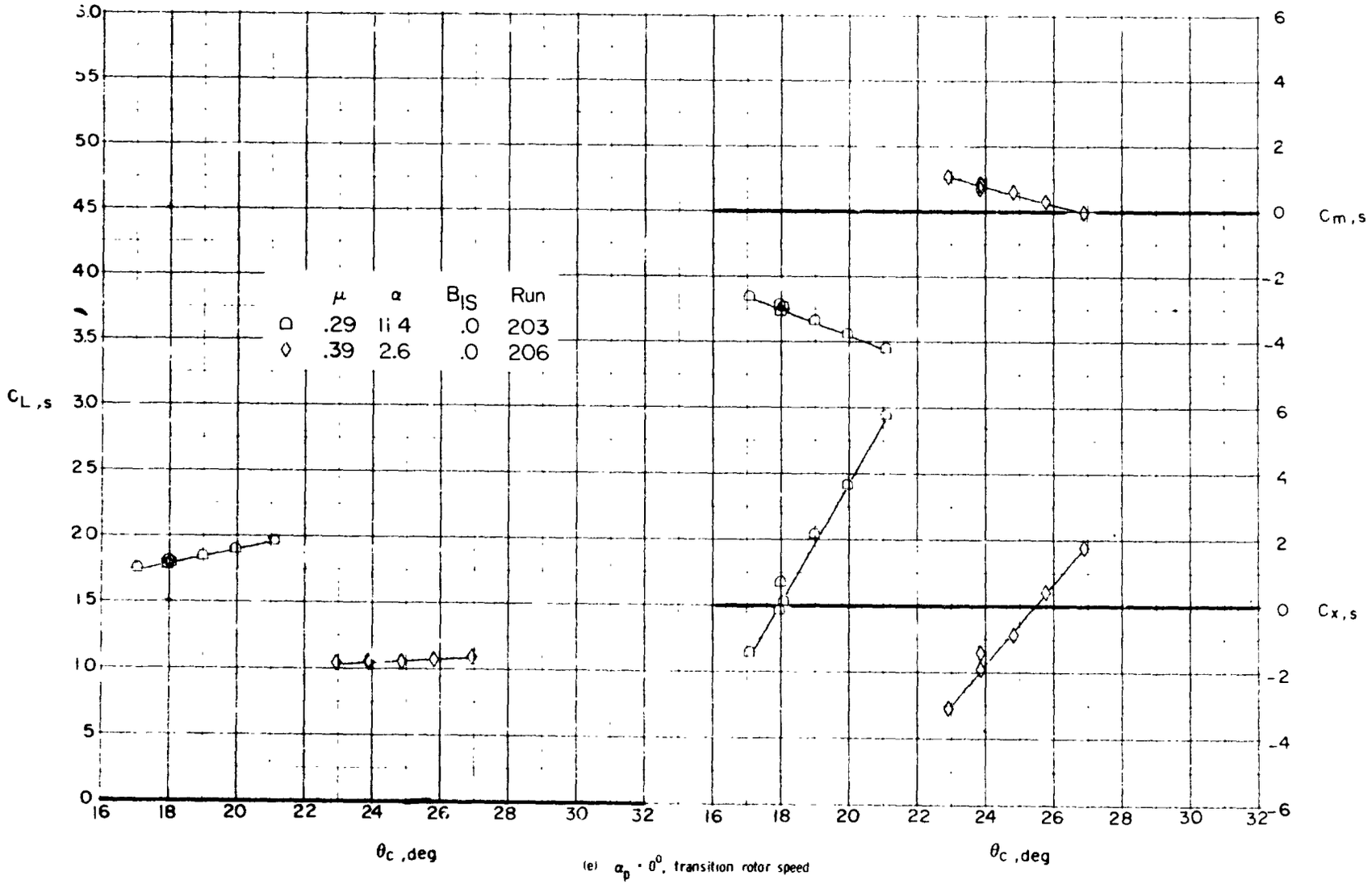

(e) $\alpha_p = 0^0$, transition rotor speed

Figure 22. - Continued.

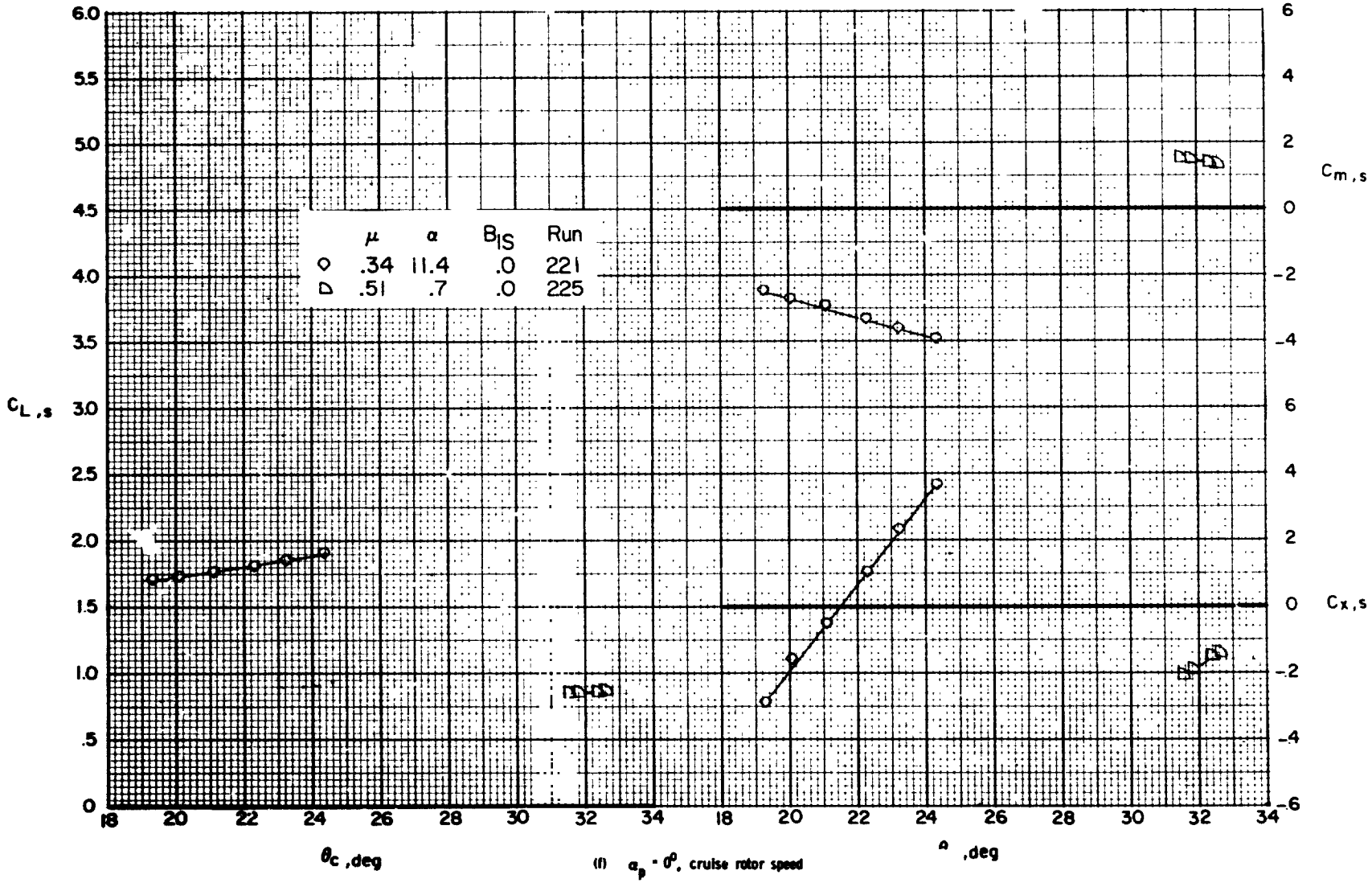

(f) $\alpha_p = 0^0$, cruise rotor speed

Figure 22. - Concluded.

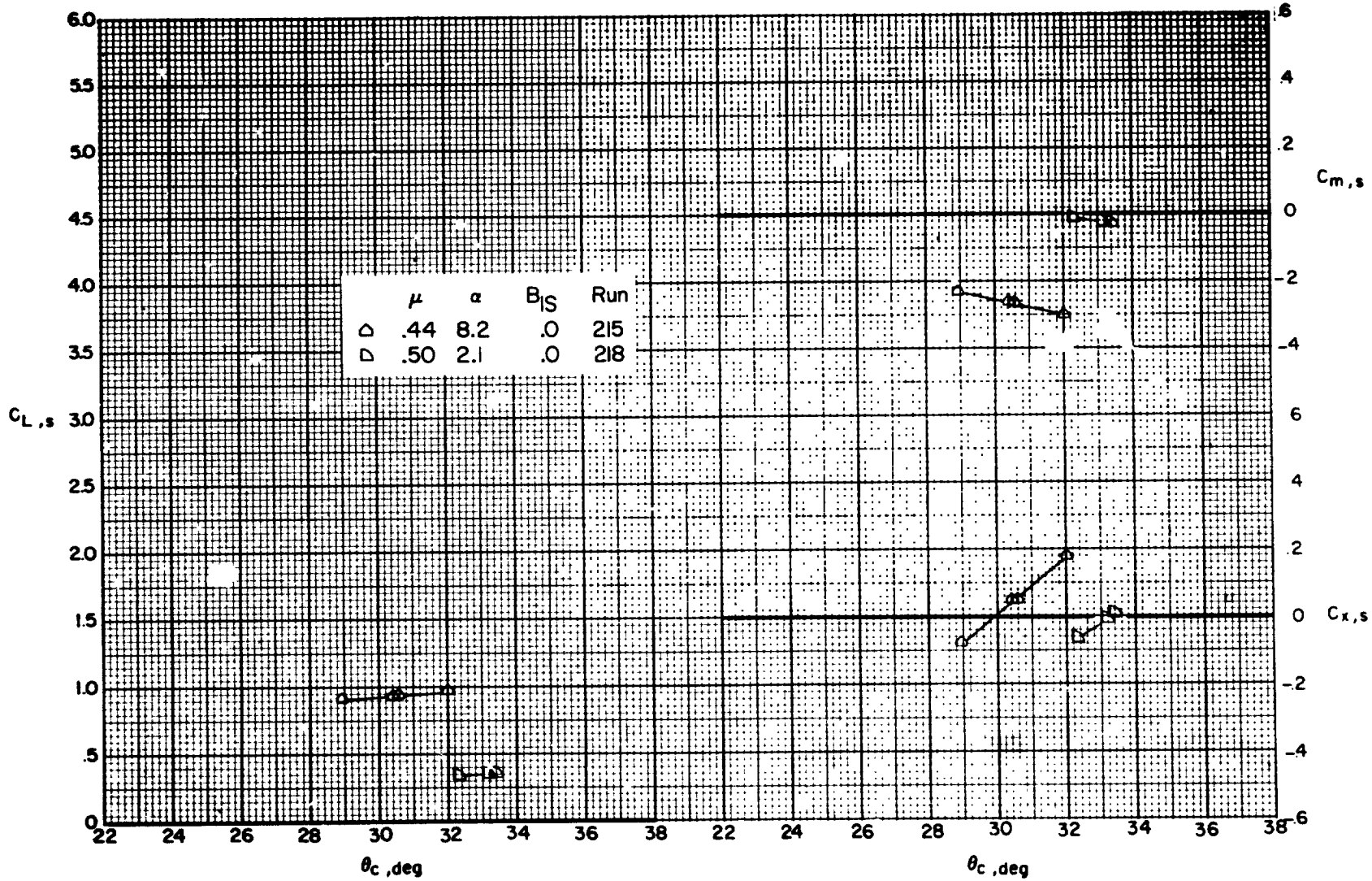

Figure 23. - Effect of collective pitch on the longitudinal aerodynamic characteristics for several forward speeds, $\alpha_p = 0^0$, $B_1 = 0^0$, $B_2 = 0^0$.

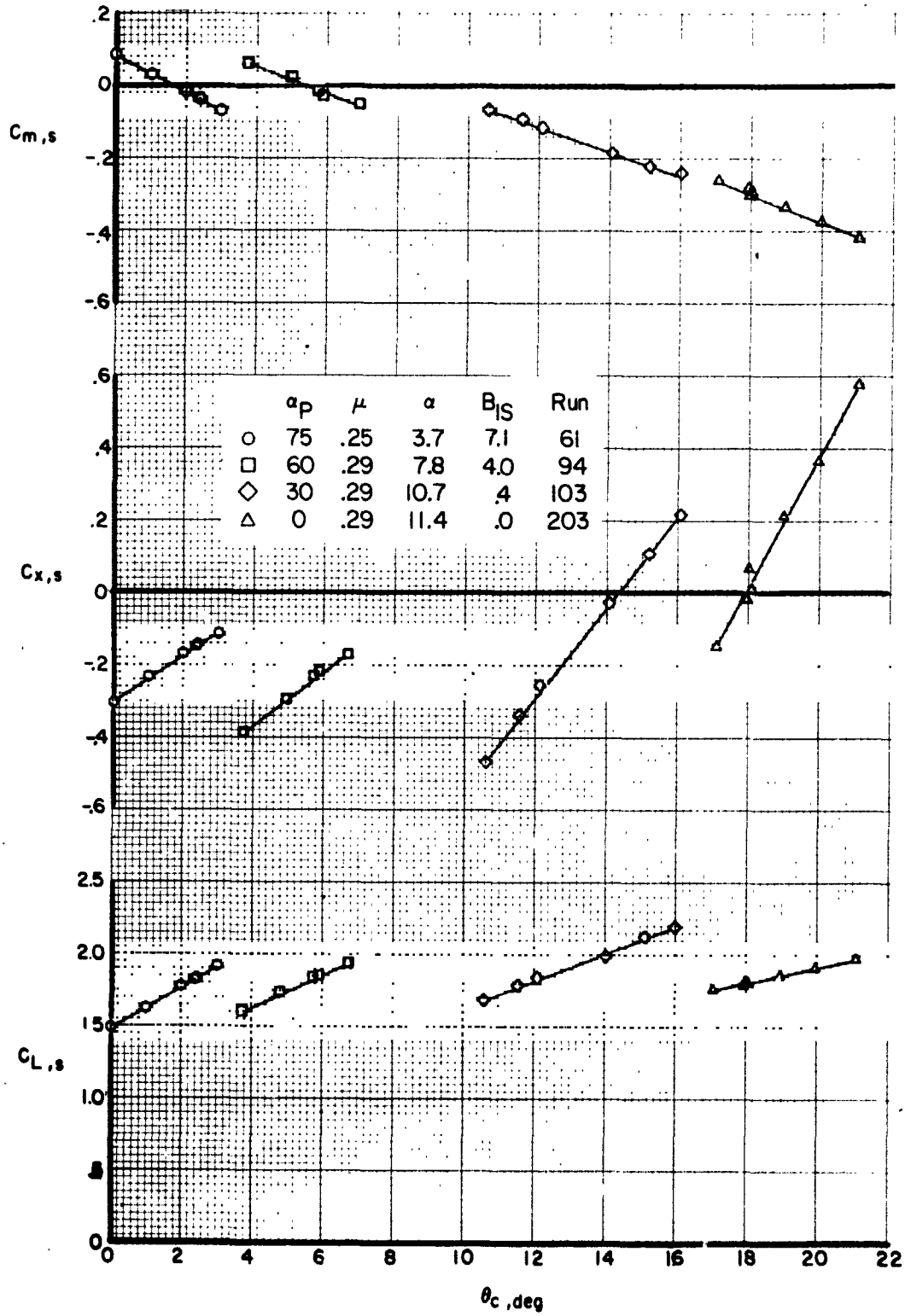

Figure 24. - Effect of collective pitch on the longitudinal aerodynamic characteristics at a full-scale flight speed of 120 knots for several pylon angles.

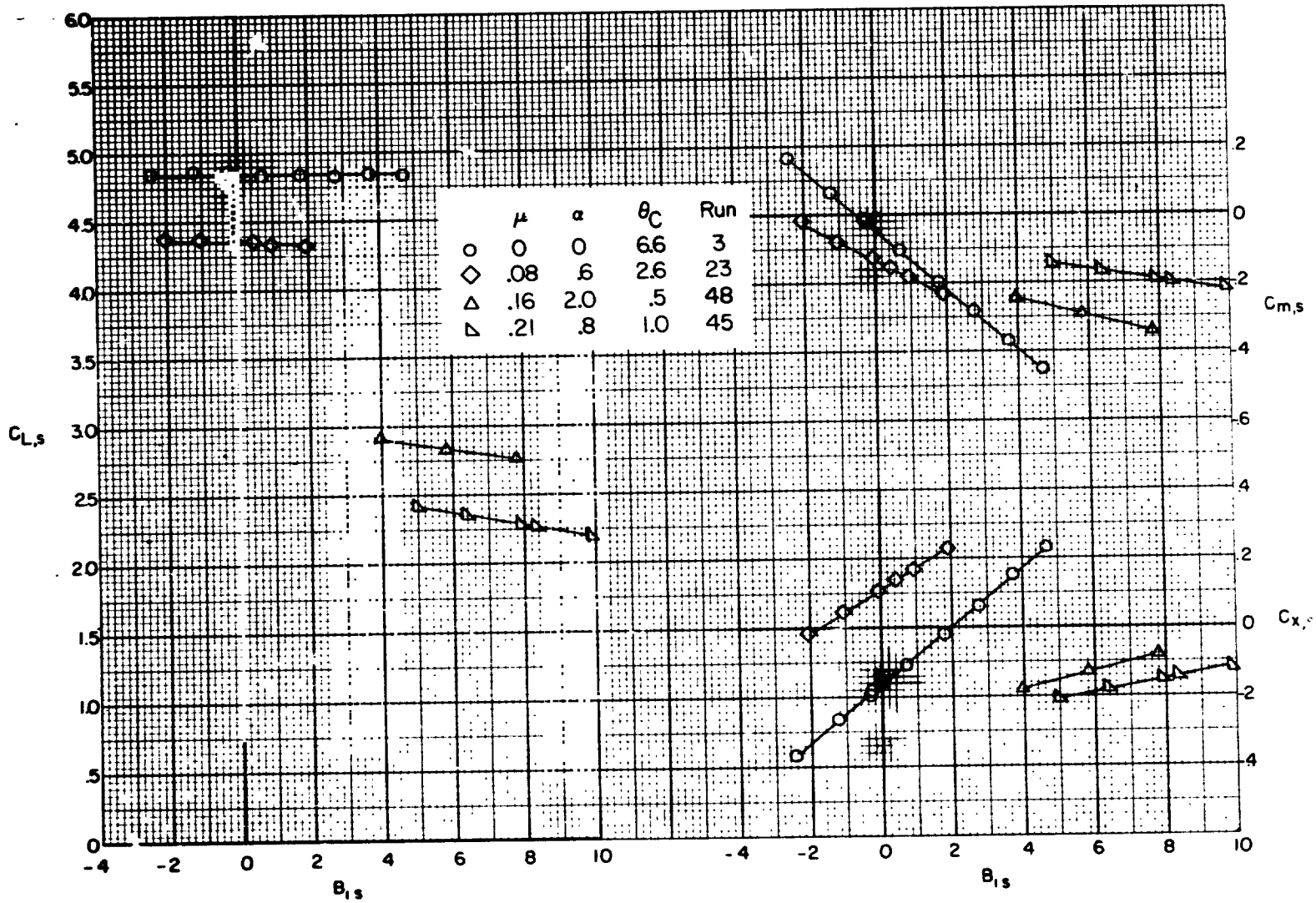

(a) $\alpha_p = 90^0$

Figure 25. - Effect of cyclic pitch on the longitudinal aerodynamic characteristics at several forward speeds.

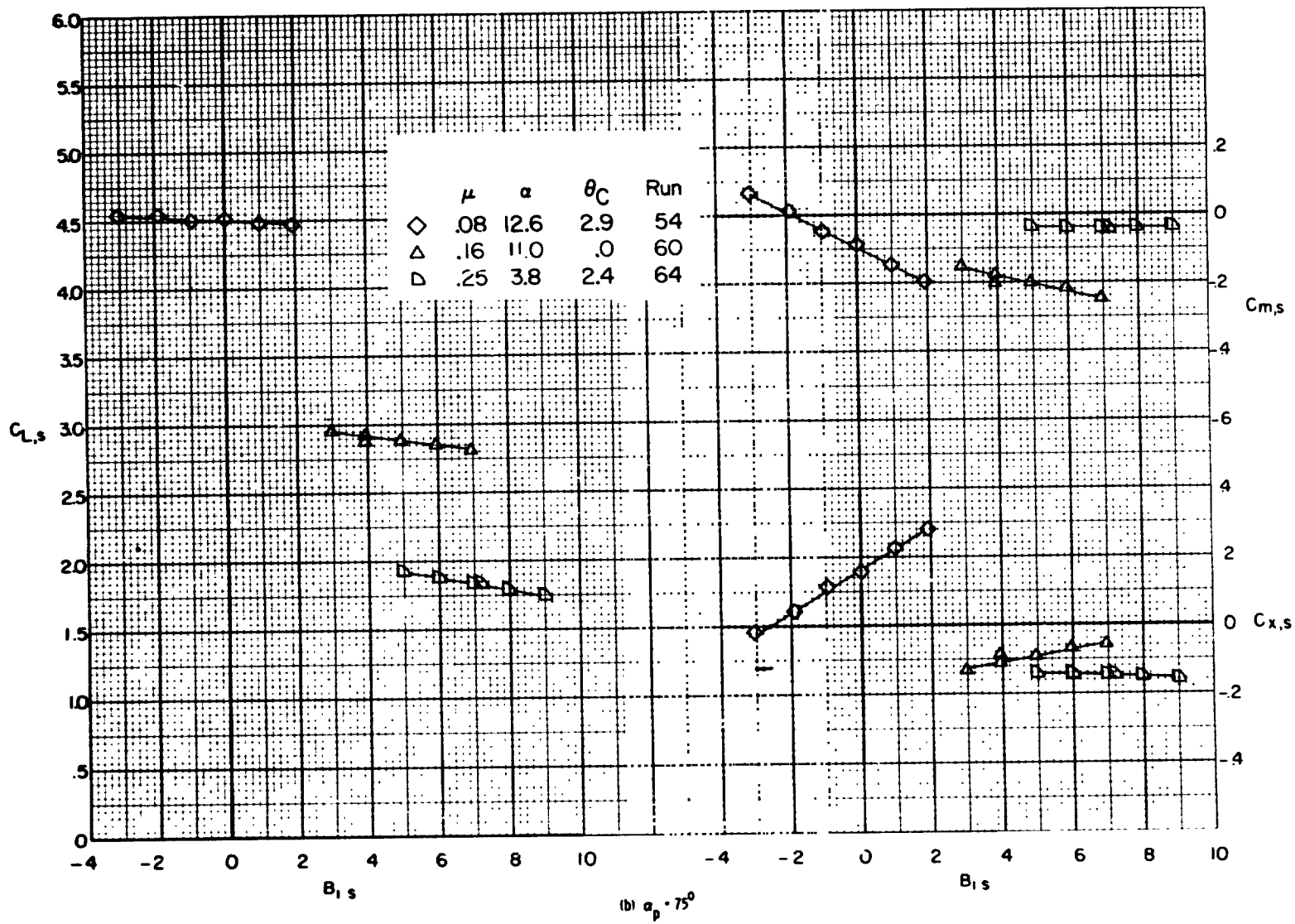

(b) $\alpha_p = 75^0$

Figure 25. - Continued.

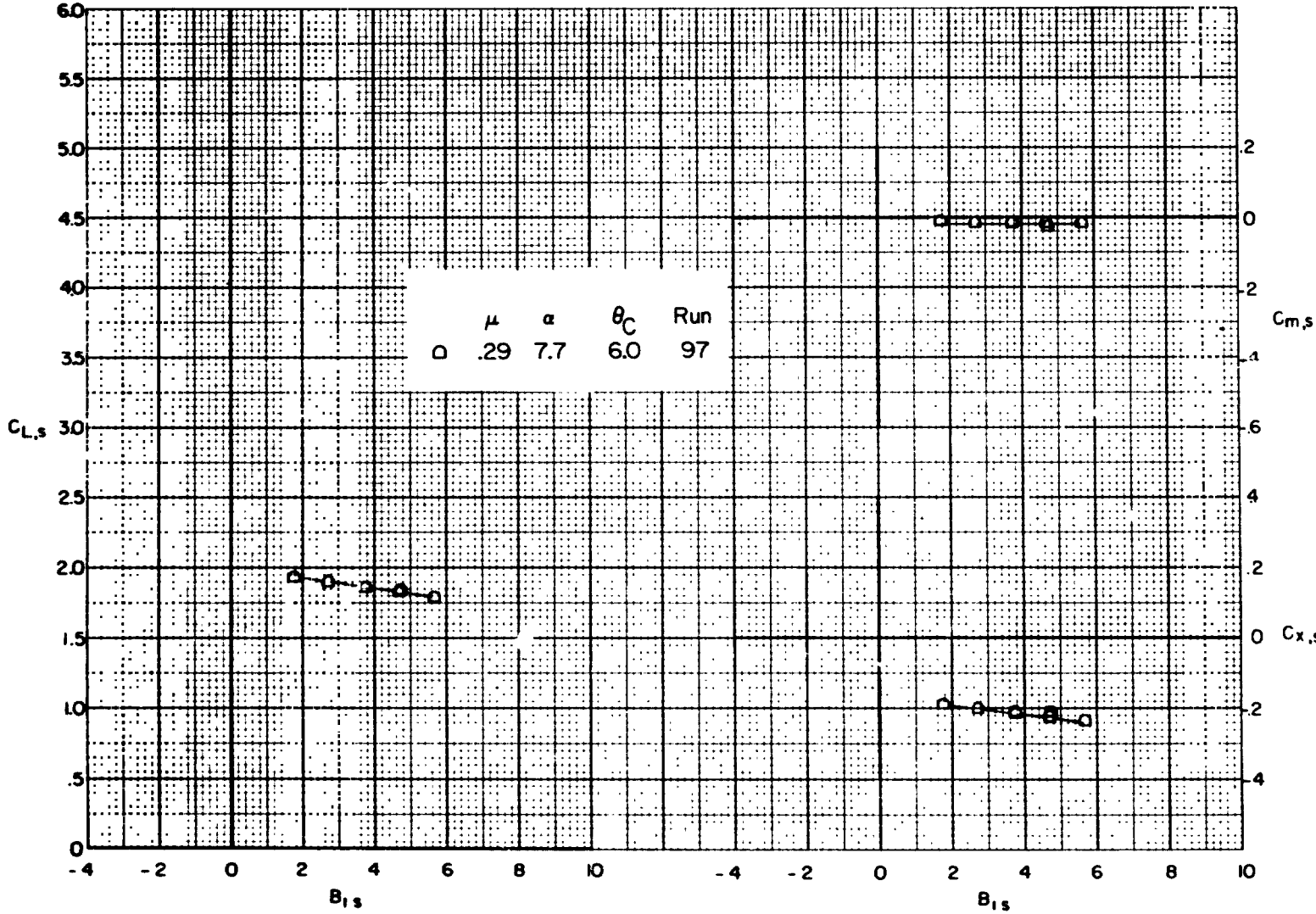

(c) $\alpha_p = 60^\circ$

Figure 25. - Continued.

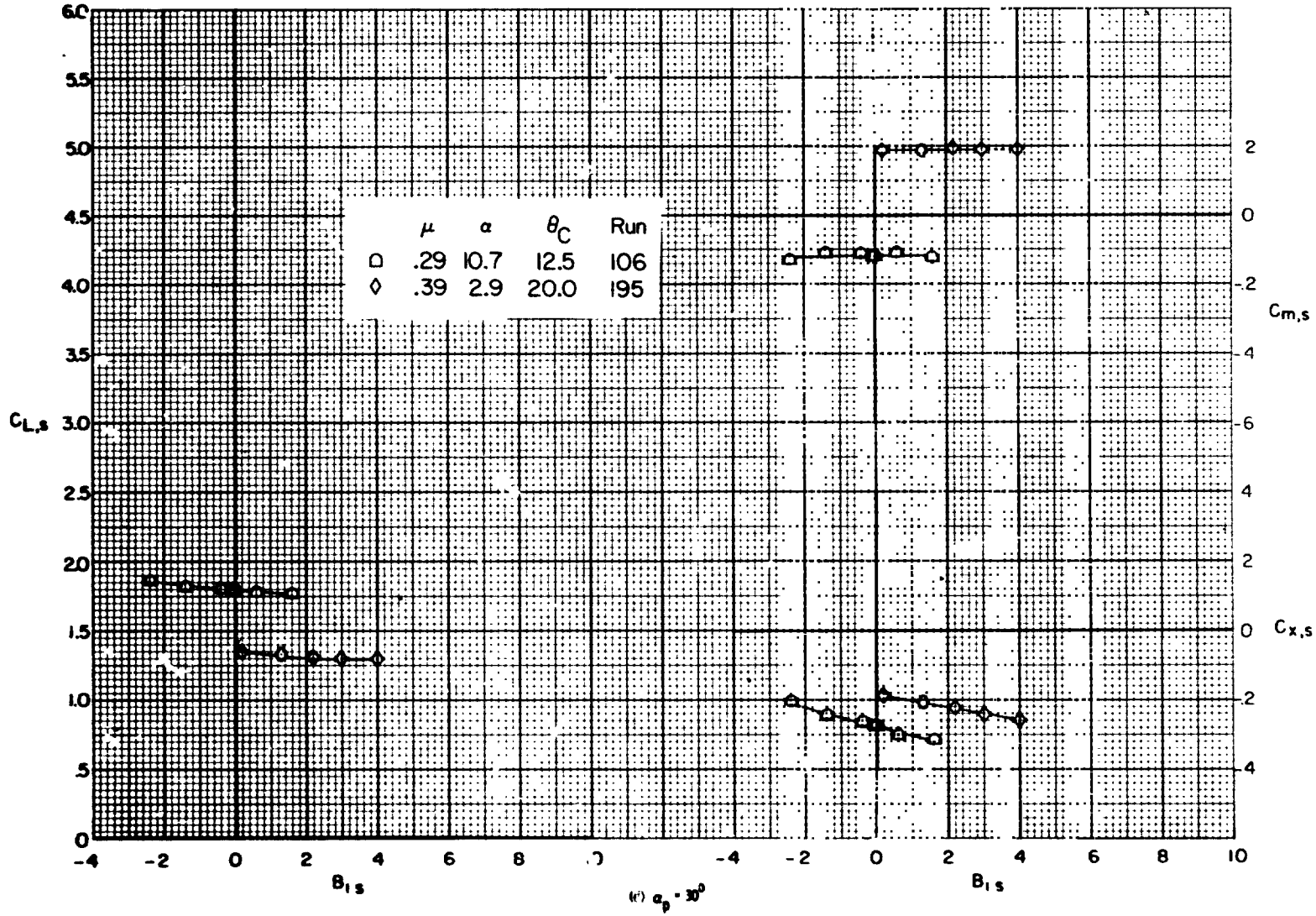

Figure 25. - Concluded.

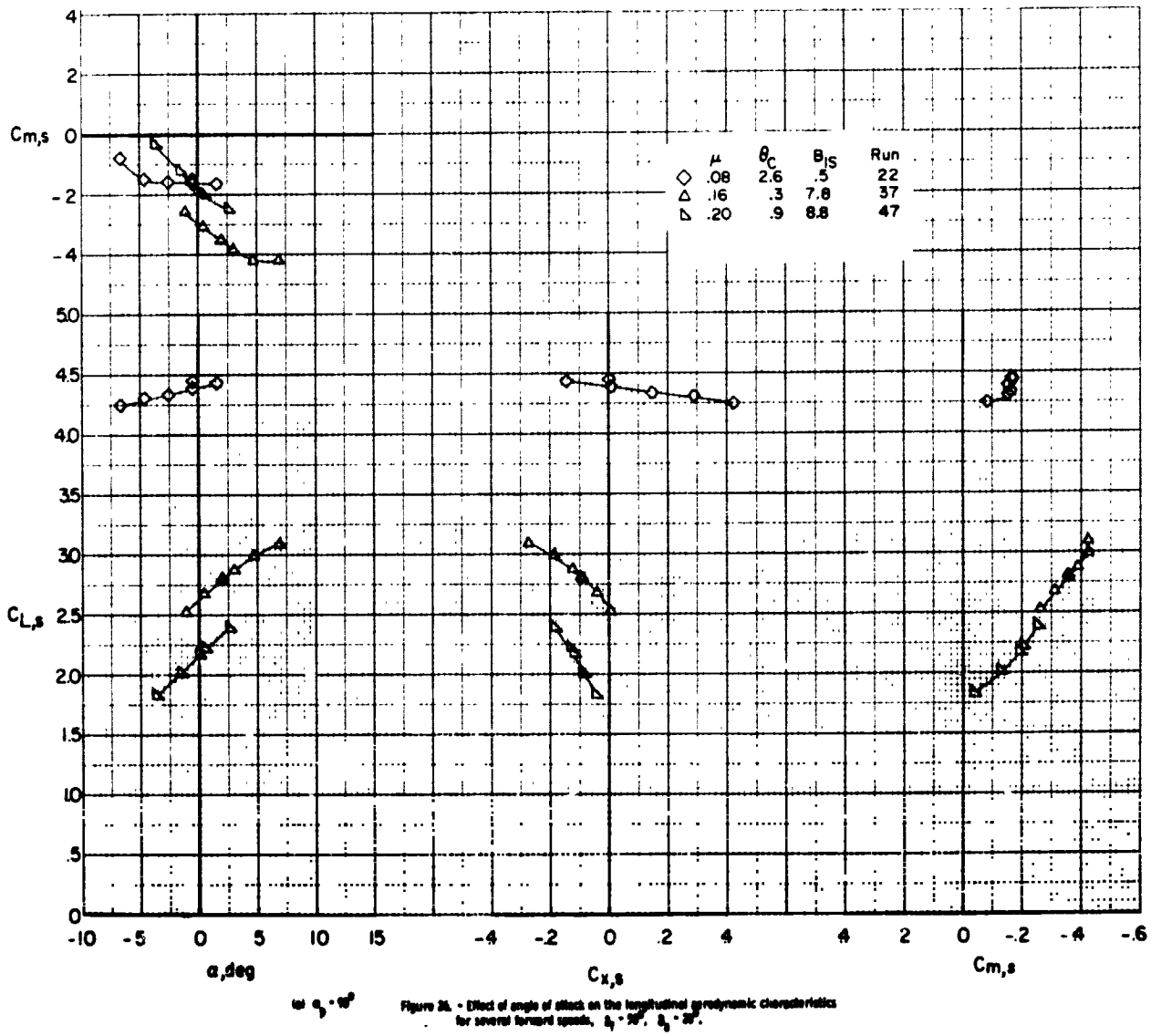

for $\delta_f = 0°$

Figure 26. - Effect of angle of attack on the longitudinal aerodynamic characteristics for several forward speeds, $i_t = 0°$, $\delta_e = 0°$.

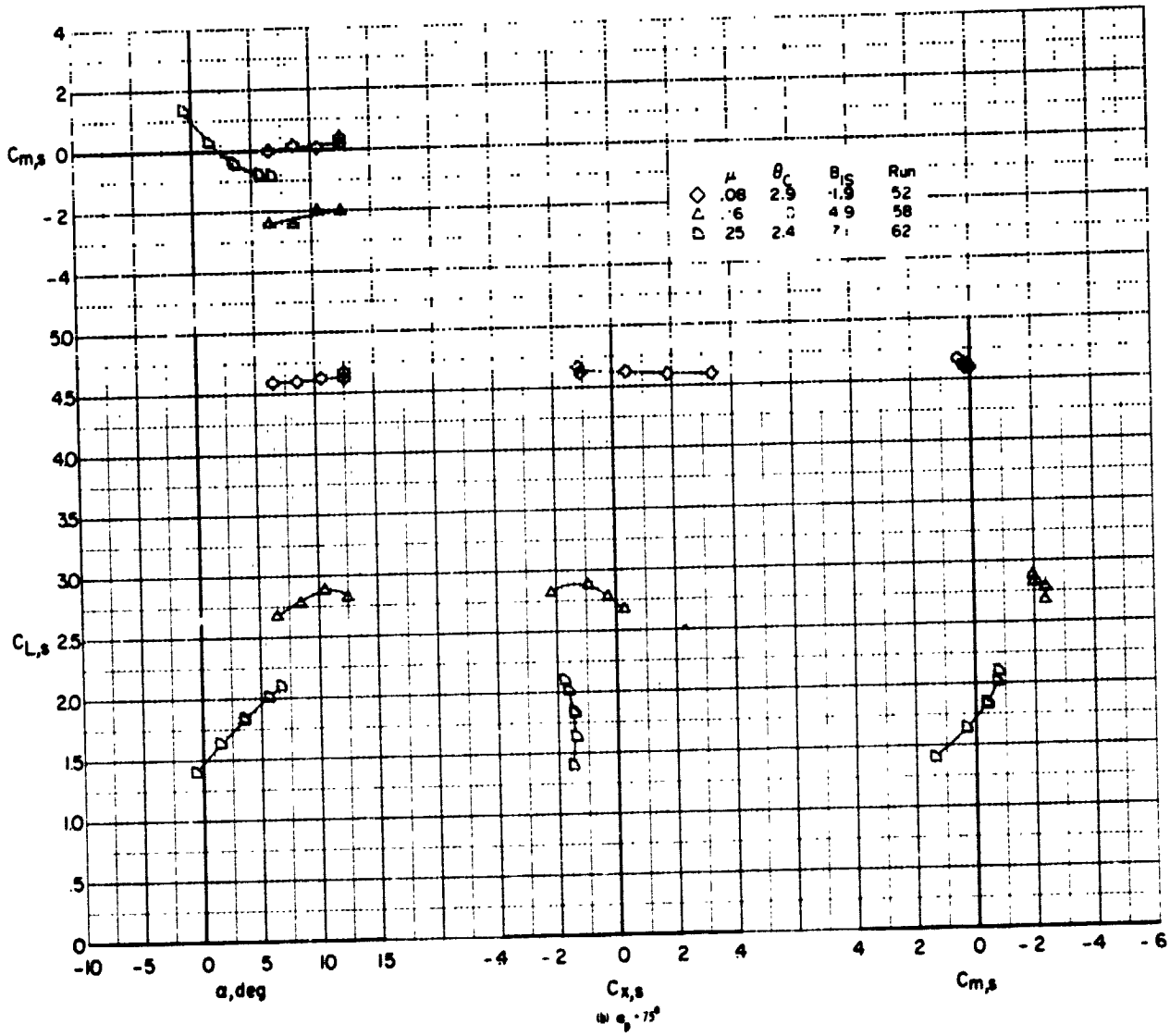

(b) $\alpha_p = 75^\circ$

Figure 26. - Continued.

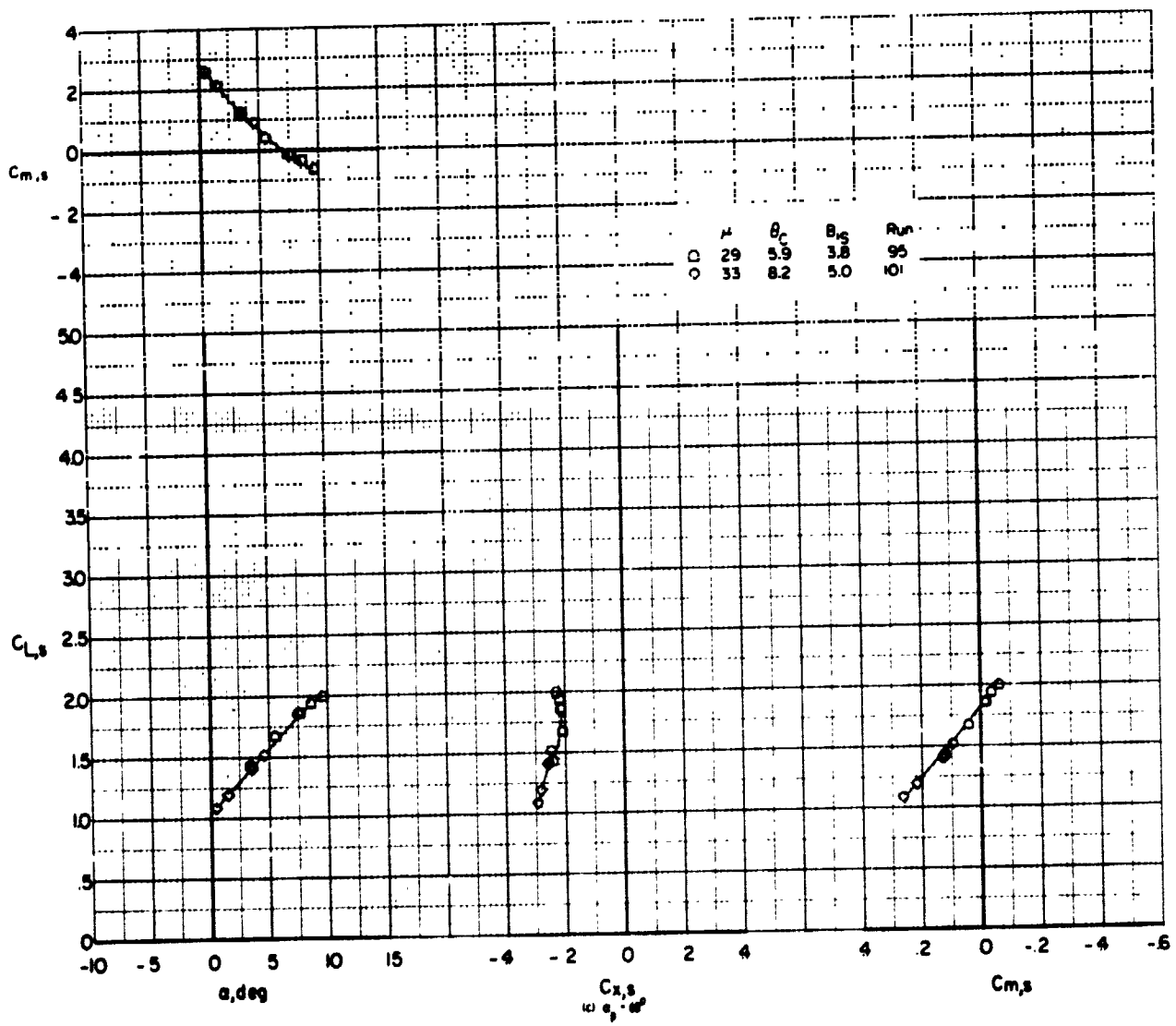

(c) $\alpha_p = 68^\circ$

Figure 26. - Continued.

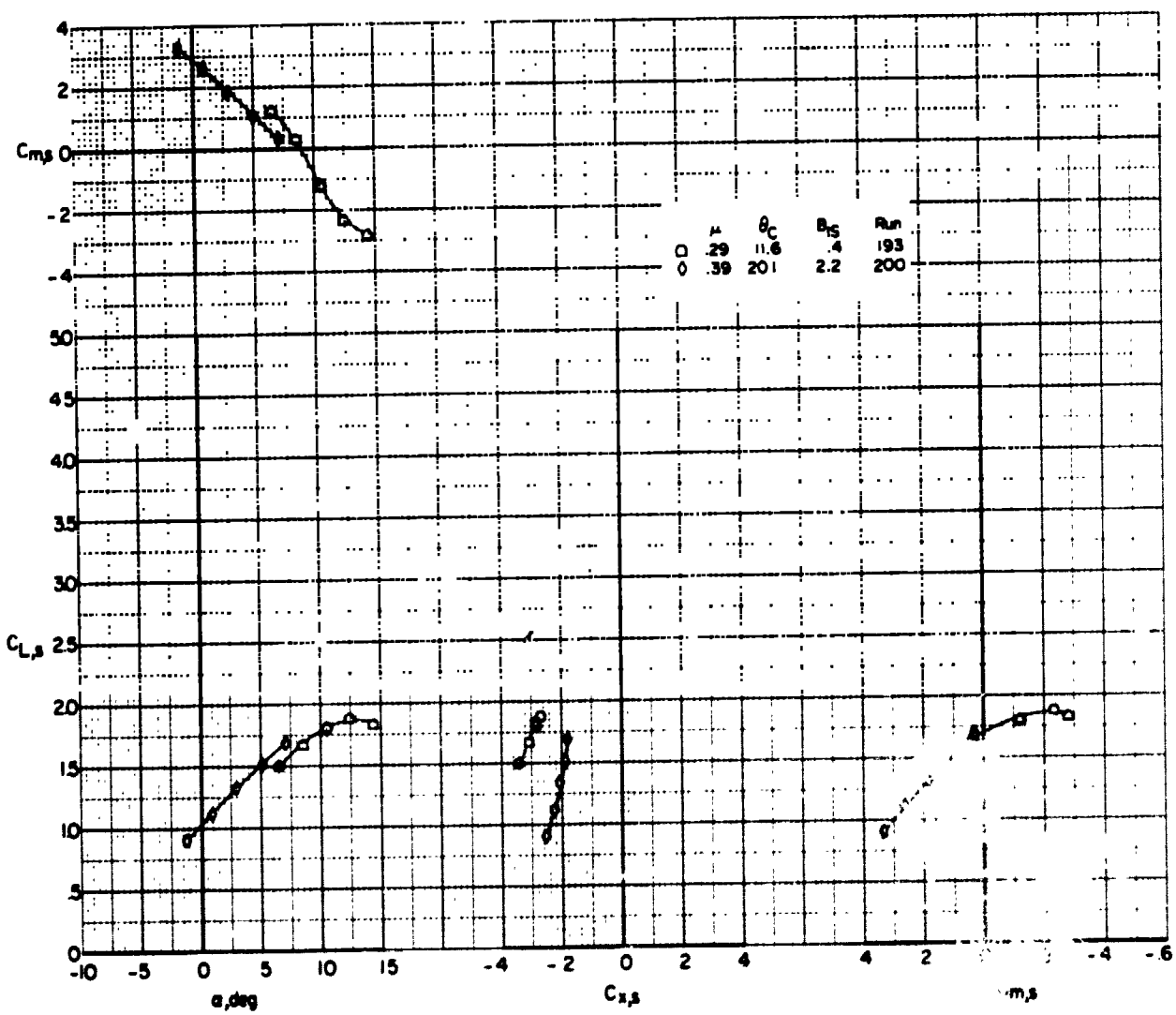

Figure 26. - Continued.

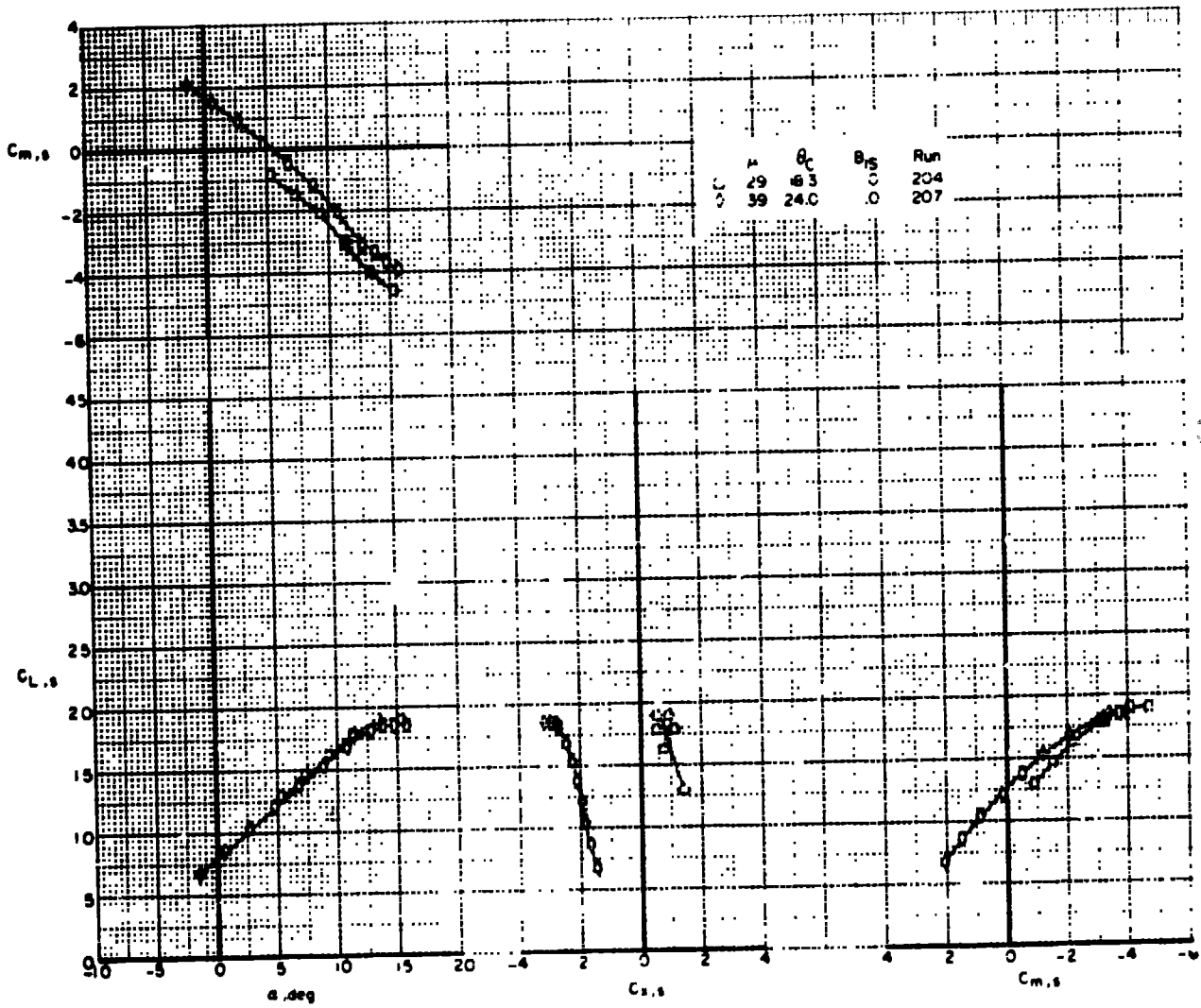

(e) $\alpha_s = 0^\circ$, transition rotor speed

Figure 28. - Concluded.

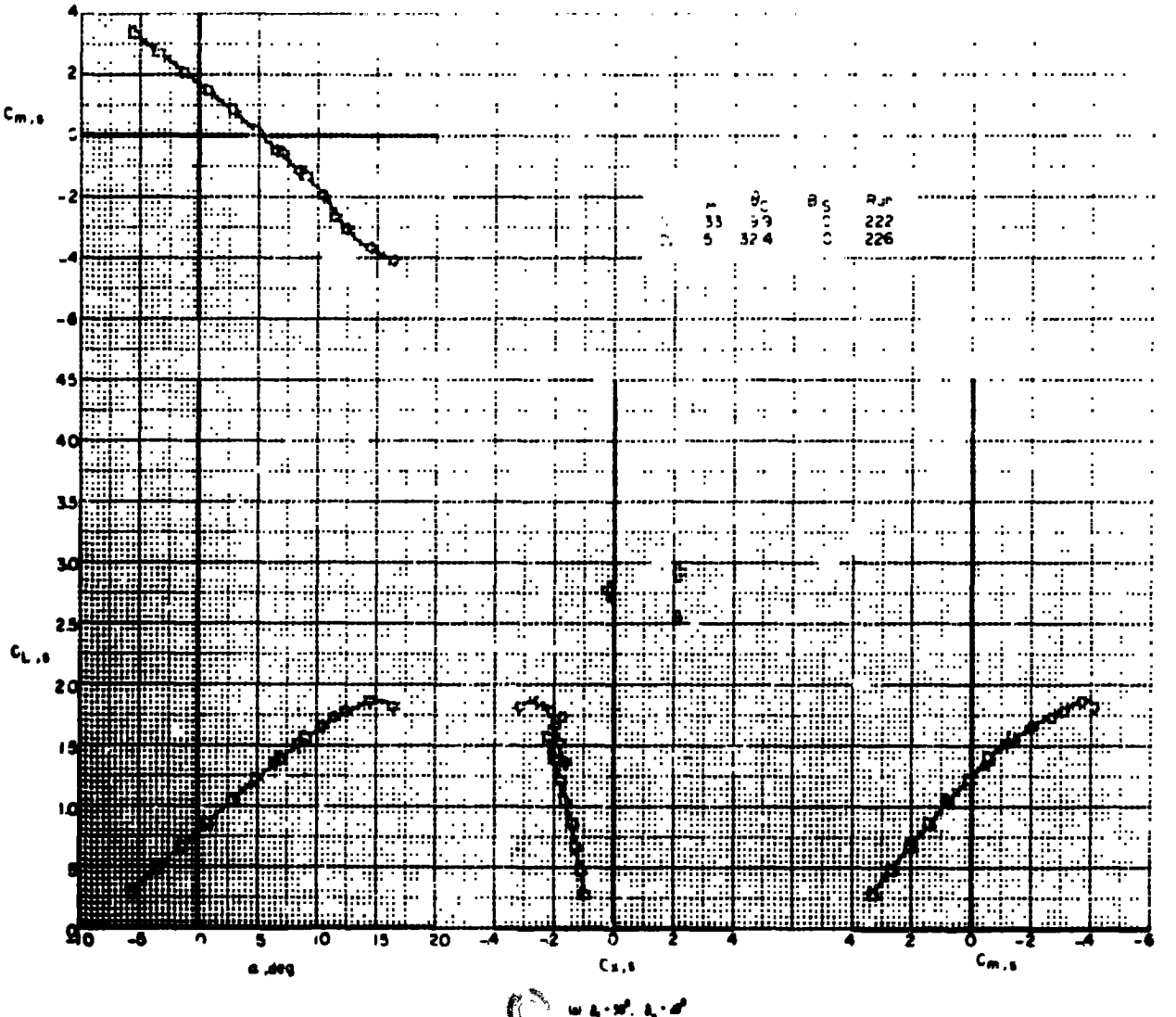
$C_{m,s}$
$C_{L,s}$
α, deg
$C_{x,s}$
$C_{m,s}$

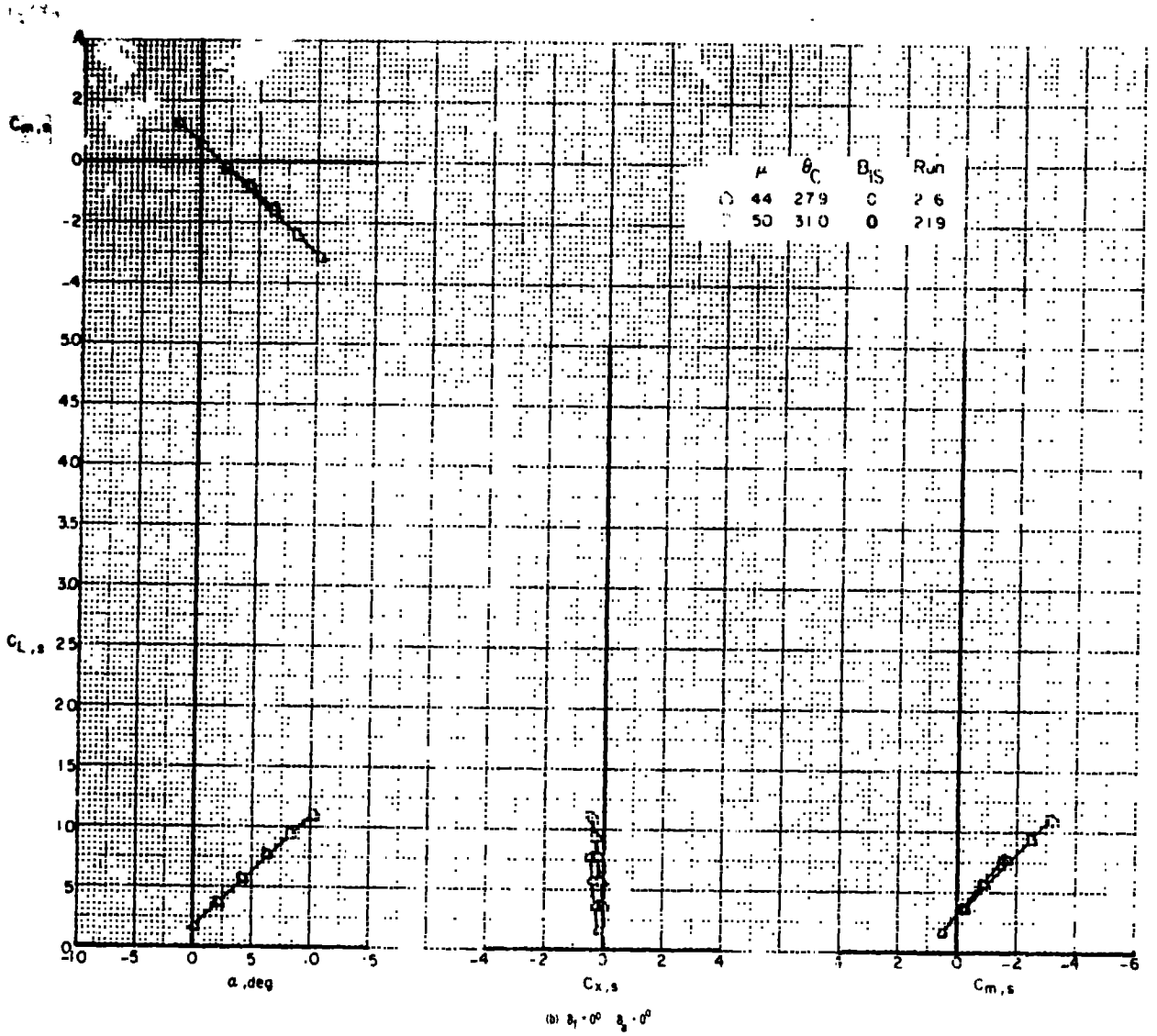

(b) $\beta_f = 0^0$ $\beta_s = 0^0$

Figure 27. - Concluded.

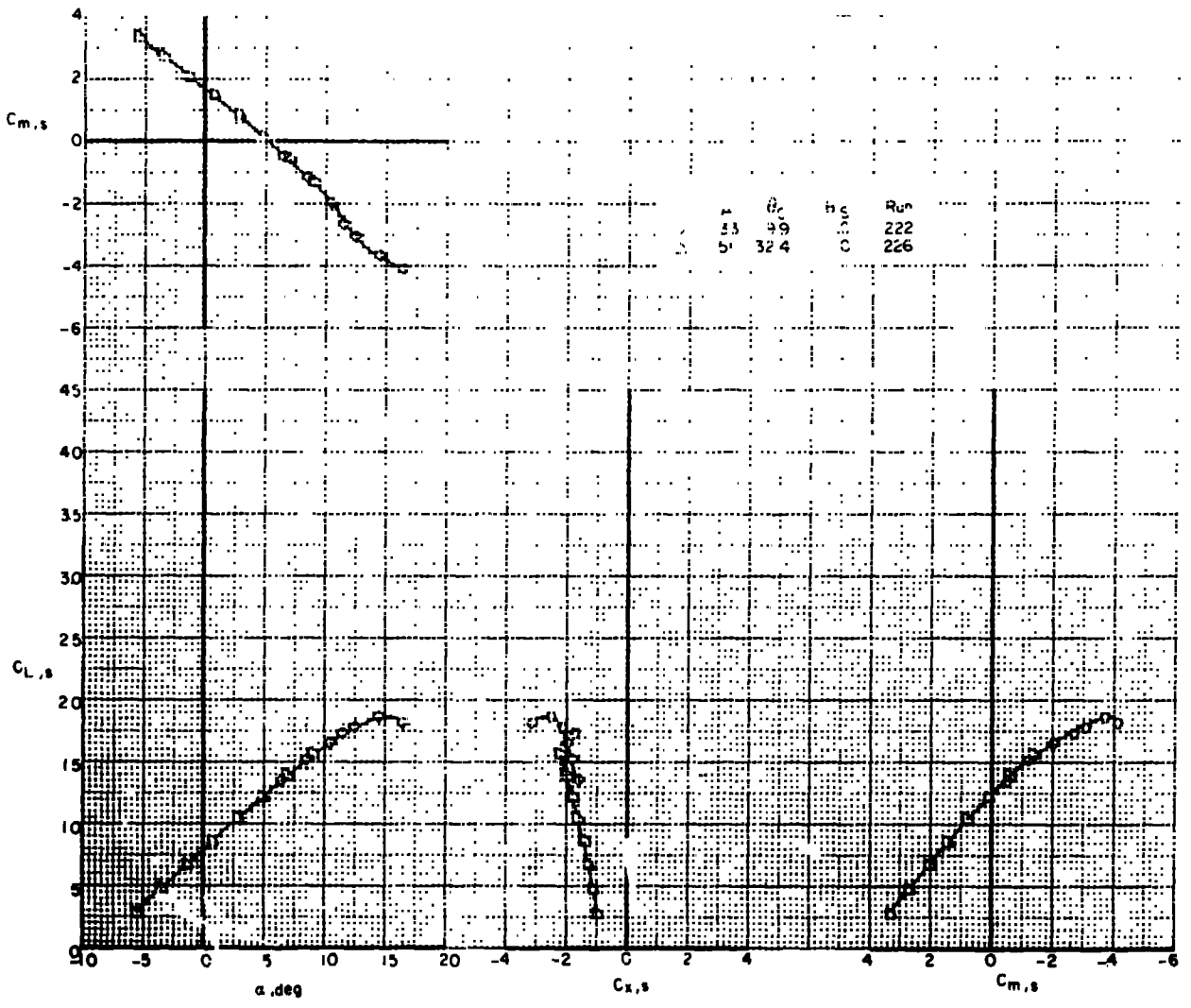

(a) $\beta_f = 50^\circ$, $\beta_s = 20^\circ$

Figure 27. - Effect of angle of attack on the longitudinal aerodynamic characteristics at several wind speeds, $\alpha_p = 0^\circ$, cruise rotor speed.

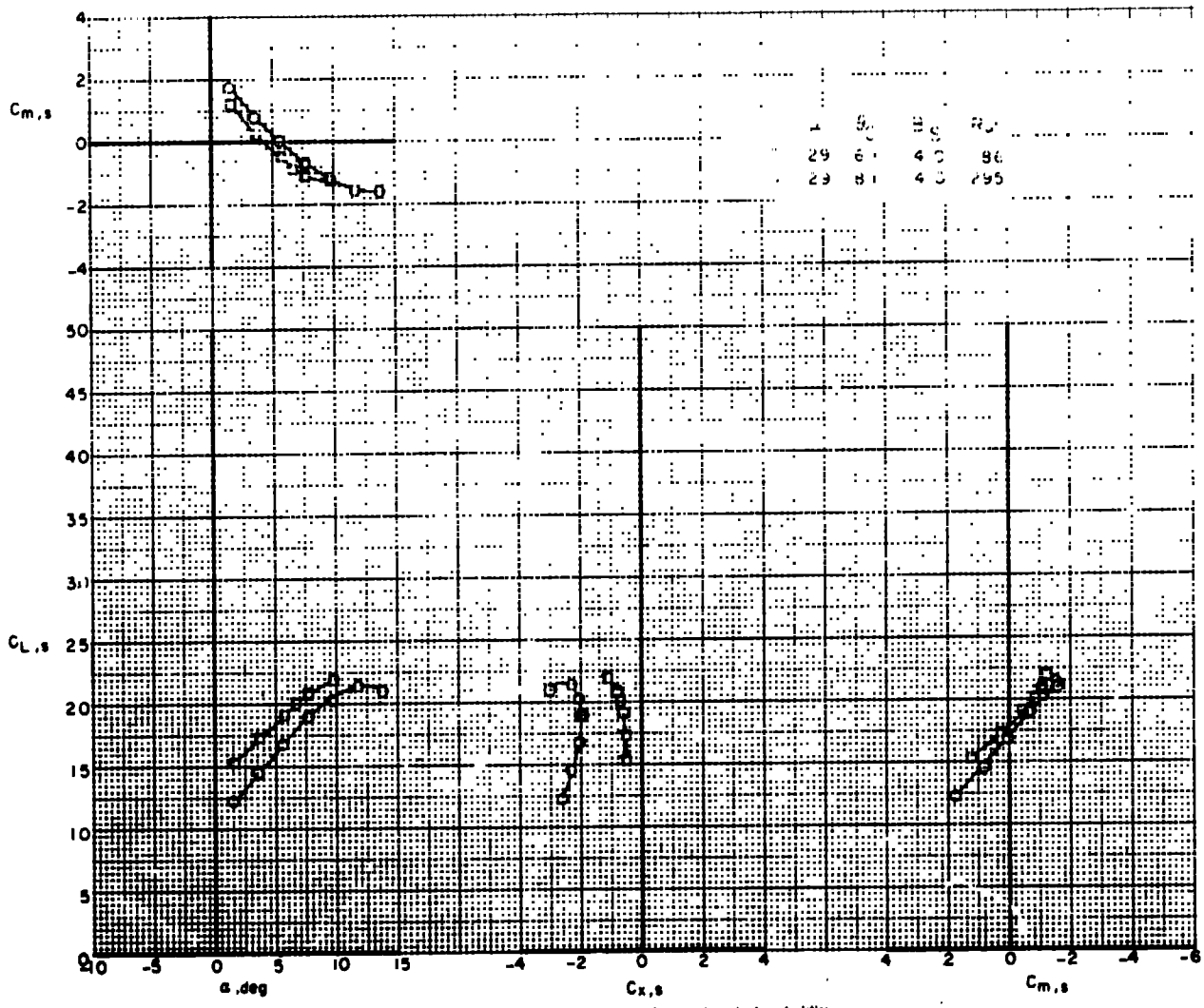

Figure 28. - Effect of angle of attack on the longitudinal aerodynamic characteristics for several collective pitch angles, θ_0 = 0°.

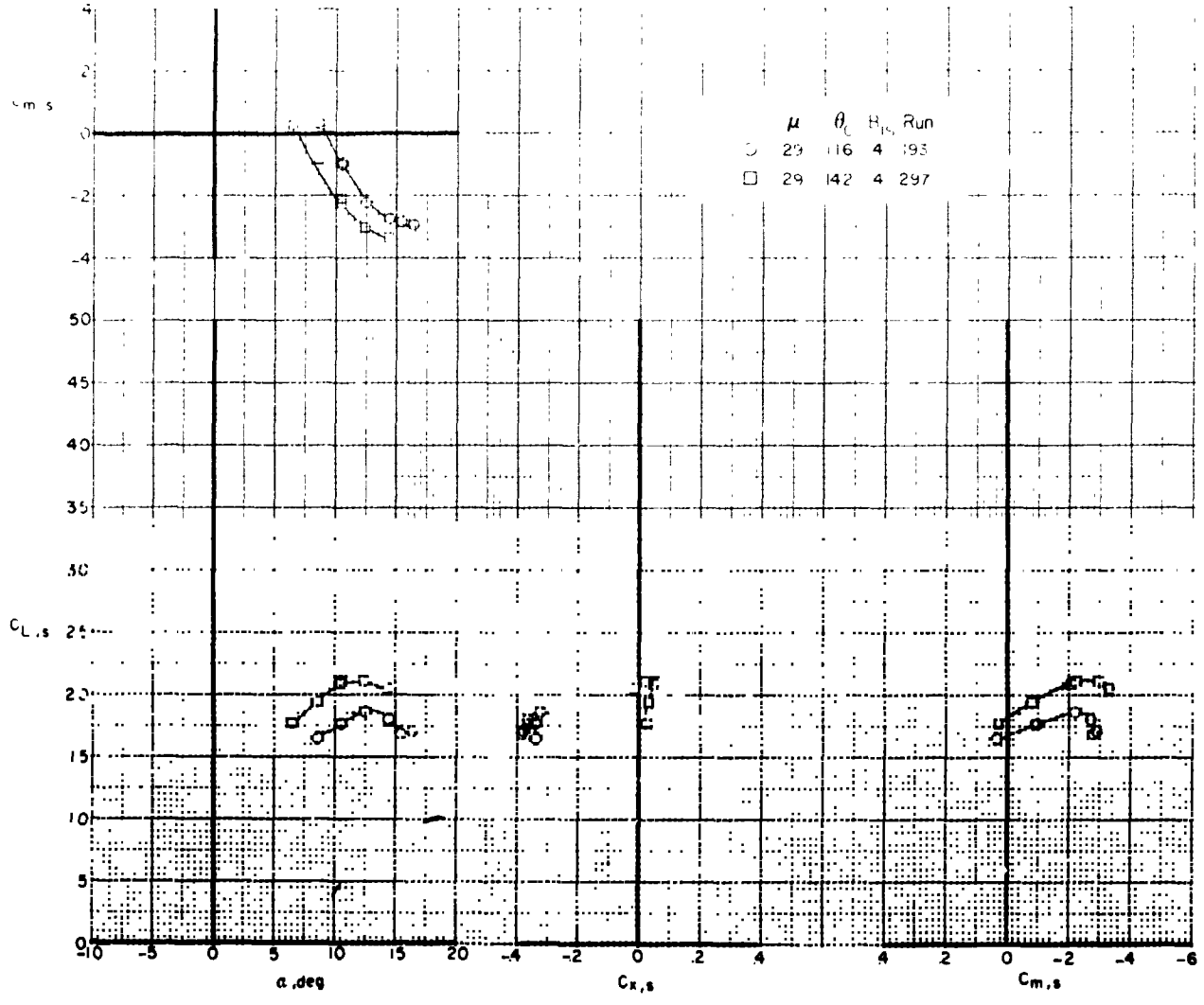

(a) $\mu = .29$

Figure 29. - Effect of angle of attack on the longitudinal aerodynamic characteristics for several collective pitch angles, $\alpha_p = 10°$.

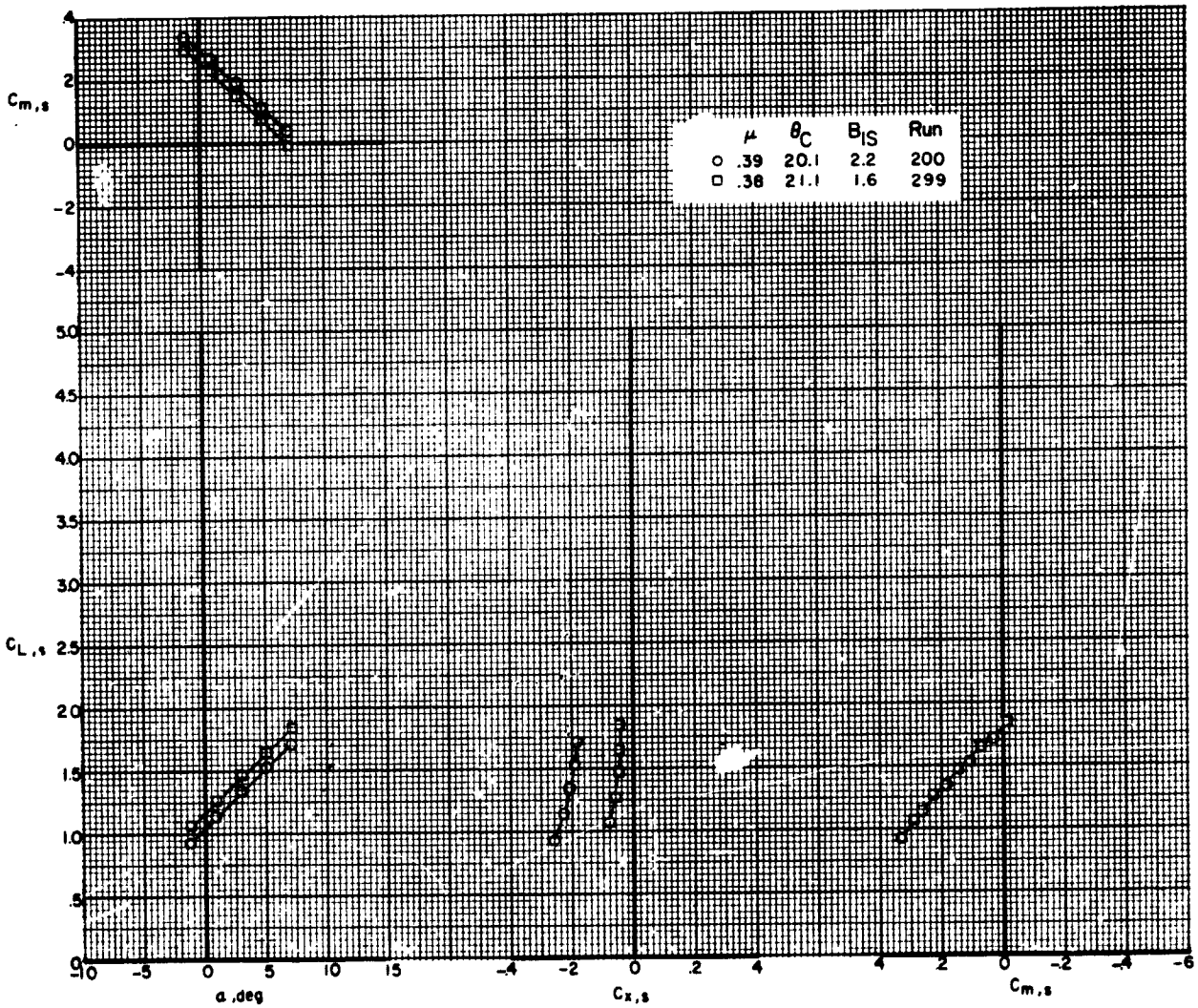

(b) $\mu = 0.38$

Figure 29. - Concluded.

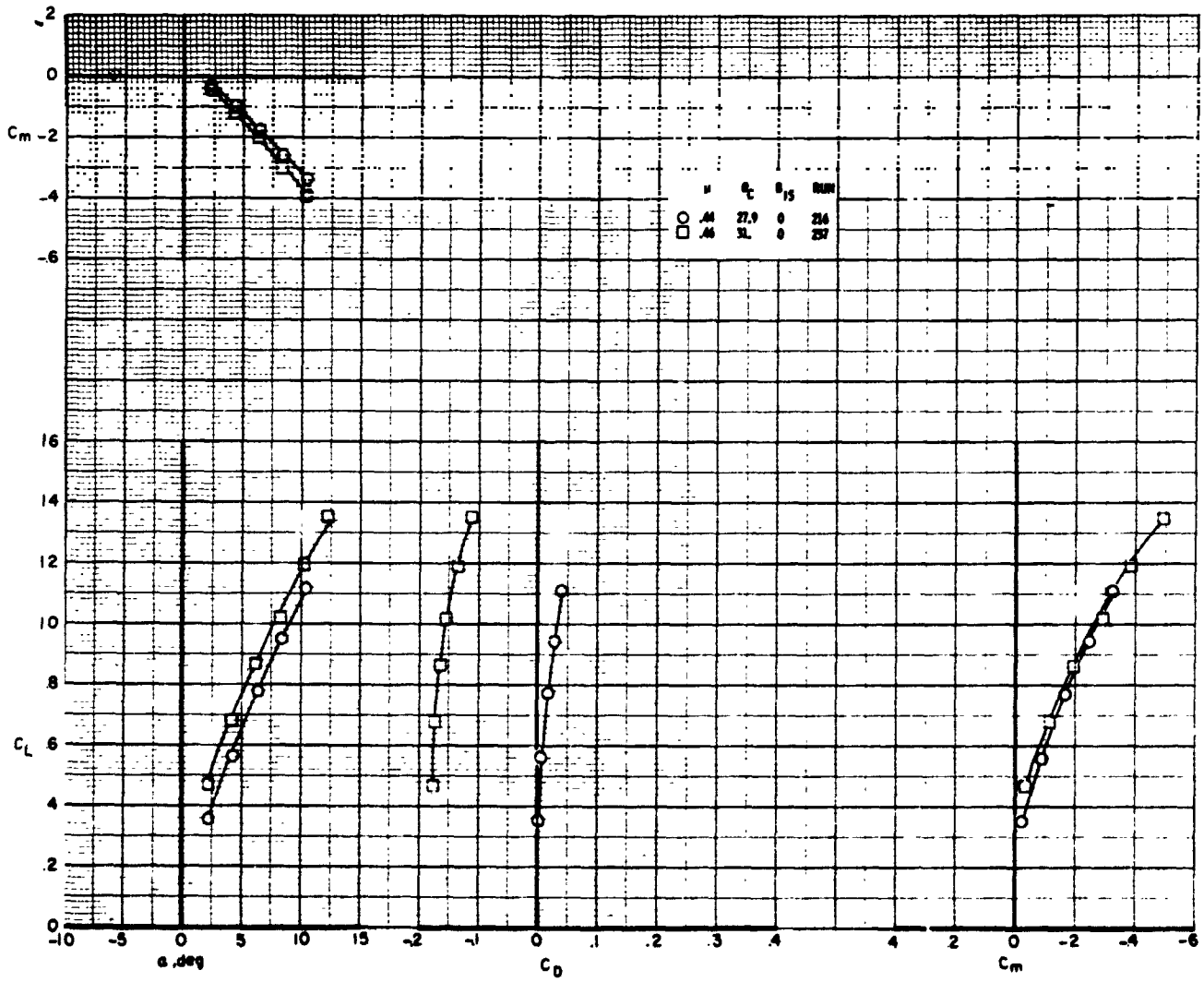

(a) V_{FS} = 300 kts

Figure 38. - Effect of angle of attack and collective pitch on longitudinal aerodynamic characteristics (stipl ream) for full-scale flight speeds of 300 and 300 knots for pylon angle 0°. $\delta_f/\delta_0 = 0^0/0^0$ and cruise rotor speed.

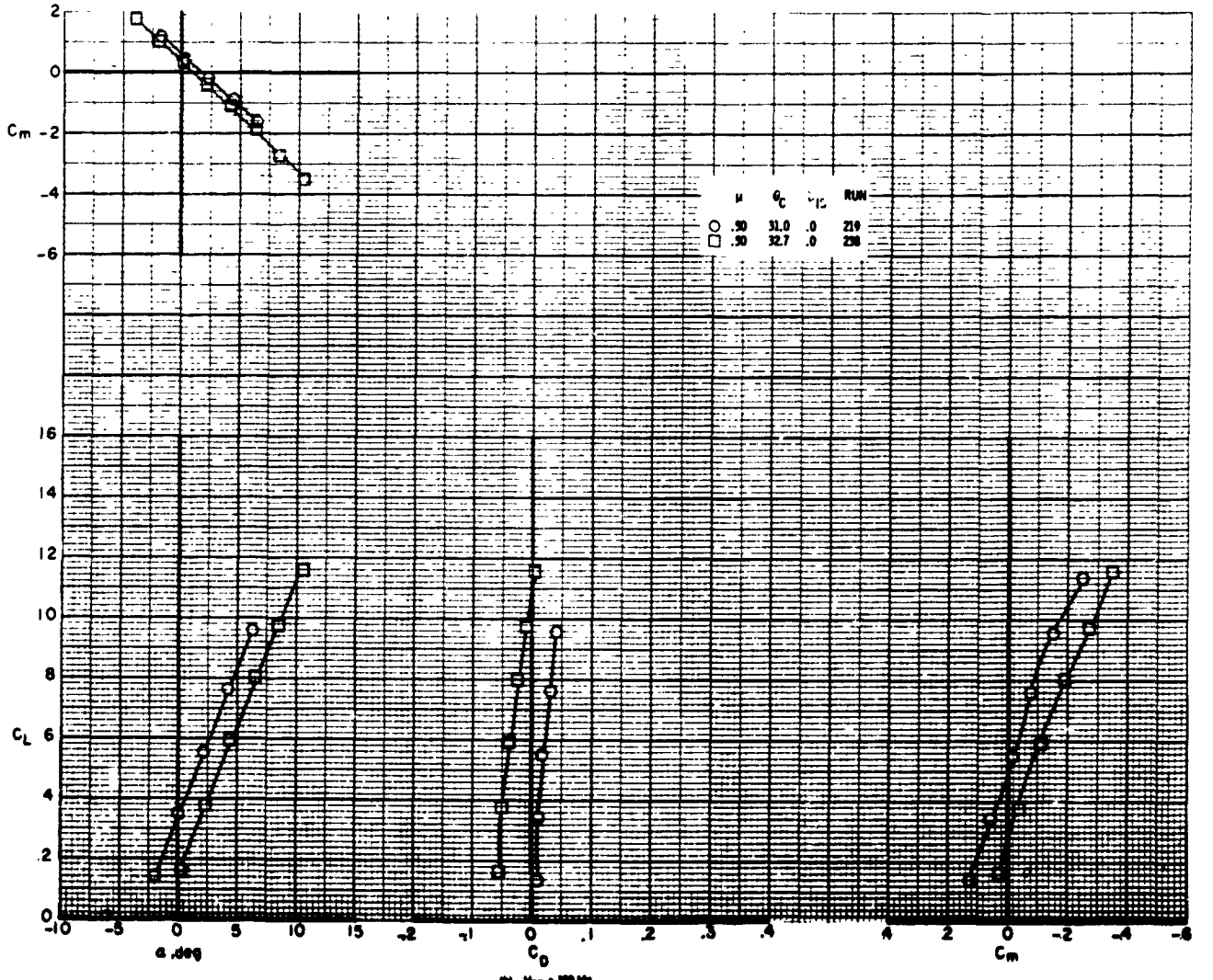

(b) V_{PS} = 100 kts

Figure 18. - Concluded.

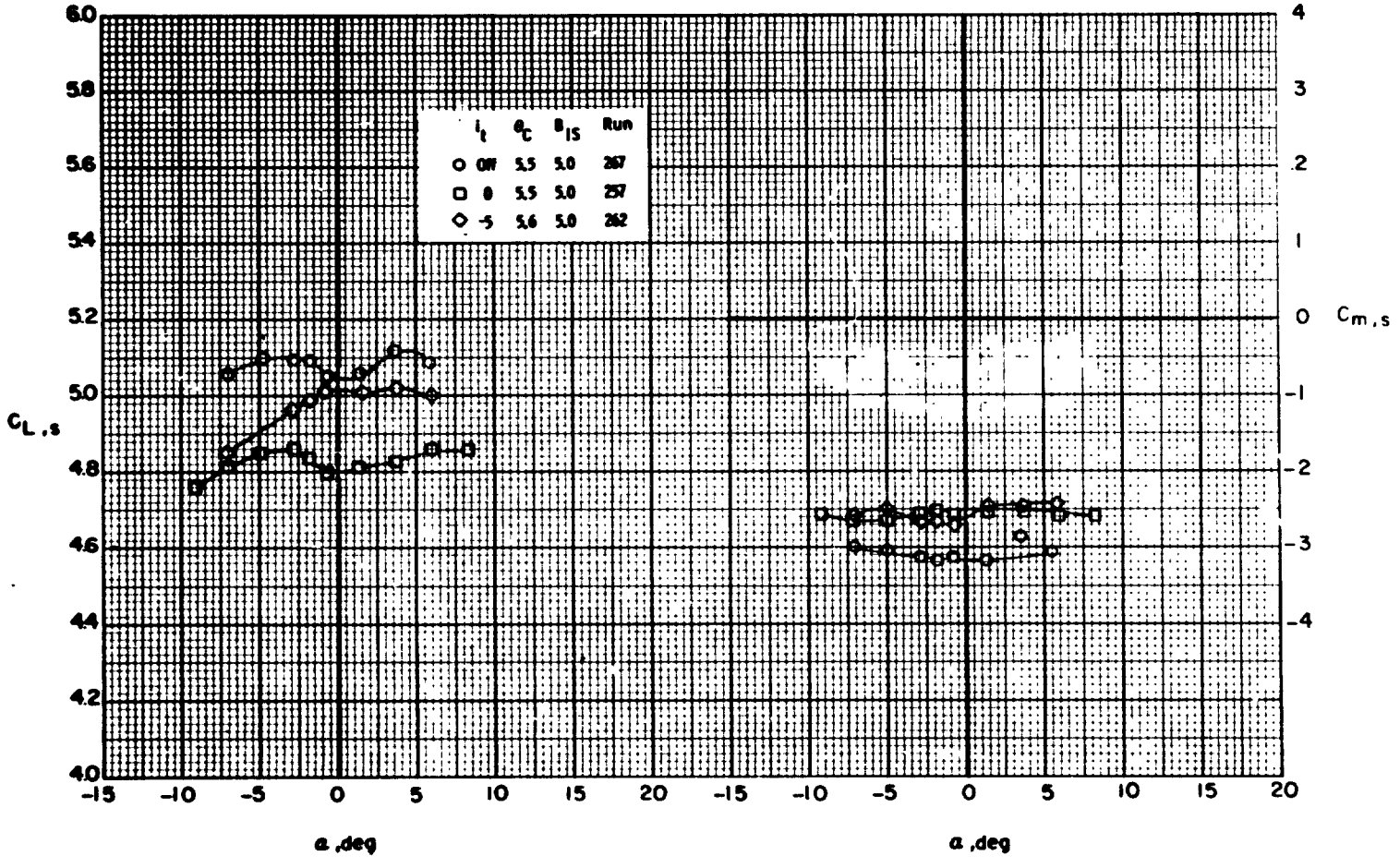

(a) $\mu = 0.04$

Figure 31. - Effect of angle of attack on the slipstream lift and pitching-moment coefficients with the horizontal tail on and off, $\alpha_p = 90^0$, $\delta_f = 50^0$, $\delta_a = 20^0$.

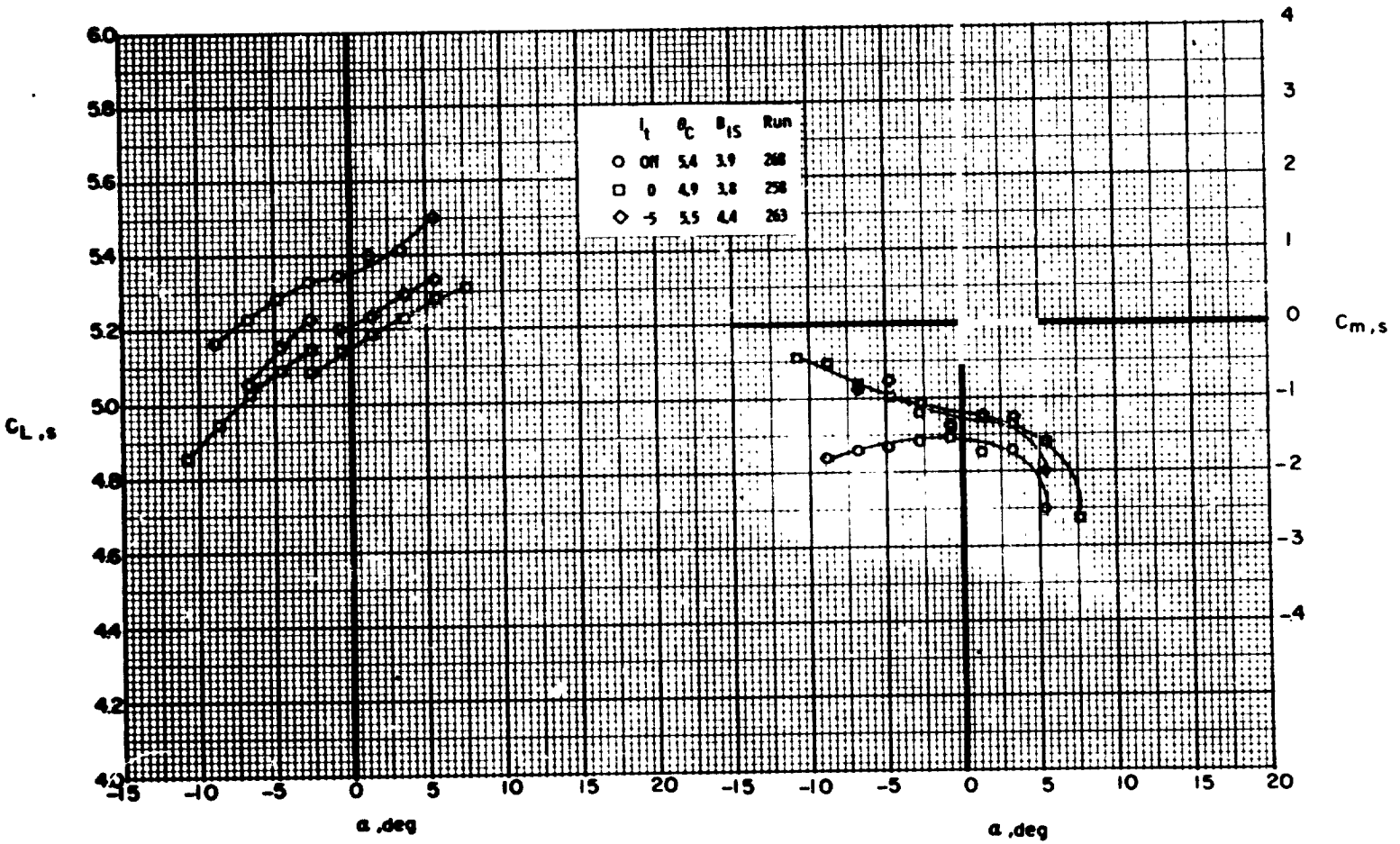

$M_\infty \beta = 0.06$

Figure 31. - Continued.

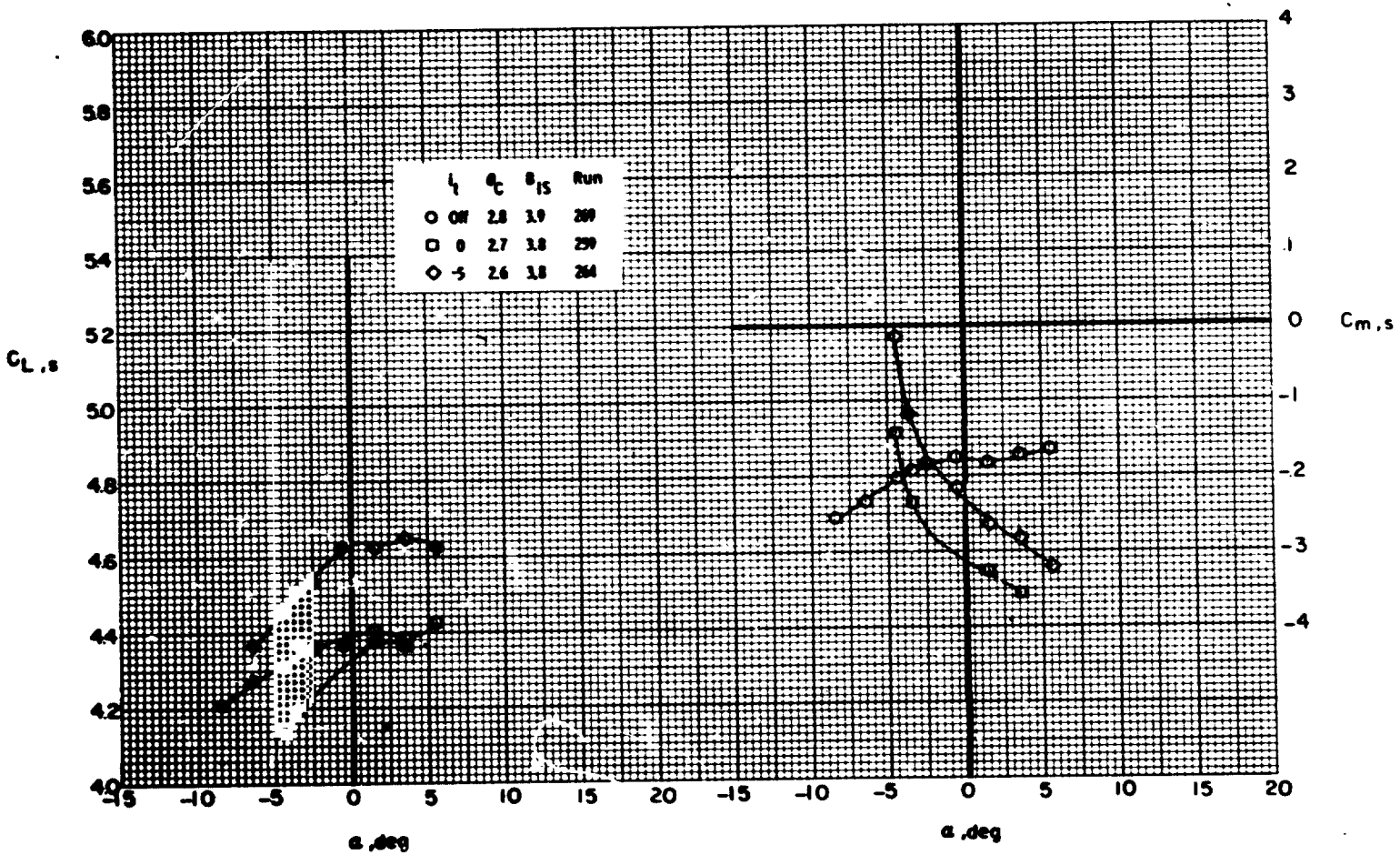

$|c|_{\mu} = 0.08$

Figure 31. - Continued.

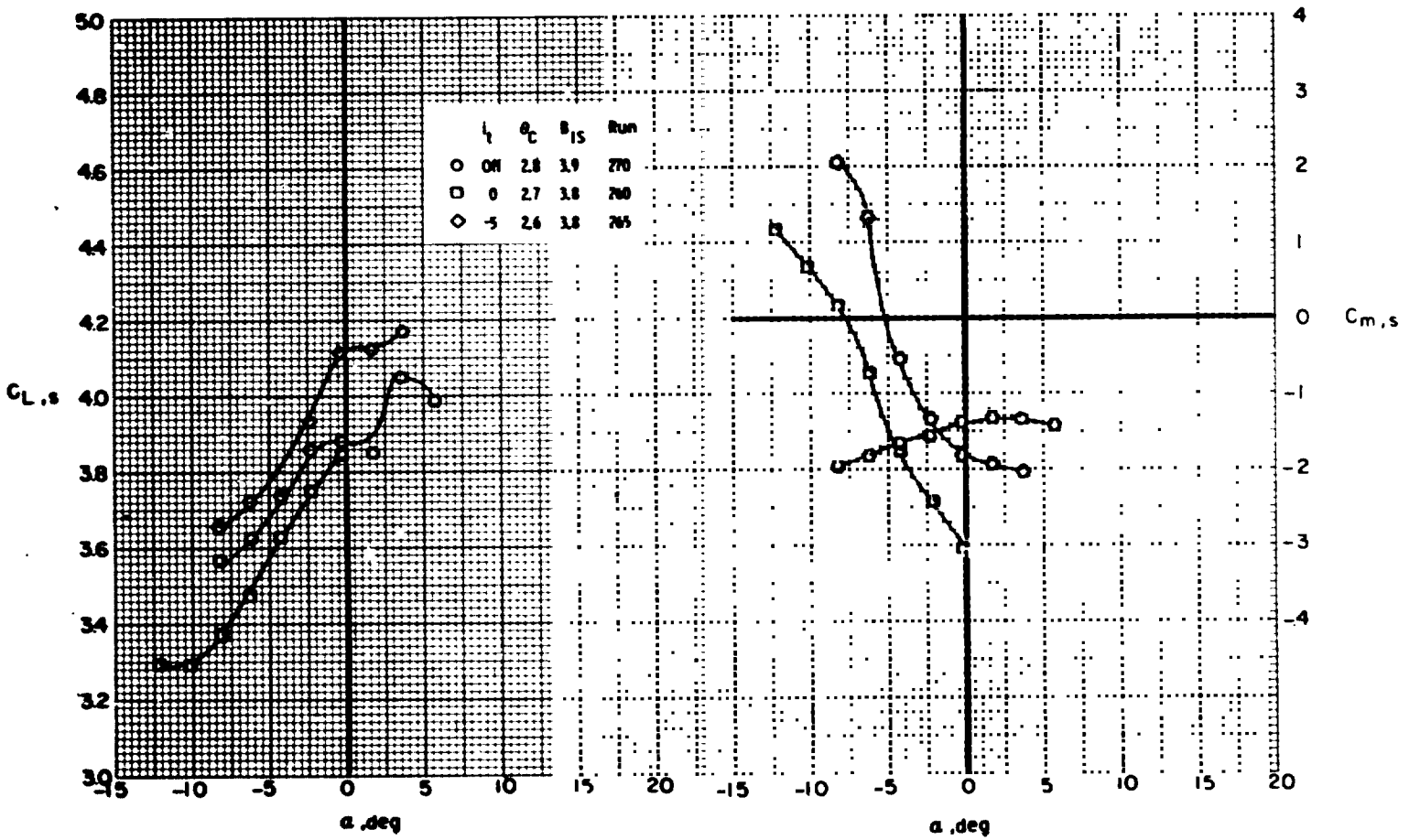

$M\beta\mu = 0.10$

Figure 31. - Continued.

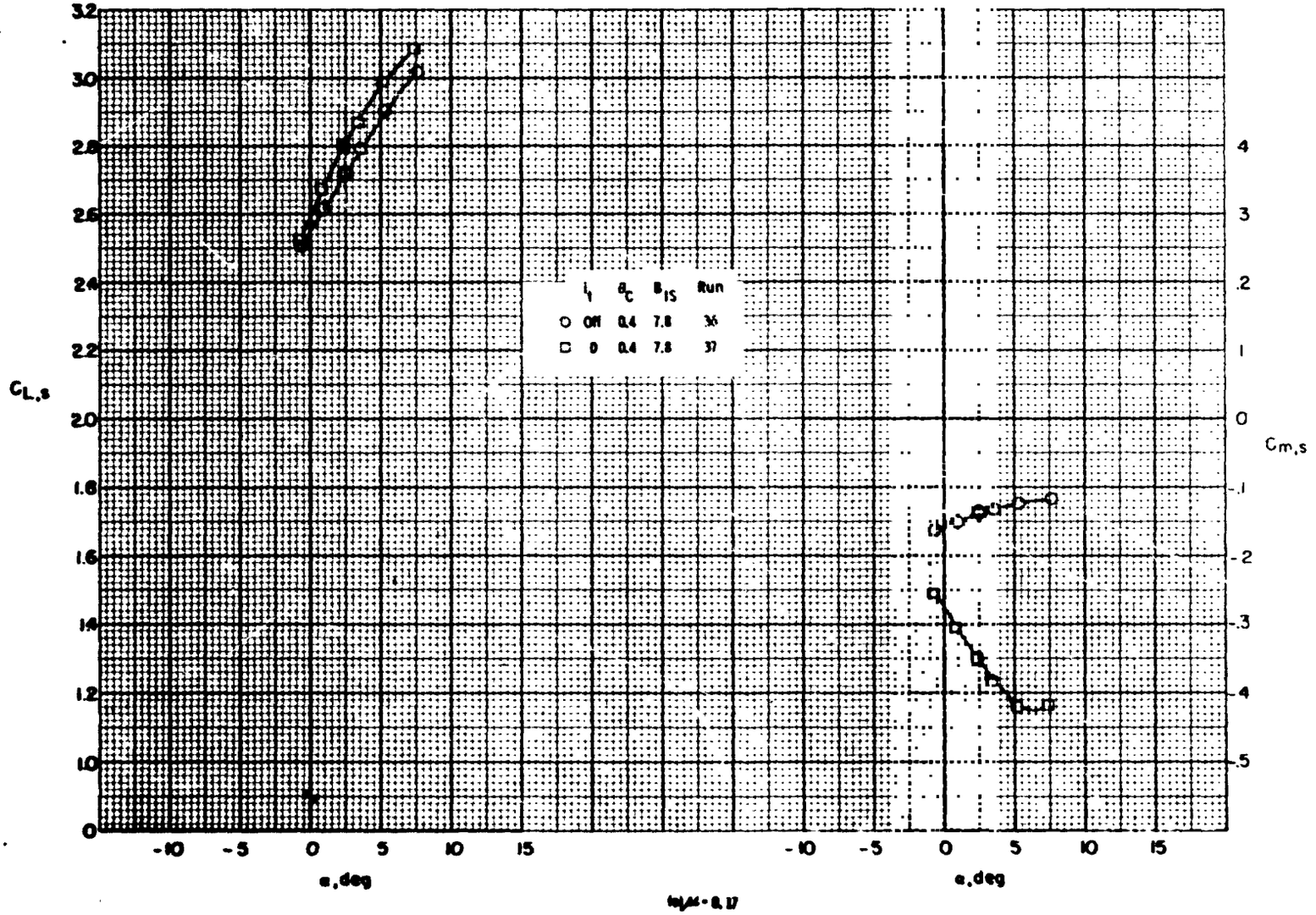

$(q/p)_\infty = 0.17$

Figure 31. - Continued.

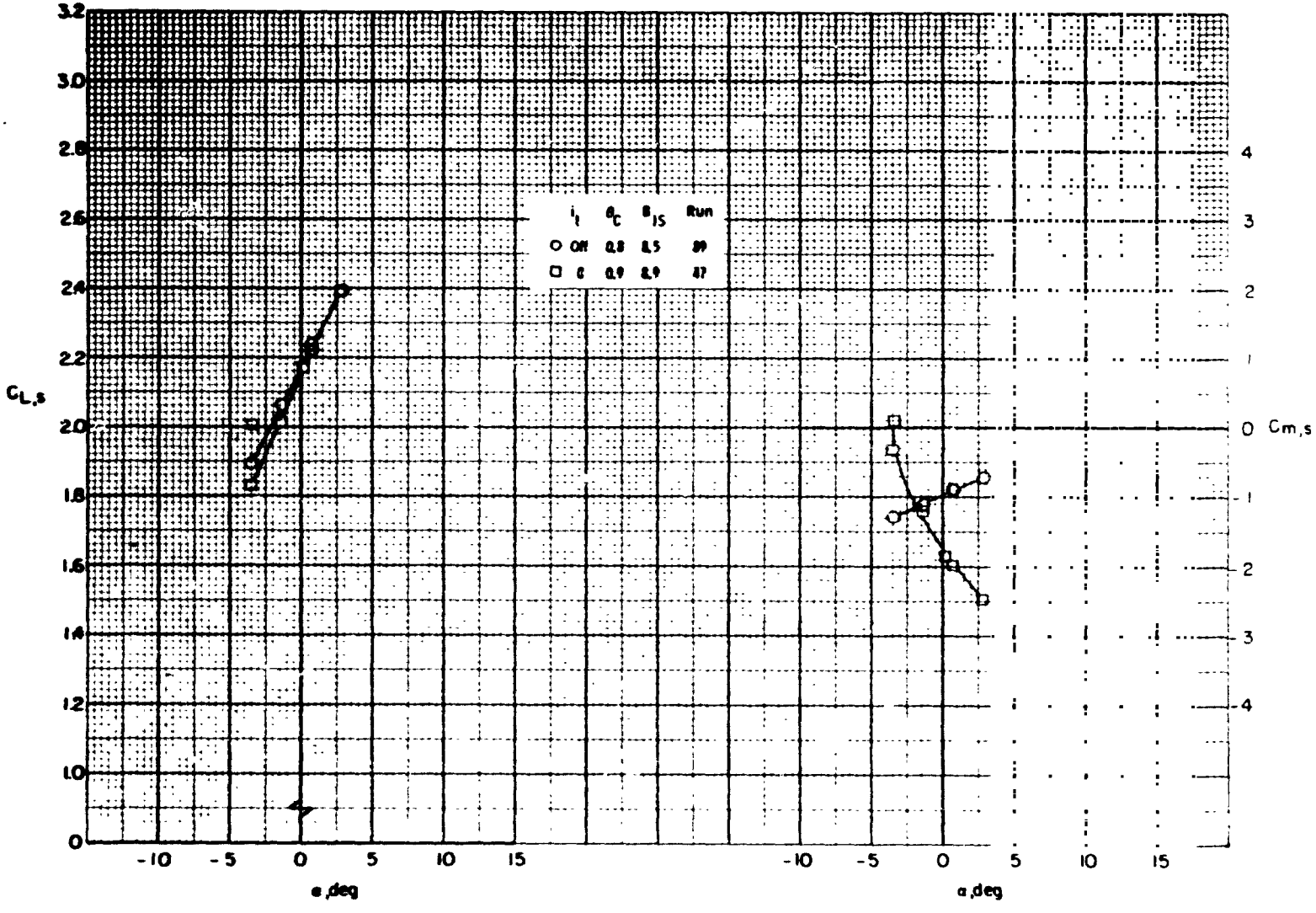

(f) $\beta = 0.20$

Figure 11. - Concluded.

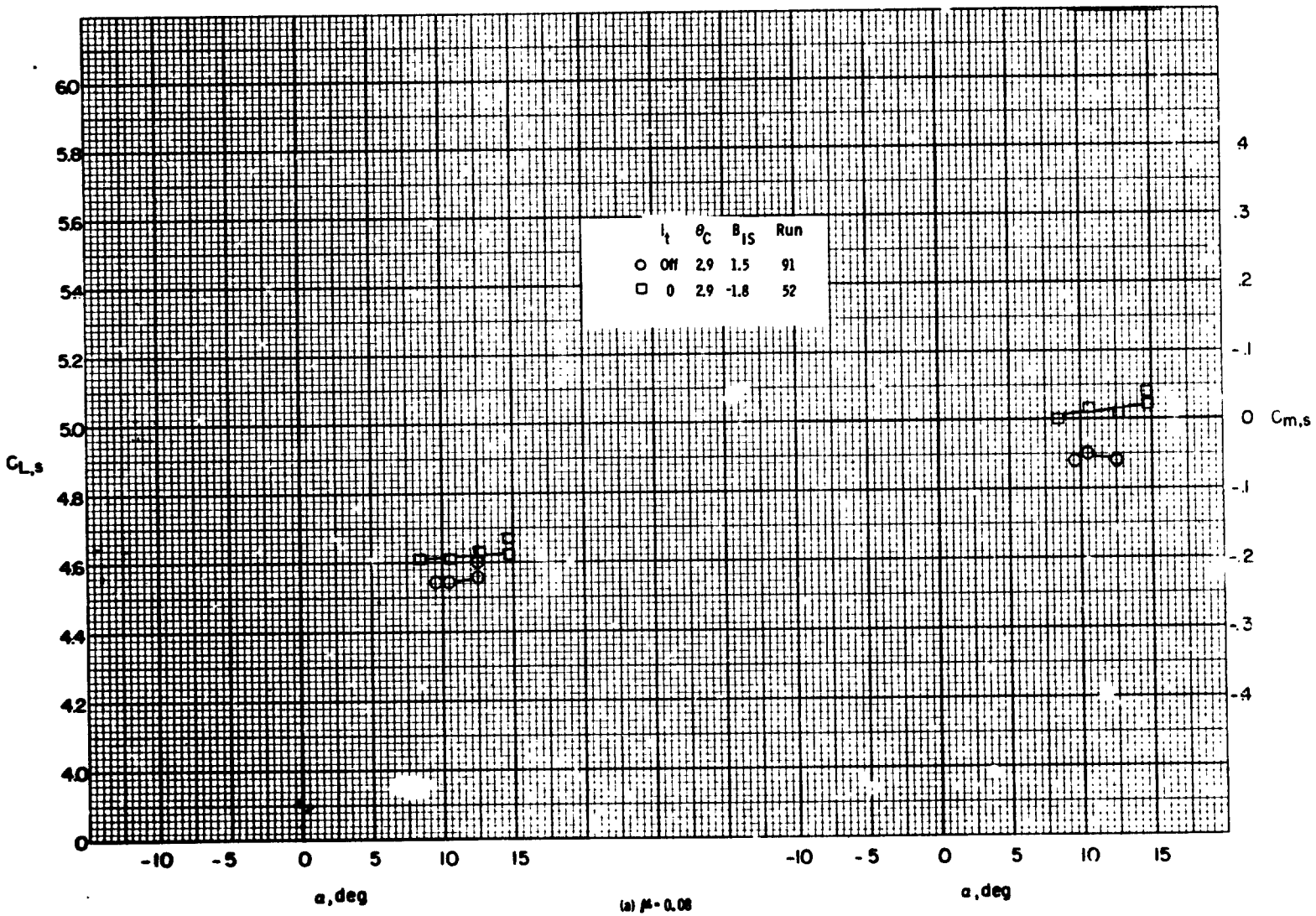

Figure 32. - Effect of angle of attack on the slipstream lift and pitching-moment coefficients with the horizontal tail on and off, $\alpha_p = 75^0$, $\delta_f = 50^0$, $\delta_a = 20^0$.

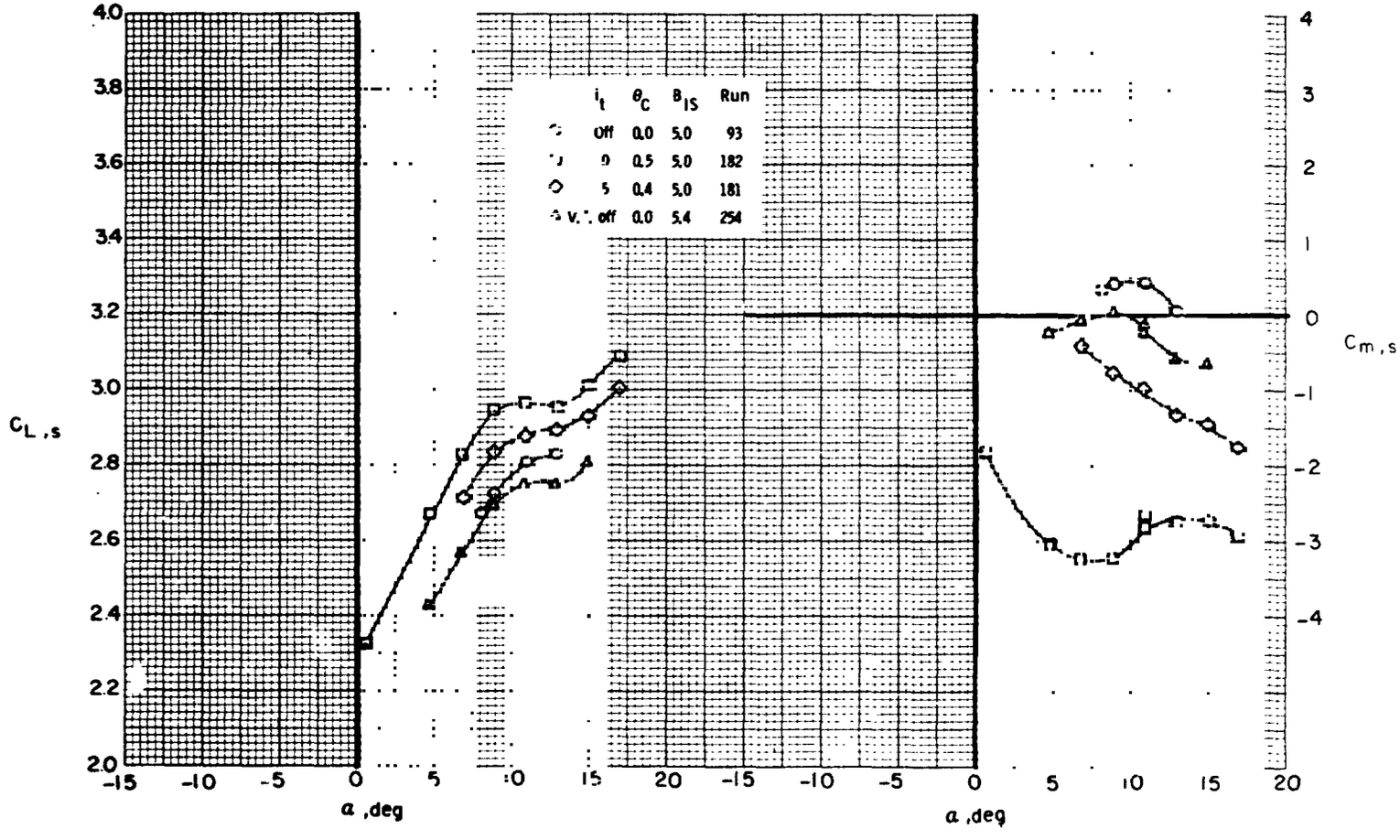

(b) μ = 0.16

Figure 32. - Continued.

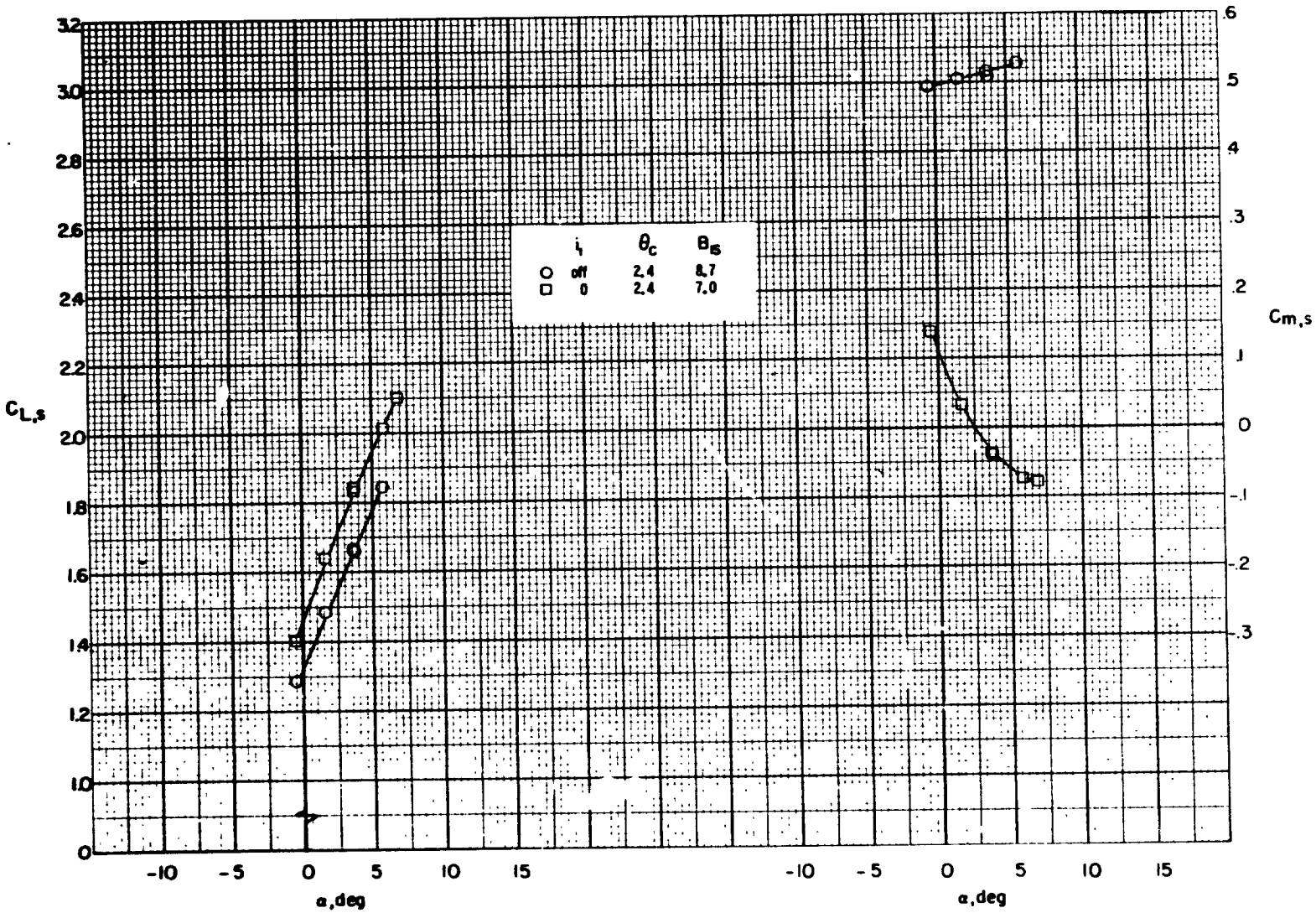

(r) $\beta = 0.25$

Figure 32. - Concluded.

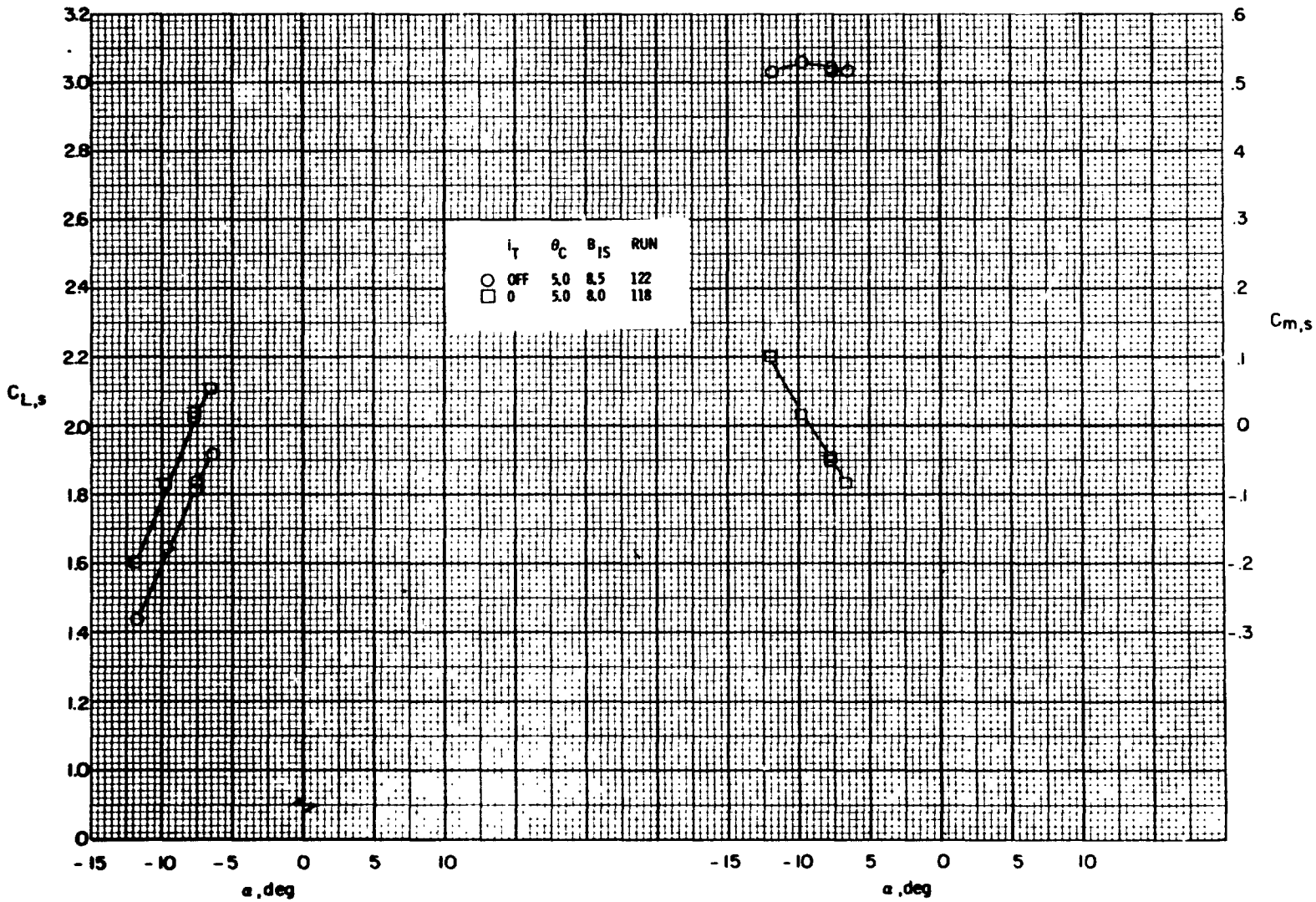

Figure 33. - Effect of angle of attack on the slipstream lift and pitching-moment coefficients with the horizontal tail on and off, $\beta = 0.16$, $\alpha_p = 75^0$, $\delta_f = 50^0$, $\delta_a = 20^0$.

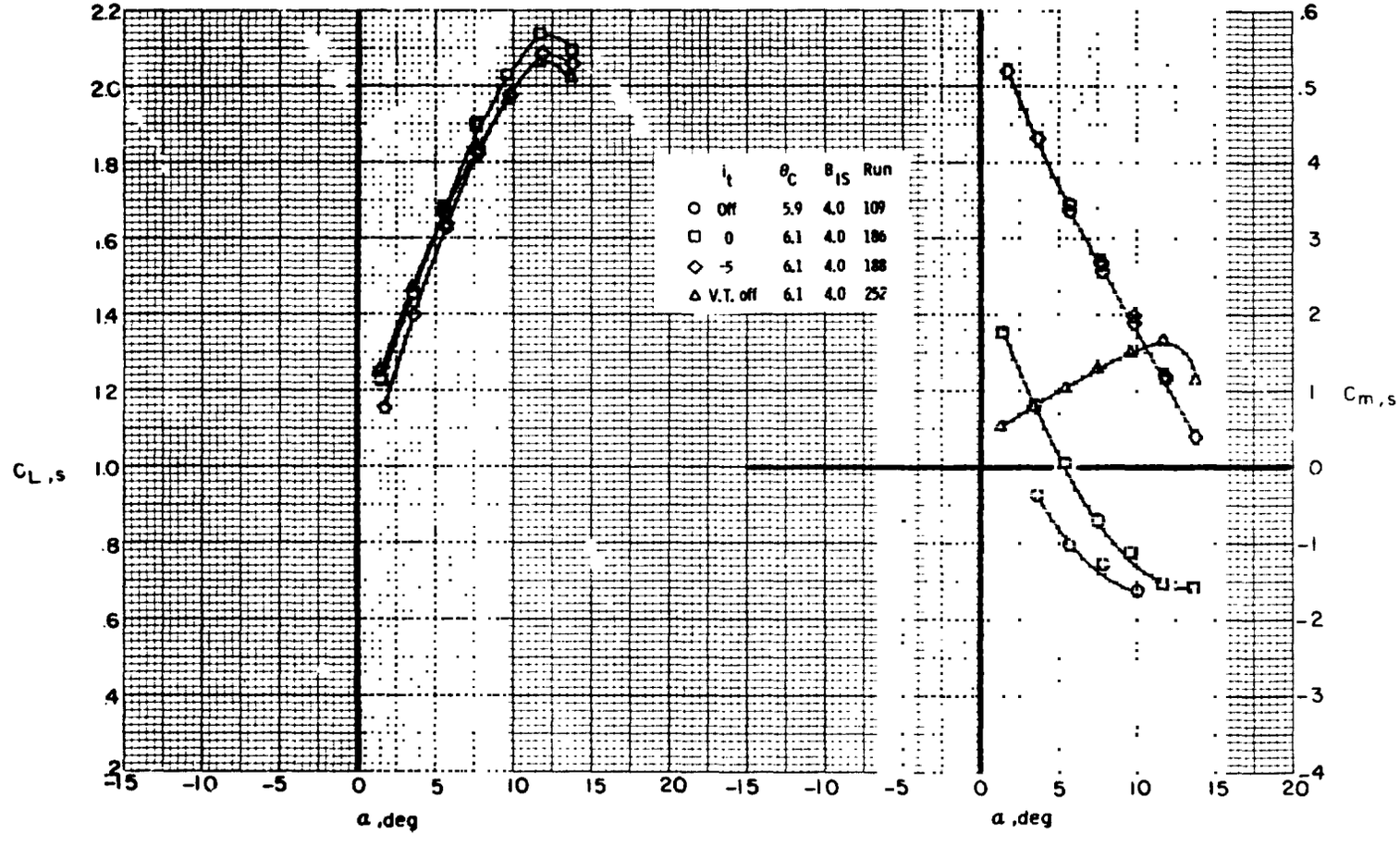

(a) $\mu = 0.29$

Figure 34. - Effect of angle of attack on the slipstream lift and pitching-moment coefficients with the horizontal tail on and off. $\alpha_p = 60^0$, $\delta_f = 50^0$, $\delta_a = 20^0$.

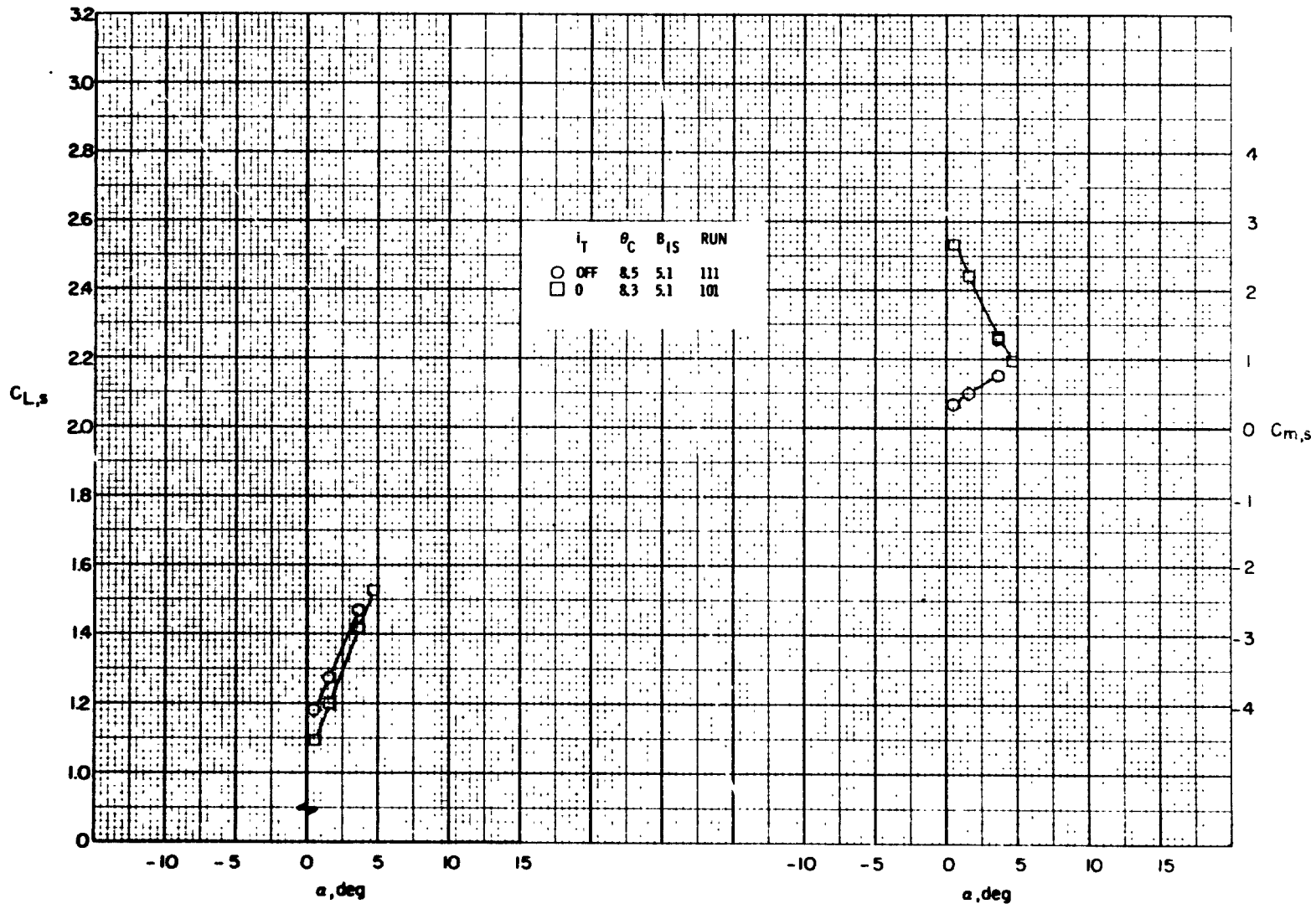

(b) $M_\infty = 0.33$

Figure 34. - Concluded.

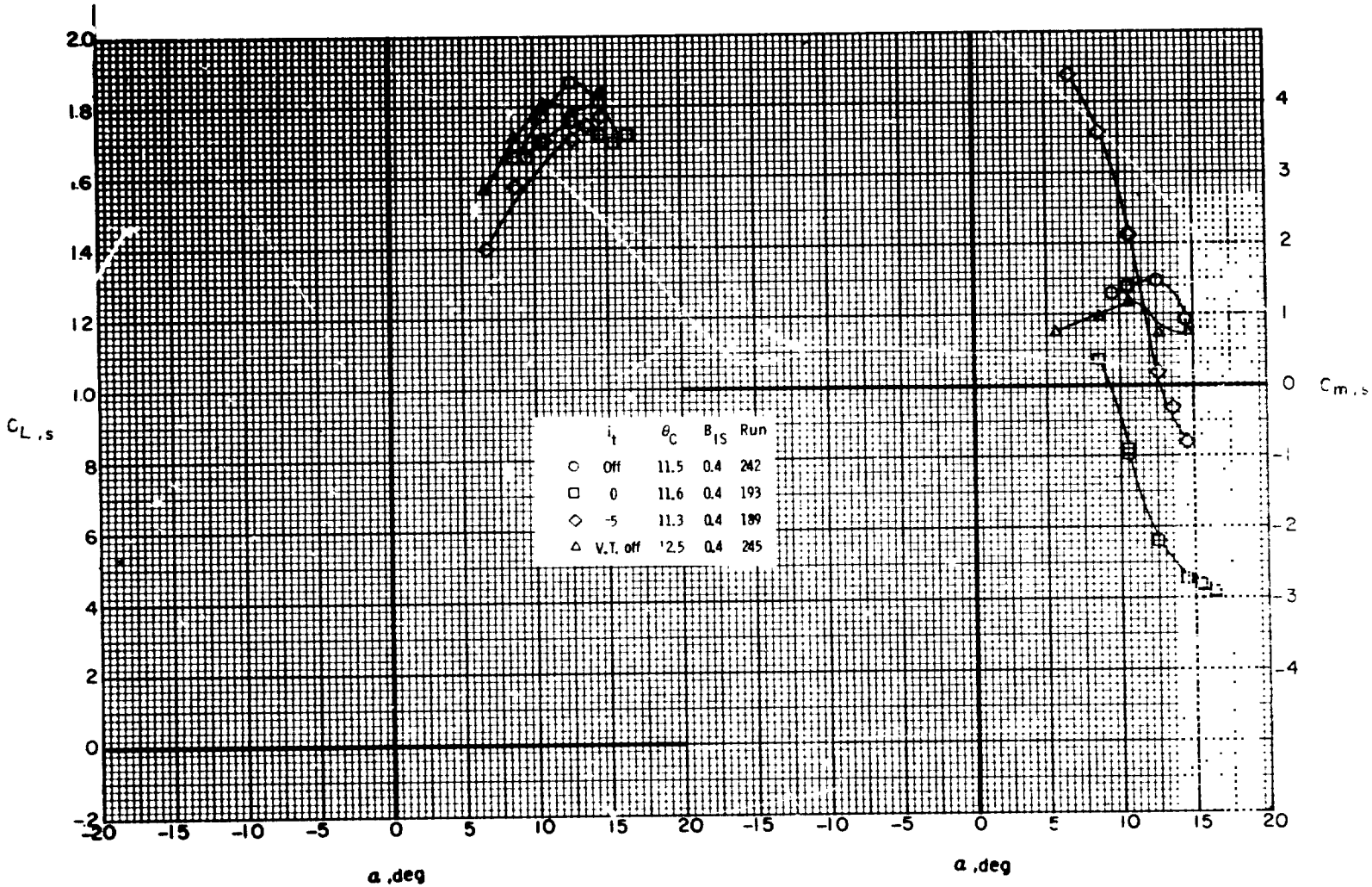

(a) $\mu = 0.29$

Figure 35. - Effect of angle of attack on the slipstream lift and pitching-moment coefficients with the horizontal tail on and off. $\alpha_p = 30^0$. $\delta_s = 50^0$. $\delta_a = 20^0$.

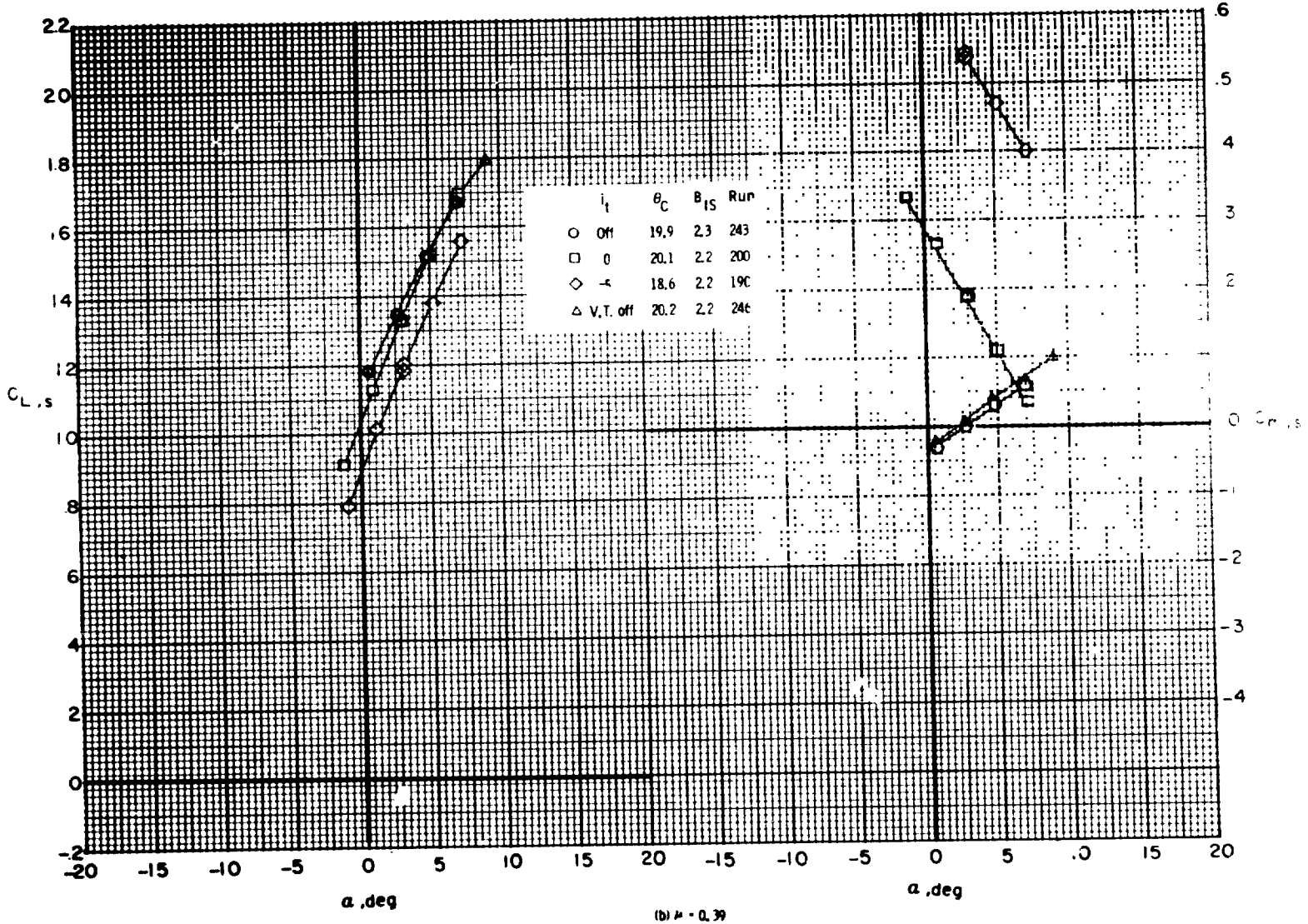

(b) μ = 0.39

Figure 35. - Concluded.

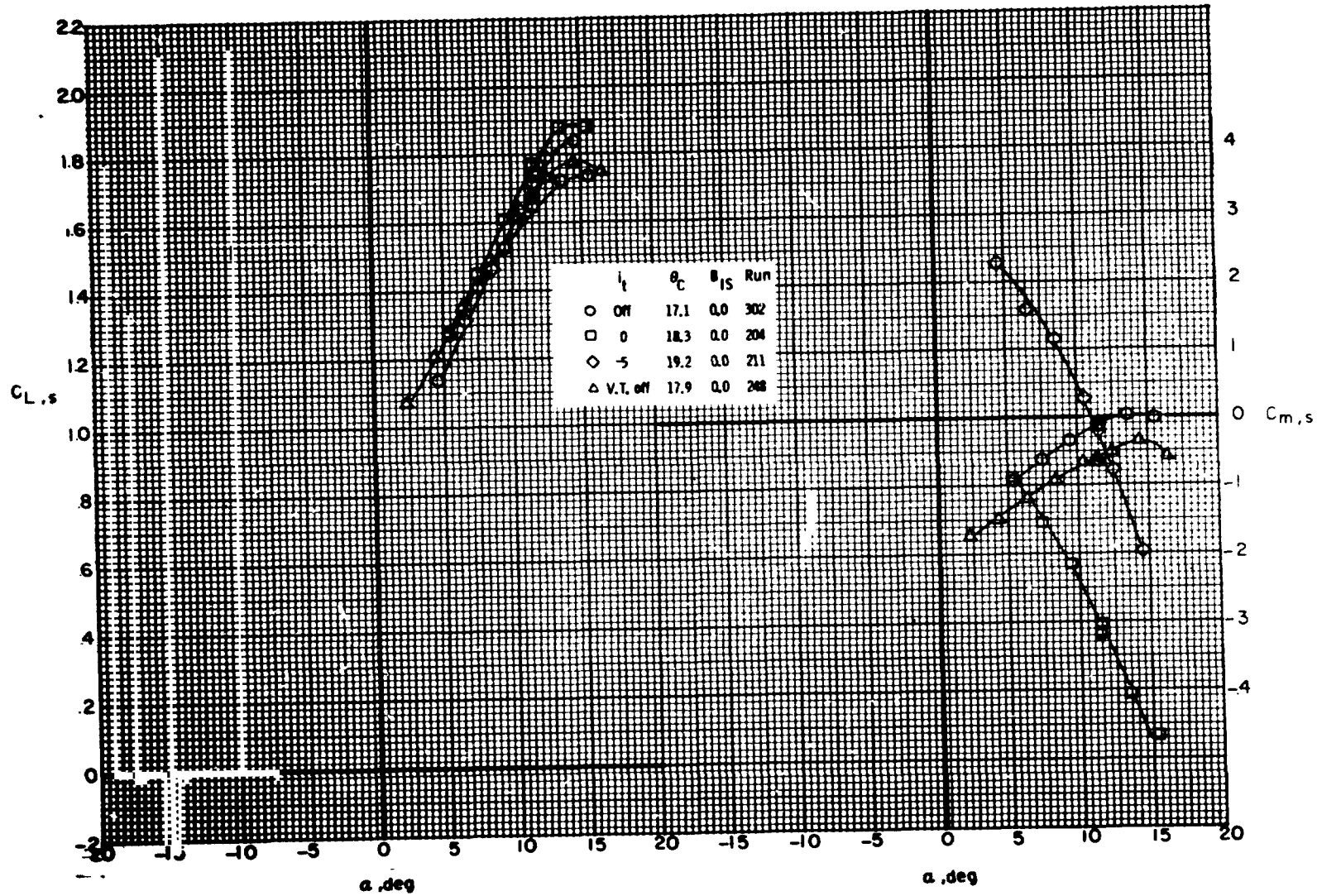

(a) $\mu = 0.29$

Figure 36. - Effect of angle of attack on the slipstream tilt and pitching-moment coefficients with the horizontal tail on and off, $\alpha_p = 0°$. θ_c = 1604 r.p.m.

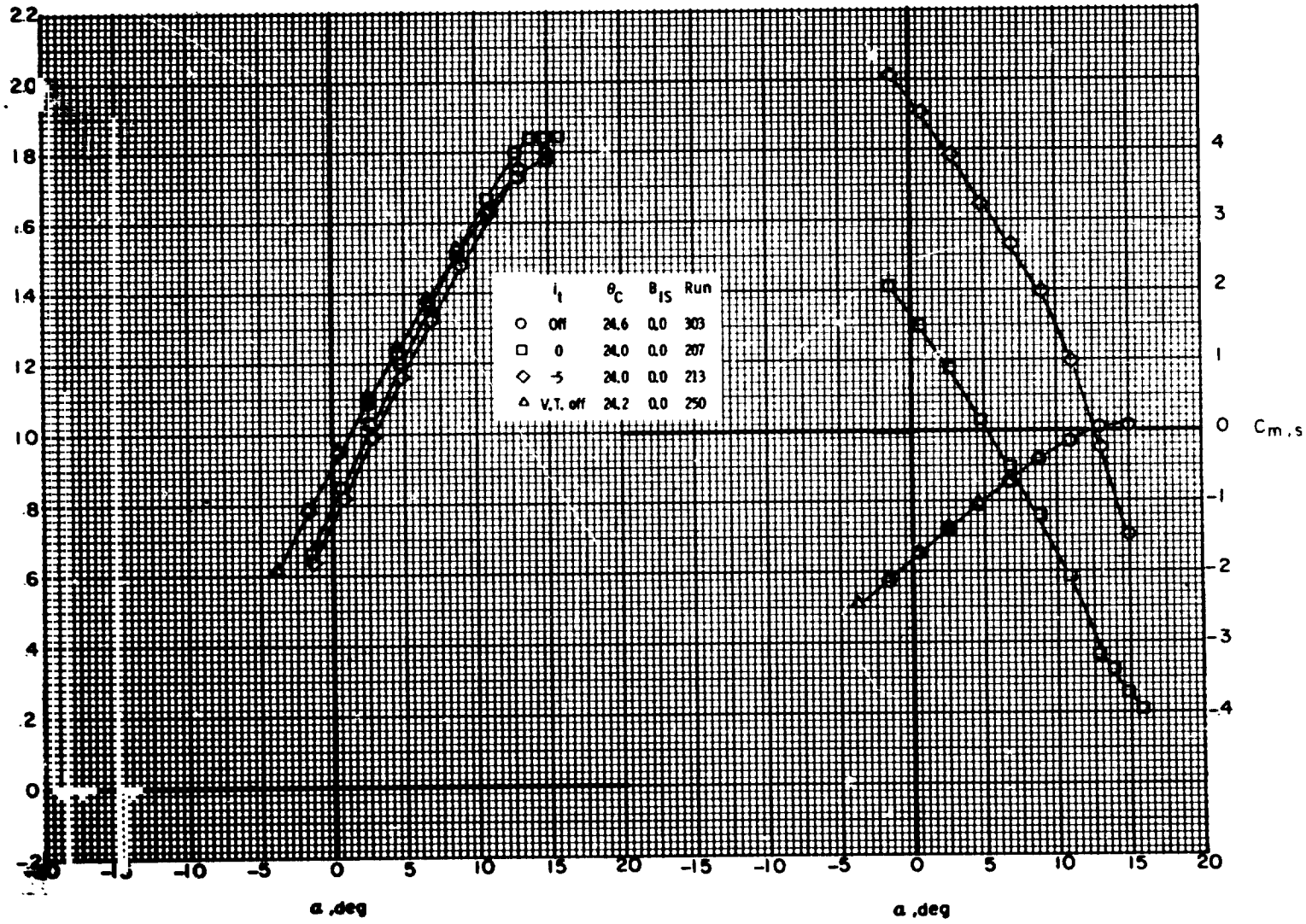

(b) $\mu = 0.39$

Figure 36. - Concluded.

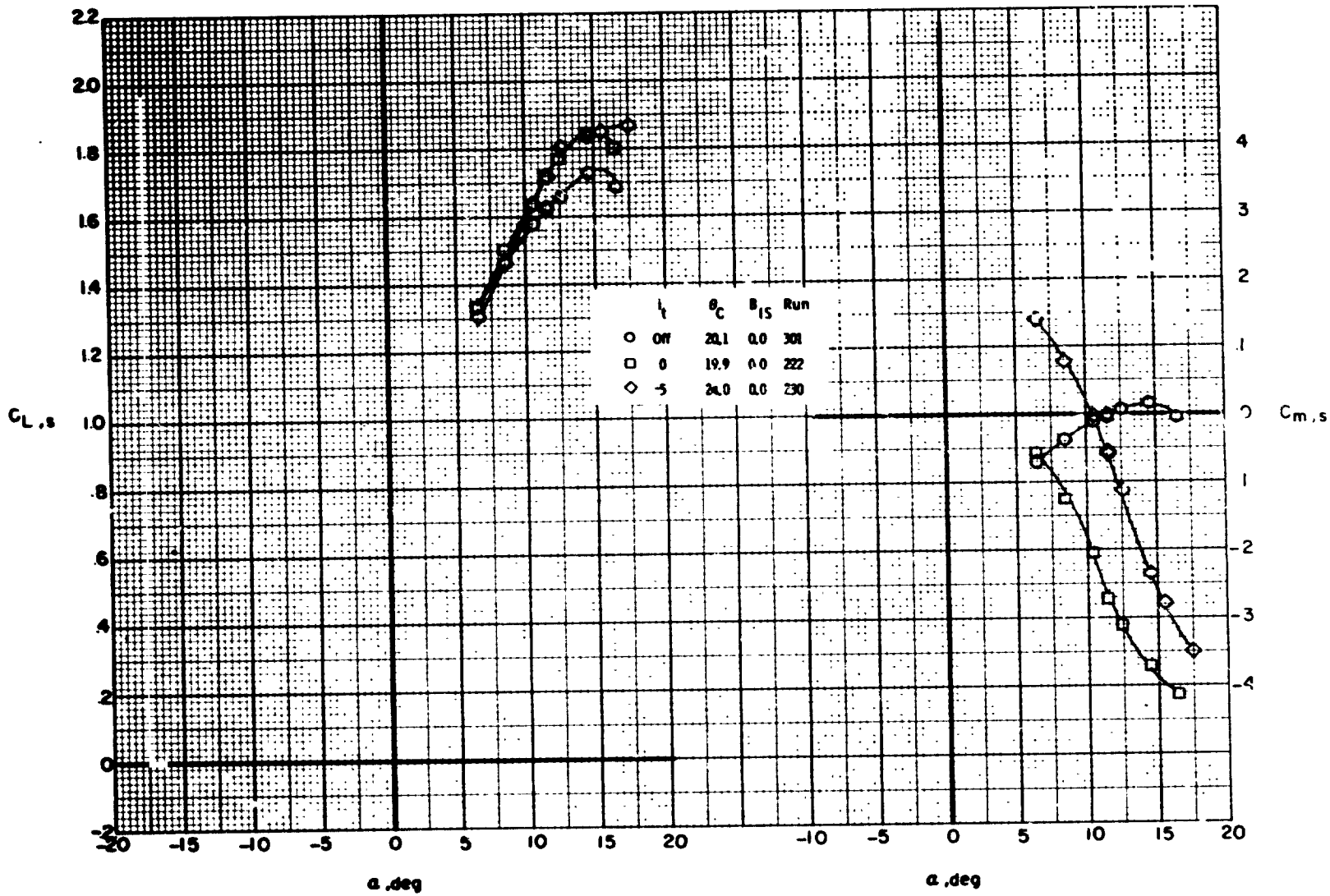

(a) $\mu = 0.34$

Figure 37. - Effect of angle of attack on the slipstream lift and pitching-moment coefficients with the horizontal tail on and off, $\alpha_p = 0^\circ$, $\delta_f = 50^\circ$, $\beta_s = 20^\circ$, cruise rotor speed.

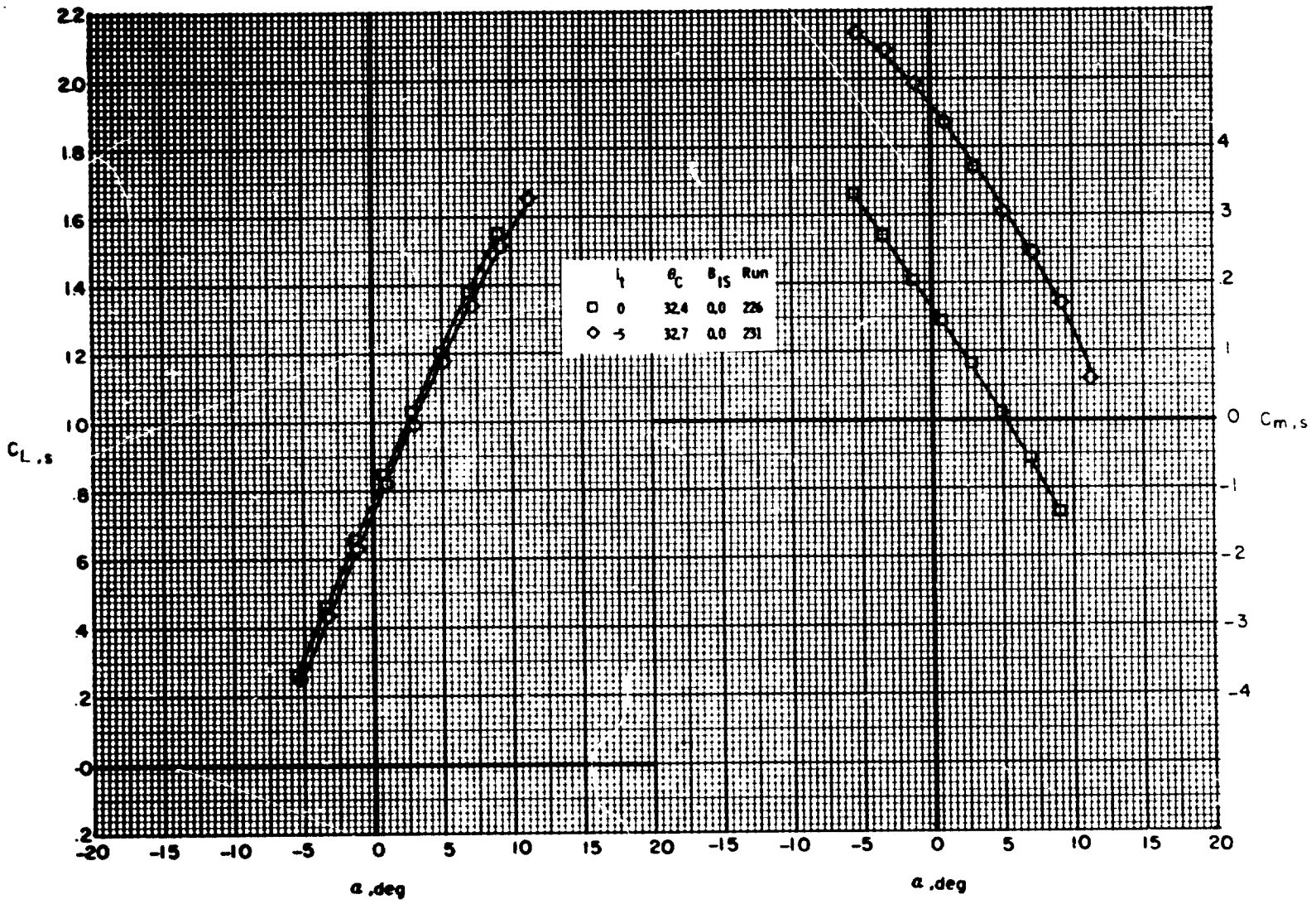

(b) $\mu = 0.50$

Figure 37. - Concluded.

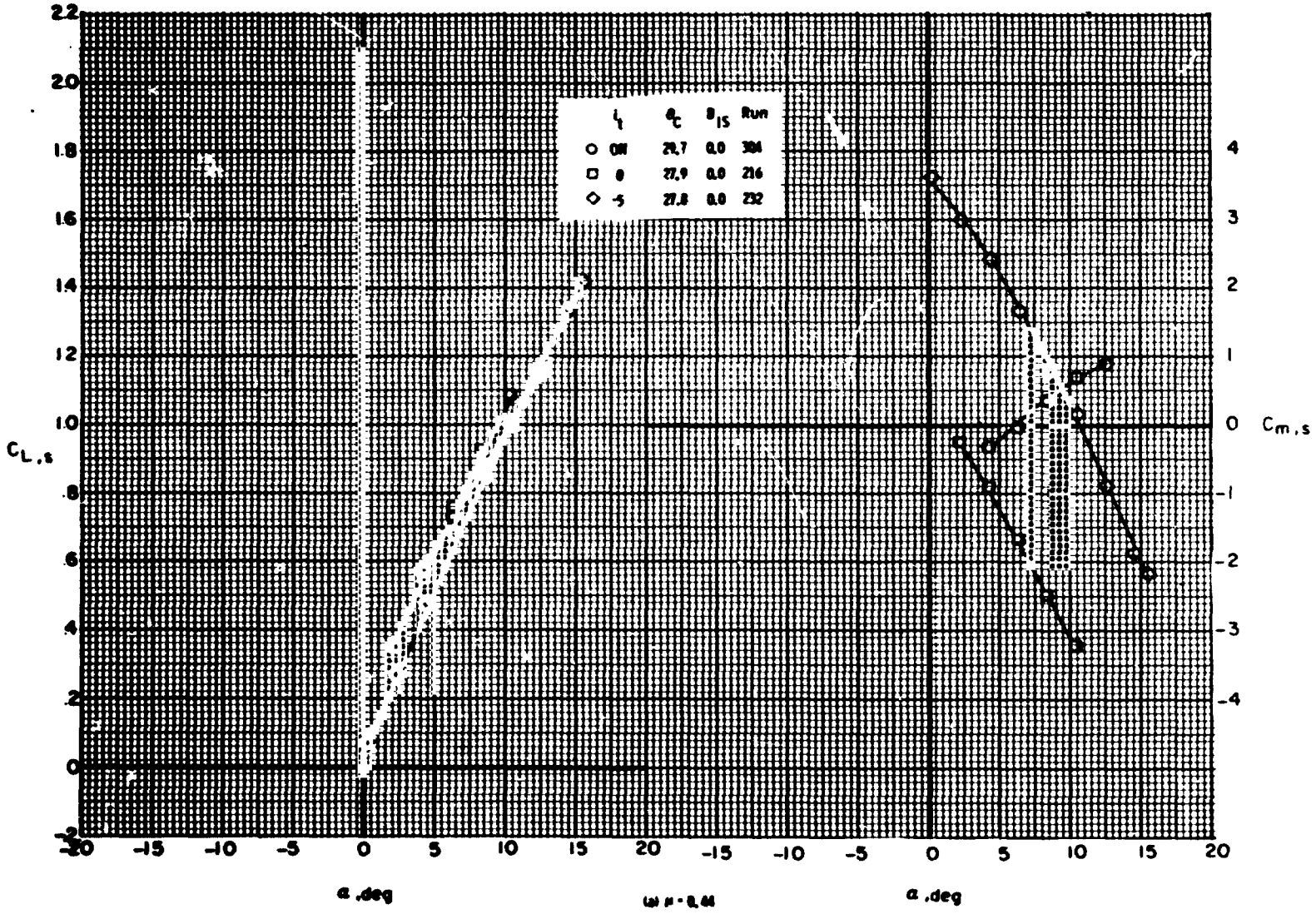

Figure 30. - Effect of angle of attack on the slipstream lift and pitching-moment coefficients with the horizontal tail on and off. α_p = 0°, δ_f = 0°, δ_a = 0°, cruise rotor speed.

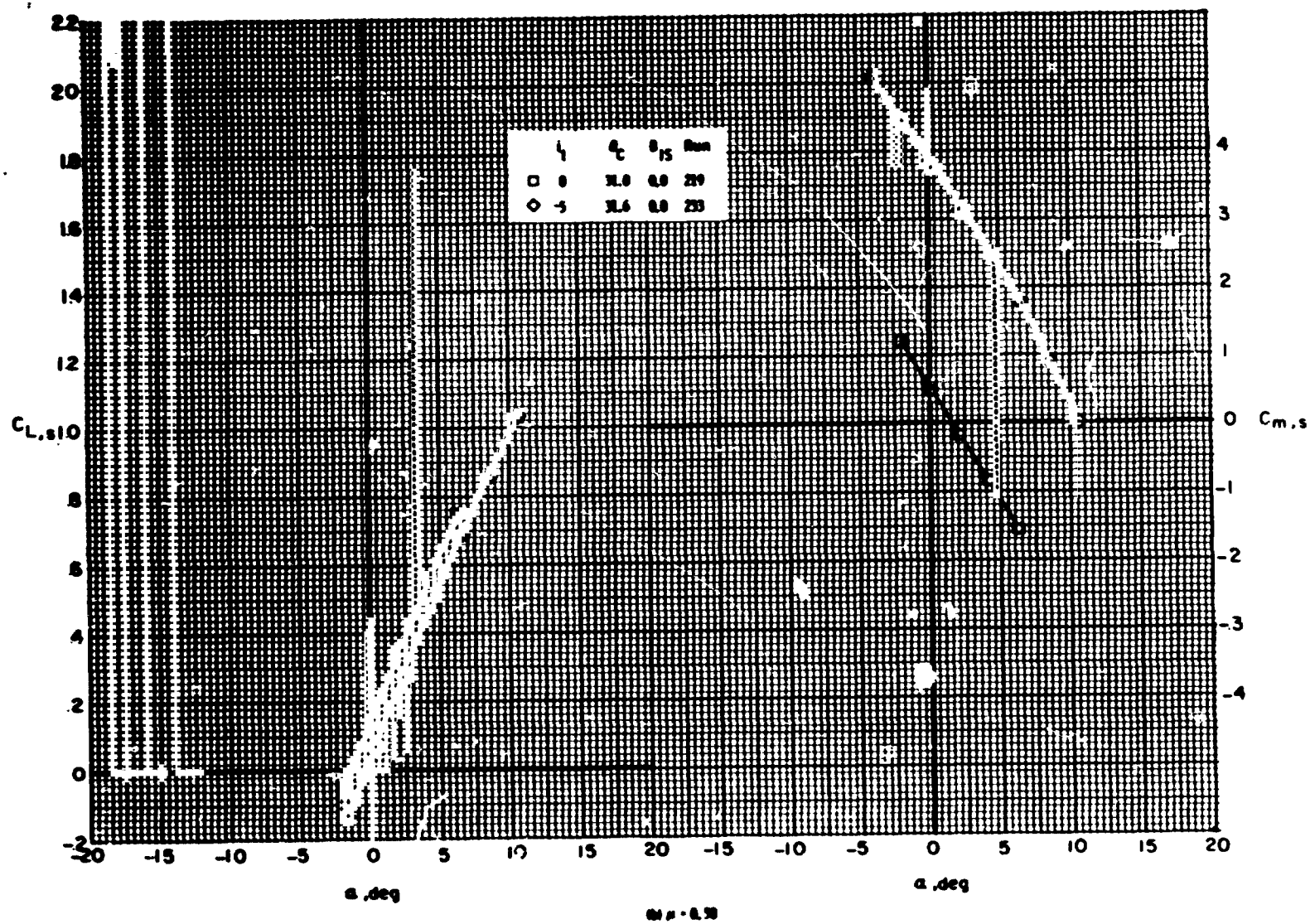

Figure 38. - Concluded.

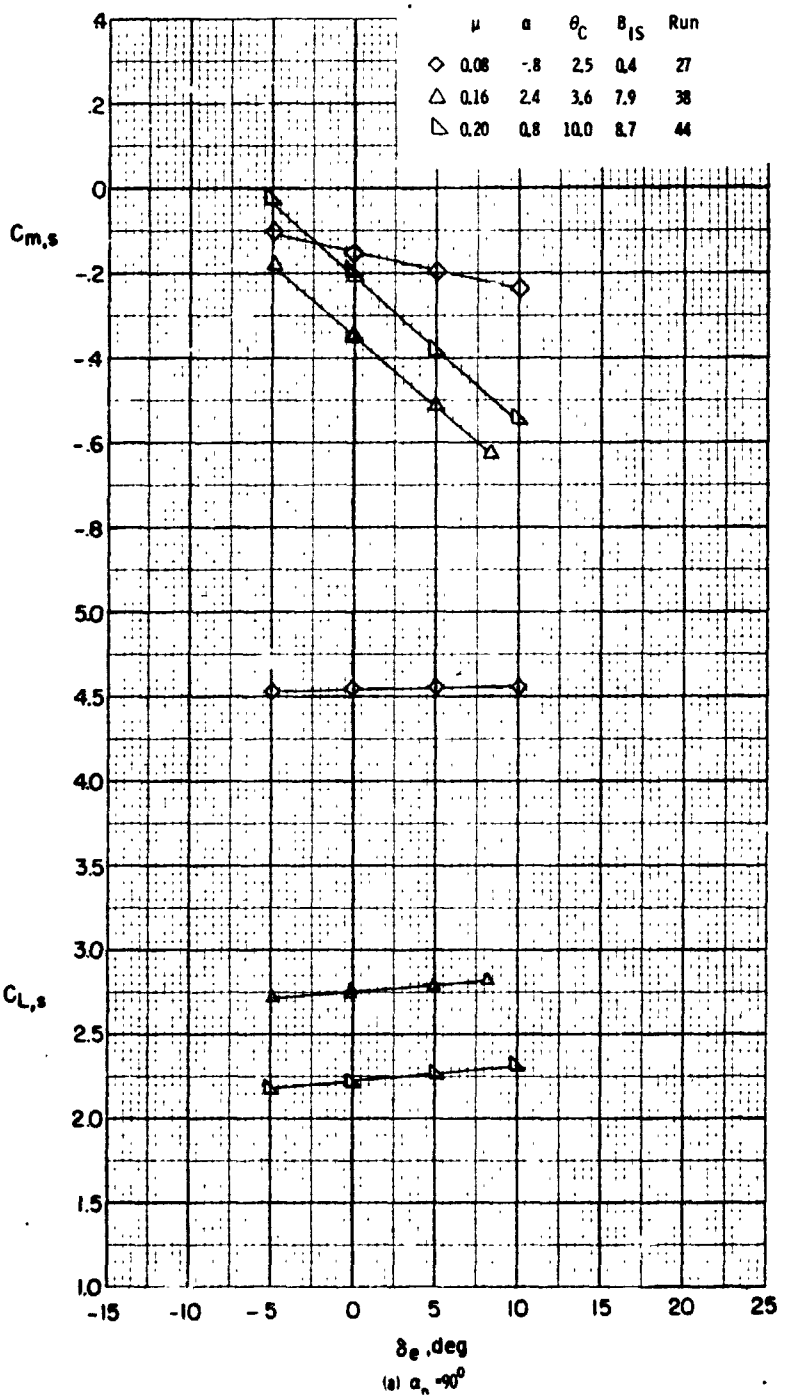

(a) $\alpha_n = 90^0$

Figure 39. - Effect of elevator deflection on the slipstream lift and pitching-moment coefficients for several wind speeds.

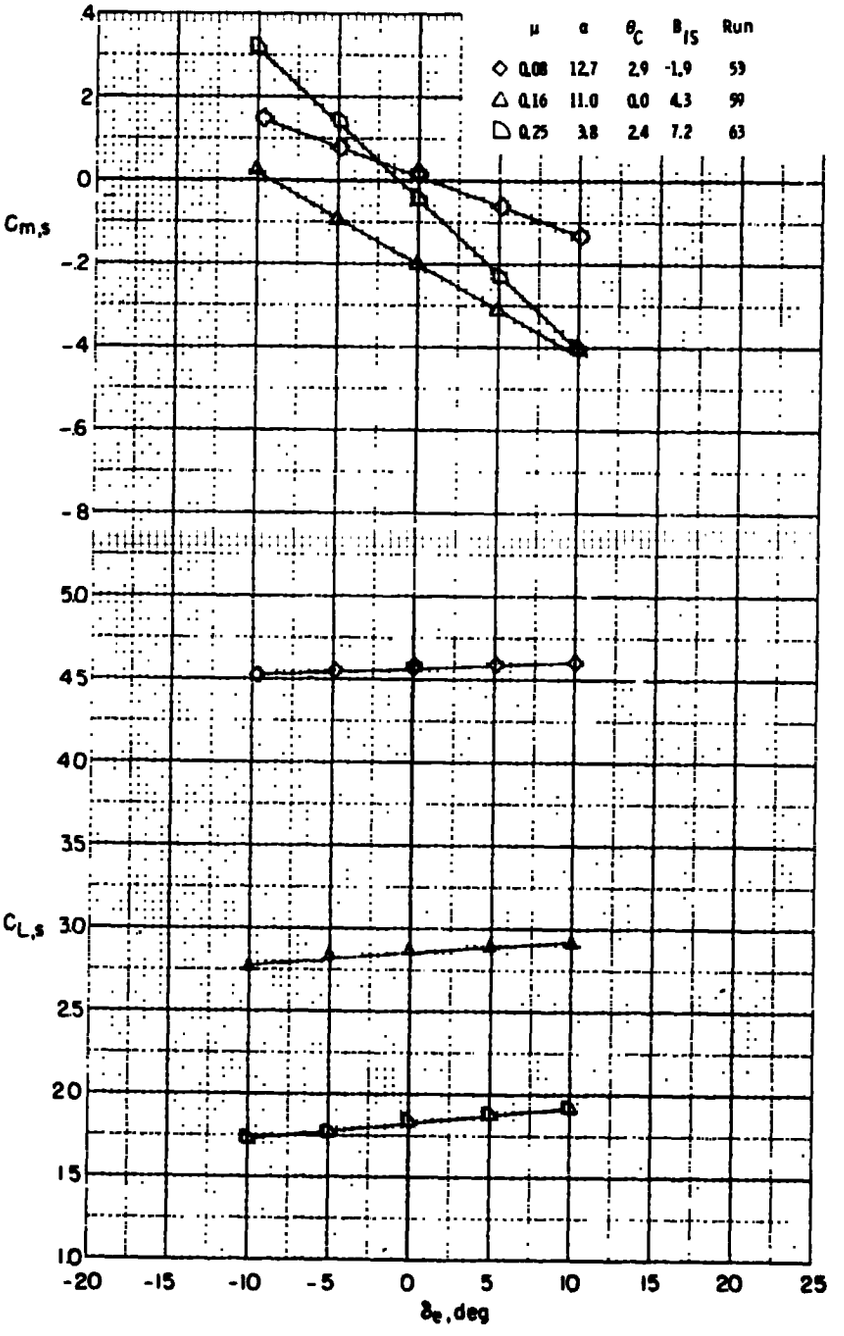

(b) $\alpha_p = 75^0$

Figure 39. - Continued.

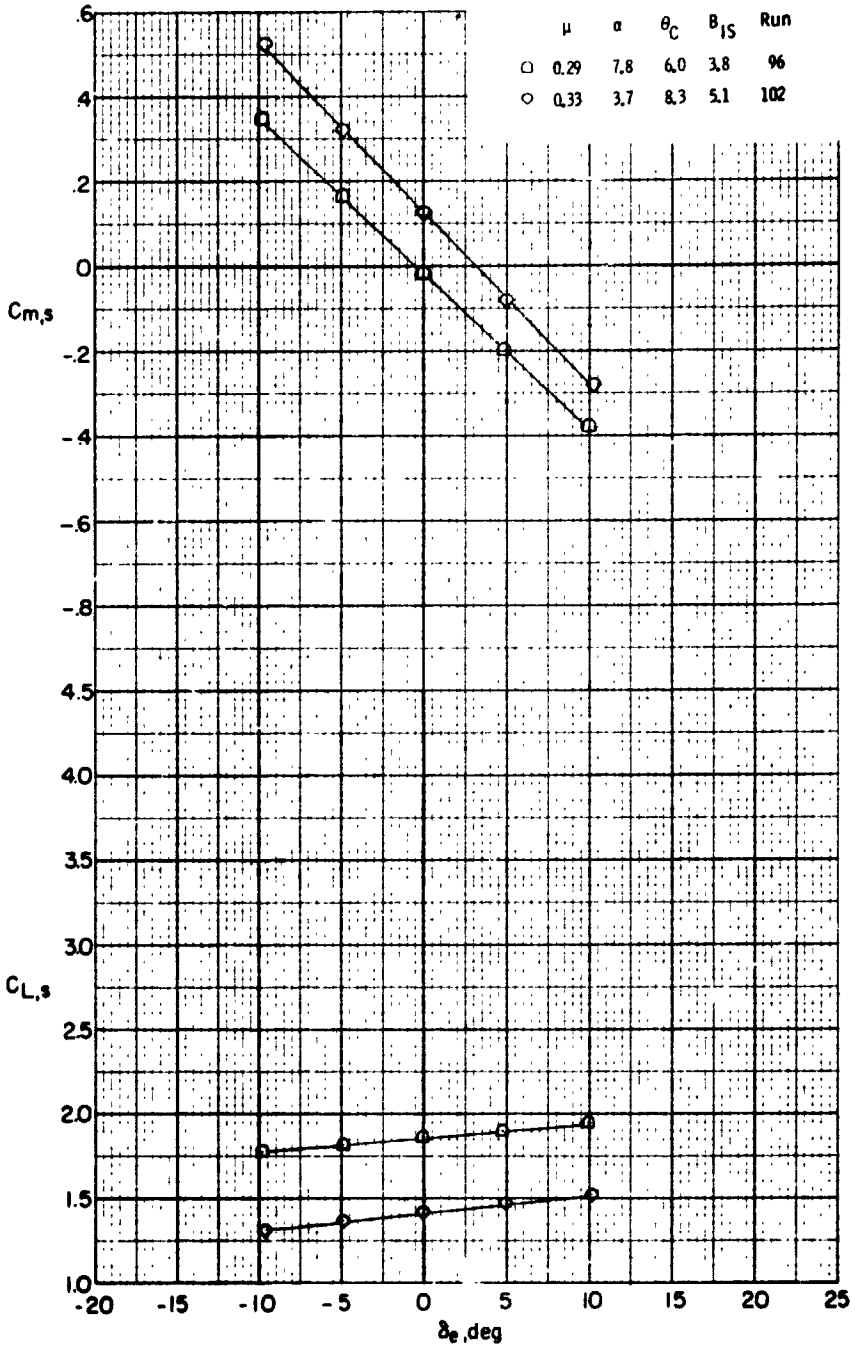

(c) $\alpha_p = 60^0$

Figure 39. - Continued.

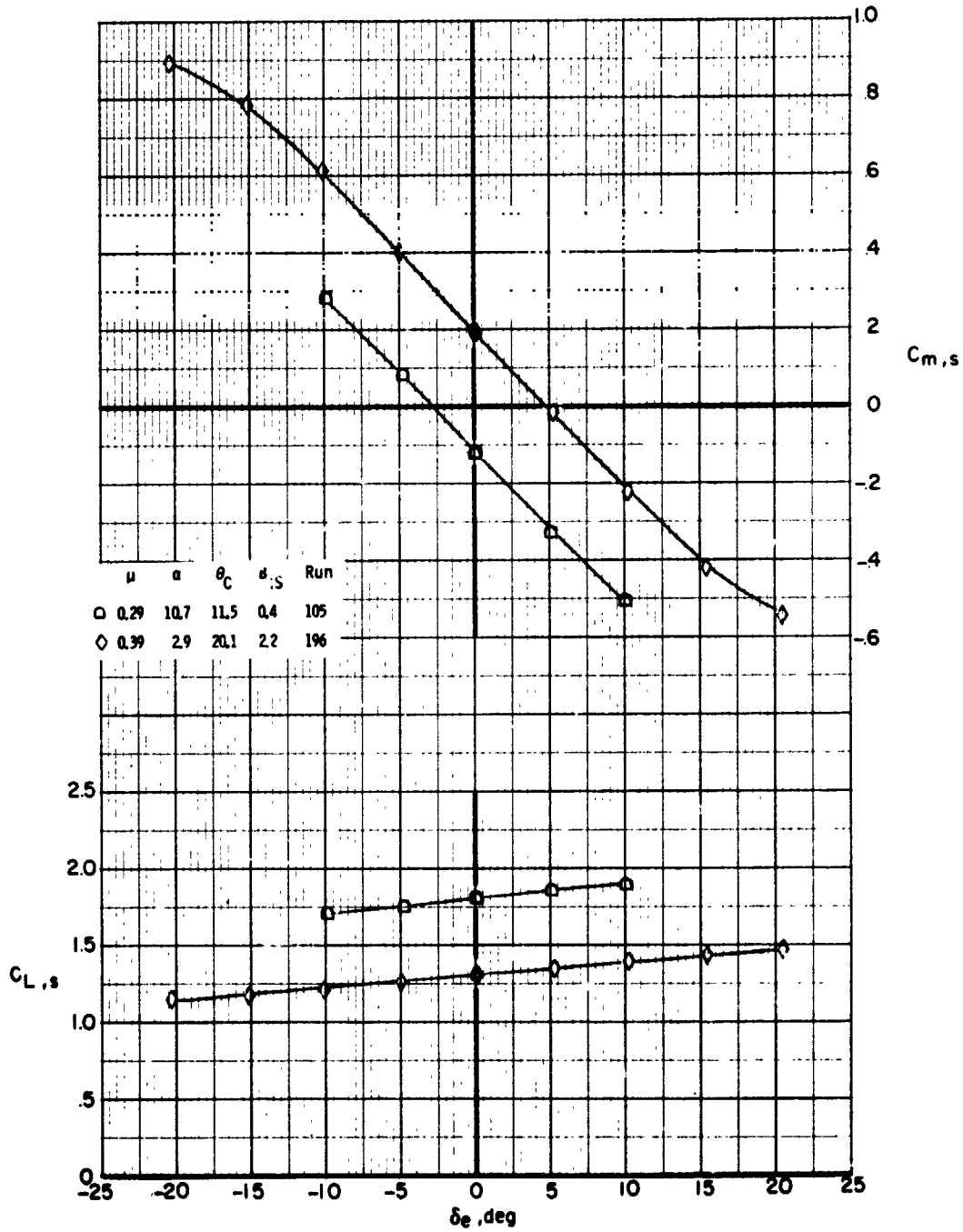

(d) $\alpha_p = 30^0$

Figure 39. - Continued.

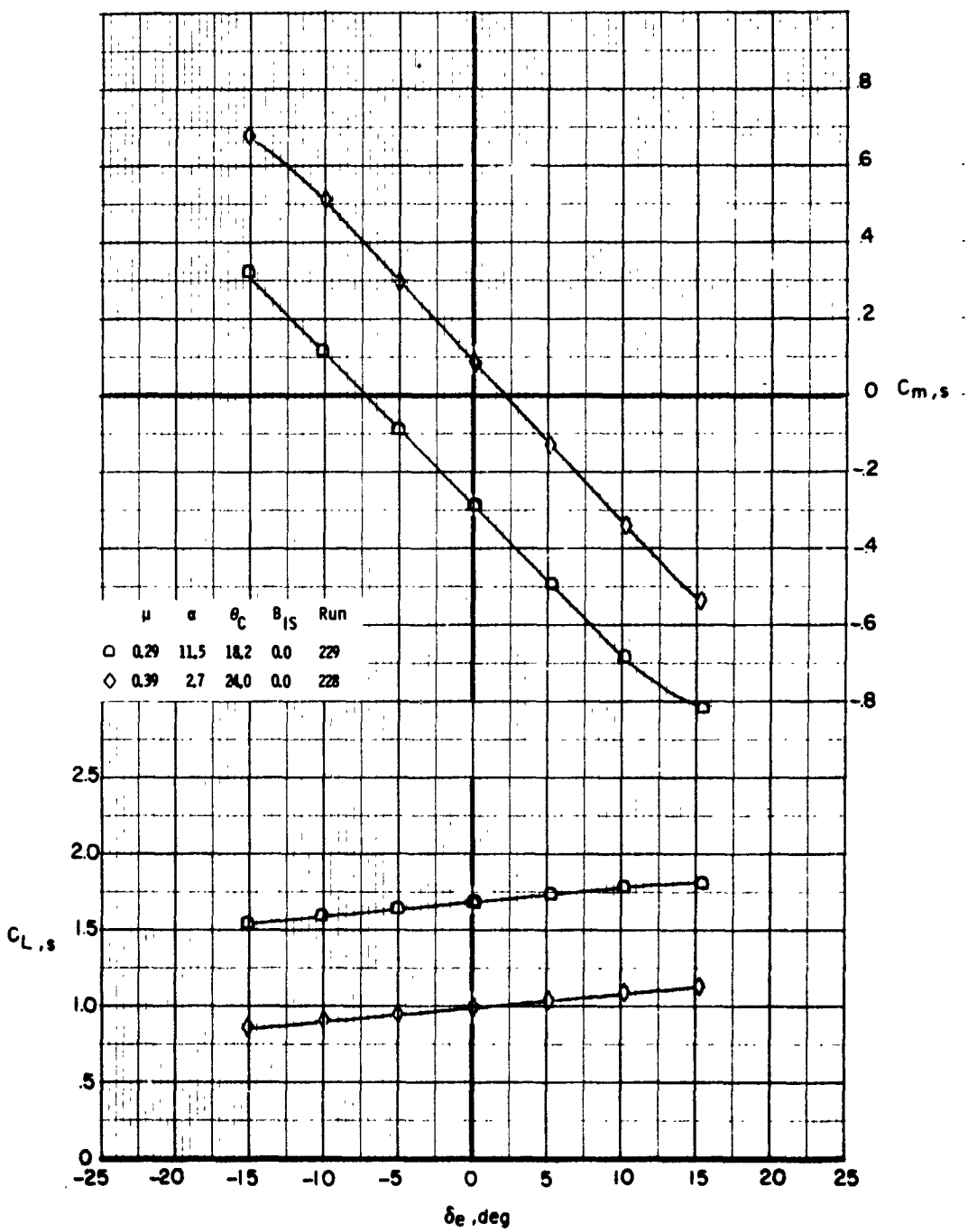

(e) $\alpha_p = 0^0$

Figure 39. - Concluded.

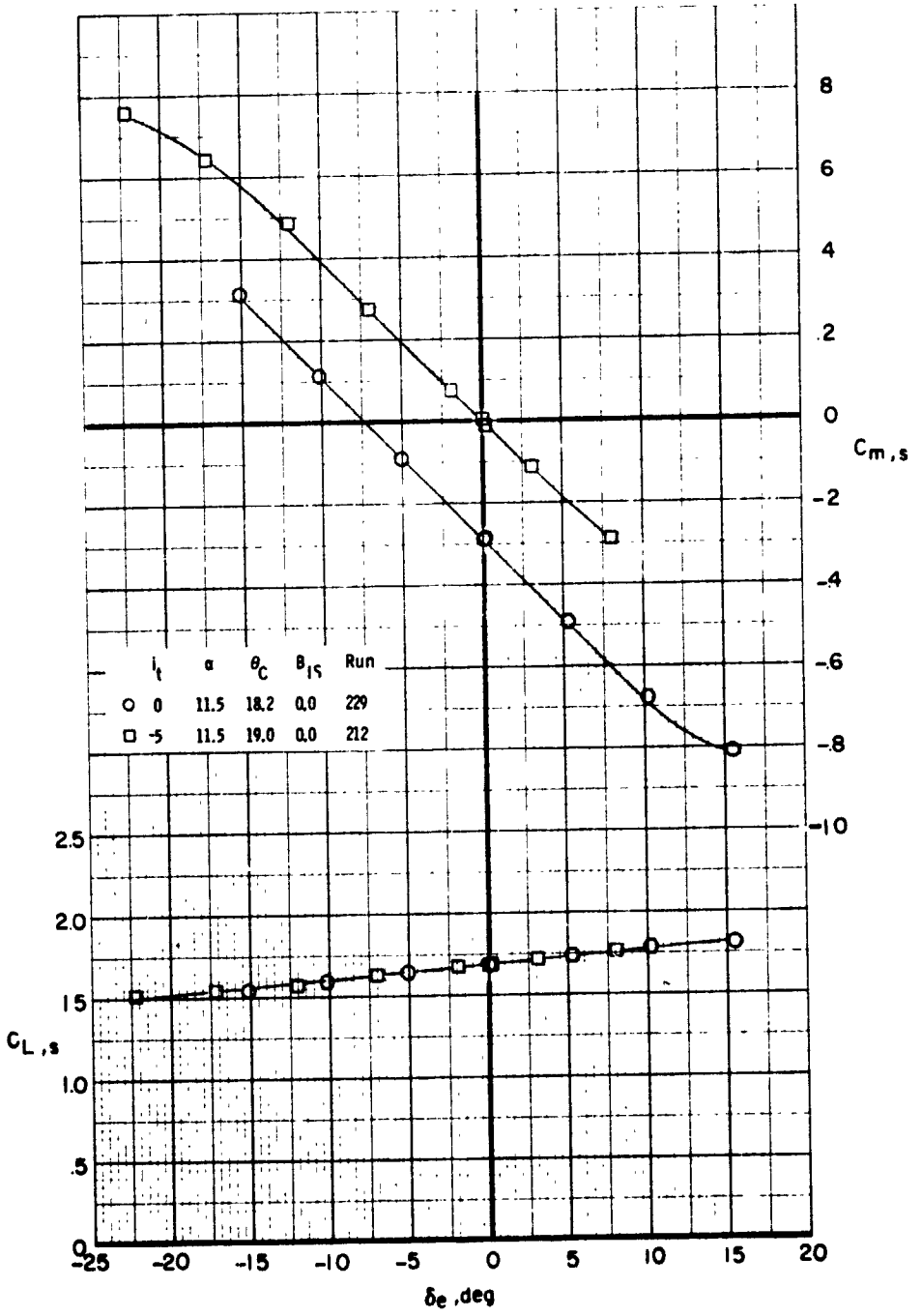

(a) $\mu = 0.29$

Figure 40. - Effect of elevator deflection on the slipstream lift and pitching-moment coefficients for two horizontal tail incidences, $\alpha_p = 90^0$.

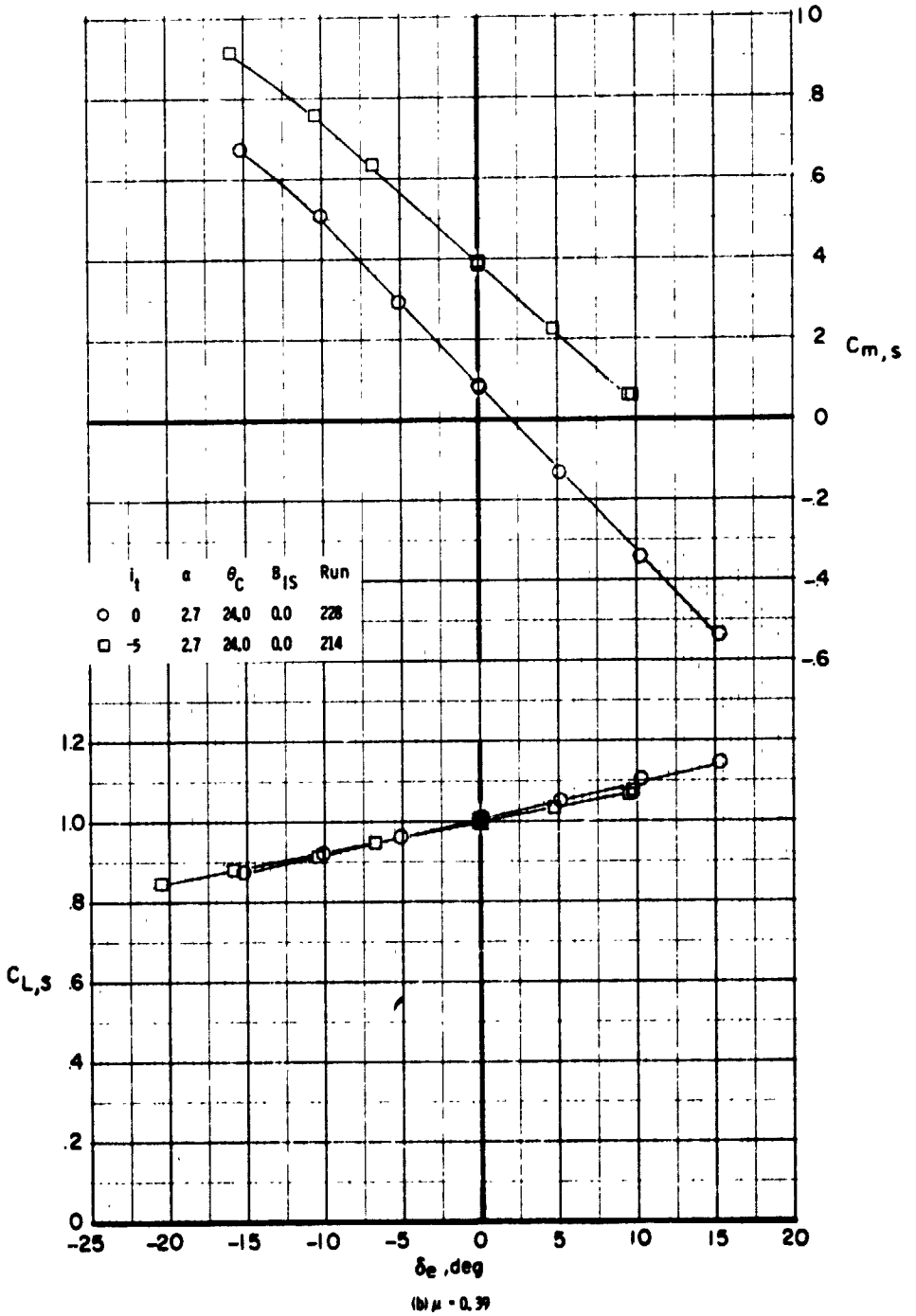

(b) μ = 0.39

Figure 40. - Concluded.

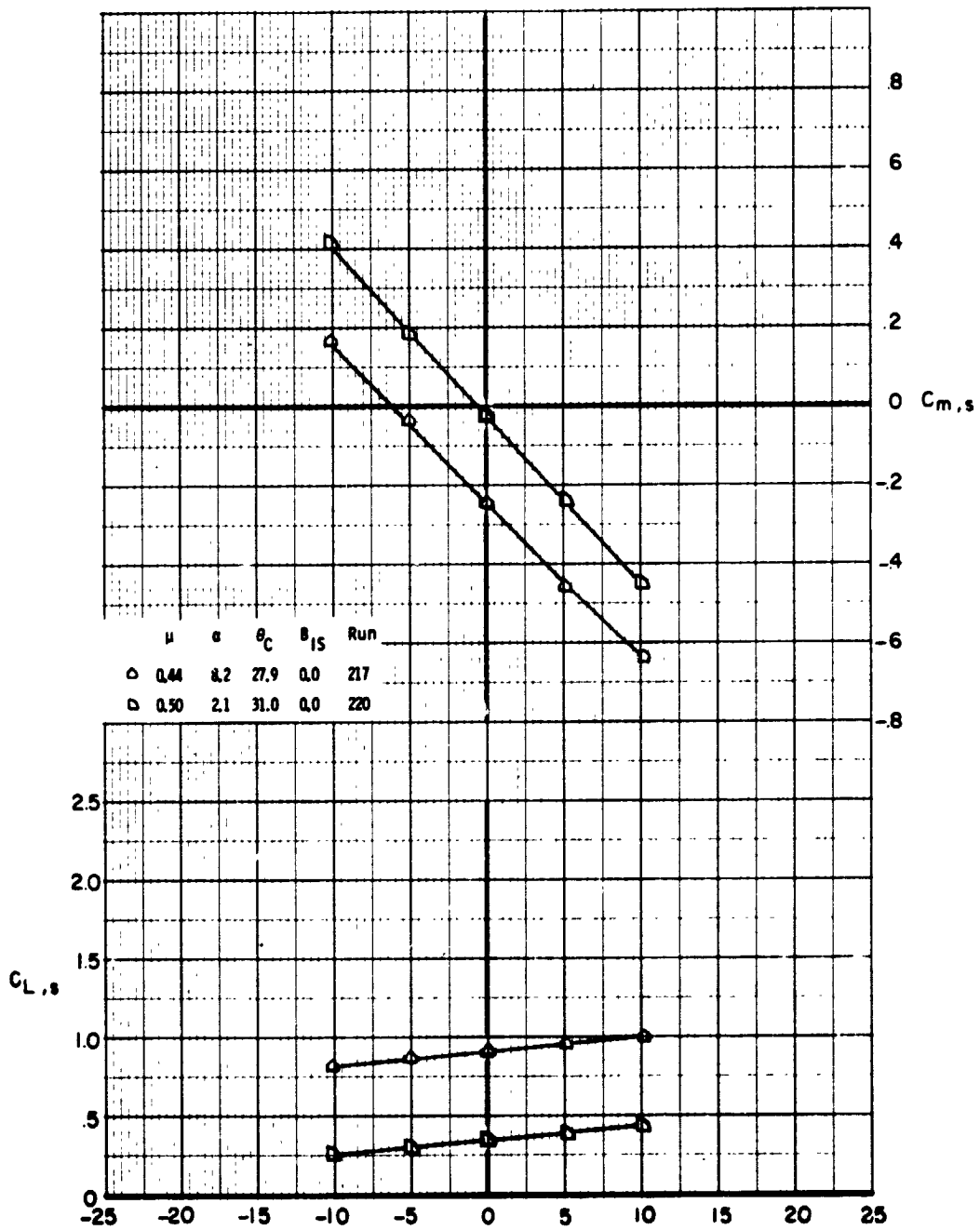

Figure 41. - Effect of elevator deflection on the slipstream lift and pitching-moment coefficient for several wind speeds, $\alpha_p = 0^\circ$, $\beta_f = 0^\circ$, $\beta_s = 0^\circ$.

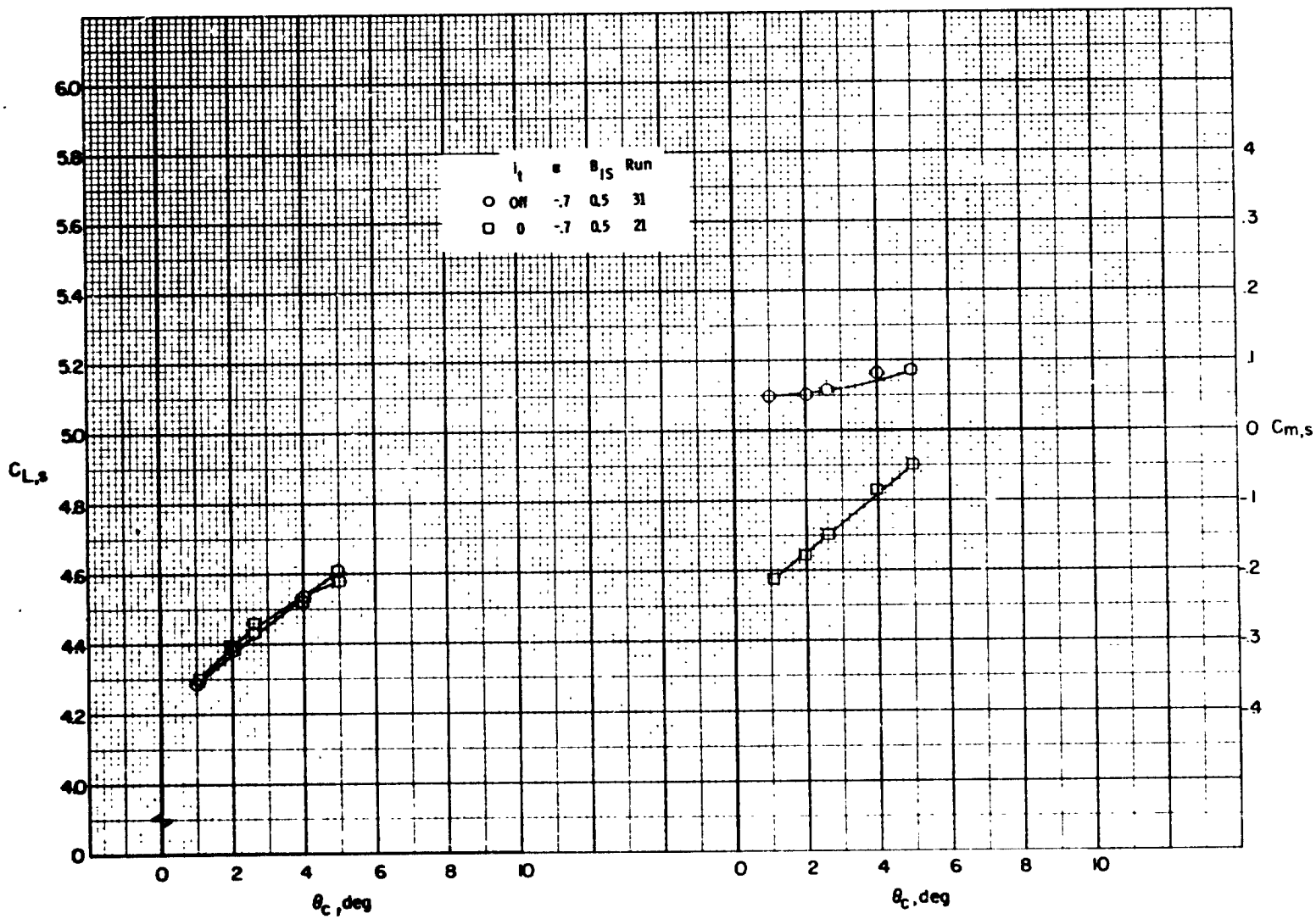

(a) $\mu_A = 0.08$

Figure 42. - Effect of collective pitch on the slipstream lift and pitching-moment coefficients with the horizontal tail on and off, $\alpha_p = 90^0$, $\delta_f = 50^0$, $\delta_a = 80^0$.

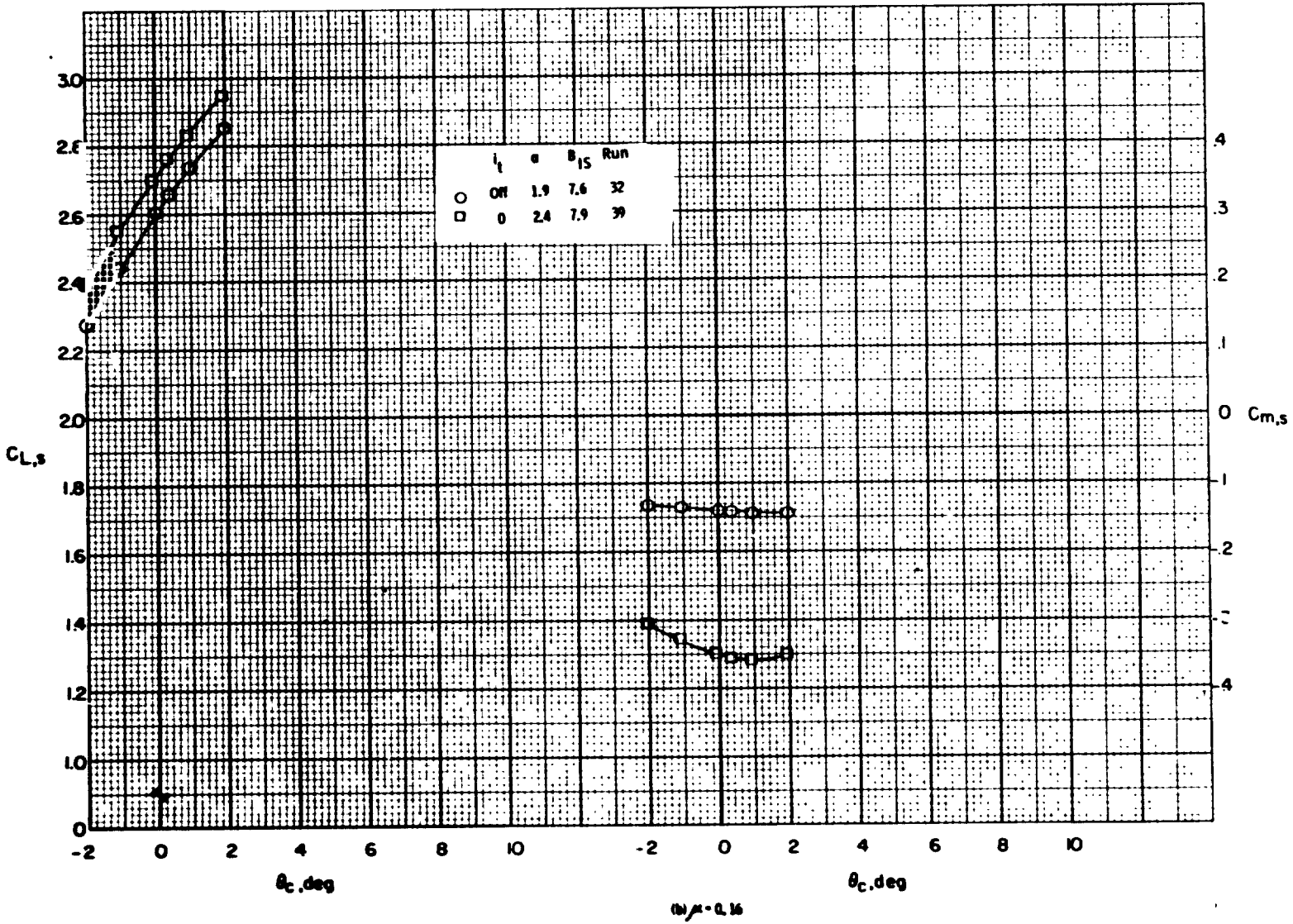

(b) $\mu = 0.16$

Figure 42. - Continued.

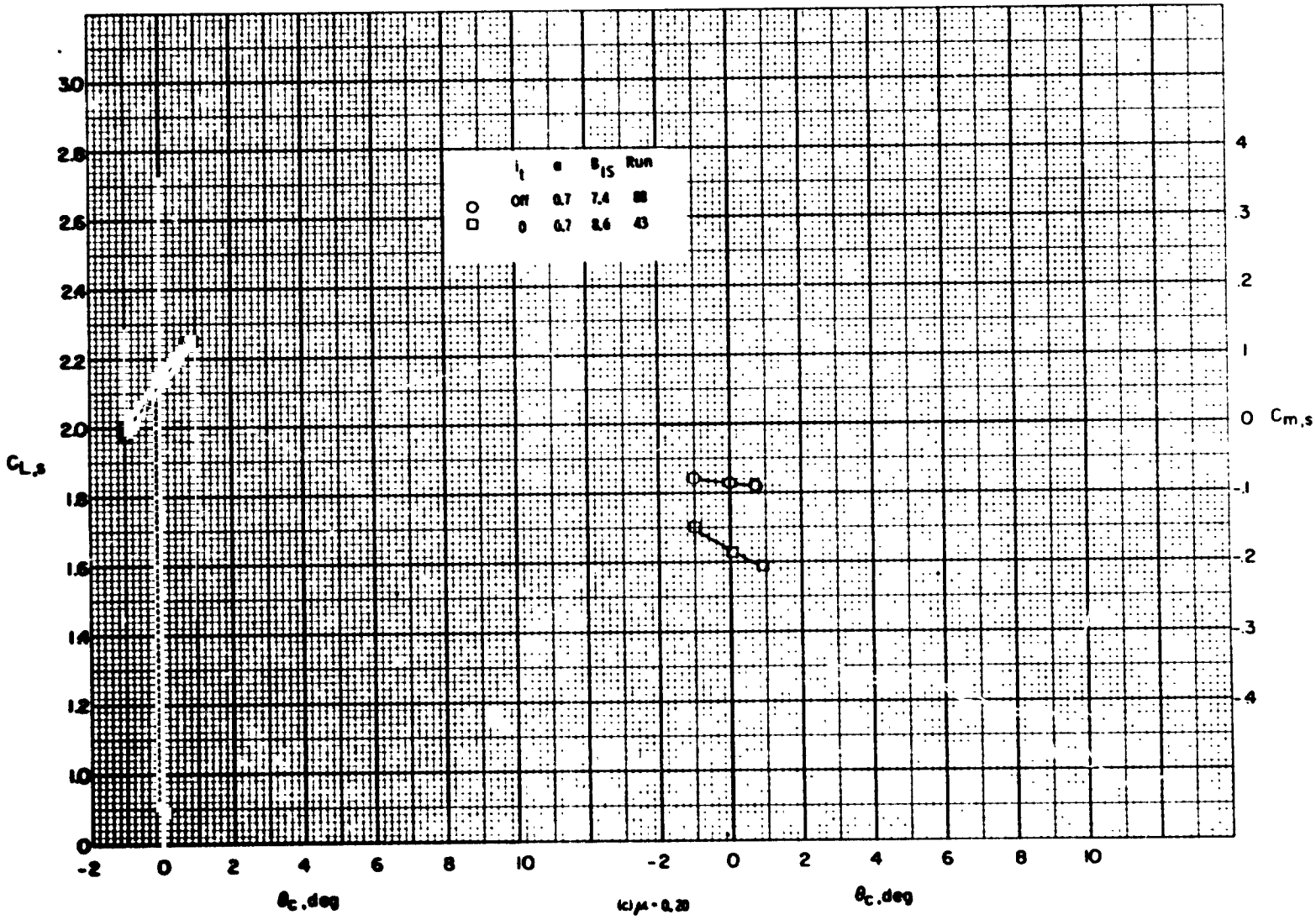

Figure 42. - Concluded.

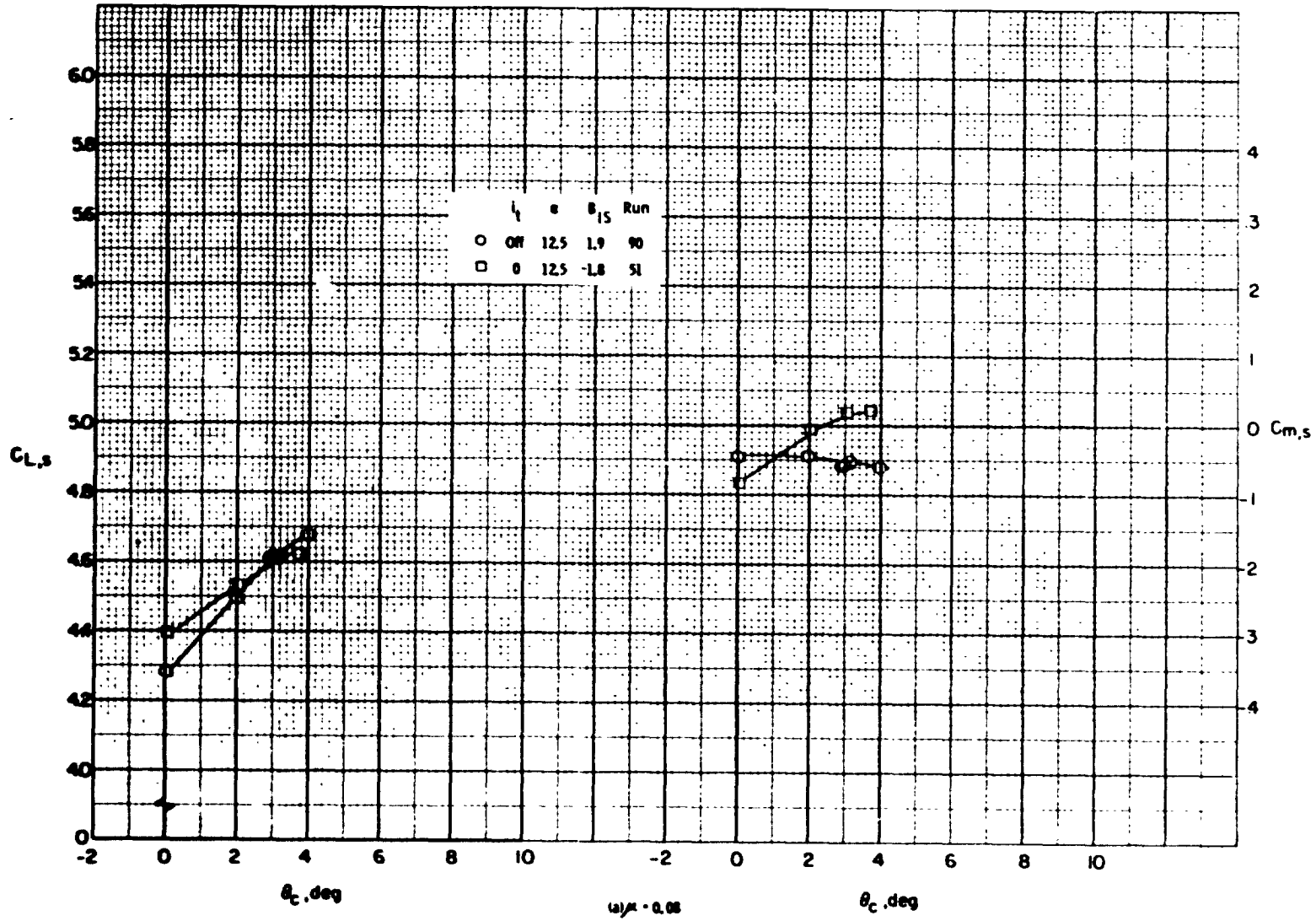

Figure 43. - Effect of collective pitch on the slipstream lift and pitching-moment coefficients with the horizontal tail on and off. $\alpha_p = 75°$, $\delta_f = 50°$, $\delta_a = 20°$.

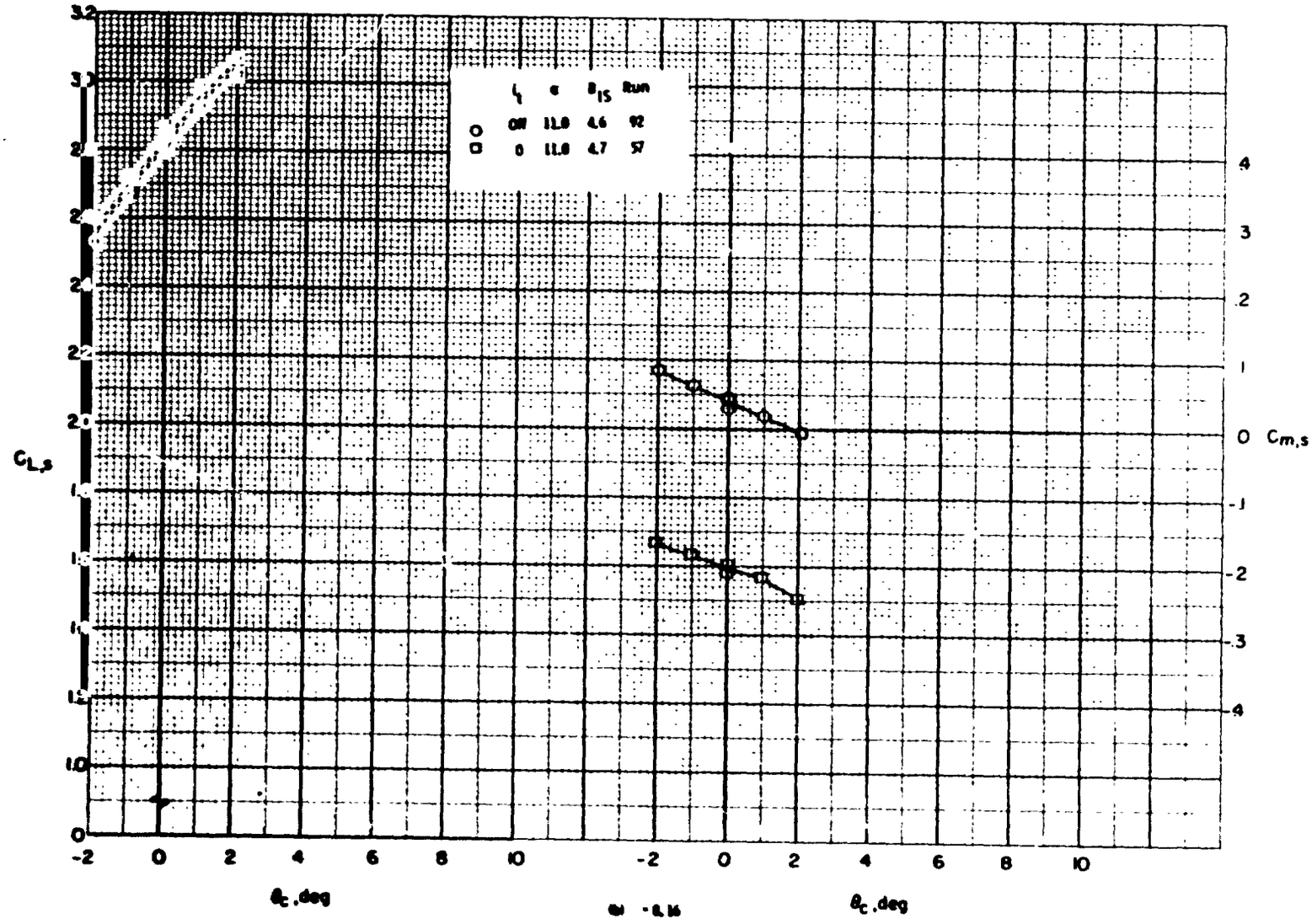

Figure 43. - Continued.

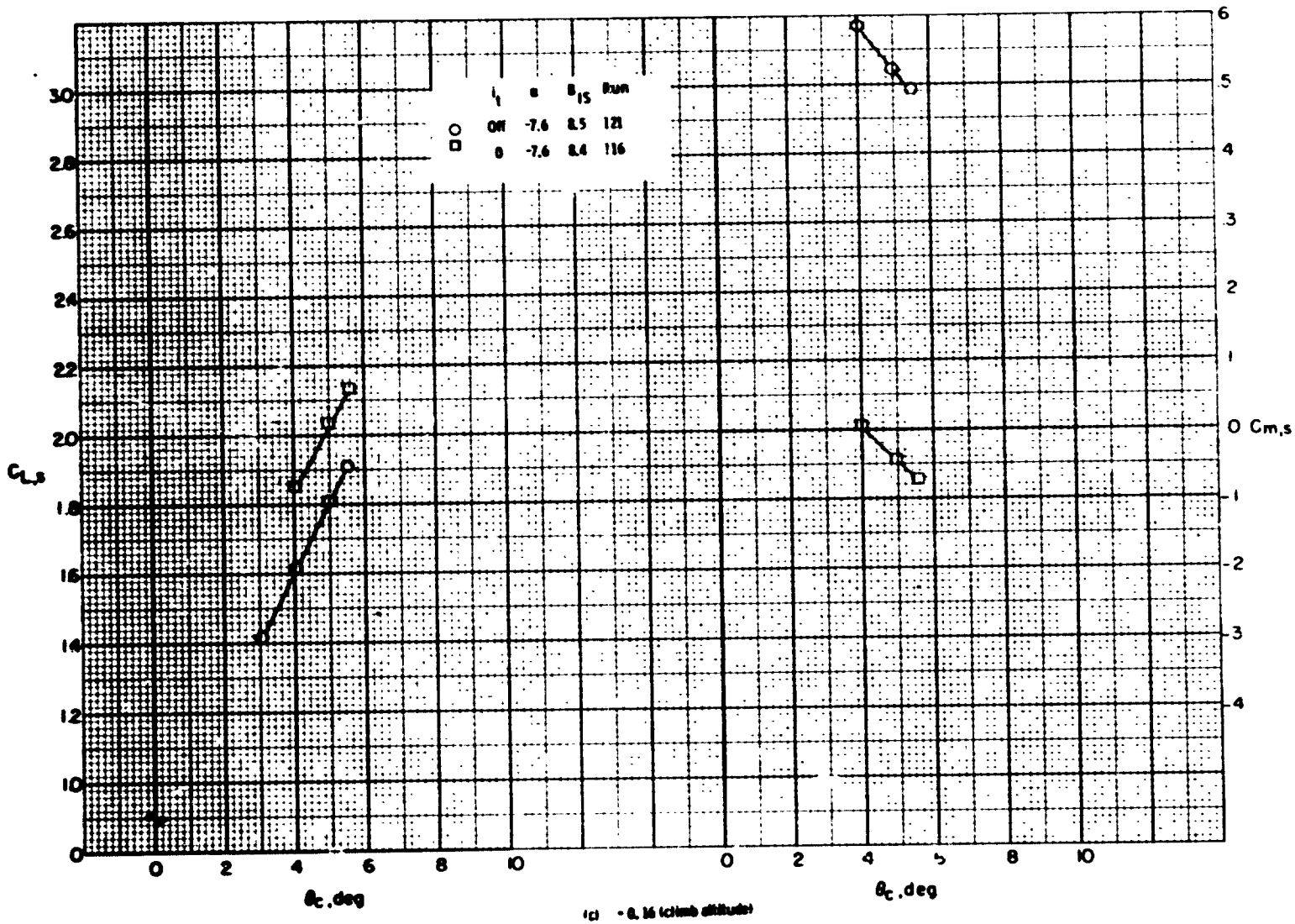

(c) δ_e 16 (climb attitude)

Figure 43. - Continued.

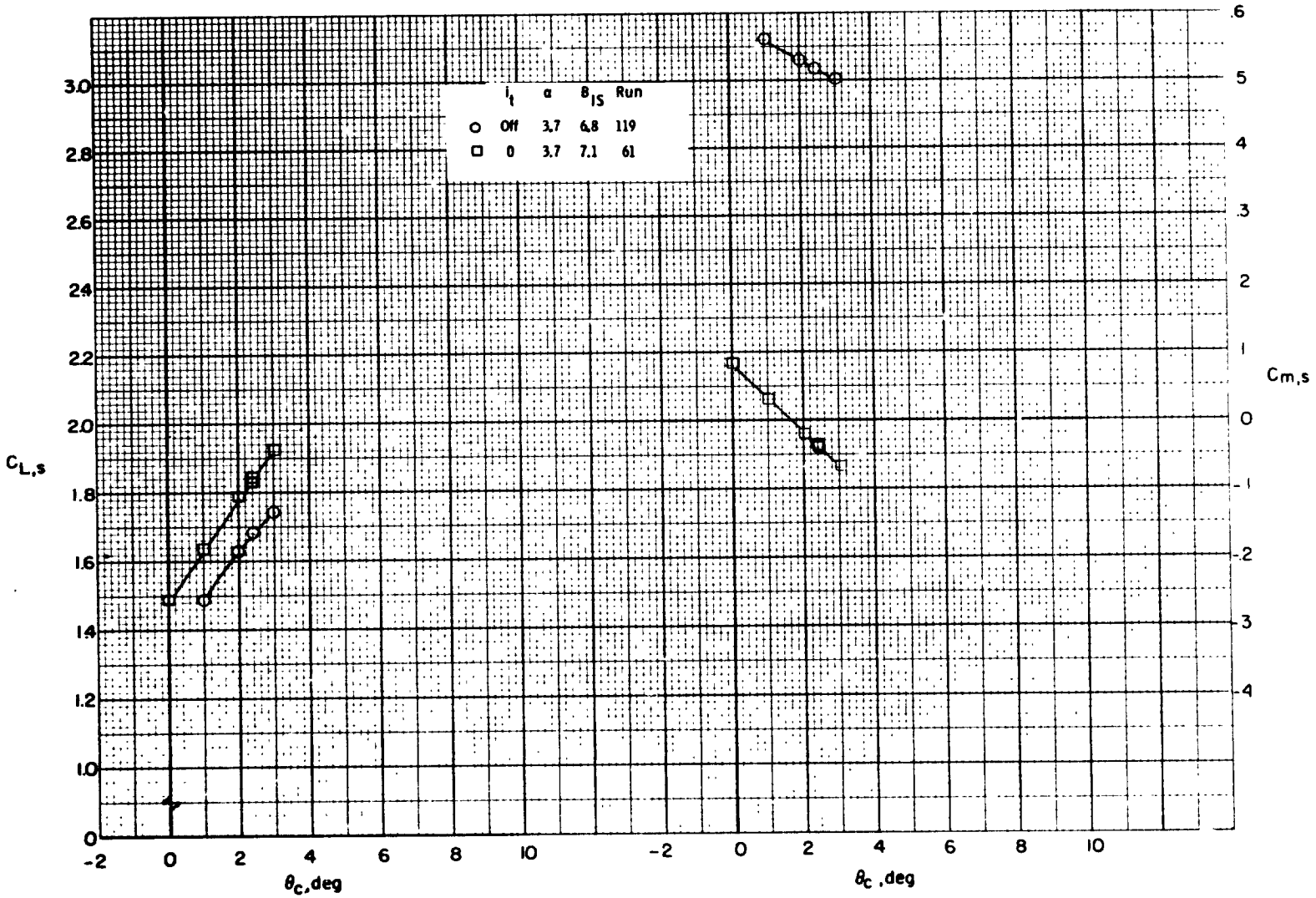

(d) $\bar{c} = 0.25$

Figure 43. - Concluded.

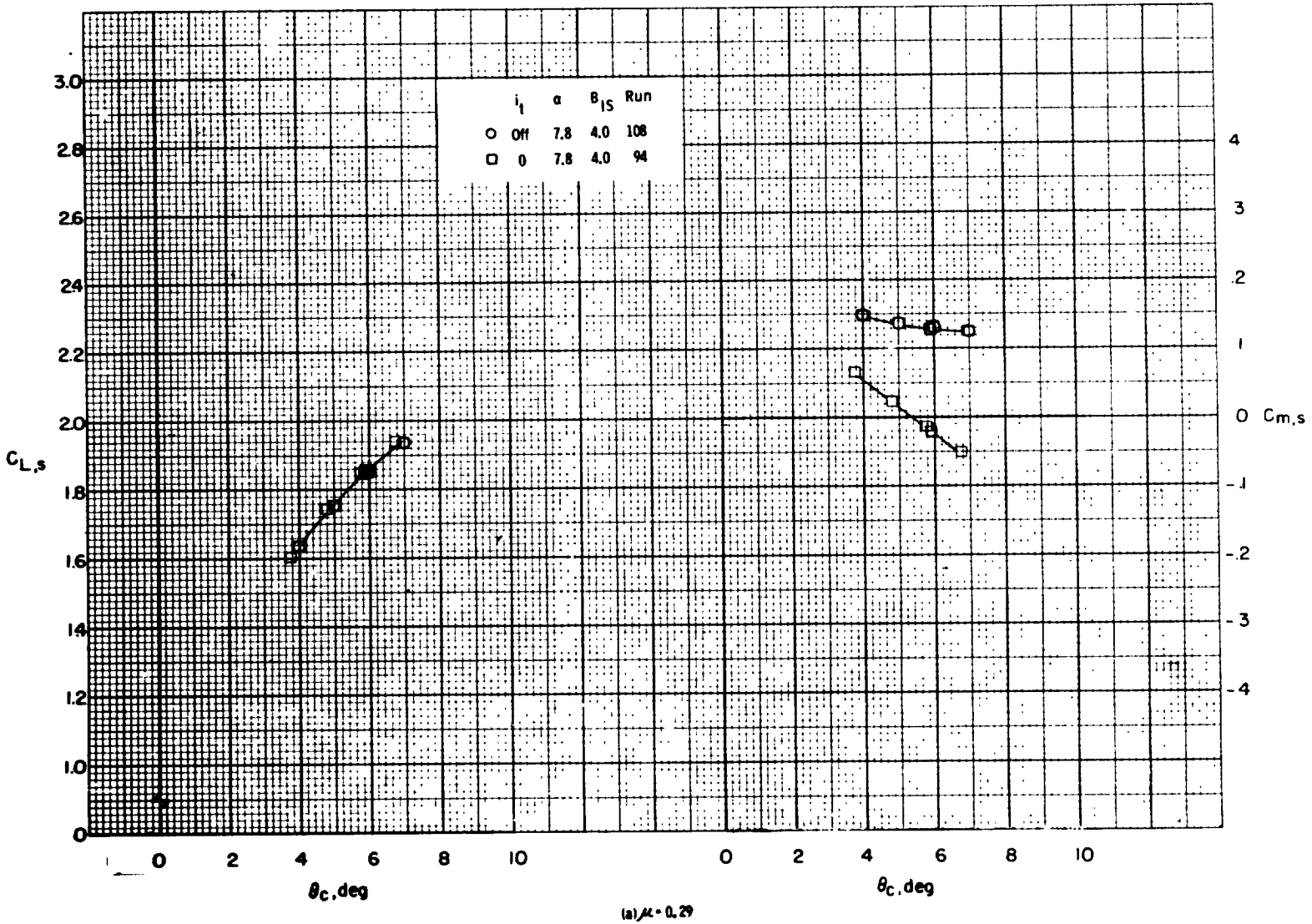

(a) $\mu = 0.29$

Figure 44. - Effect of collective pitch on the slipstream lift and pitching-moment coefficients with the horizontal tail on and off, $\alpha_p = 60^0$, $\beta_f = 50^0$, $\beta_a = 20^0$.

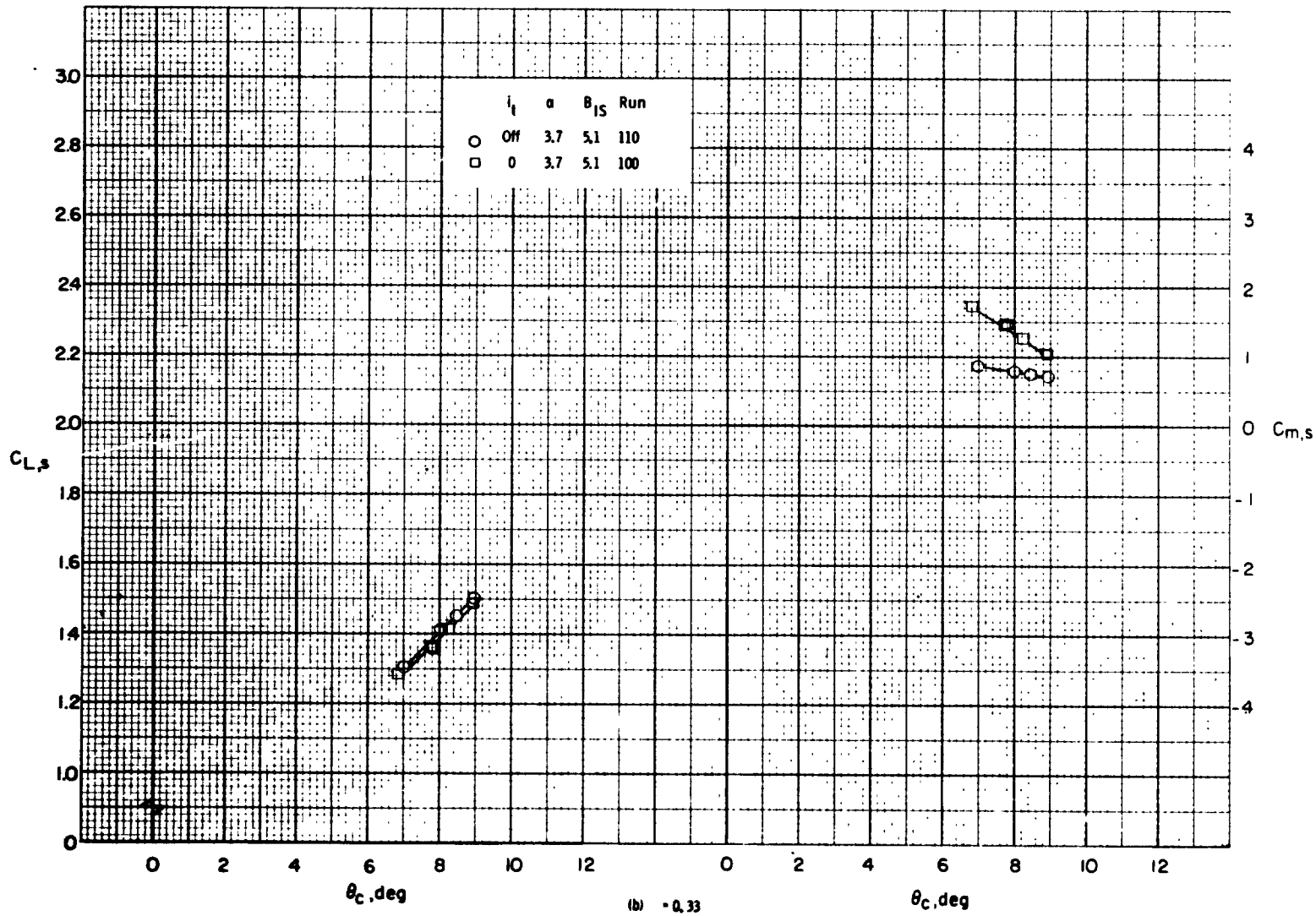

(b) $\bar{x} = 0.33$

Figure 44. - Concluded.

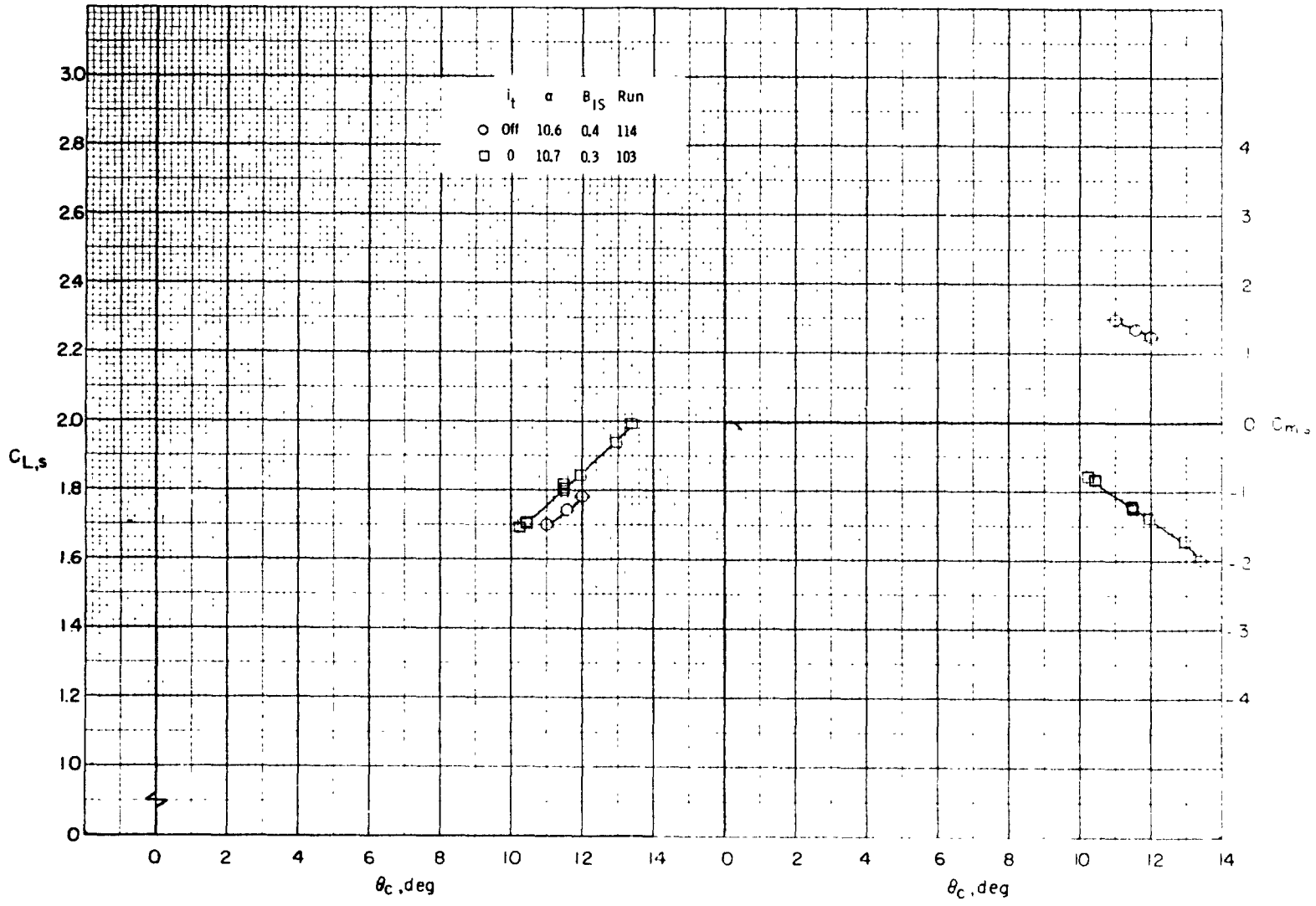

Figure 45. - Effect of collective pitch on the slipstream lift and pitching-moment coefficients with the horizontal tail on and off, $\alpha_p = 30^0$, $\delta_f = 50^0$, $\delta_a = 20^0$, $\mu = 0.29$.

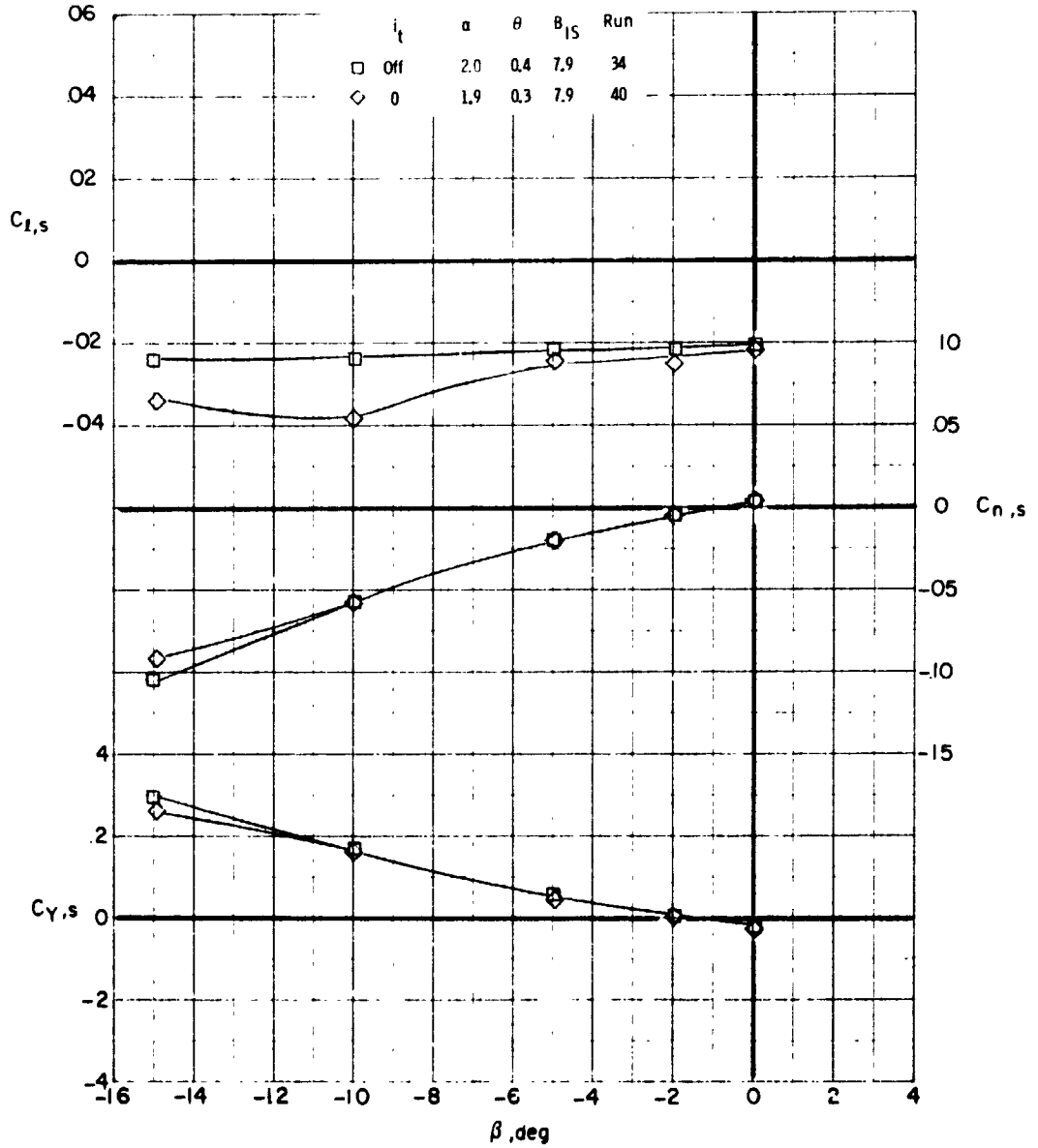

Figure 46. - Effect of sideslip angle on the lateral aerodynamic characteristics with the horizontal tail on and off at a full-scale flight speed of 80 knots, $\mu = 0.16$, $\alpha_p = 90^0$.

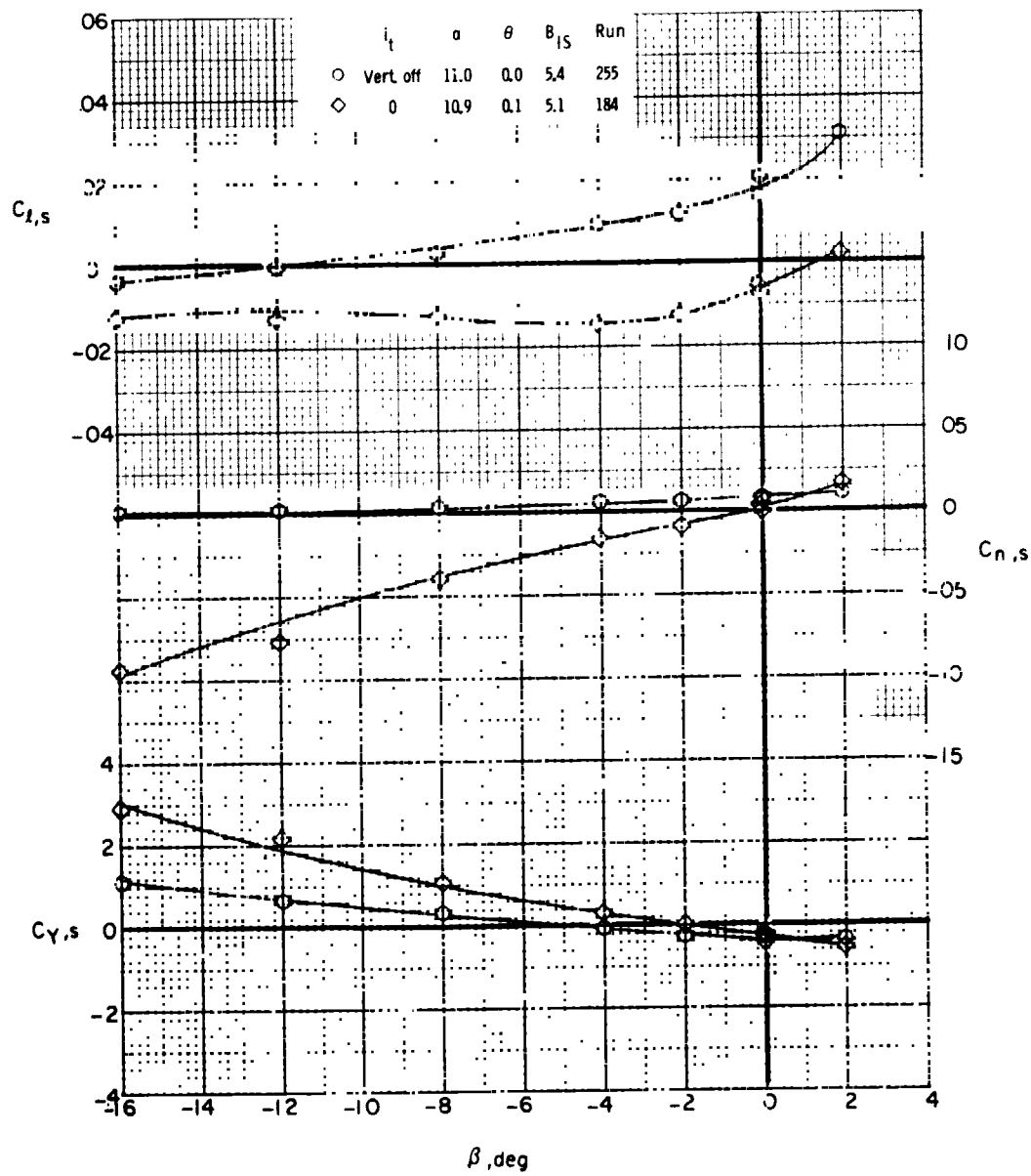

Figure 47. - Effect of sideslip angle on the lateral aerodynamic characteristics with the vertical tail on and off at a full-scale flight speed of 80 knots, $\alpha_p = 75^0$.

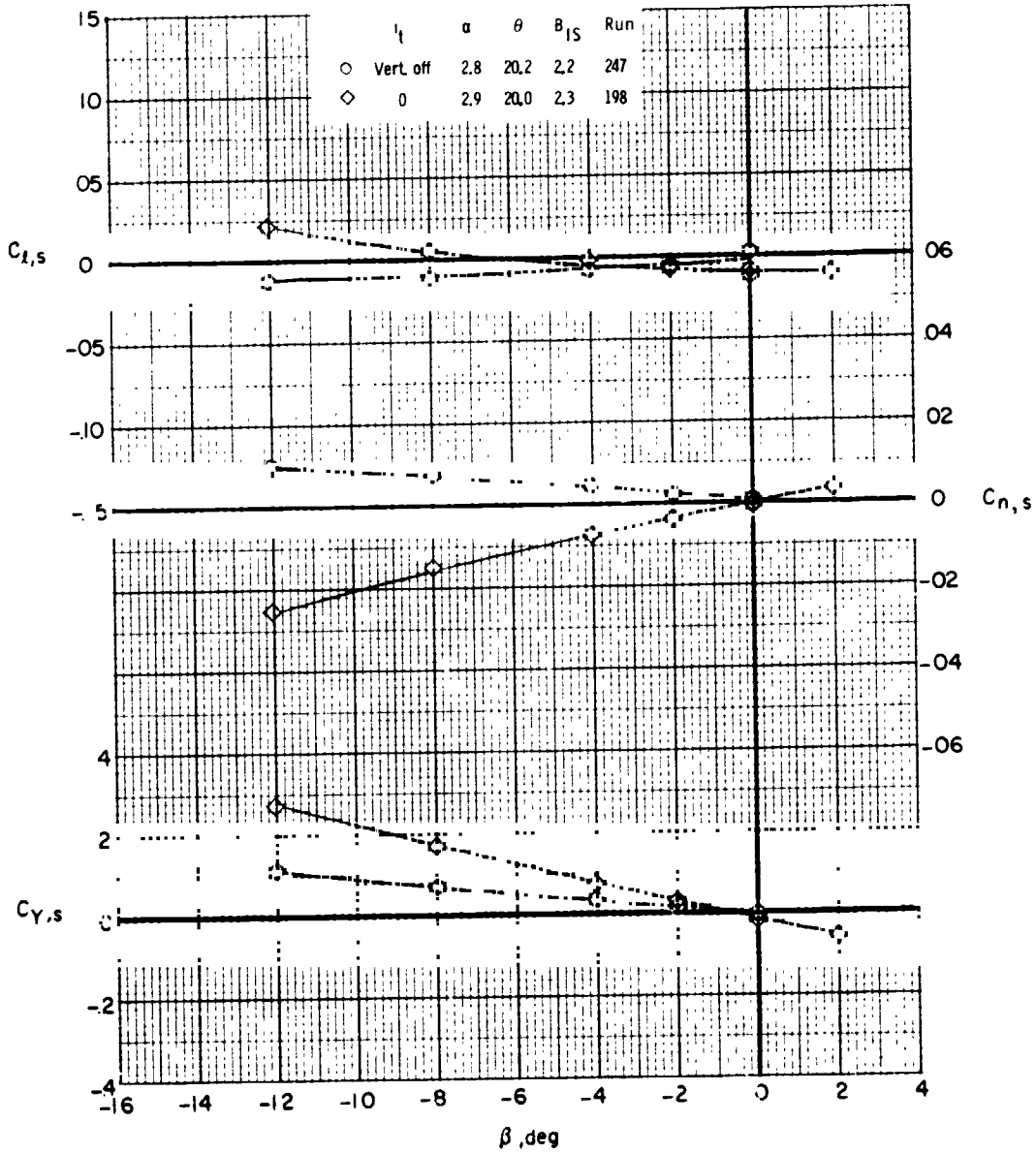

(b) $\mu = 0.39$

Figure 47. - Concluded.

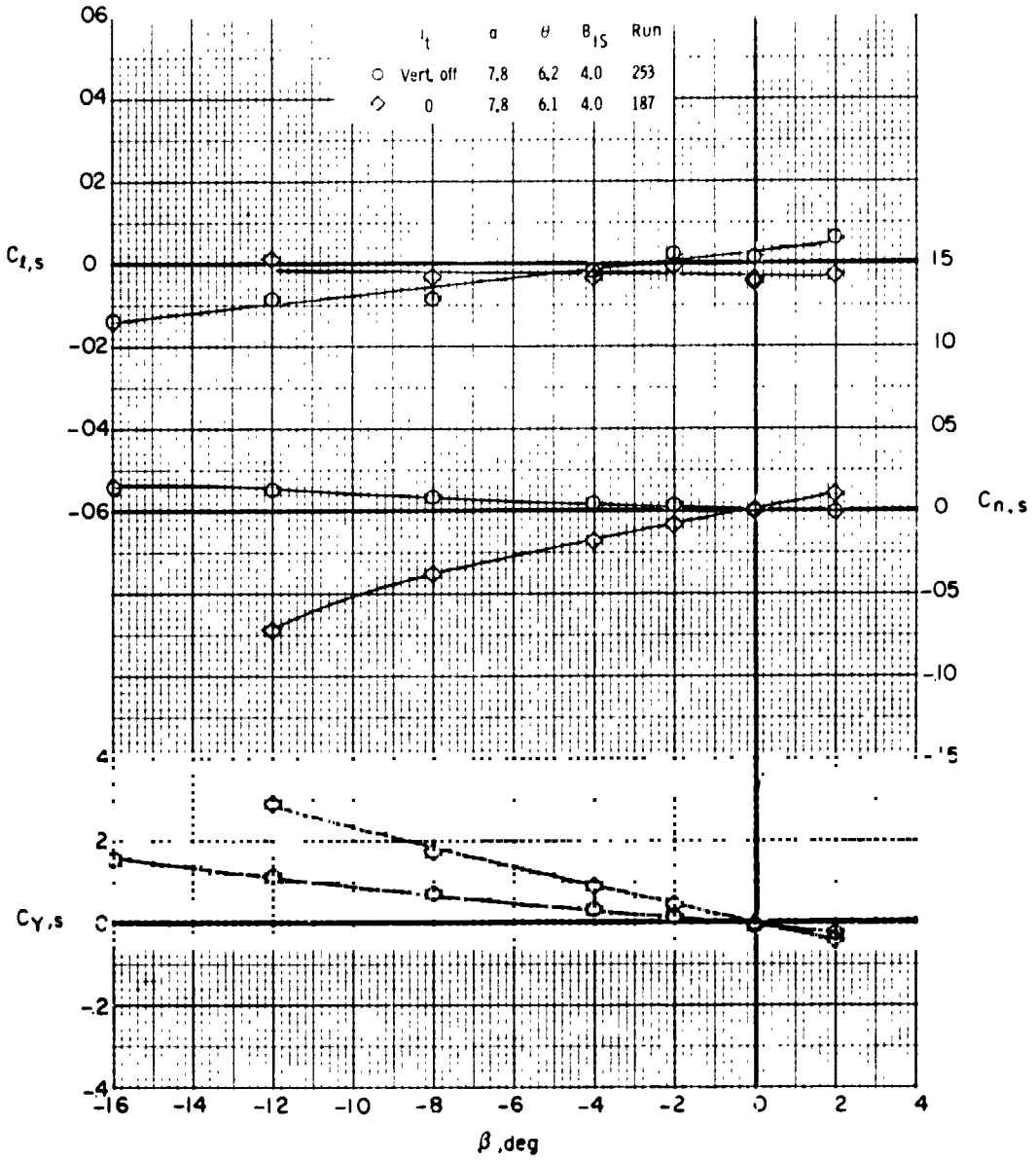

Figure 48. - Effect of sideslip angle on the lateral aerodynamic characteristics with the vertical tail off and on at a full-scale flight speed of 120 knots, $\mu = 0.29$, $\alpha_p = 60^\circ$.

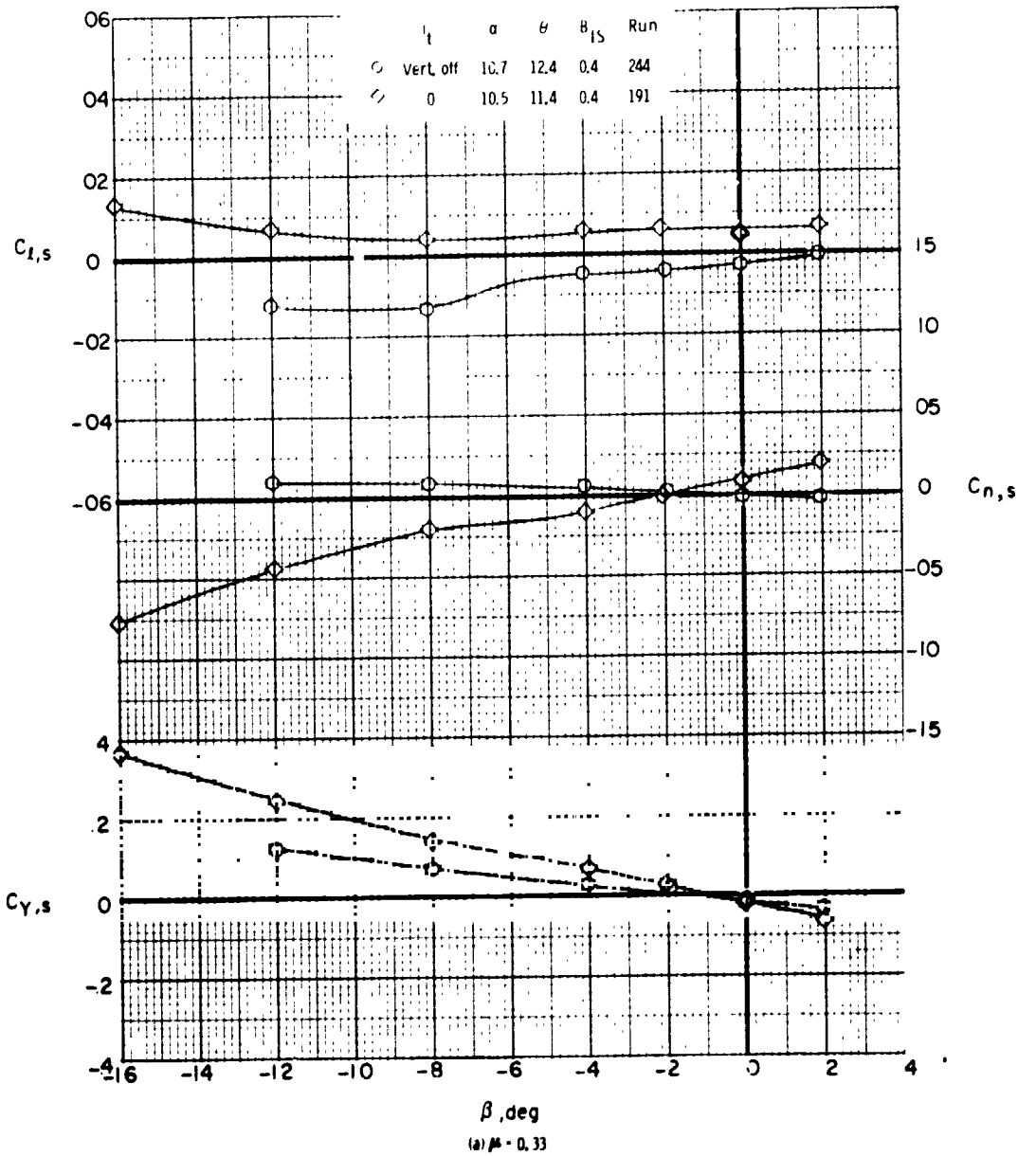

(a) $M = 0.33$

Figure 49. - Effect of sideslip angle on the lateral aerodynamic characteristics with the vertical tail on and off, $\alpha_p = 30^0$.

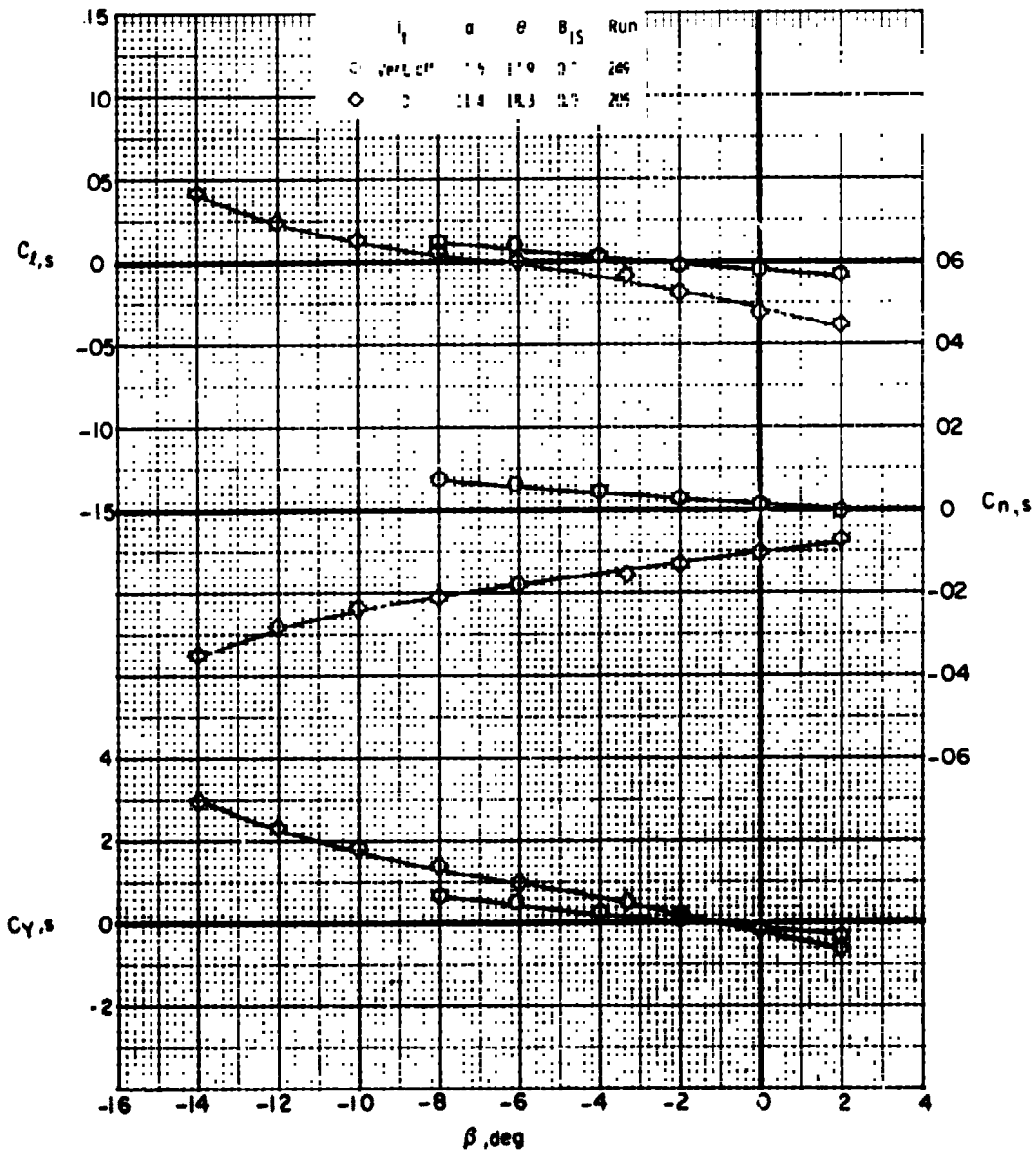

(a) $\beta = 0.2\theta$

Figure 50. - Effect of sideslip angle on the lateral aerodynamic characteristics with the vertical tail on and off, $\alpha_b = 0^\circ$

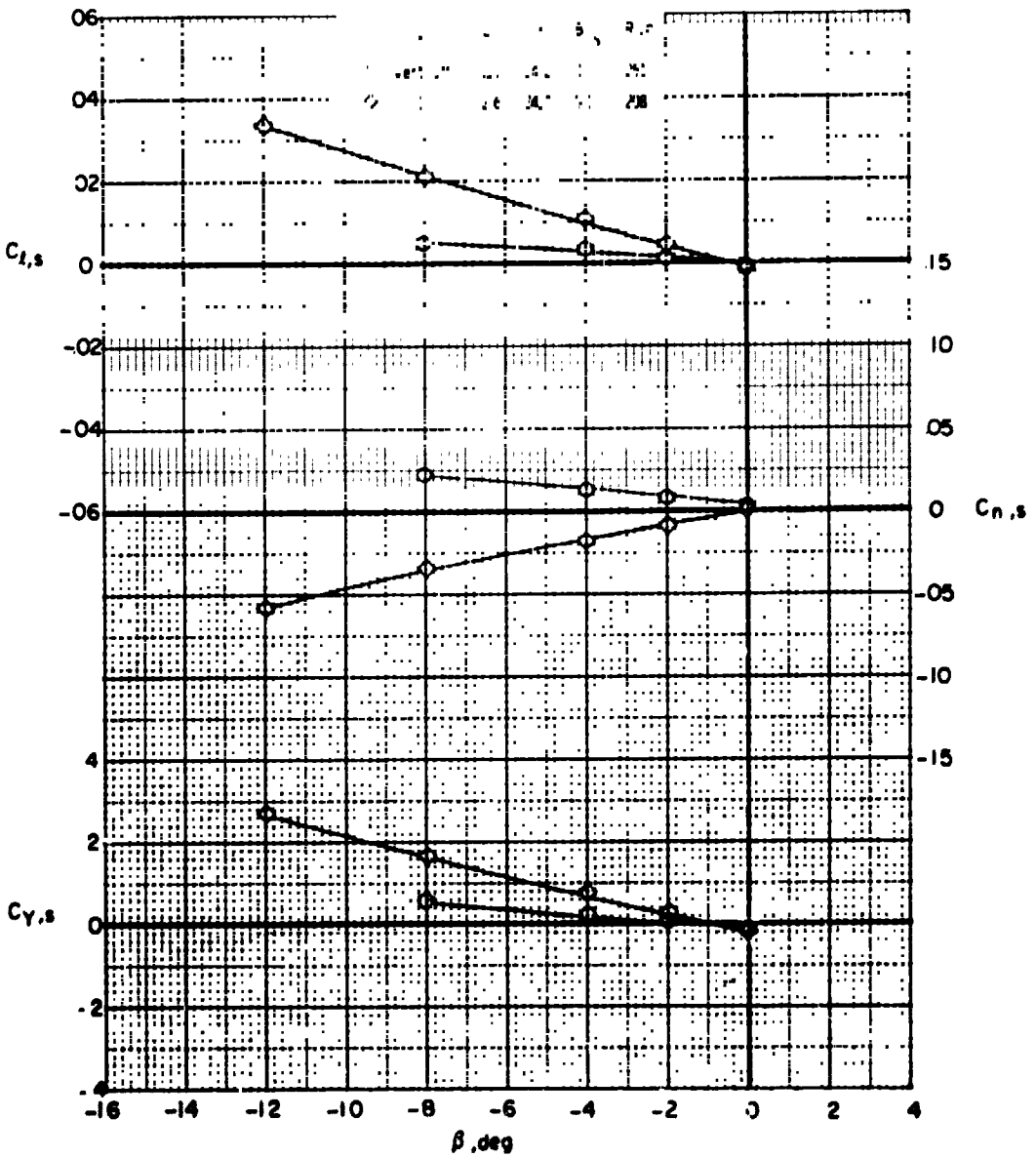

(b) $\mu = 0.39$

Figure 58. - Concluded.

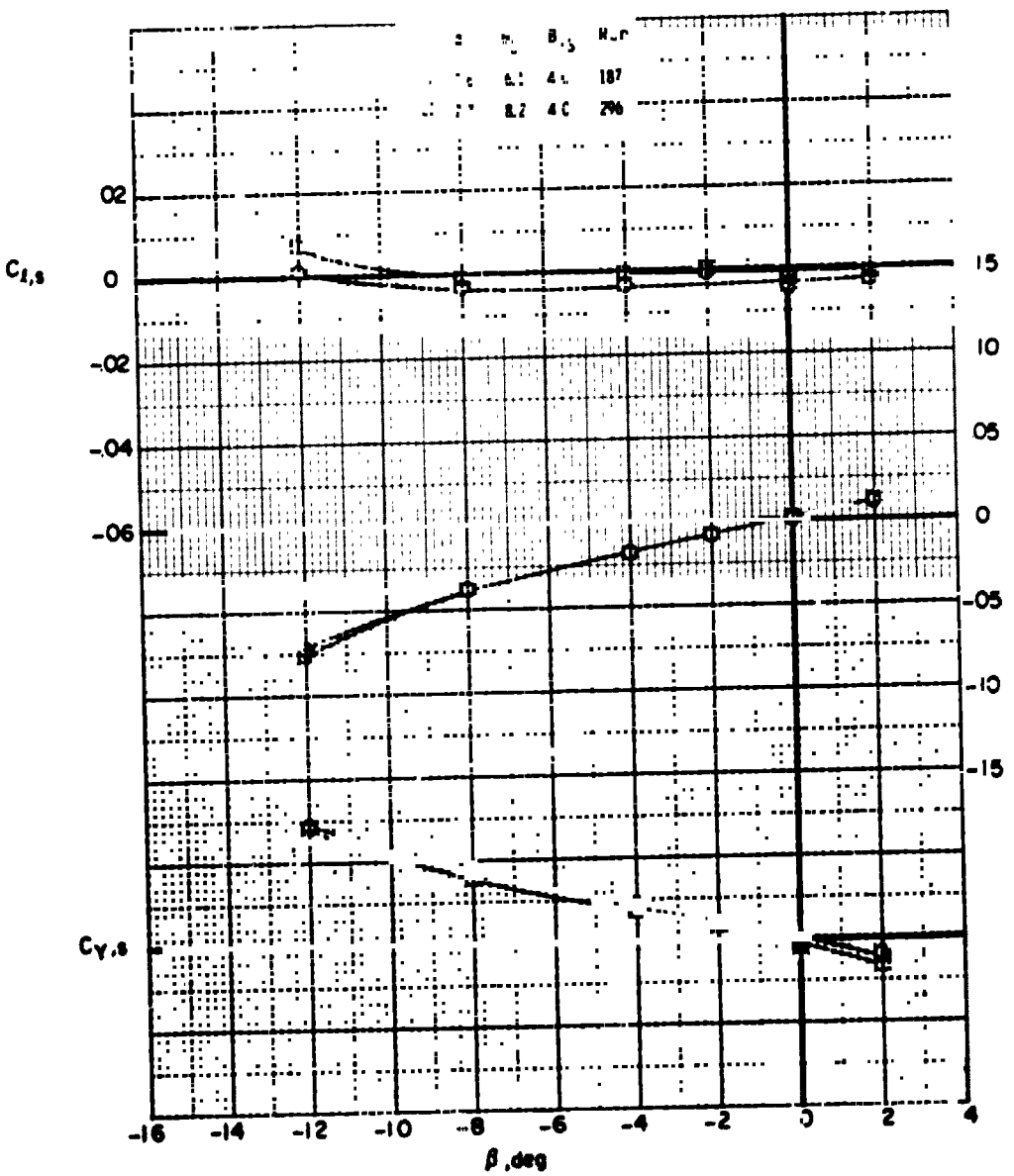

(a) $\alpha_s = 6^0, \mu = 0.29$

Figure 51. - Effect of sideslip angle on the lateral aerodynamic characteristics at different rotor collective pitch settings.

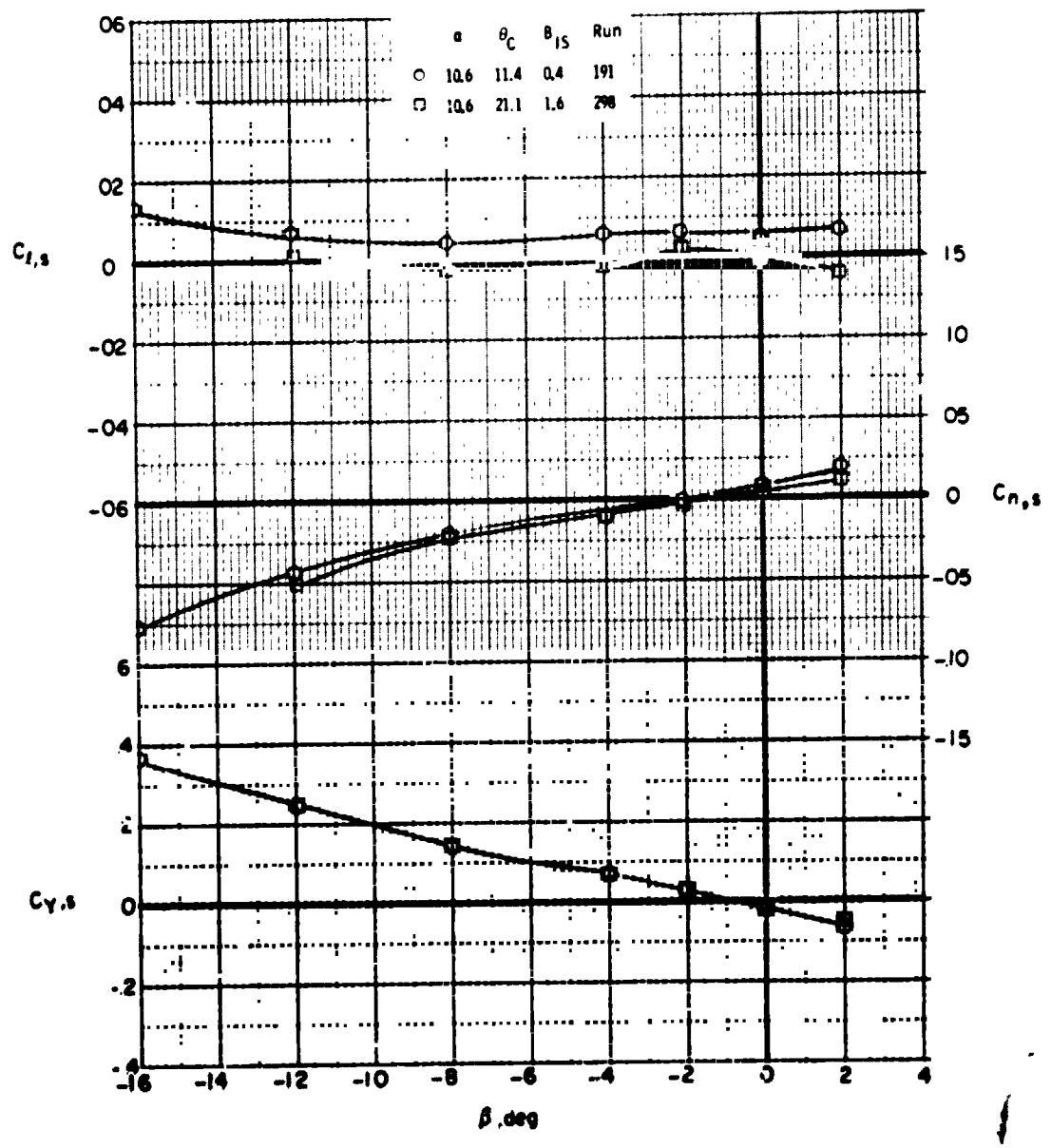

(b) $\alpha_p = 30^\circ$, $\delta_{IS} = 0.4^\circ$

Figure 51. - Continued.

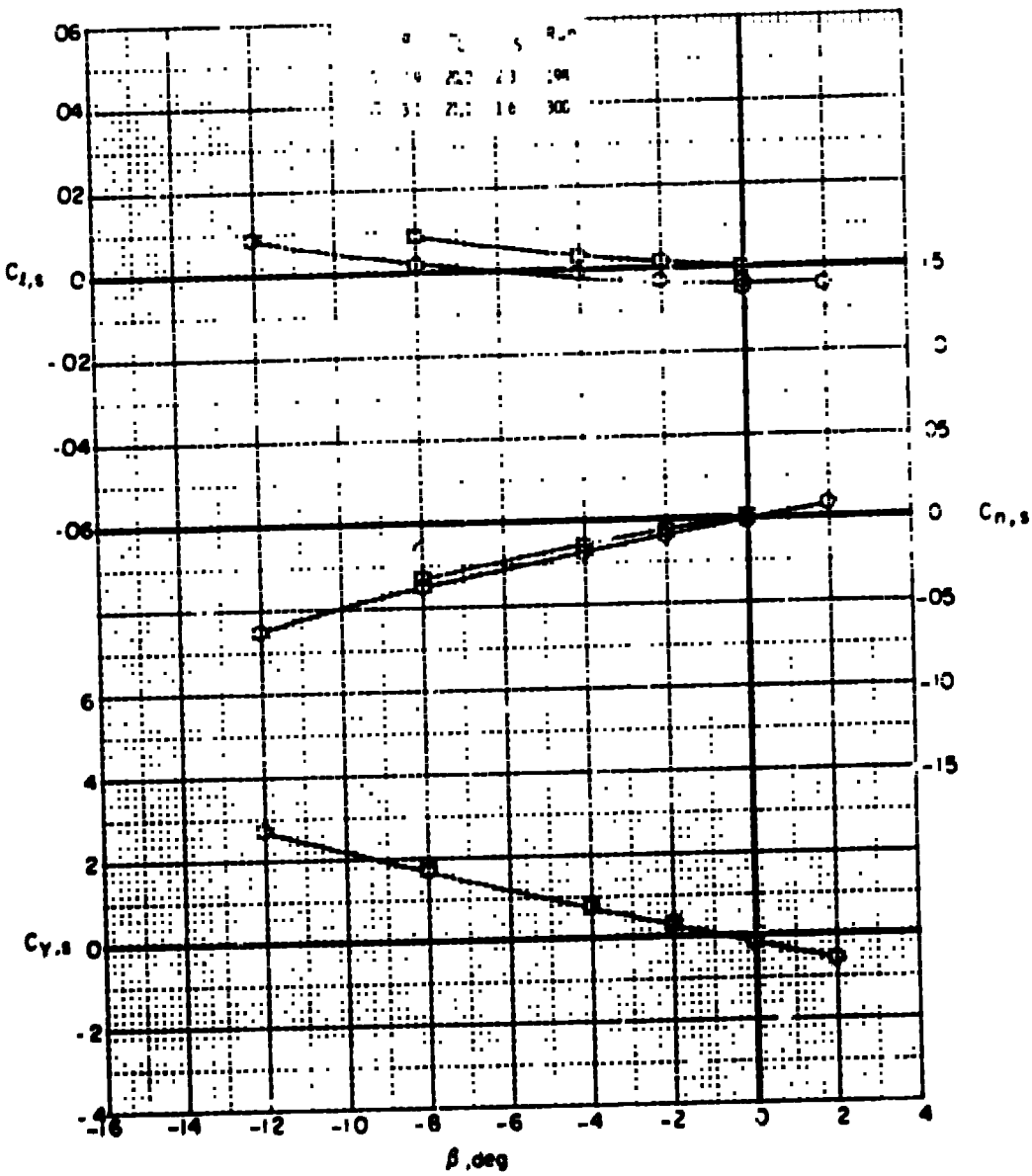

(c) $\alpha_p = 30^\circ$, $M = 0.30$

Figure 51. - Concluded.

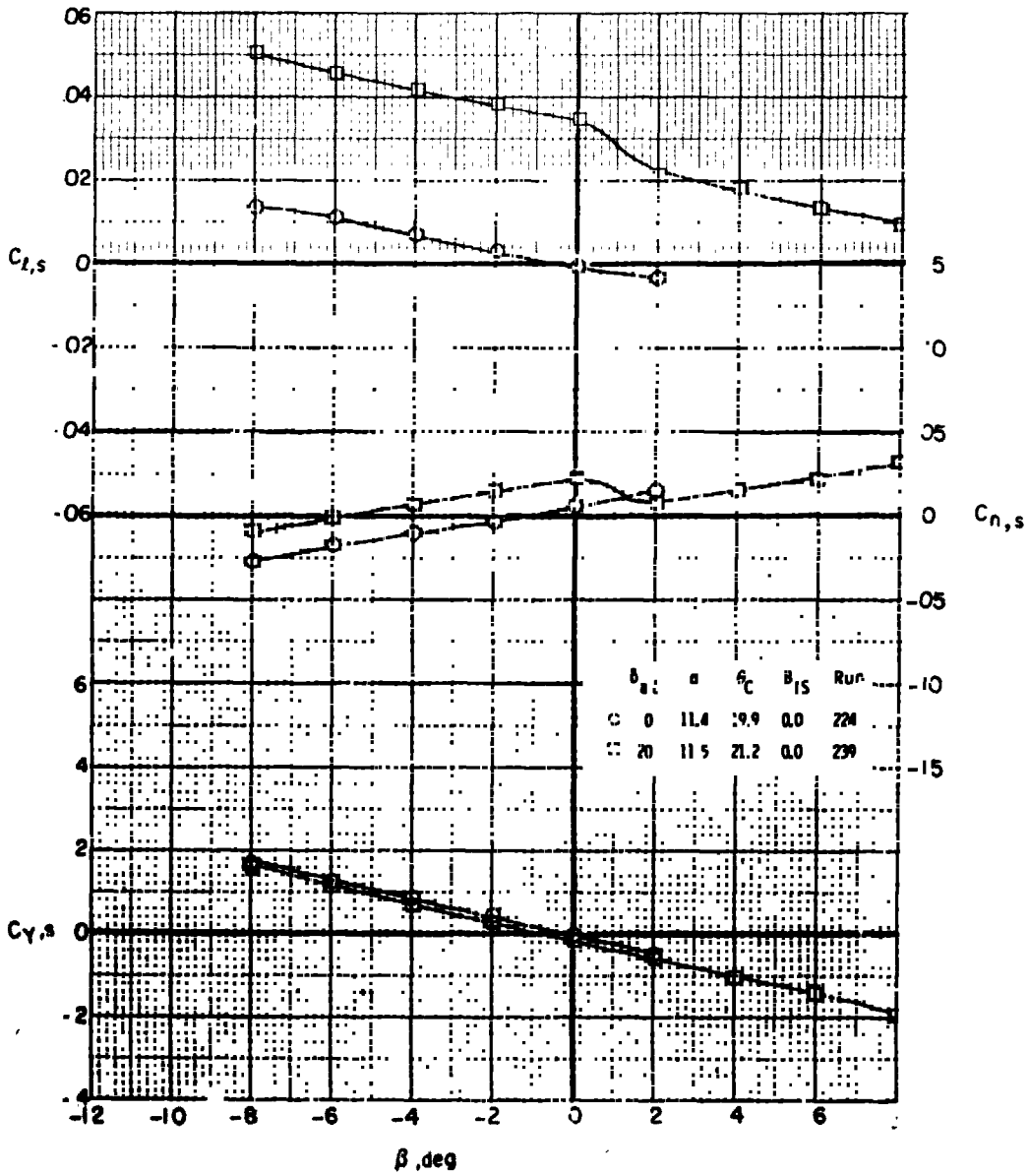

Figure 52. - Effect of sideslip angle on the lateral aerodynamic characteristics for different aileron deflections, $\alpha_p = 0^0$, $\delta_f = 50^0$, $\mu = 0.34$.

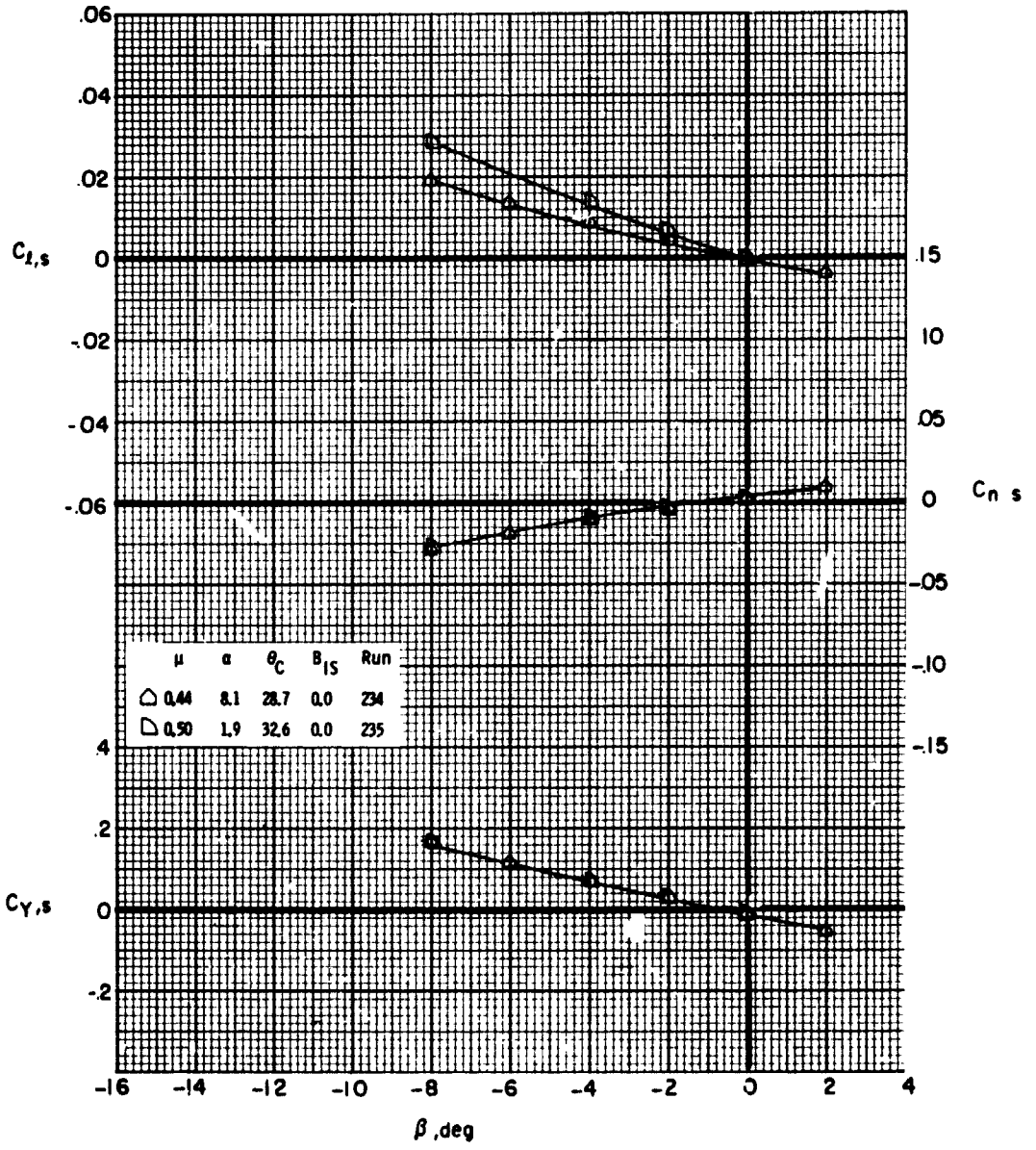

Figure 53. - Effect of sideslip angle on the lateral aerodynamic characteristics for several forward speeds, $\alpha_p = 0^\circ$, $\delta_f = 0^\circ$, $\delta_s = 0^\circ$.

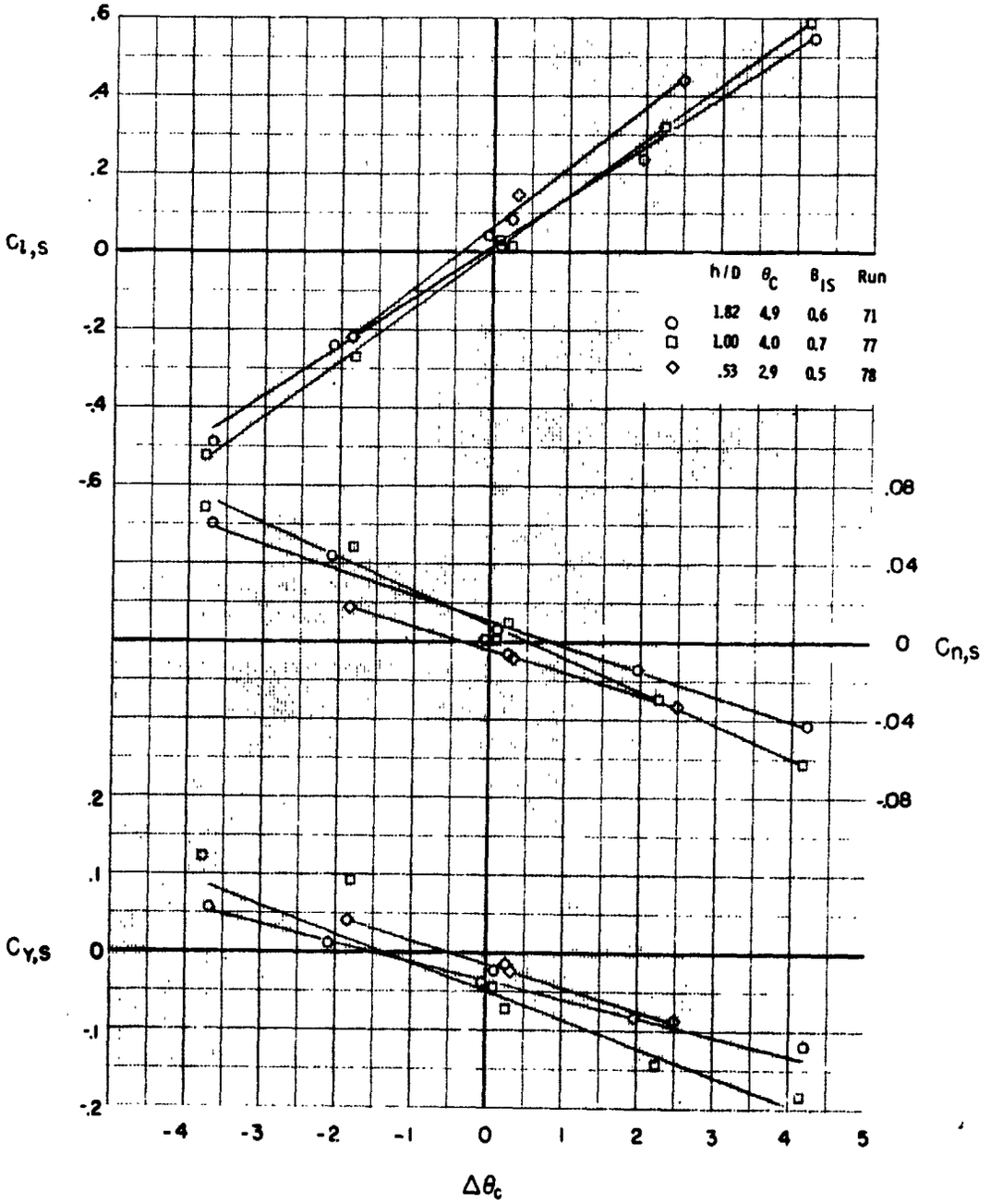

Figure 54. - Effect of differential collective pitch on the lateral aerodynamic characteristics in hover and out of ground effect, $\alpha_p = 90^0$

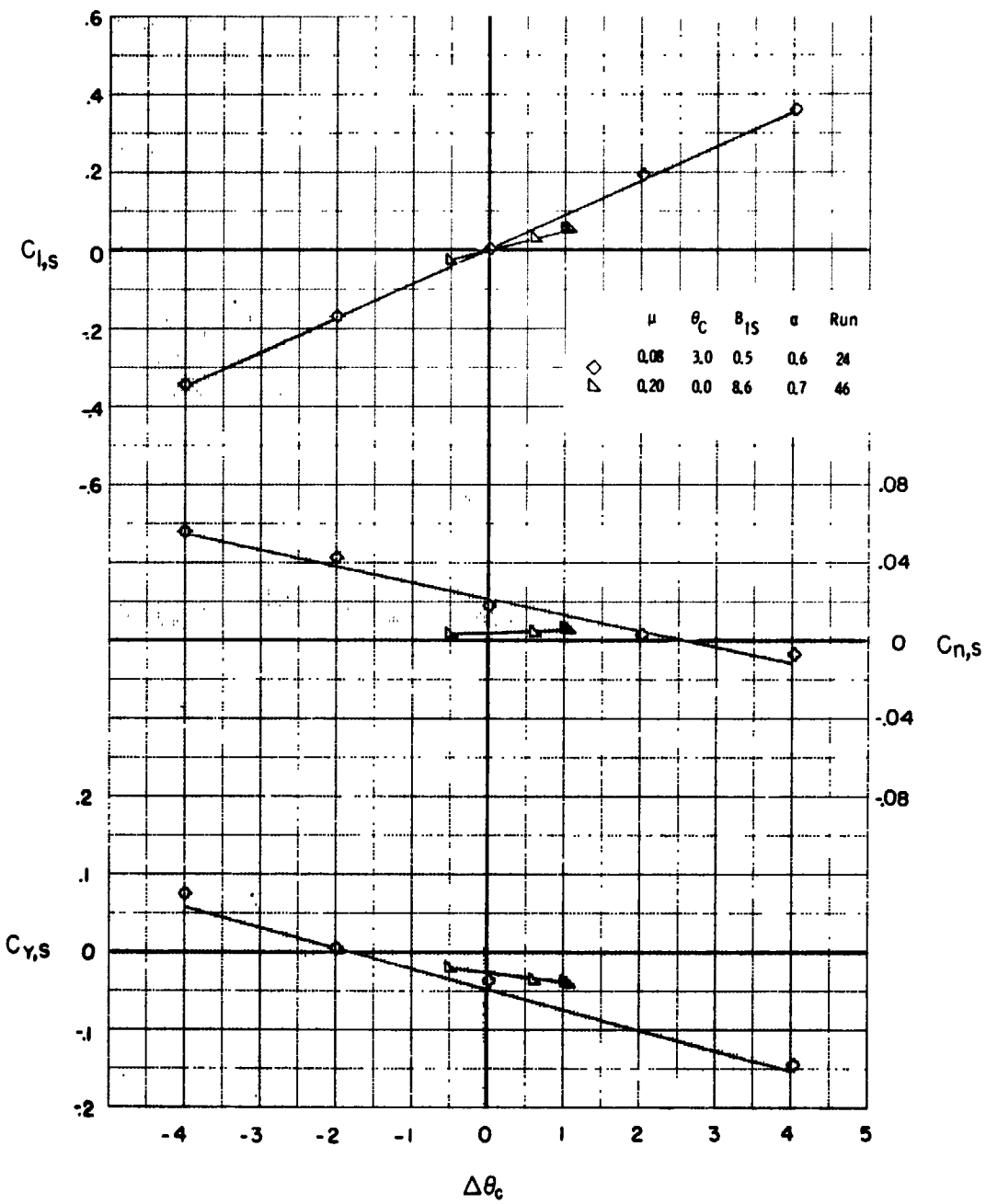

(a) $\alpha_p = 90^0$

Figure 55. - Effect of differential collective pitch on the lateral aerodynamic characteristics for several flight speeds.

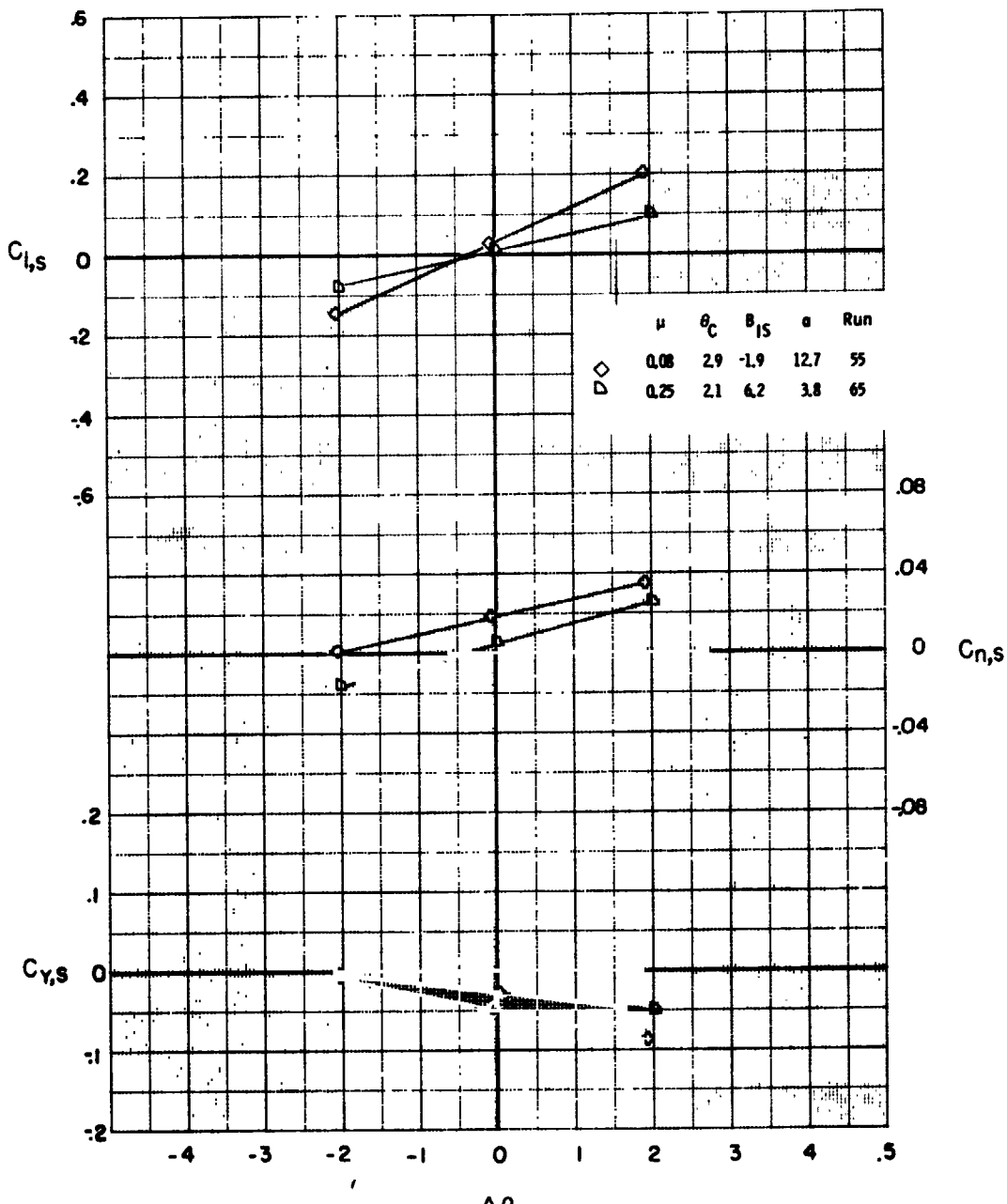

(b) $\alpha_p = 75^0$

Figure 55. - Continued.

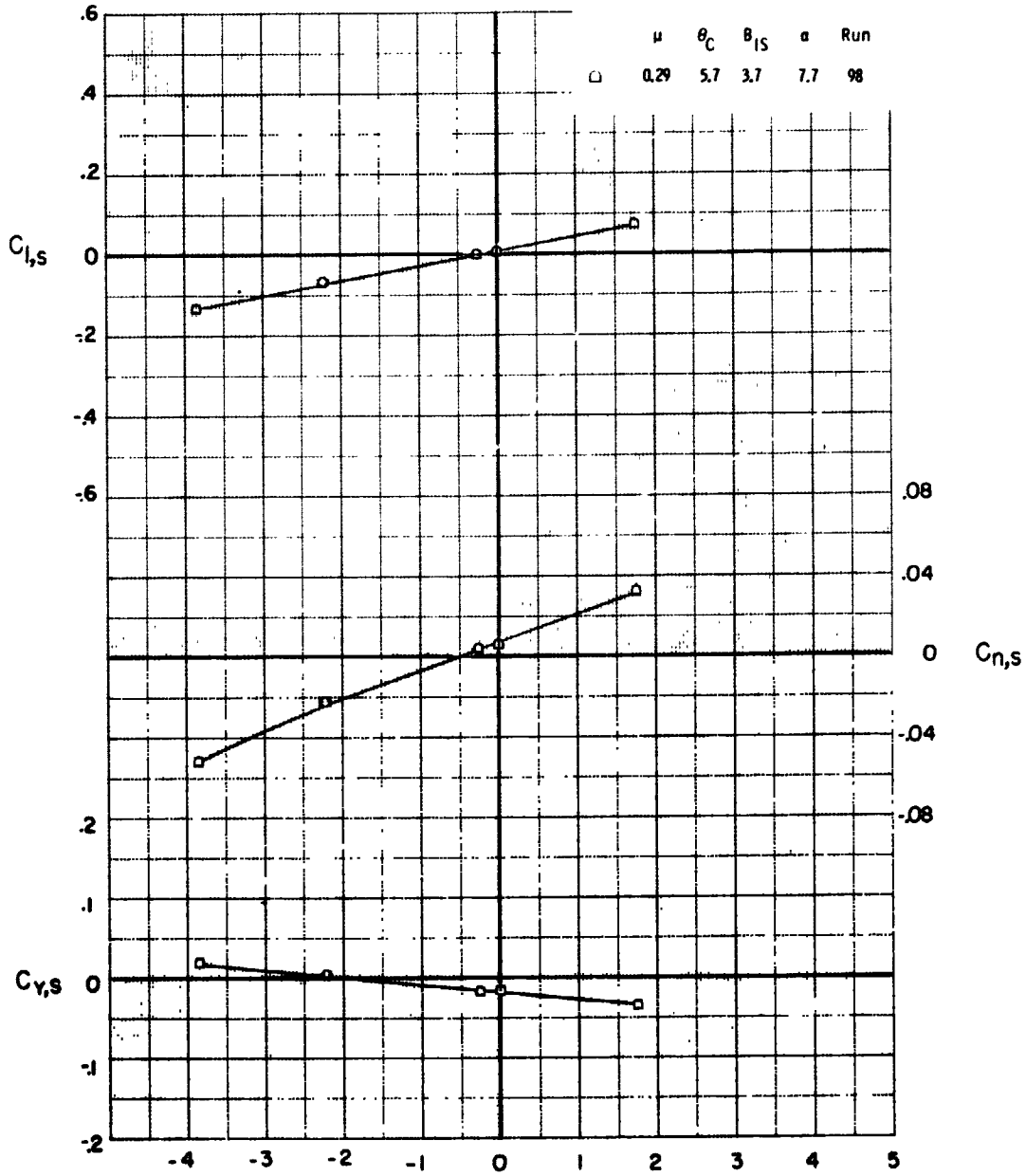

(c) $\alpha_p = 60^0$

Figure 55. - Concluded.

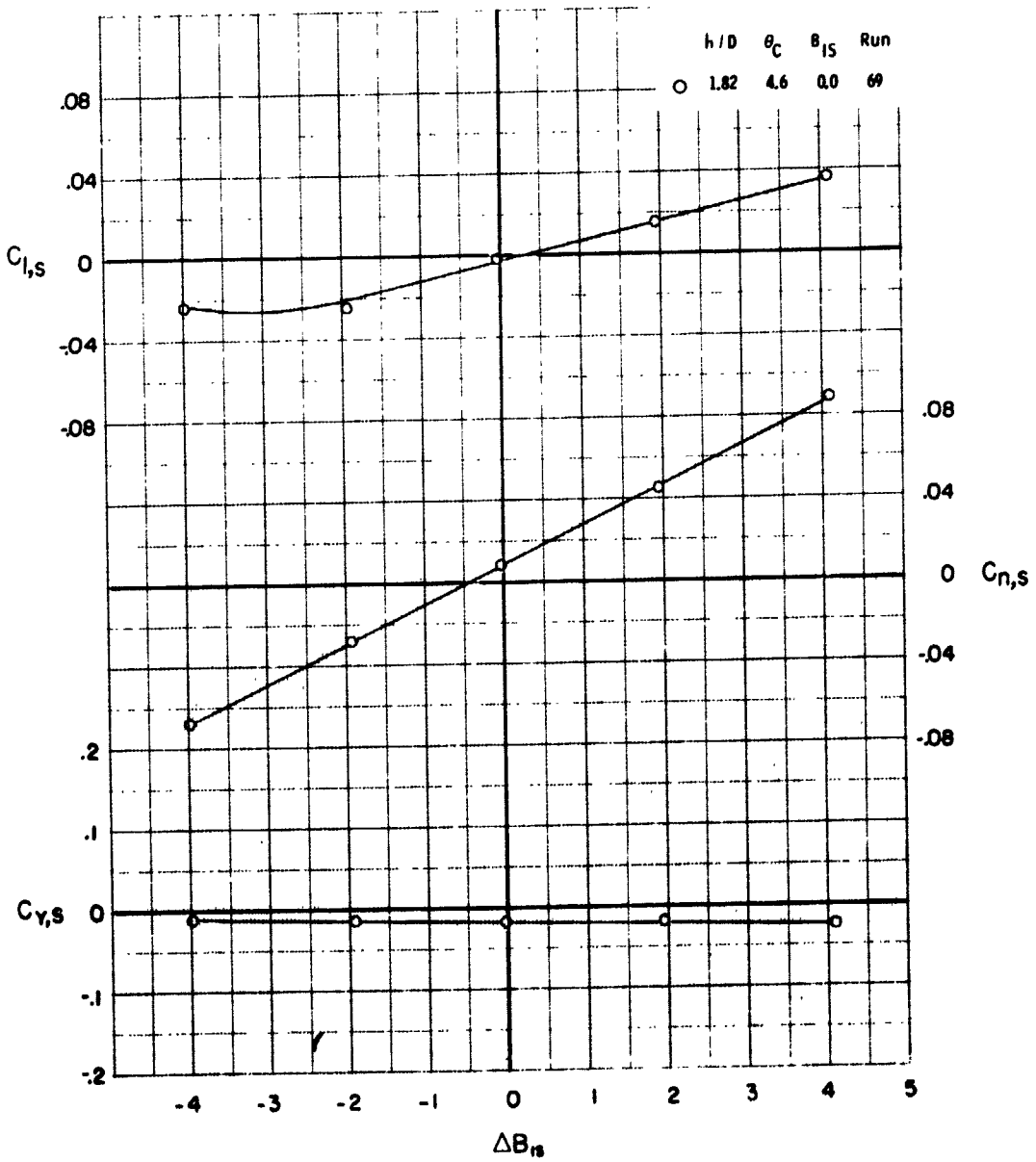

Figure 56. - Effect of differential cyclic pitch on the lateral aerodynamic characteristics in hover out of ground effect, $\alpha_p = 90°$.

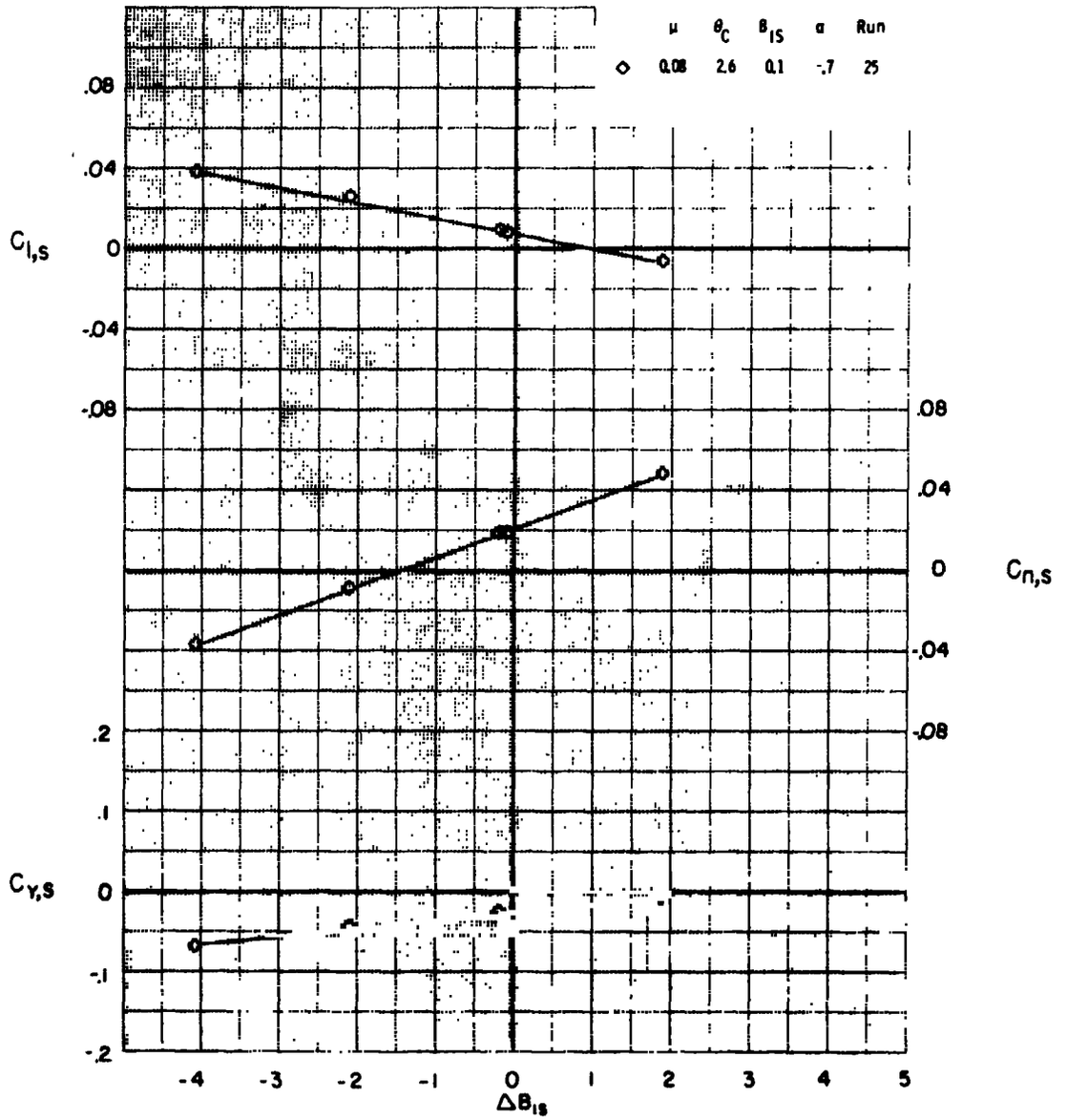

(a) $\alpha_p = 90^0$

Figure 57. - Effect of differential cyclic pitch on the lateral aerodynamic characteristics at several wind speeds.

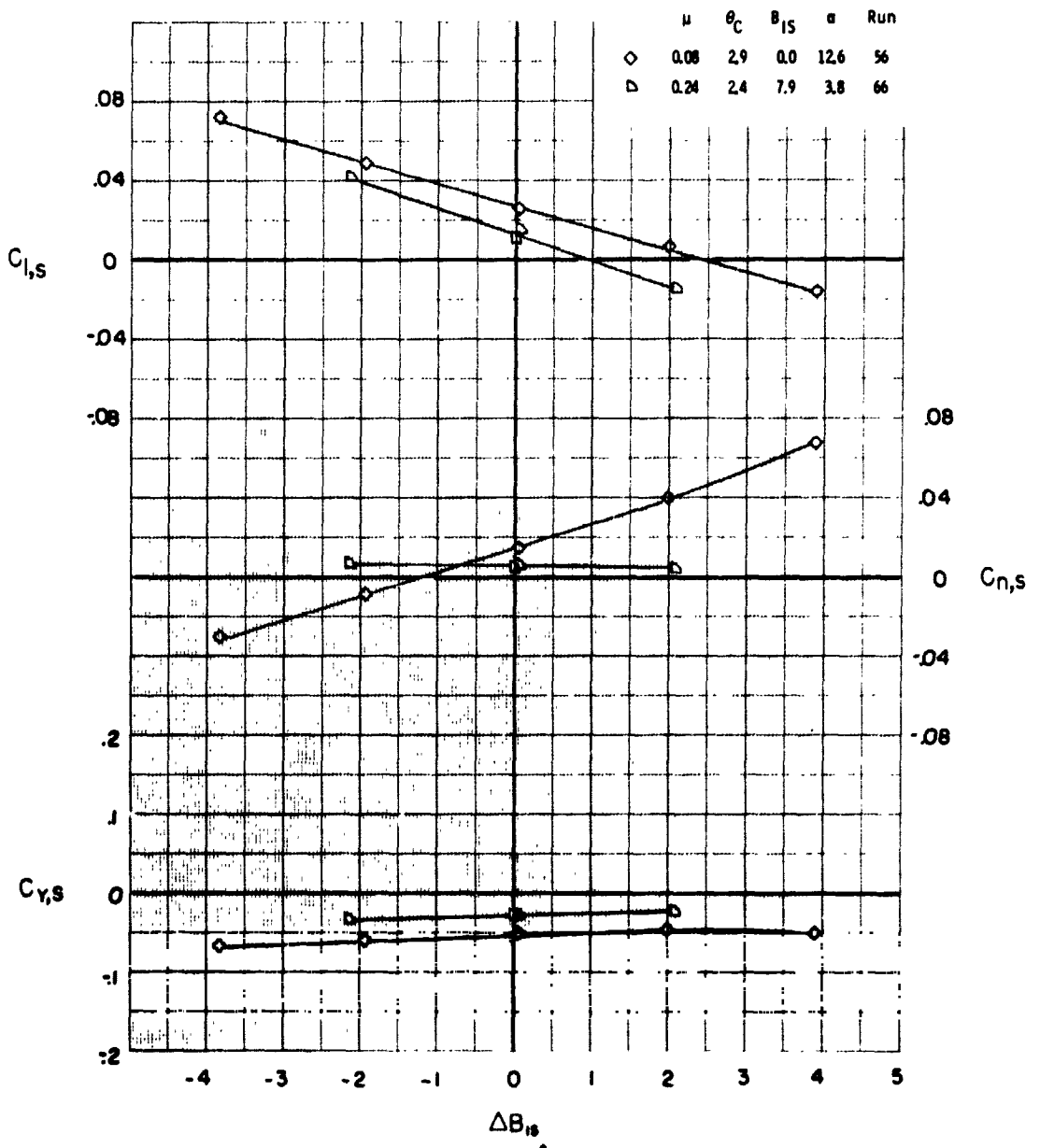

(b) $\alpha_p = 75^0$

Figure 57. - Continued.

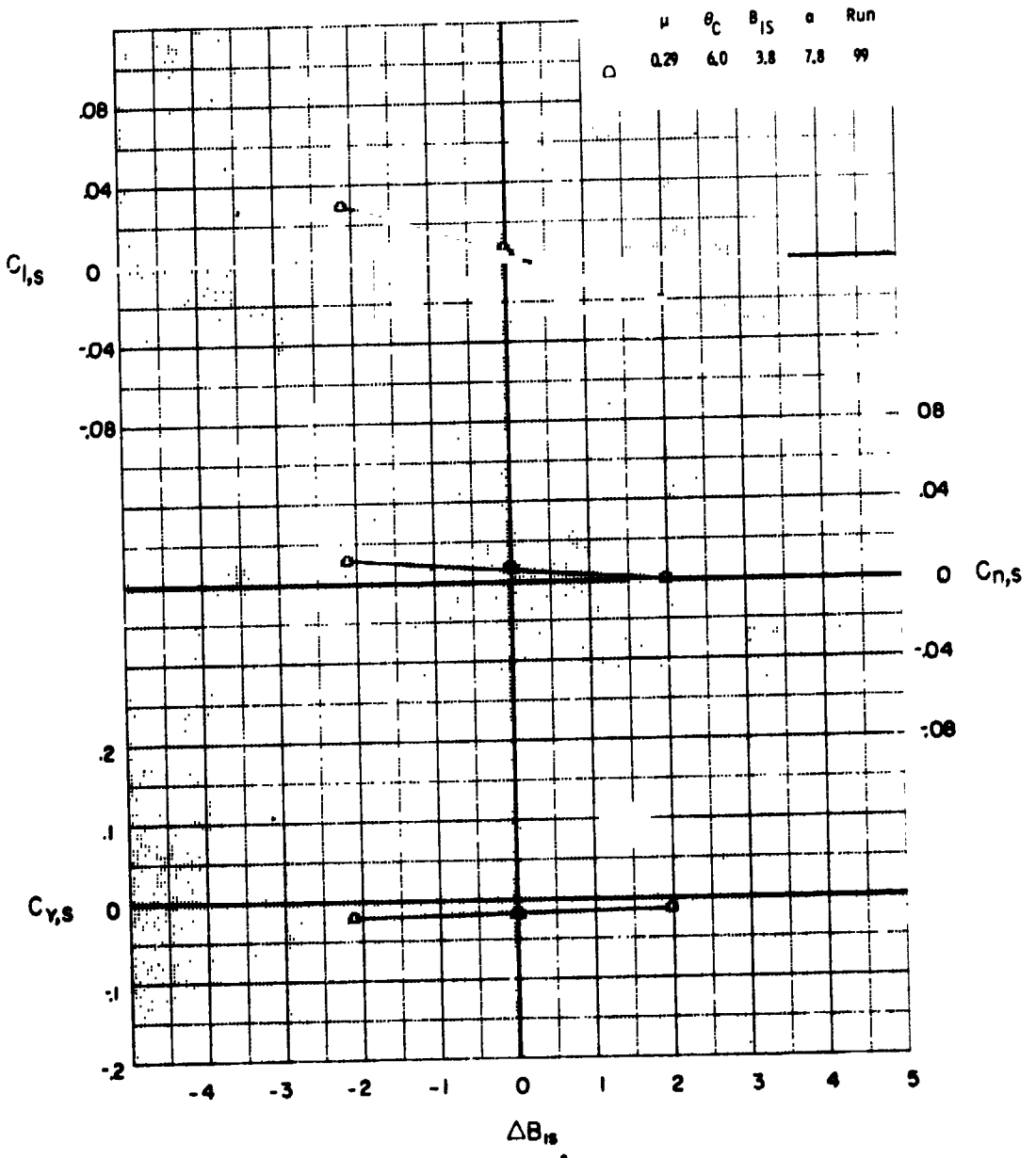

(c) $\alpha_p = 60^0$

Figure 57. - Continued.

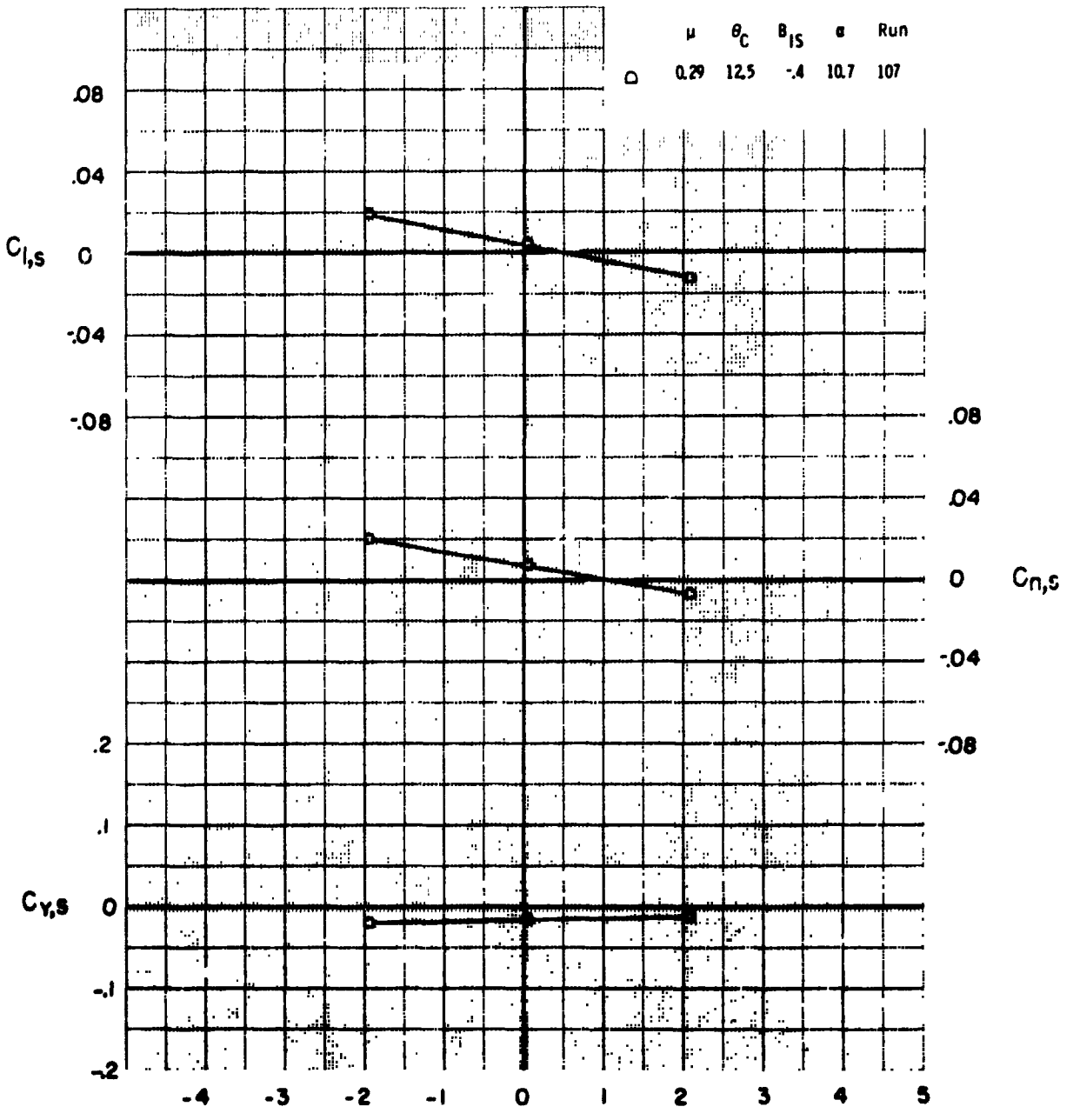

(a) $\alpha_p = 30^0$

Figure 57 - Concluded.

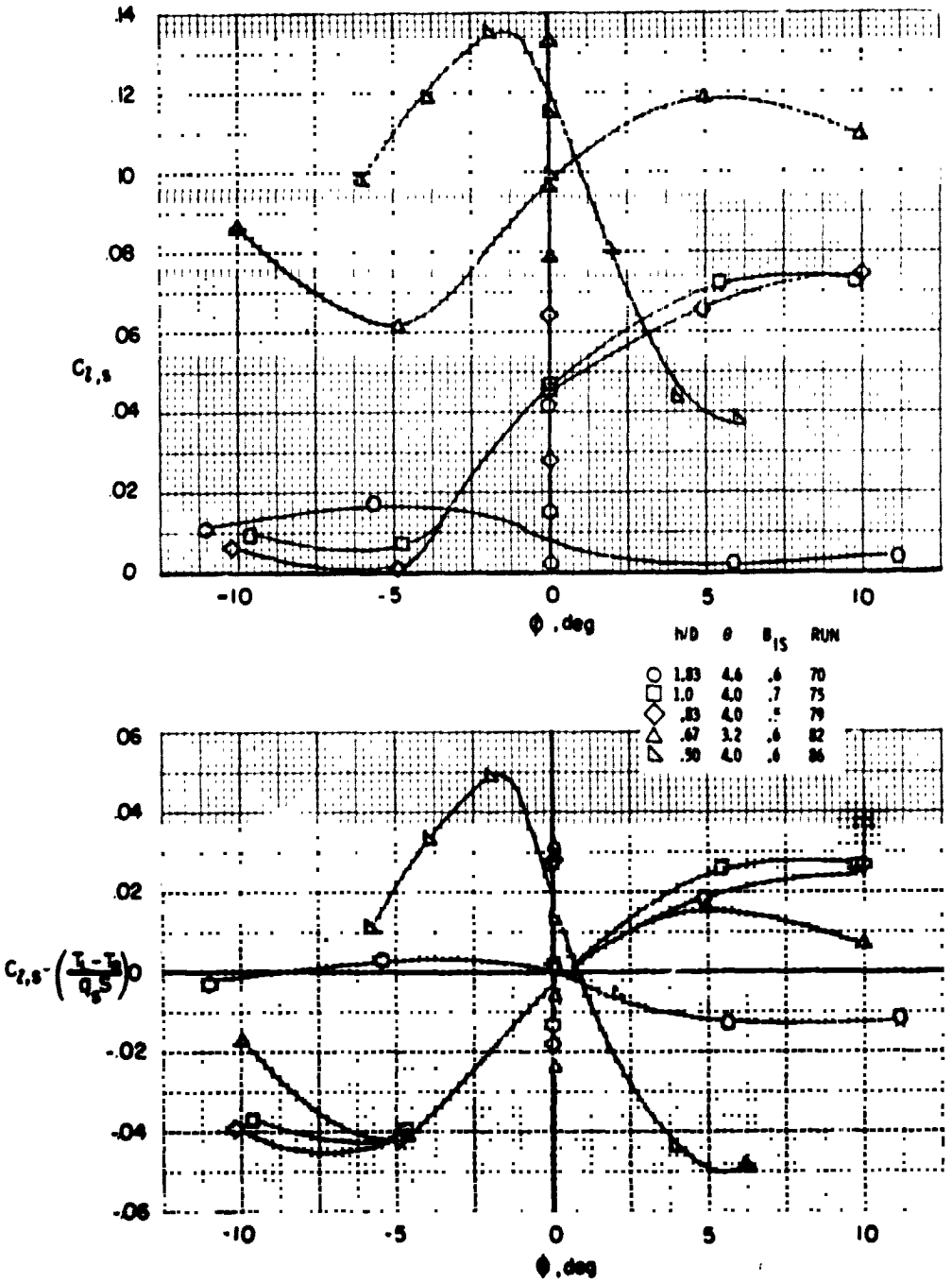

Figure 58. - Effect of roll angle on roll moment coefficient (slipstream) for hover at various heights above ground, $\alpha_p = 90°$.

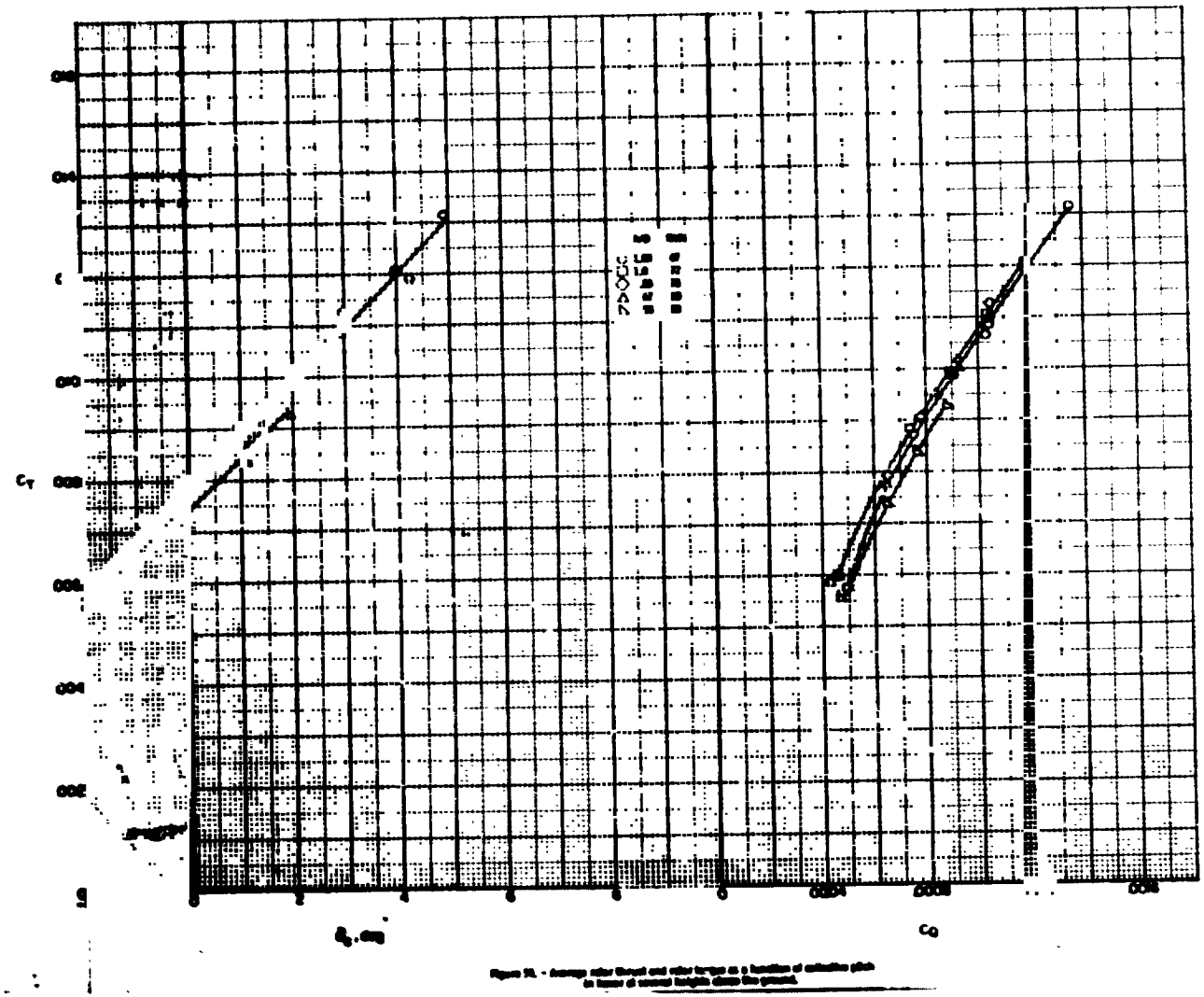
C_T
C_0

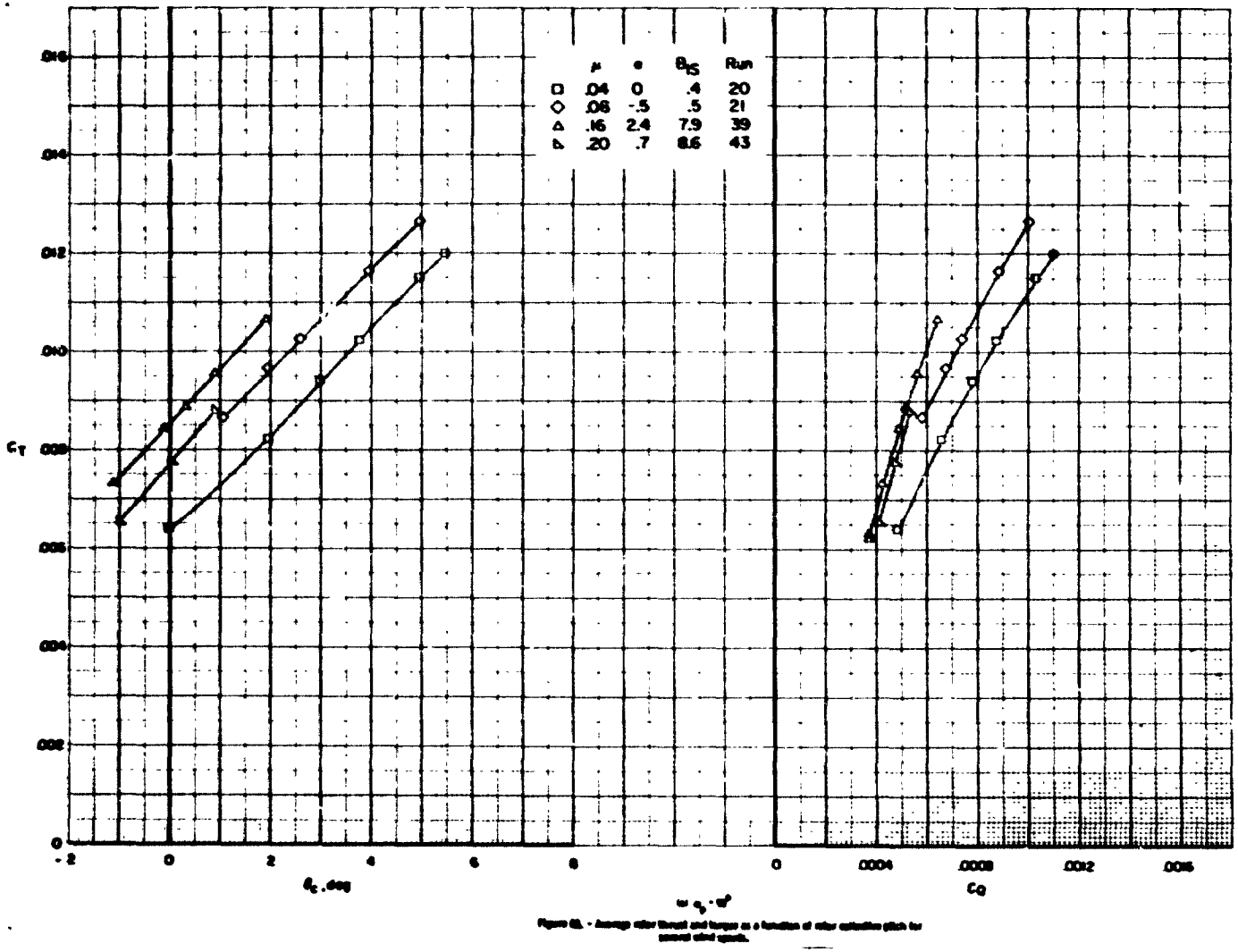
μ α B_{1S} Run
□ .04 0 .4 20
◇ .06 -.5 .5 21
△ .16 2.4 7.9 39
▷ .20 .7 8.6 43
C_T
θ_c, deg
C_Q

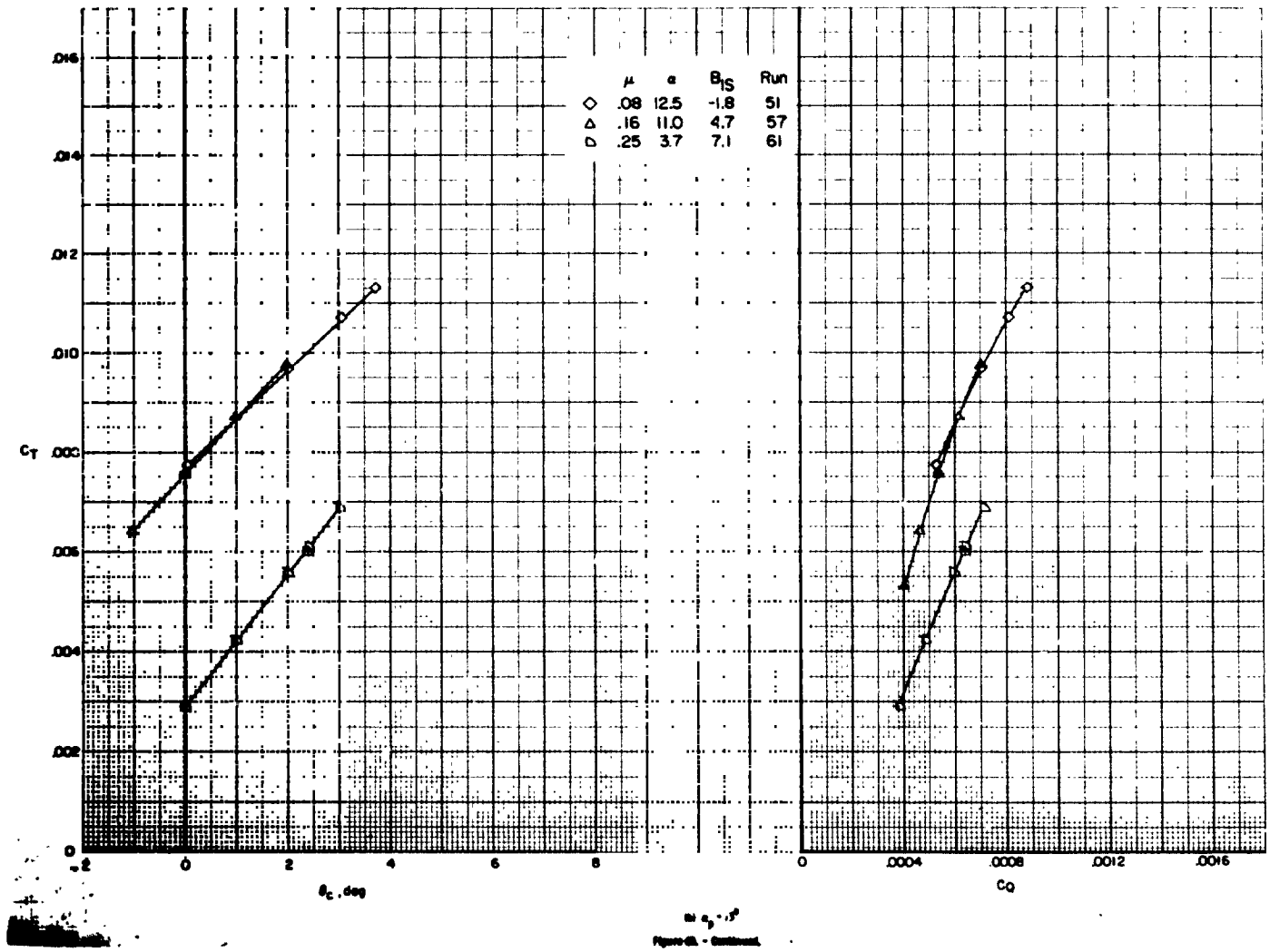

at $\alpha_p = -1°$

Figure 6b. - Continued.

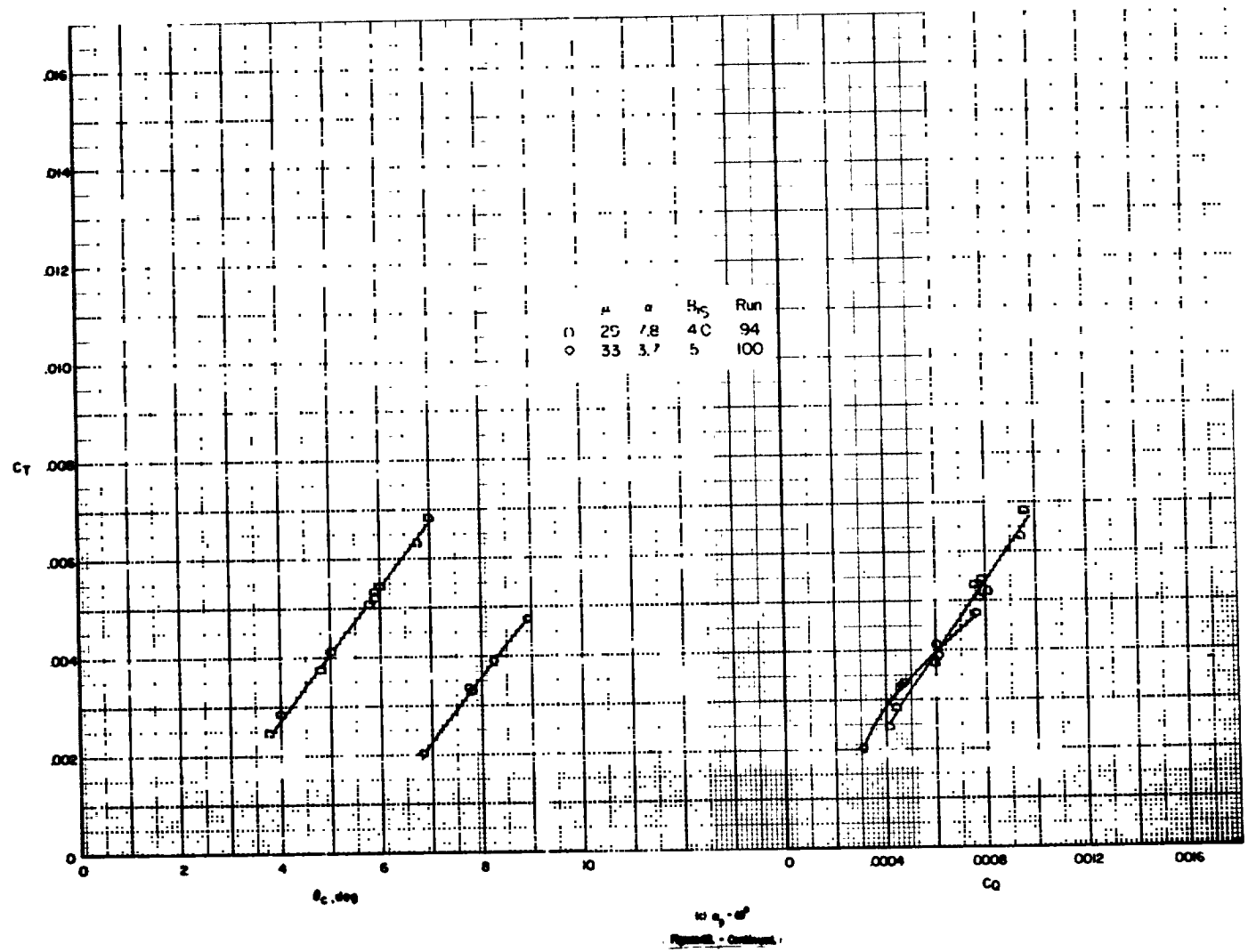
μ α H_{KS} Run
□ .25 7.8 4C 94
◇ .33 3.7 5 100
C_T
θ_c, deg
C_Q
to α_s - deg

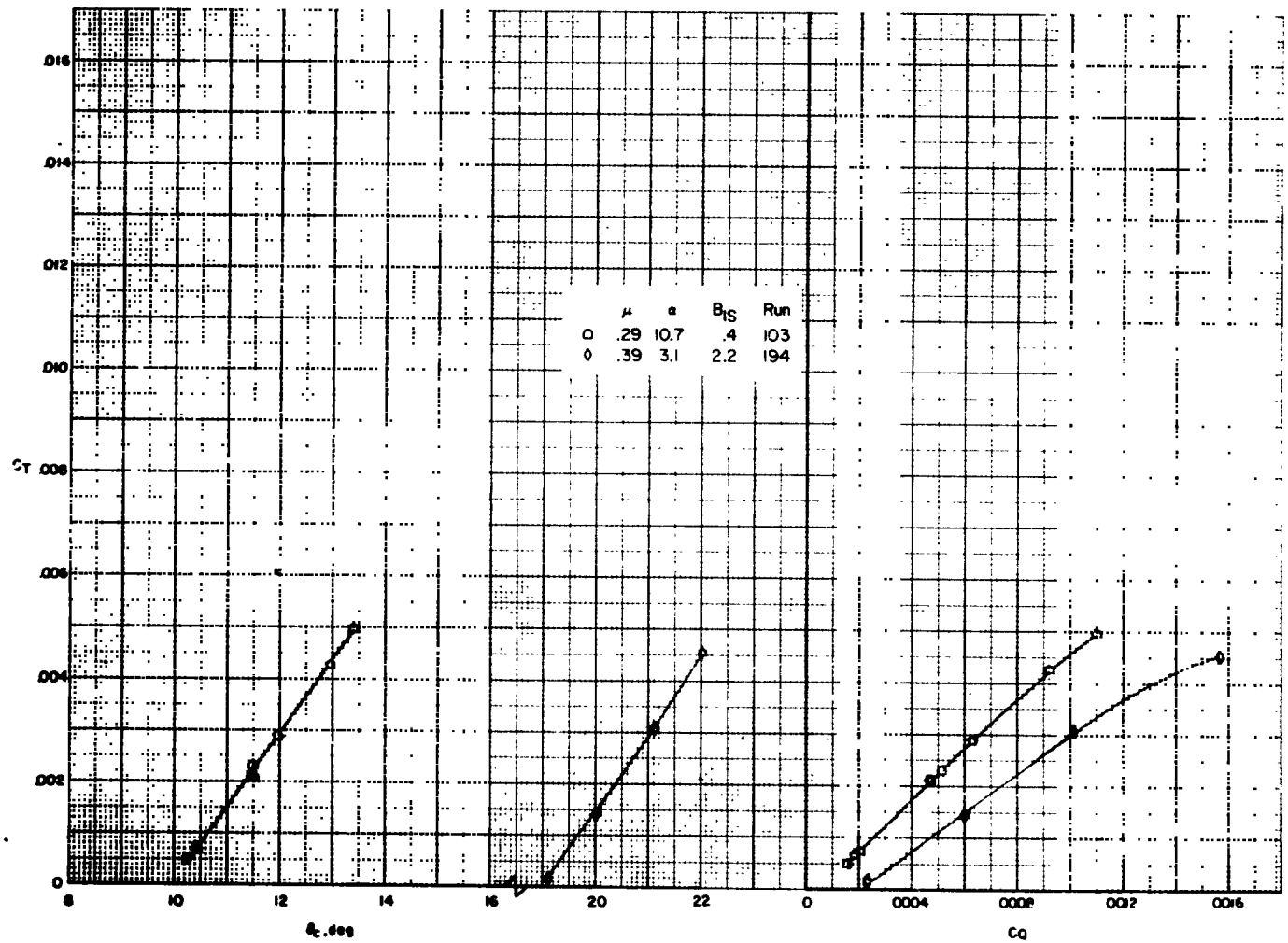

@ a_s = 0°

Figure 68. - Continued.

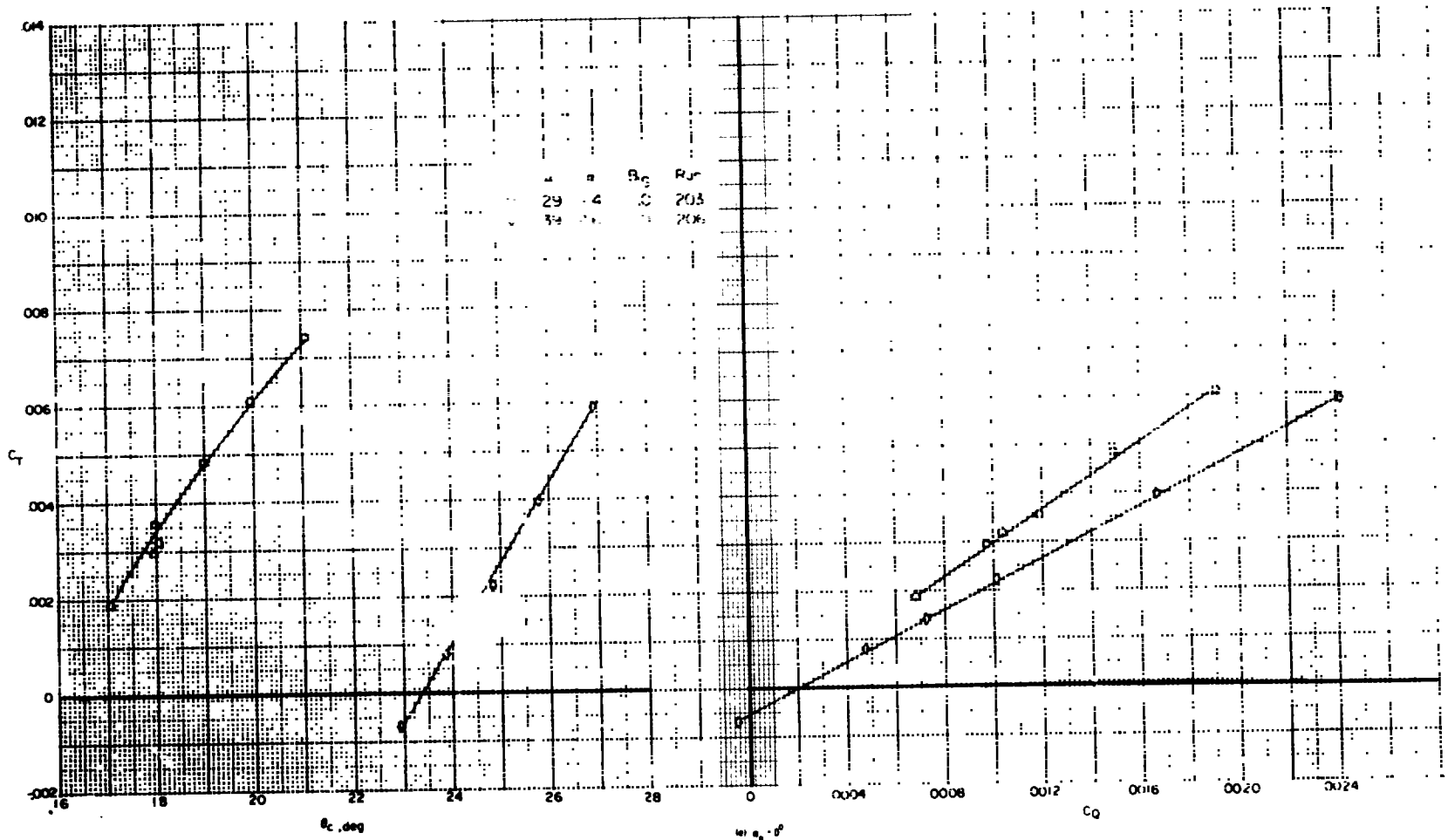

(c) $\alpha_p = 0°$

Figure 66. - Concluded.

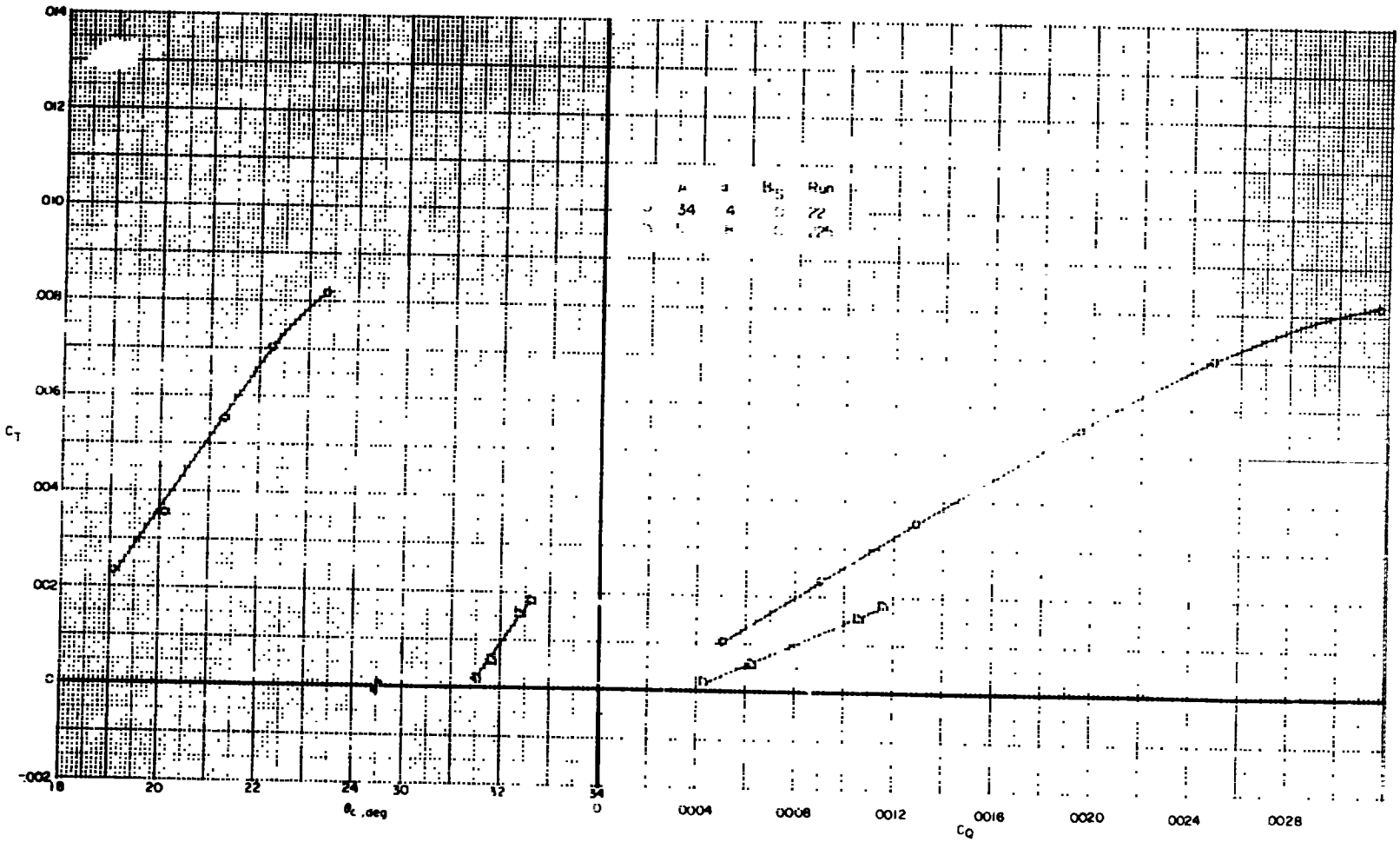

(a) $\delta_1 = 50^0$, $\delta_3 = 20^0$

Figure 61. - Average rotor thrust and torque as a function of collective pitch for several wind speeds, $\alpha_s = 0^0$, cruise r.p.m.

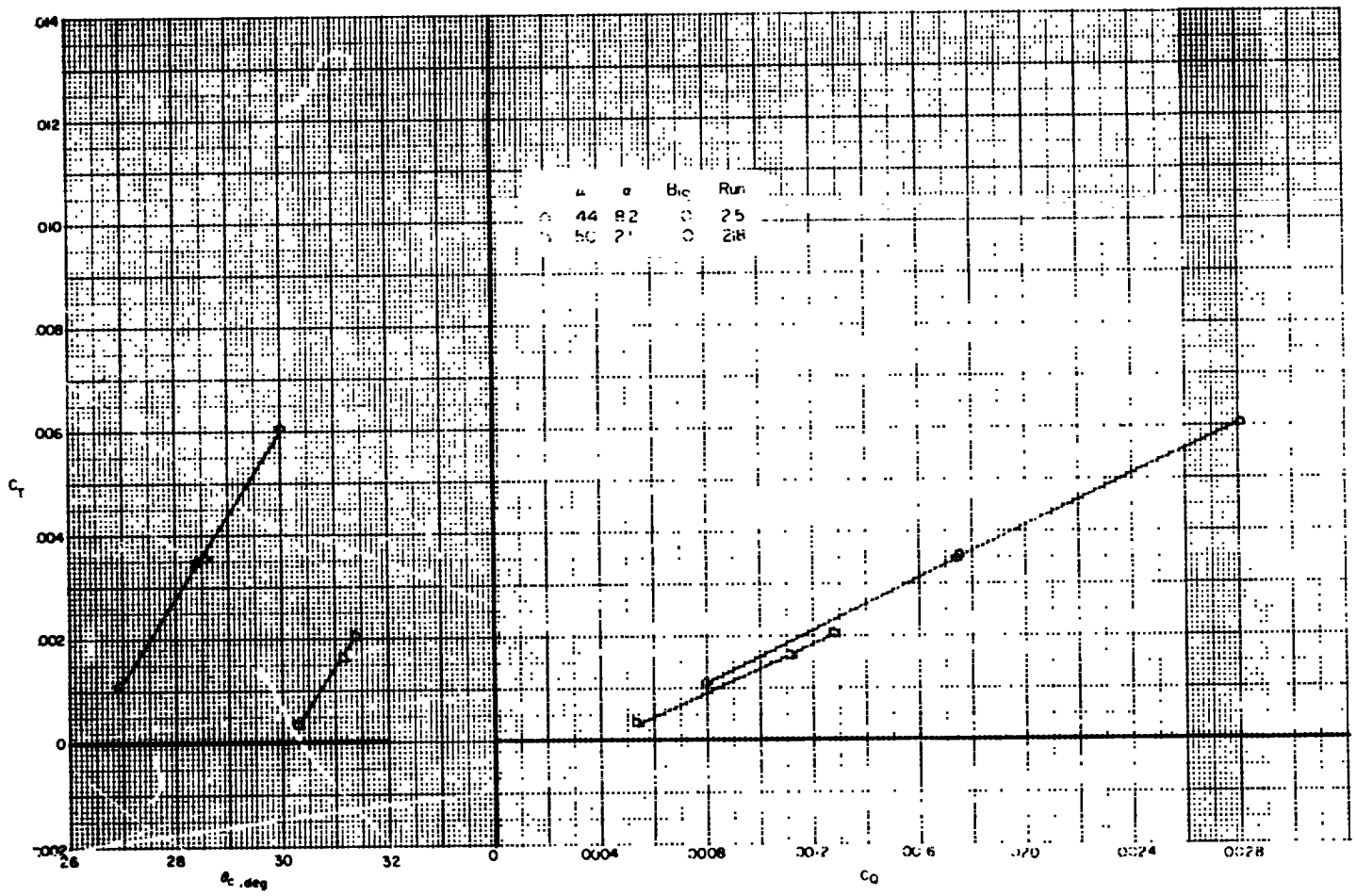

(b) $\delta_1 = 0^\circ$, $\delta_0 = 0^\circ$

Figure 61. - Concluded.

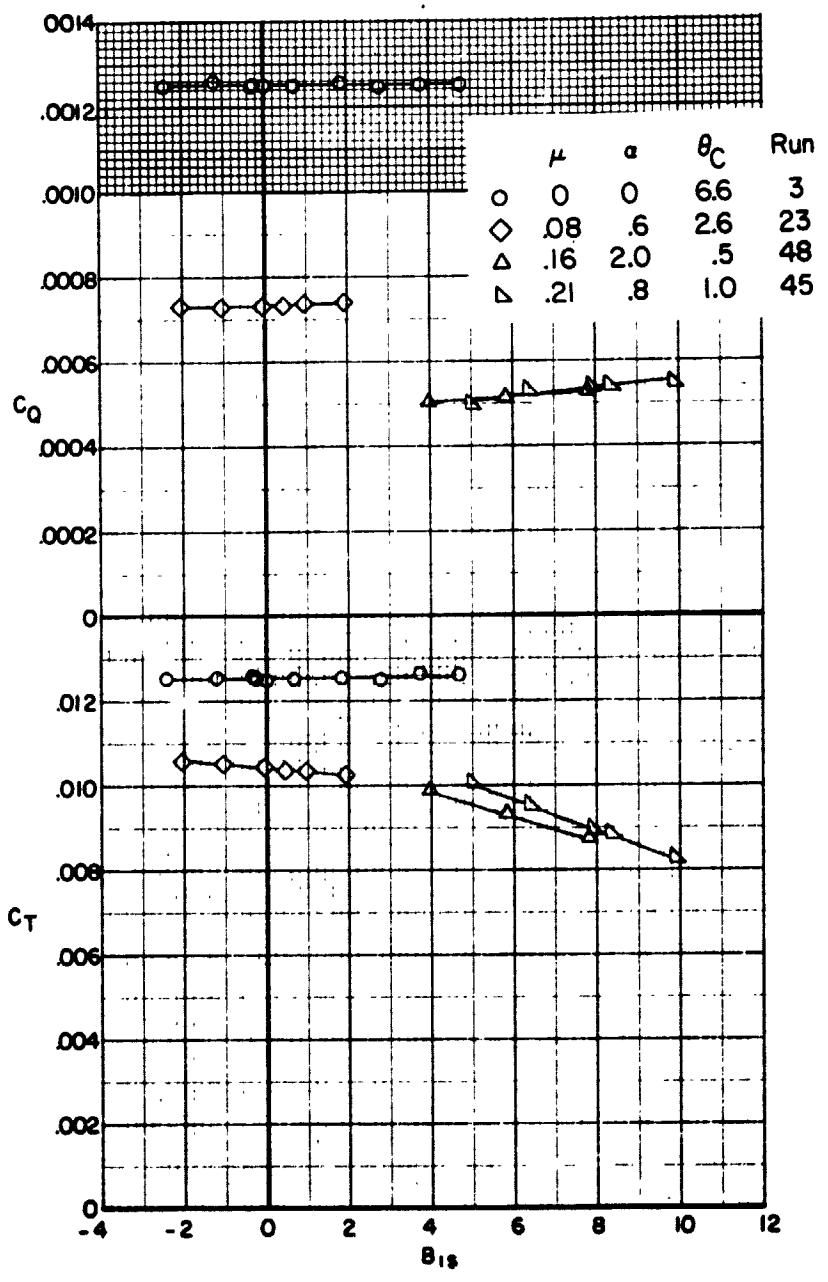

(a) $\alpha_p = 18^0$

Figure 62. - Average rotor thrust and torque as a function of cyclic pitch for several wind speeds.

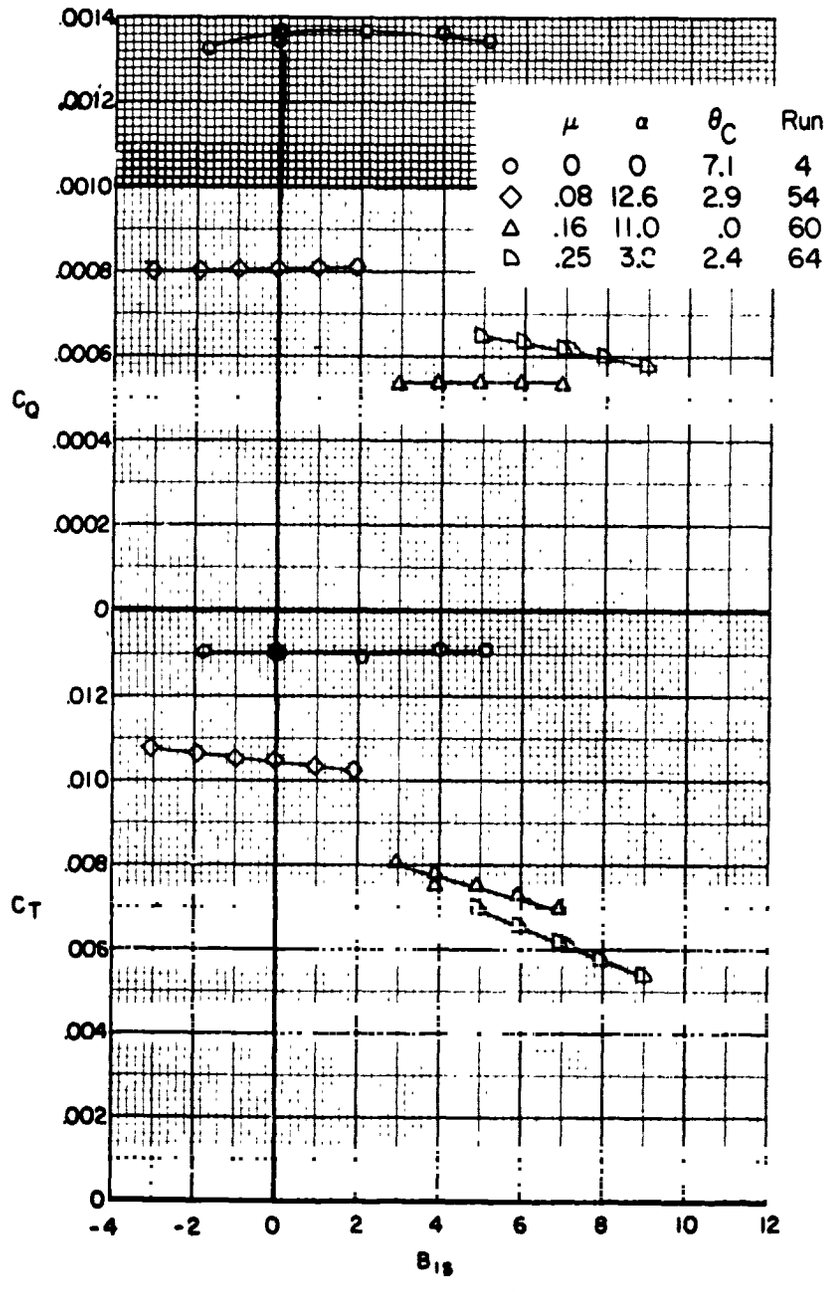

(b) $\alpha_p = 75^0$

Figure 62. - Continued.

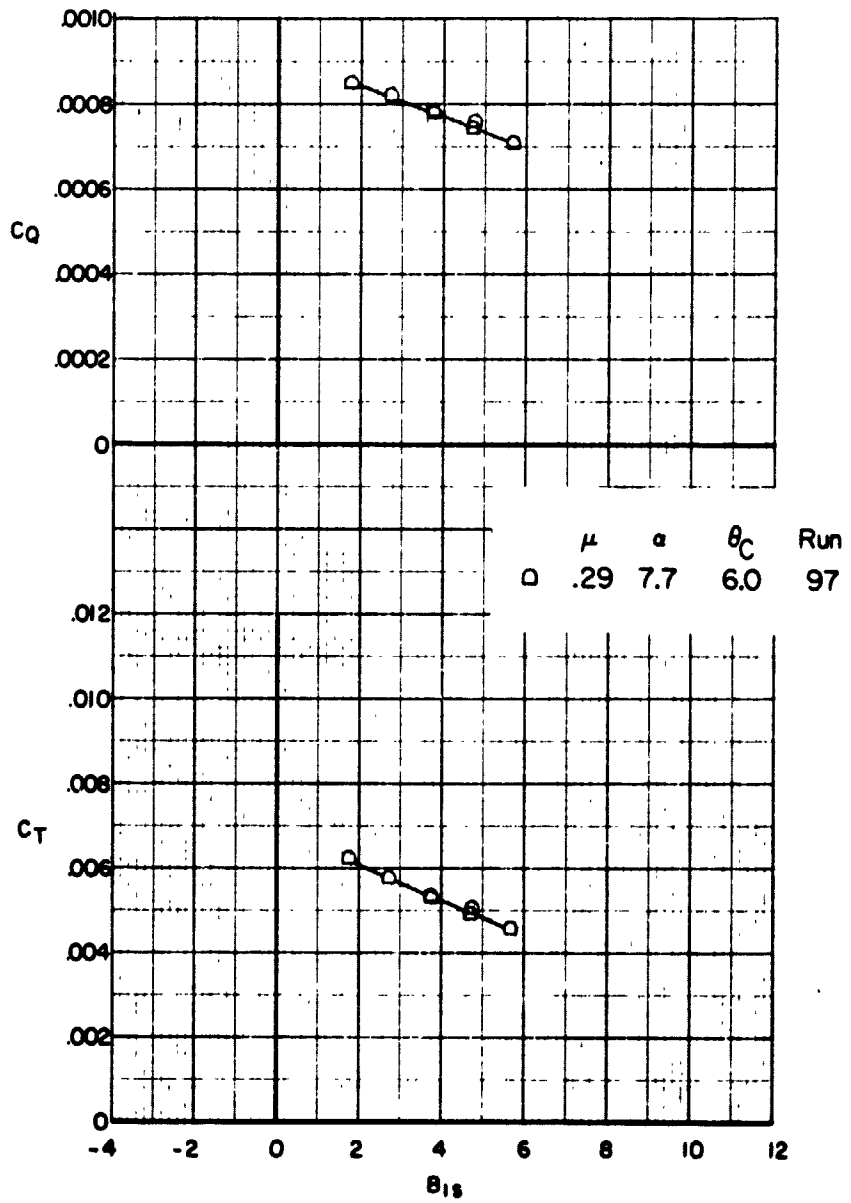

(c) $\alpha_p = 6^\circ$

Figure 68 - Continued.

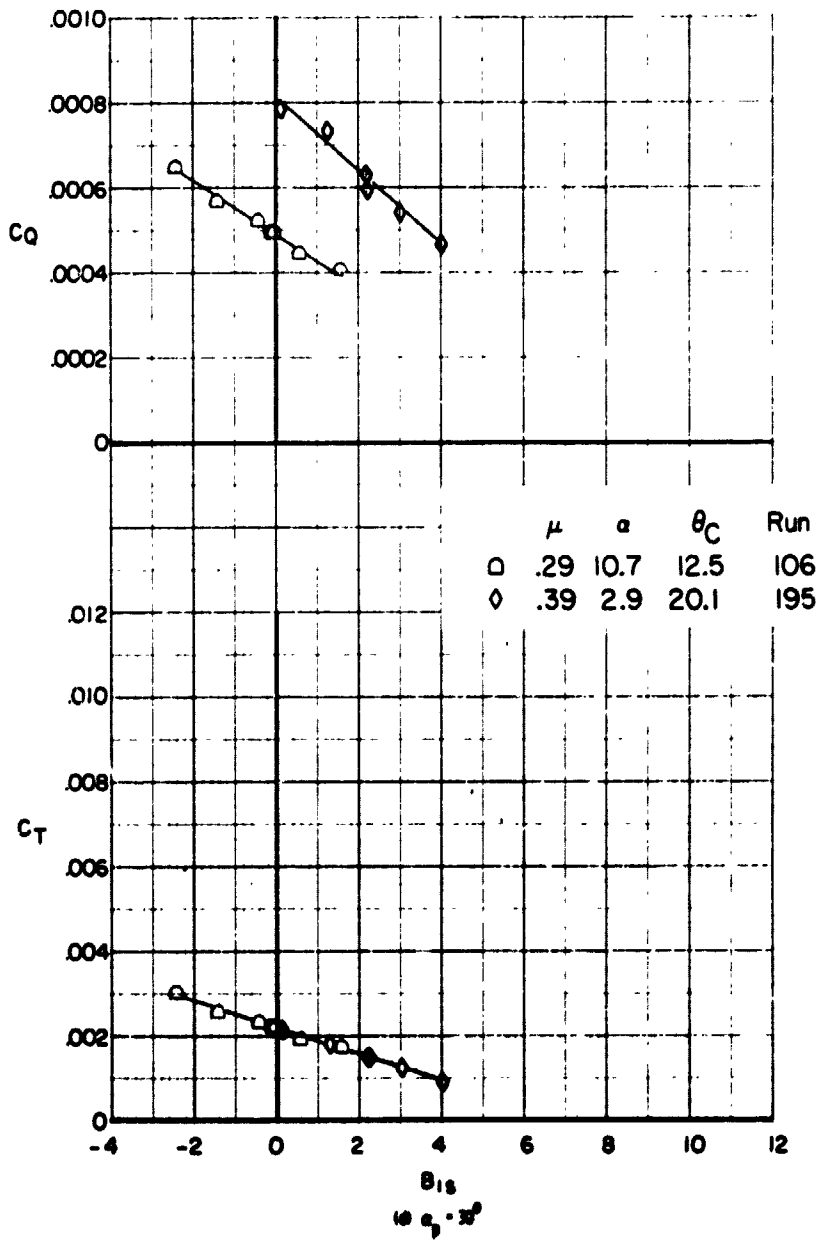

Figure 62. - Concluded.

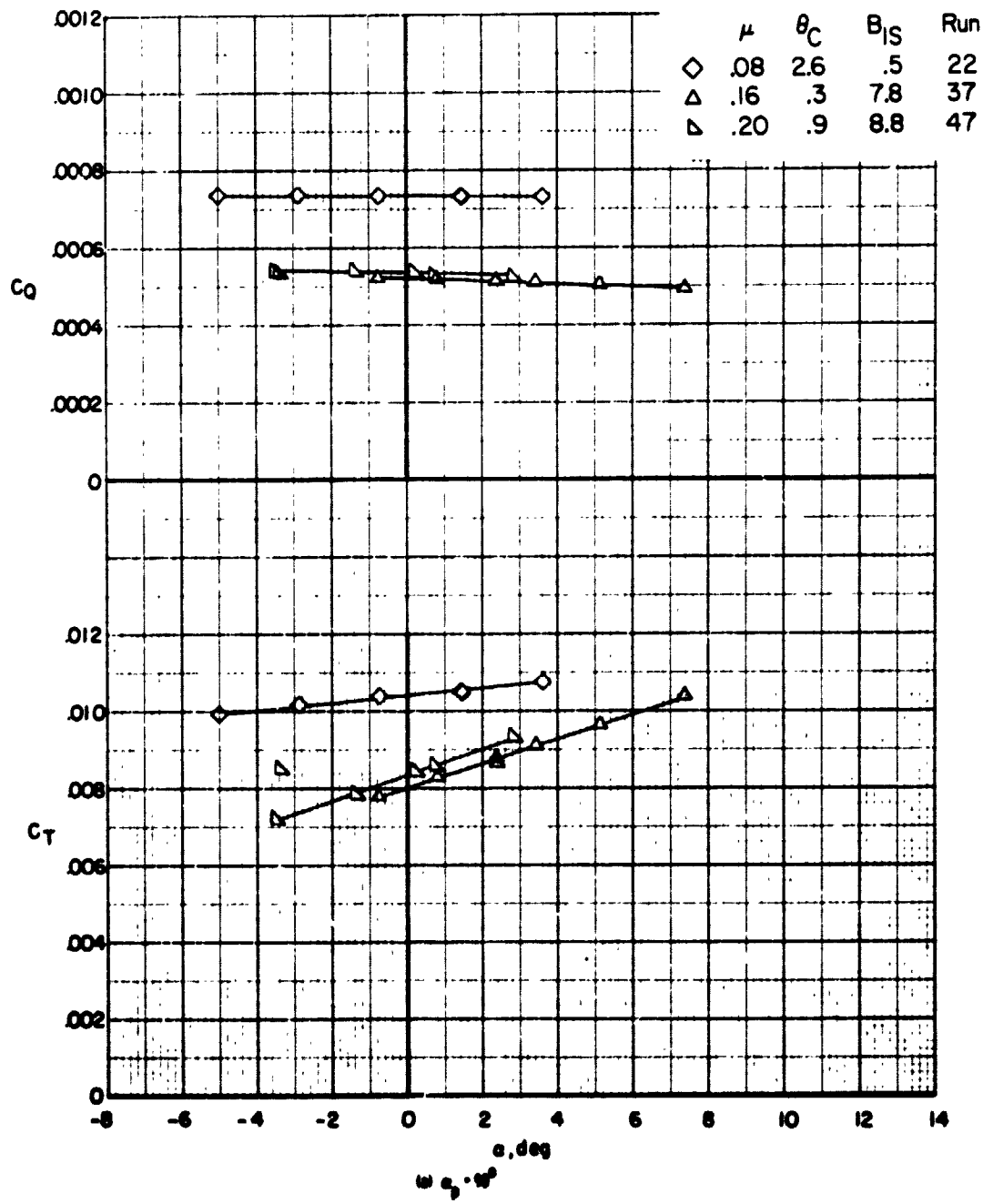

Figure 63. - Average rotor thrust and torque as a function of angle of attack for several wind speeds.

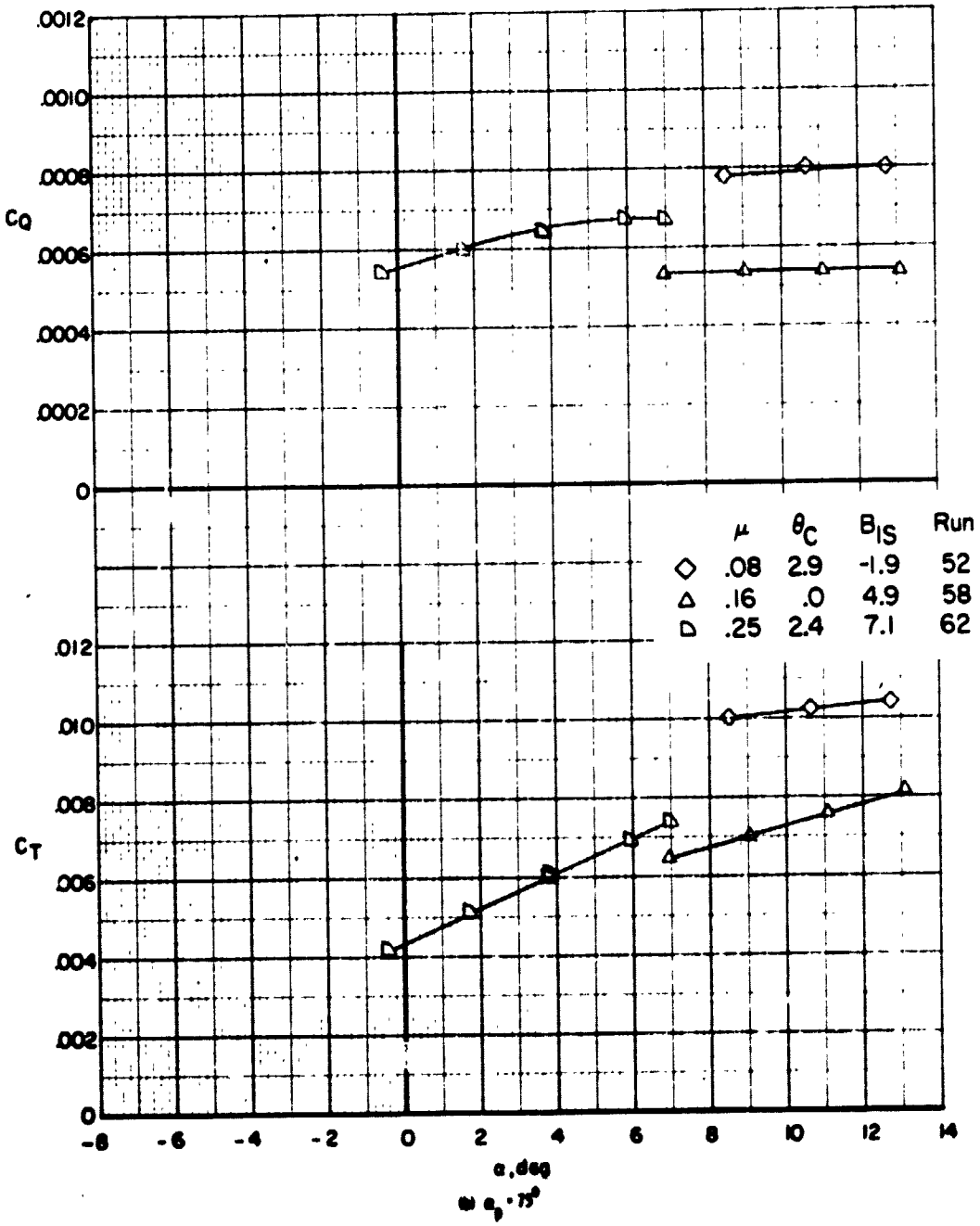

Figure 63. - Continued.

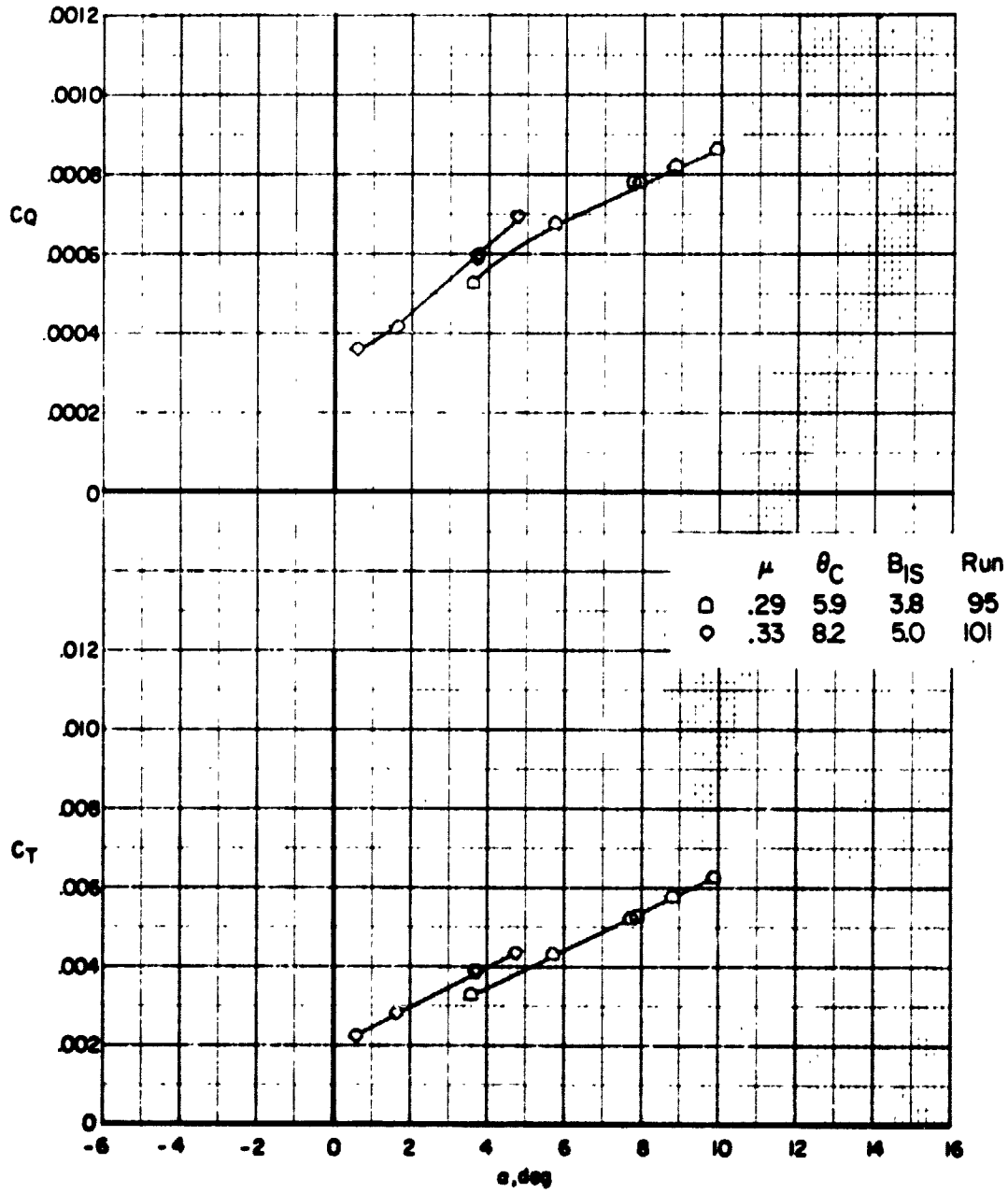

(c) $\alpha_p = 0^\circ$

Figure 63. - Continued.

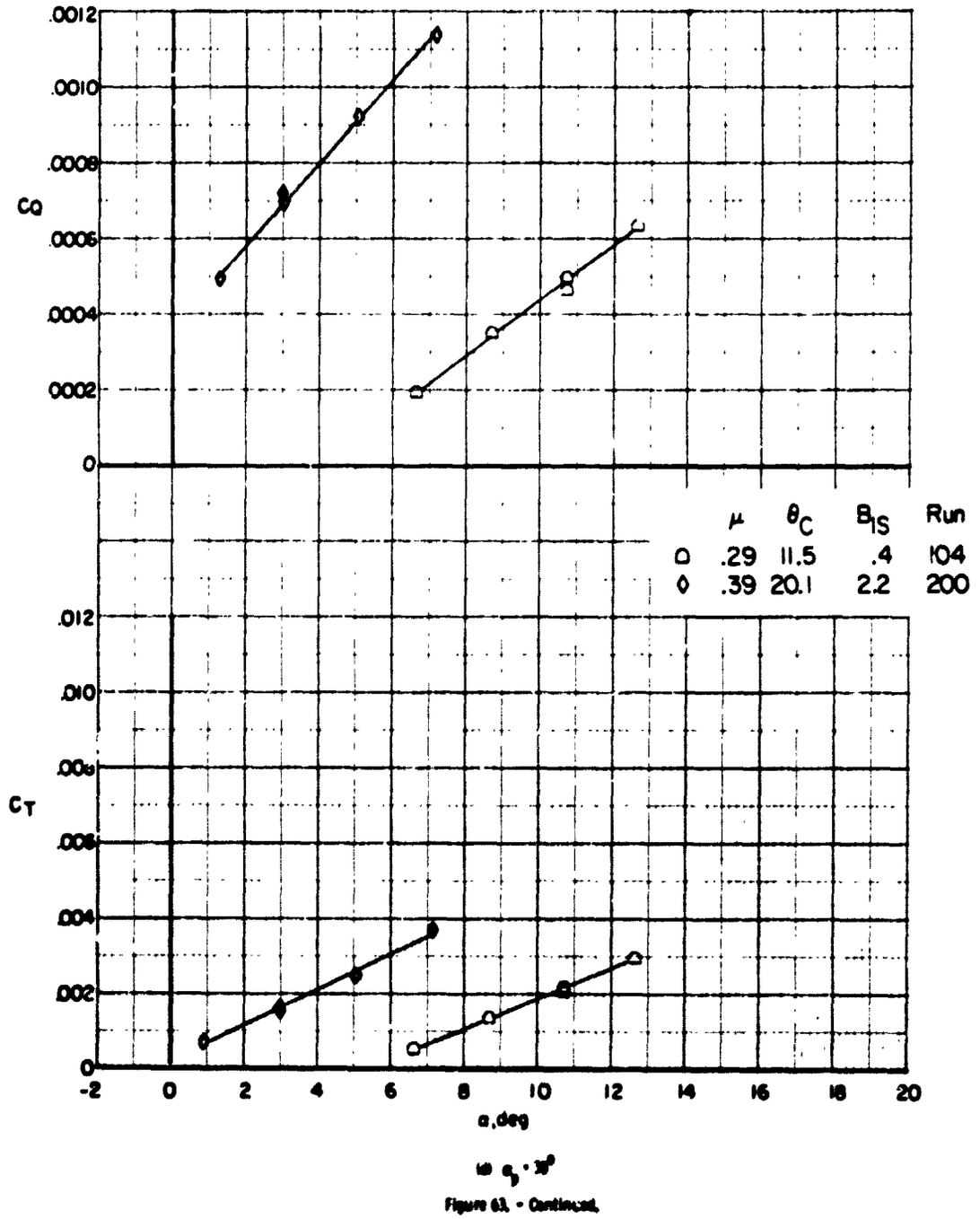

(a) $\phi_p = 30°$

Figure 63. - Continued.

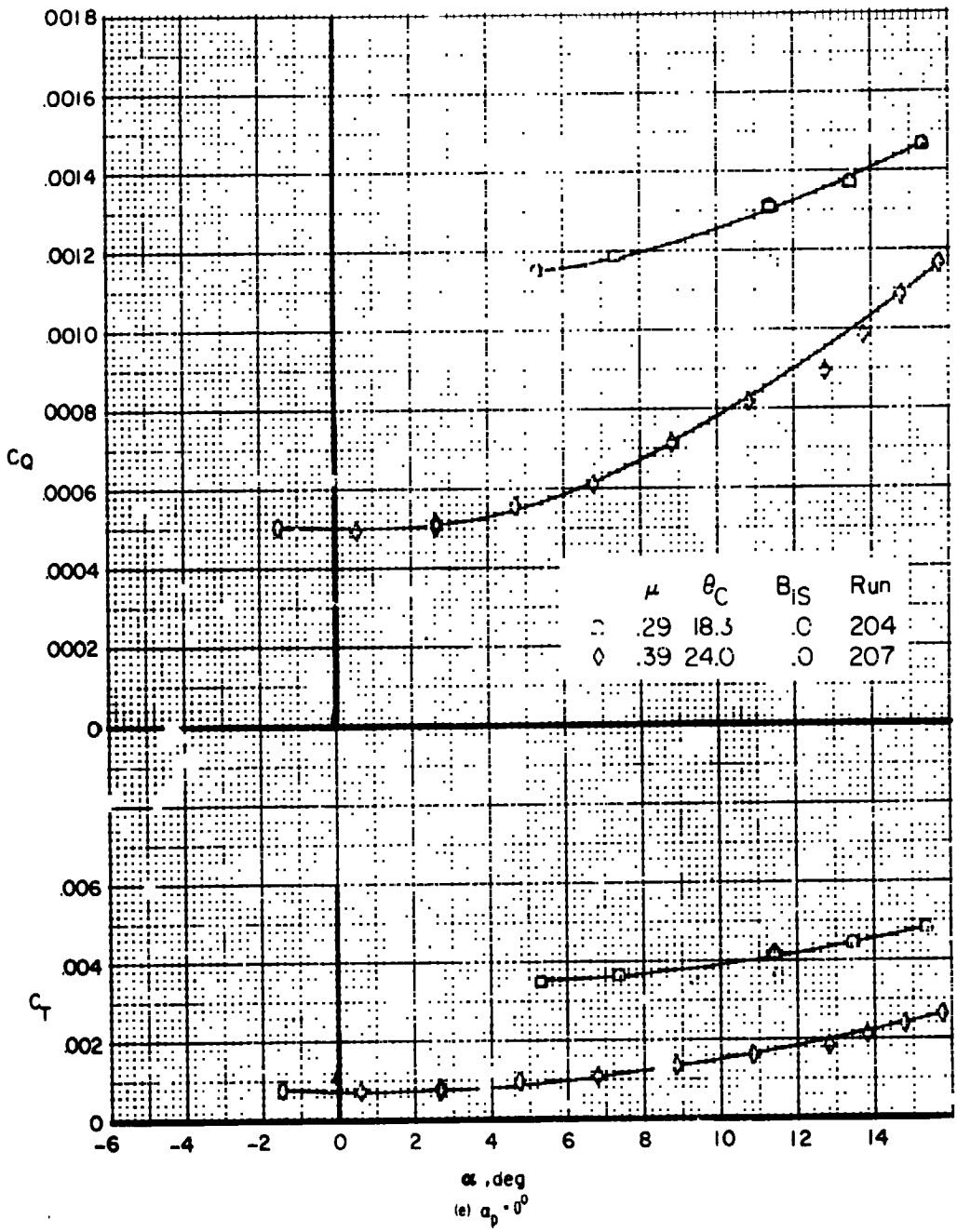

(e) $\alpha_p = 0^0$

Figure 63. - Concluded.

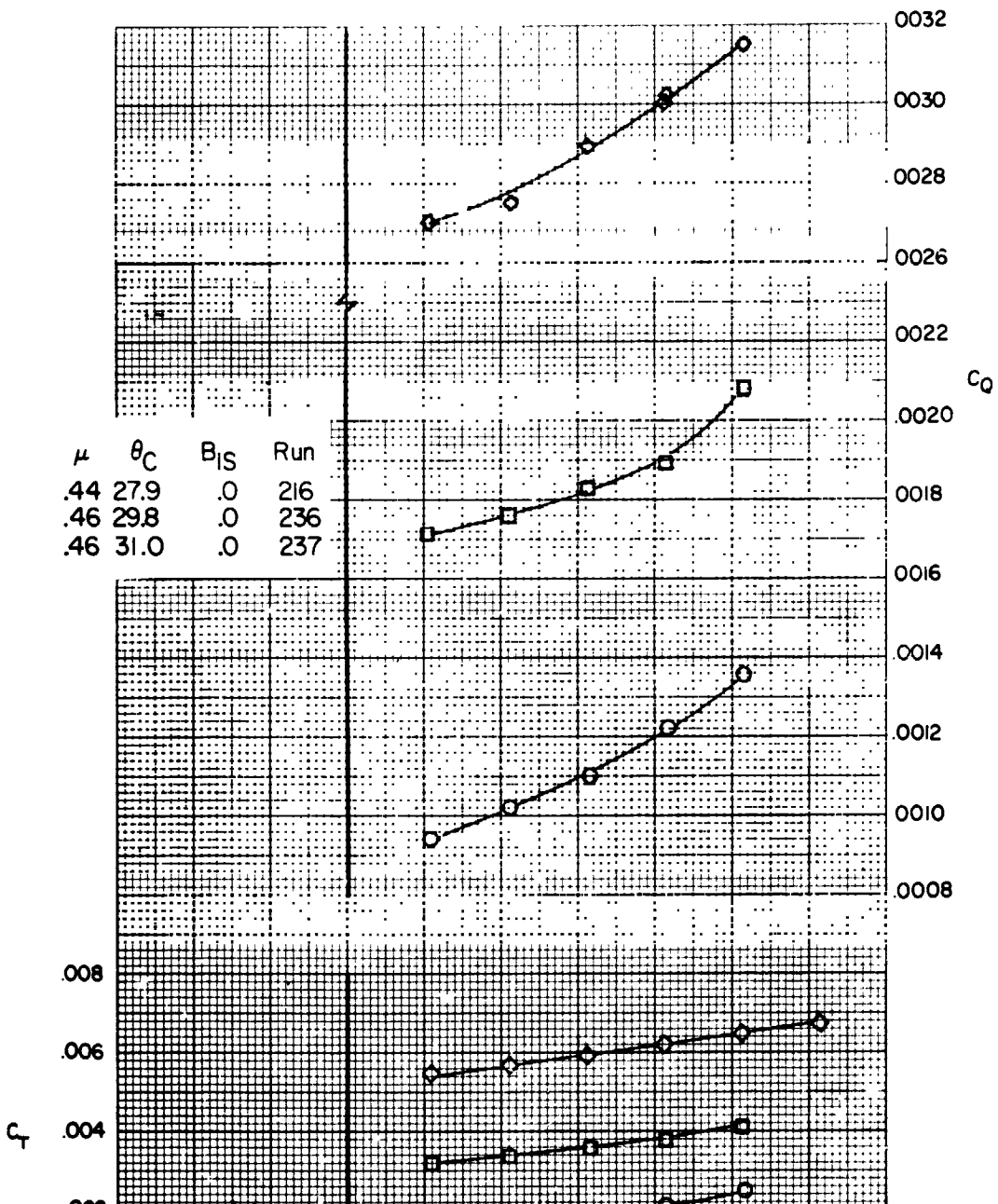

(a) $\mu = .45$.

Figure 64. - Average rotor thrust and torque as a function of angle of attack for several collective pitch settings.

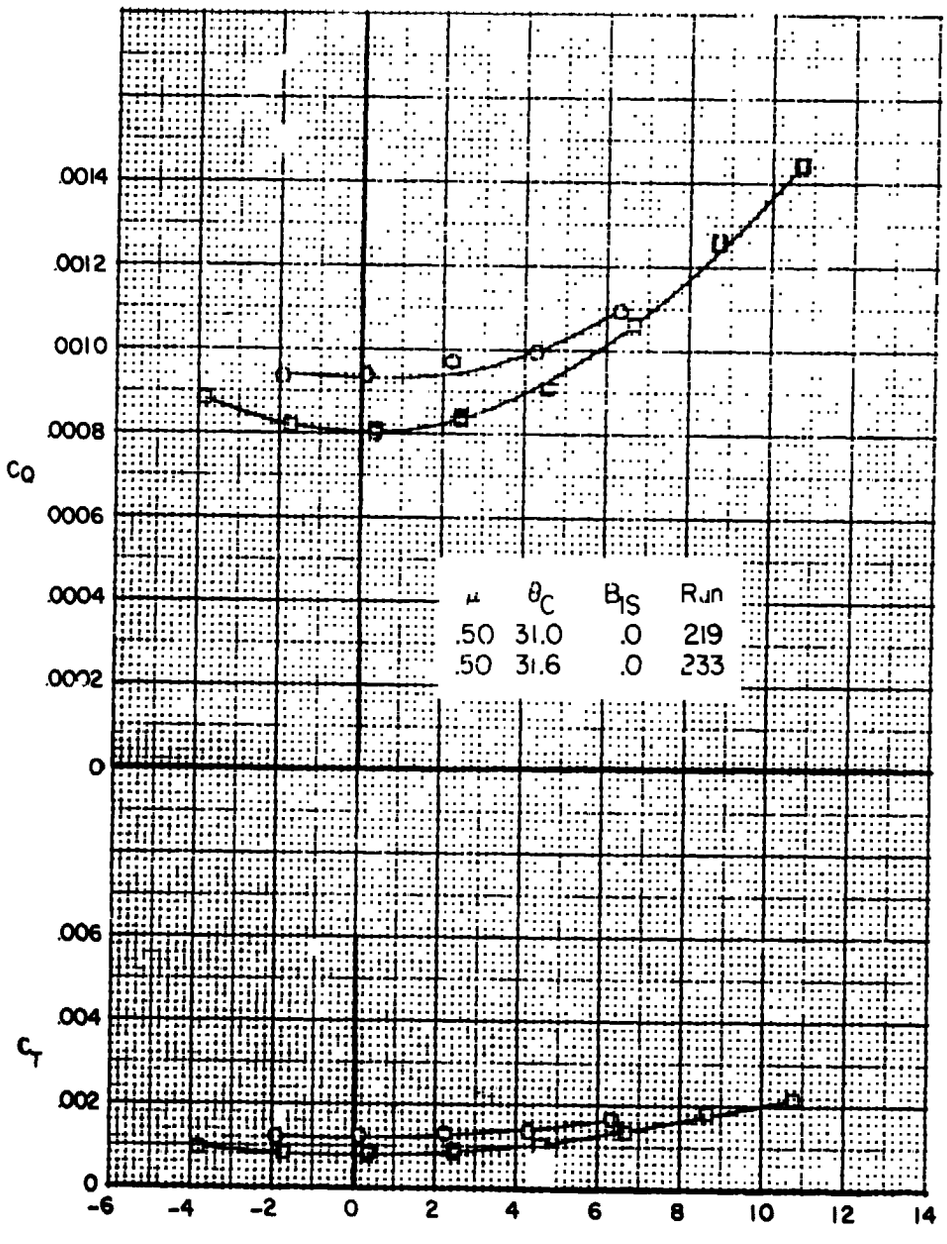

(b) $\mu = 0.50$

Figure 64. - Concluded.

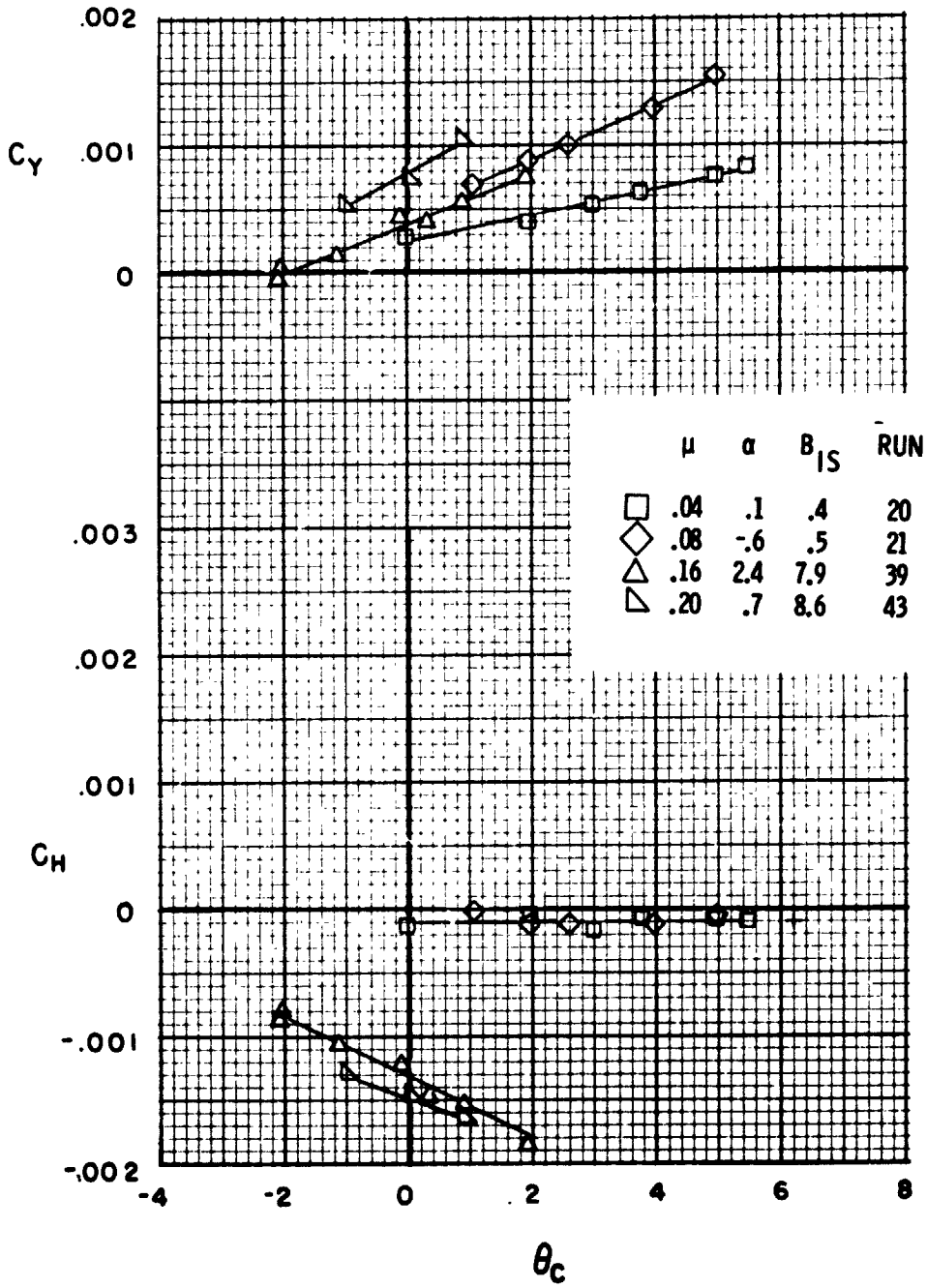

(a) $\alpha_p = 90^0$.

Figure 65 - Effect of collective pitch on the average rotor H force and Y force at several wind speeds.

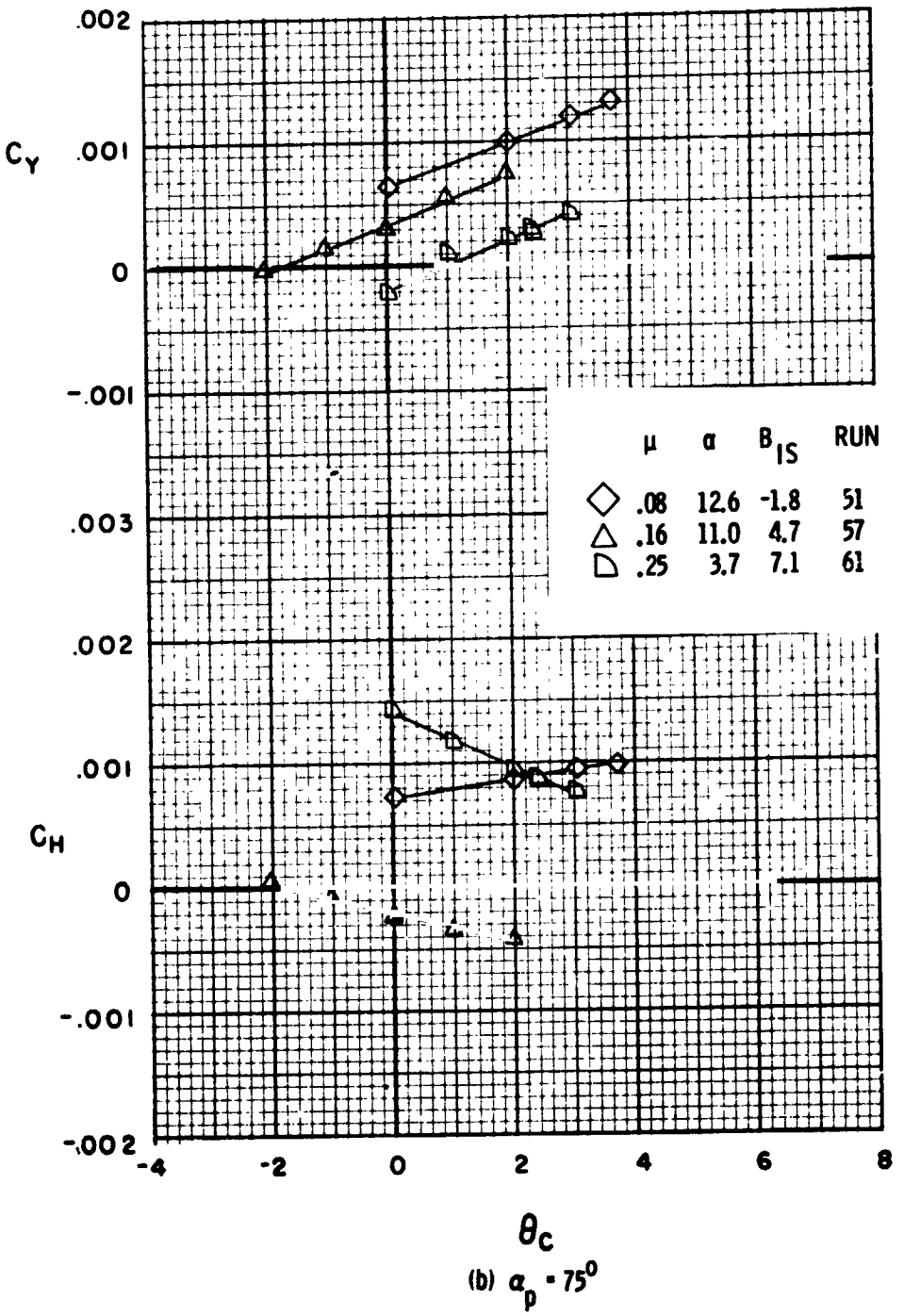

(b) $\alpha_p = 75^0$

Figure 65. - Continued.

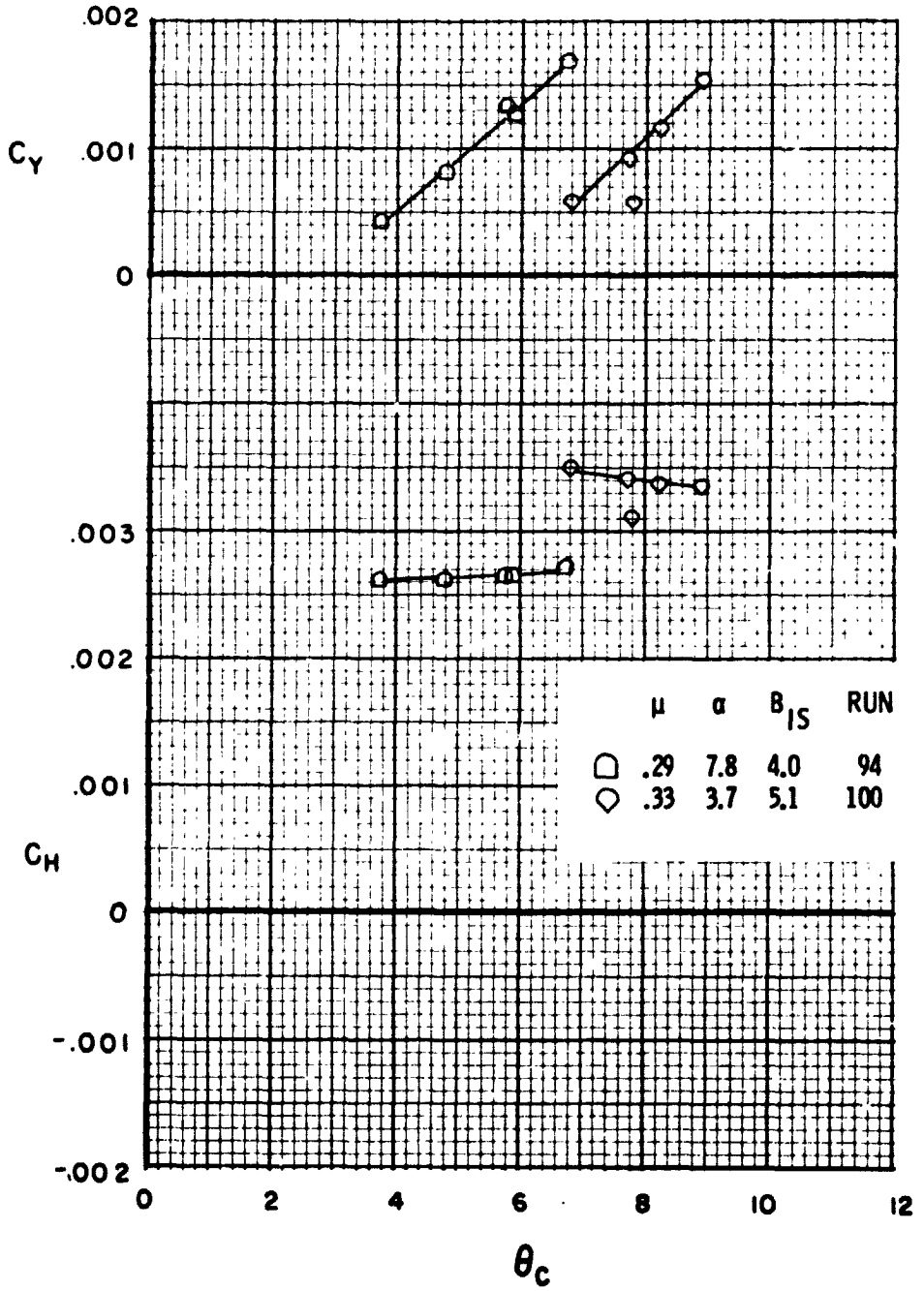

(c) $\alpha_p = 60^0$

Figure 65. - Continued.

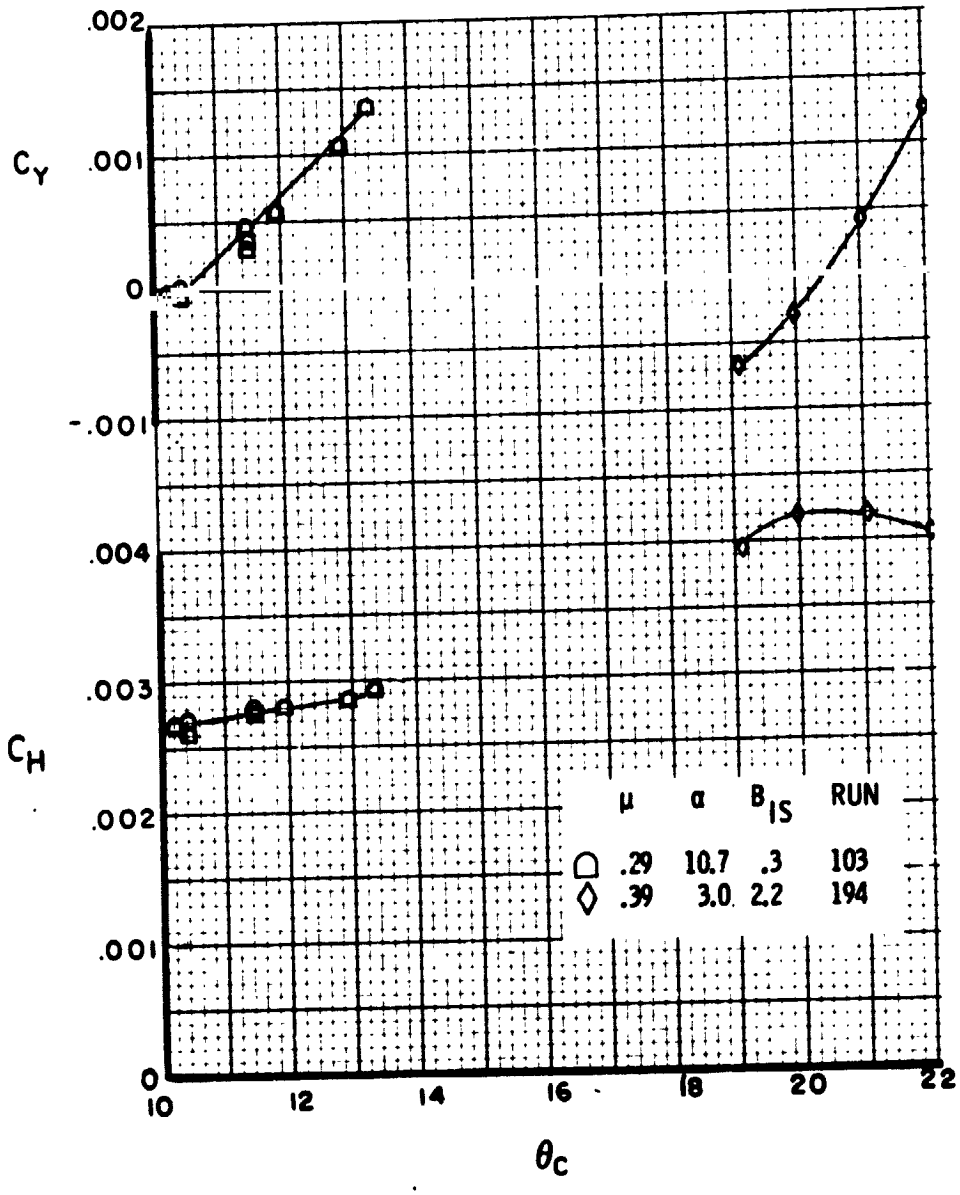

(d) $\alpha_p = 30^0$

Figure 65. - Continued.

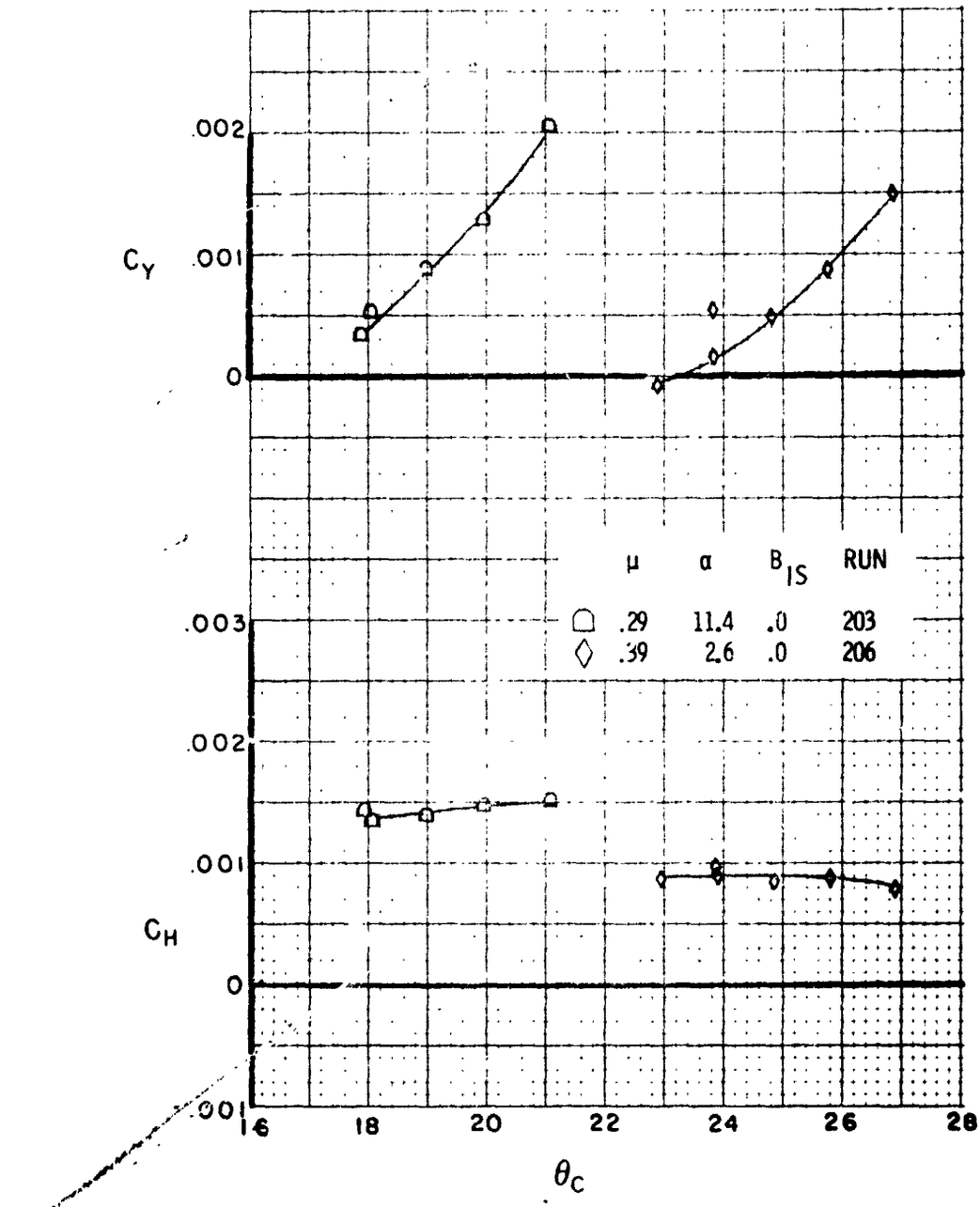

(e) $\alpha_p = 0°$

Figure 65. - Concluded.

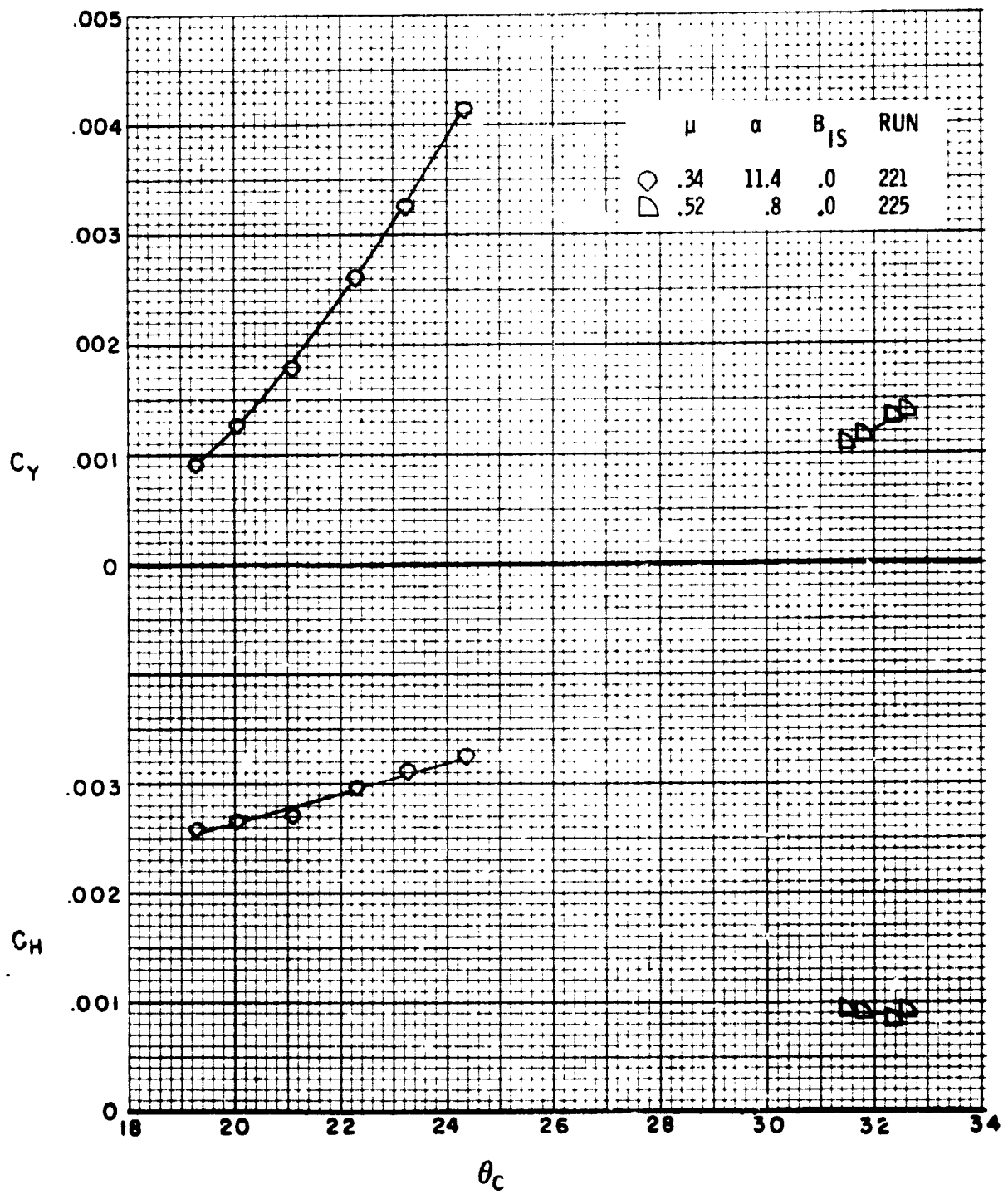

(a) $\delta_f = 50^0$, $\delta_a = 20^0$

Figure 66. - Effect of collective pitch on the average rotor H force and Y force at several wind speeds.

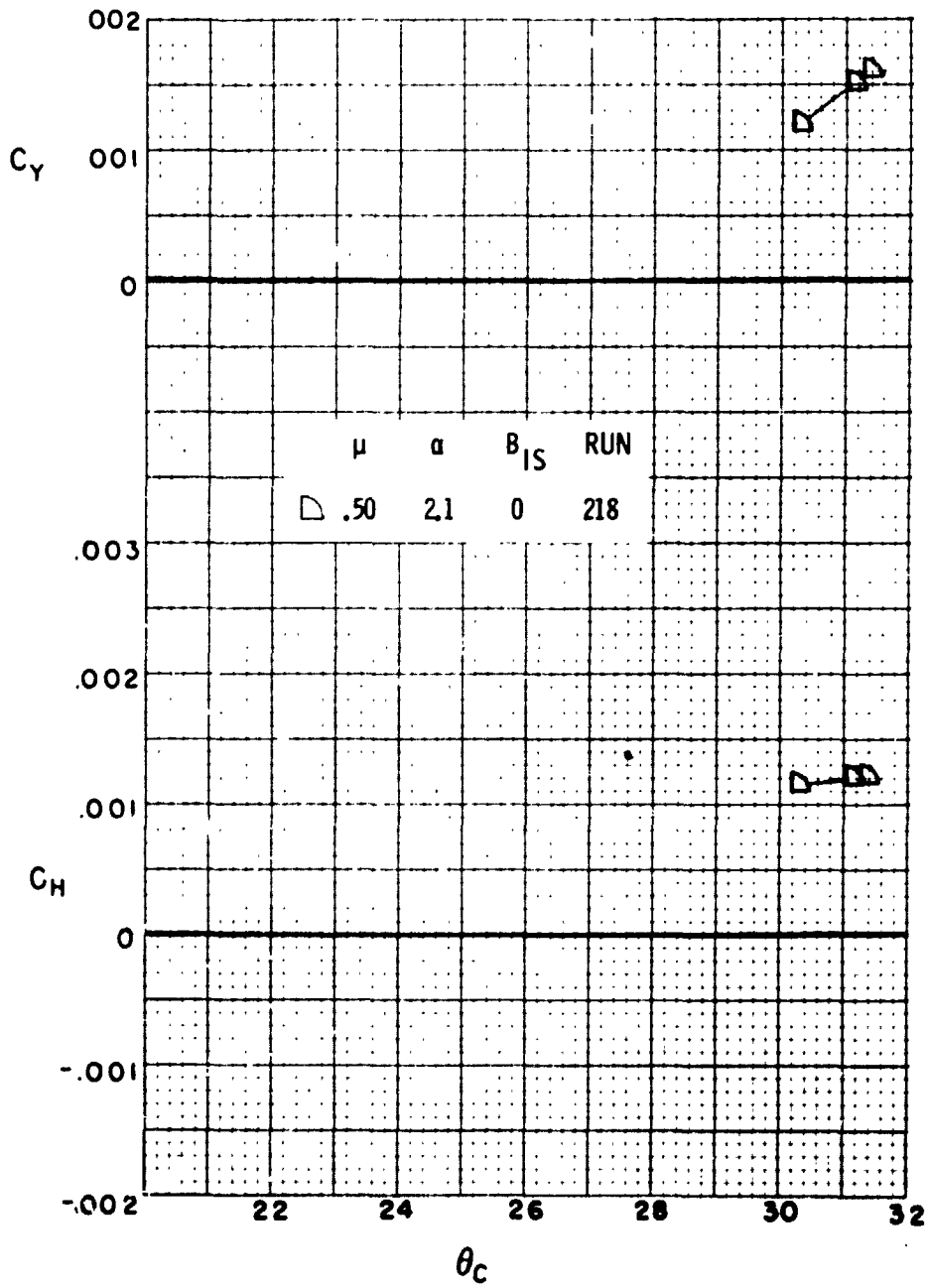

(b) $\delta_f = 0^0$, $\delta_a = 0^0$

Figure 66. - Concluded.

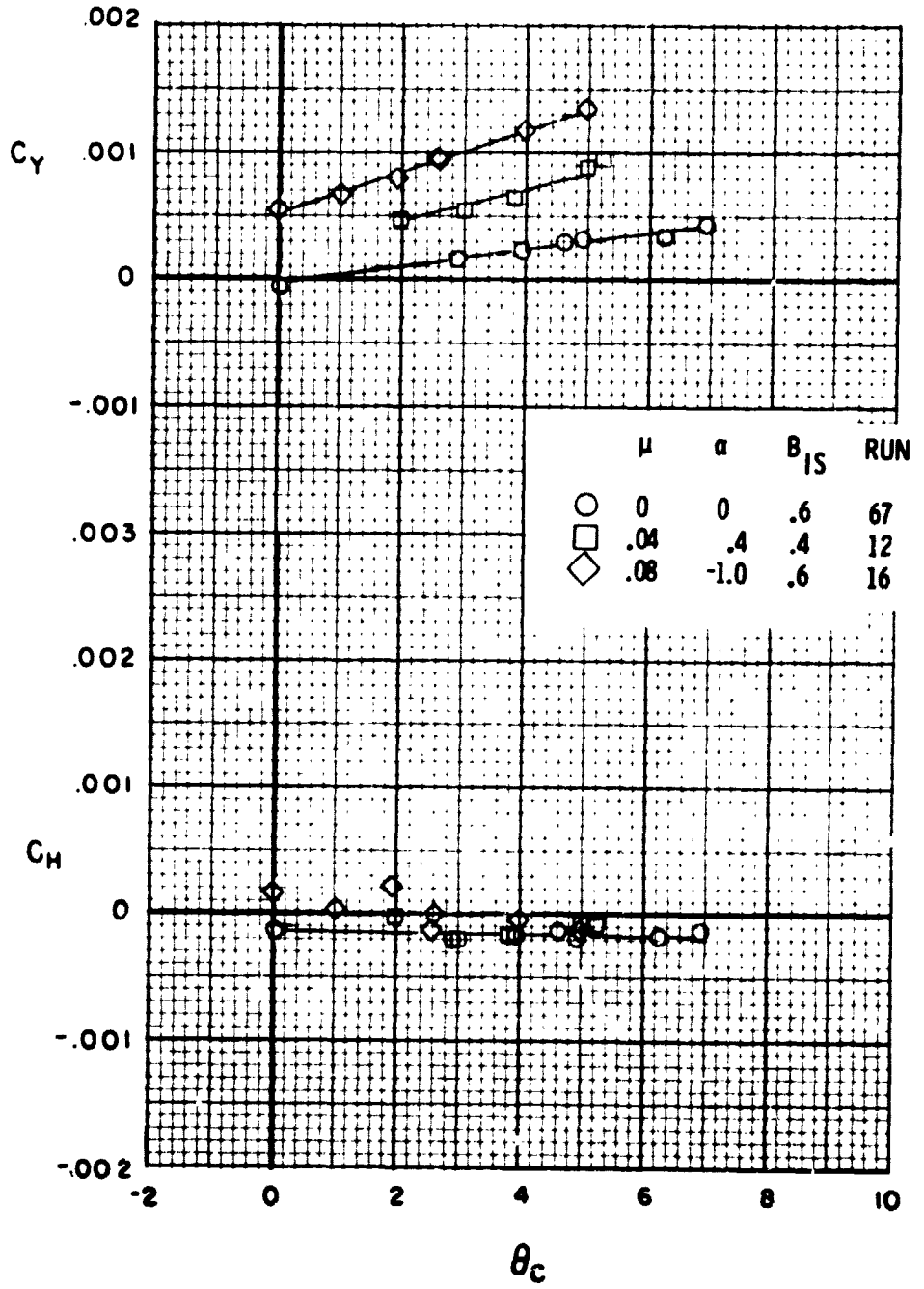

Figure 67. - Effect of collective pitch on the average rotor H and Y force for several low wind speeds with the tunnel walls up.

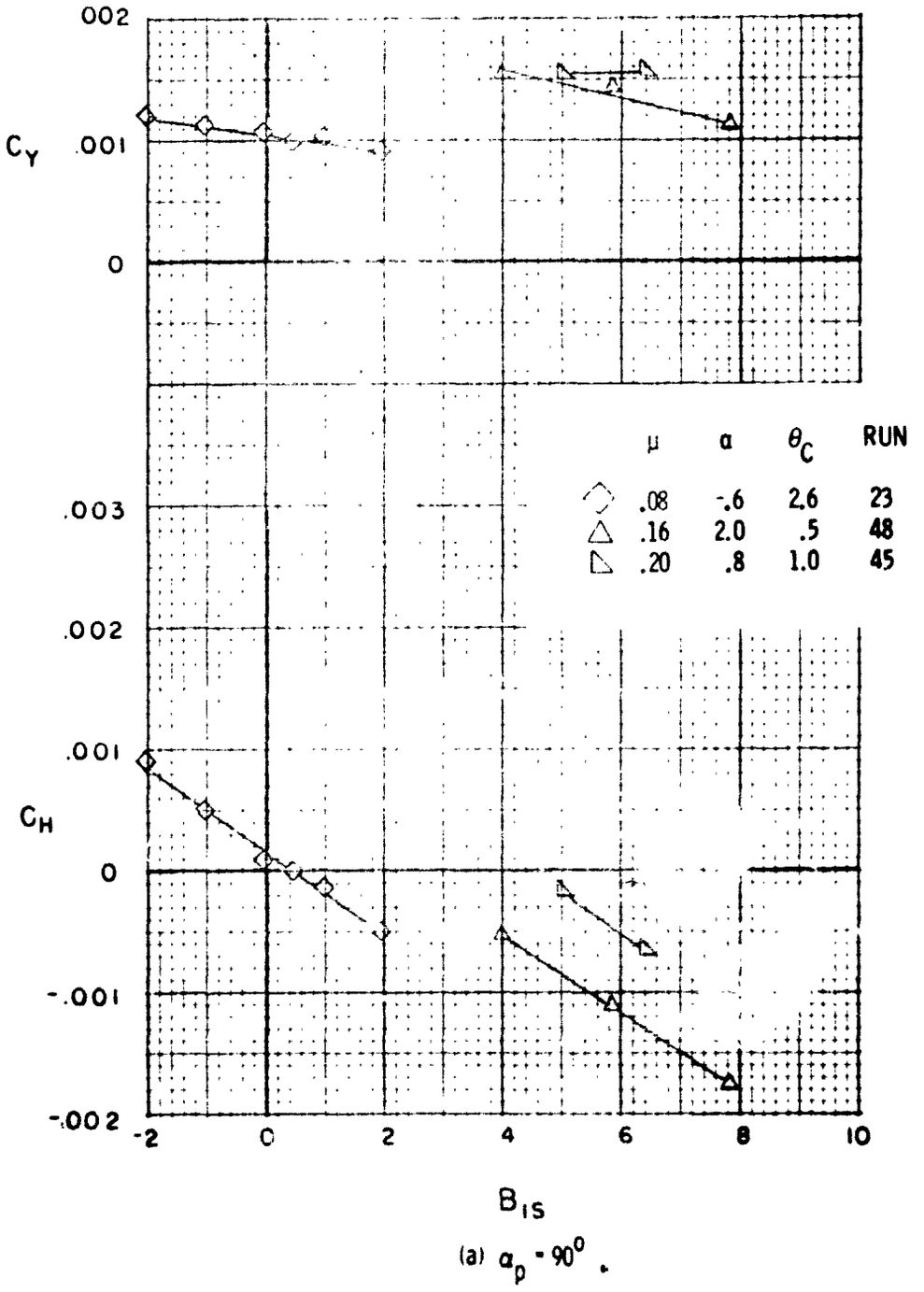

(a) $\alpha_p = 90^0$.

Figure 68. - Effect of cyclic pitch on the average rotor H and Y force at several wind speeds.

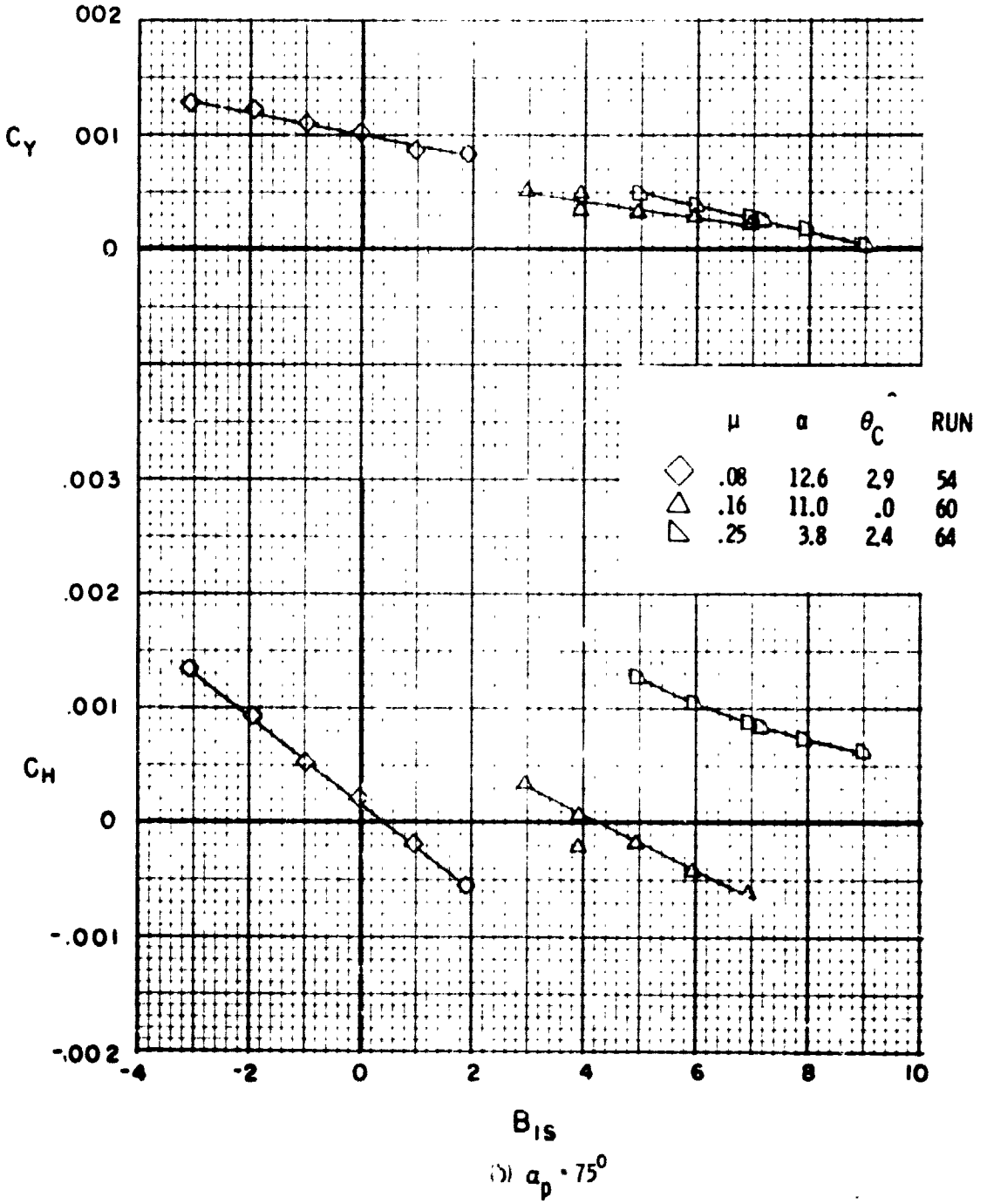

(b) $\alpha_p = 75^0$

Figure 68. - Continued.

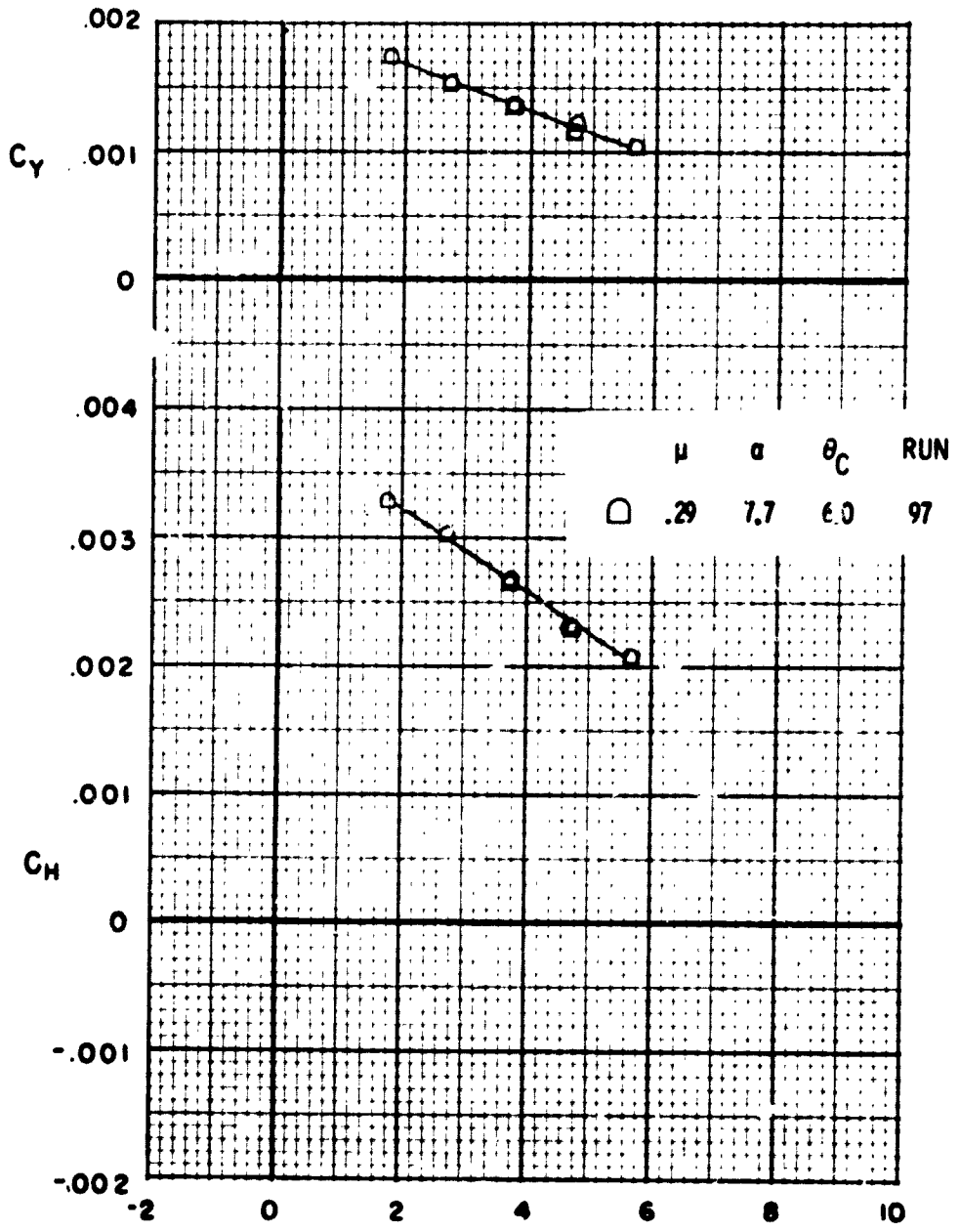

(c) $\alpha_p = 60^0$

Figure 68. - Continued.

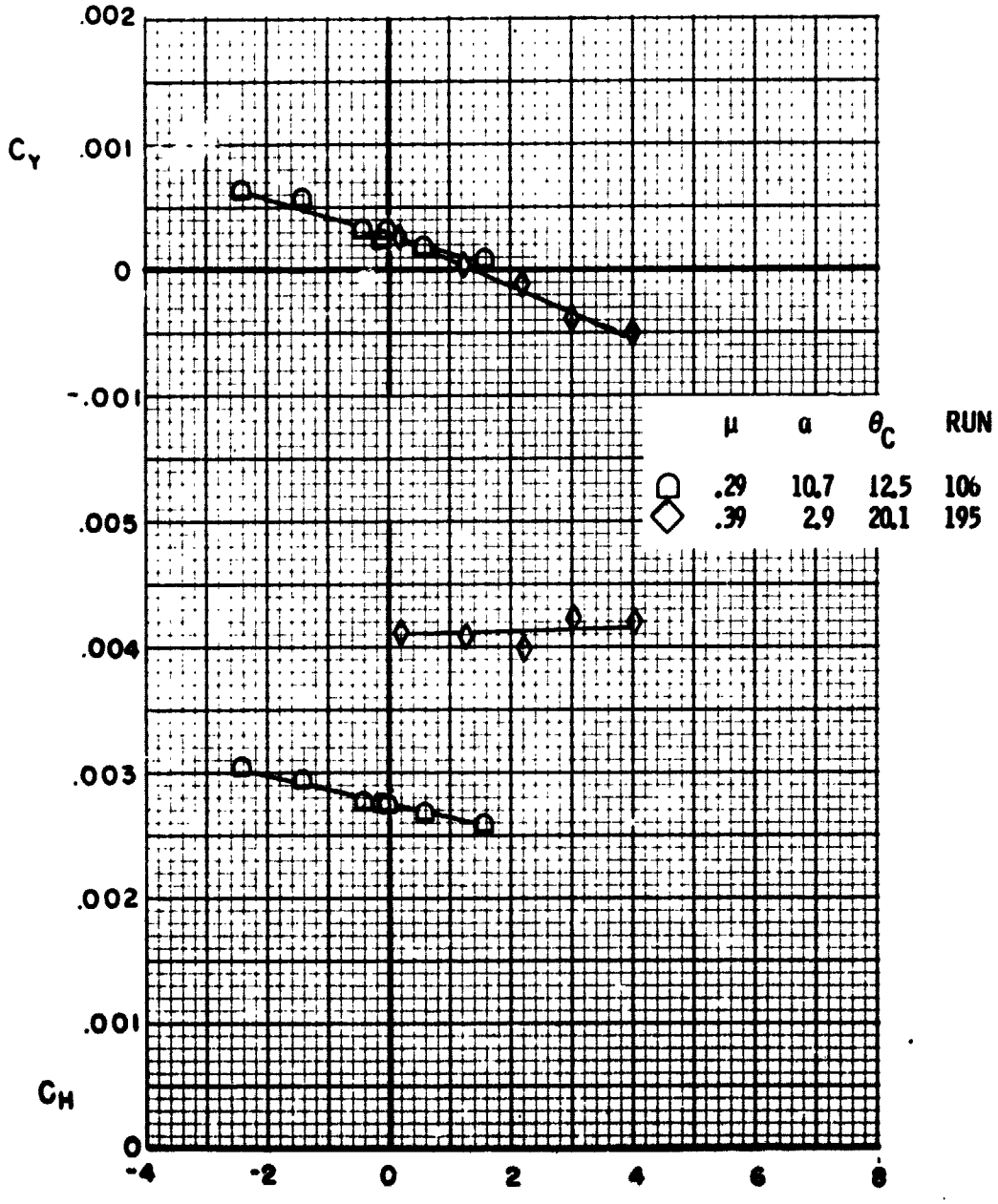

(d) $\alpha_0 = 30^0$

Figure 68. - Concluded.

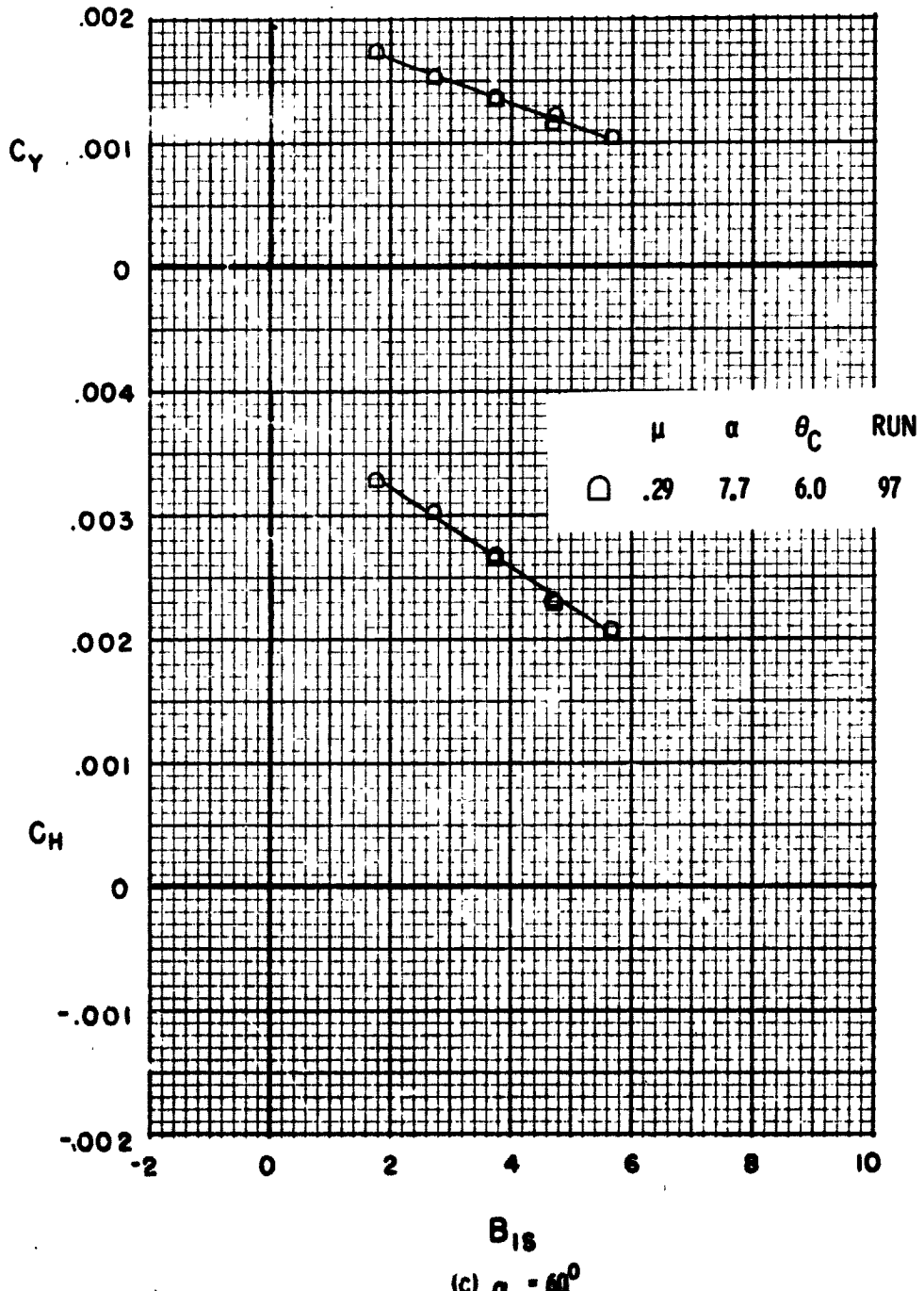

(c) $\alpha_p = 60^0$

Figure 68. - Continued.

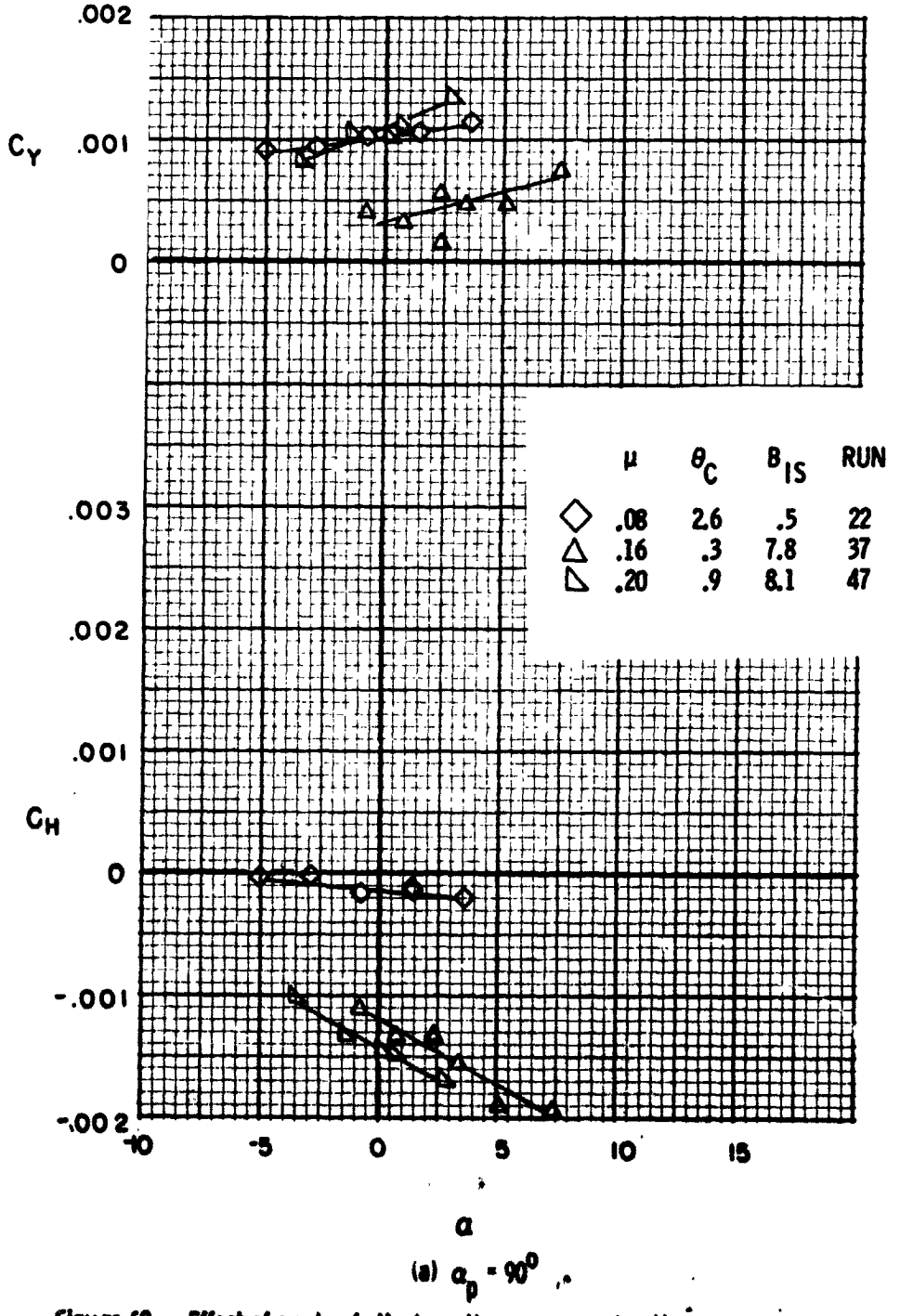

(a) $\alpha_p = 90^0$

Figure 69. - Effect of angle of attack on the average rotor H and Y force at several forward speeds.

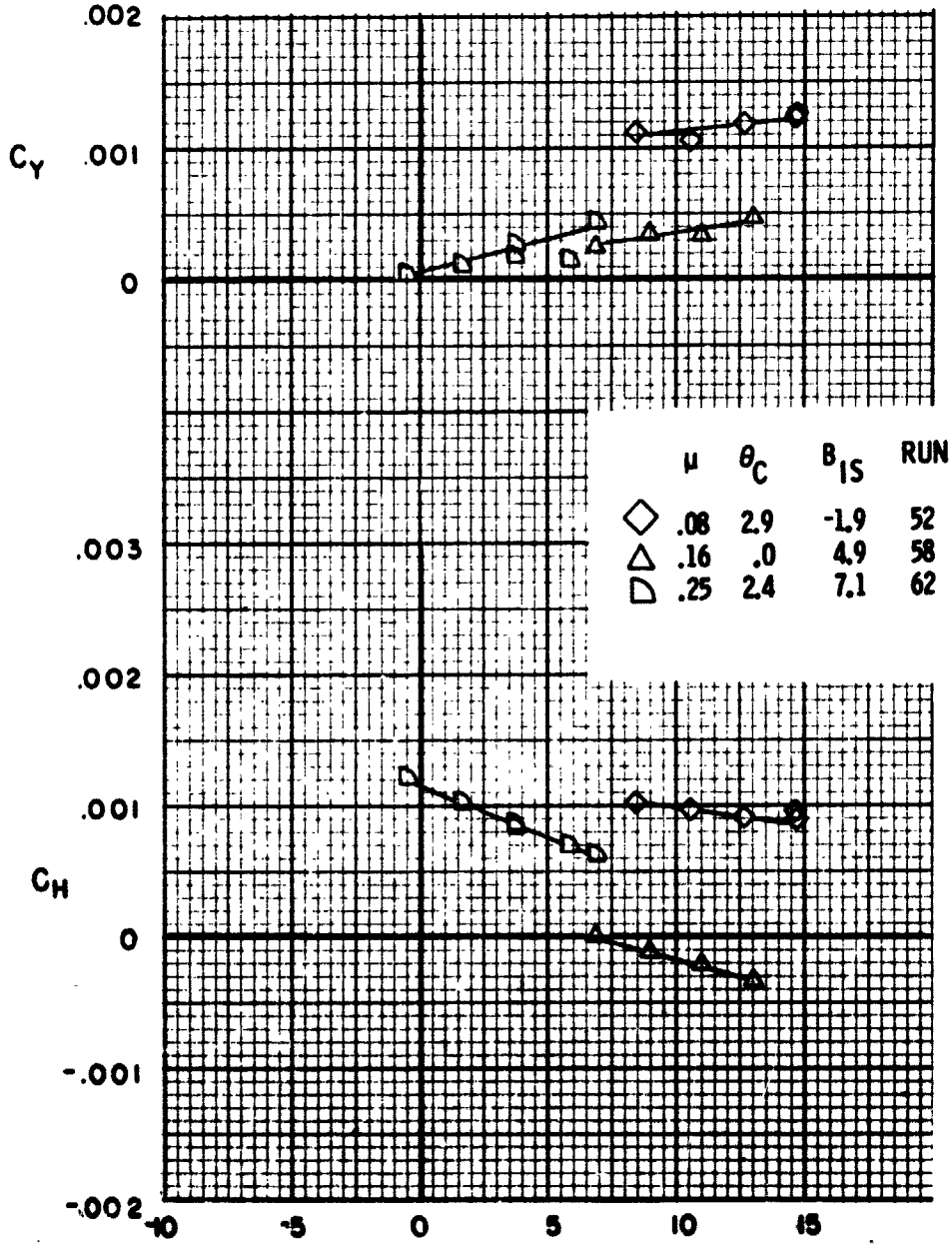

(b) $\alpha_p = 75^0$

Figure 69. - Continued.

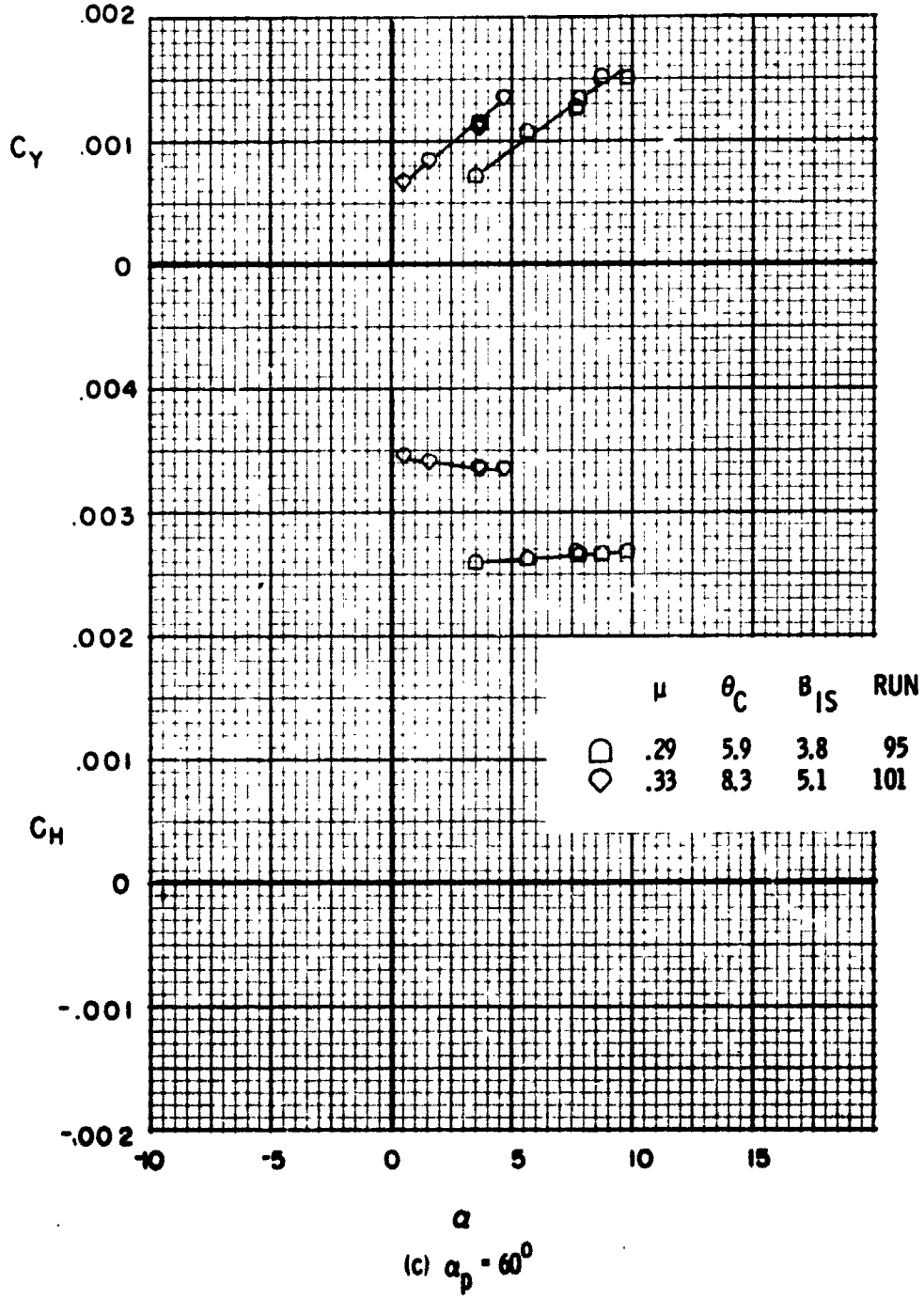

(c) $\alpha_p = 60^0$

Figure 69. - Continued.

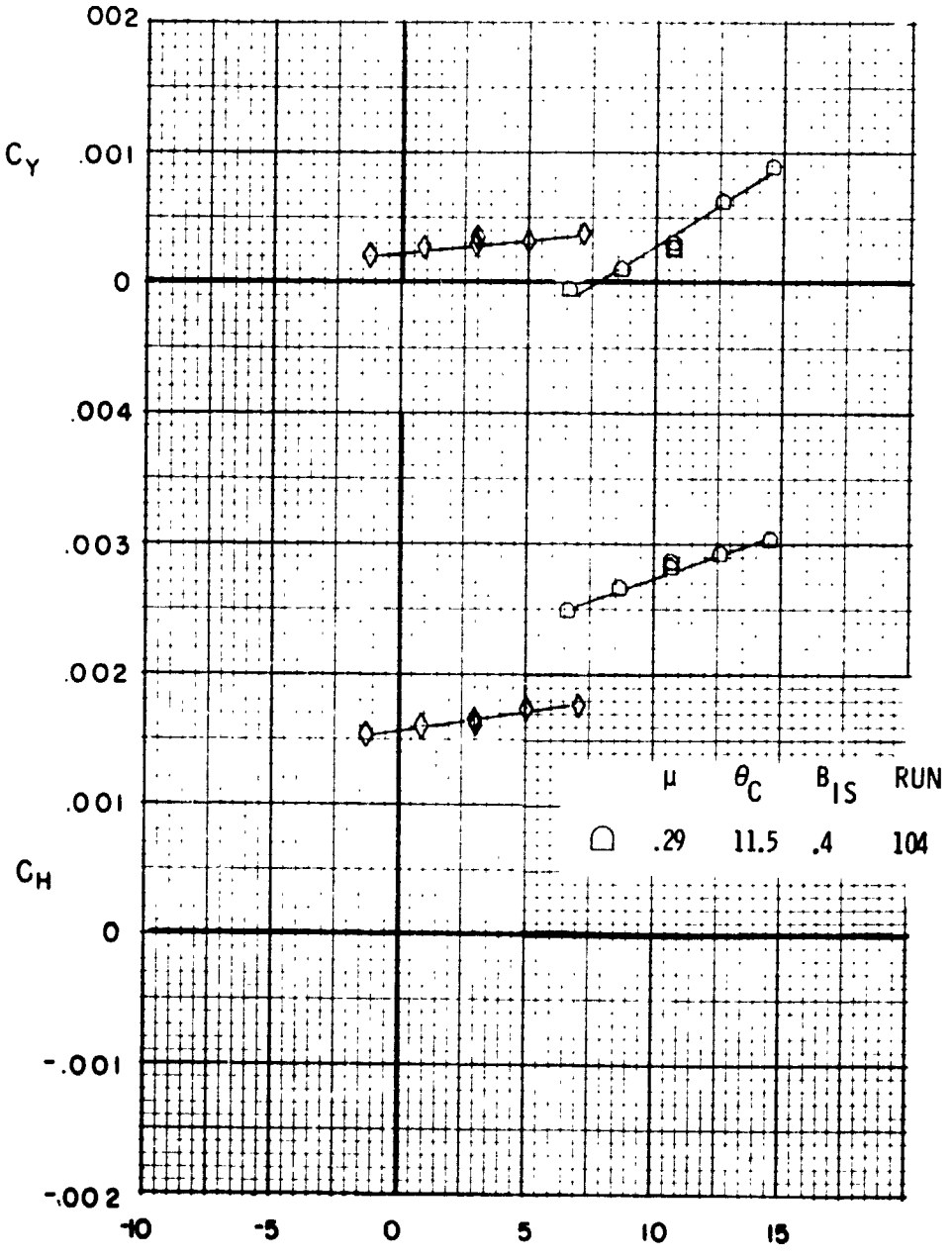

(d) $\alpha_p = 30^0$

Figure 69. - Continued.

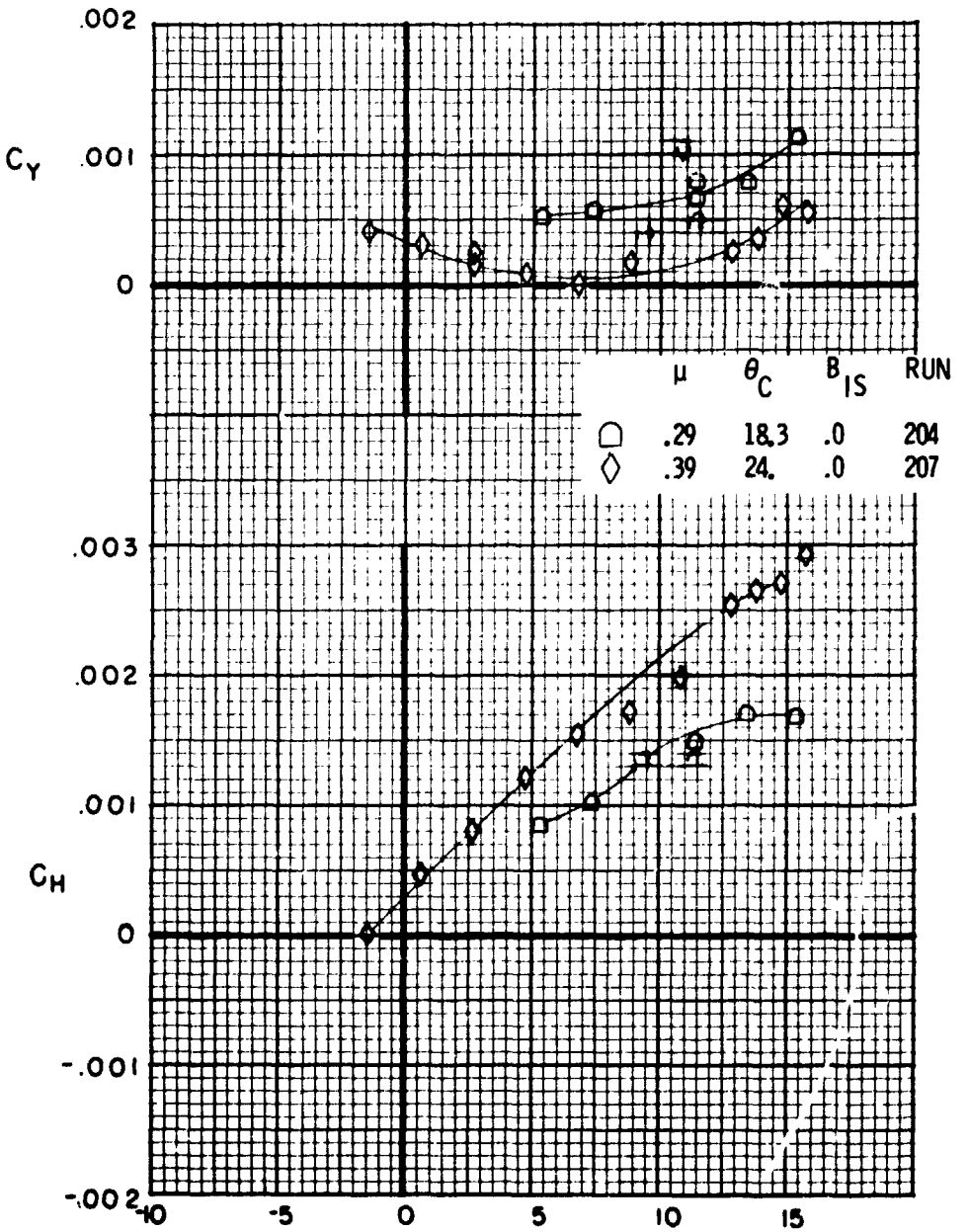

(e) $\alpha_p = 0^0$

Figure 69. - Concluded.

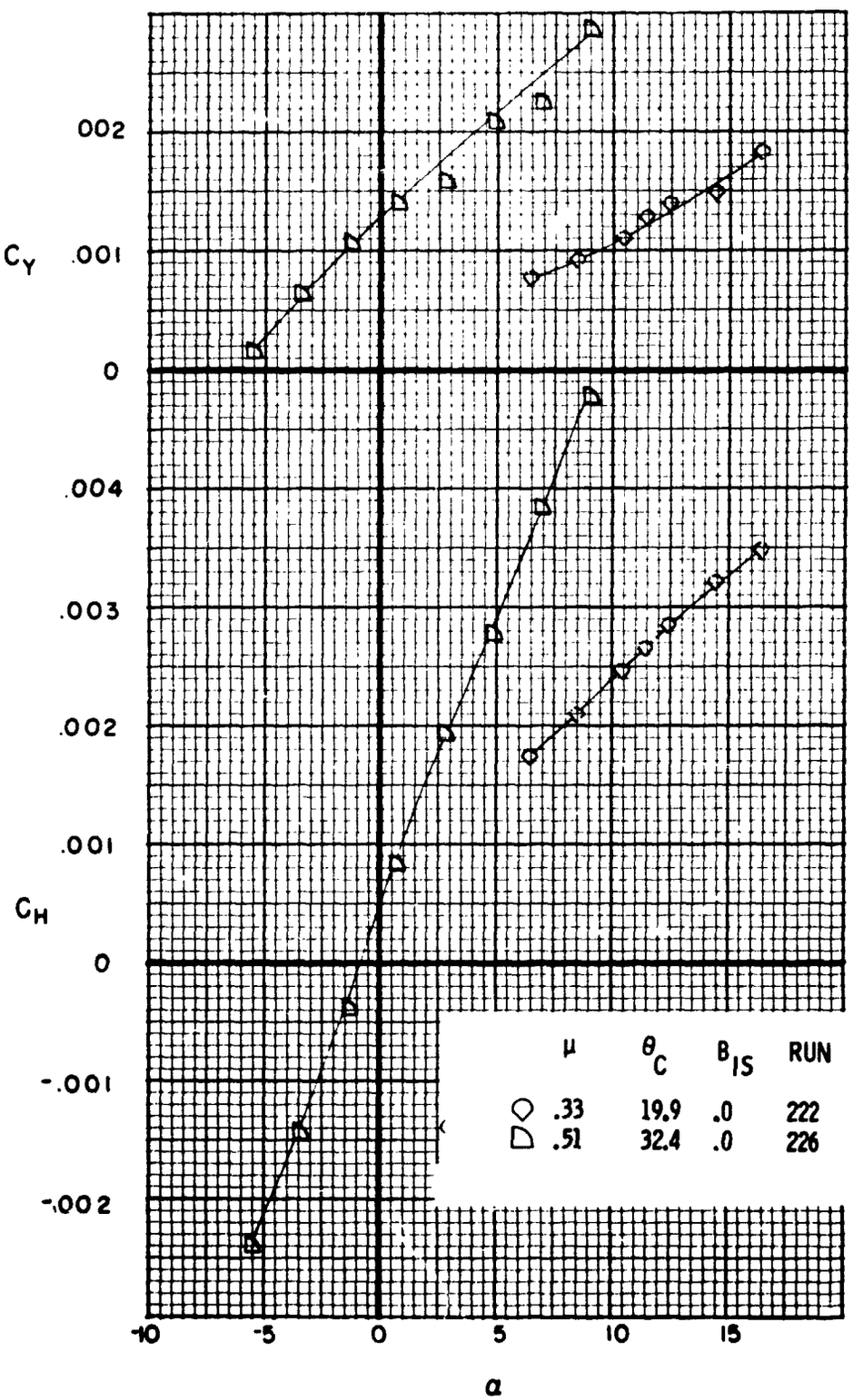

(a) $\delta_f = 50^0$, $\delta_d = 20^0$

Figure 70. - Effect of angle of attack on the average rotor H and Y force at several wind speeds for cruise r.p.m.

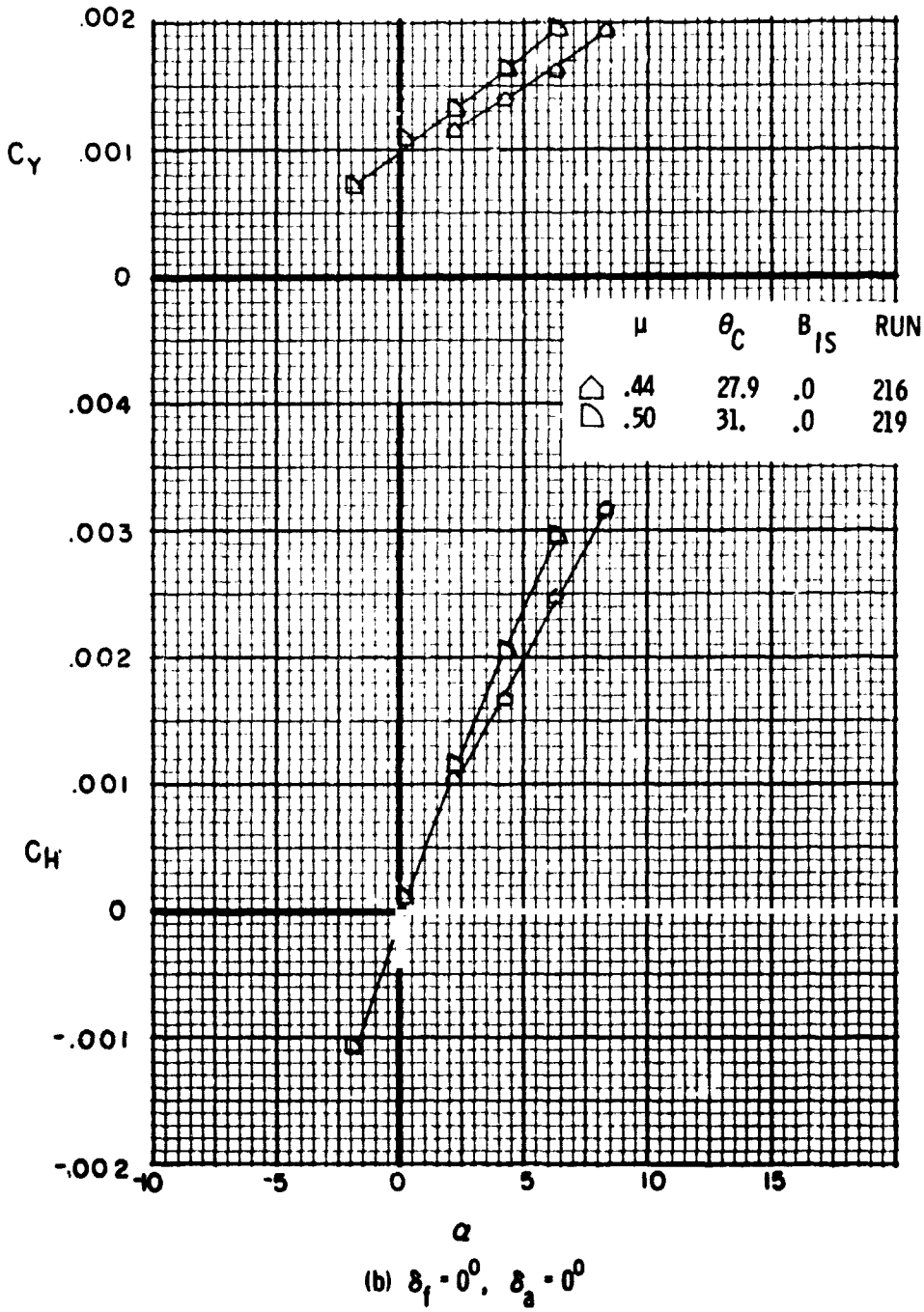

(b) $\delta_f = 0^0$, $\delta_a = 0^0$

Figure 70. - Concluded.

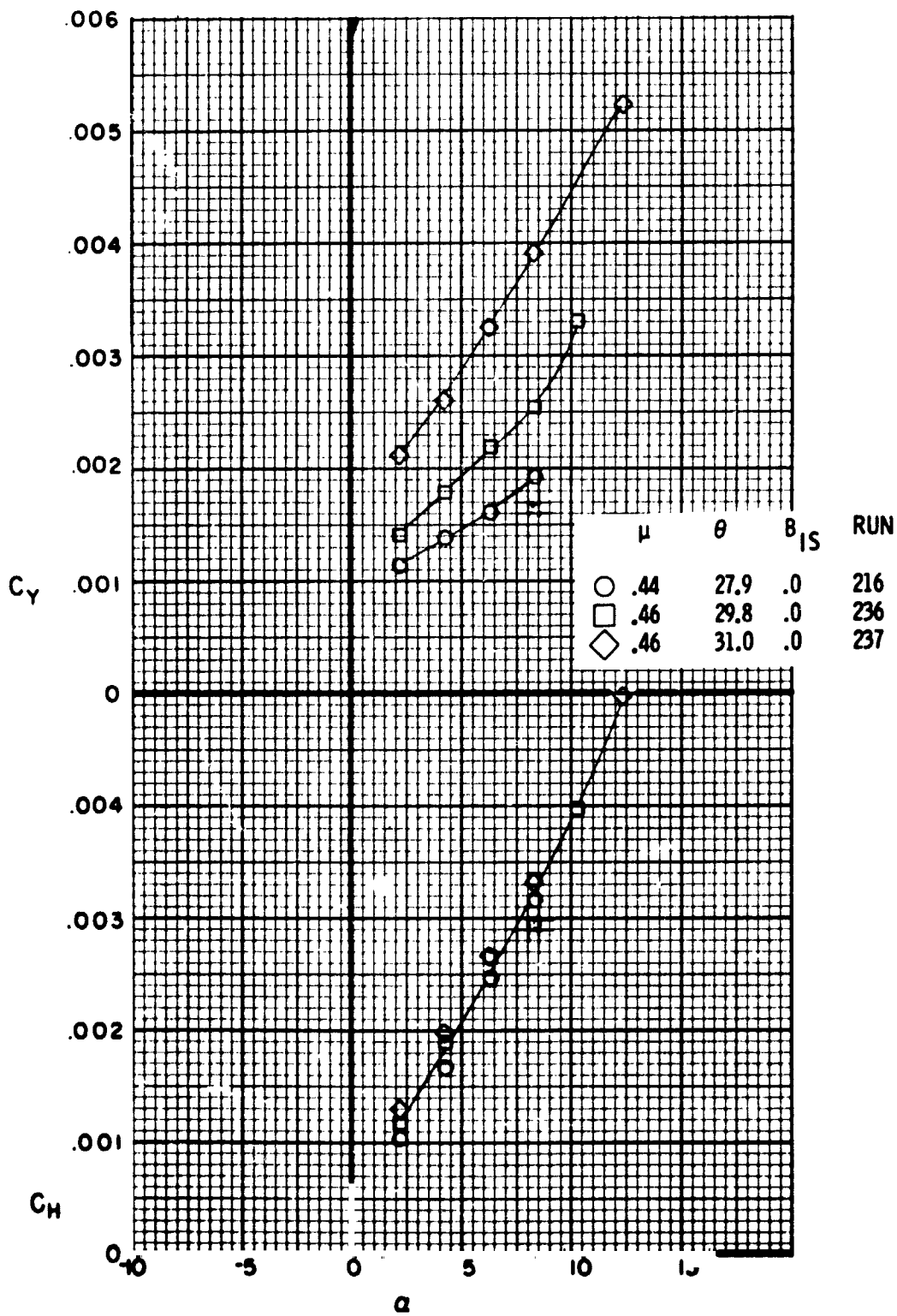

Figure 71. - Effect of angle of attack on the average rotor H and Y force at several collective pitch angles, μ 0.46, $\delta_f = 0^0$, $\delta_s = 0^0$

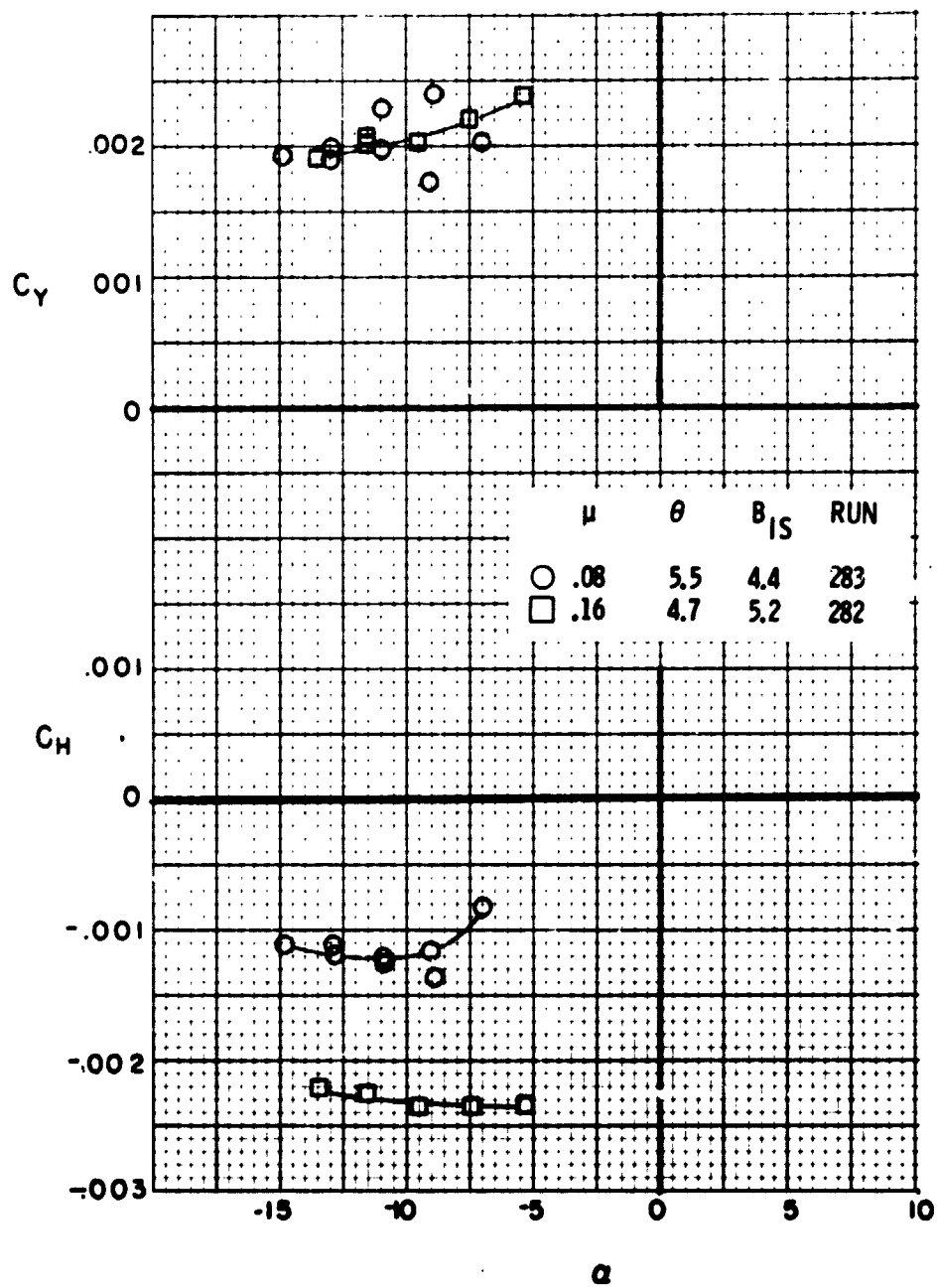

Figure 72. - Effect of angle of attack on the average rotor H and Y force at several wind speeds in climbing flight, $\alpha_p = 90^0$.

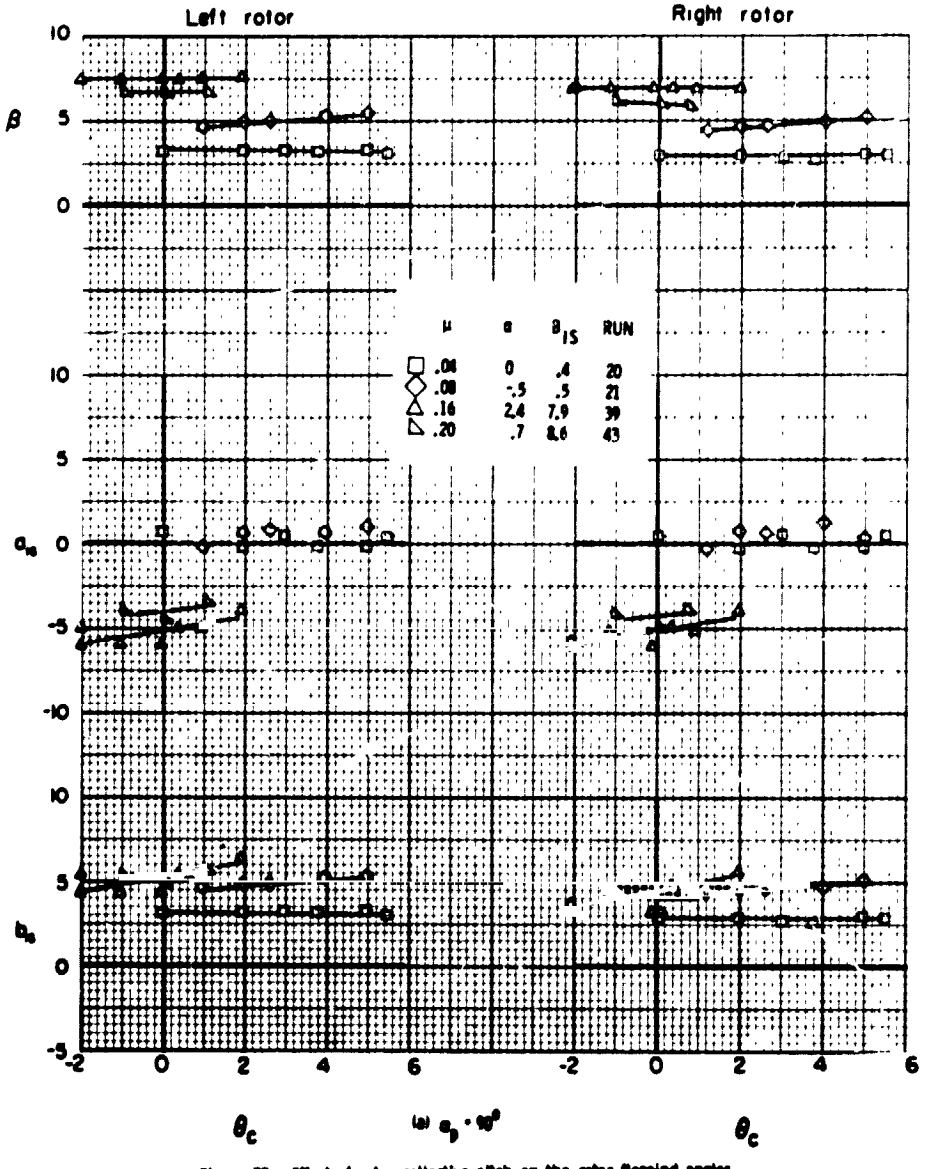

Figure 73 - Effect of rotor collective pitch on the rotor flapping angles at several wind speeds.

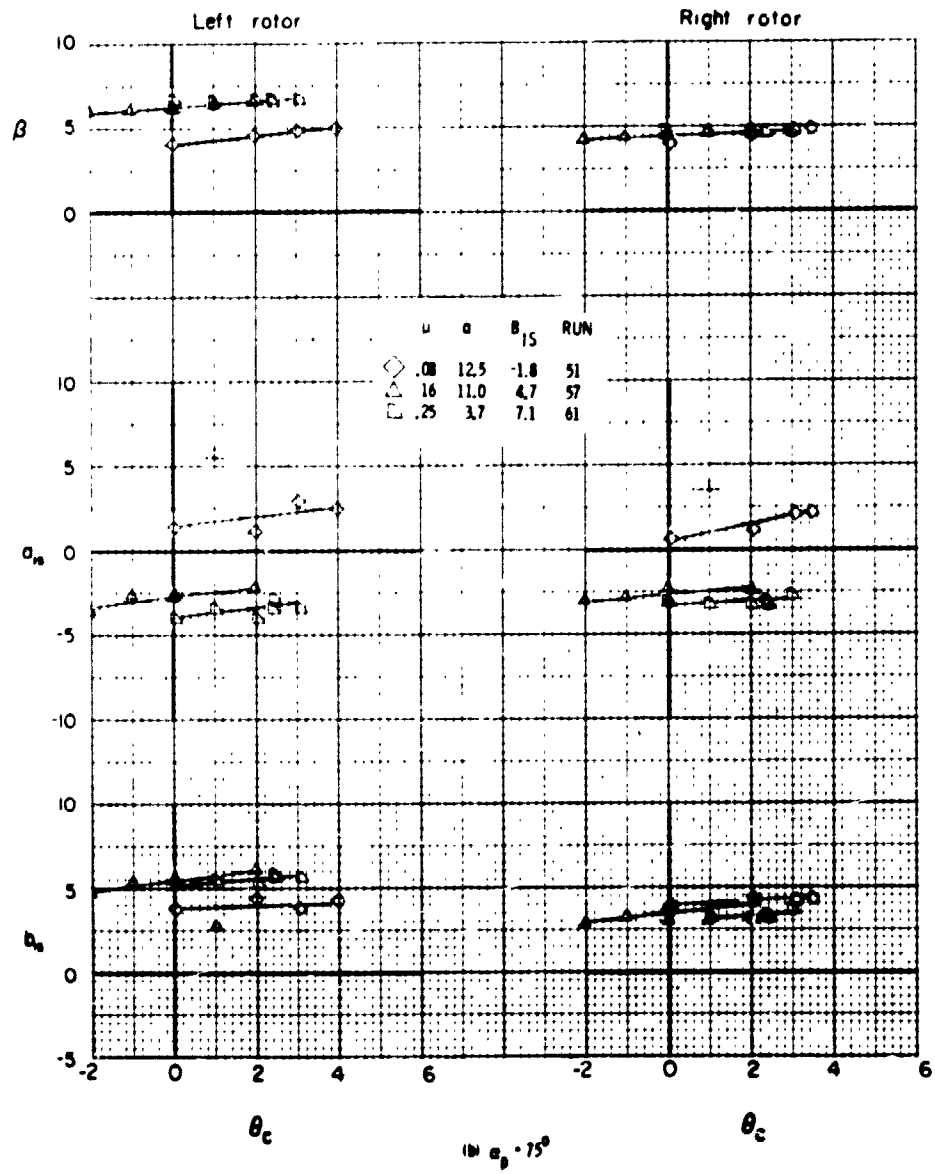

Figure 73. - Continued.

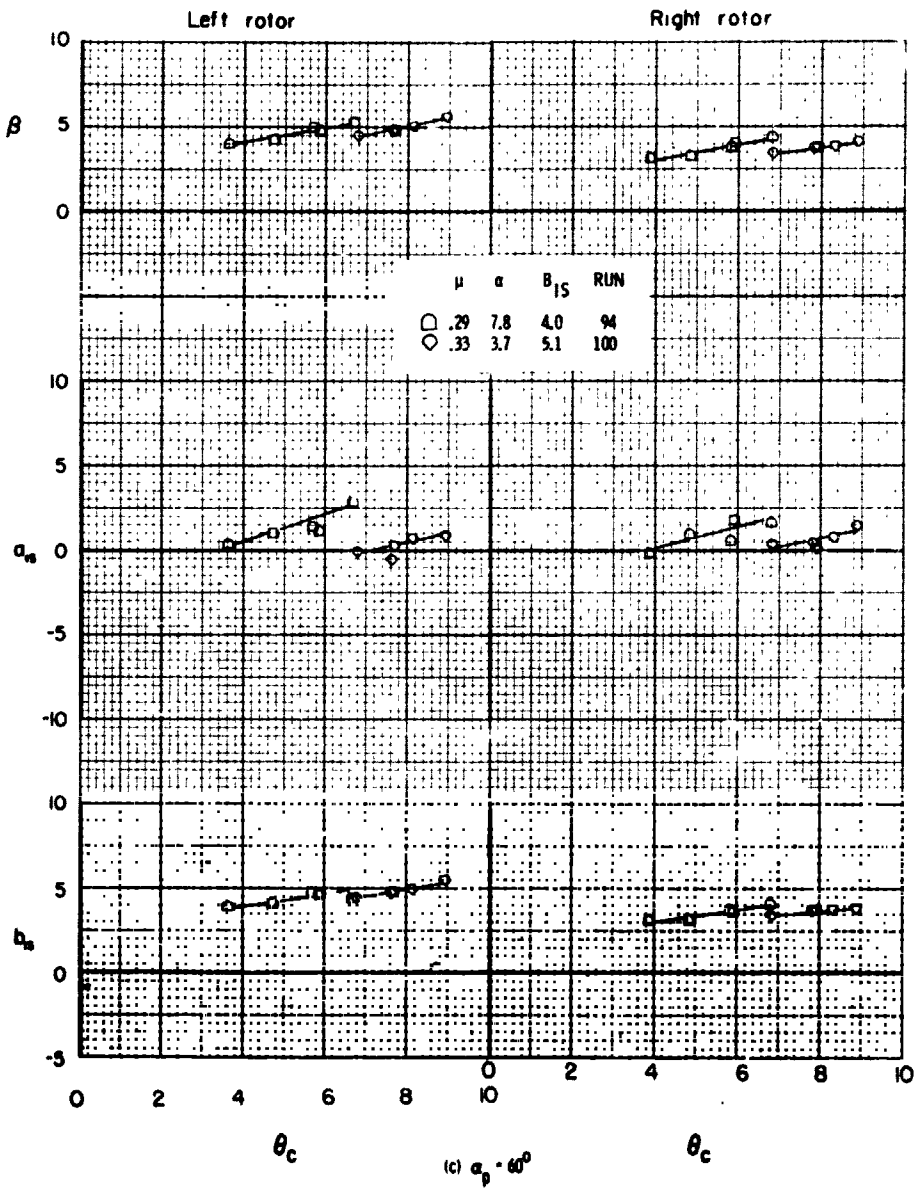

(c) $\alpha_p = 60^0$

Figure 73. - Continued.

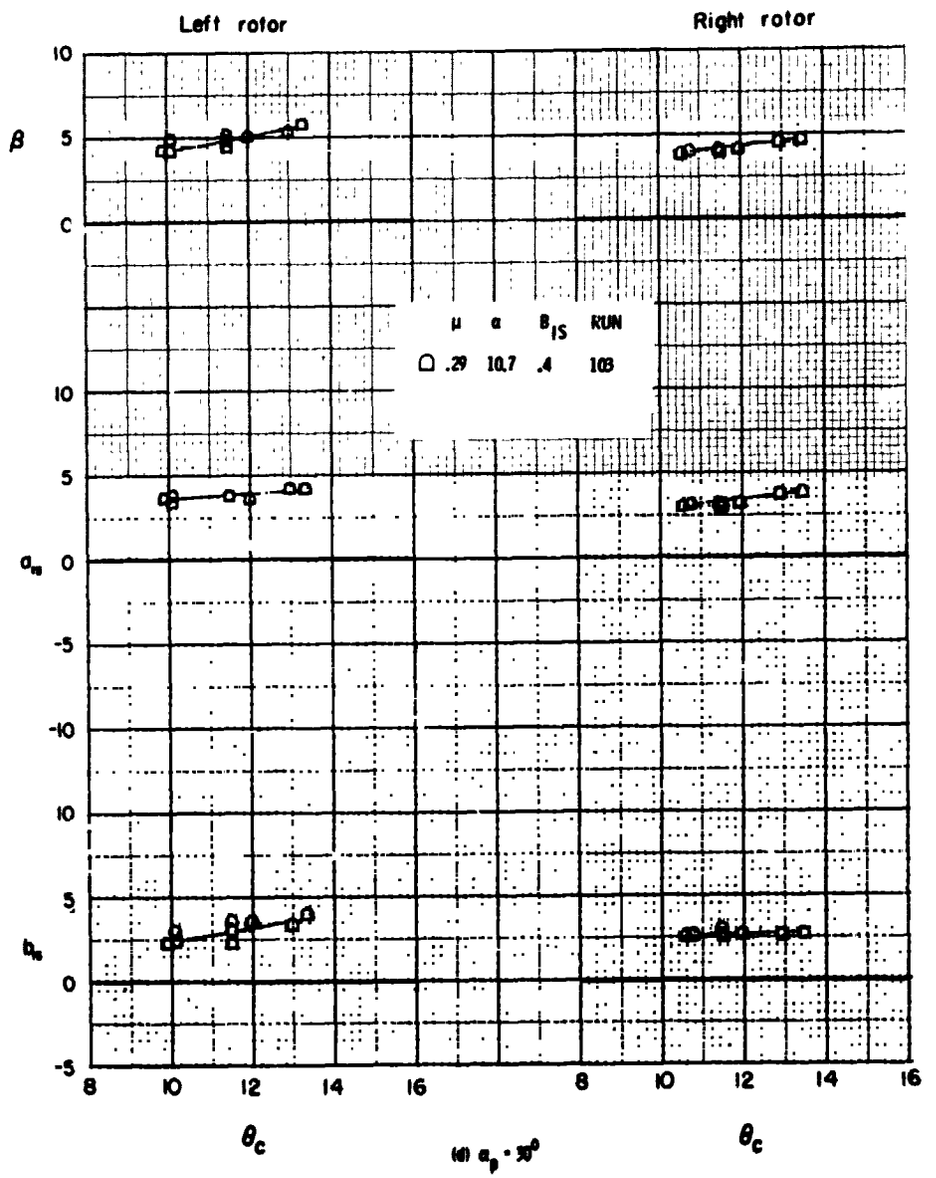

(d) $\alpha_p = 30^0$

Figure 73. - Concluded.

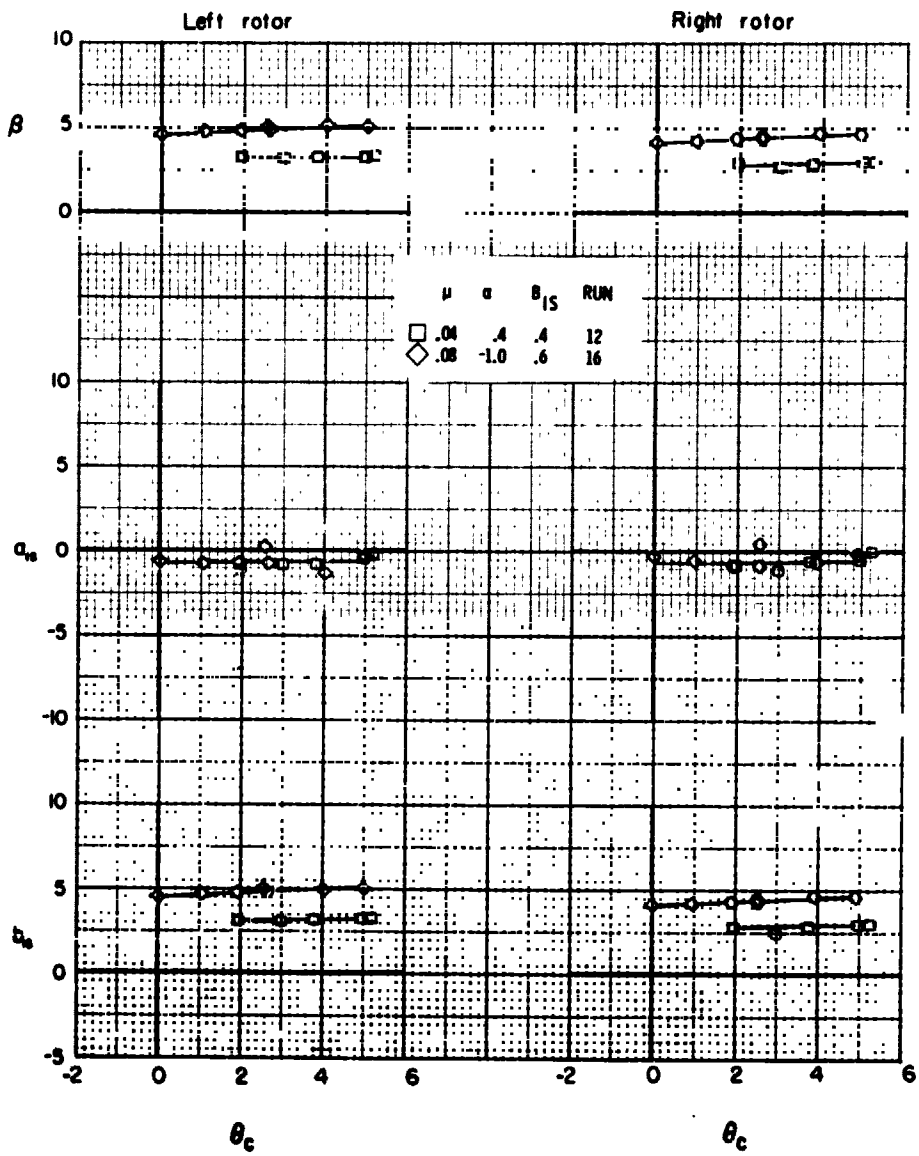

Figure 74. - Effect of collective pitch on the flapping angles at low wing wind speeds with the tunnel walls up, $\alpha_p = 90°$.

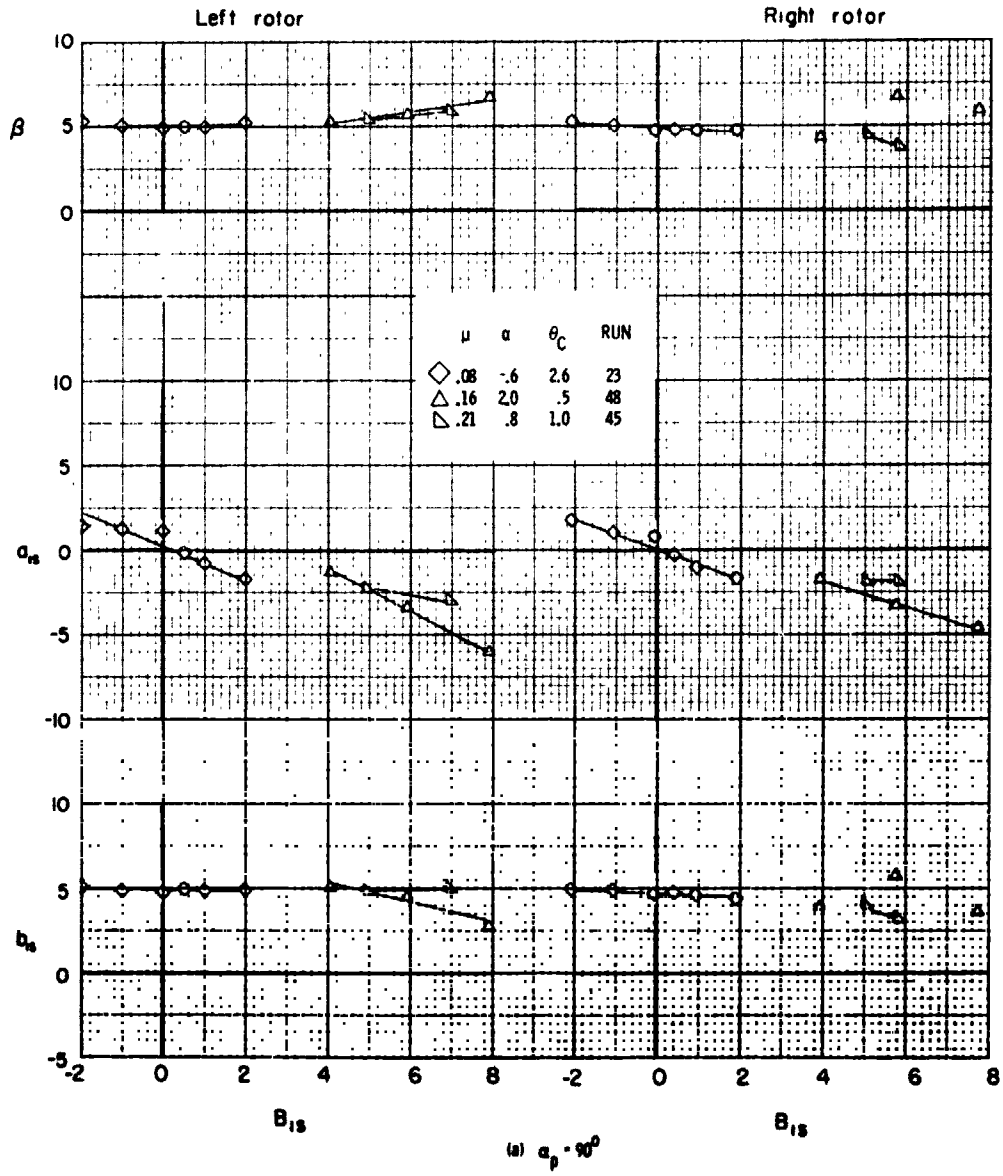

(a) $\alpha_p = 90^0$

Figure 75. - Effect of cyclic pitch on the flapping angles for several wind speeds.

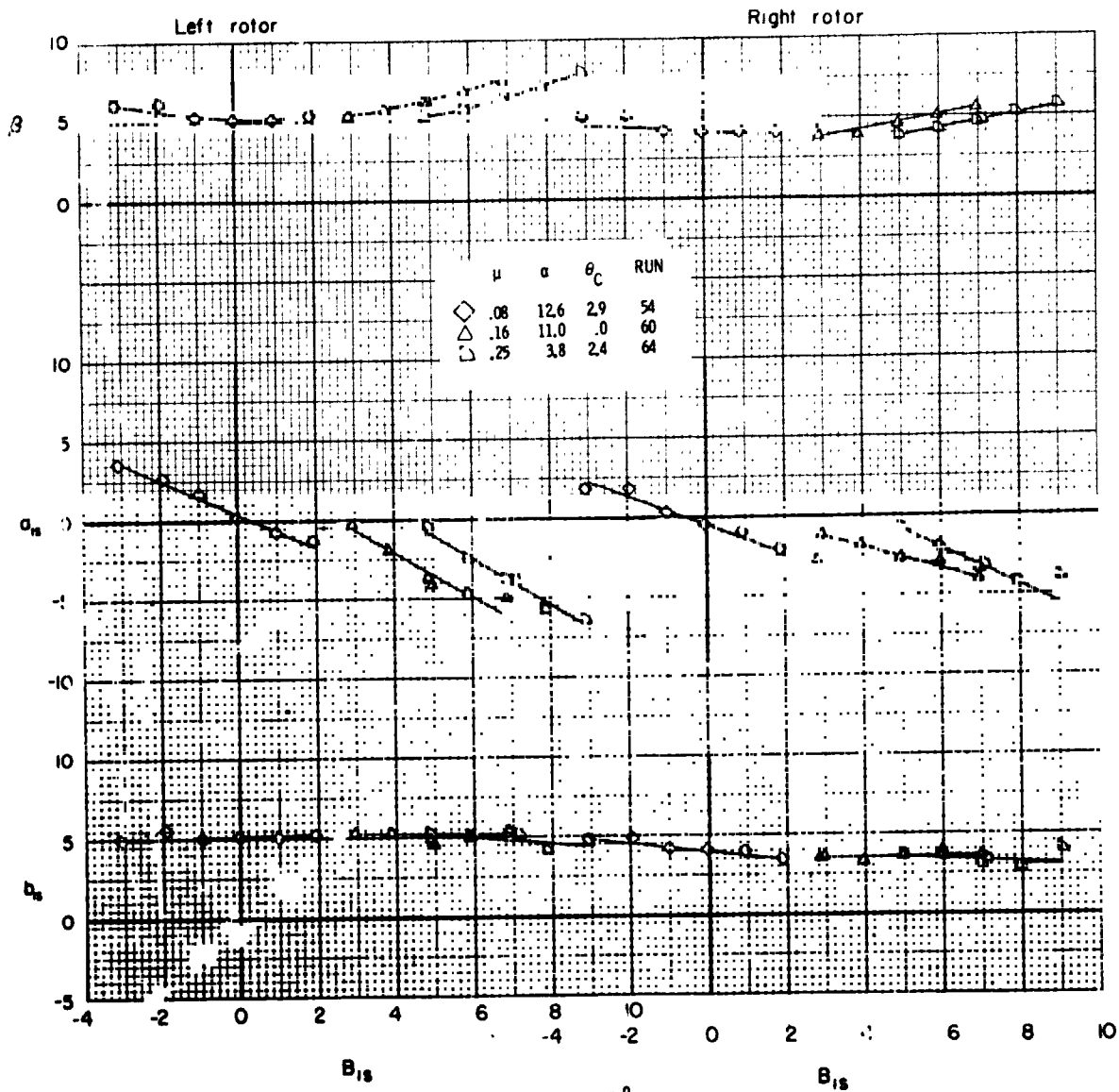

(b) $\alpha_p = 75^0$

Figure 75. - Continued.

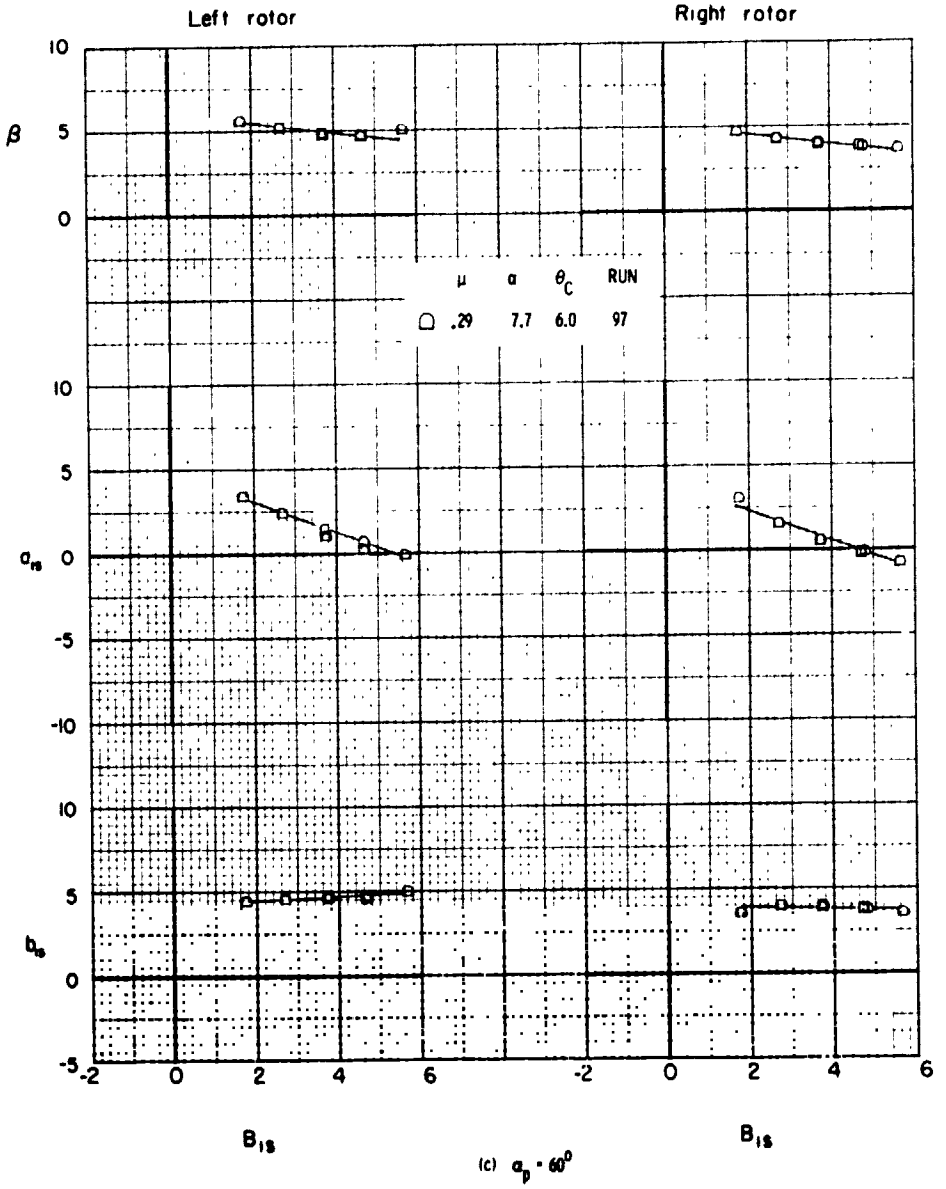

(c) $\alpha_p = 60^0$

Figure 75. - Continued.

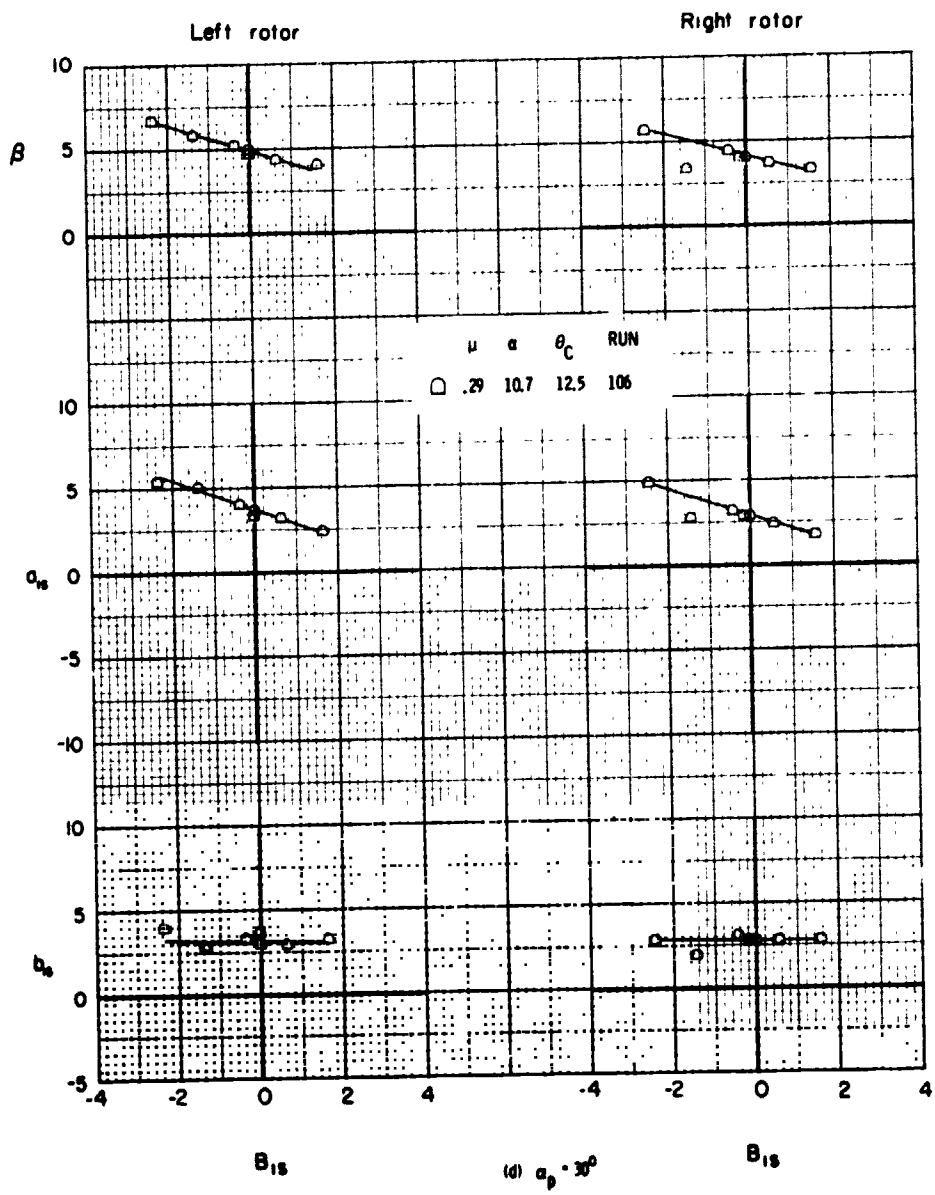

Figure 75. - Concluded.

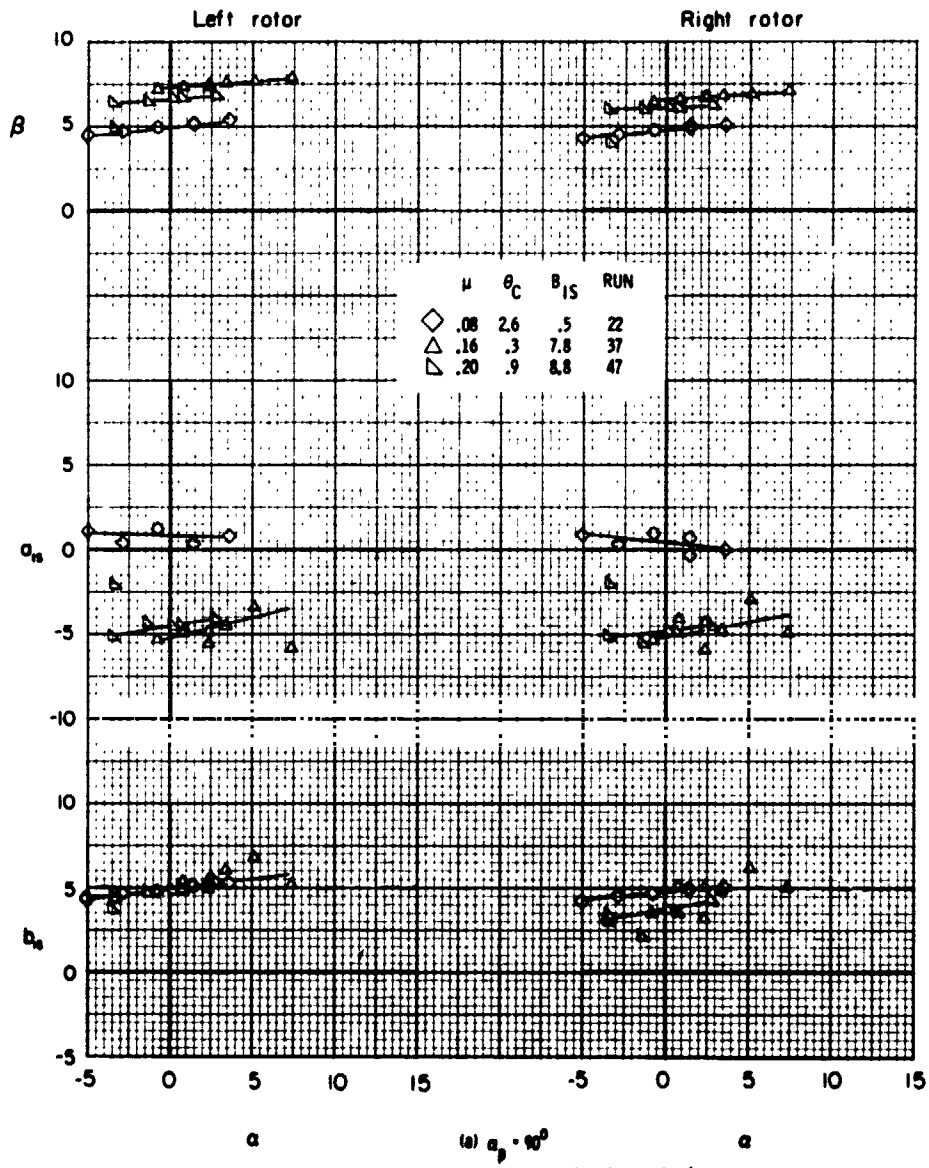

Figure 76. - Effect of angle of attack on the flapping angles for several forward speeds.

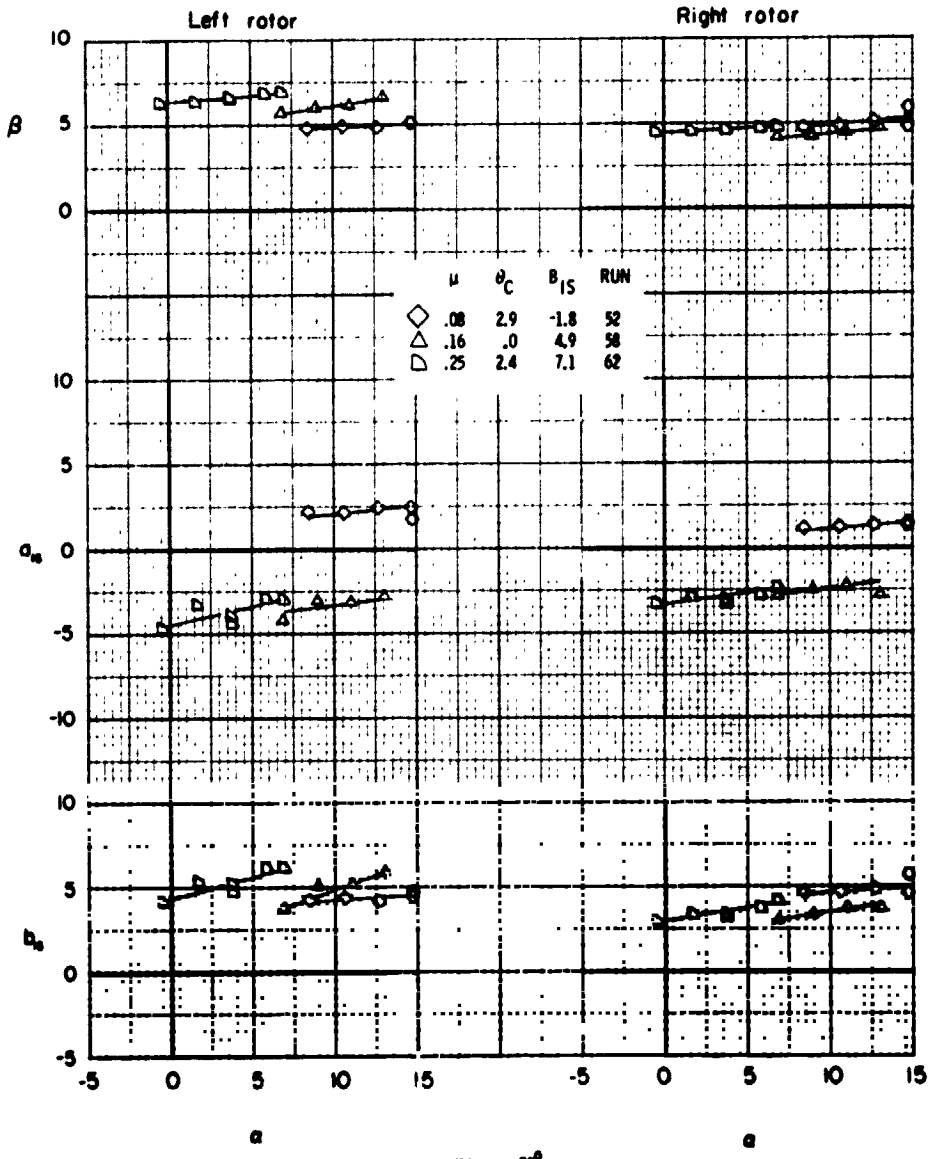

(b) $\alpha_p = 75^0$

Figure 76. - Continued.

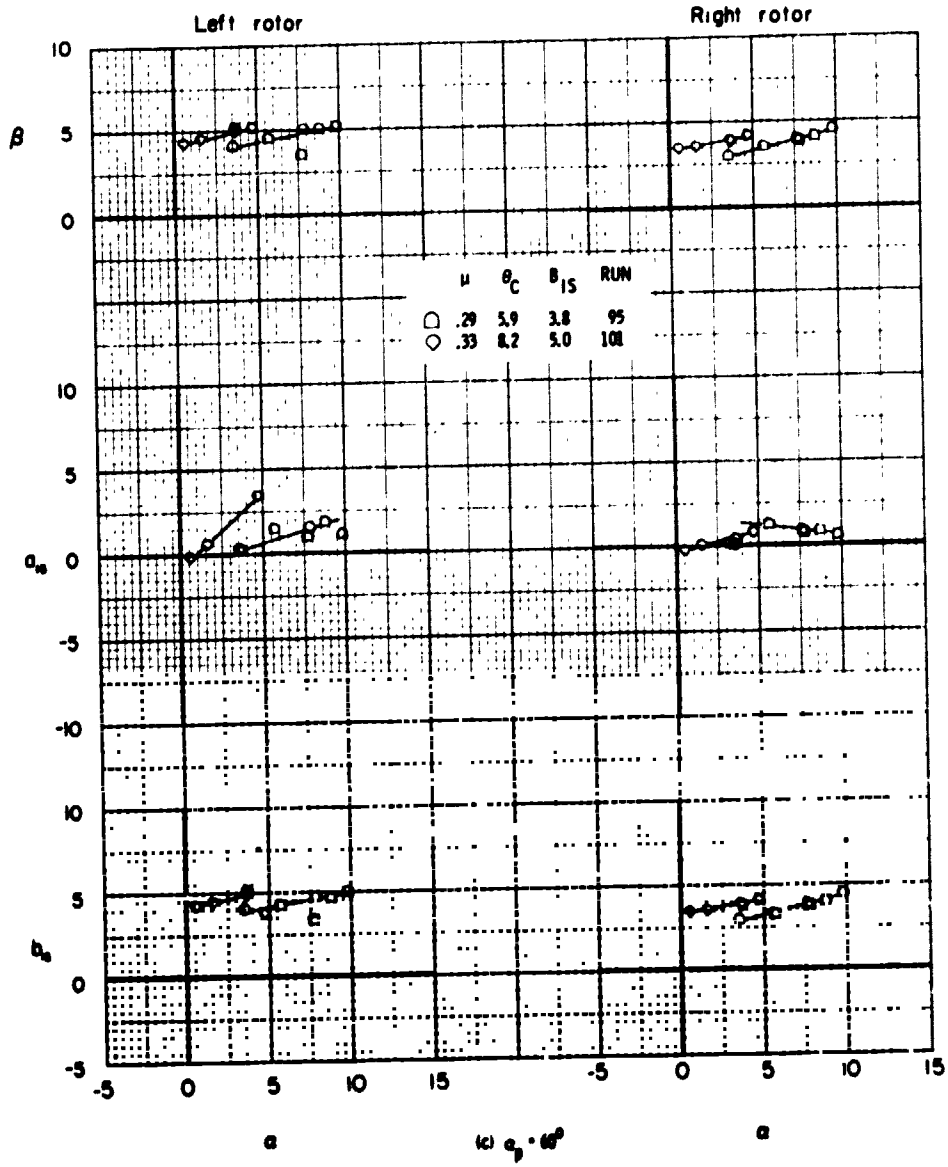

Figure 76. - Continued.

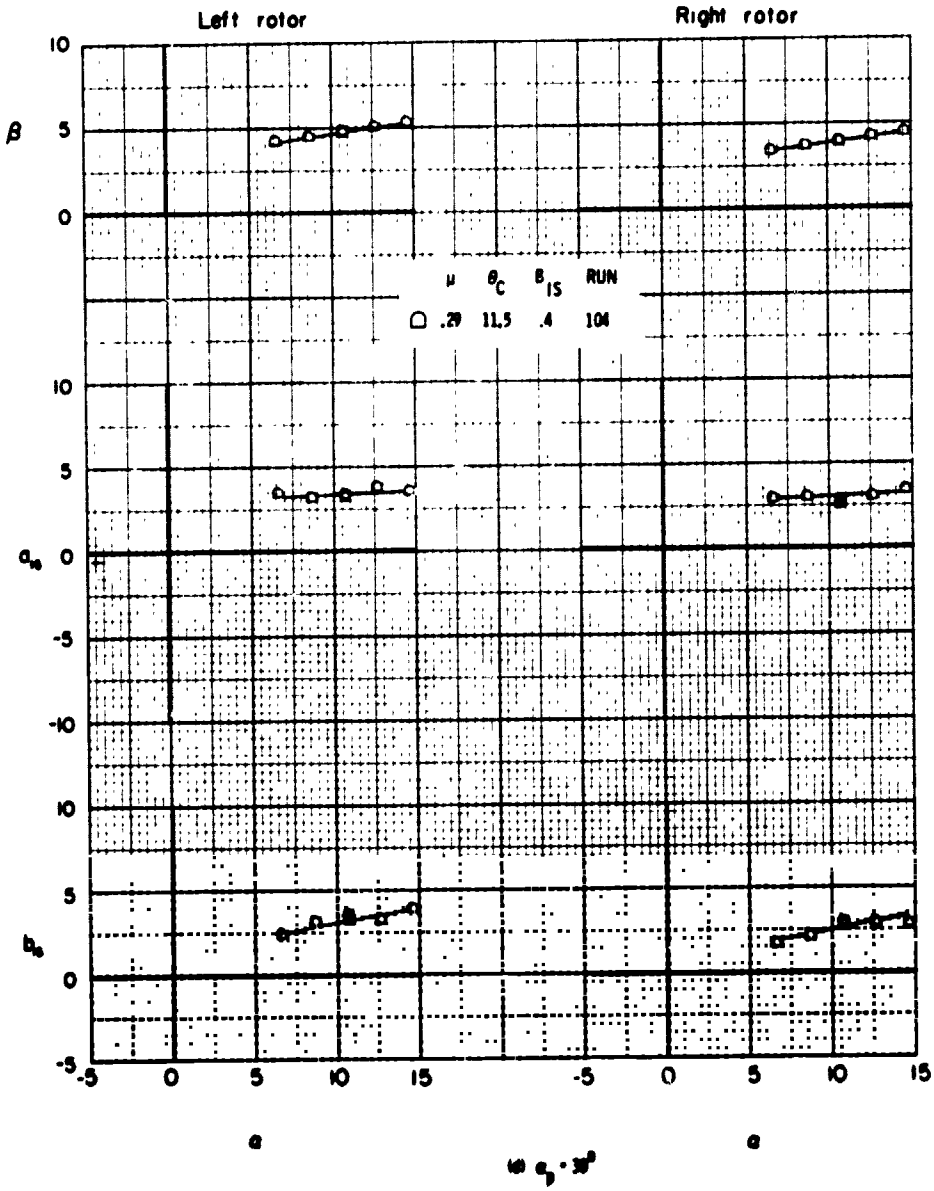

Figure 76. - Concluded.

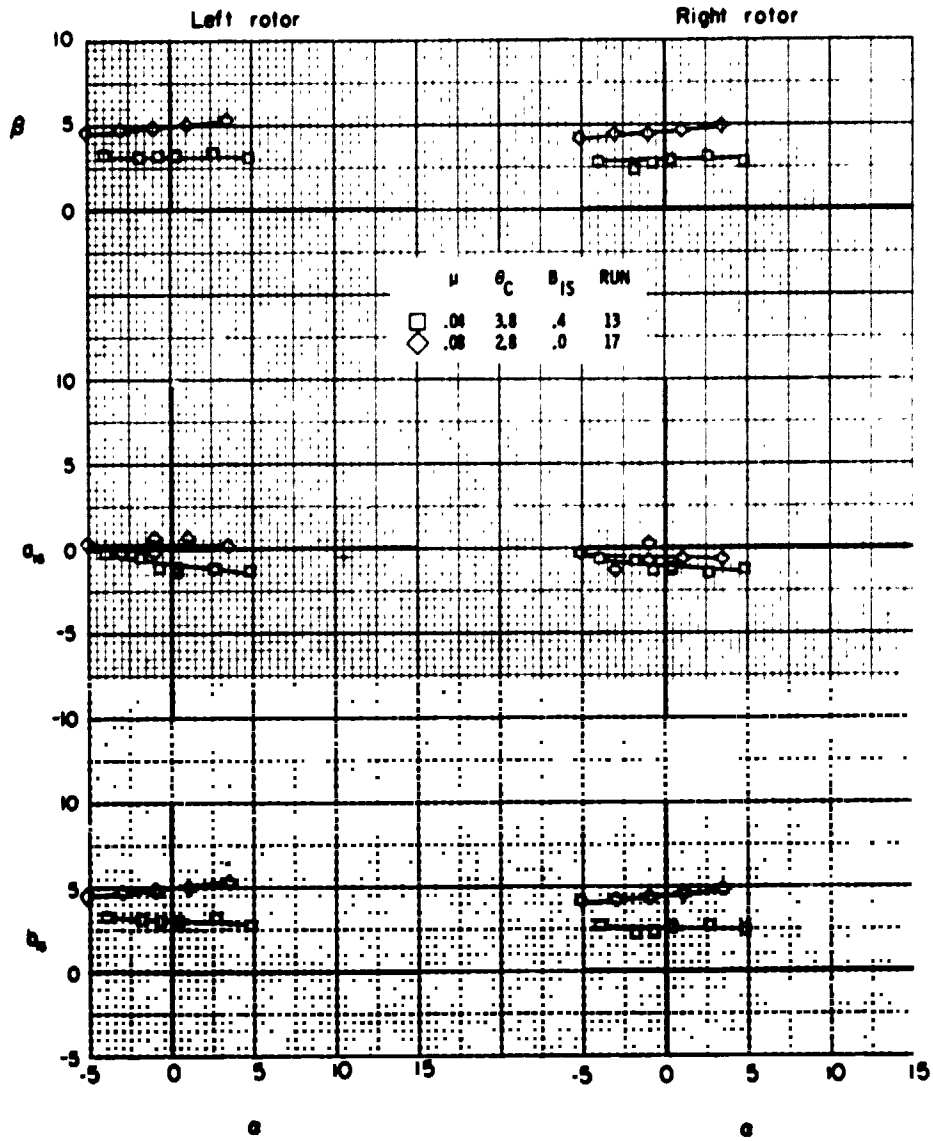

Figure 77. - Effect of angle of attack on the flapping angles at several forward speeds with the tunnel walls up. α_s -90°.

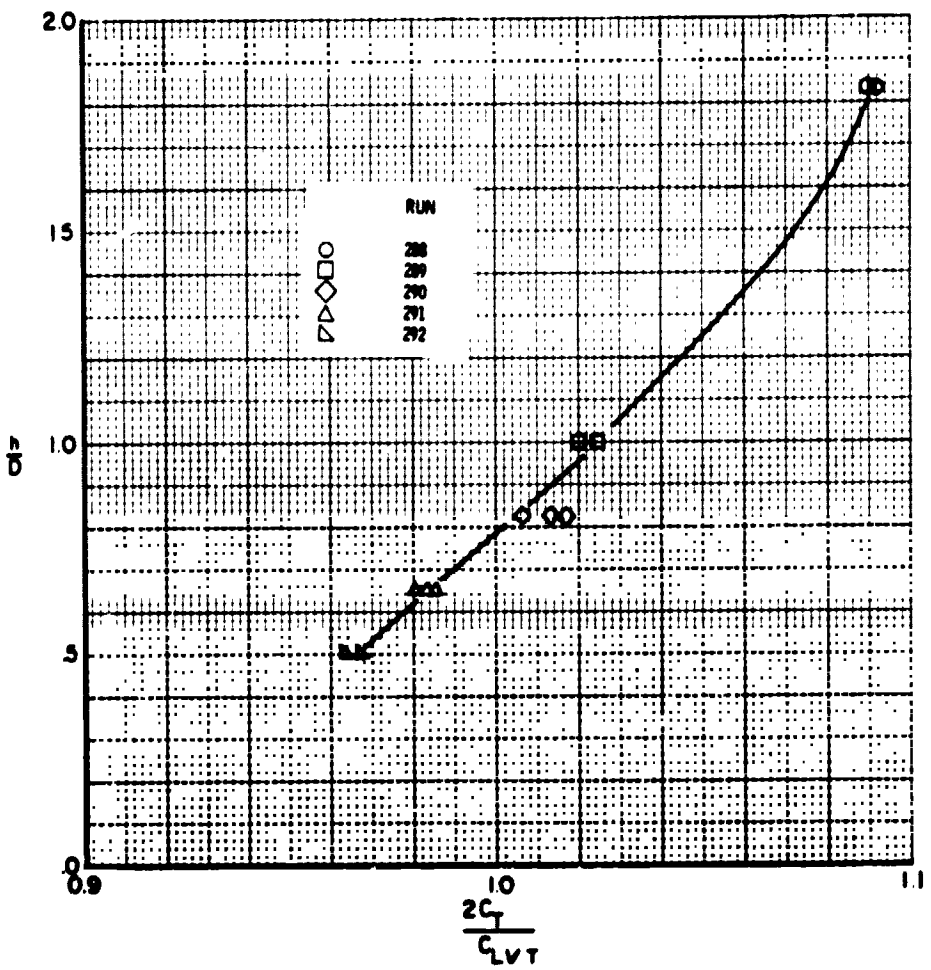

Figure 78. - Effect of hover height above ground on thrust required to hover, $\delta_0/\delta_f = 30°/30°$.

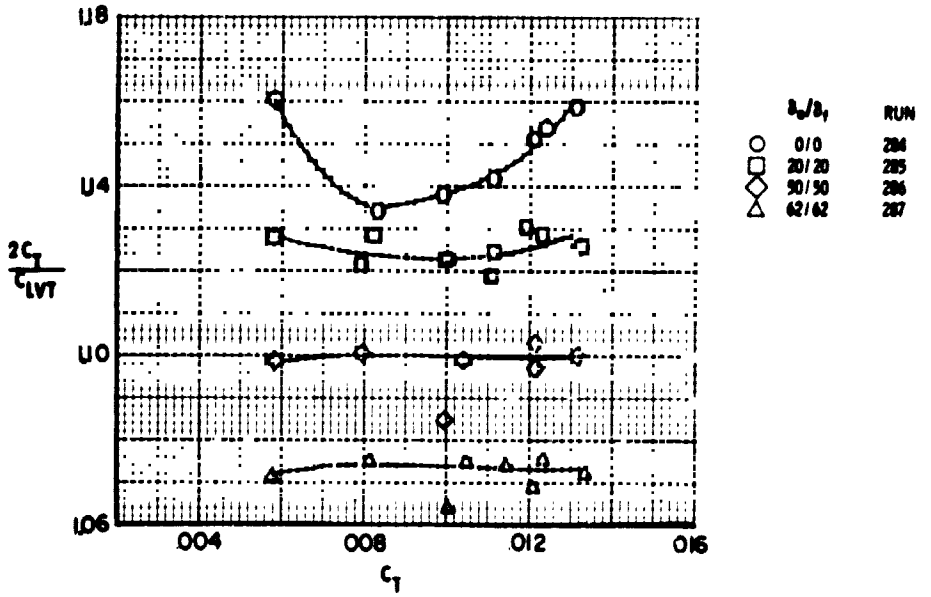

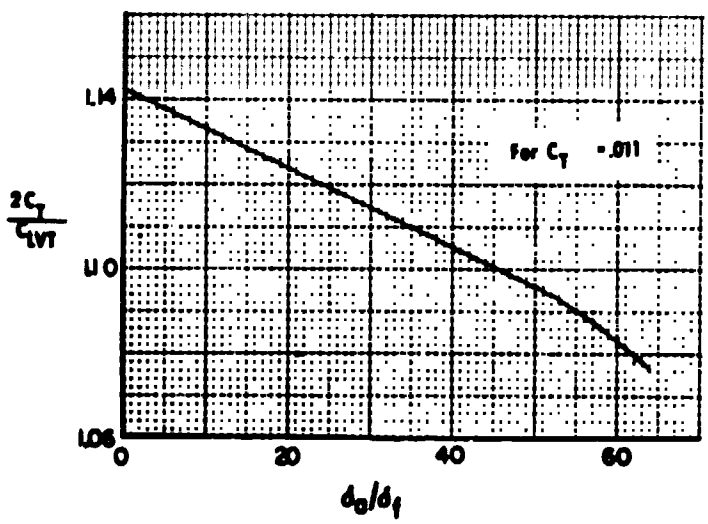

Figure 78. - Effect of aileron/flap deflection on thrust required to hover out of ground effect, h/B = 1.83.

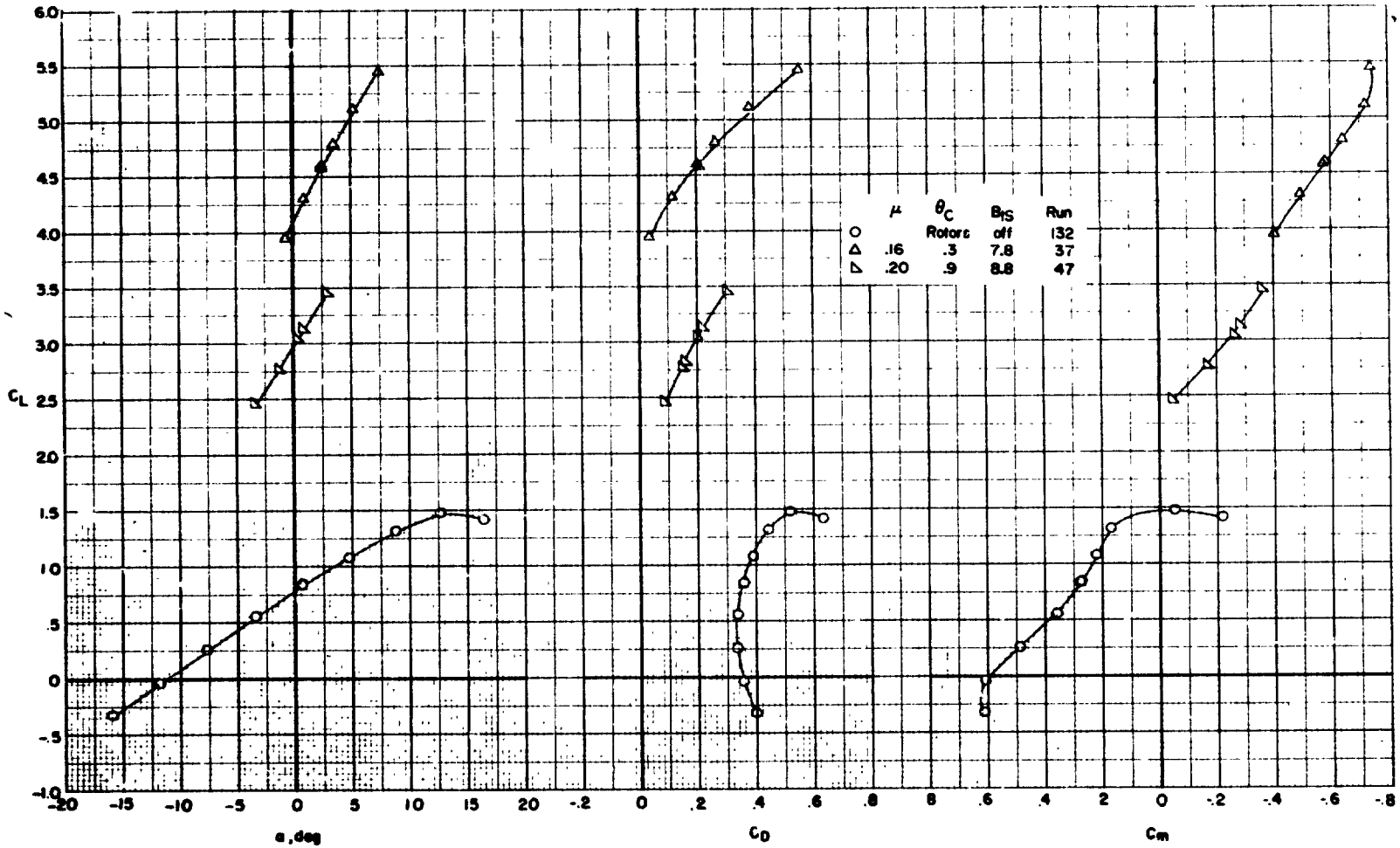

(a) Horizontal tail on

Figure 88. - Effect of angle of attack on the longitudinal aerodynamic characteristics with the rotors on and off for the horizontal tail on and off.

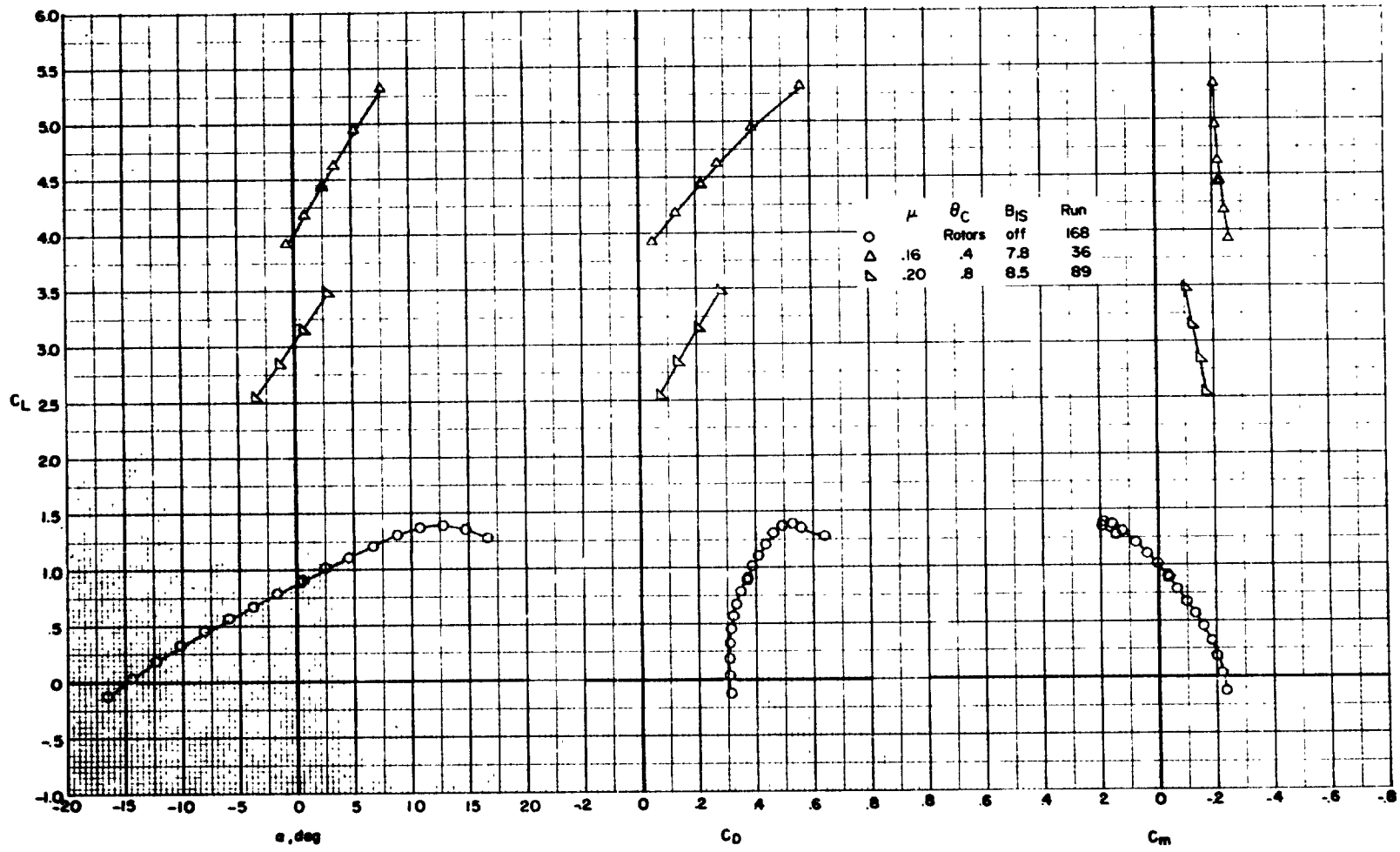

Figure 80. - Concluded. (b) Horizontal tail off

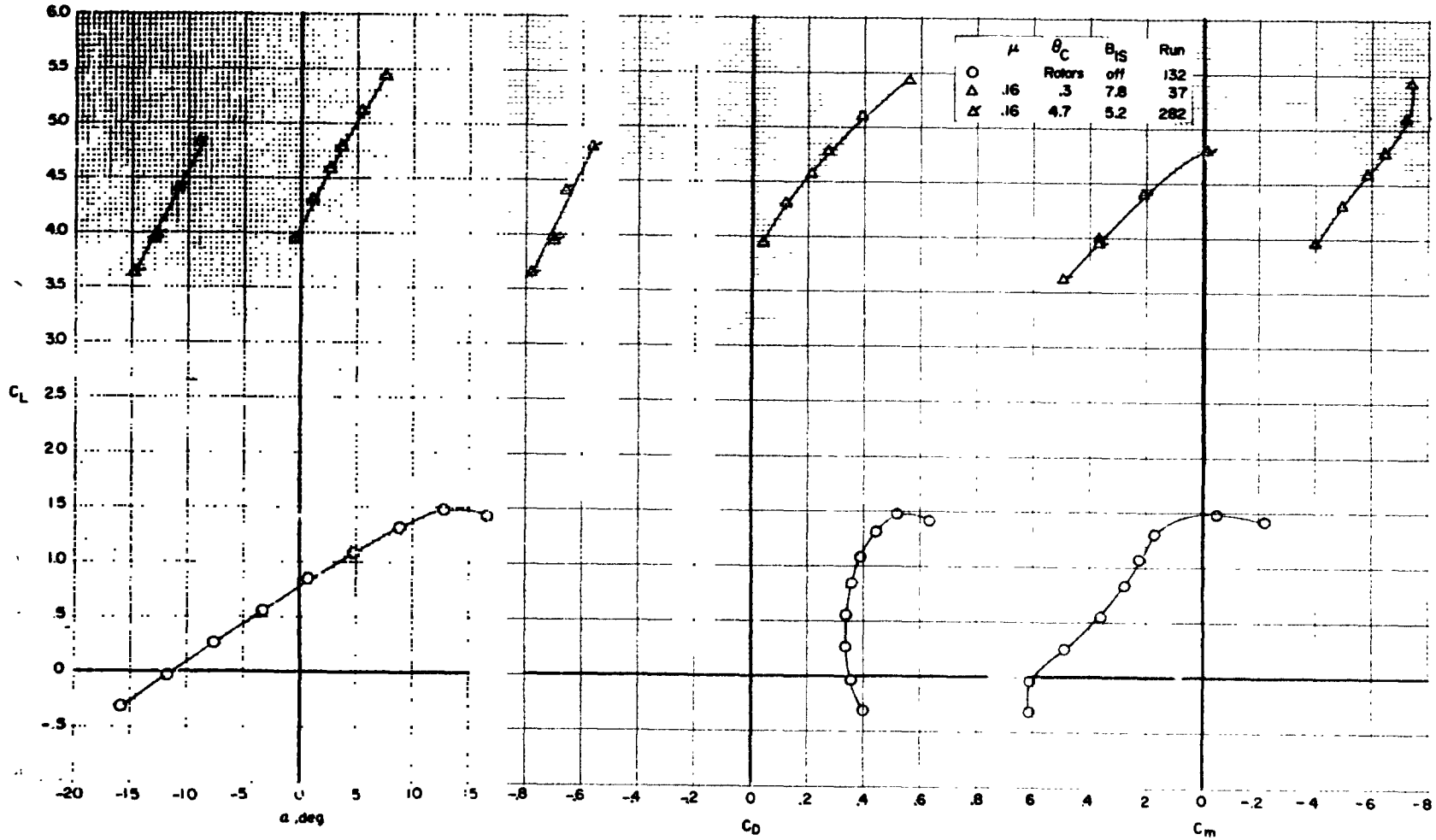

Figure 81. - Comparison of rotor thrust effects on longitudinal aerodynamic characteristics in positive and negative (climb attitude) angle of attack ranges for pylon angle 90° at full-scale flight speed of 80 knots.

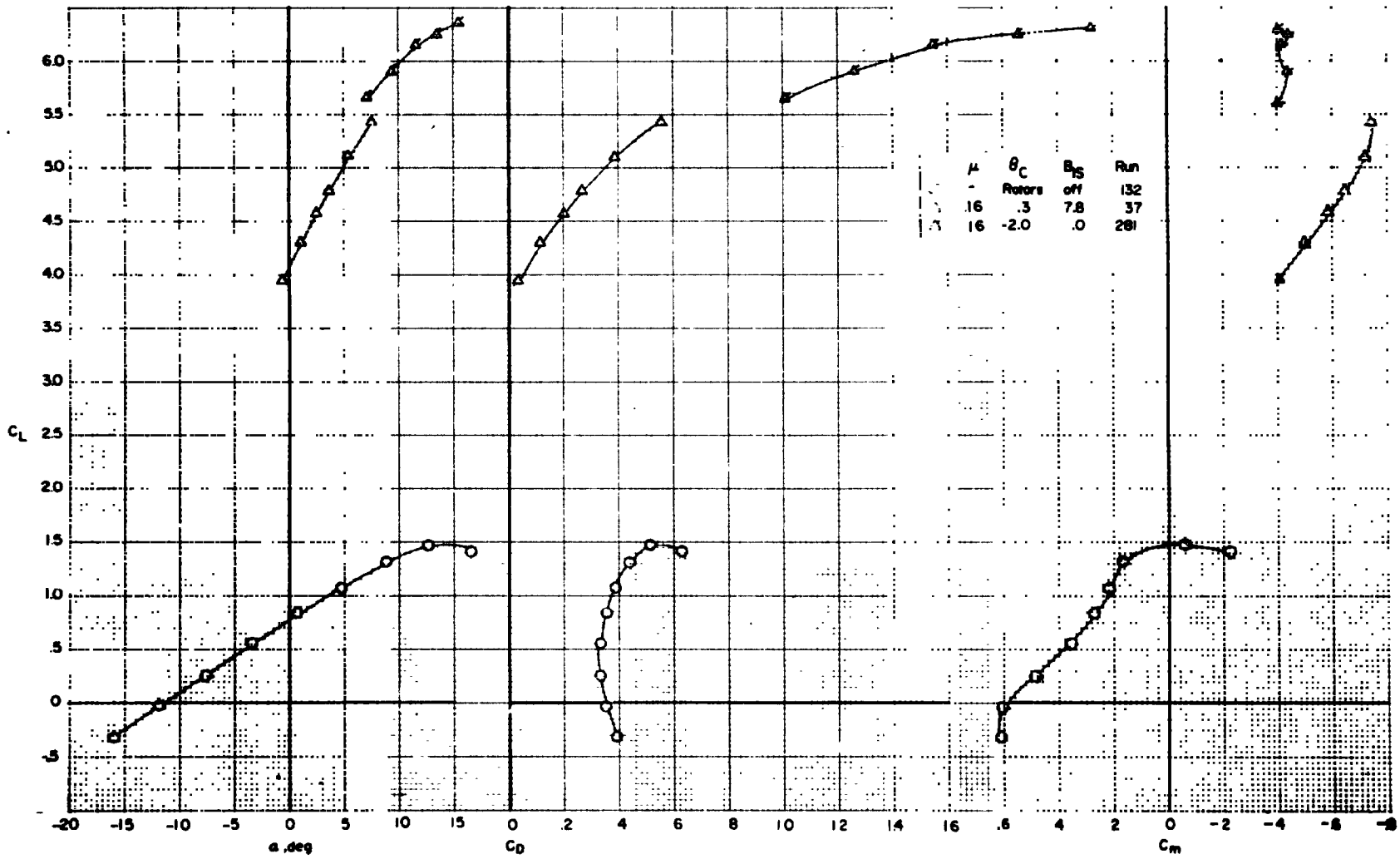

Figure 82. - Comparison of rotor thrust effects on longitudinal aerodynamic characteristics for near autorotation, pylon angle 90°, full-scale flight speed of 80 knots.

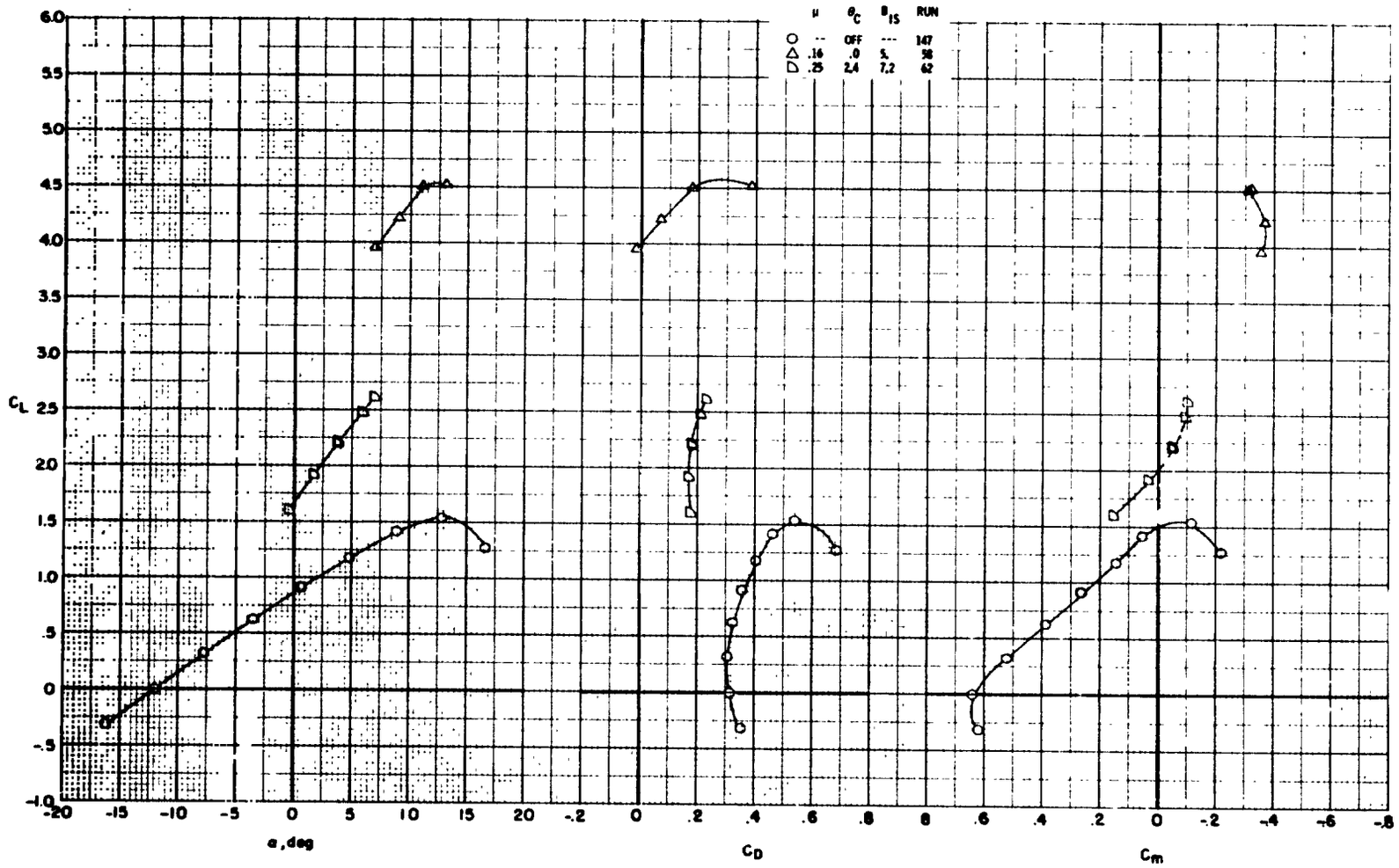

(a) Horizontal tail on

Figure 83. - Effect of rotor thrust and angle of attack on longitudinal aerodynamic characteristics for pylon angle 75°, horizontal tail on and off.

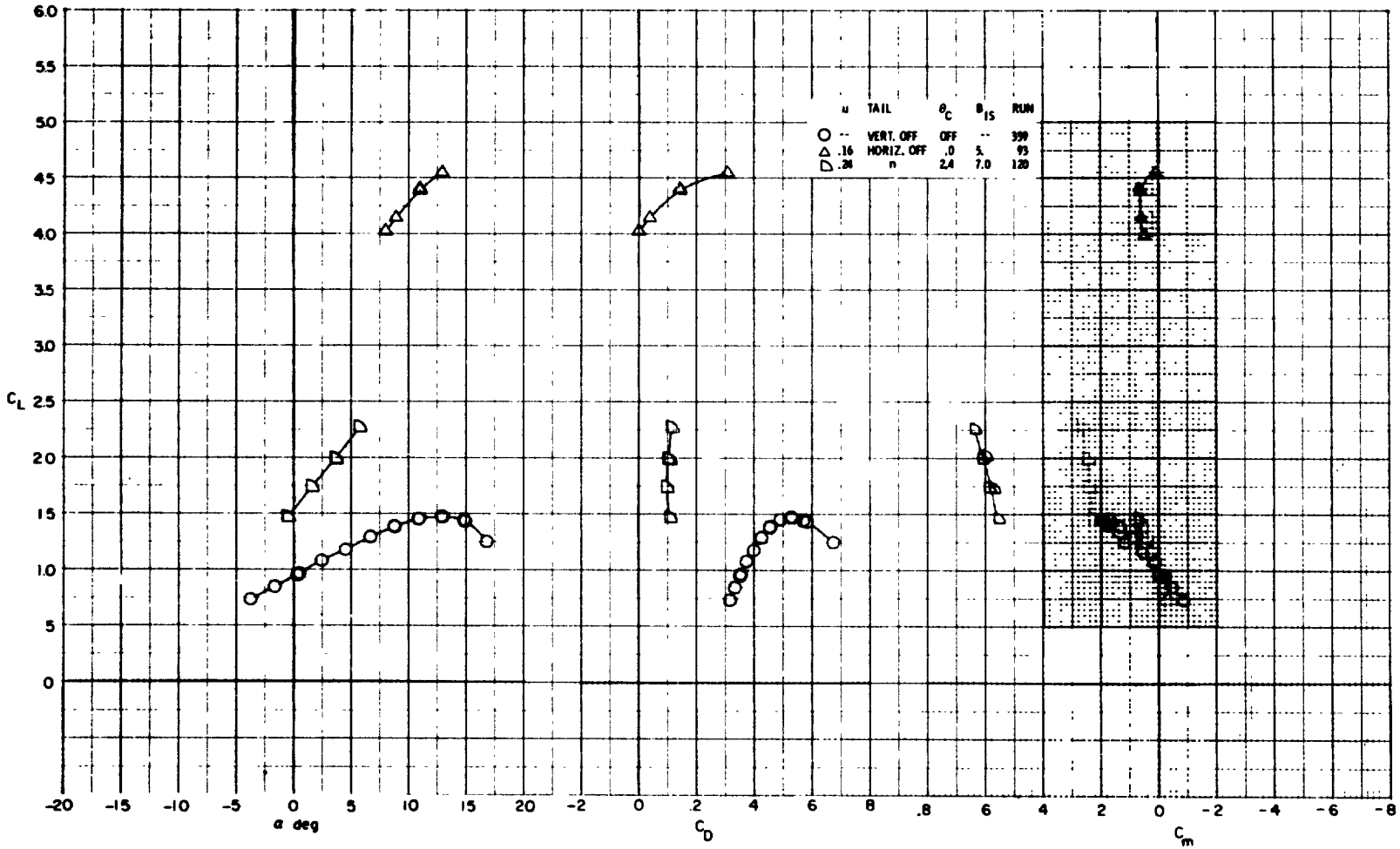

(b) Horizontal tail off

Figure 83. - Continued.

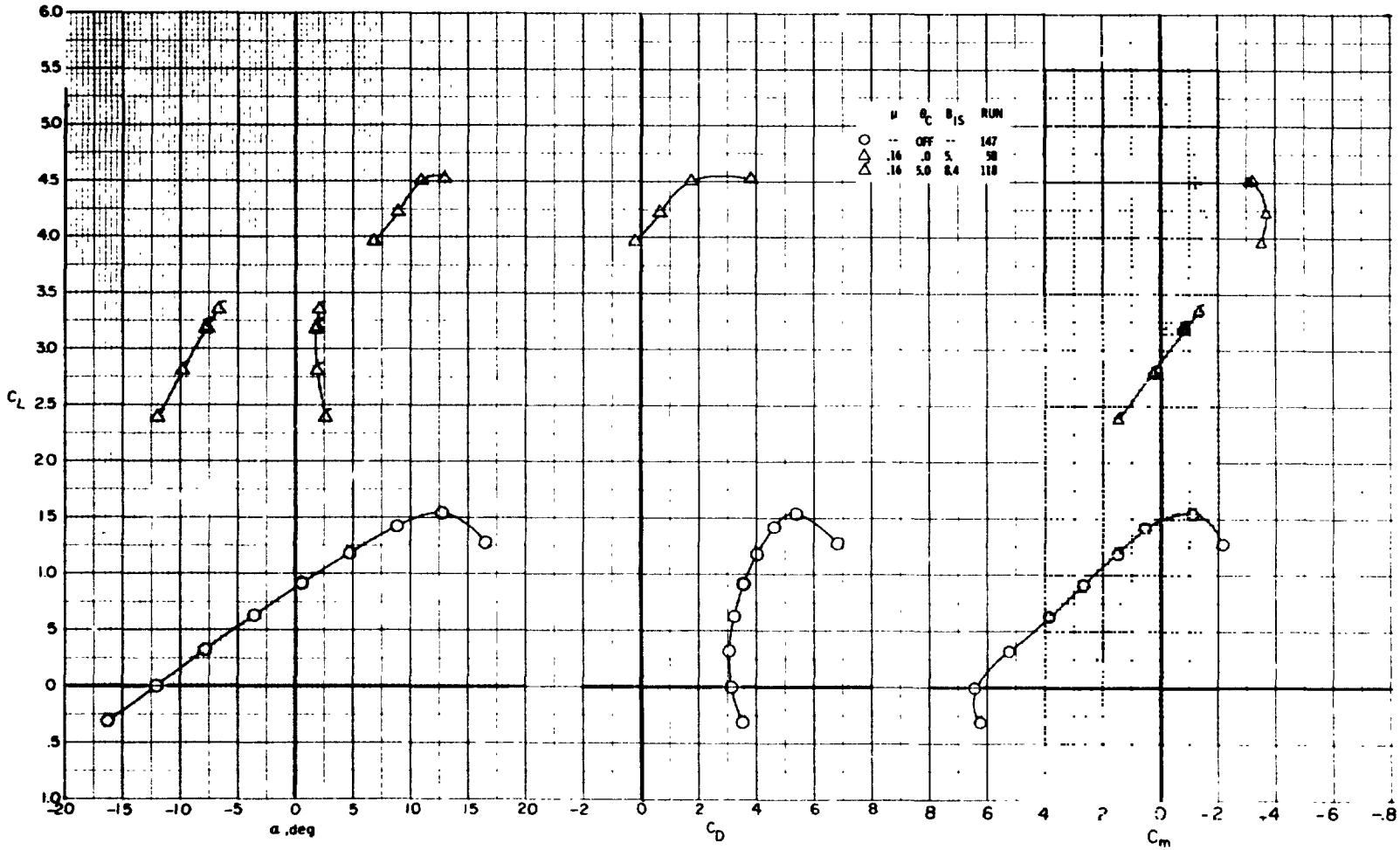

(a) Horizontal tail on

Figure 84. - Comparison of rotor thrust effect on longitudinal aerodynamic characteristics in positive and negative angle of attack for pylon angle 75°.

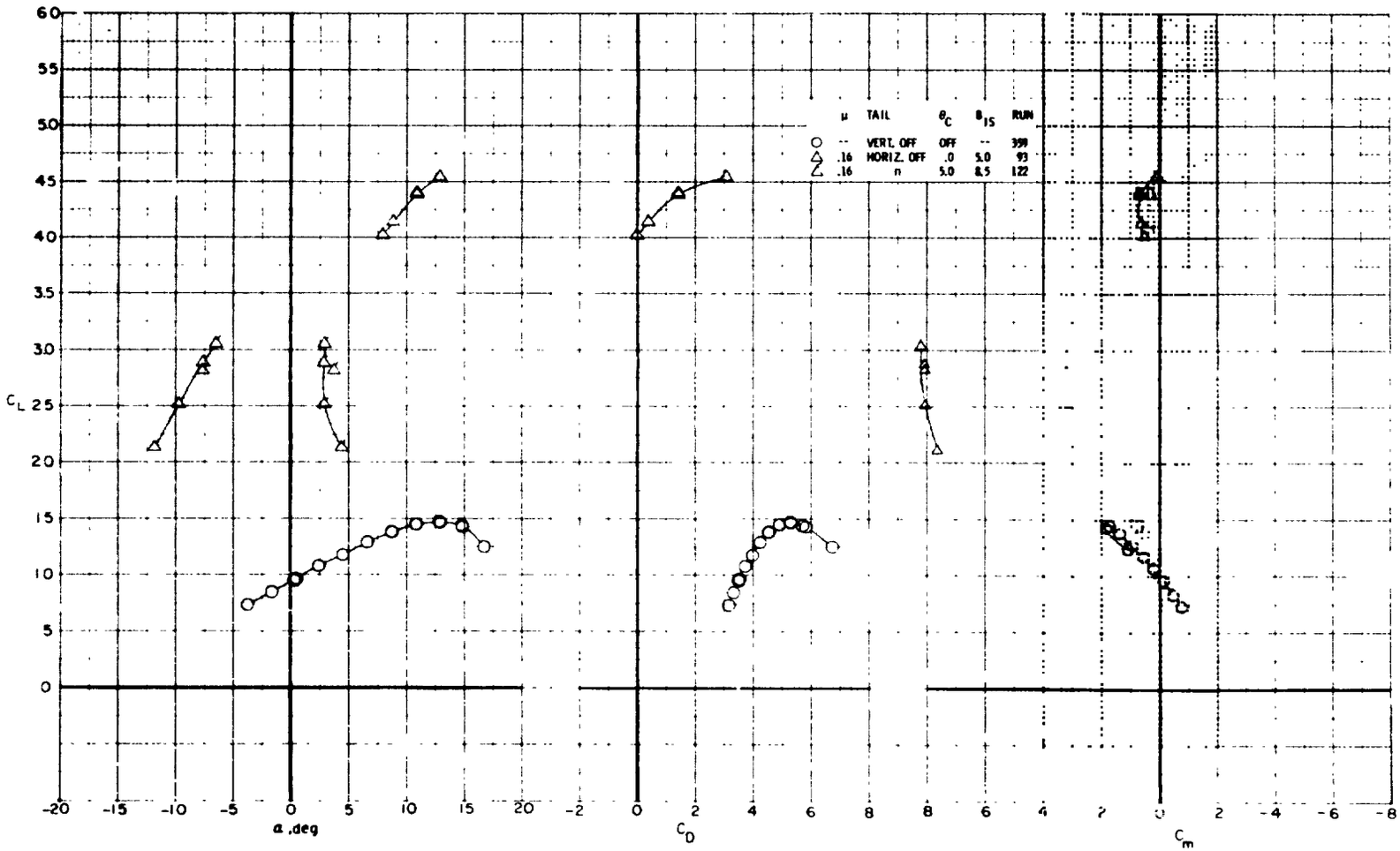

(b) Horizontal tail off

Figure 84. - Concluded.

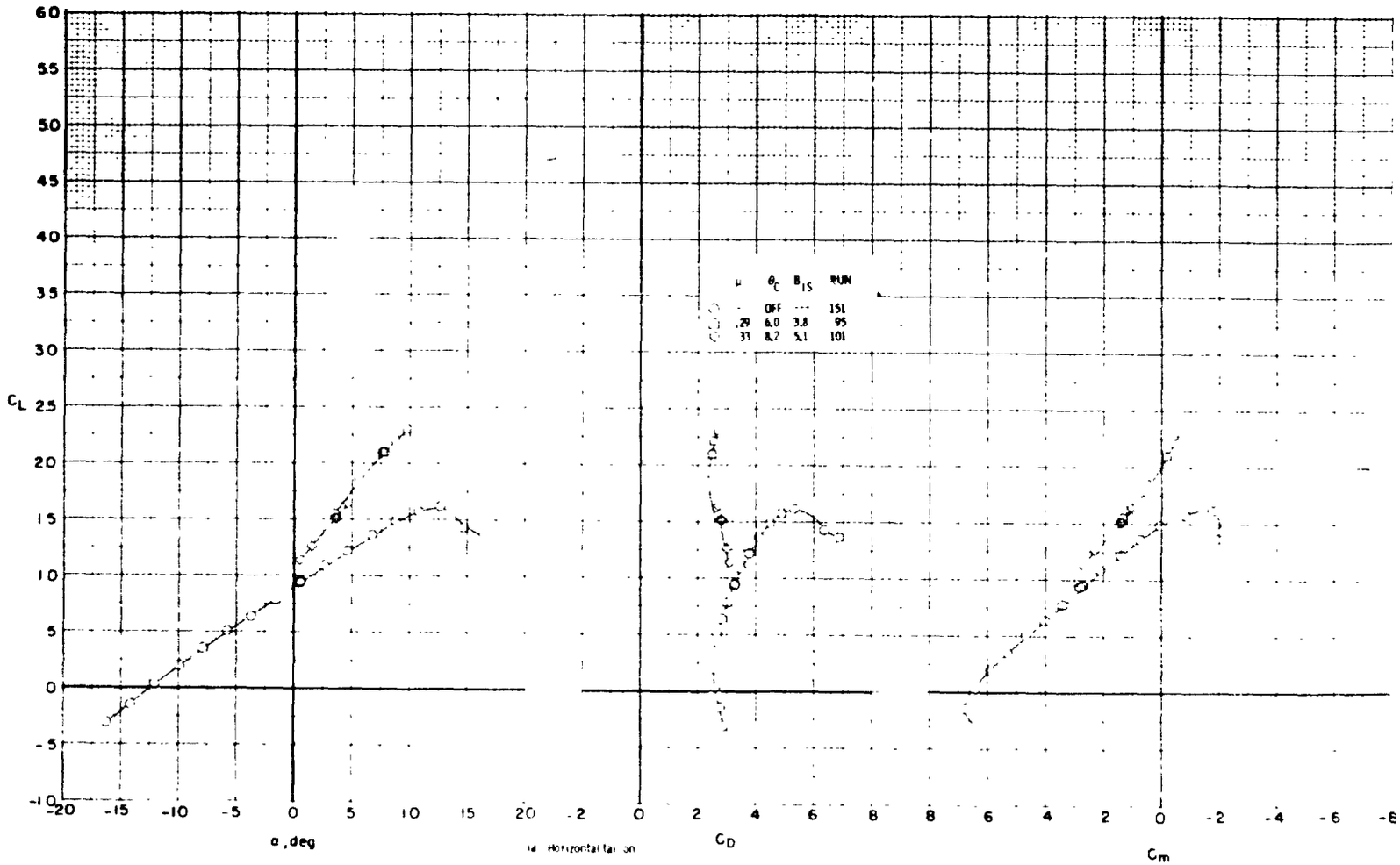

Figure 85 - Effect of rotor thrust and angle of attack on longitudinal aerodynamic characteristics for pylon angle 60°, horizontal tail on and off

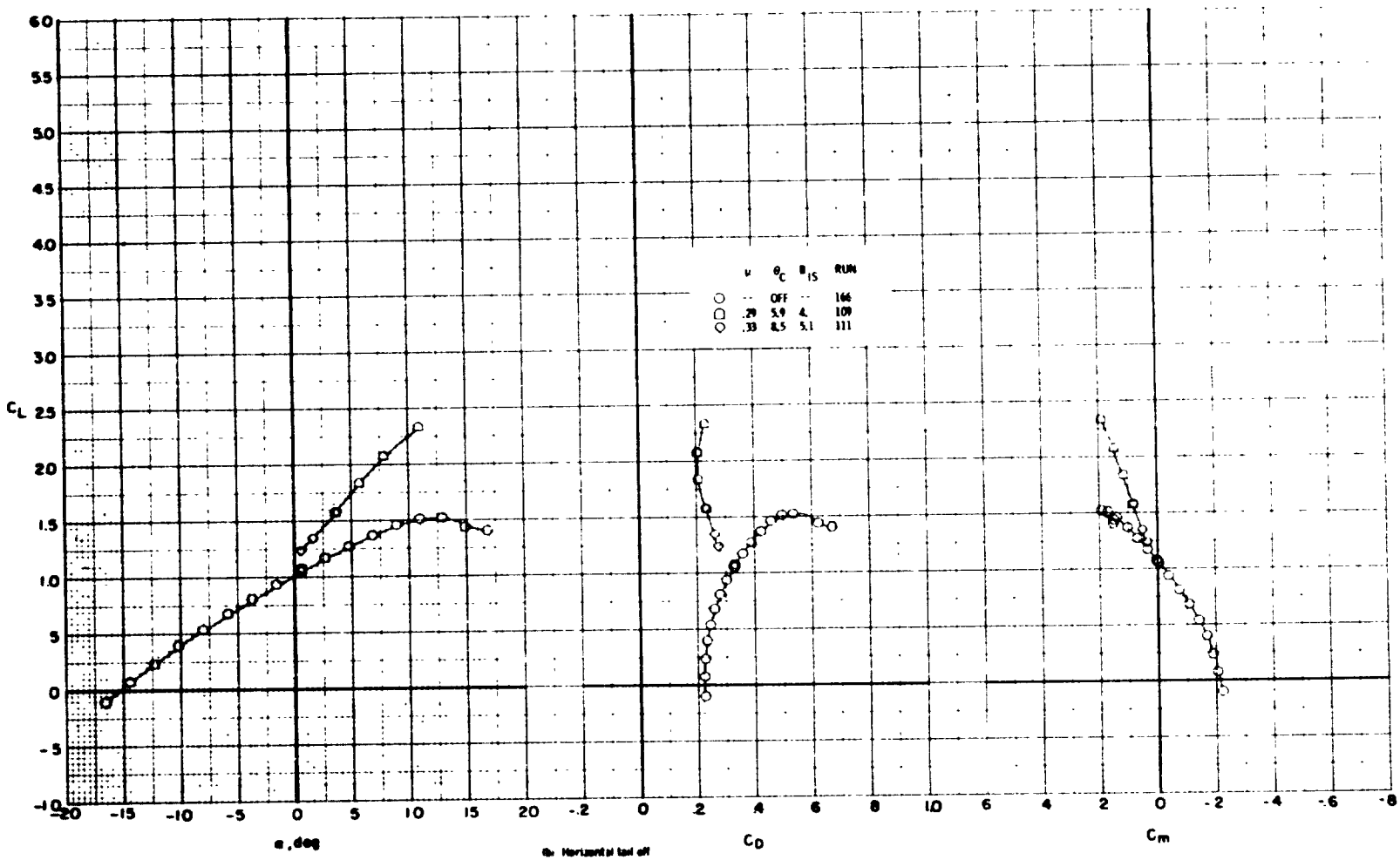

(b) Horizontal tail off

Figure 85. - Concluded.

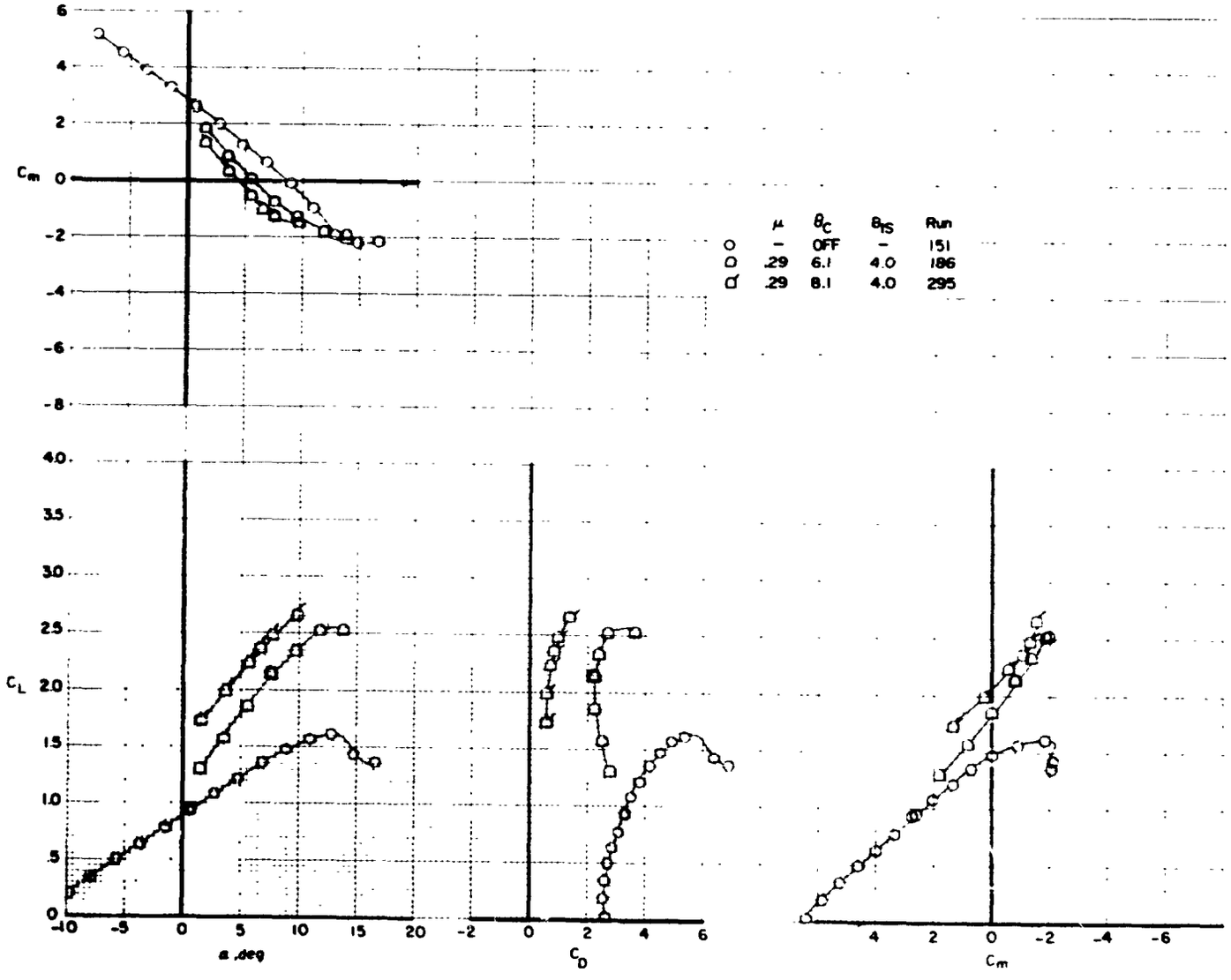

Figure 86. - Comparison of rotor thrust effects (δ_c = 6.1° and 8.1°) on longitudinal aerodynamic characteristics for rotor angle 65° for full-scale flight speed of 120 knots.

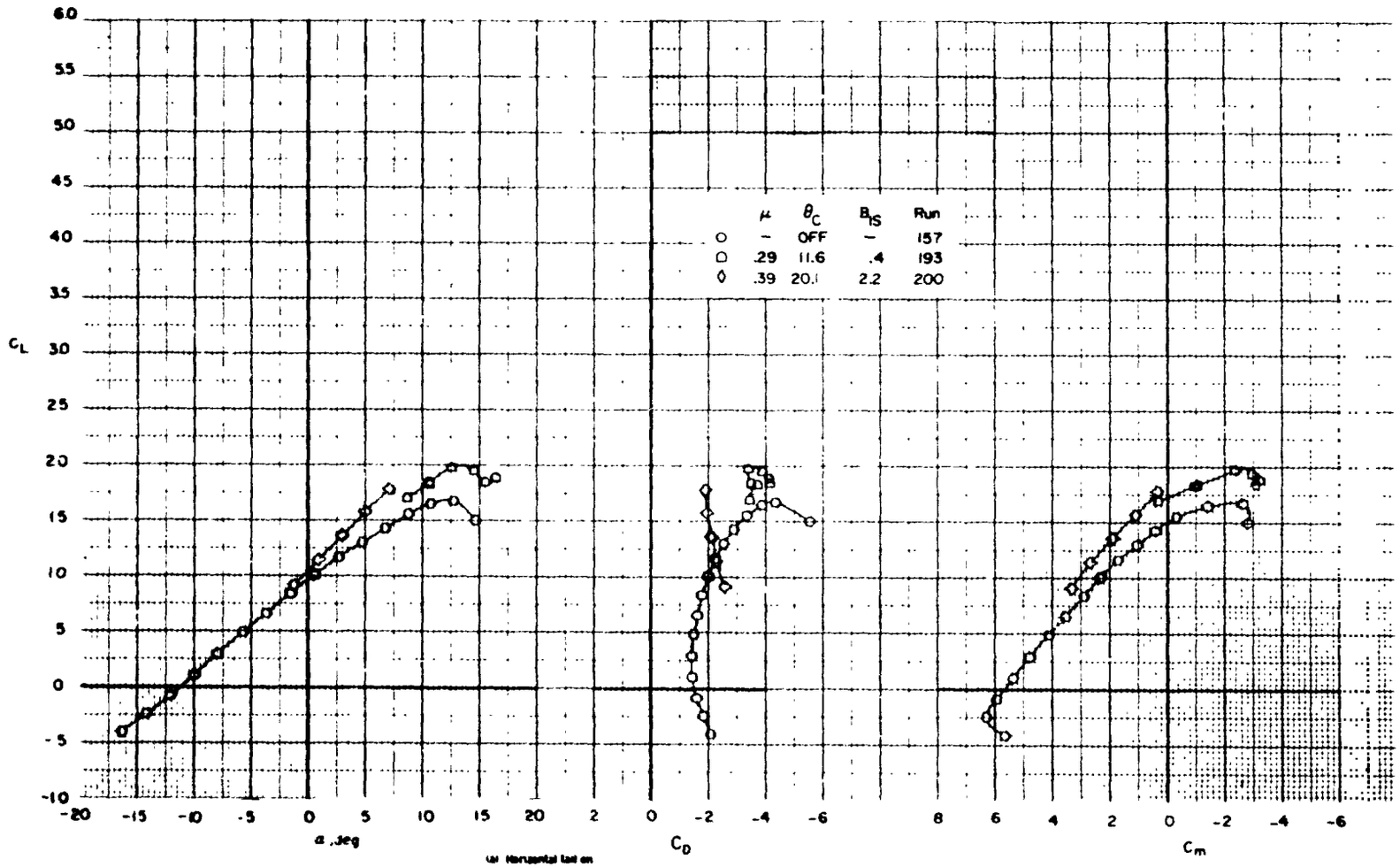

(a) Horizontal tail on

Figure 17. - Effect of rotor thrust and angle of attack on longitudinal aerodynamic characteristics for pylon angle 39°, horizontal tail on and off.

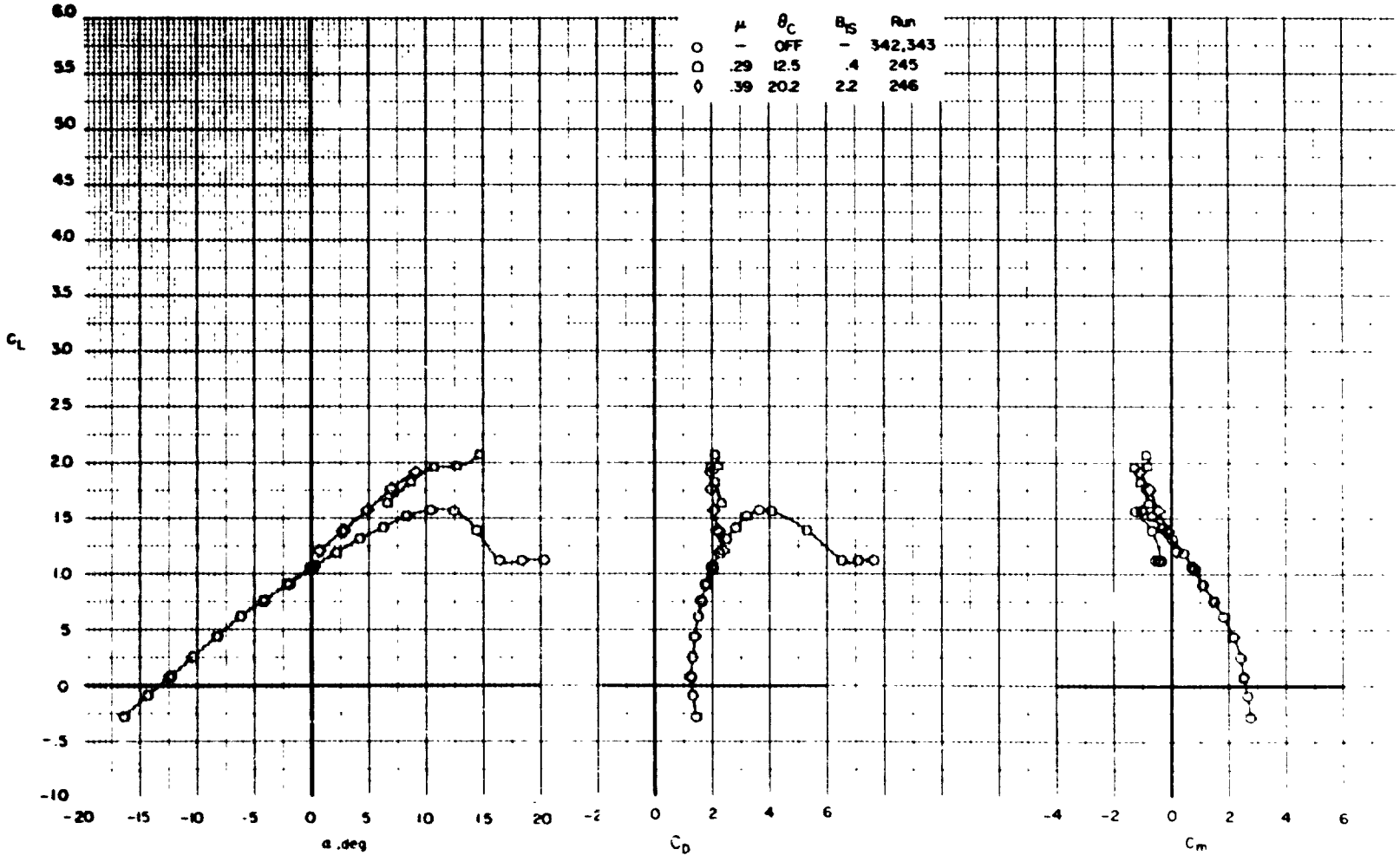

(b) Horizontal tail off

Figure 87. - Concluded.

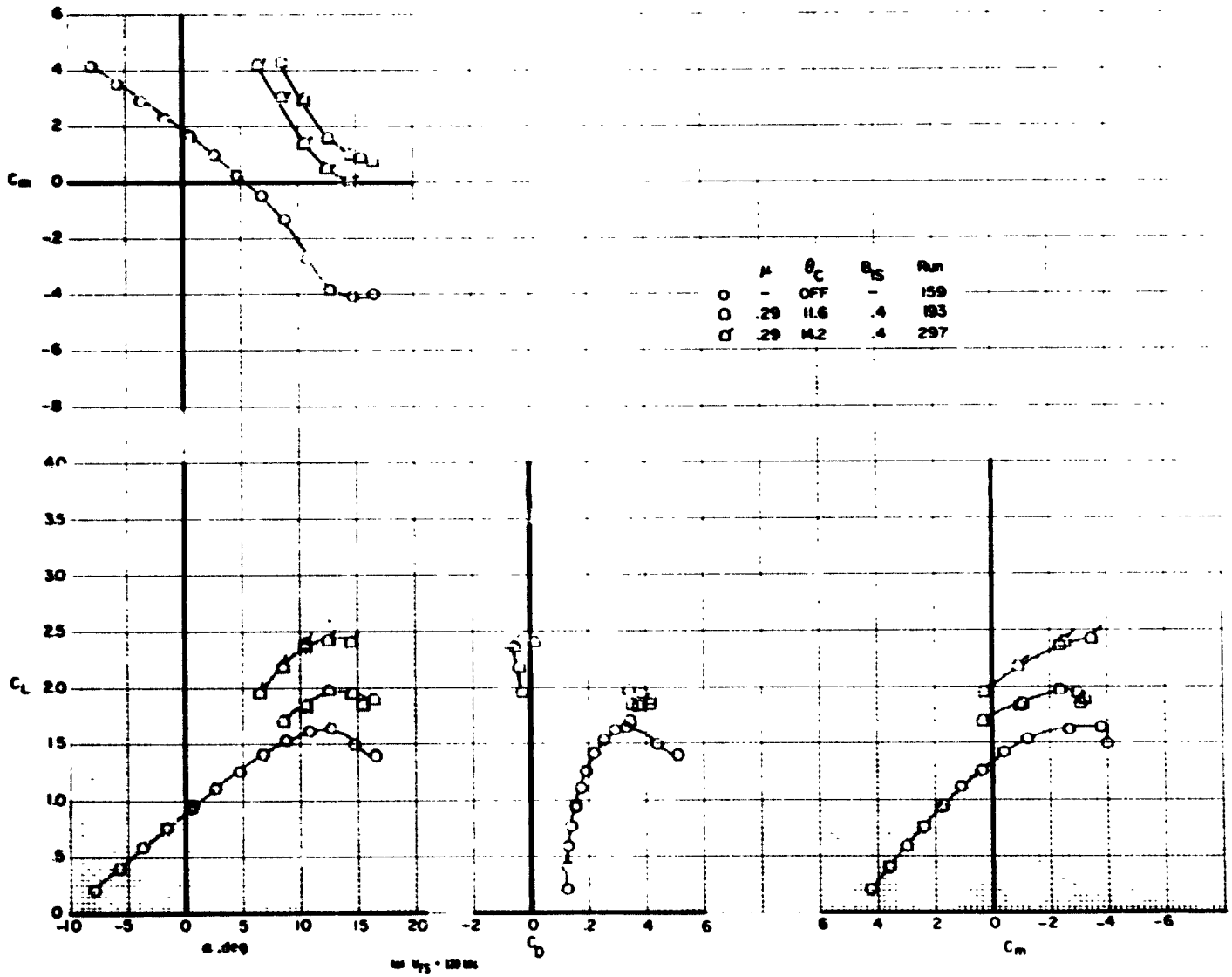

Figure 68. - Comparison of rotor thrust effects (θ_c = 11.6° and 14.2°) on longitudinal aerodynamic characteristics for pylon angle 30° and full-scale flight speeds of 120 and 180 knots.

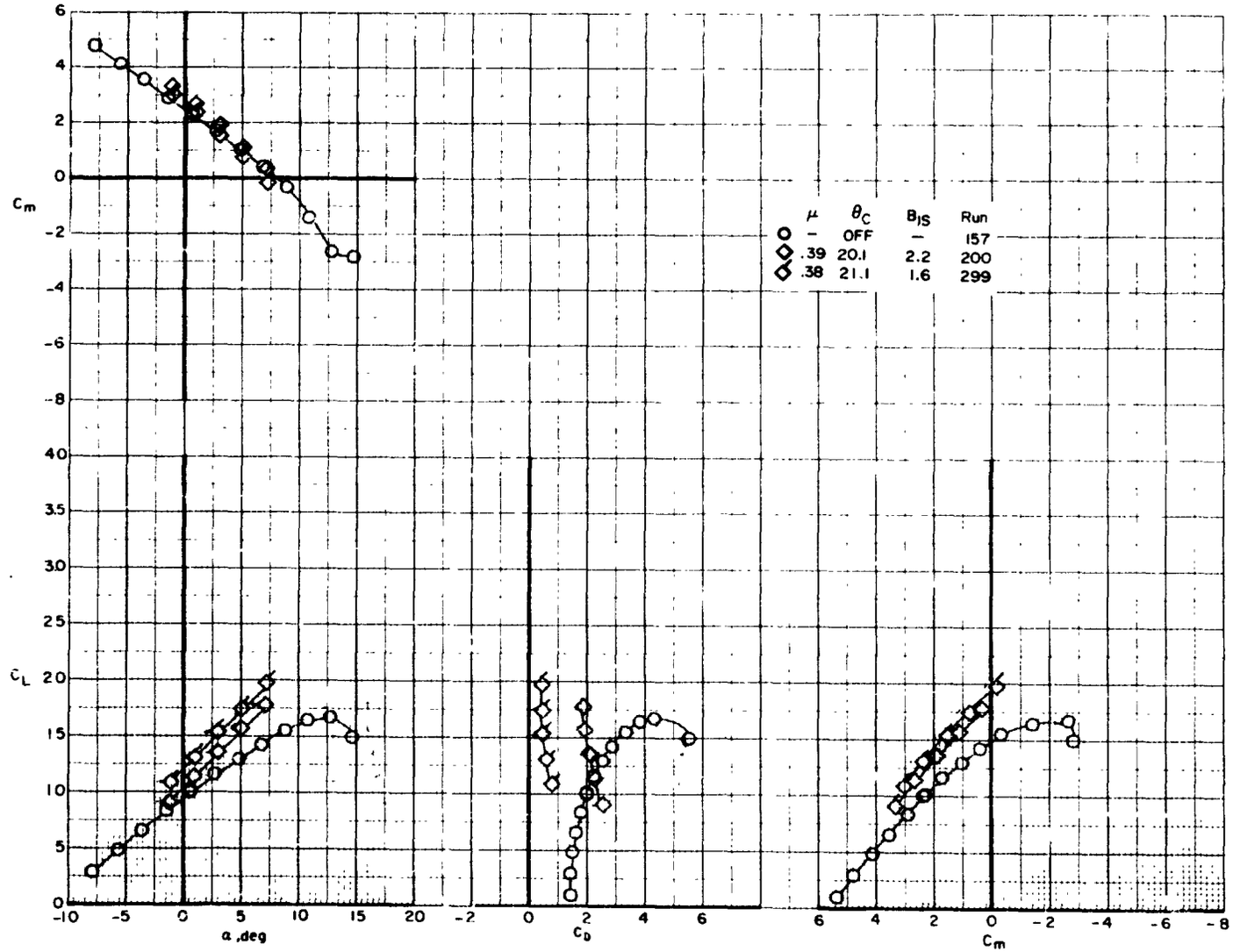

(b) V_{FS} = 160 kts

Figure 88. - Concluded.

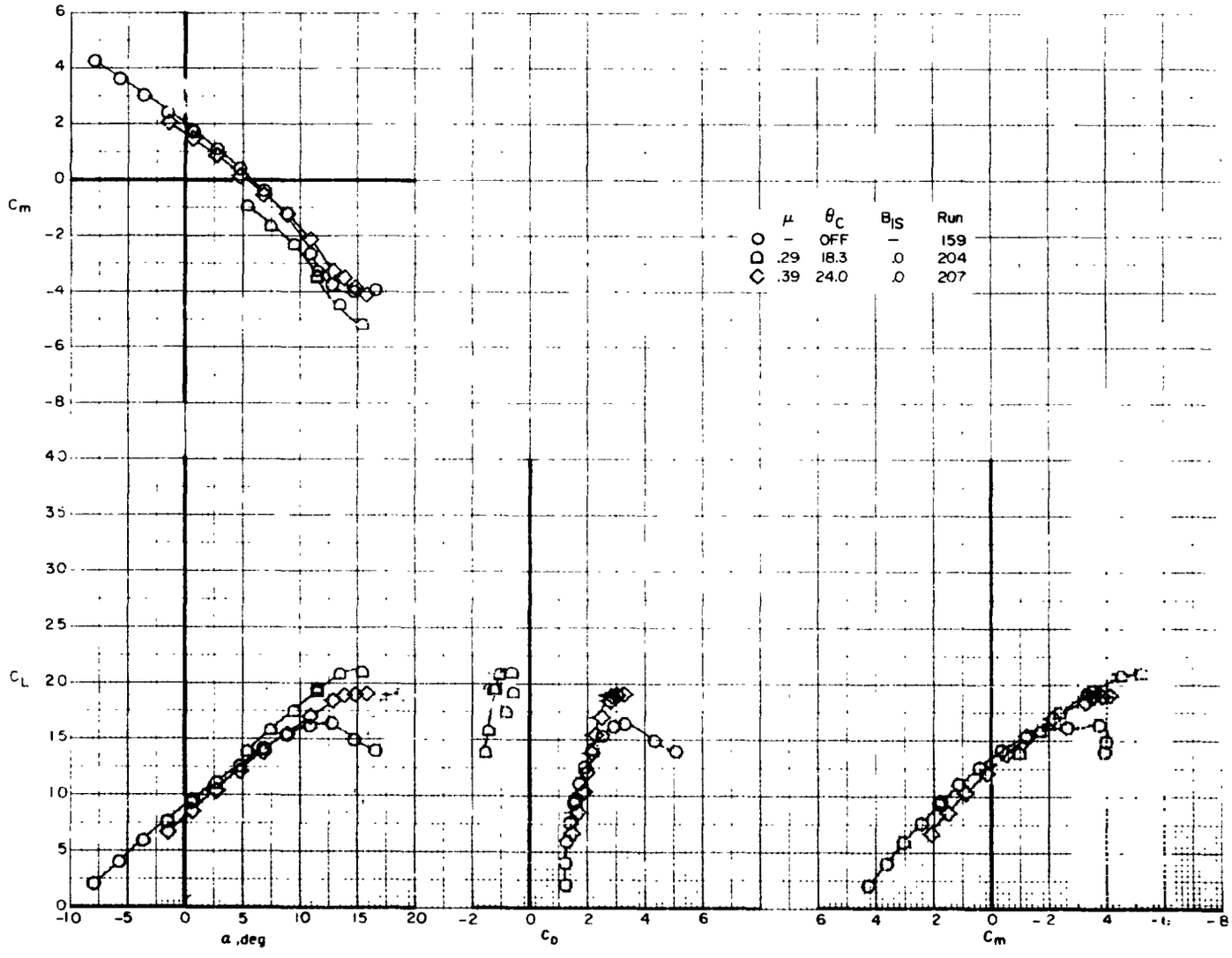

(a) 1604 r.p.m.

Figure 89. - Effect of rotor thrust and angle of attack on longitudinal aerodynamic characteristics for pylon angle 0° and transition and cruise r.p.m.

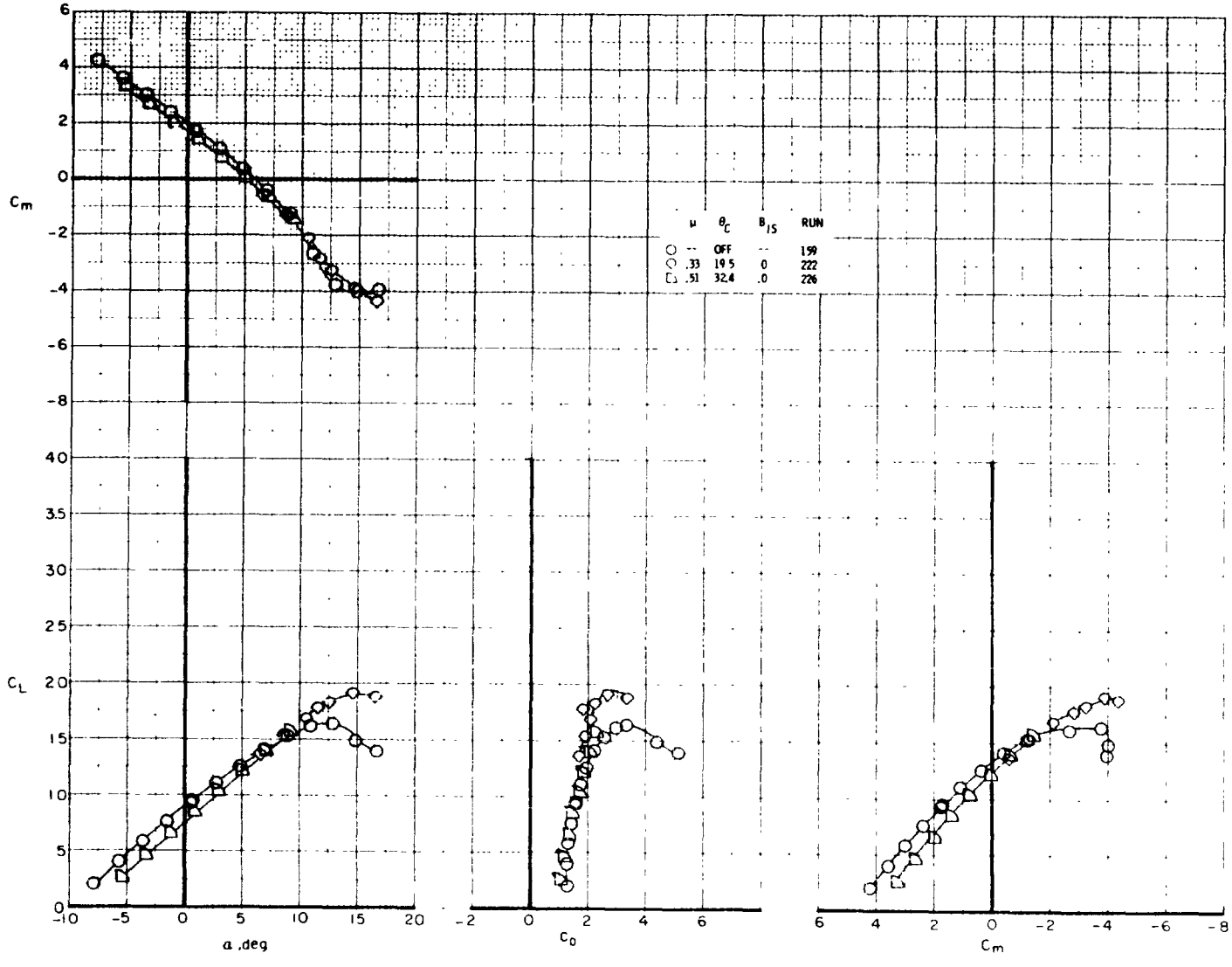

(b) 1372 r.p.m

Figure 89. - Concluded.

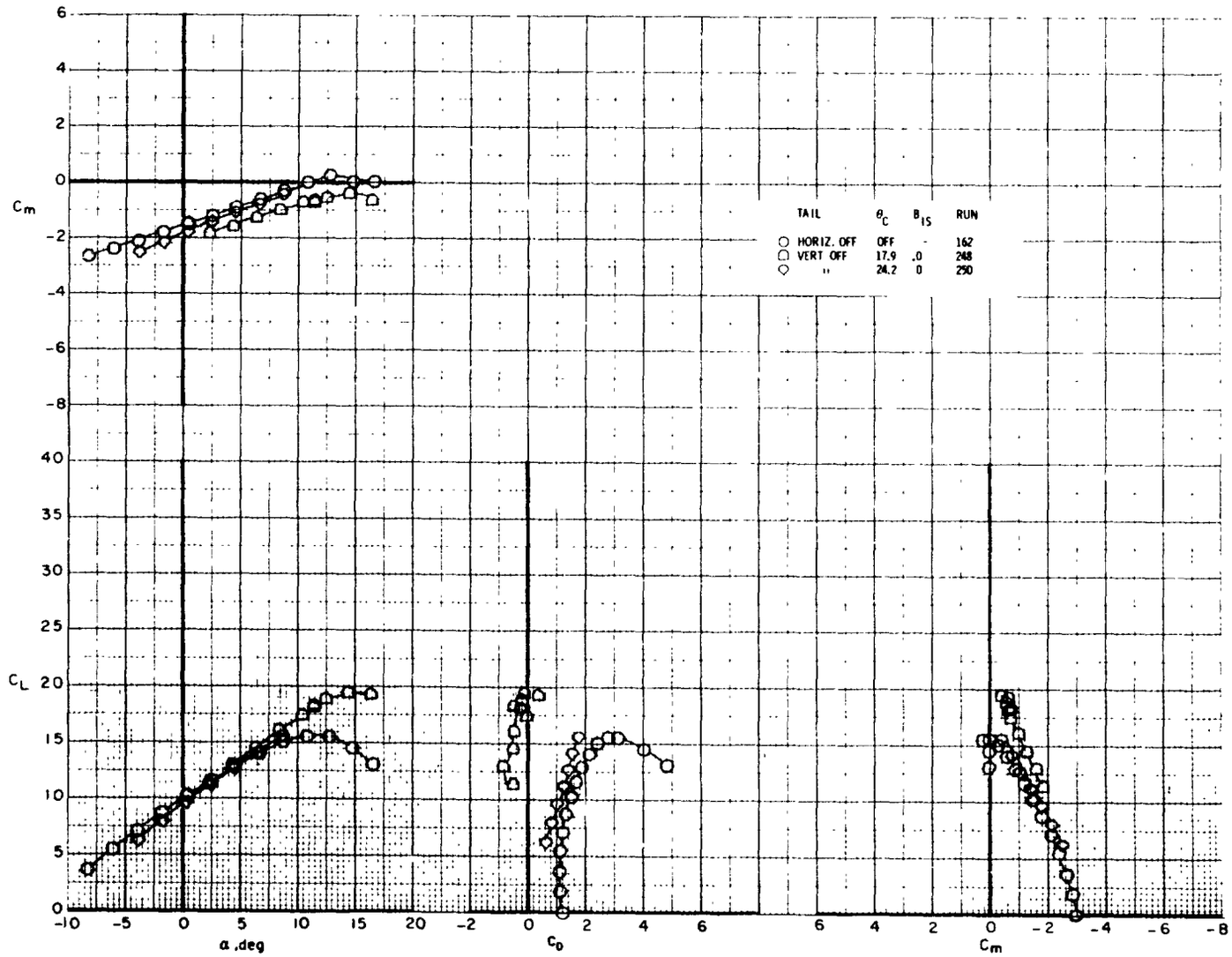

(a) 1604 r.p.m.

Figure 90. - Effect of rotor thrust and angle of attack on longitudinal aerodynamic characteristics for pylon angle 0°, tail off, and transition and cruise r.p.m.

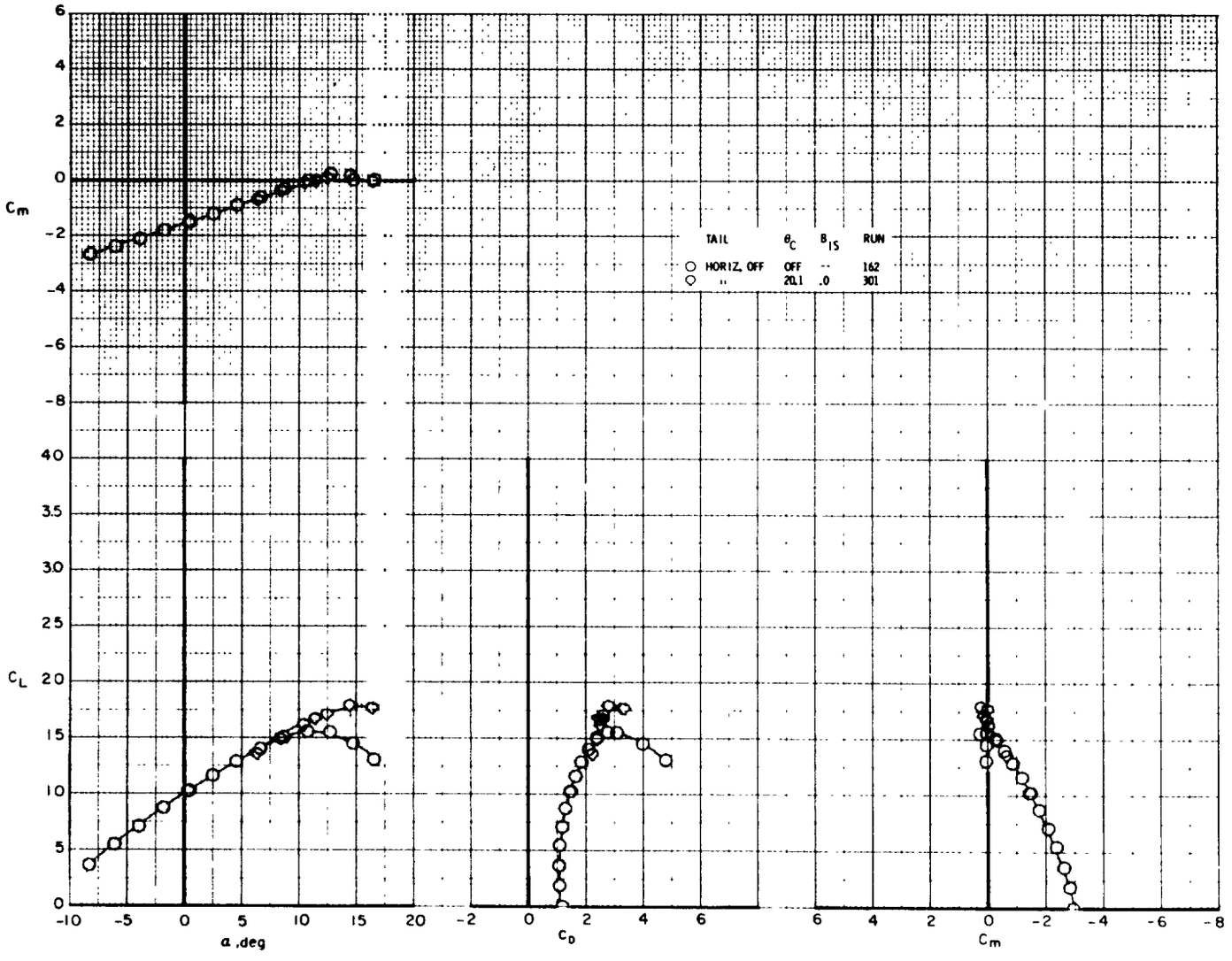

(b) 1372 r.p.m.

Figure 90 - Concluded.

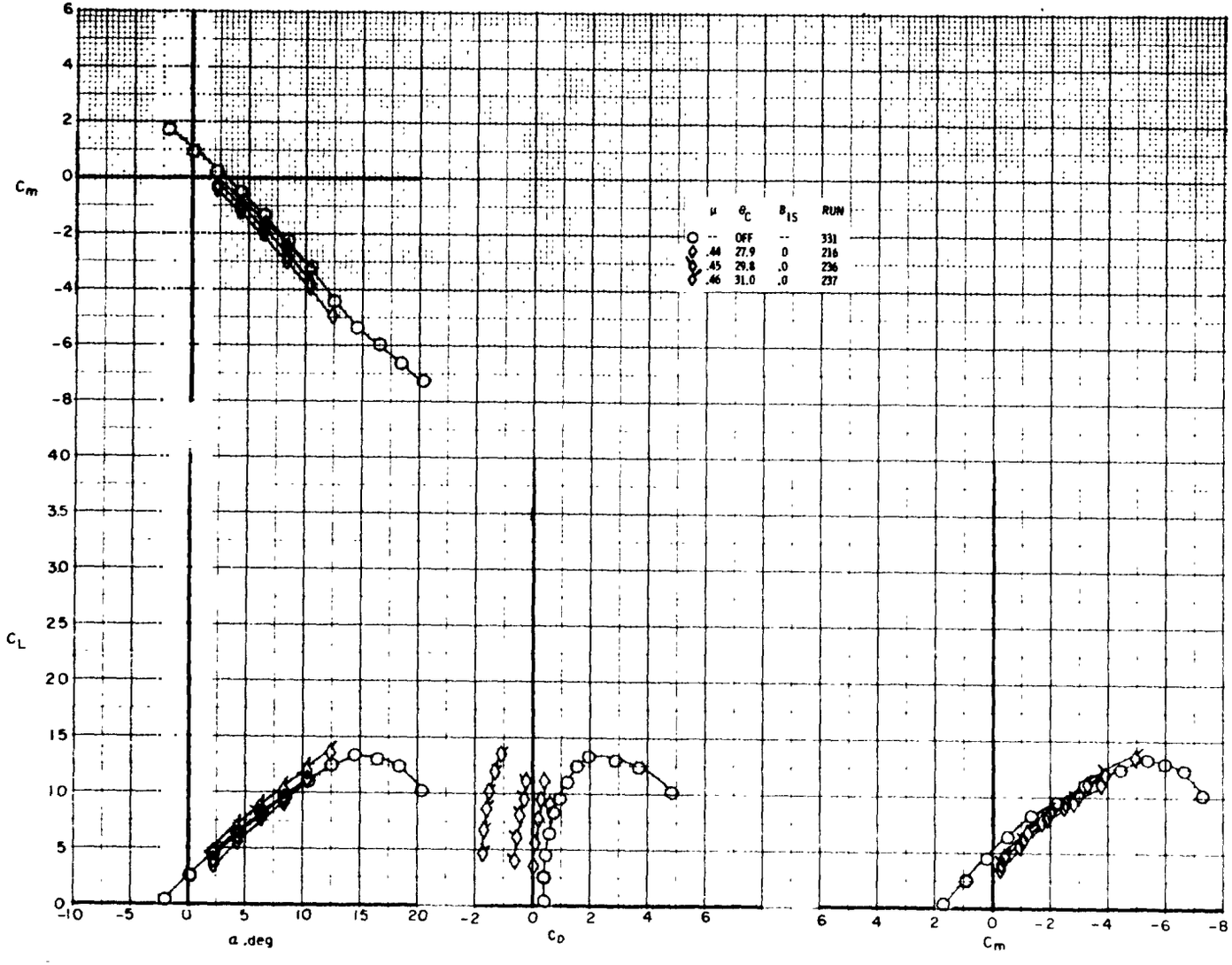

(a) V_{FS} = 160 kts

Figure 91. - Effect of rotor thrust and angle of attack on longitudinal aerodynamic characteristics for pylon angle 0° and for full-scale flight speeds of 160 and 180 knots. B_f/B_a = 0/0, transition rotor speed.

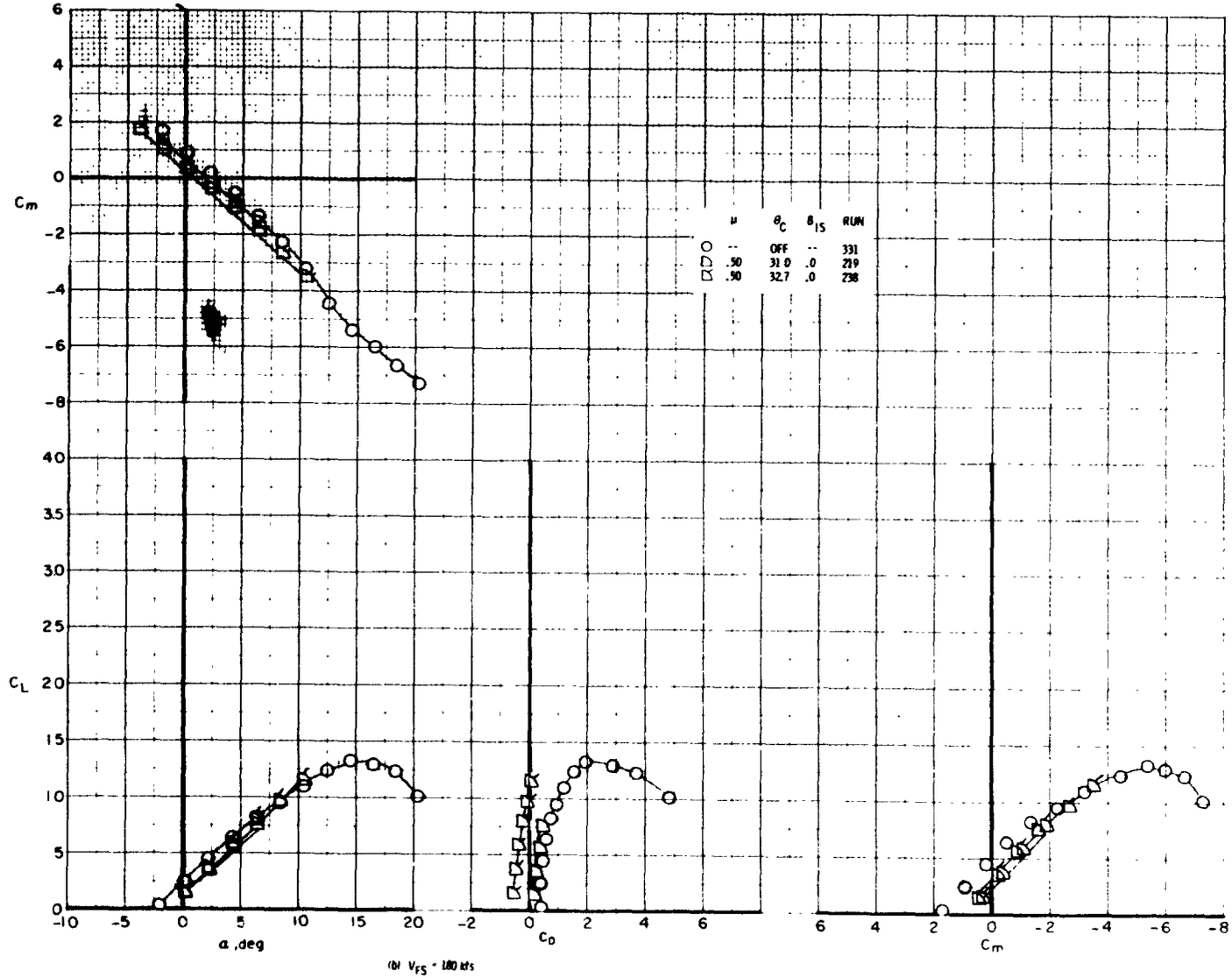

(b) V_{FS} = 180 kts

Figure 91. - Concluded.

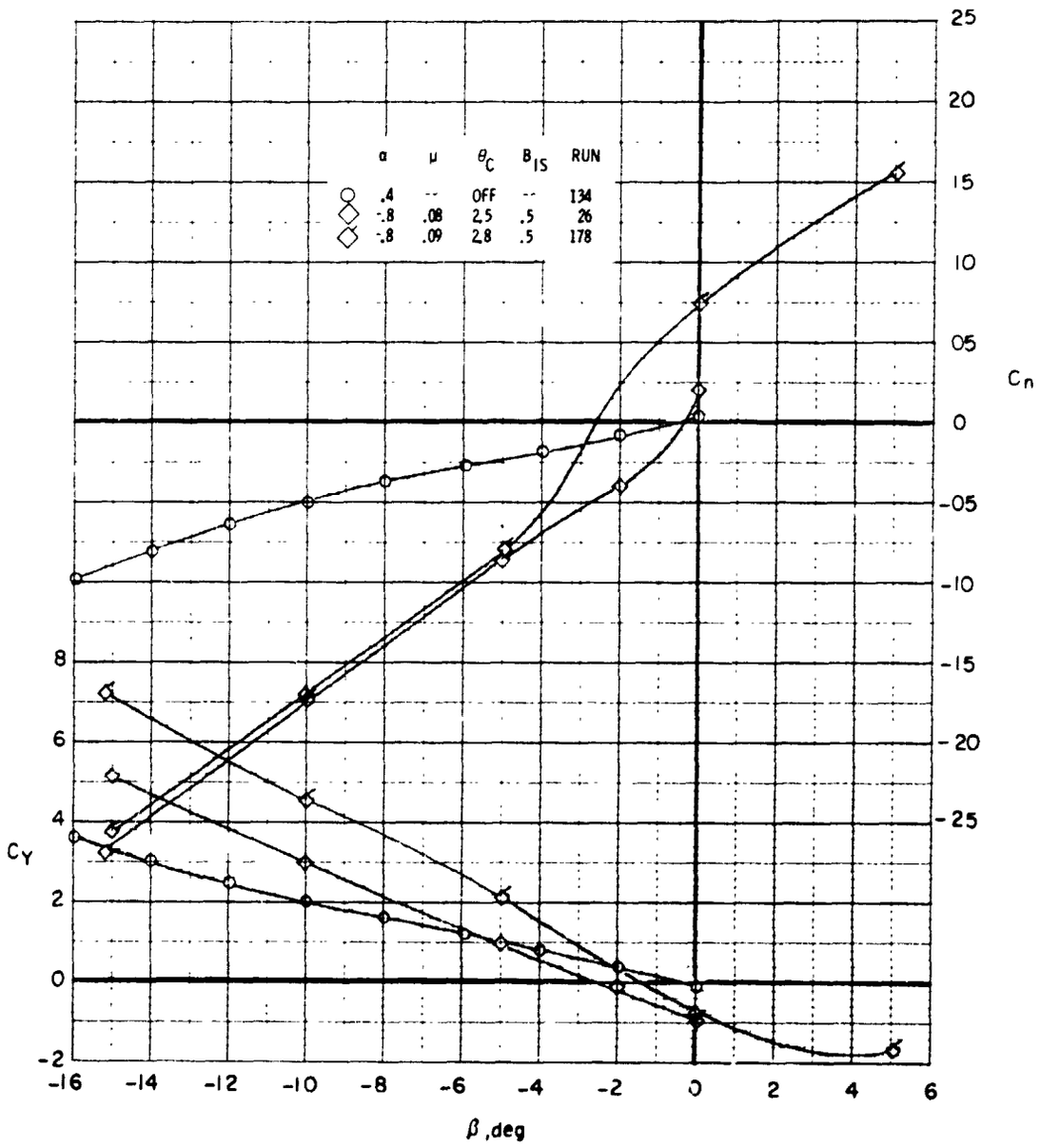

(a) V_{FS} = 40 kts, μ = 0.08

Figure 92. - Effect of rotor thrust and sideslip angle on lateral aerodynamic characteristics for full-scale flight speeds of 40 and 80 knots for pylon angle 90°.

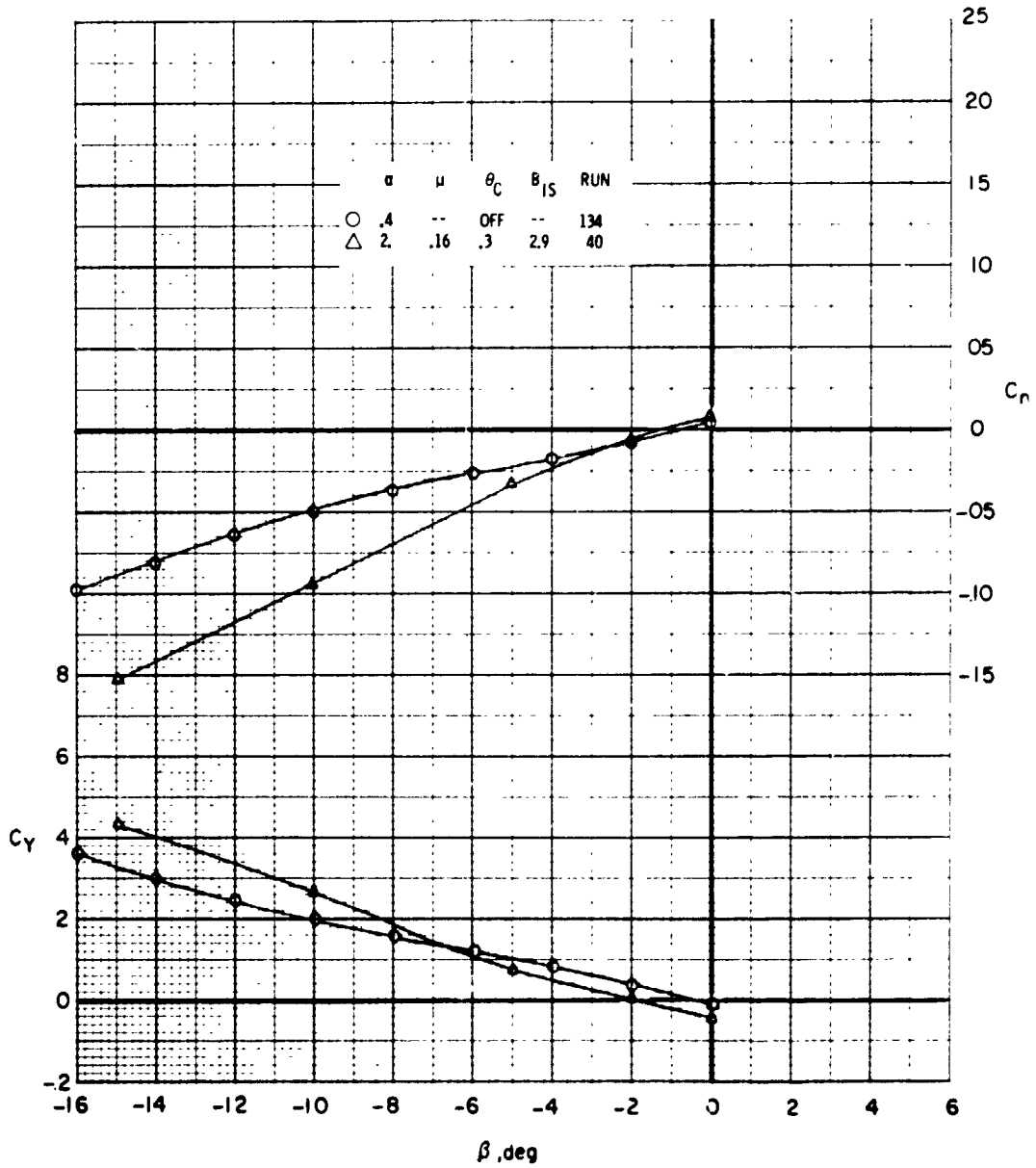

(b) V_{FS} = 80 kts, μ = 0.16

Figure 92. - Concluded.

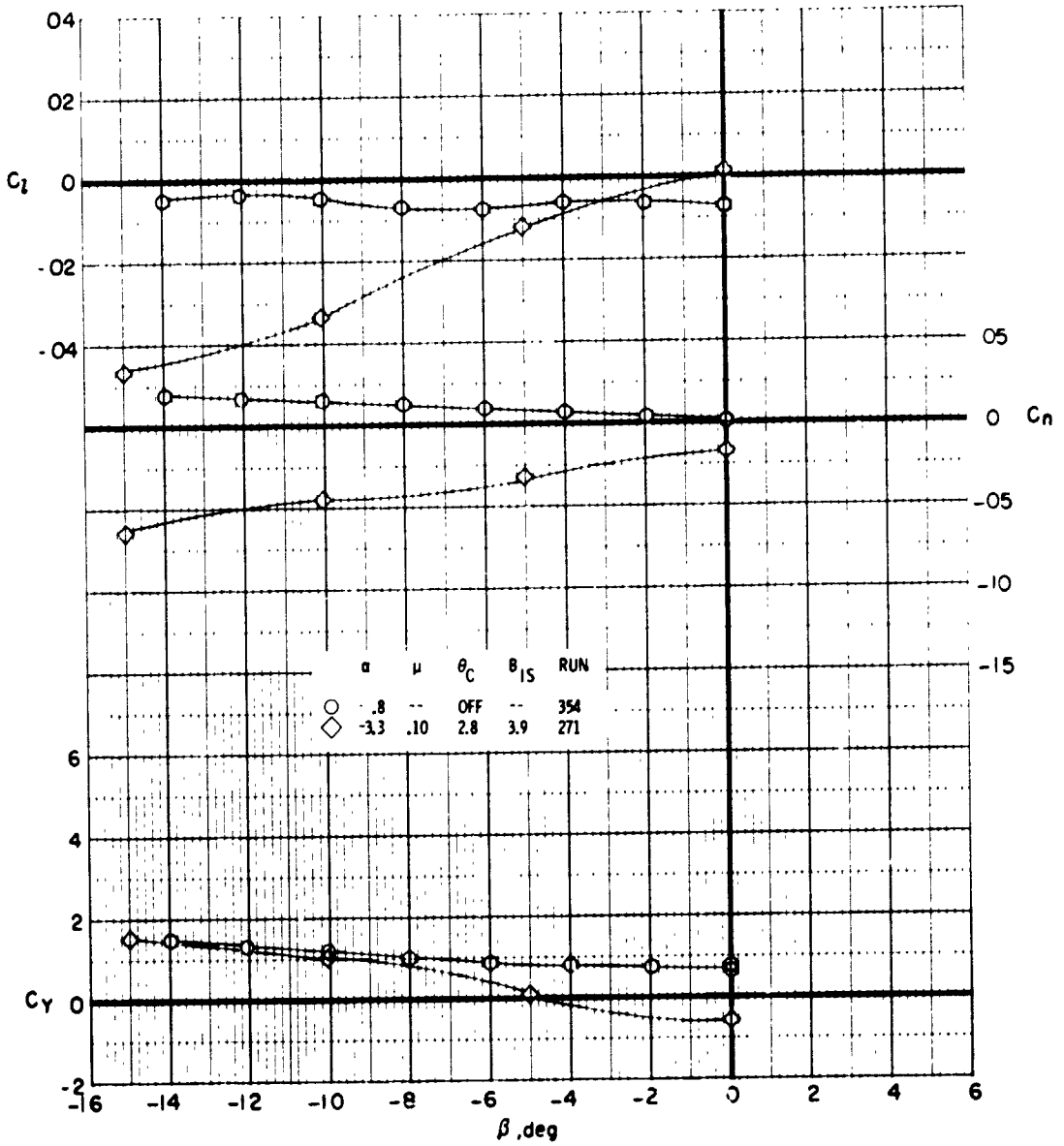

(a) V_{FS} = 60 kts, vertical tail off

Figure 93. - Effect of rotor thrust and sideslip angle on lateral aerodynamic characteristics for full-scale flight speeds of 50 and 80 knots, pylon angle 90°, tail off.

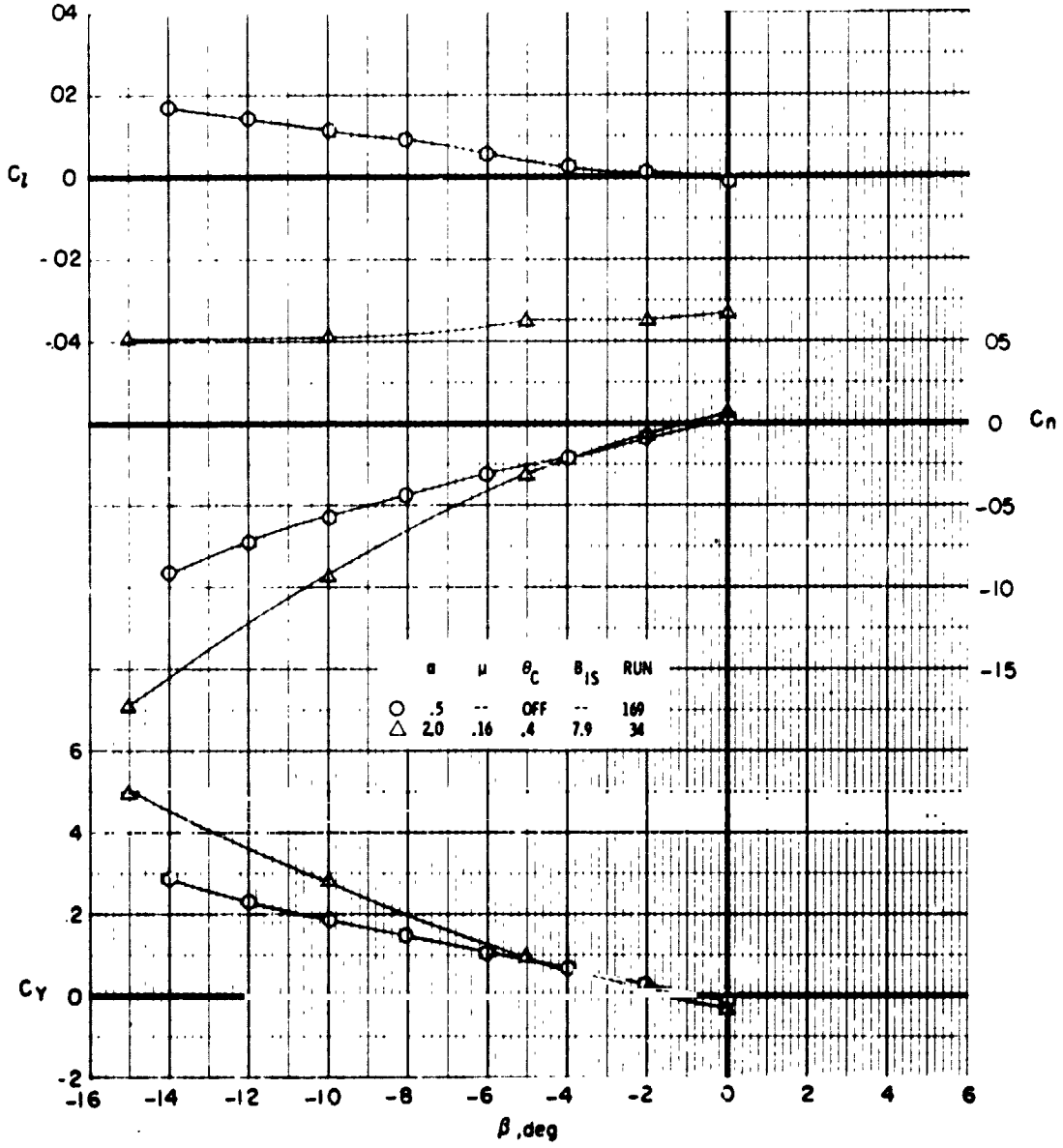

(b) V_{FS} = 80 kts, horizontal tail off

Figure 93. - Concluded.

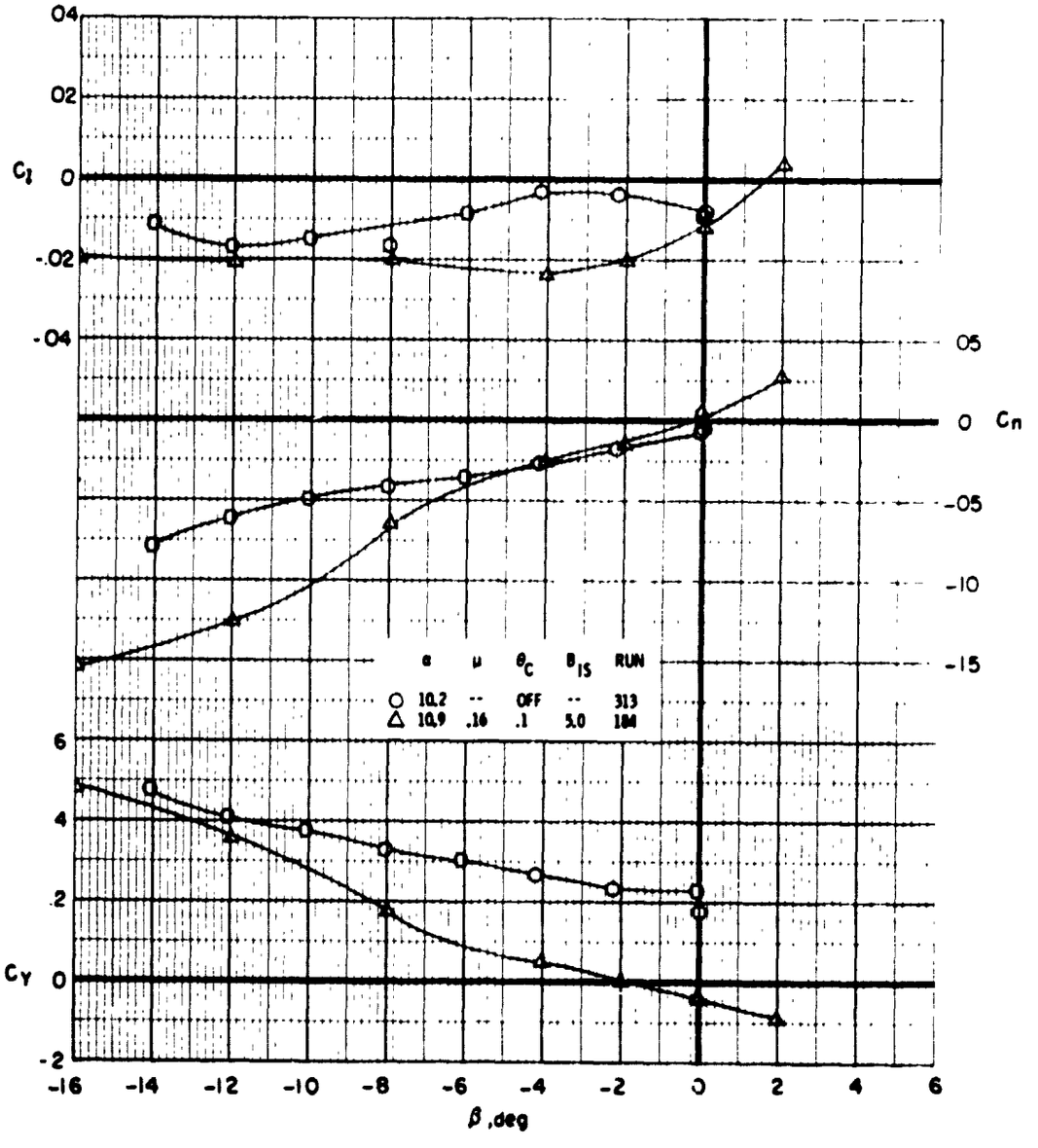

(a) Vertical tail on

Figure 96. - Effect of rotor thrust and sideslip angle on lateral aerodynamic characteristics for full-scale flight speeds of 80 knots, pylon angle 75°, vertical tail on and off.

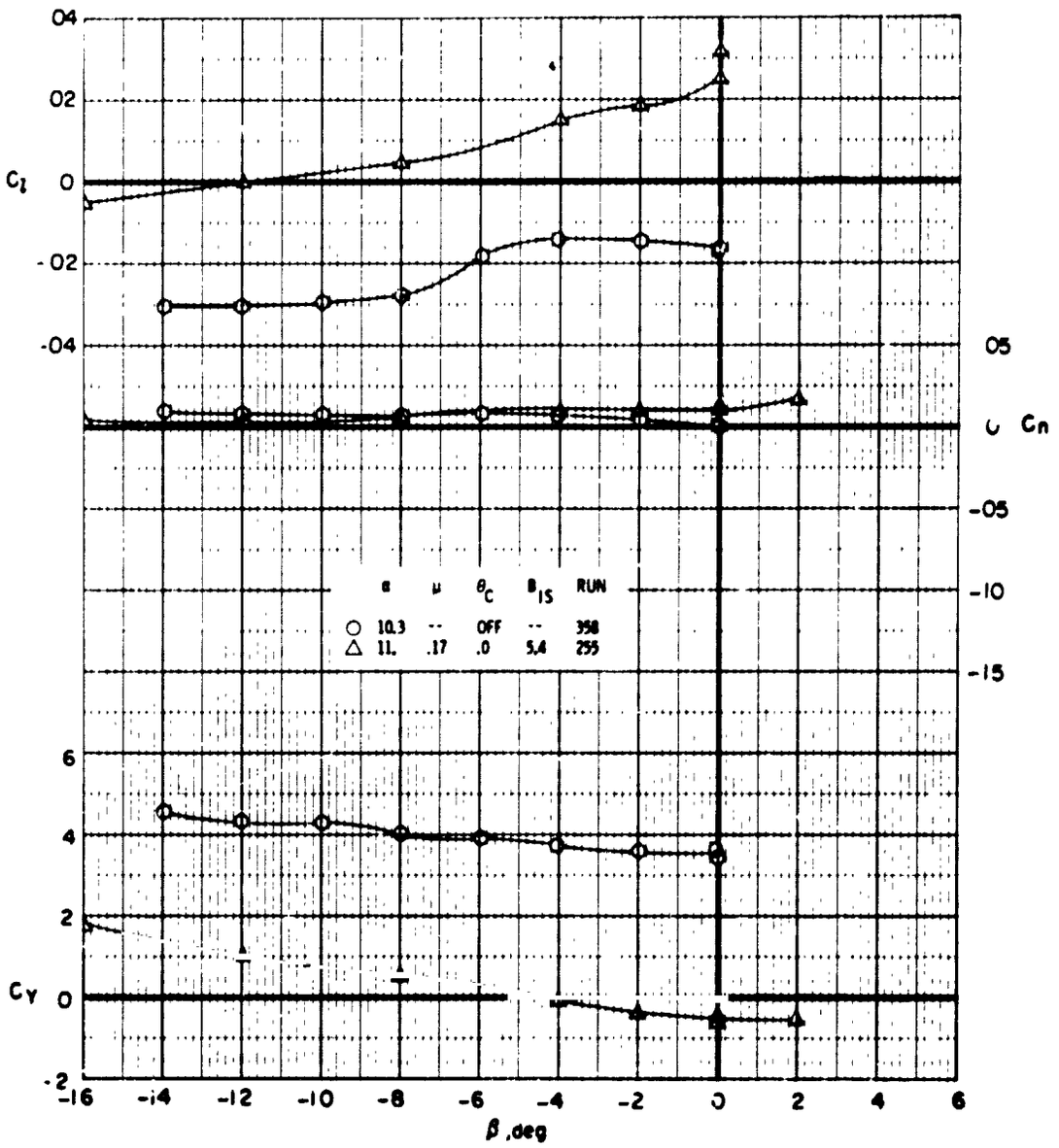

(b) Vertical tail off

Figure 9L. - Concluded.

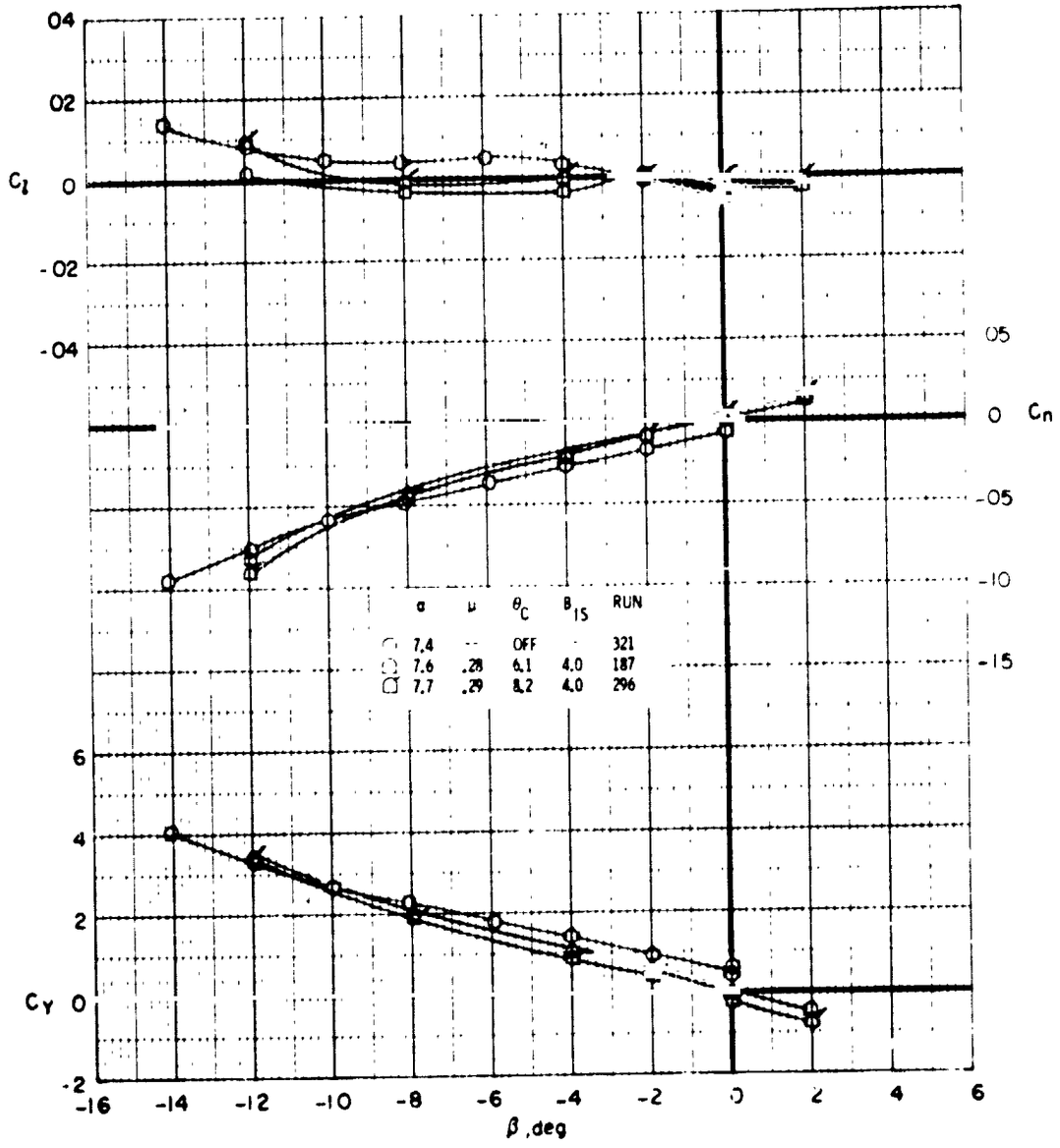

(a) Vertical tail on

Figure 95. - Effect of rotor thrust and sideslip angle on lateral aerodynamic characteristics for full-scale flight speed of 120 knots, pylon angle 60°, vertical tail on and off.

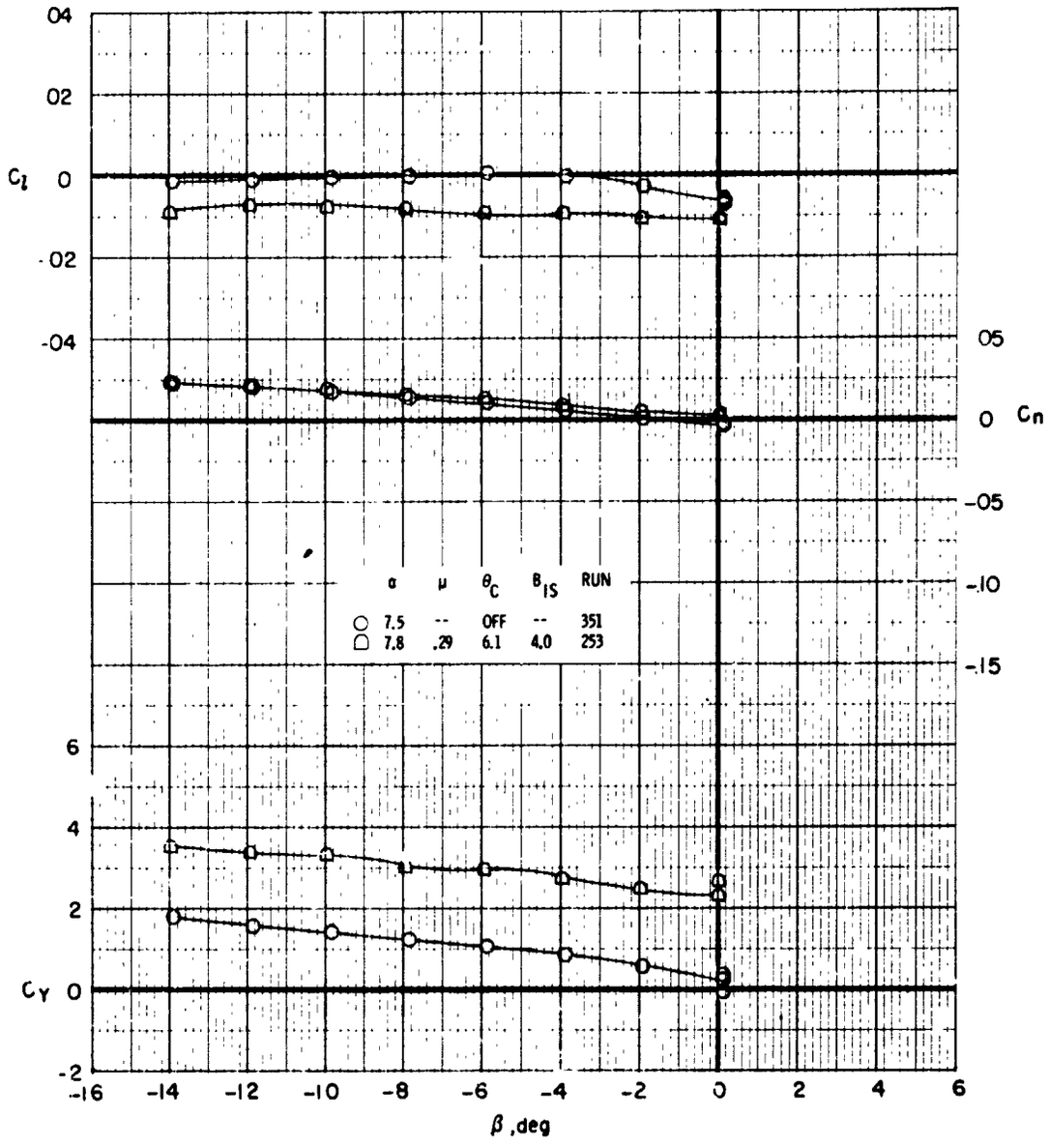

(b) Vertical tail off

Figure 95. - Concluded.

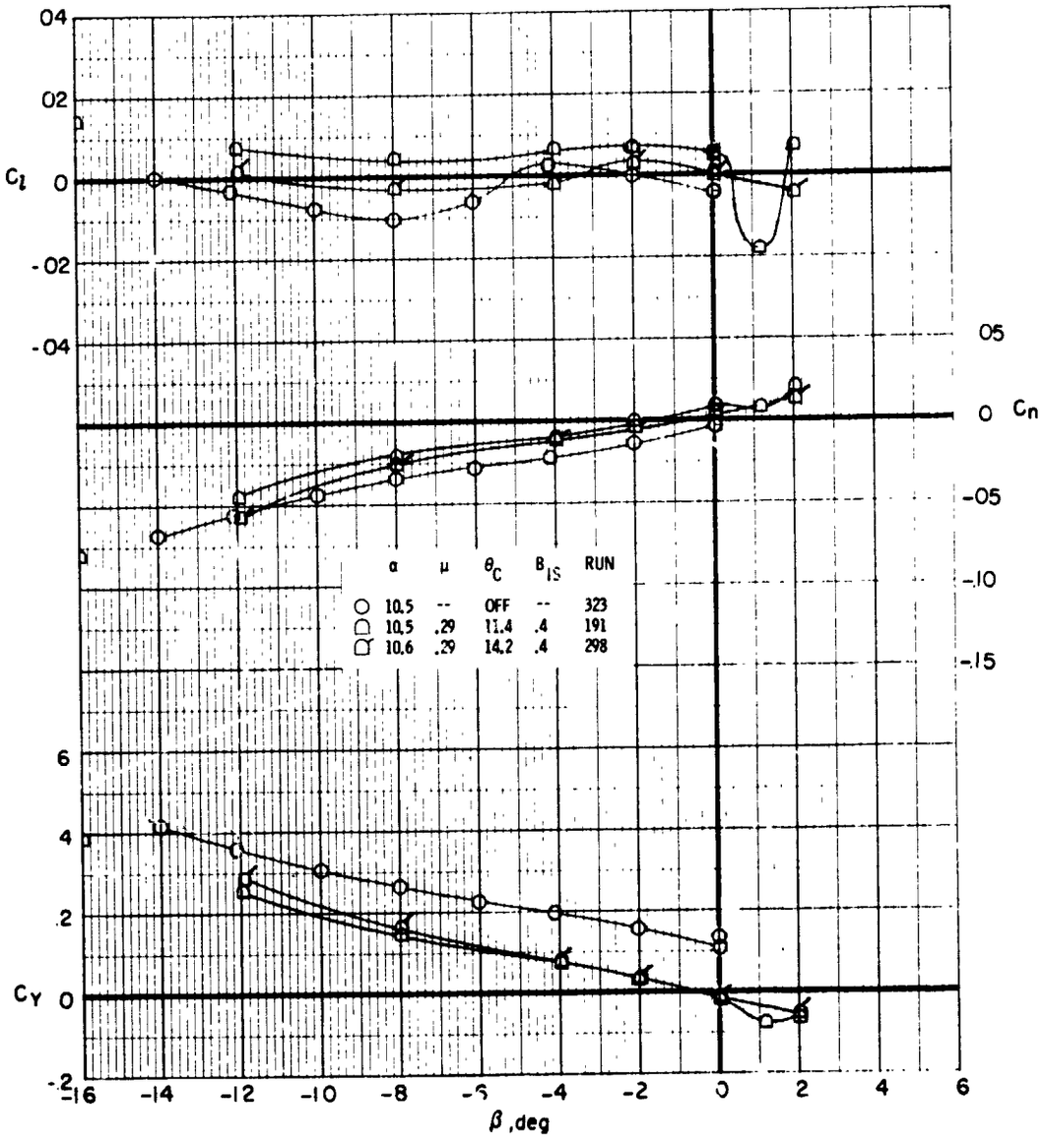

(a) V_{FS} = 120 kts

Figure 96. - Effect of rotor thrust and sideslip angle on lateral aerodynamic characteristics for full-scale flight speeds of 120 and 160 knots for pylon angle 30°.

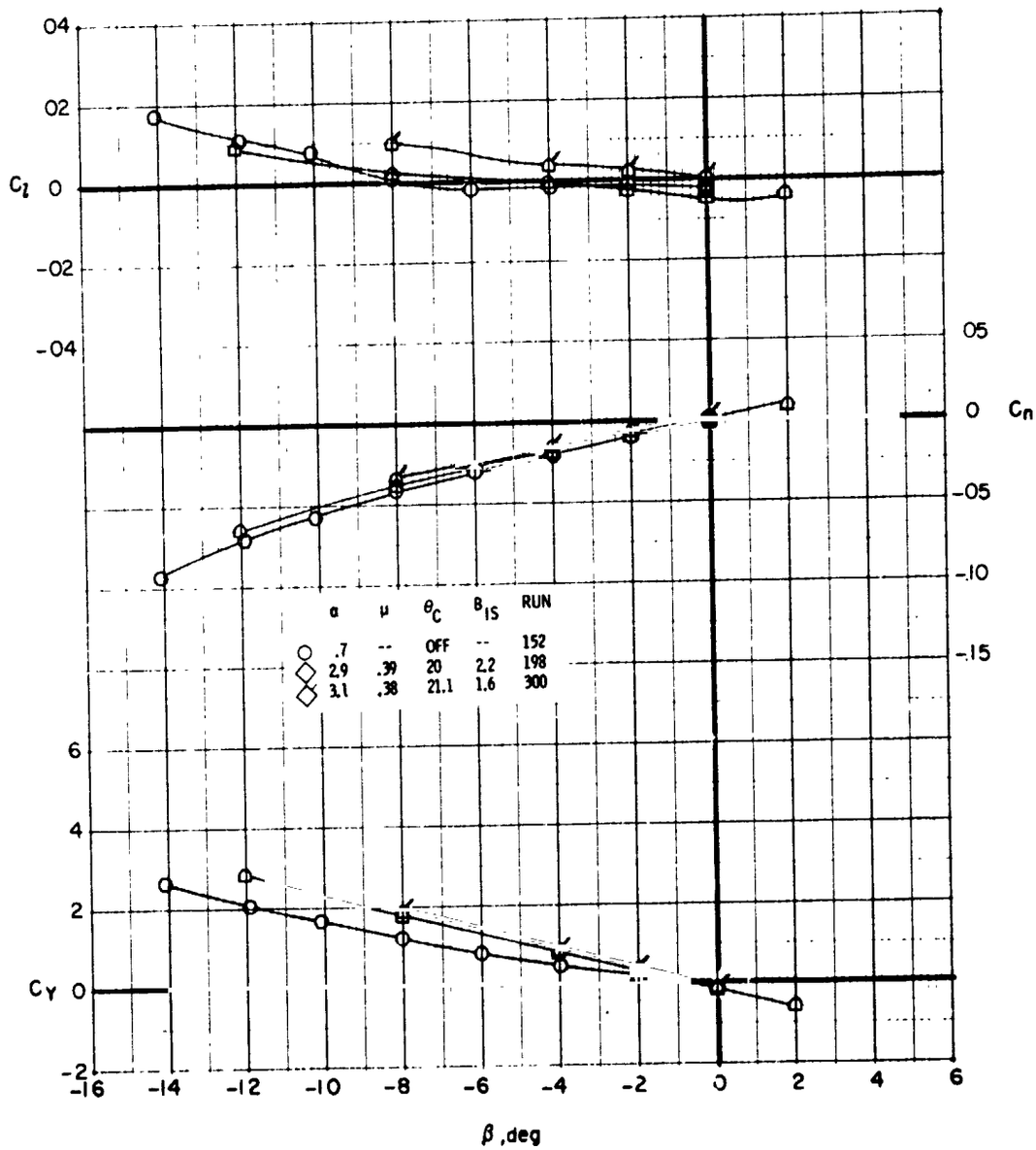

(b) V_{FS} = 160 kts

Figure 96. - Concluded.

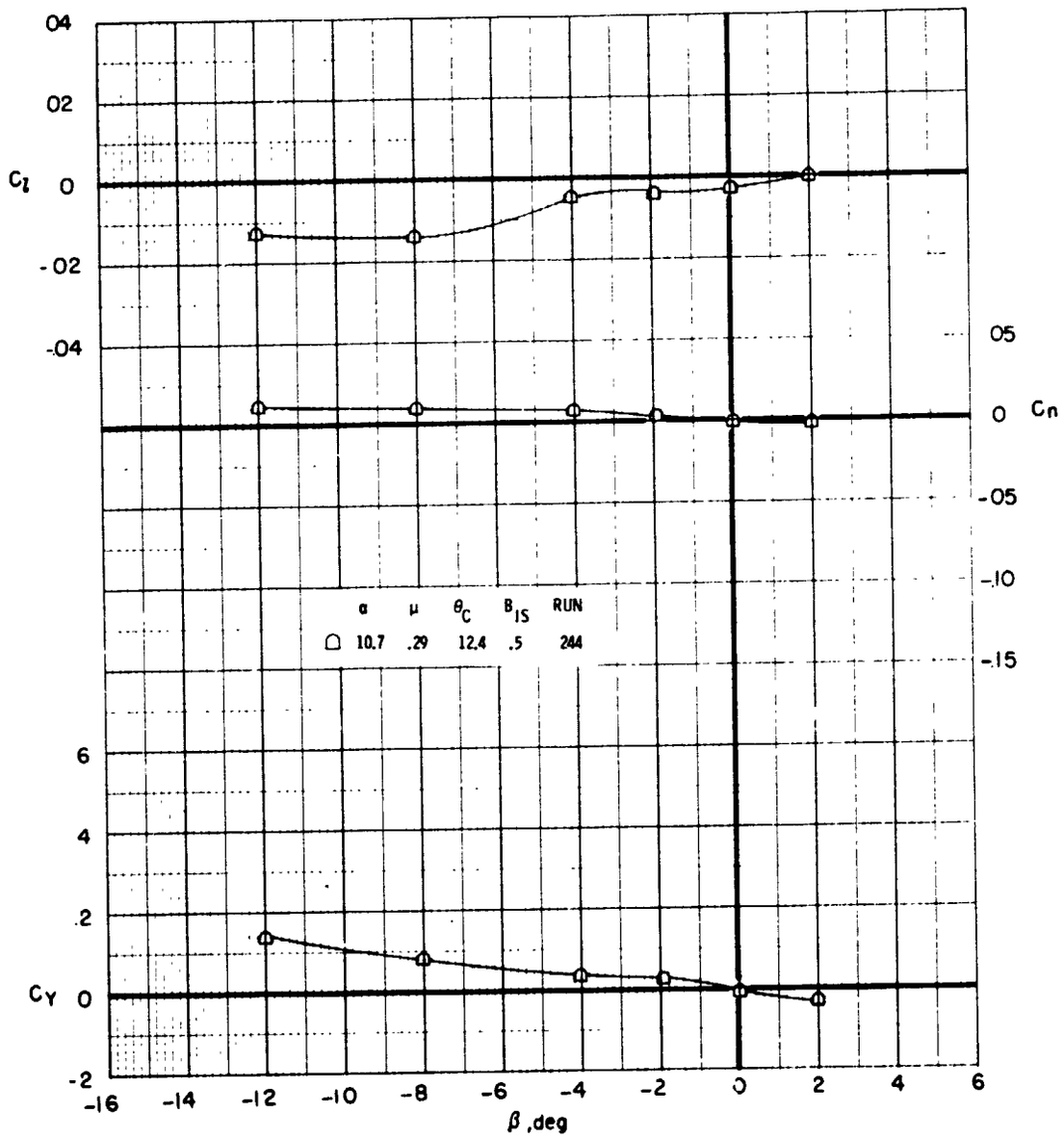

(a) V_{FS} = 120 kts

Figure 97. - Effect of rotor thrust and sideslip angle on lateral aerodynamic characteristics for full-scale flight speeds of 120 and 160 knots, pylon angle 30°, vertical tail off.

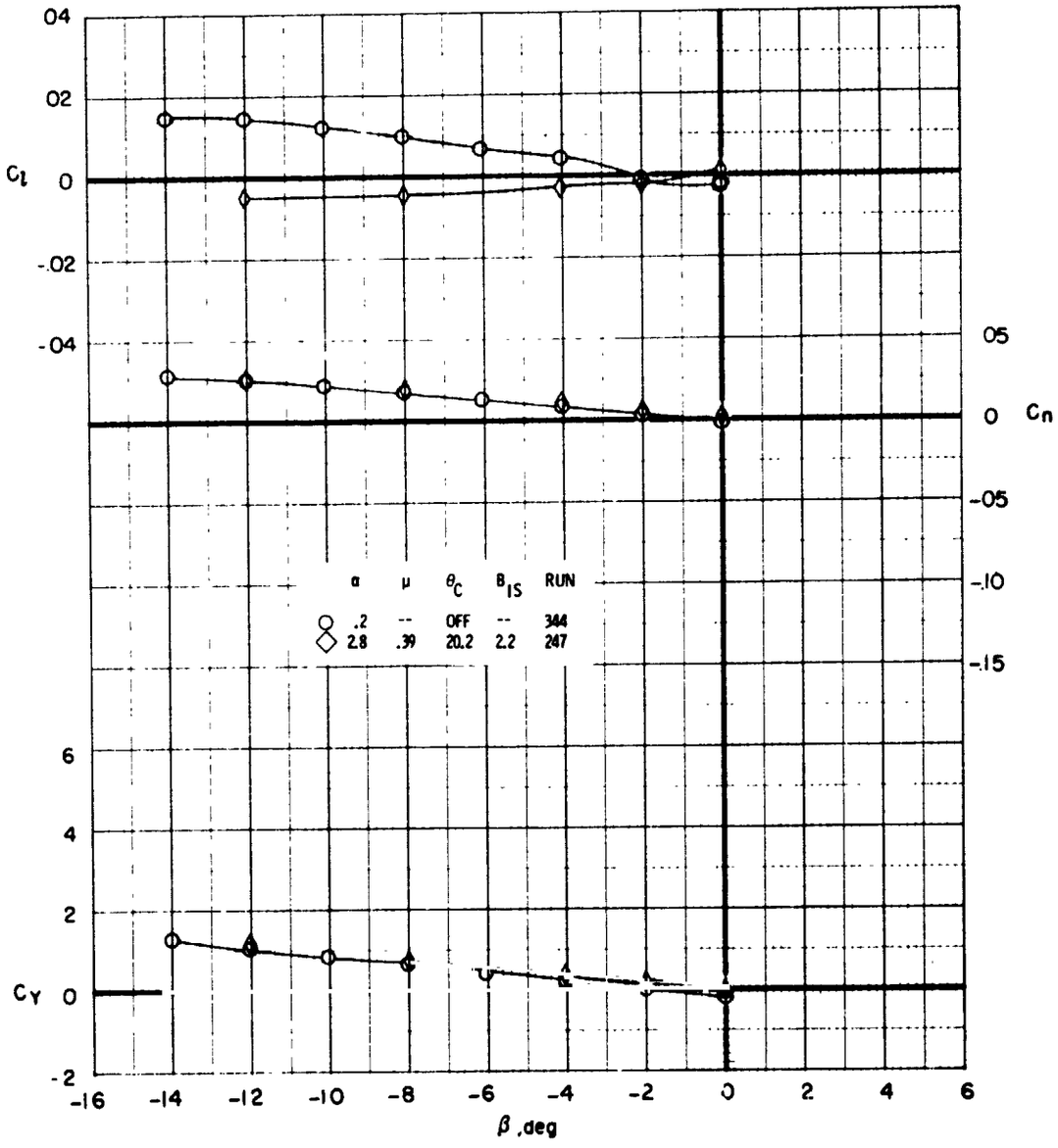

(b) V_{FS} = 160 kts

Figure 97. - Concluded.

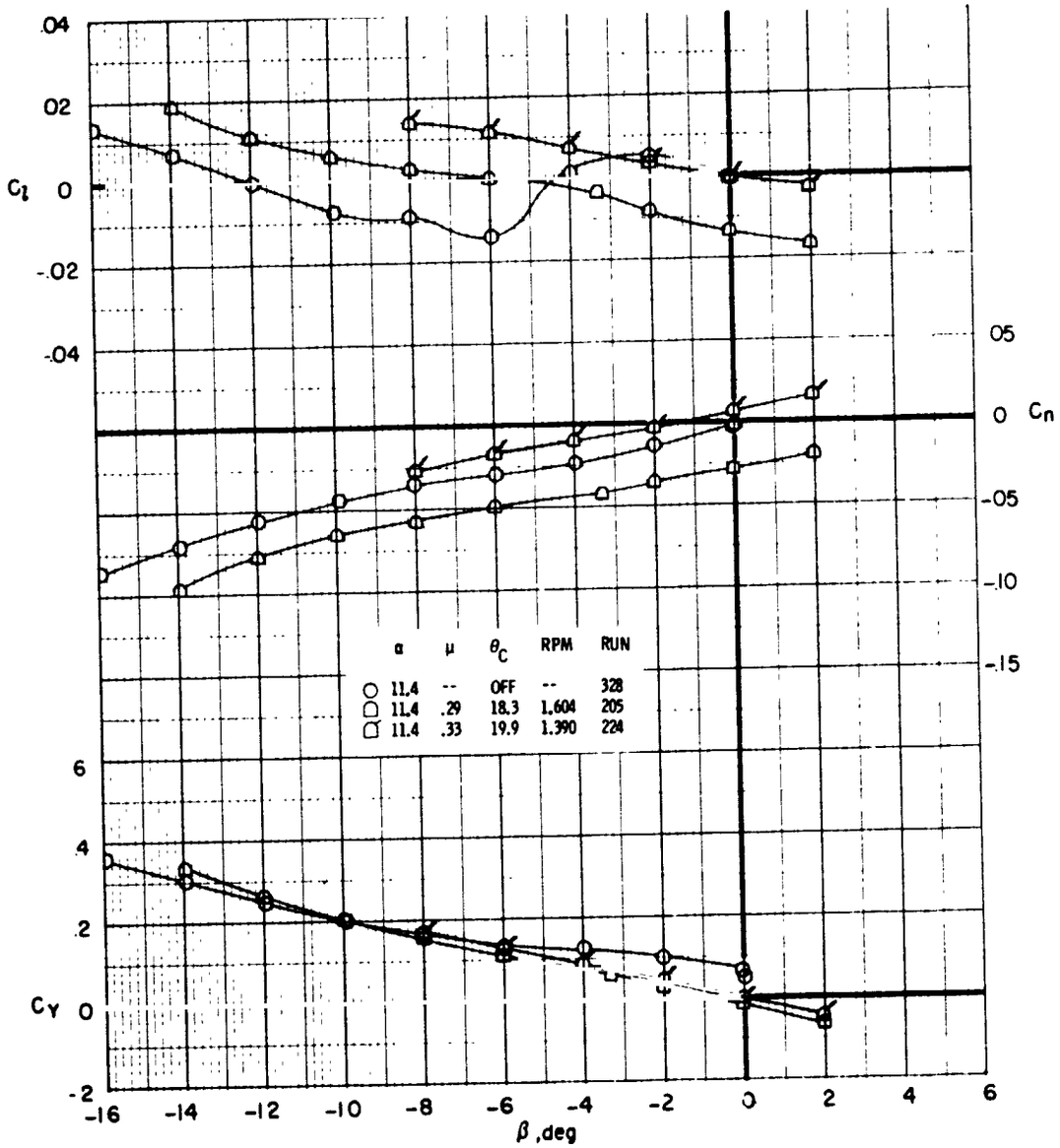

(a) V_{FS} = 120 kts

Figure 98. - Effects of rotor thrust and sideslip angle on lateral aerodynamic characteristics for full-scale flight speeds of 120, 160, and 180 knots for pylon angle 0°.

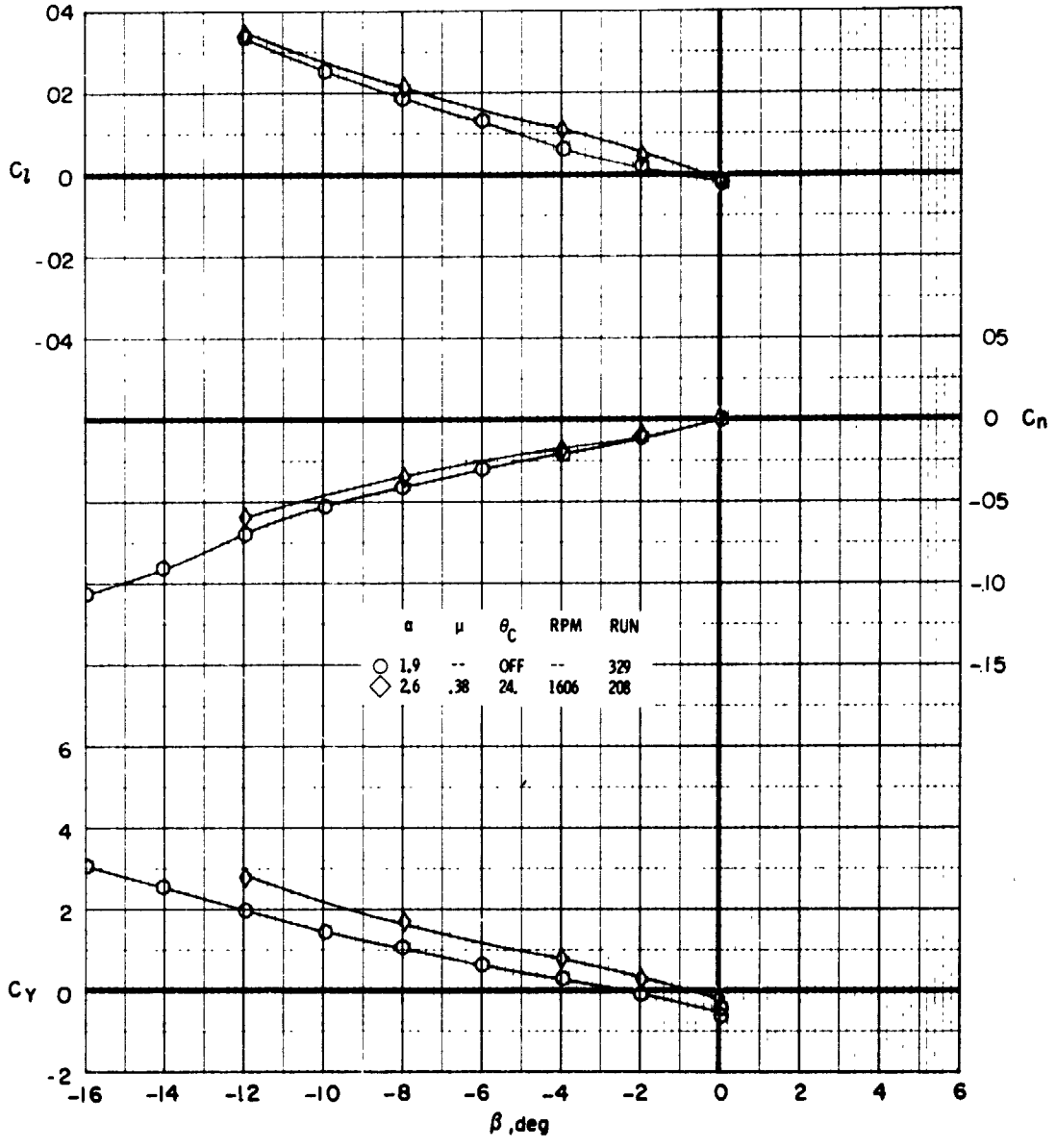

(b) V_{FS} = 160 kts

Figure 98. - Continued.

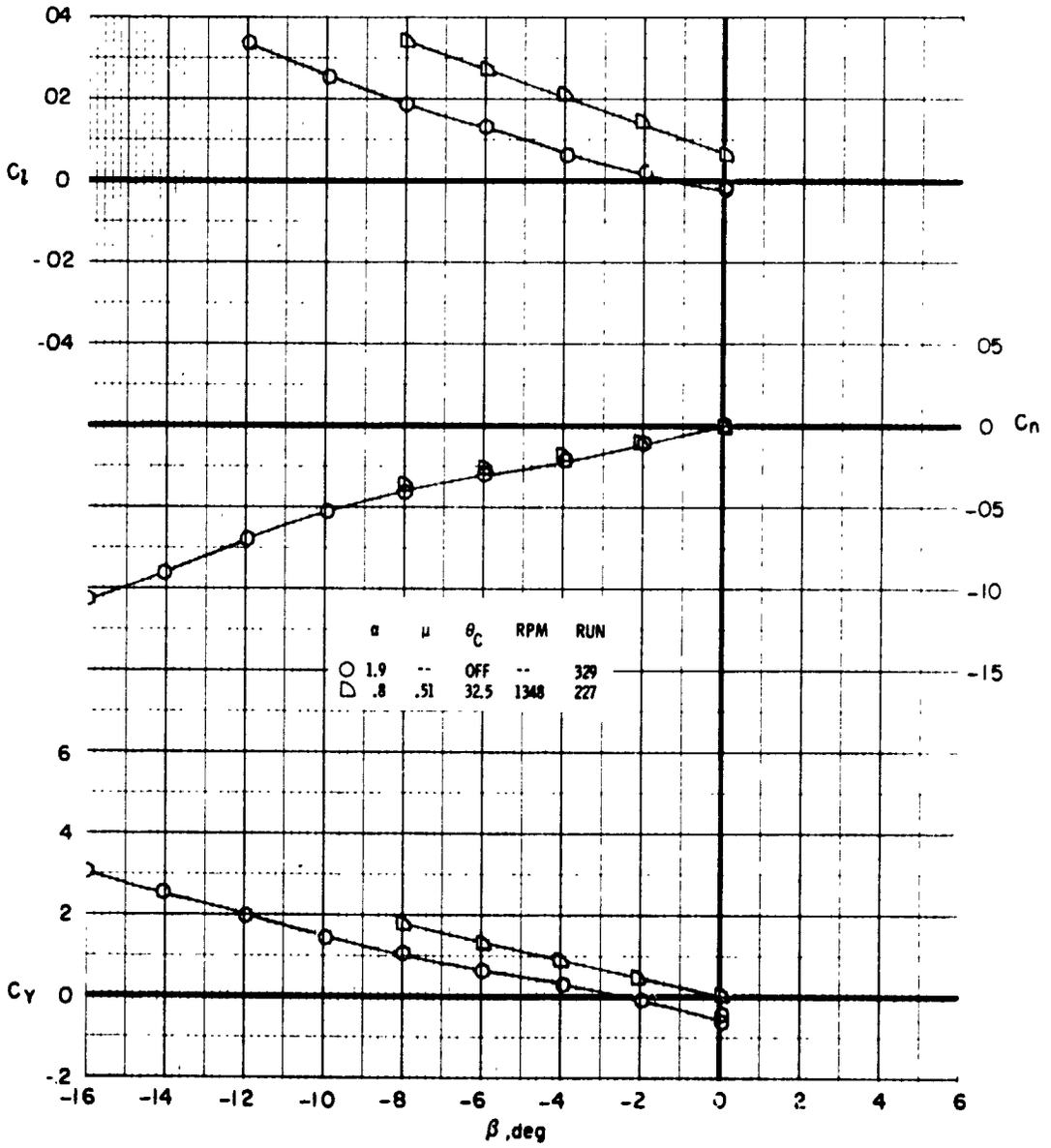

(c) V_{FS} = 180 kts

Figure 98. - Concluded.

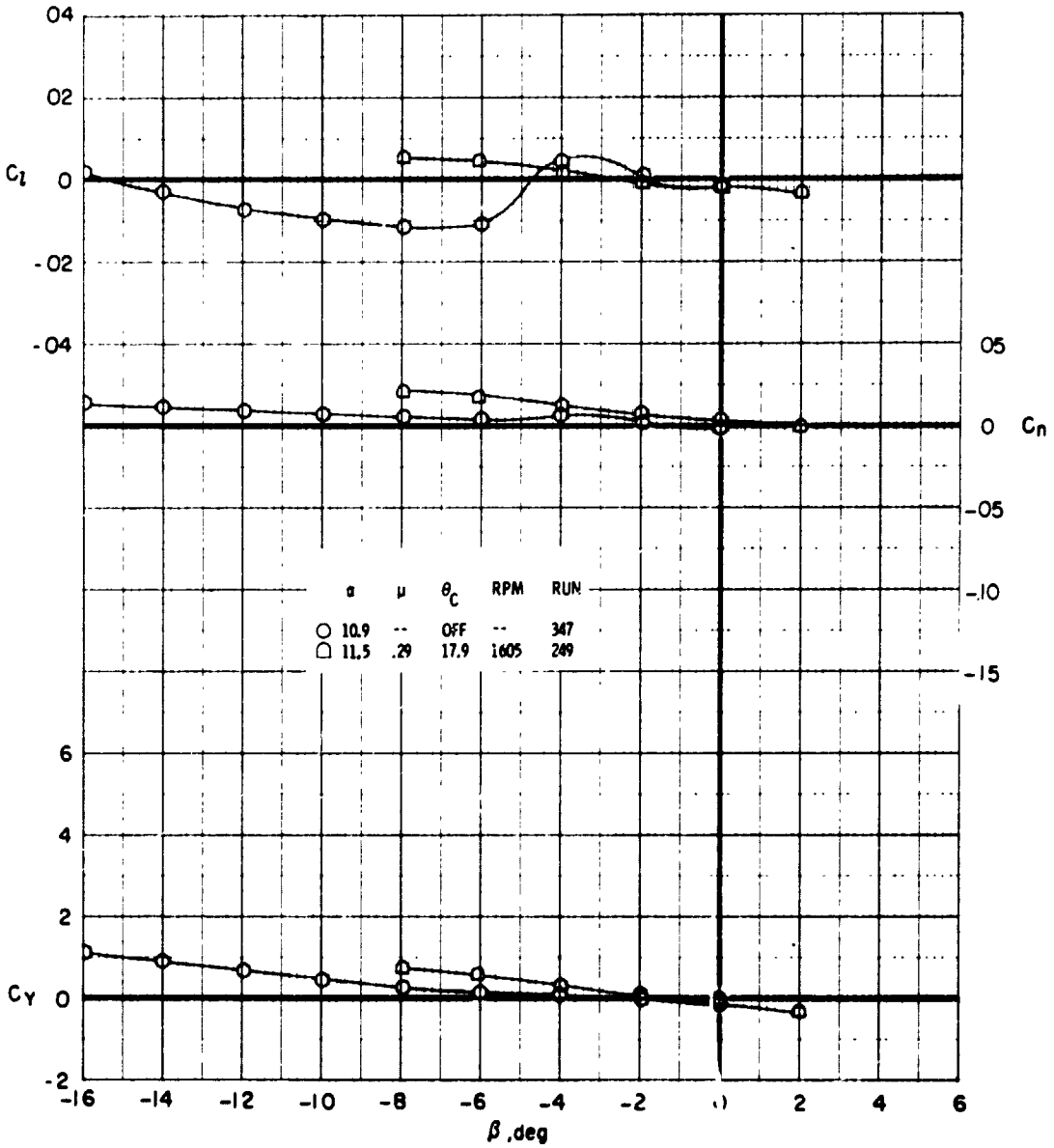

(a) V_{FS} = 120 kts

Figure 99. - Effects of rotor thrust and sideslip angle on lateral aerodynamic characteristics for full-scale flight speeds of 120 and 160 knots for pylon angle 0° and vertical tail off.

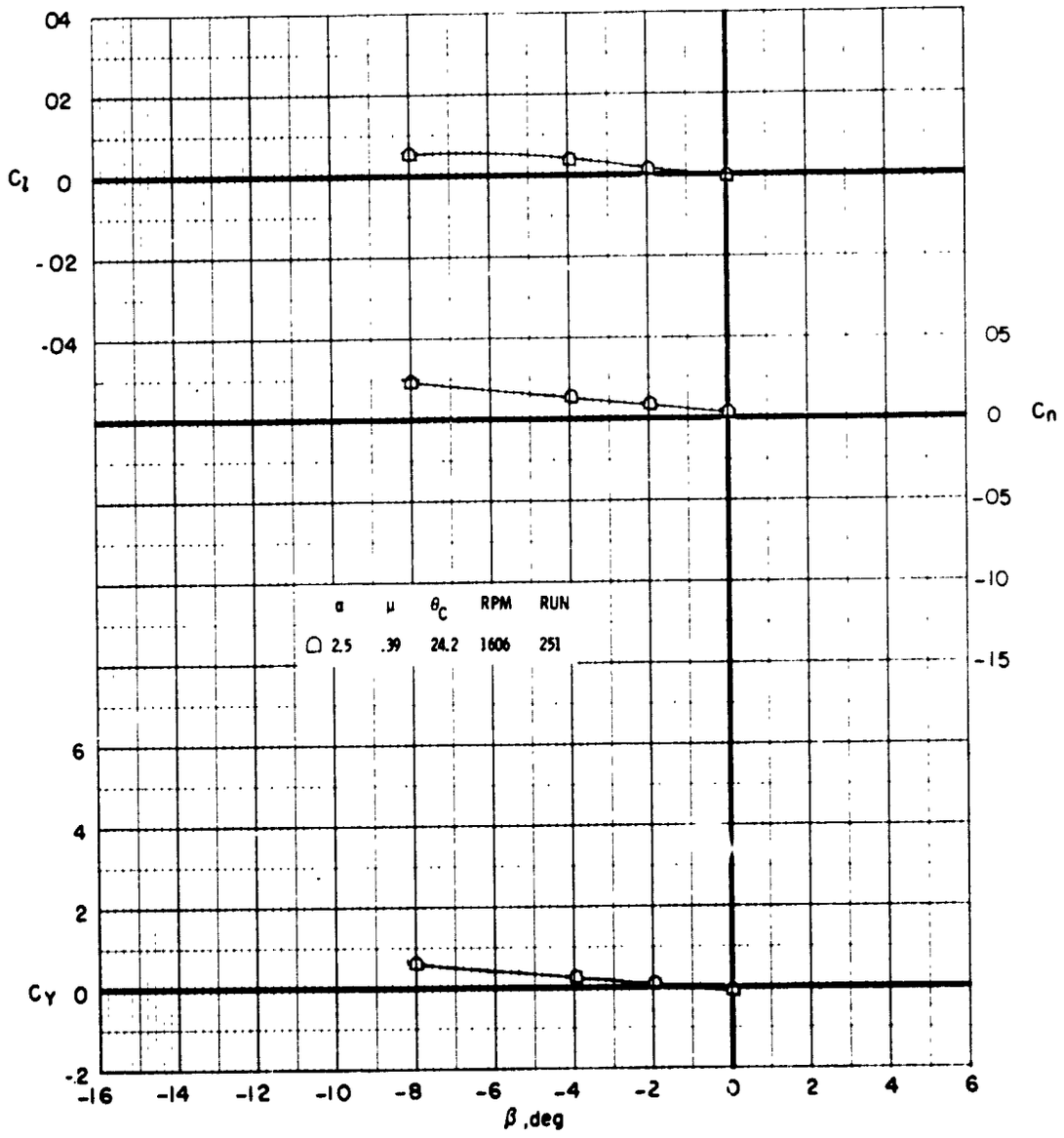

(b) V_{FS} = 160 kts

Figure 99. - Concluded.

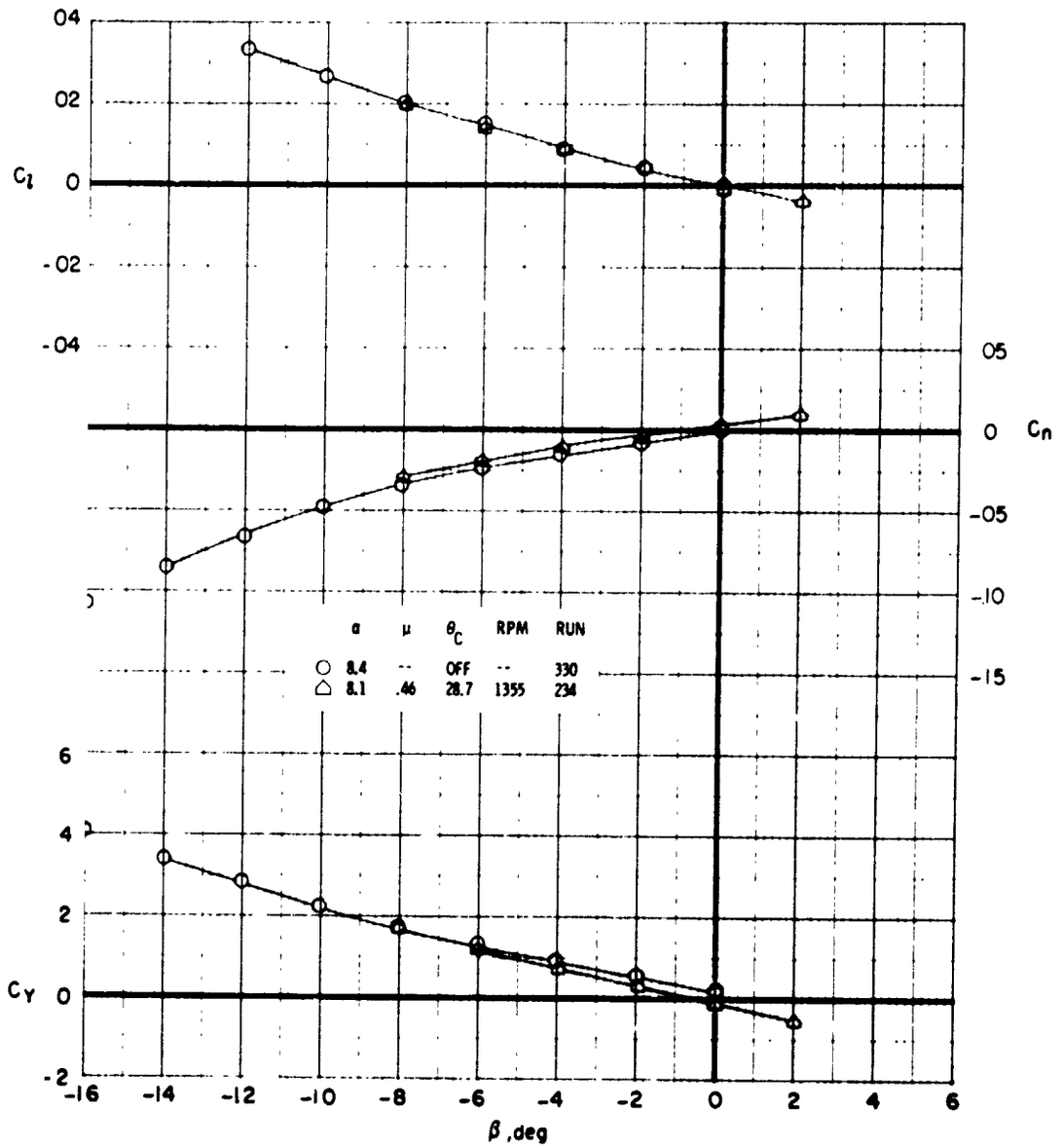

(a) V_{FS} = 160 kts

Figure 100. - Effects of rotor thrust and sideslip angle on lateral aerodynamic characteristics for full-scale flight speeds of 160 and 180 knots for pylon angle 0^0 and flap/aileron deflection $0^0/0^0$.

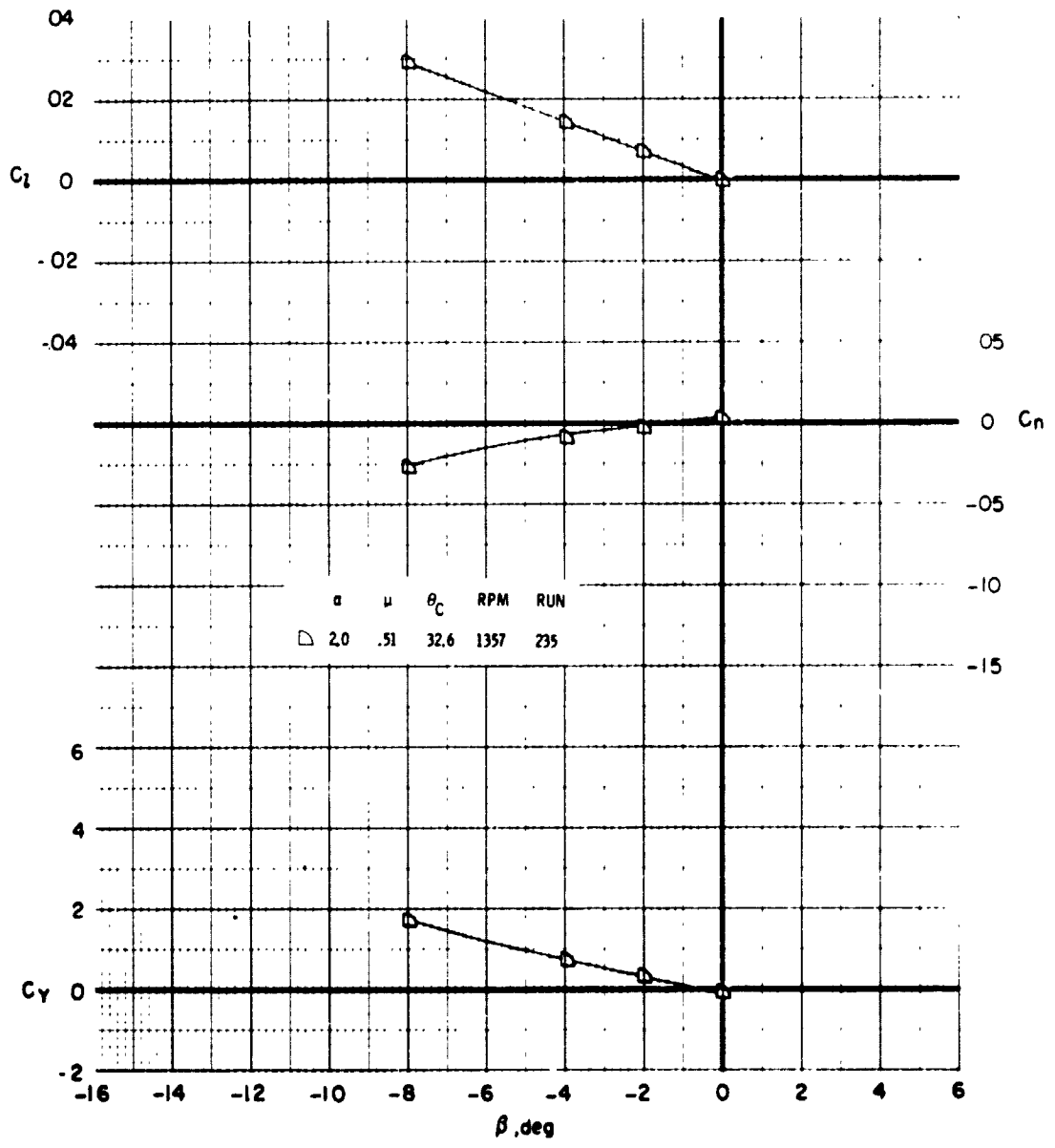

(b) V_{FS} = 180 kts

Figure 100. - Concluded.

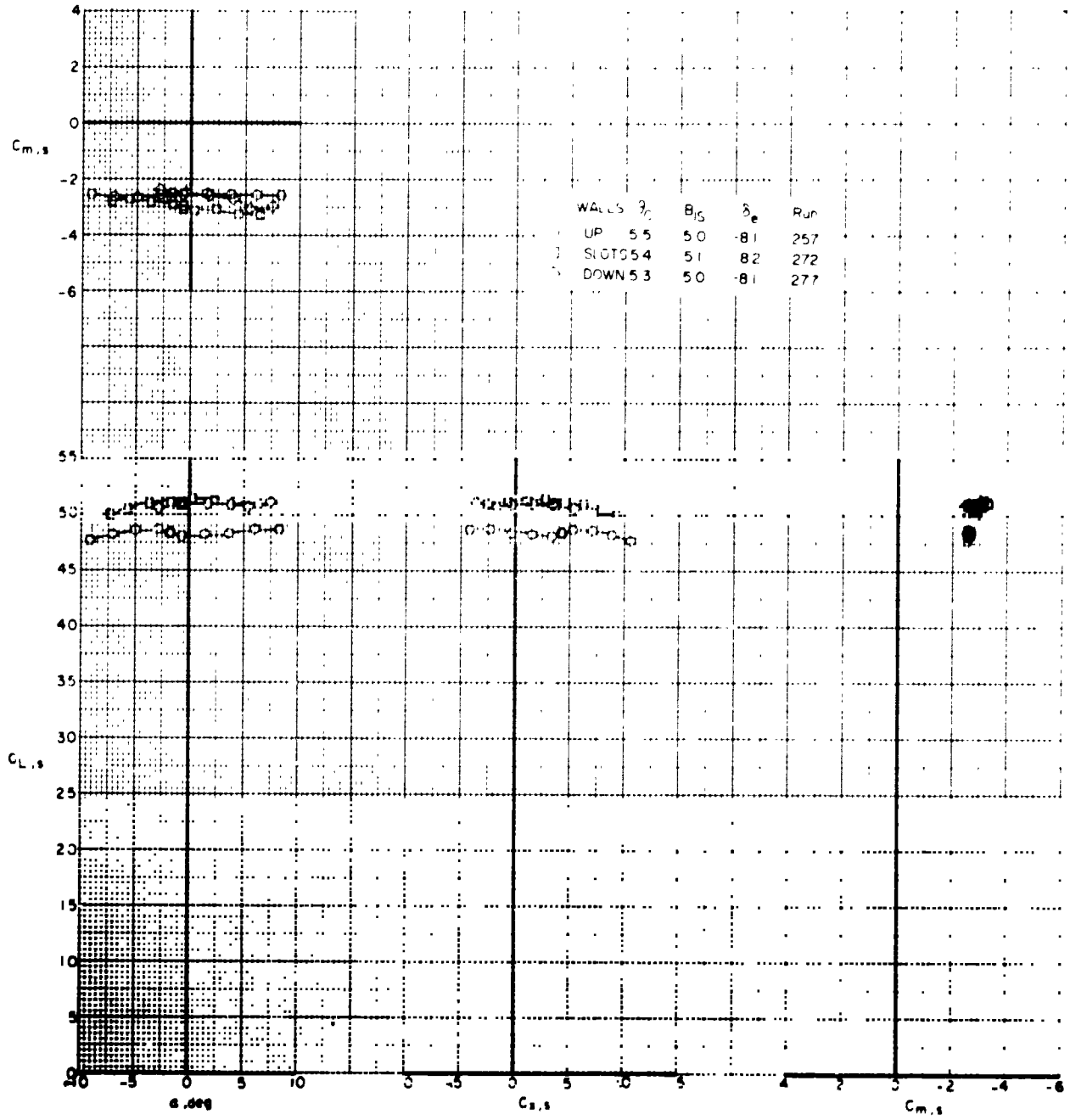

(a) V_{FS} = 20 kts (β = 0.08)

Figure 101. - Effect of wind-tunnel test section configuration on longitudinal aerodynamic characteristics at low full-scale flight speeds (20 to 60 kts) for pylon angle 90°.

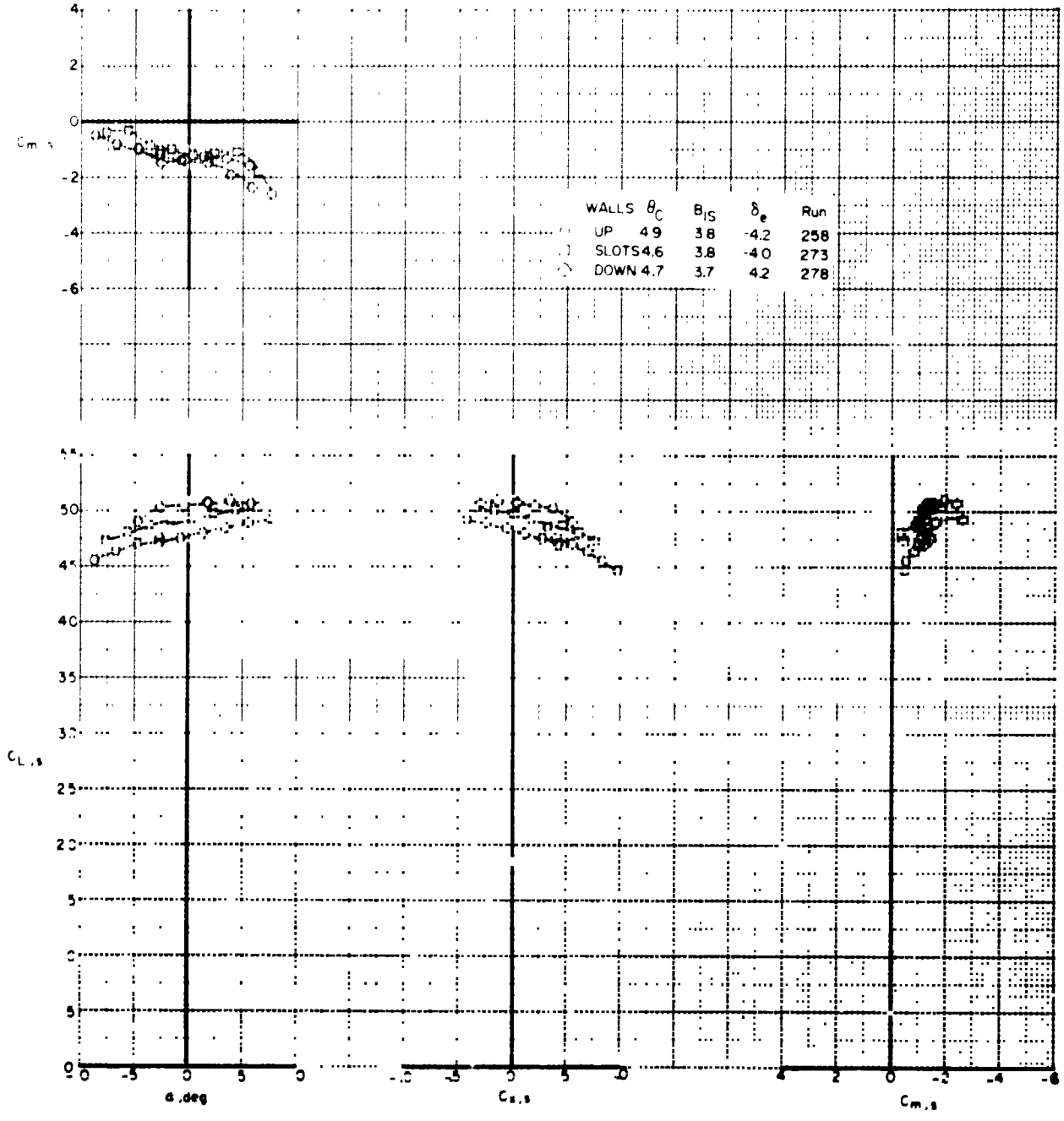

(b) V_{FS} = 30 kts (β = 0.0)

Figure 10L - Continued.

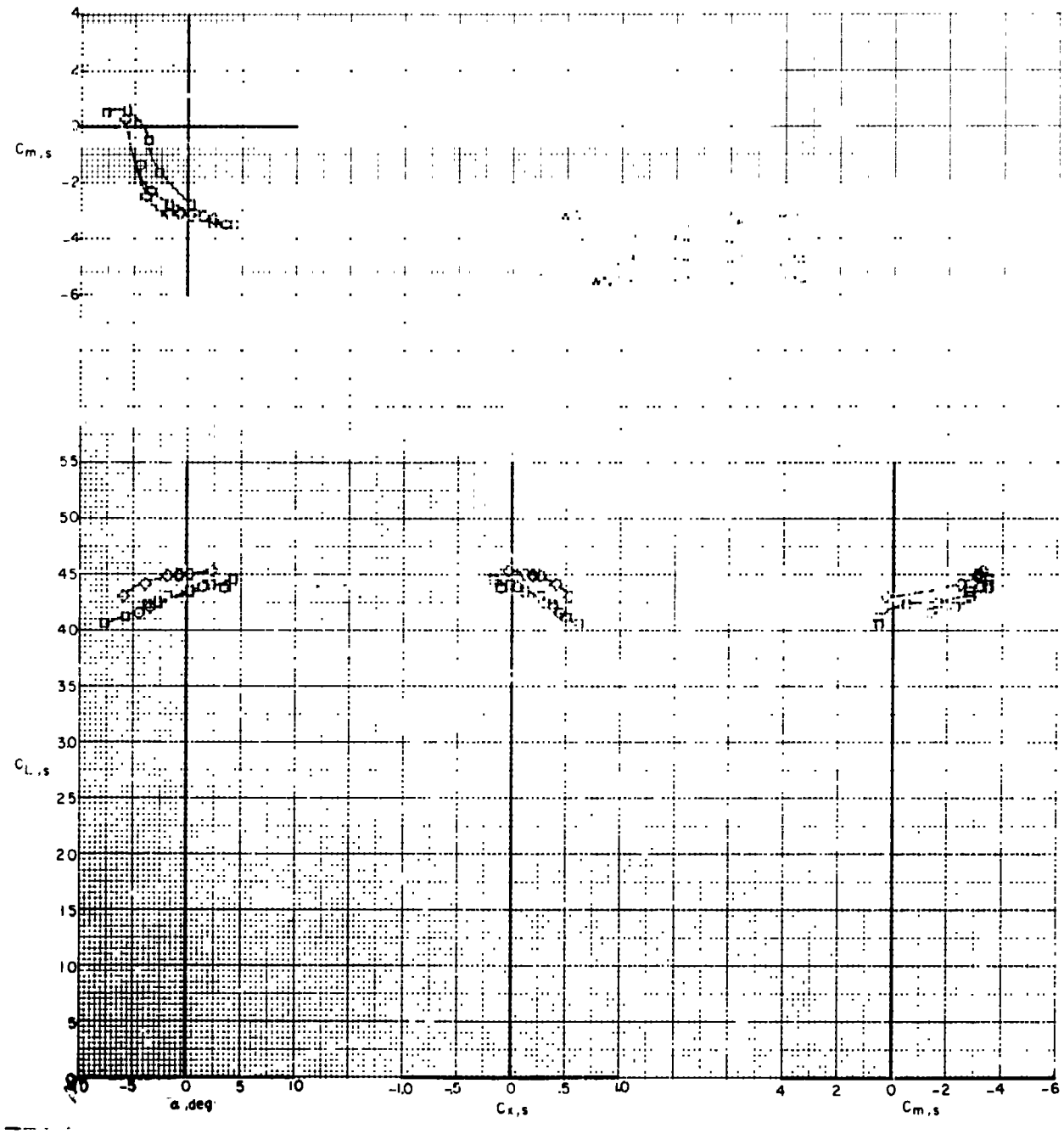

(c) V_{FS} = 40 kts (μ = 0.08

Figure 101. - Continued.

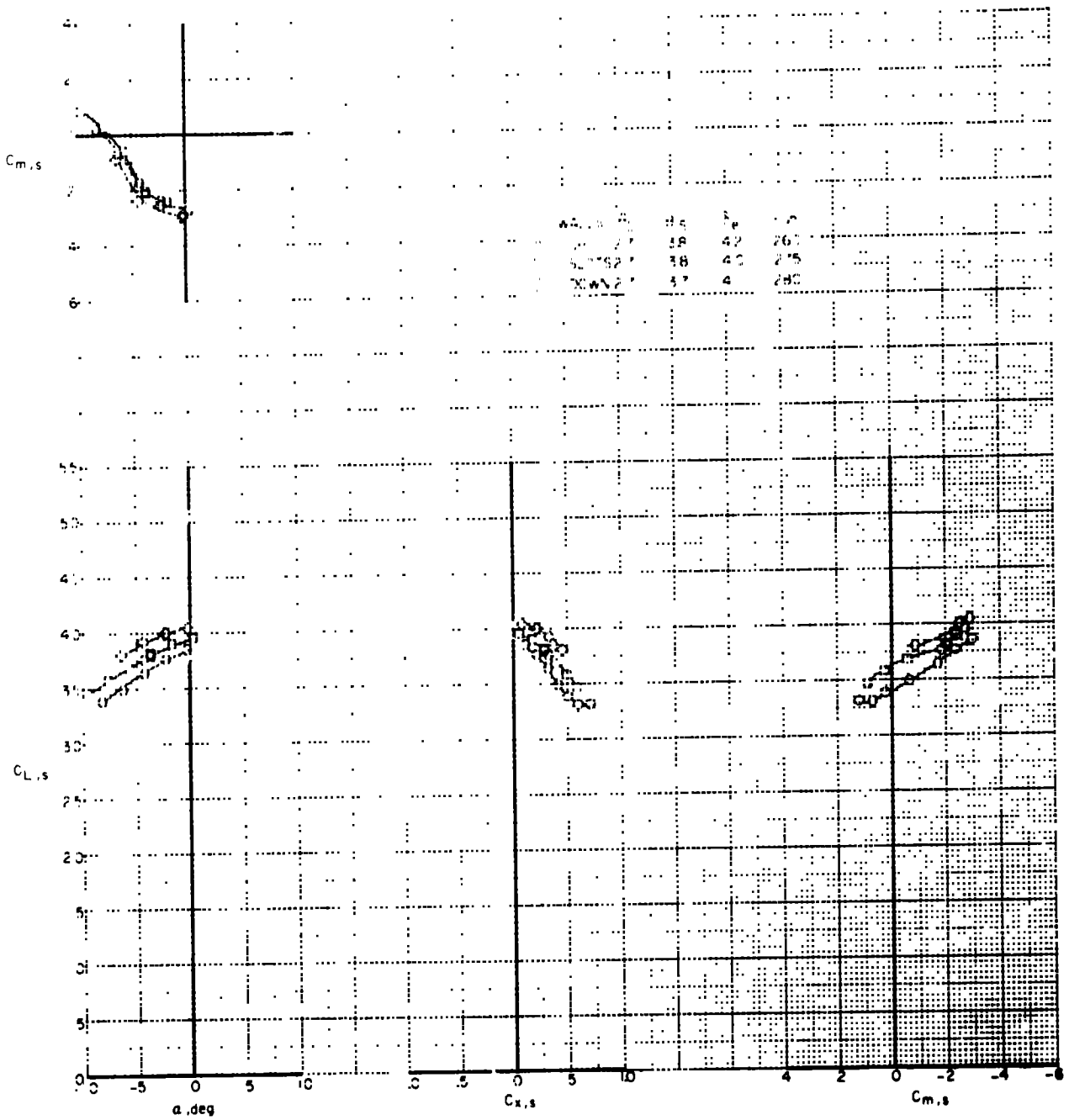

(d) V_{FS} = 50 kts (β = 0, 10)

Figure 101. - Continued.

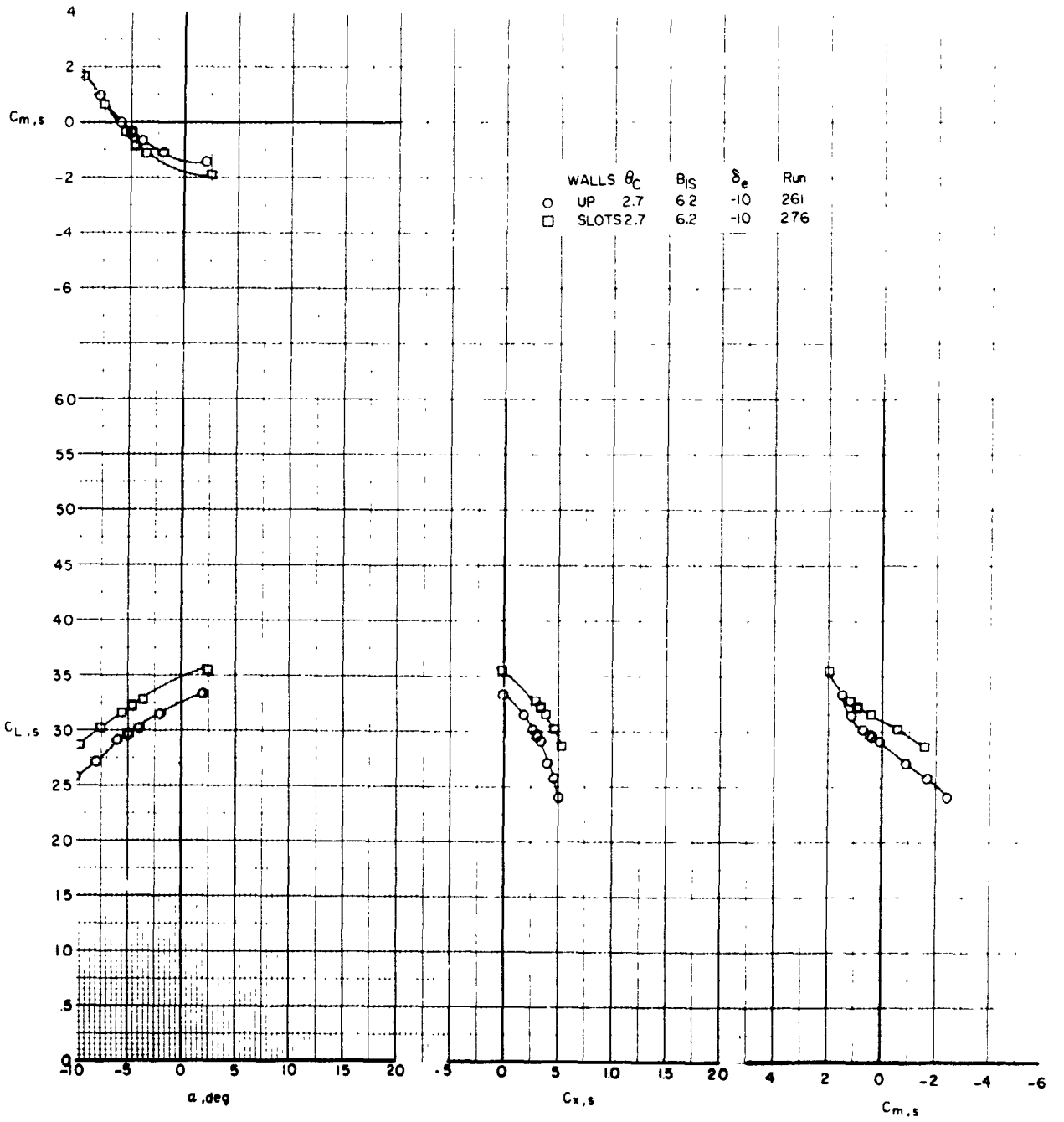

(e) V_{FS} = 63 kts (μ= 0.13)

Figure 10L - Concluded.

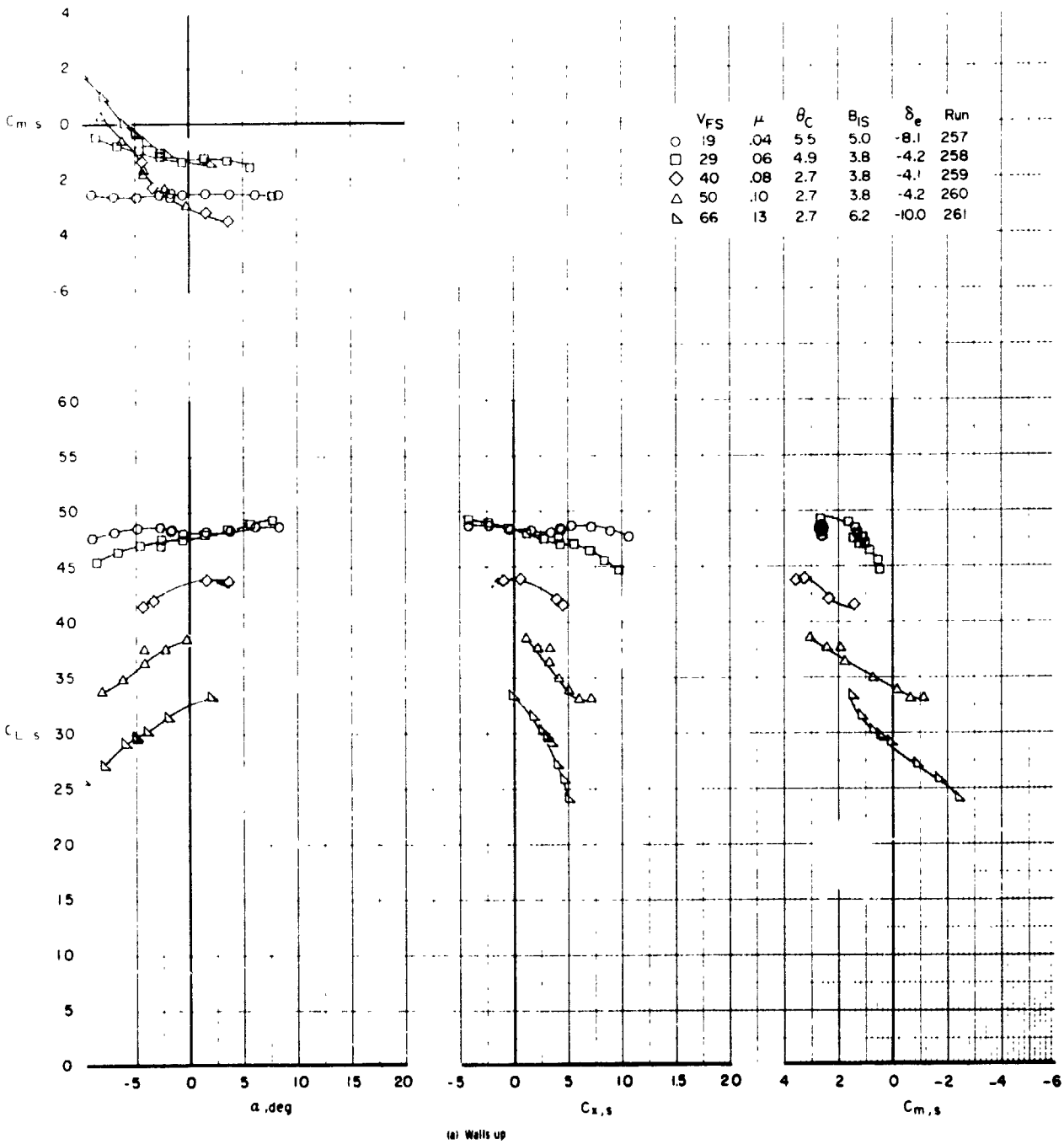

(a) Walls up

Figure 102. - Effect of ic · full-scale flight speeds and angle of attack on longitudinal aerodynamic characteristics as determined in three wind-tunnel test sections configurations for pylon angle 90°.

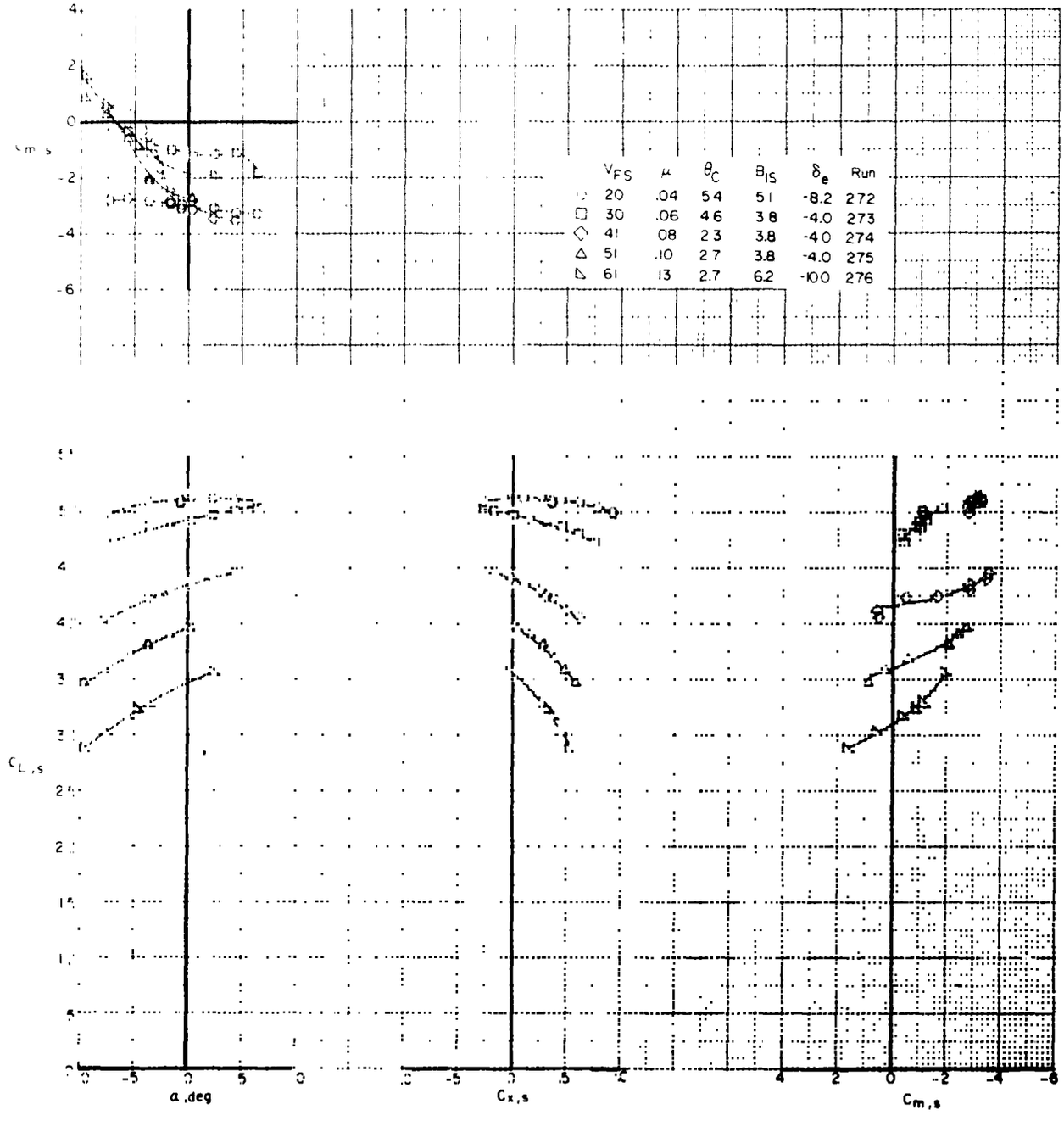

(b) Slotted walls

Figure 102. - Continued.

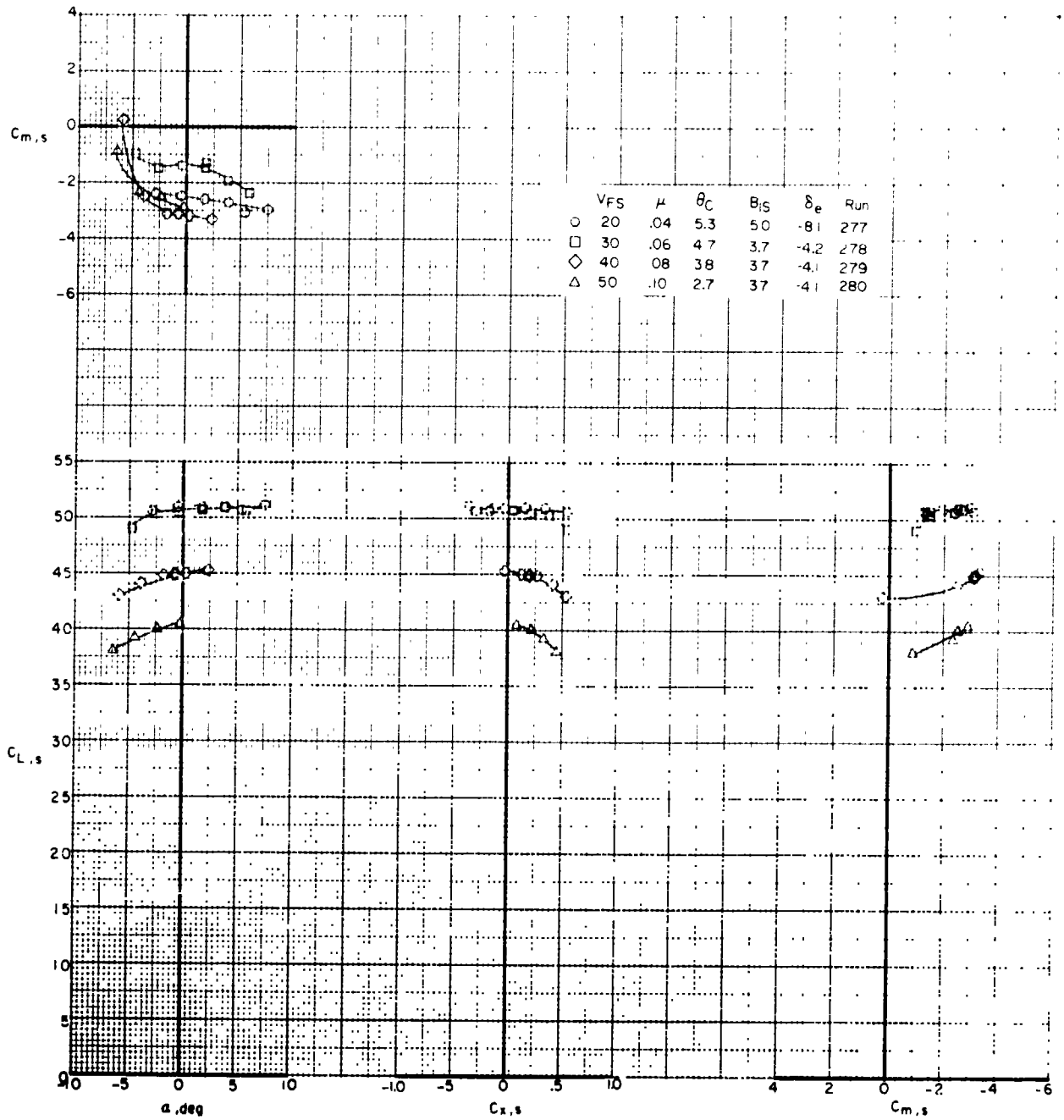

(c) Walls down

Figure 102. - Concluded.

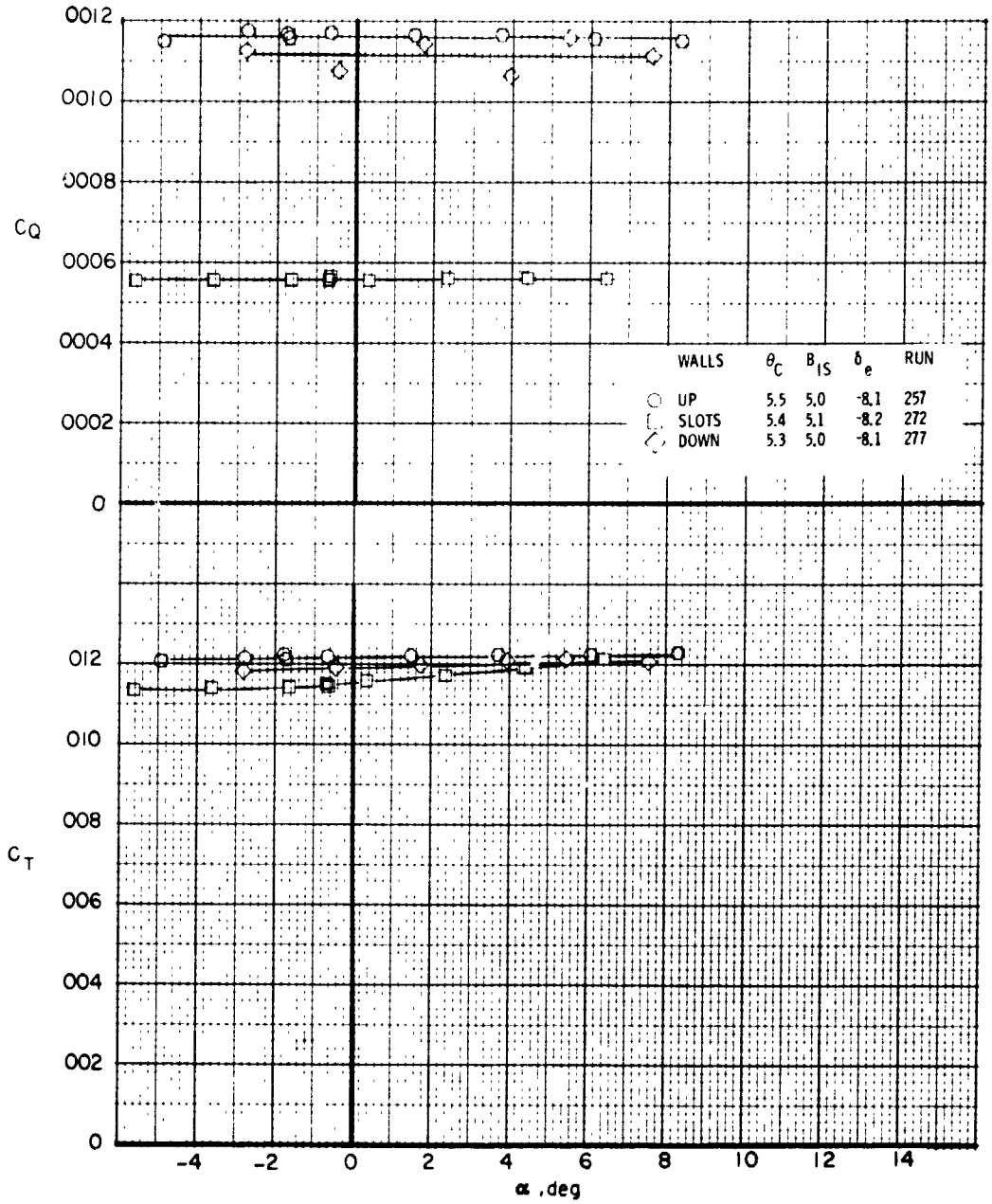

(a) V_{FS} = 20 kts (μ = 0.04)

Figure 103. - Effect of wind-tunnel test section configuration on the rotor thrust and torque at low full-scale flight speeds. $\alpha_p = 90^0$.

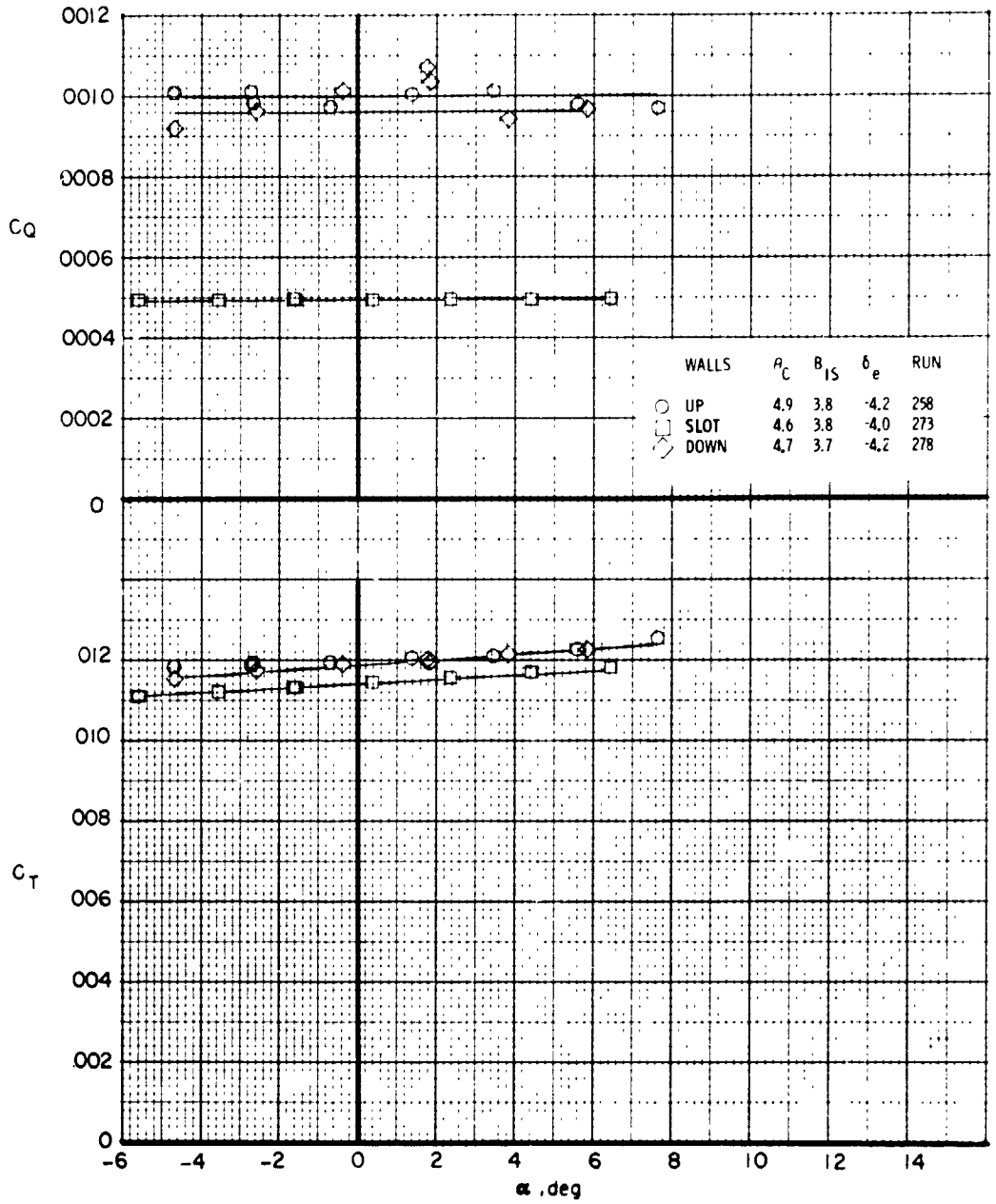

(b) V_{FS} = 30 kts (μ = 0.06)

Figure 103. - Continued.

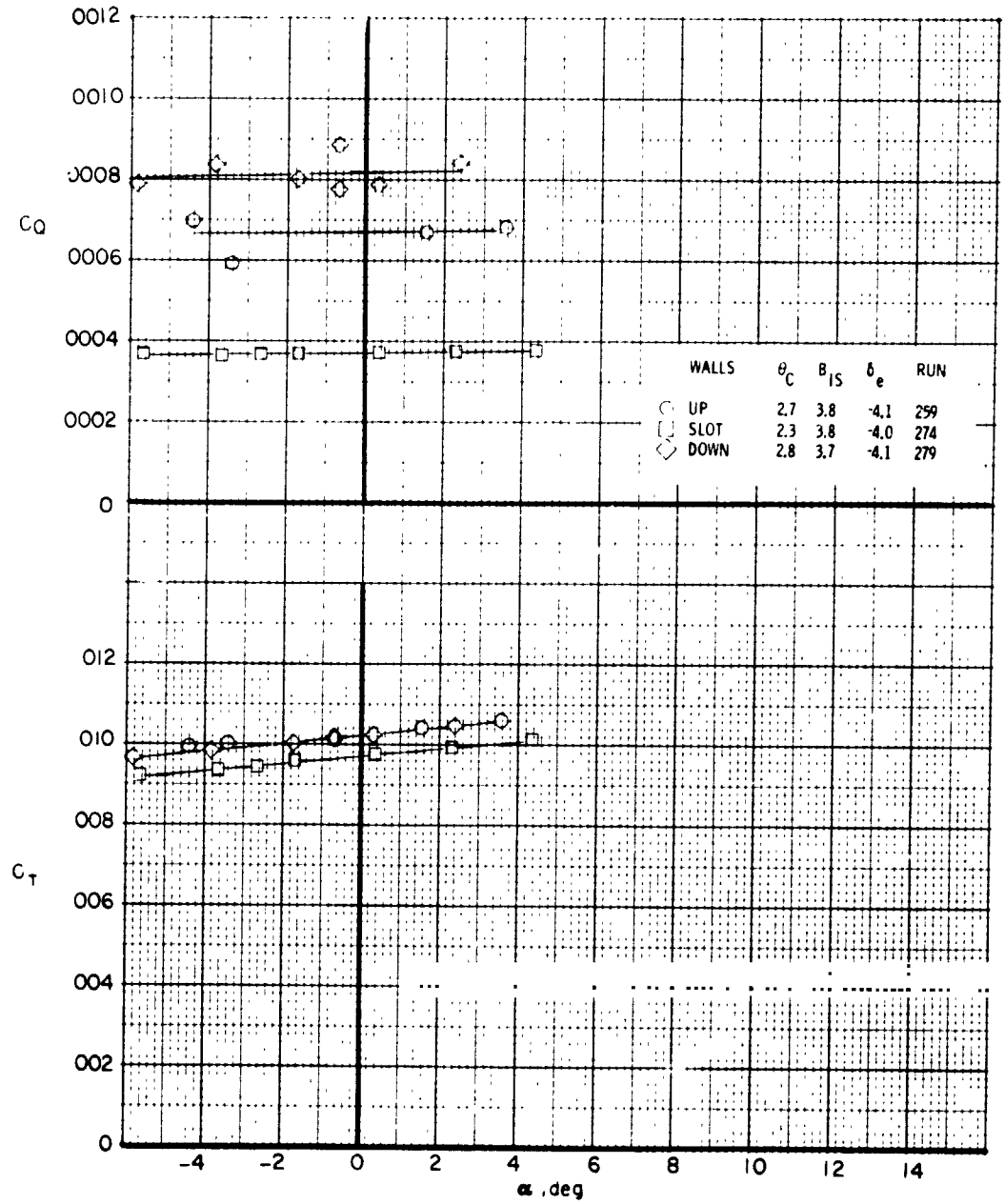

(c) V_{FS} = 40 kts (μ = 0.08)

Figure 103. - Continued.

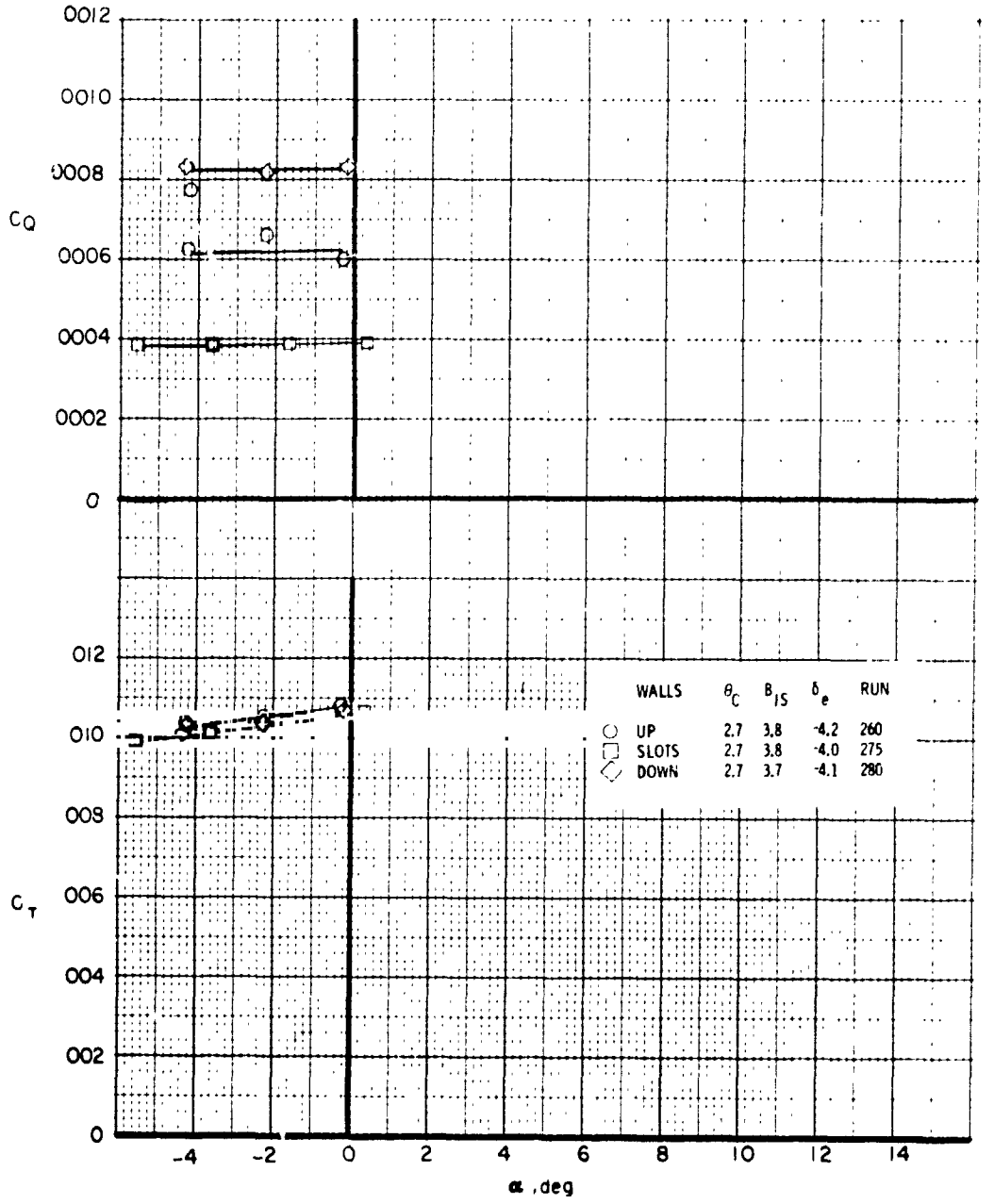

(d) V_{FS} = 50 kts (μ = 0.10)

Figure 103. - Continued.

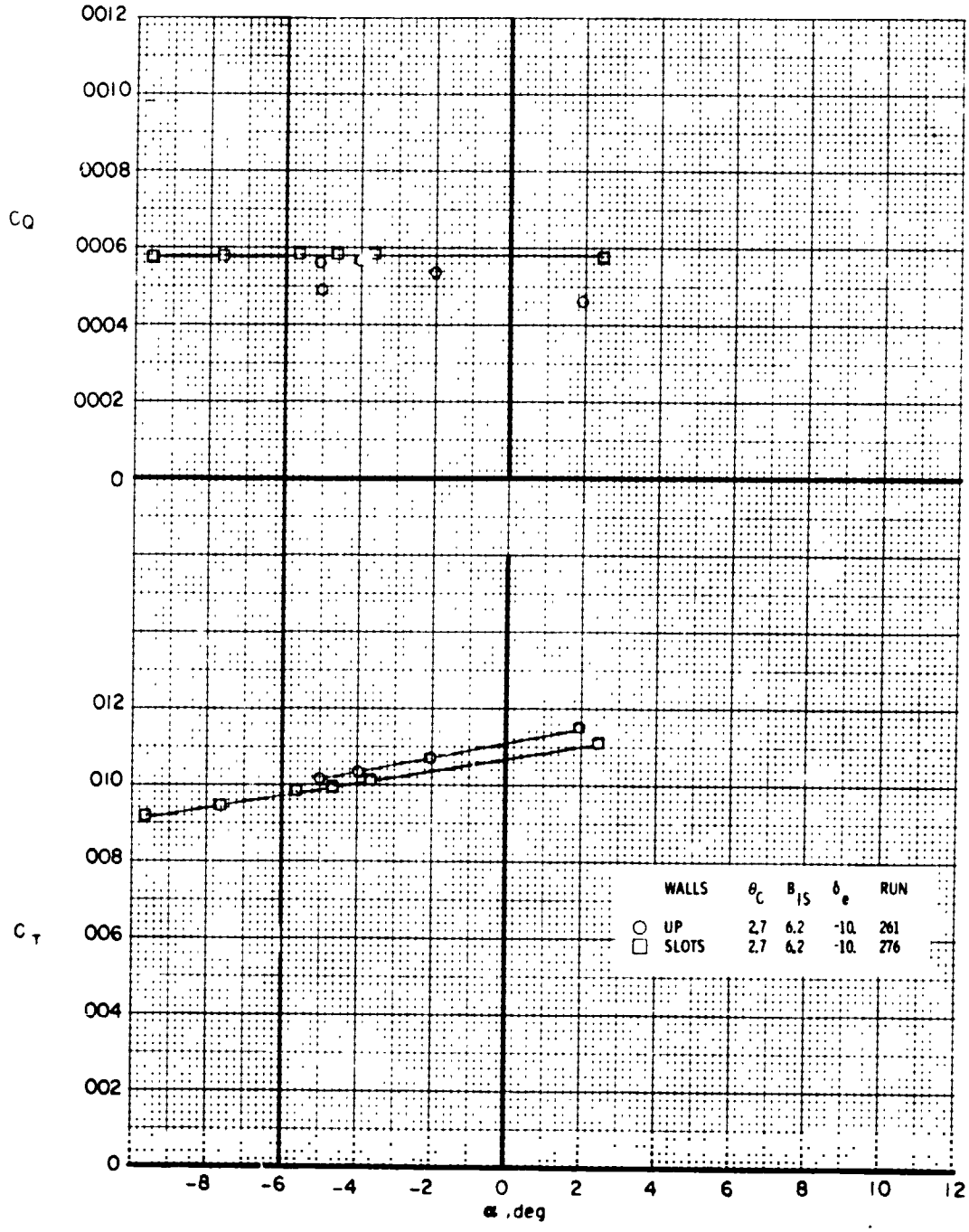

(e) V_{FS} = 60 kts (μ = 0.12)

Figure 103. - Concluded.